UNIVERSITÉ DE MONTRÉAL

THERMODYNAMIC MODELING OF ALUMINUM-MAGNESIUM-RARE EARTH SYSTEMS

LILING JIN

DÉPARTEMENT DE GÉNIE CHIMIQUE

ÉCOLE POLYTECHNIQUE DE MONTRÉAL

THÈSE PRESENTÉE EN VUE DE L'OBTENTION

DU DIPLÔME DE PHILOSOPHIAE DOCTOR

(GÉNIE MÉTALLURGIQUE)

AOÛT 2012

UNIVERSITÉ DE MONTRÉAL

ÉCOLE POLYTECHNIQUE DE MONTRÉAL

Cette thèse intitulée:

THERMODYNAMIC MODELING OF ALUMINUM-MAGNESIUM-RARE EARTH
SYSTEMS

présentée par : JIN Liling

en vue de l'obtention du diplôme de : Philosophiae Doctor

a été dûment acceptée par le jury d'examen constitué de :

M. PELTON Arthur D., Ph. D., président

M. CHARTRAND Patrice, Ph. D., membre et directeur de recherche

M. JUNG In-Ho, Ph. D., membre

Mme KATTNER Ursula R., Ph. D., membre

DEDICATION

To My Beloved Family

ACKNOWLEDGEMENTS

I would like to express my deepest gratitude toward my research supervisor Prof. Patrice Chartrand, for providing me such a wonderful opportunity to deepen my scientific knowledge and for his guidance and support throughout my studies.

I would also like to thank the Center for Research in Computational Thermochemistry (CRCT) at École Polytechnique de Montréal, where this project has been completed.

I am also grateful to Prof. Mamoun Medraj, Dr. Dmytro Kevorkov, Mr. Mazen Samara, Mr. Tian Wang and Mr. Yi-Nan Zhang from Concordia Universtiy, without whom the diffusion couple and key experiments could not have been done.

I would like to give my special thanks to Prof. Ping Wu and Dr. Kewu Bai at Institute of High Performance Computing (IHPC), Singapore for their training of the First-Principles calculations.

I am indebted to Prof. Arthur D. Pelton, Prof. Christopher Bale, and Dr. Youn-bae Kang for their helpful advice and discussions. I am very grateful to Dr. Aimen Gheribi for the discussion and support on First-Principles and Miedema's model. I would like to thank Dr. Christian Robelin for french translation of the abstract.

I would like to show my appreciation to Prof. In-Ho Jung from McGill University, who provided neodymium metal for my experiments. I would like to thank Dr. Lang Shi from McGill University for his help with electron probe microanalysis (EPMA) experiments.

I would like to thank all the members of CRCT, Dr. Christian Robelin, Dr. Aimen Gheribi, Dr. Jacques Melançon, Mme Catherine Boucher, Mme Éve Belisle, Dr. Wan-Yi Kim, Mr. Adarsh Shuklar, Dr. Guillaume Lambotte, Mr. Zhi-jun Zhu, Mr. Jian Wang, *etc*, for their friendship and kindness. I would like to express my deepest gratitude to Luc for his support and encouragement.

Last but not least, financial support from General Motors of Canada Ltd. and the Natural Sciences, Engineering and Research Council of Canada through the CRD grant program, REGAL and FQRNT are gratefully acknowledged.

RÉSUMÉ

Le magnésium et ses alliages sont les matériaux métalliques structuraux les plus légers et, de ce fait, jouent un rôle croissant dans les domaines de l'automobile, de l'aérospatial et de l'électronique. Bien que le magnésium puisse être recyclé aisément et ait une conductivité thermique élevée et de bonnes propriétés de protection électromagnétique, il présente des inconvénients : une force insuffisante, une faible résistance à la corrosion et au fluage,… L'utilisation d'alliages de magnésium est l'une des méthodes fréquemment utilisées pour améliorer les propriétés du magnésium. L'ajout de terres rares (RE : «*Rare Earth*») à des alliages de magnésium peut améliorer leur force et leur résistance au fluage à température élevée en formant des précipités stables à base de Mg (RE_yMg_x), Al (RE_yAl_x) ou Zn (RE_yZn_x).

Parallèlement au développement d'alliages de Mg, les alliages Al–RE (aluminium-terre rare) sont d'intérêt en science des matériaux dans le cadre du développement d'alliages légers. Les terres rares sont des éléments d'alliage d'importance croissante pour les alliages d'aluminium à cause de leur capacité à améliorer les propriétés à haute température et les caractéristiques de moulage. De plus, les alliages Al–RE rapidement solidifiés offrent aussi la possibilité d'obtenir un meilleur comportement en corrosion.

Les méthodes calculatoires sont des outils importants et puissants pour la sélection et l'élaboration de nouveaux alliages de magnésium. Elles aident à comprendre le comportement des matériaux et réduisent significativement la quantité de travail expérimental requise. De plus, les terres rares pures sont très coûteuses.

Jusqu'à présent, il n'existait aucun diagramme de phases pour les systèmes Mg-Al-Mischmetal optimisé à l'aide du modèle quasichimique (prenant en compte l'ordre à courte distance) pour la phase liquide, à l'exception de quelques optimisations récentes (Al–Ce, Al–Y, Al–Sc) effectuées par le Dr. Youn-Bae Kang au CRCT de l'Ecole Polytechnique de Montréal. De plus, certains systèmes (Al–Mg–Pr, Al–Mg–Nd, Al–Mg–Tb, Al–La–Nd, Al–Pr–Nd, Al–La–Pr, Al–Ce–La et Al–Ce–Pr) n'avaient pas encore été optimisés thermodynamiquement.

L'objectif principal de cette thèse est de développer une banque de données thermodynamiques pour le système Al–Mg–La–Ce–Pr–Nd–Sm–Gd–Tb–Dy–Ho–Er. Ainsi, des modèles

thermodynamiques pour le liquide, les solutions solides et les composés stœchiométriques ont été proposés; les diagrammes de phases et les propriétés thermodynamiques des systèmes binaires Al–RE, Mg–RE et RE'–RE'', ainsi que des systèmes ternaires Mg–Al–RE et Al–RE'–RE'' ont été optimisés à l'aide des données expérimentales et / ou théoriques. Le second objectif consiste à faire des expériences clés dans la région riche en magnésium afin de vérifier les équilibres des phases, car cela est très important pour la conception de nouveau alliage à base de magnésium. L'étude expérimentale a été effectuée pour les systèmes ternaires Al–Mg–La, Al–Mg–Ce, Al–Mg–Pr et Al–Mg–Nd afin d'obtenir les phases en équilibres ainsi que les informations concernant les solubilités des solutions solides. Le troisième objectif de la recherche consiste à développer des méthodes originales pour estimer les données thermodynamiques absentes de la littérature scientifique pour les phases contenant des terres rares.

Nous avons tout d'abord optimisé les systèmes binaires Al–RE (RE= La, Ce, Pr, Nd, Sm, Gd, Tb, Dy, Ho, Er) à partir d'une revue de la littérature pour les solides (composés intermétalliques, structures cristallographiques, températures de fusion, chaleurs de formation, températures de transformation,…), pour les propriétés du liquide (enthalpie de mélange intégrale, enthalpie de mélange partielle, activités des composants, capacités calorifiques, solubilités à l'état solide,…) et pour les données expérimentales de diagrammes de phases. Une approche systématique a été adoptée au cours des optimisations thermodynamiques. Puisque les terres rares sont chimiquement proches, une comparaison avec les terres rares voisines et une analyse systématique de la température de fusion des composés a facilité l'optimisation du système Al–Tb pour lequel peu de données expérimentales étaient disponibles.

Deuxièmement, pour les systèmes Mg–RE pour lesquels les données expérimentales étaient rares ou contradictoires, des calculs de premier principe ont été utilisés pour évaluer l'enthalpie de formation de certains composés ainsi que l'enthalpie de mélange pour les phases FCC et HCP à l'aide de la technique "*supercell*". En parallèle, des estimations ont été faites à l'aide du modèle semi-empirique de Miedema puis ont été comparées aux calculs de premier principe. Il a été suggéré que le modèle semi-empirique de Miedema peut fournir un bon estimé initial pour l'enthalpie de formation des composés et l'enthalpie de mélange de solutions sans un coût élevé

en calculs. Ainsi, le modèle de Miedema a été utilisé pour estimer l'enthalpie de formation des composés ternaires et des phases métastables dans les systèmes ternaires Mg–Al–RE.

Troisièmement, en ce qui concerne les systèmes ternaires Mg–Al–RE, leurs propriétés thermodynamiques et leurs équilibres de phase ont été moins étudiés comparativement aux autres systèmes métalliques. Les évaluations et optimisations thermodynamiques des systèmes Al–Mg–RE (RE= La, Ce, Pr, Nd, et Sm) ont été effectuées systématiquement sur la base de l'information disponible dans la littérature et de nos résultats expérimentaux. Dans ce travail, des expériences-clés ont été réalisées pour les systèmes Mg–Al–La, Mg–Al–Ce, Mg–Al–Pr, et Mg–Al–Nd pour vérifier les équilibres de phases dans le coin riche en Mg et les solubilités à l'état solide. Les estimations à l'aide du modèle de Miedema de l'enthalpie de formation pour les composés ternaires ont été utilisées pour les optimisations thermodynamiques de tous les systèmes Mg–Al–terre rare. Dans les systèmes Mg–Al–Gd (Dy, Ho), des compromis ont été faits entre les données expérimentales (température du liquidus) et les optimisations en considérant la fiabilité limitée des expériences à haute température (1200 K et plus). Nous n'avons pas jugé nécessaire l'utilisation de nombreux paramètres ternaires en excès pour le liquide pour bien reproduire les données expérimentales. Le système Mg–Al–Tb a été estimé en supposant des similarités avec les systèmes Mg–Al–Gd (Dy), et les résultats correspondants ont été présentés pour la première fois dans la présente étude. Une technique d'interpolation de type Kohler a été utilisée, considérant le fait que les enthalpies de mélange des liquides Al–Mg, Al–RE et Mg–RE sont très différentes les unes des autres.

Quatrièmement, pour les systèmes Al–RE'–RE", les systèmes binaires RE'–RE" (La–Ce, La–Pr, La–Nd, Ce–Pr, Ce–Nd, Pr–Nd) ont été optimisés à partir de l'information expérimentale disponible. A l'exception des systèmes La–Nd et Ce–Pr, aucun paramètre en excès n'a été utilisé pour le liquide. Des données expérimentales ne sont disponibles que pour le système Al–Ce–Nd. Les autres systèmes Al–RE'–RE" ont été optimisés en supposant des propriétés thermodynamiques similaires à celles du système Al–Ce–Nd.

Finalement, des applications de la banque de données thermodynamiques ont été montrées.

La banque de données thermodynamiques pour les systèmes Mg–Al–RE fournira une ligne directrice claire pour la sélection et l'élaboration d'alliages de Mg et de Al; ce qui permettra d'éviter des expériences à long-terme improductives portant sur des alliages ayant moins de potentiel pour des applications pratiques.

ABSTRACT

As the current lightest structural metallic material, magnesium and its alloys play an increasingly important role in automotive, aerospace and electronic consumer products. Although magnesium has excellent recyclability, high thermal conductivity, good electromagnetic shielding characteristics and so on, it suffers from its shortcomings: insufficient strength, poor corrosion and low creep resistance, *etc*. Alloying magnesium is one of the frequently used methods to improve its properties. Adding Rare Earth (RE) metals to magnesium alloys can improve their strength and creep resistance at elevated temperatures by forming stable precipitates with Mg, for example, (RE_yMg_x), Al (RE_yAl_x) or Zn (RE_yZn_x).

Parallel to Mg alloys development, Al–RE (aluminum – rare earths) alloys have been of interest to materials scientists who want to develop light weight alloys. Rare earths have an increasing importance as alloying elements in aluminum alloys because of their ability to enhance the high temperature properties and casting characteristics. Moreover, rapidly solidified Al–RE alloys also offer the possibility of obtaining better corrosion behavior.

Computational methods are important and powerful tools in the selection and design of new magnesium alloys. These methods help our understanding of materials behavior, while they significantly reduce extensive and time-consuming experimental work. Furthermore, pure rare earth metals are expensive.

Up to the present, few phase diagrams for Mg–Al–Mischmetal systems have been optimized using the quasichemical model (which takes into account short-range ordering) for the liquid phase except some recent optimizations (Al–Ce, Al–Y, and Al–Sc) by Dr. Youn-Bae Kang of CRCT at École Polytechnique de Montréal. Furthermore, some systems (Al–Mg–Pr, Al–Mg–Nd, Al–Mg–Tb, Al–La–Nd, Al–Pr–Nd, Al–La–Pr, Al–Ce–La, and Al–Ce–Pr) have not yet been thermodynamically optimized.

The main objective of this thesis is to build a thermodynamic database for Al–Mg–La–Ce–Pr–Nd–Sm–Gd–Tb–Dy–Ho–Er systems. To this end, thermodynamic models of liquid and solid solutions and stoichiometric compounds have been proposed; phase diagrams and thermodynamic properties of binary Al–RE, Mg–RE, RE'–RE" systems, ternary Mg–Al–RE and Al– RE'– RE" systems have been optimized based on experimental and/or theoretical data. The secondary objective of this research is to do key experiments in the magnesium-rich corners of ternary systems to check phase equilibrium, since this is very important for Mg alloy design. Key experimental investigations have been performed for the Al–Mg–La, Al–Mg–Ce, Al–Mg–Pr and Al–Mg–Nd ternary systems in order to obtain phase equilibria and solid solubilities information. The third objective in this work is to find or develop proper methods for estimating the missing thermodynamic data for the binary and ternary phases which include rare earth elements.

First, Al–RE (RE= La, Ce, Pr, Nd, Sm, Gd, Tb, Dy, Ho, Er) binary systems were optimized, based on literature review for the solids (intermetallic compounds, their crystal structures, melting points, enthalpy of formation, transformation temperature, *etc*), liquid properties (integral enthalpy of mixing, partial enthalpy of mixing, activities of the components, heat capacities, solid solubility and so on) and experimental phase diagram data. A systematic approach has been used in the course of thermodynamic optimizations. Since rare earths are chemically similar, comparision with neighboring rare earth elements and systematic analysis of melting point of compounds helped in the optimization of the Al–Tb system, in which few experimental data are available.

Second, for the Mg–RE systems in which the experimental data were scarce or contradictory, First-Principles were employed to calculate the enthalpy of formation of certain compounds and enthalpy of mixing for the FCC and HCP phases using the supercell technique. Meantime, estimations from the semi-empirical Miedema model were made and compared to First-Principles calculations. It was suggested that the semi-empirical Miedema model can provide a good initial guess for the enthalpy of formation of compounds and the enthalpy of mixing for solutions for thermodynamic optimizations, without high computing cost. Therefore, the Miedema model was

used to estimate the enthalpy of formation of the ternary compounds and metastable phases in Mg–Al–RE ternary systems.

Third, as for Mg–Al–RE ternary systems, less research has been done on the thermodynamic properties and phase equilibria of these systems compared to other metallic systems. Thermodynamic evaluations and optimizations of the Al–Mg–RE (RE= La, Ce, Pr, Nd, Sm) systems have been systematically carried out on the basis of literature information and our experimental results. In this work, key experiments were performed for the Mg–Al–La, Mg–Al–Ce, Mg–Al–Pr, and Mg–Al–Nd systems to check phase equilibria in the Mg-rich corners and solid solubilities. The estimations of enthalpy of formation for the ternary compounds from Miedema model were used for thermodynamic optimizations of all the Mg–Al–rare earth systems. In the Mg–Al–Gd (Dy, Ho) systems, careful weighting was made between the experimental data (liquidus temperature) and optimization results, considering the restricted accuracy of experimental results at high temperatures (1200 K and more). It was judged unnecessary to use many excess ternary parameters for the liquid to fit satisfactorily the experimental data. The Mg–Al–Tb system was estimated by assuming similarities to the Mg–Al–Gd (Dy) systems and is presented for the first time in the present study. The Kohler-type interpolation method was used, seeing that the enthalpies of mixing of the liquid in the Al–Mg, Al–RE, and Mg–RE systems differ significantly.

Fourth, RE'–RE" (La–Ce, La–Pr, La–Nd, Ce–Pr, Ce–Nd, Pr–Nd) binary systems were optimized based on the available experimental information. Except for the La–Nd and Ce–Pr systems, no excess parameters were used for the liquid. For the Al–RE'–RE" systems, experimental data are available only for the Al–Ce–Nd system. Other Al– RE'–RE" systems were optimized assuming thermodynamic properties similar to those of the Al–Ce–Nd system.

Finally, some applications of this thermodynamic database were shown.

The thermodynamic database of the Mg–Al–RE systems will provide clear guidelines for Mg and Al alloy selection and design, thereby avoiding unproductive long-term experiments with alloys which have less potential for practical applications.

CONDENSÉ EN FRANÇAIS

Les alliages à base de magnésium sont parmi les plus légers matériaux structuraux et dont les applications commerciales sont importantes (industrie automobile et aérospatiale par exemple). L'addition d'éléments chimiques comme les terres rares (RE) dans les alliages de magnésium pourrait améliorer certaines de leurs propriétés physiques et mécaniques. Les terres "rares" ne sont pas rares. Par exemple, Ce est plus abondant dans la croûte terrestre que Sn, tandis que Y et Nd sont plus abondants que Pb. Cependant, les terres rares sont généralement présentes à de très faibles concentrations et coexistent toujours avec d'autres terres rares puisque ces éléments sont chimiquement proches. Suite à leur forte affinité mutuelle, les terres rares sont extrêmement difficiles à séparer l'une de l'autre. On distingue quinze éléments : La, Ce, Pr, Nd, Sm, Eu, Gd, Dy, Ho, Er, Tm, Yb et Lu. Pour des raisons pratiques, les terres rares incluent souvent le scandium (Sc) et l'yttrium (Y) puisque ces deux éléments ont des caractéristiques similaires à celles des lanthanides. Les terres rares sont souvent divisées en deux sous-groupes : les éléments légers (de La à Sm) et les éléments lourds (de Gd à Lu).

La prédiction des propriétés thermodynamiques et des équilibres de phases pour les systèmes Mg–Al–RE une étape très importante lors du développement de nouveaux alliages à base de magnésium. Dans un alliage multi-constitué et multiphasique, il est très utile de développer des banques de données thermodynamiques, contenant les informations relative à chaque phase du système, afin de mieux comprendre et prédire les propriétés thermodynamiques, et les relations de phases pour des systèmes plus complexes.

L'objectif principal de cette thèse consiste en la modélisation des propriétés thermodynamiques et des équilibres de phase des systèmes Mg–Al–RE. Le second objectif consiste à faire des expériences clés dans la région riche en magnésium afin de vérifier les équilibres des phases, car cela est très important pour la conception de nouveaux alliages à base de magnésium. L'étude expérimentale a été effectuée pour les systèmes ternaires Al–Mg–La, Al–Mg–Ce, Al–Mg–Pr et Al–Mg–Nd afin d'obtenir les phases en équilibres ainsi que les informations concernant les solubilités des solutions solides. Des expériences de type « couples de diffusion » ont également été effectuées pour vérifier les phases en équilibres dans les systèmes ternaires étudiés. Le troisième objectif de la recherche consiste à développer des méthodes originales pour estimer les données thermodynamiques absentes de la littérature scientifique pour les phases contenant des

terres rares. Ces données sont par exemple les entropies et les enthalpies de formation des composés stœchiométriques binaires. La première approche fut la systématisation des propriétés thermodynamiques (enthalpies de mélange) en fonction des numéros atomiques des terres rares formant le mischmétal. Par la suite, des modèles basés sur des principes physiques tels que les calculs *ab initio* ou le modèle de Miedema ont été utilisés pour estimer les enthalpies de formation des composés stœchiométriques binaires, ainsi que les enthalpies de mélange des solutions solides : (Al)-FCC et (Mg)-HCP.

Une des hypothèses de la modélisation thermodynamique de ce travail est que le modèle quasichimique modifié avec l'approximation des paires, où la fonction d'enthalpie libre rend compte de l'ordre à courte distance, peut reproduire le comportement d'une solution liquide avec un fort ordonnancement. La présente modélisation est réalisée sous trois contraintes: i) les énergies de Gibsb de référence (g^0) d'éléments purs doivent être ceux de la base de données SGTE (ou de publications antérieurs de notre groupe de recherche pour quelques terres rares), et les g^0 des composés de références (tel que Al_2Mg, Mg_2Mg, Mg_2Al, Al_2Al dans la phase de Laves_C15) doivent être ceux de la banque de données FTlite existante. ii) la base de données thermodynamique a été construite en se basant sur celle dite des « éléments légers » (FTlite) déjà existante et disponible dans le logiciel FactSage. iii) les nombres de coordination des liquides métalliques purs (Al, Mg, RE) doivent être identiques à ceux de la banque de données existante (FTLite).

La présente étude fait partie d'un grand projet de recherche au sein du CRCT (Centre de recherche en Calcul Thermochimique de l'École Polytechnique de Montréal) afin de développer une nouvelle banque de données thermodynamiques d'alliages à base de magnésium en incluant des éléments d'addition susceptibles d'être bénéfiques pour diverses propriétés physiques, mécaniques et de moulage.

La modélisation des propriétés thermodynamiques des alliages de type : Mg–Al–RE a été effectuée en respectant les étapes suivantes :

1- Revue de la littérature en vue de l'obtention des données expérimentales des équilibres de phases et des propriétés thermodynamiques. Pour l'optimisation thermodynamique d'un diagramme de phase, la première étape consiste à recueillir et à classer toutes les données expérimentales pour le système d'intérêt. Ces données sont : les enthalpies intégrales de

mélange, les enthalpies partielles de mélange, les activités des composants, les capacités calorifiques, la solubilité des constituants dans les solutions solides, les structures cristallines ainsi que les points de fusion des composés intermétalliques, les enthalpies de formation et les températures de transitions de phases. Parfois, des données utiles peuvent être disponibles uniquement pour des systèmes d'ordre supérieur (systèmes ternaires, quaternaires, etc...).

2- Évaluer les données expérimentales. L'évaluation critique des données expérimentales avant de procéder à l'optimisation thermodynamique est nécessaire pour éliminer les données contradictoires ou jugées peu fiables. Cela nécessite une connaissance des différentes méthodes expérimentale. L'évaluation critique des données expérimentales peut également être basée sur diverses règles (Gibbs-Konovalov pour les phases intermédiaires, relation de Van't Hoff entre les pentes du liquidus et du solidus, des valeurs empirique pour l'entropie et l'enthalpie, etc.).

3- Développer des techniques d'analyse systématiques. Il est connu que, dans la famille des terres rares, les propriétés thermodynamiques, voire les équilibres de phase, changent selon un modèle systématique, et on observe que certaines propriétés de ces éléments ou des composés qui y sont liés sont représentées par des lois empiriques. L'enthalpie de formation, la température de fusion des composés, l'enthalpie et l'entropie de fusion, etc, seront systématiquement analysées en fonction du numéro atomique, des rayons atomiques, ou de l'électronégativité de la terre rare afin de trouver une tendance acceptable. Par la suite, les quelques données manquantes peuvent être interpolées ou extrapolées.

4- Évaluer les données absentes de la littérature par des calculs *ab initio* ou des estimations par des modèles semi-empiriques tels que le modèle de Miedema. Les calculs *ab initio* et les estimations via le modèle Miedema ont été utilisées pour estimer les enthalpies de formation des phases binaires, l'enthalpie de mélange des phases (Al)-FCC et (Mg)-HCP. Ces calculs théoriques sont très importants parce que certaines des données enthalpiques sont rares et difficiles à mesurer. Dans le cadre de ce projet, les calculs *ab initio* on été effectués lors d'un stage en collaboration avec l'Institut de Calcul Haute Performance (IHPC, Prof. Ping Wu) à Singapour (février-mai 2009). Les enthalpies de formation pour

certaines phases métastables et certaines phases stœchiométriques ternaires sont calculées par le modèle semi-empirique de Miedema.

5- Choix du modèle thermodynamique le plus approprié pour les diverses phases. Pour construire une banque de données précise et fiable pour un système multi-constitué, il est crucial de choisir le modèle thermodynamique pour la phase basé sur sa structure cristalline (le nombre et le type de sous-réseaux..) afin de permettre la prédiction pour des systèmes à multi-constitué à partir des paramètres du modèle des sous-systèmes.

6- Optimiser les paramètres du modèle des systèmes binaires et ternaires. Après l'évaluation des données expérimentales et les choix des modèles thermodynamiques appropriés les paramètres du modèle sont optimisés afin de reproduire toutes les données expérimentales fiables. Dans la présente étude, le logiciel de calcul thermodynamique Factsage^{TM} (Bale, et al., 2002) a été utilisé. Les diagrammes de phases ternaires correspondants peuvent être optimisés en utilisant des modèles géométriques appropriés et les fonctions thermodynamique des sous-systèmes binaires. Dans certain cas, un terme d'excès de l'enthalpie libre (mineur en général) est ajouté afin de raffiner les paramètres. En général, les données expérimentales ternaires disponibles pour le liquide ont été reproduites de façon satisfaisante à l'aide des paramètres binaires seulement.

Dans le Chapitre 2, nous décrivons brièvement la méthode CALPHAD (Calculation of Phase Diagrams), la minimisation de l'énergie libre de Gibbs d'un système, et les différents modèles thermodynamiques utilisés dans ce travail. Pour décrire la propriété de la phase liquide, le Modèle Quasichimique Modifié (MQM) développé à l'École Polytechnique de Montréal a été utilisé. Ce modèle thermodynamique de solution est physiquement réaliste en considérant l'ordre à courte distance.

Dans le Chapitre 3, nous décrivons brièvement la méthodologie adoptée dans cette thèse : La méthode *ab initio*, le modèle semi-empirique (Miedema model), les méthodes expérimental et systématique ainsi que la technique d'estimation des enthalpies et entropies de formation des composes stœchiométriques. La méthode *ab initio* qui est un outil indispensable aujourd'hui est utilisé pour calculer des enthalpies de formation dans le système Mg–RE, où il n'y a pas ou peu

de données expérimentales rapportées dans la littérature ou bien dans certains cas les données expérimentales sont très différentes. De plus, le modèle semi-empirique (Miedema model) est utilisé pour estimer les enthalpies de formation et enthalpies de mélange dans les solutions solides (Al)-FCC et (Mg)-HCP.

Dans le Chapitre 4, la façon d'organiser les articles dans cette thèse est décrite. A l'aide des modèles thermodynamiques décrits dans le Chapitre 2 et les données expérimentales publié dans la littérature ou calculé par les méthodes décrites dans le Chapitre 3, nous avons modélisé les phases solides et liquides de 21 systèmes binaires (Al–La, Al–Ce, Al–Pr, Al–Nd, Al–Sm, Al–Gd, Al–Tb, Al–Dy, Al–Ho, Al–Er, Mg–La, Mg–Ce, Mg–Pr, Mg–Nd, Mg–Sm, La–Ce, La–Pr, La–Nd, Ce–Pr, Ce–Nd, Pr–Nd), et 16 systèmes ternaires (Al–Mg–La, Al–Mg–Ce, Al–Mg–Pr, Al–Mg–Nd, Al–Mg–Sm, Al–Mg–Gd, Al–Mg–Tb, Al–Mg–Dy, Al–Mg–Ho, Al–Mg–Er, Al–La–Ce, Al–La–Pr, Al–La–Nd, Al–Ce–Pr, Al–Ce–Nd, Al–Pr–Nd). Les résultats sont présentés dans les Chapitre 5 à 9 et l'annexe III. Les propriétés thermodynamiques des systèmes multi-constitués peuvent donc être estimées et prédites avec une bonne précision selon des paramètres des modèles obtenus pour les systèmes binaires et ternaires.

Les trois articles des Chapitres 5 à 7 sont publiés dans le journal de Calphad. Le premier (Chapitre 5) présente les optimisations thermodynamiques des systèmes : Al–La, Al–Ce, Al–Pr, Al–Nd, et Al–Sm de la façon systématique et doit être lus en relation avec l'article du Chapître 6 qui y fait suite. La phase liquide de la solution Al–RE a été modélisée à l'aide du Modèle Quasichimique Modifié avec l'approximation de paires. Les solutions solides quand à elles ont été modélisées à l'aide du modèle des sous-réseaux ou «Compound Energy Formalism». La procédure d'optimisation a été orientée en mettant l'accent sur les tendances observées dans les propriétés thermodynamiques des systèmes Al–RE. Il est montré que le modèle Quasichemique Modifié utilisé pour les alliages liquides nous permet d'obtenir des entropies de mélange qui sont plus fiables que celles basées sur un modèle statistique de mélange aléatoire (Bragg - Williams) qui ne prend pas des en compte l'ordonnancement à courte distance.

Le deuxième article (Chapitre 6) présente, en suite de l'article précédent, les optimisations thermodynamiques des systèmes Al–Gd, Al–Tb, Al–Dy, Al–Ho, et Al–Er. Une technique

systématique (proposé par Gschneidner) a été utilisée pour estimer le diagramme de phase Al–Tb en raison du manque de données expérimentales. Les valeurs de (H_T-H_{273K}) pour le composé stœchiométrique Al₂Er ont été reportées dans la littérature, en considérant ces données, la capacité calorifique d'excès (ΔC_p) de cette phase a pu être estimée. La différence de capacité calorifique (ΔC_p) des autres composés intermétalliques ont été interpolées linéairement entre Al pur et Al₂Er ou Er pur et Al₂Er. Les paramètres optimisés du modèle pour toutes les phases reproduise de manière très satisfaisante toutes les données expérimentales fiables.

Le troisième article (Chapitre 7) présente les optimisations thermodynamiques des systèmes Mg–La, Mg–Ce, Mg–Pr, Mg–Nd, et Mg–Sm. La solubilité des RE dans la solution solide Mg – HCP a été soigneusement évalué en considérant la tendance linéaire (ln x_{RE} versus 1/T) selon l'équation $\ln x_{RE}^{HCP} = \frac{\Delta G^0}{nRT} - \ln \gamma_{RE}^{HCP}$ et calcul d'enthalpie de formation des composés intermétalliques (Mg₁₂La, Mg₁₂Ce, Mg₁₂Pr, Mg₄₁Nd₅, Mg₄₁Sm₅) a été évalué par le Modèle Miedema et les simulations *ab initio*. Les résultats de ces deux approches sont comparables. Les optimisations thermodynamiques des systèmes Mg–La, Mg–Ce, Mg–Pr, Mg–Nd, et Mg–Nd été effectuées de façon systématique. Les paramètres optimisés du modèle pour toutes les phases reproduise de manière très satisfaisante toutes les données expérimentales fiables.

Le quatrième article (Chapitre 8) présente les optimisations thermodynamiques des systèmes Mg–Al–La, Mg–Al–Ce, Mg–Al–Pr, Mg–Al–Nd, et Mg–Al–Sm avec les donné expérimentales obtenues au cours de cette étude ainsi que les donné expérimentales disponibles dans la littérature. Dix expériences ont été réalisées afin de vérifier les équilibres de phases dans les systèmes ternaires, spécialement dans les régions riches en Mg. Les solubilités dans les composés LaMg₁₂, CeMg₁₂ et PrMg₁₂ et Nd₅Mg₄₁ sont vérifiées. Deux expériences de type « couples de diffusion » ont été aussi effectuées. Les paramètres optimisés du modèle pour toutes les phases sont en accord avec nos données expérimentales et les données dans issues de la littérature.

Le Chapitre 9 présente les optimisations thermodynamiques des systèmes ternaires Mg–Al–Gd, Mg–Al–Tb, Mg–Al–Dy, Mg–Al–Ho, et Mg–Al–Er. Pour la première fois, le système Mg–Al–Tb

a été estimé. L'estimation est basée sur la méthode systématique. Assumant des similarités entre les systèmes Mg–Al–Gd et Mg–Al–Dy, un composé ternaire (Al_4MgTb) est postulé. Son enthalpie de formation est calculée par le Modèle Miedema, tout comme d'autres composés ternaires.

Les propriétés physiques des éléments terres rares qui viennent de la littérature sont présentées dans l'Annexe I.

Dans l'Annexe III, les optimisations thermodynamiques des systèmes Al–La–Ce, Al–La–Pr, Al–La–Nd, Al–Ce–Pr, Al–Ce–Nd et Al–Pr–Nd sont présentées.

Finalement, quelques exemples d'utilisation de cette banque de donnée thermodynamique sont présentés.

TABLE OF CONTENTS

LIST OF TABLES

LIST OF FIGURES

LIST OF SYMBOLS

c_p	Molar heat capacity (J/mol-K)
G_i^0	Standard Gibbs energy of i (J)
ΔG	Gibbs energy change (J)
G^E	Excess Gibbs energy of a solution (J)
g_i^0	Molar Gibbs energy of component i (J/mol)
H_i^0	Standard enthalpy of i (J)
n_i	Number of moles of component i (mol)
n_{ij}	Number of moles of i-j pairs in a solution (mol)
g_{AB}^{ij}	Excess interation parameter between A and B (J/mol)
R	Ideal gas constant (8.31451 J/mol-K in FactSage)
S_i^0	Standard entropy of component i (J/K)
ΔS^{config}	Configurational entropy of mixing of a solution (J/K)
T	Absolute temperature (K)
wt.%	Weight percent
at.%	Atomic percent
X_i	Mole fraction of i
X_{ij}	Pair fraction of i-j pairs
y_i	Site fraction of component i
Y_i	"Coordination-equivalent" fraction of i
Z_i	Coordination number of i, when all the nearest neighbors of an i are i's
Z_{ij}^i	Coordination number of i, when all the nearest neighbors of an i are j's

ΔH^{chem} Chemical contribution to the enthalpy in Miedema's model (J/mol)

$\Delta H^{elastic}$ Elastic contribution to the enthalpy in Miedema's model (J/mol)

ΔH^{struct} Structure contribution to the enthalpy in Miedema's model (J/mol)

G_B Shear modulus of B (Pa)

K_A Compressibility of A (Pa^{-1})

V_i^* Molar volumes of i (m^3)

$\vec{R}$ Nuclei coordinates

$\vec{r}$ Electron coordinates

$\hat{H}$ Hamiltonian operator

E Total energy of the system (eV)

$B_0^{'}$ Bulk modulus pressure derivative

r_{temp} Reduced temperature

r_{vol} Volume ratio relative to a selected rare earth (La)

LIST OF ABBREVIATIONS

CALPHAD   CALculation of PHAse Diagram

CEF   Compound Energy Formalism

DFT   Density Functional Theory

DSC   Differential Scanning Calorimetry

DTA   Differential Thermal Analysis

EMF   Electromotive Force

EPMA   Electron Probe Microanalysis

ES   Excess stability function

GGA   Generalized Gradient Approximation

LDA   Local Density Approximation

MQM   Modified Quasichemical Model

PAW   Projector Augmented plane Wave

PBE   Perdew-Burke-Ernzerhof gradient approximation

SGTE   Scientific Group Thermodata Europe

SRO   Short-Range Ordering

VASP   Vienna Ab initio Simulation Package

XRD   X-Ray Diffraction

LIST OF APPENDICES

CHAPTER 1   **INTRODUCTION**

Magnesium is the lightest metal used as a structural material. Use of magnesium alloys is attractive, particularly in transportation industries (*eg*. automotive and aircraft), because of their low density and potentially high strength/weight ratios (the density of magnesium at 25 $^\circ$C is ~1.738 g/cm^3). Magnesium is 35% lighter than aluminum (~2.698 g/cm^3), 62% lighter than titanium (~4.540 g/cm^3), and 78% lighter than iron (~7.874 g/cm^3). Its high strength-to-weight ratio makes it even more attractive than steel in many applications. Due to limited fossil fuel resources and environmental issues, there is a compelling tendency in the automotive industry to make cars lighter to reduce fuel consumption and greenhouse gas emission. World consumption of magnesium alloys in the automotive industry increased 15% per year for more than a decade (Liu, 2008). Moreover, magnesium is easily recycled; it also has high thermal conductivity, good electromagnetic shielding characteristics, high damping characteristics, good machinability, high dimensional stability and favorable environmental properties (Froes et al., 1998). These advantageous properties make Mg alloys an excellent choice for a number of applications, like computer housings and cell phone cases. Magnesium – aluminum – based alloys are widely used because of their low density, high strength-to-weight ratio, specific rigidity, satisfactory salt-spray corrosion resistance and good ductility. Although magnesium alloys offer light weight, high stiffness, excellent machinability and the best alternative for weight reduction, their use for engineering applications is restricted to a few structural parts in the automotive and other transport industries due to their poor creep resistance at elevated temperatures (above 150 $^\circ$C), which has made them inadequate for engine blocks or powertrain applications. Automatic transmission cases can operate up to 175 $^\circ$C, engine blocks up to 200 $^\circ$C, and engine pistons up to 300 $^\circ$C (Yang et al., 2008). Adding rare earth (RE) elements in Mg–Al alloys (*i.e.* AE41, AE42 alloys) may improve the creep resistance (Pettersen et al., 1996) and strength at elevated temperatures due to the precipitation of the intermetallic phases (*eg*. Al$_{11}$RE$_3$) and suppression of the detrimental Mg$_{17}$Al$_{12}$ phase in the interdendritic or grain boundary region. Several alloys series have been studied in the development of creep resistant magnesium die-casting alloys. The first investigated alloys for automotive applications were Mg–Al–Si alloys by Volkswagen in the 1970's (Pekguleryuz & Kaya, 2003). Mg$_2$Si precipitates, which are deemed to improve the creep

resistance by the pinning effect (to pin discloations and grain boundaries), have a low density, high hardness and much higher melting temperature than $Mg_{17}Al_{12}$ phase. However, the addition of Si cannot suppress the formation of the brittle $Mg_{17}Al_{12}$ phase for a given level of aluminum. Ca addition to the Mg–Al binary system can increase the creep resistance at elevated temperatures by precipitating Al_2Ca phase, which has stability at high temperatures and by suppression of $Mg_{17}Al_{12}$ phase (Pekguleryuz & Renaud, 2000). However, Ca can enhance hot crack tendency (Nakaura et al., 2006). Mg–Al–Sr alloys are a new addition to creep resistant magnesium alloys.

Parallel to Mg alloy development, Al–RE (aluminum – rare earths) alloys have been of interest to materials scientists who want to develop light weight alloys. Rare earths are important alloying elements in aluminum alloys because of their ability to enhance the high temperature properties and casting characteristics (Nie et al., 2002). Moreover, rapidly solidified Al–RE alloys also offer the possibility of obtaining better corrosion behavior (Borzone et al., 2001).

As to the rare earth elements, they are actually not rare except synthetic promethium (Pm). For example, cerium (Ce) is the twenty-sixth most abundant of all existing elements in the earth's crust, being five times as abundant as lead (Pb) and half as abundant as chlorine (Cl). Even thulium (Tm), the rarest after Pm, is rather more abundant than iodine (I) in the earth's crust (Greenwood & Earnshaw, 1998).

It is of great interest to study rare earth-based bulk metallic glasses (BMGs) and Al-based BMGs in recent years because of their physical properties, such as high glass-forming ability (GFA), special magnetic properties (Luo et al., 2006), superplasticity in the supercooled liquid region, and high fracture strength and ductility (Li et al., 2008; Zhang et al., 2009), which show promising potential applications.

Rare earth metals are also technologically important in other applications due to their special properties. For example, the misch-metal (a mixture of mainly Ce, La, Pr and Nd) are added in high-alloy steels; Y, Eu, Tb and Ce are used in fluorescent materials; Nd, Sm and Gd are

important metals for the magnets; Ce is used with Fe in lighter flints and as oxygen getters in order to lower the oxygen partial pressure; rare earth oxides Ce_2O_3 and La_2O_3 can be added to ceramics; solid oxide fuel cells can contain rare earth-doped ceria or yttria-stabilized zirconia (YSZ) electrolyte materials. Pr, Nd, Tm, Er, Ho and Yb can be used in fiber lasers and fiber amplifiers. They even have applications in superconductors and glasses.

Rare earth elements are chemically similar. Due to high affinity among the rare earths, the individual elements are extremely difficult to separate chemically. They include fifteen elements: La, Ce, Pr, Nd, Sm, Eu, Gd, Dy, Ho, Er, Tm, Yb, and Lu. For practical reasons, the rare earth elements often include scandium and yttrium, since these two elements have similar characteristics as the lanthanides. Rare earth elements are often divided into two subgroups: the light rare earths (from La to Sm) and the heavy rare earths (from Gd to Lu, except Yb).

It has been well known that rare earths show certain trends and similar regularities as a function of the atomic number in several constitutional properties of the pure elements and of their alloys across the lanthanide series (from La to Lu all of which form trivalent rare earth ions upon oxidation, except Eu and Yb which form divalent ions upon oxidation). Such similarity and trends of the physical and chemical properties are shown in lanthanides with another common metal [like Ag (Ferro & Delfino, 1979), Al(Buschow & Van Vucht, 1967; Ferro et al., 1993; Saccone et al., 1998), Mg (Ferro et al., 1993), In (Delfino et al., 1984), Sn (Borzone et al., 1983), Tl (Saccone et al., 1988)) and non-metals (like lanthanide oxides (Cordfunke & Konings, 2001b), Lanthanide trihalides (Cordfunke & Konings, 2001a), Lanthanide carbides, Lanthanide silicides (Meschel & Kleppa, 2001)]. Regularities in the structure and properties of Mg–RE alloys were presented by Rokhlin (Rokhlin, 1978, 2007); the general properties of Al–RE alloys were summerized by Saccone et al. (Ferro et al., 1993; Saccone et al., 1998).

Most aluminum alloys are used as wrought alloys that are shaped by plastic deformation, while more than 90% of magnesium alloys are used as cast products made by different casting methods (Yang et al., 2008). Some casting alloys may undergo subsequent heat-treatments to improve properties. Plastic deformation of Mg alloys with a hexagonal lattice is more difficult than Al

alloys with cubic lattice. However, research on wrought Mg alloys is increasing and has been more extensive in recent years. As is known, in material science, one of the ultimate goals is to control and design the microstructure in order to achieve the desired properties and performance. The microstructure depends on temperature, pressure, chemical composition and thermal history of the material. One of the most important guides for the materials scientist is the appropriate phase diagram. The phase diagram may be regarded as a road map, describing the state of equilibrium in the system under various experimental conditions, *i.e.* temperature, pressure and chemical composition. According to thermodynamics, the phase assemblage with the lowest Gibbs energy determines the equilibrium state at given conditions. With the help of computational thermochemistry, not only binary and ternary systems, but also multi-component systems can be investigated properly.

Over the last 30 years, advances in thermodynamic modeling have resulted in the development of computer databases containing thermodynamic properties, as functions of temperature and composition, of hundreds of multi-component alloy phases. These databases are developed by critical evaluation of all available thermodynamic and phase diagram data for binary, ternary and even higher order systems, thermodynamic modeling and optimizations. Optimized model parameters are obtained which reproduce the data within experimental error limits. The models are then used to predict the properties of multi-component phases from the stored parameters for the binary and ternary sub-systems. The models can be refined through additional ternary parameters if data for ternary or higher-order systems are available. Gibbs energy minimization software, such as Thermo-Calc (Sundman et al., 1985), Pandat (Chen et al., 2002), Factsage^{TM} (Bale et al., 2002) can employ these databases to calculate the amounts and compositions of all phases at equilibrium in a given system, as well as the crystallization paths, solid solubilities, temperatures and enthalpies of phase transformations, or non-equlibrium cooling [like Scheil-Gulliver cooling (Gulliver, 1913)], *etc*.

As for the thermodynamic database development of Mg–Al–RE systems, less research has been done on the thermodynamic properties of these systems compared to other metallic systems. Only few thermodynamic experimental data are available in the literature, which makes it necessary to

develop some theoretical estimation techniques (First-Principle calculations, semi-empirical Miedema model, interpolation or extrapolation methods and systematic analysis). Fortunately, the rare earth elements are chemically very similar and often one can make good predictions by studying tendencies in the periodic table.

The thermodynamic database of the Mg–Al–RE systems will provide clear guidelines for Mg and Al alloy selection and design, avoiding unproductive long-term experiments with alloys which have less potential for practical applications.

As part of ongoing projects in our laboratory to develop thermodynamic databases for multi-component Mg– and Al– based alloys, the aim of this work is to evaluate and optimize systematically ten binary systems Al–RE (Al–La, Al–Ce, Al–Pr, Al–Nd, Al–Sm, Al–Gd, Al–Tb, Al–Dy, Al–Ho, Al–Er), ten Mg–Al–RE (Mg–Al–La, Mg–Al–Ce, Mg–Al–Pr, Mg–Al–Nd, Mg–Al–Sm, Mg–Al–Gd, Mg–Al–Tb, Mg–Al–Dy, Mg–Al–Ho, Mg–Al–Er) ternary systems and six Al–RE'–RE" (Al–Ce–La, Al–Ce –Pr, Al–Ce–Nd, Al–La–Pr, Al–La–Nd, Al–Pr–Nd) ternary systems. The Al–Ce, Al–Y, and Al–Sc systems were previously optimized by Kang et al (Kang et al., 2008b). The optimization procedure is deliberately biased by putting strong emphasis on the observed trends in the thermodynamic properties of Al–RE, Mg–RE, and Al–Mg–RE systems. With respect to the enthalpies of formation and of mixing this can enable 1) estimation of some missing thermodynamic properties and 2) ensuring that the mathematical optimization of model parameters do not significantly differ from one chemical system to an other. The Modified Quasichemical Model, which takes short–range ordering into account, is used for the liquid solution and the Compound Energy Formalism is used for the solid solutions. Equilibrated key alloy experiments are carried out for Mg–Al– (La, Ce, Pr, and Nd) systems in order to validate the modeling parameters. First-Principles calculations are performed for the dilute enthalpies of mixing in the Al–RE systems and for enthalpies of formation of certain compounds in the Al–RE and Mg–RE (RE: Ce, La, Pr, Nd) binary systems. Moreover, Miedema model is also used to estimate the enthalpies of formation of binary and ternary intermetallic compounds.

CHAPTER 2   **LITERATURE REVIEW**

In this chapter, a general review of the computational thermodynamic CALPHAD (calculation of phase diagrams) method, thermodynamic models used for the liquid and solids, and the extension to the ternary and higher-order systems will be introduced. The literature related to specific systems presented in papers is not reviewed in this chapter, but will be covered in the scientific papers presented in Chapters 4 to 9.

2.1   CALPHAD Method

CALPHAD is an abbreviation for the CALculation of Phase Diagrams. It could be better described as "the Computer Coupling of Phase Diagrams and Thermochemistry".

One of the fundamental efforts in metallurgical engineering is to study the relationship among the alloy's chemical compositions, the processing conditions, the resulting microstructure, and the alloy's final physical, mechanical, and/or chemical properties; phase diagrams are the roadmap for alloy design, processing and basic understanding. Almost all the real engineering materials are multi-component in nature. Experimentally determined phase diagram information is usually available for most binary systems, very limited for ternary systems, and is rather rare for higher-order systems. This is where the CALPHAD method comes in with the pioneering work of Dr. Larry Kaufman (Spencer, 2008). This method is based on the concept of deriving the thermodynamic functions of stable and metastable phases from all available experimental data in a given system. Such functions include enthalpy of formation of compounds, enthalpy of mixing in liquids, heat capacity and so on. The thermodynamic Gibbs energy can be expressed as mathematical functions of temperature and chemical composition. The parameters of these functions are obtained by a numerical Gibbs minimization technique using the data obtained after a process of critical evaluation, which analyses the techniques and reliability on how the experiments (or estimations) have been carried out. All other thermodynamic properties (*i.e.* enthalpy, entropy) can be then derived from Gibbs energy functions. It is possible to calculate the multi-component phase diagrams if the thermodynamic properties are known. Thermodynamic descriptions of binary systems are combined to extrapolate ternary and higher-order systems using proper extrapolation techniques. The model parameters can be refined if the experimental data are available for the ternary systems by adding ternary parameters, if

necessary. However, a good model should be able to describe the thermodynamic behavior of a system as close as possible to true behaviour, resulting in the sparing use of very small ternary terms. The Gibbs energy of a phase is represented by a proper thermodynamic model that contains a relatively small number of model parameters. Experimental data such as calorimetric data (heat capacities, enthalpies of formation, *etc*), phase equilibria data (liquidus temperature, solidus temperature, phase transformation temperatures, solid solubility, *etc*), chemical potentials and activities data would be used for thermodynamic optimization.

With the help of computational thermochemistry, not only the computation of multi-component phase diagrams, but also tracking of alloys during heat treatment or solidification is possible. The calculation of the amount and composition of the phases precipitated helps in understanding the microstructural evolution of alloys. In an alloy with several alloying elements, the phase relationships are very complex. In order to investigate effectively and understand these complex phase relationships, it will be very useful to develop a database containing model parameters, giving the thermodynamic properties of all the involved phases as functions of temperature and composition. Such a thermodynamic database will provide clear guidelines for selection of these alloys, avoiding unproductive long-term experiments with alloys having less potential for commercial purposes.

Several thermodynamic research groups have been formed using the CALPHAD method. The THERMODATA group and IRSID/Arcelor Research group in France, the Thermo-Calc group (Sundman et al., 1985) at KTH in Sweden, the MTDATA group (Davies et al., 2002) at National Physical Laboratory (NPL) in the UK, the thermochemical group (NIST, 2002) at National Institute of Standards and Technology (NIST) in the USA, the CaTCalc group (Shobu, 2009) at national institute of Advanced Industrial Science and Technology (AIST) in Japan, the FACTSAGE group (Bale et al., 2002) (led by A. Pelton and C. Bale in collaboration with G. Eriksson at GTT Technology in Germany) at Ecole Polytechnique de Montréal in Canada and the PANDAT group (Chen et al., 2002) in USA may be mentioned, among other thermodynamic softwares.

Using these databases with Gibbs energy minimizing software like FactSage™ (FactSage 2008), one will be able to calculate the amounts and compositions of all phases at equilibrium at any

temperature and composition in multicomponent alloys, to follow the course of equilibrium or nonequilibrium (Scheil-Gulliver) cooling, to calculate corresponding heat effects, *etc.*

The total Gibbs energy of a system reaches minimum when phase equilibria are established for a given temperature, composition and pressure. It can be expressed by Eq. (2.1)

$$G = \sum_{\varphi} n^{\varphi} g^{\varphi} = \text{minimum} \tag{2.1}$$

where

n^{φ} is number of moles of phase φ

g^{φ} is molar Gibbs functions of phase φ

The chemical potential of system component i, μ_i, is defined as

$$\mu_i = g_i = (\partial G / \partial n_i)_{T,P,n_j} \tag{2.2}$$

where G is the Gibbs energy of a solution, n_i is the number of moles of component i, and the derivative is taken at constant temperature, pressure and $n_j (j \neq i)$. g_i is the partial molar Gibbs energy of component i.

When phase equilibria of a system are reached for given temperature, pressure, and overall composition, the chemical potential of each component i, μ_i, is equal in all phases, φ. That is,

$$\mu_i^1 = \mu_i^2 = ... = \mu_i^{\varphi} \tag{2.3}$$

Then, the total Gibbs energy at equilibrium in Eq. (2.1) can be written as

$$G = \sum_i n_i \mu_i \tag{2.4}$$

At equilibrium, the total G in Eq. (2.4) at constant temperature, pressure, and overall composition is minimized under mass balance constraints by Solgasmix algorithm using Lagrangian multipliers. In terms of the l independent system components and φ phases, these mass balance equations (Eriksson, 1975) may be written as

$$\sum_{\varphi}\sum_{j} n_j^{\varphi} a_{ji}^{\varphi} = b_i \qquad (i=1, 2, \ldots, l) \tag{2.5}$$

where n_j^{φ} is the amount of the jth constituent of phase φ, a_{ji}^{φ} is a coefficient of the stoichiometry matrix composed of the constituents of phase φ, and b_i is the total amount of the ith system component.

Under given set of constraints, like constant temperature, pressure, and overall composition, the Gibbs energy minimization algorithms search and obtain a set of mole numbers of each phase φ and compositions of each solution phase which minimize the total Gibbs energy of given system.

The Gibbs energy of a phase can be described by a variety of models that take into account contributions from temperature and composition, pressure and magnetism. For the condensed systems at normal pressure, the pressure contribution to the Gibbs energy is usually ignored.

For pure elements or stoichiometric phases without magnetism, the Gibbs energy is usually expressed as a power series of T, as follows:

$$G - H^{SER} = a + b \cdot T + c \cdot T \cdot \ln(T) + \sum d_n \cdot T^n \tag{2.6}$$

where $G - H^{SER}$ is the Gibbs energy relative to a standard element reference state (SER). T is the absolute temperature in Kelvin. H^{SER} is the enthalpy of the element in its stable state at temperature of 298.15 K and pressure of 10^5 Pascal. The typical numbers of 2, 3, -1 and 7 or -9 (Dinsdale, 1991) are often used as the n exponent.

The enthalpy and entropy can be expressed as functions of heat capacity C_p by

$$H(T) = H^0_{29815} + \int_{29815}^{T} C_p dT \tag{2.7}$$

$$S(T) = S^0_{29815} + \int_{29815}^{T} \frac{C_p}{T} dT \tag{2.8}$$

For the pure elements, $H^0_{298.15}$ can be considered to be zero, while $S^0_{298.15}$ comes from the integration of Cp at low temperatures from 0 K to 298.15 K according to the third law of thermodynamics.

Generally, for A–B binary liquid solution, The Gibbs energy of a solution can be described as:

$$G_m = g_A^0 n_A + g_B^0 n_B - T\Delta S^{config} + G_{mix}^{ex} \tag{2.9}$$

where G_m is the Gibbs energy of the solution; g_A^0 is the molar Gibbs energy of component A, $-T\Delta S^{config}$ is generally the ideal mixing contribution to the Gibbs energy, G_{mix}^{ex} is the excess Gibbs energy.

For solid solutions, the Compound Energy Formalism (CEF) (Hillert, 2001) can be used to express the Gibbs energy of the phases.

The configurational entropy change in Eq. (2.9) can be described by ideal solution behavior (Bragg-William mixing) and the excess Gibbs energy can be expressed by polynomial model for the binary systems that do not show a large deviation from the ideality. However, a large number of interaction parameters are often needed in this simple polynomial based model to adequately represent all the thermodynamic properties of the systems that show strong short-range ordering in liquids. The same problems also arise for the thermodynamic properties of higher-order systems extrapolated directly from the model parameters of the lower-order sub-systems, where large arbitrary parameters are often needed in these higher-order systems to reproduce the available data. As pointed out by Pelton and Blander (Pelton & Blander, 1986), for systems which exhibit short range ordering, i.e. SiO_2-CaO-FeO, the above-mentioned ideal behavior for the configurational entropy and polynomial model for the excess Gibbs energy to describe liquid behavior are not satisfactory even if a large number of model parameters are used.

Taking the characteristics of the liquid phase into account, Pelton and co-workers (Pelton et al., 2000) and Pelton and Chartrand (Chartrand & Pelton, 2001a; Pelton & Chartrand, 2001a) developed the Modified Quasichemical Model (MQM) by improving the configurational entropy term of the model taken into account short-range ordering. Other modifications (*i.e.* cocordination number changes with compositions) were also made to make the MQM model more flexible and applicable for more complex systems.

2.2 Modified Quasichemical Model (MQM) for the Liquids

2.2.1 Binary Solutions

The MQM in the pair approximation (Pelton et al., 2000) was used to model the thermodynamic properties of the liquid solution in the present study. A detailed description of the MQM and its associated notation is given by Pelton et al. (Pelton et al., 2000). The same notation is used in the present article. The MQM has been successfully applied to alloy solutions (Kang et al., 2007b, 2007c), molten oxides (Jung et al., 2005; Kang et al., 2004), molten salts (Chartrand & Pelton, 2001b; Pelton & Chartrand, 2001b), and molten sulphides (Waldner & Pelton, 2004). A brief summary of this model for binary solutions is given below. The following pair exchange reaction between atoms A and B distributed over the sites of a quasilattice is considered in the MQM:

$$(A - A)_{pair} + (B - B)_{pair} = 2\ (A - B)_{pair}\ , \qquad \Delta g_{AB} \tag{2.10}$$

Where $(i - j)_{pair}$ represents a first-nearest-neighbor pair of atoms. The Gibbs energy change for the formation of 1 mole of $(A - B)$ pairs is $\Delta g_{AB}/2$. Let n_A and n_B be the number of moles of A and B, n_{AA}, n_{BB}, and n_{AB} be the number of moles of $(A - A)$, $(B - B)$, and $(A - B)$ pairs. And Z_A and Z_B are the coordination numbers of A and B. The Gibbs energy of the solution is given by:

$$G = (n_A g^o_A + n_B g^o_B) - T\Delta S^{config} + (n_{AB}/2)\Delta g_{AB}\ , \tag{2.11}$$

where g^o_A and g^o_B are the molar Gibbs energies of the pure component A and B, and given by randomly distributing the $(A - A)$, $(B - B)$ and $(A - B)$ pairs in the one $-$ dimensional Ising approximation (Pelton et al., 2000):

$$\Delta S^{config} = -R\ (n_A \ln X_A + n_B \ln X_B) - R\ (n_{AA} \ln \frac{X_{AA}}{Y_A^2} + n_{BB} \ln \frac{X_{BB}}{Y_B^2} + n_{AB} \ln \frac{X_{AB}}{2Y_A Y_B}). \tag{2.12}$$

Where X_{AA}, X_{BB} and X_{AB} are pair fractions of the (A − A), (B − B) and (A − B) pairs; Y_A, and Y_B are equivalent fractions of A and B:

$$X_{ij} = \frac{n_{ij}}{n_{AA} + n_{BB} + n_{AB}} \qquad (i, j = \text{A or B}) \qquad (2.13)$$

$$Y_i = \frac{Z_i n_i}{Z_A n_A + Z_B n_B} \qquad (i = \text{A or B}) \qquad (2.14)$$

Moreover, the following mass balance equations can be written:

$$Z_A n_A = 2n_{AA} + n_{AB} \qquad (2.15)$$

$$Z_B n_B = 2n_{BB} + n_{AB} \qquad (2.16)$$

It may be noted that there is no exact expression for the configurational entropy in three dimensions. Although Eq. (2.12) is only an approximate expression in three dimensions, it is exact one-dimensionally (when $Z = 2$) (Pelton et al., 2000). As explained in Pelton et al. (Pelton et al., 2000), one is forced by the approximate nature of Eq. (2.12) to use nonphysical values of the coordination numbers in order to yield good fits between the experimental data and calculated ones. The mathematical approximation of the one-dimensional Ising model of Eq. (2.12) can be partially compensated by selecting values of Z_A and Z_B which are smaller than the experimental values (Kang et al., 2008b). The MQM model is sensitive to the ratio of coordination numbers, but less sensitive to their absolute values. From a practical standpoint for the development of large thermodynamic databases, values of Z_A and Z_B of the order of 6 have been found necessary for the solutions with a small or medium degree of ordering (*i.e.* alloy solutions). The MQM has been successfully applied in many alloy systems(Aljarrah & Medraj, 2008; Kang et al., 2008b; Kang et al., 2007b, 2007c; Shukla et al., 2008, 2009; Spencer et al., 2008; Wasiur-Rahman & Medraj, 2009).

Δg_{AB} in Eq. (2.10) and Eq. (2.11) is expanded in terms of the pair fractions X_{AA} and X_{BB}:

$$\Delta g_{AB} = \Delta g_{AB}^0 + \sum_{i \geq 1} g_{AB}^{i0} X_{AA}^i + \sum_{j \geq 1} g_{AB}^{0j} X_{BB}^j \ , \tag{2.17}$$

where Δg_{AB}^0, g_{AB}^{i0}, g_{AB}^{0j} are the parameters of the model which can be functions of temperature (typically $a+bT$). The equilibrium state of the system is obtained by minimizing the total Gibbs energy at constant composition, temperature and pressure. The equilibrium pair distribution is calculated by setting

$$(\frac{\partial G}{\partial n_{AB}})_{n_A, n_B} = 0, \tag{2.18}$$

This gives the "equilibrium constant" for the "quasichemical pair reaction" of Eq. (2.10):

$$\frac{X_{AB}^2}{X_{AA} X_{BB}} = 4 \exp(-\frac{\Delta G_{AB}}{RT}) \ . \tag{2.19}$$

Moreover, the model permits Z_A and Z_B to vary with compositions as follows (Pelton et al., 2000):

$$\frac{1}{Z_A} = \frac{1}{Z_{AA}^A} (\frac{2n_{AA}}{2n_{AA} + n_{AB}}) + \frac{1}{Z_{AB}^A} (\frac{n_{AB}}{2n_{AA} + n_{AB}}) \tag{2.20}$$

$$\frac{1}{Z_B} = \frac{1}{Z_{BB}^B} (\frac{2n_{BB}}{2n_{BB} + n_{AB}}) + \frac{1}{Z_{BA}^B} (\frac{n_{AB}}{2n_{BB} + n_{AB}}) \ , \tag{2.21}$$

Where Z_{AA}^A and Z_{AB}^A are the values of Z_A when all nearest neighbours of an A are As, and when all nearest neighbours of an A are Bs, and where Z_{BB}^B and Z_{BA}^B are defined similarly.

The composition of maximum short–range ordering (SRO) is determined by the ratio of the coordination numbers Z_{AB}^A / Z_{AB}^B. This composition is very often identified as very close to the composition of the more negative enthalpy of mixing of the liquid.

2.2.2 Multicomponent Solutions

A detailed description of the MQM in the pair approximation for multicomponent solutions and its associated notation is given by Pelton and Chartrand (Pelton & Chartrand, 2001a). The same notation is used in the present article. A brief summary of this model for multicomponent solutions is given below. The following pair exchange reaction between atoms m and n in a ternary 1- 2- 3 solution distributed over the sites of a quasilattice is:

$$(m\text{-}m)_{\text{pair}} + (n\text{-}n)_{\text{pair}} = 2\,(m\text{-}n)_{\text{pair}}; \qquad \Delta g_{mn} \qquad (2.22)$$

where m and $n =$1, 2, 3; $(m\text{-}m)_{\text{pair}}$, $(n\text{-}n)_{\text{pair}}$ and $(m\text{-}n)_{\text{pair}}$ represent the first-nearest-neighbor (FNN) pairs.

Similar to the binary solutions, the mass balance constrains for the multicomponent solutions are:

$$Z_m n_m = 2n_{mm} + \sum_{n \neq m} n_{mn} \qquad (2.23)$$

where Z_m and n_m are the coordination number of m and the number of moles of m, respectively. n_{mm} and n_{mn} are the number of moles of $(m\text{-}m)$ pair and $(m\text{-}n)$ pair, respectively.

The pair fraction (X_{mn}), overall mole (or site) fraction (X_m) and "coordination-equivalent" fractions (Y_m) are defined as:

$$X_{mn} = n_{mn} / \sum n_{ij} \qquad\qquad (i, j = 1, 2, 3) \qquad (2.24)$$

$$X_m = n_m / \sum n_i \qquad\qquad (i = 1, 2, 3) \qquad (2.25)$$

$$Y_m = Z_m n_m / \sum (Z_i\, n_i) \qquad\qquad (i= 1, 2, 3) \qquad (2.26)$$

The Gibbs energy of the solution is expressed as:

$$G = \sum_m n_m g_m^0 - T\Delta S^{config} + \sum_{n>m}\sum n_{mn}(\Delta g_{mn}/2) \qquad (2.27)$$

where g_m^0 is the molar Gibbs energy of the pure component m, and ΔS^{config} is an approximate configurational entropy of mixing, which can be given by:

$$\Delta S^{config} = -R\sum_m (n_m \ln X_m) - R\left(\sum n_{mm} \ln(X_{mm}/Y_m^2) + \sum_{n>m}\sum n_{mn} \ln(X_{mn}/2Y_m Y_n)\right) \qquad (2.28)$$

In the present study, Δg_{mn} is given by a polynomial in terms of pair of fractions. Then the Δg_{mn} term is proposed according to the symmetric model or asymmetric model used for the ternary subsystems.

In a symmetric ternary system, the Kohler-type interpolation (Chartrand & Pelton, 2000; Kohler, 1960) is used. Δg_{mn} can be expressed as:

$$\Delta g_{12} = \Delta g_{12}^0 + \sum_{(i+j)\geq 1} g_{12}^{ij}\left(\frac{X_{11}}{X_{11}+X_{22}+X_{12}}\right)^i\left(\frac{X_{22}}{X_{11}+X_{22}+X_{12}}\right)^j + \sum_{\substack{i\geq 0 \\ j\geq 0 \\ k\geq 0}} g_{12(3)}^{ijk}\left(\frac{X_{11}}{X_{11}+X_{22}+X_{12}}\right)^i\left(\frac{X_{22}}{X_{11}+X_{22}+X_{12}}\right)^j Y_3^k \qquad (2.29)$$

In practice, it is sufficient to include only terms with $i = 0$ or $j = 0$.

In an asymmetric ternary system, the Kohler-Toop interpolation is used. Let 1 be an asymmetric component for 1-2 system. That is, the energy of forming (1-2) nearest-neighbor pairs is assumed to be constant as component 2 is replaced by component 3 in the 1-2-3 ternary system. Then the following equation can be written:

$$\Delta g_{12} = \Delta g_{12}^0 + \sum_{(i+j)\geq 1} g_{12}^{ij}(X_{11})^i(X_{22}+X_{23}+X_{33})^j + \sum_{\substack{i\geq 0 \\ j\geq 0 \\ k\geq 0}} g_{12(3)}^{ijk}(X_{11})^i(X_{22}+X_{23}+X_{33})^j\left(\frac{Y_3}{Y_2+Y_3}\right)^k \qquad (2.30)$$

In a ternary 1-2-3 system, Toop-interpolation (Toop, 1965) can be chosen for all three binary sub-systems. For example, Let 1 be an asymmetric component for 1-2 binary system, 2 be an asymmetric component for 2-3 binary system, and 3 be an asymmetric component for 1-3 system. Then three equations for $\Delta g_{23}, \Delta g_{13}$ can be similarly written as Δg_{12} in Eq. (2.30). In this case, the energy of forming (1-2) nearest-neighbor pairs, (2-3) nearest-neighbor pairs and (1-3) nearest-neighbor pairs are assumed to be constant as component 2 is replaced by component 3, as component 3 is replaced by component 1, and as component 1 is replaced by component 2, respectively, in the 1-2-3 ternary system. The liquid of Al–Mg system, Al–RE system and Mg–

RE system behaves differently: the minimum of Gibbs energy of mixing at 1273 K in Al–Mg liquid is -7.9 kJ/mol, while in Al–RE and Mg–RE liquids it is around -38 kJ/mol and -13 kJ/mol, respectively. In the present study, Kohler-type interpolation is chosen for liquid in Mg–Al–RE ternary systems.

In multicomponent systems, the excess Gibbs energy contribution from the binary subsystems and ternary subsystems are interpolated in a specific way which was introduced by Pelton and Chartrand (Pelton & Chartrand, 2001a). No additional model parameters are added.

2.3 Compound Energy Formalism (CEF) for Solid Solutions

The compound energy formalism was introduced (Hillert, 2001) to describe the Gibbs energy of solution phases with sub-lattices. Ideal mixing of sublattice species on each sublattice site is assumed. A Laves phase is taken as an example as follows.

Example: A Laves_C15 phase, in its simplest form $(A, B)_2{}^a(X, Y)_1{}^b$, has two sublattices, a and b
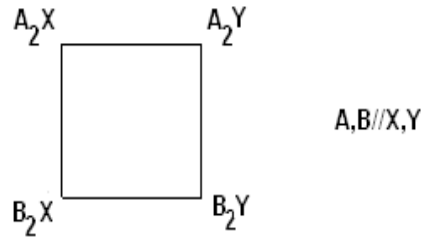
In the CEF, its Gibbs energy will be given by:

$$
\begin{aligned}
G &= y_A y_X G_{A_2 X} + y_A y_Y G_{A_2 Y} + y_B y_X G_{B_2 X} + y_B y_Y G_{B_2 Y} \\
&+ 2RT(y_A \ln y_A + y_B \ln y_B) + RT(y_X \ln y_X + y_Y \ln y_Y) \\
&+ \sum_i {}^i L_{AB/X}(y_A - y_B)^i y_A y_B y_X + \sum_i {}^i L_{AB/Y}(y_A - y_B)^i y_A y_B y_Y \\
&+ \sum_i {}^i L_{A/XY}(y_X - y_Y)^i y_A y_X y_Y + \sum_i {}^i L_{B/XY}(y_X - y_Y)^i y_B y_X y_Y \\
&+ L_{AB/XY} y_A y_B y_X y_Y
\end{aligned}
\tag{2.31}
$$

where A_2X, B_2X, A_2Y, B_2Y are the end-members.

y_A , y_B are site fractions of component A and B on sublattice a, where $y_A + y_B = 1$.

y_x , y_y are site fractions of component A and B on sublattice b, where $y_x + y_y = 1$.

$G_{A_2X}, G_{A_2Y}, G_{B_2X}, G_{B_2Y}$ are Gibbs energies of end-members A$_2$X, A$_2$Y, B$_2$X, B$_2$Y in Laves_C15 structure respectively.

$L_{AB/X}$ and $L_{AB/Y}$ are interaction parameters between components A and B on the a sublattice when the b sublattice is occupied only by X or by Y, respectively.

$L_{A/XY}$ and $L_{B/XY}$ are interaction parameters between components X and Y on the b sublattice when the a sublattice is occupied only by A or by B, respectively.

$L_{AB/XY}$ is the reciprocal interaction parameter when one sublattice is occupied by A and B; the other sublattice is occupied by X and Y.

2.4 Extension to ternary solution phases

Thermodynamic properties of a ternary solution can be estimated by the Kohler or Toop or Muggianu or other extrapolation techniques using optimized data for its binary sub-systems and ternary terms, if needed. The thermodynamic characteristics and structural properties in the given ternary solution will be considered when one proper geometric model is chosen. Figure 2.1 shows some geometric models for estimating ternary thermodynamic properties from optimized binary parameters (Pelton, 2001).
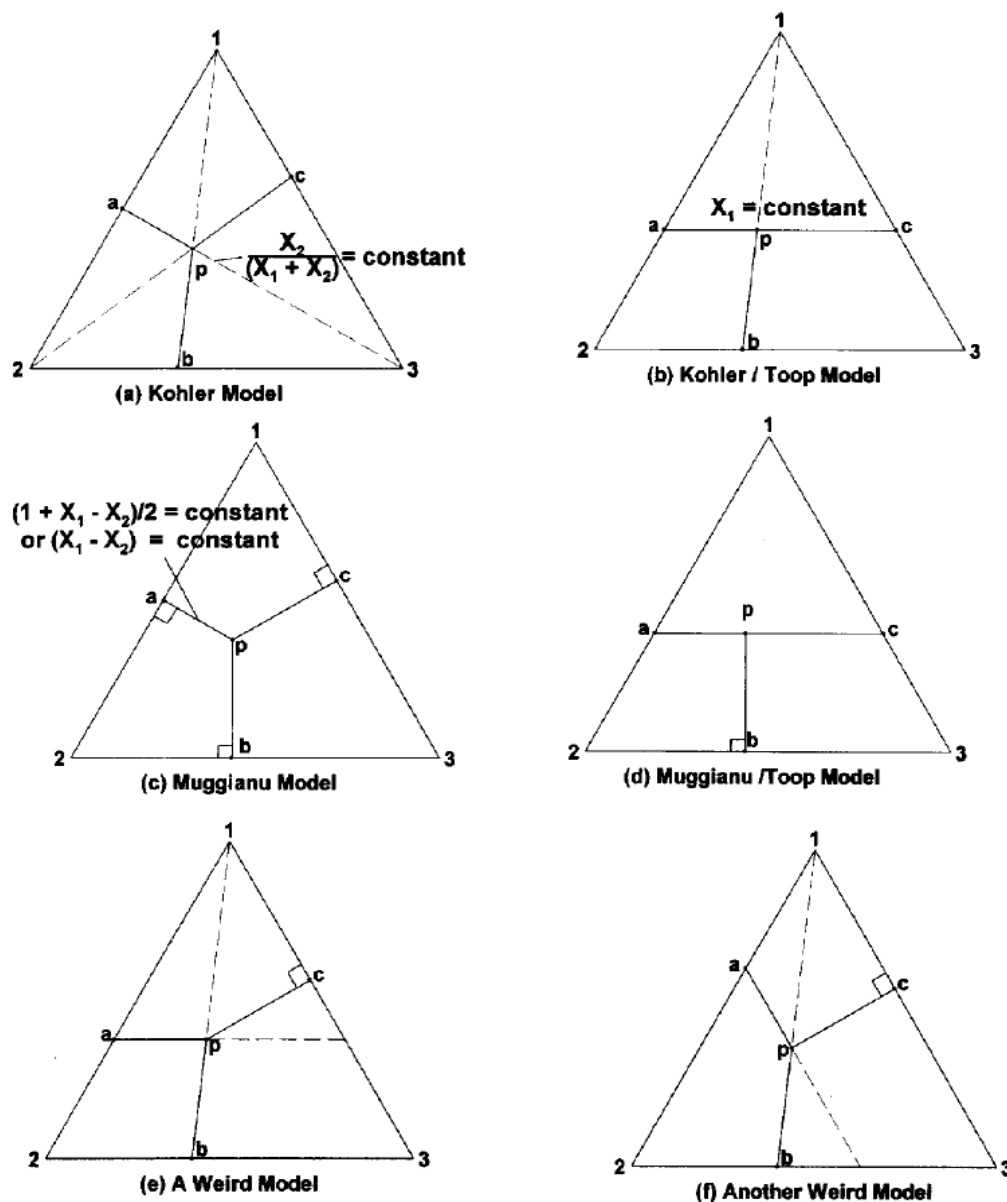
Figure 2.1 Some geometric models for estimating ternary thermodynamic properties from optimized binary parameters (Pelton, 2001)

2.5 Thermodynamic Evaluation and Optimization Procedure

The whole project will be divided into two main parts: 1) the experiments and theoretical calculations (ab-initio and Miedema model) to obtain data, and 2) assessment (modeling) of the systems. Since not all the key experimental data are available for all the systems, the question is how to obtain those key data. In the present study, the systematic analysis, calculations from

First-Principle and Miedema model and some key experiments will be performed in order to obtain complete thermodynamic data. As for assessment of the systems, many techniques and tactics will be considered, such as, which proper thermodynamic model should be chosen for each phase, how to assess the data according to the quality and credibility of the experimental methods, how to extrapolate or interpolate the thermodynamic data to the ranges needed.

The procedure can be realized by the following steps:

1) Collection of the experimental data

For the thermodynamic optimization of a phase diagram, the first step is to collect and categorize all the experimental data for the system of interest including integral enthalpy of mixing, partial enthalpy of mixing, activities of the components, heat capacities, solid solubility, crystal structures of the intermetallic compounds, melting points, enthalpy of formation, transformation temperature, physical properties, *etc.* Sometimes, useful data may be available from the higher-order systems of which the studied one is a sub-system.

2) Evaluation of the experimental data

The critical evaluation of the experimental data before doing the thermodynamic optimization is necessary to eliminate contradictory or unreliable data. Considerable expertise and familiarity with the different experimental methods is required.

3) Development of systematic analytical techniques

It is known that within the rare earth family, several thermodynamic properties change according to a systematic pattern, and it is observed that some constitutional properties of the alloys formed by similar elements enable empirical regularities to be discerned. Enthalpy of formation, melting temperature of the compound, entropy of fusion, enthalpy of fusion, *etc*, will be systematically analyzed according to atomic number, radii of rare earths, or electronegativities of the rare earths in order to discover regular and reasonable trends. Then some missing data can be interpolated or extrapolated.

4) Evaluation of the missing data by First-Principles or the semi-empirical Miedema model

First-Principles calculations and the semi-empirical Miedema model have been used to estimate the enthalpies of formation of the binary phases, enthalpies of mixing of rare earth elements in Al–FCC phase and Mg–HCP phase. These theoretical calculations are very important because some of the enthalpy data are missing and are experimentally difficult to measure. Collaboration with the Institute of High Performance Computing (IHPC) in Singapore for First-Principle calculations was obtained for the period from Feb, 2009 to May, 2009. The enthalpies of formation for some metastable phases and ternary stoichiometric phases are calculated by the semi-empirical Miedema model.

5) Choice of the appropriate thermodynamic model for the phases

To construct an accurate and reliable multi-component database, it is very crucial to choose a proper thermodynamic model for the phase based on its structure (number of sublattices, which species are mixing on the specific sublattices, *etc*.) in order to yield a reliable prediction for the multi-component systems from the model parameters of their sub-systems.

Solid solution and liquid databases have been built using the compound energy formalism and the modified quasi-chemical model (Pelton & Chartrand, 2001c) for the present study.

6) Optimization of the model parameters of binary and ternary systems

After the evaluation of the experimental data is completed and the appropriate thermodynamic models are chosen, the model parameters are optimized in order to reproduce all the reliable experimental data. Afterwards, all the thermodynamic properties can be back-calculated. In the present study, the Factsage^{TM} thermodynamic software was used (Bale et al., 2002).

CHAPTER 3   **OBJECTIVES AND METHODOLOGY**

3.1   Objectives

The main objective of the present study is to construct a consistent thermodynamic and phase equilibrium model and its database for Mg and Al alloys with additions of rare earths. Rare earth elements are chemically similar (except Eu and Yb). Numerous binary and ternary systems in the Mg–Al–La–Ce–Pr–Nd–Sm–Gd–Tb–Dy–Ho–Er group were critically evaluated and systematically optimized. The Al–Tm, Al–Lu and Al–Pm binary systems, in which few experimental data are available in the literature, are not included in this work. The Al–Eu and Al–Yb binary systems, which are quite dissimilar from other Al–RE systems, are not considered, since Eu and Yb elements show anomalies across the rare earth elements. The Al–Sc and Al–Y systems, which were optimized previously by Kang *et al.* (Kang et al. 2008) using MQM for liquids, are not included. The systematic modeling of all these Mg–RE, Al–RE binary systems and Mg–Al–RE ternary systems, using the modified quasi-chemical model (MQM) that takes into account the short-range ordering effect in liquids, has never been realized previously.

The secondary objective of this research is to do key experiments in the magnesium-rich corners to check phase equilibria, since this is very important for the Mg alloy design. Key experimental investigations have been performed for the Al–Mg–La, Al–Mg–Ce, Al–Mg–Pr and Al–Mg–Nd ternary systems in order to obtain information on phase equilibria and solid solubilities. Diffusion couples have also been made to verify phase equilibria in ternary systems.

The third objective in this work is to find or develop proper methods for estimating missing thermodynamic data for binary and ternary phases involving rare earth elements. These thermodynamic data include enthalpy of formation and entropy of formation. For systems where thermodynamic data are scarce or experimental data are contradictory, First-Principles (including supercell technique for dilute solutions) and the semi-empirical Miedema model have been employed. These methods are used to calculate the enthalpies of formation of binary and ternary stoichiometric compounds and enthalpy of mixing in (Mg)-HCP and (Al)-FCC solutions. Estimation techniques for enthalpy of formation based on systematic studies of trends across rare earth elements have been performed and used for thermodynamic optimizations.

The main hypothesis of this work is that the modified quasi-chemical model (MQM) can well describe liquid solutions and realistic results can be obtained for phase equilibria in multi-component systems even without ternary parameters. The present study was performed under three constraints :1) the g^0 of pure elements was directly taken from Scientific Group Thermodata Europe (SGTE) database or from Kang *et al*. (Kang, 2008; Kang et al., 2012), and the g^0 of fixed end-members (such as Al_2Mg, Mg_2Mg, Mg_2Al, Al_2Al in Laves_C15 phase) was taken from the existing FTlite database. 2) the present thermodynamic database was constructed from and partially based on the existing FTlite database in Factsage software. 3) the coordination numbers for the pure liquids (Al, Mg, RE) were set to the same values as those in the existing alloy database (*i.e*. FTLite database), for purposes of compatability.

In the following, a brief introduction on the First-Principles, Miedema model, experiments, and estimation techniques based on systematic studies used in this work are presented.

3.2 First-Principles Calculations

A solid can be considered as an assemblage of interacting positively charged nuclei and negatively charged electrons (Liu, 2009). Theoretically, the properties of solids can be obtained without any empirical parameters by solving the many-body Schrödinger equation involving both the nuclei and the electrons:

$$\hat{H}\Psi(\vec{R_1}, \vec{R_2}, \cdots \vec{R_N}, \vec{r_1}, \vec{r_2}, \cdots \vec{r_n}) = E\Psi(\vec{R_1}, \vec{R_2}, \cdots \vec{R_N}, \vec{r_1}, \vec{r_2}, \cdots \vec{r_n}) \tag{3.1}$$

where the $\vec{R}$'s are the nuclei coordinates, the $\vec{r}$'s are the electron coordinates, $\hat{H}$ is the Hamiltonian operator, E is the total energy of the system, N is the total number of nuclei and n is the total number of electrons in the system.

However, although theoretically exact, it is extremely difficult to solve this equation due to its many-body characteristics. As a matter of fact, the only system that can be solved analytically is the single-electron hydrogen atom. Thus several approximations have to be introduced to reduce the complexity. One is the Born-Oppenheimer Approximation (Born & Oppenheimer, 1927).

Due to the fact that the nuclei are much heavier than the electrons, it is reasonable to assume that the electrons are always in the instantaneous ground state with the nuclei. The other is the one-electron approximation. Each electron moves independently in the field of an average potential generated by all the other electrons. Most modern electronic calculations for solids are based on the density functional theory (DFT) proposed by Kohn and Sham (Kohn & Sham, 1965). According to DFT, the total energy of a system is a function of the electron charge density. There are the Local Density Approximation (LDA) and the Generalized Gradient Approximation (GGA). The original many-electron Schrödinger equation is then converted into a set of one-electron Schrödinger equations, one for each electron in the system. Nevertheless, the exact form of the exchange correlation energy remains unknown.

It is worth noting that there is only one LDA exchange correlation functional, *i.e.* the one by Ceperley and Alder (Ceperley & Alder, 1980). Nevertheless, there are many versions of GGA due to the freedom of choice in incorporating the gradient term in the exchange correlation energy.

The actual First-Principles total energy calculations were performed in a self-consistent iteration. An educated guess is given for the initial charge density function. By solving the Schrödinger equations, a new charge density is obtained. The iteration stops when the new charge density (or the new total energy) does not differ much from the previous one, which means that the iteration has converged. In practice, it is nesscessary to relax the nuclei into their equilibrium positions until the quantum-mechanical forces acting on each of them vanish. Such structural relaxations are usually performed numerically, such as according to a conjugate-gradient or a quasi-newton scheme. The final total energies obtained can be used to extract the formation enthalpies of stable, metastable or even unstable structures at T = 0 K using the following equation:

$$\Delta H\left(A_{1-x}B_x\right) \ = \ E\left(A_{1-x}B_x\right) - \ \left(1-x\right)\cdot E\left(A\right) \ - \ x\cdot E\left(B\right) \tag{3.2}$$

where the *E*'s are the First-Principles calculated total energies of structure $A_{1-x}B_x$ and pure elements A and B, each fully relaxed to their equilibrium (zero-pressure) geometries, respectively.

All electronic structure calculations were performed by the means of the periodic density functional theory (DFT) using the Vienna Ab initio Simulation Package (VASP) (Kresse et al.). The Kohn-Sham equations were solved using the projector augmented plane wave (PAW) method (Blochl, 1994; Kresse & Joubert, 1999) with the generalized gradient approximation (GGA). The Perdew-Burke-Ernzerhof (PBE) gradient approximation was chosen to describe the exchange-correlation interaction. The interaction between ions and electrons were described by the standard frozen-core potentials which combine the accuracy of augmented plane wave method and the flexibility of pseudopotentials approach. For La, Ce, Pr and Nd elements, 5s, 5p, 6s, 5d electrons were treated within the valence band while the other electrons were kept frozen in the core; this is based on the assumption that electrons (including 4f electrons) of rare earths in the deep atomic core states are very localised and generally do not participate in the bonding of molecules and solids. Spin polarization with collinear magnetization were not considered in the calculations, since no significant magnetic contribution to the total energy was found after our comparison studies. It was also pointed out by Gao *et al*. (Gao et al., 2007) that the magnetic contribution to the total energy is zero or negligible when the trivalent potentials for La, Ce, Pr and Nd elements are used. The plane wave cutoff energy (Ecut) of 300eV magnitude was set up after the convergence test. The total energy converged to within 5 meV/atom. For the Brilloin zone intergration, the Monkhort-Pack grid (Monkhorst & Pack, 1976) and Gamma-centered grid (for hexagonal structures) were used. Reciprocal space (*k*-point) meshes were increased until the total energy converged to within 5 meV/atom.

The lattice constant, equilibrium volume, bulk modulus, and cohesive energy can be obtained by performing energy calculations on different volumes and then fitting data to the following Birch-Murnaghan equation of state.

$$E(V) = \frac{B_0 V}{B_0^{'}(B_0^{'}-1)}[B_0^{'}(1-\frac{V_0}{V}) + (\frac{V_0}{V})^{B_0^{'}} - 1] + E_0(V_0) \qquad (3.3)$$

V_0 is equilibrium volume. $E_0(V_0)$ is the equilibrium energy at equilibrium volume V_0. $B_0^{'}$ is the bulk modulus pressure derivative, $B_0^{'} = (\dfrac{\partial B}{\partial P})_T$.

The supercell method was employed for the solid solutions. For example, for the Al-fcc and Mg-hcp solid solutions, the mixing energies were determined by relaxations for a single RE-substituted atom in a 96-atom (4*4*3) Mg supercell and in a 108-atom (3*3*3) Al supercell. The atomic positions are relaxed until the total energy converged to less than 5 mev/atom.

3.3 Miedema Model

The Miedema model has been formulated (Bakker, 1998; Boer et al., 1988; Miedema et al., 1980) to predict enthalpy effects in alloys with the accuracy comparable to that of the experimentally observed quantities. With respect to the understanding of phase diagrams, the prediction of enthalpies of formation is as important as experimental measurements. An essential point in the formation of the empirical Miedema model is that qualitative experimental information has been used to obtain the semi-empirical equations and parameters.

The Miedema enthalpies of formation (Bakker, 1998; Boer et al., 1988) for an A-B solution starts with Eq. (3.4)

$$\Delta H^{mix} = X_A X_B (X_B^S \Delta H^{\mathrm{int}erfacial}(AinB) + X_A^S \Delta H^{\mathrm{int}erfacial}(BinA)). \tag{3.4}$$

Where ΔH^{mix} is the chemical enthalpy for the A-B solution, X_A and X_B are mole fractions of A and B. $\Delta H^{\mathrm{int}erfacial}(AinB)$ indicates the enthalpy upon alloying, X_A^S and X_B^S are surface fractions of A and B.

$\Delta H^{\mathrm{int}erfacial}(AinB)$ can be described by the following form in Eq. (3.5):

$$\Delta H^{\text{interfacial}}(AinB) = \frac{2PV_A^{2/3}}{\frac{1}{n_{WS_A}^{1/3}} + \frac{1}{n_{WS_B}^{1/3}}} \cdot [-(\phi_B^* - \phi_A^*)^2 + \frac{Q}{P}(n_{WS_A}^{1/3} - n_{WS_B}^{1/3})^2 - a \times \frac{R}{P}]$$

(3.5)

Moreover, X_A^S, can be obtained by Eq. (3.6):

$$X_A^S = \frac{X_A V_A^{2/3}}{X_A V_A^{2/3} + X_B V_B^{2/3}}$$

(3.6)

In principle, the actual calculation of X_A^S should change upon alloying. The volume upon alloying is estimated by eq. (3.7):

$$(V_A^{2/3})alloy = [1 + \mu_A f_B^A (\varphi_A - \varphi_B)](V_A^{2/3})_{pureA}$$

(3.7)

while

$$f_B^A = X_B^S \qquad \text{for disordered alloys}$$

(3.8)

$$f_B^A = X_B^S[1 + 8(X_A^S X_B^S)^2] \qquad \text{for ordered alloys}$$

(3.9)

In general, Eq. (3.6) has to be solved by itineration techniques. It can be expressed as Eq. (3.10) by substitution of Eqs. (3.5)-(3.8) into Eq. (3.4):

For disordered alloys:

$$\Delta H_{AB} = f_{AB} \frac{x_A(1 + \mu_A x_B(\phi_A - \phi_B))x_B(1 + \mu_B x_A(\phi_B - \phi_A))}{x_A V_A^{2/3}[1 + \mu_A x_B(\phi_A - \phi_B)] + x_B V_B^{2/3}[1 + \mu_B x_A(\phi_B - \phi_A)]}$$

(3.10)

For ordered alloys:

$$(\Delta H_{AB})_{order} = \Delta H_{AB}\left[1 + \gamma\left(\frac{V_A^{2/3}V_B^{2/3}\Delta H_{AB}}{f_{AB}\{x_A V_A^{2/3}[1 + \mu_A x_B(\phi_A - \phi_B)] + x_B V_B^{2/3}[1 + \mu_B x_A(\phi_B - \phi_A)]\}}\right)^2\right]$$

(3.11)

$$f_{AB} = \frac{2PV_A^{2/3}V_B^{2/3}}{\dfrac{1}{n_{WS_A}^{1/3}} + \dfrac{1}{n_{WS_B}^{1/3}}} \cdot [-(\phi_B^* - \phi_A^*)^2 + \frac{Q}{P}(n_{WS_A}^{1/3} - n_{WS_B}^{1/3})^2 - a \times \frac{R}{P}] \tag{3.12}$$

where x_i, ϕ_i, V_i, n_{WS_i} are the mole fraction, chemical potential (or work function), mole volume, and the electronic density at the Winger-Seitz cell boundary of component i, respectively. a, P, $\frac{R}{P}$, $\frac{Q}{P}$, μ_i, and γ are the semi-empirical parameters evaluated and reported in Miedema (Boer et al., 1988). The P empirical parameter assumes different values according to whether A and B are both transition, both non-transition, or transition and non-transition elements; Q/P is assumed to be constant (equal to 9.4) (Boer et al., 1988).

The formation enthalpy of a crystalline solid solution can be described as (Sun et al., 2010) :

$$\Delta H^{cryst} = \Delta H^{chem} + \Delta H^{elastic} + \Delta H^{struct} \tag{3.13}$$

where ΔH^{chem} is the chemical contribution due to the mixing of two components; $\Delta H^{elastic}$ is the elastic contribution due to the atom-size mismatch effect; ΔH^{struct} is the structure contribution due to the valence and crystal structure difference of the two components.

$$\Delta H^{elastic} = x_A \cdot x_B (x_A \Delta H_{BinA}^{elastic} + x_B \Delta H_{AinB}^{elastic}) \tag{3.14}$$

where $\Delta H_{BinA}^{elastic}$ and $\Delta H_{AinB}^{elastic}$ are the atom-size mismatch contributions to the solution enthalpy in a binary system. It can be evaluated by:

$$\Delta H_{AinB}^{elastic} = \frac{2G_B(V_A^* - V_B^*)^2}{3V_B^* + 4G_B K_A V_A^*} \tag{3.15}$$

$$(V_i^*)^{2/3} = V_i^{2/3}(1 + \mu_i(\phi_i - \phi_j)) \qquad (i, j = \text{A, B}) \qquad (3.16)$$

where G_B is the shear modulus of the solvent; K_A is the compressibility of the solute; V_i^* (i=A, B) are the molar volumes of the solute or the solvent.

The contribution of formation enthalpies from two different structures has minimal effect and can be neglected.

$$\Delta H^{struct} \approx 0. \qquad (3.17)$$

The calculation for a ternary alloy is similar to that of a binary alloy. However, it has involved interpolation from three sub-binary systems. There are methods for interpolating, such as the Kohler, Muggianu and Toop models. The choice of the interpolation model should be made according to the thermodynamic properties of the three sub-binary alloys. In the current study, the thermodynamic properties (like enthalpy of mixing in the liquid) of the three binary systems Al-Mg, Al-RE and Mg-RE are quite different among themselves. The Kohler model was chosen for the present study.

The Kohler model can be expressed as

$$\Delta H_{ijk}^{cryst} = (1-x_i)\Delta H_{jk}^{cryst}(\frac{x_j}{x_j+x_k}, \frac{x_k}{x_j+x_k}) + (1-x_j)\Delta H_{ik}^{cryst}(\frac{x_i}{x_i+x_k}, \frac{x_k}{x_i+x_k})$$
$$+ (1-x_k)\Delta H_{ij}^{cryst}(\frac{x_i}{x_i+x_j}, \frac{x_j}{x_i+x_j}) \qquad (3.18)$$

where i, j, k are the three components in a ternary system, x_i, x_j or x_k is the mole fraction of each component, ΔH_{ij}^{cryst}, ΔH_{jk}^{cryst}, ΔH_{ik}^{cryst} and ΔH_{ijk}^{cryst} are the contributions (chemical, elastic and

structural contributions) of the three sub-binary systems and ternary system, respectively. The chemical and elastic enthalpies of ternary alloys can be extrapolated similarly from those of sub-binary systems by the Eq. (3.18).

3.4 Experiments

The use of diffusion couples in phase diagram studies is based on the assumption that local equilibria are established and maintained at the phase interfaces in the diffusion zone (Zhao, 2007). That is, an infinitesimal layer adjacent to the interface in such a diffusion zone is in thermodynamic equilibrium with its neighboring layer on the other side of the interface (Kirkaldy, 1958; Zhao, 2007). A diffusion couple is an assembly of two different materials in intimate interfacial contact. It is usually subjected to high temperature annealing for a long period of time to promote thermal inter-diffusion to form layers (solid solutions and intermetallic compounds). The local equilibria at the phase interfaces enables determination of phase equilibrium information from diffusion couples or diffusion multiples.

In this work, the solid–solid diffusion couple for the Al–Mg–La system was prepared from two blocks of Mg and Al alloys with La foil in between. The blocks' facing surfaces and La foil were pre-grinded up to 1200 grit using SiC paper and polished up to 1 mm using diamond paste. The blocks were pressed together using a hydraulic press, placed in a Ta container and sealed in a quartz tube under protective argon atmosphere. The prepared samples were annealed at 673 K for four weeks. The annealed samples were well grinded and polished before being subjected to electron probe microscopy analysis (EPMA) using point and line scans. The solid–liquid diffusion couple for Al–Mg–Ce system was prepared using two prepared alloys ($Ce_{0.333}Mg_{0.667}$ alloy and $Ce_{0.333}Al_{0.667}$ alloy). The block ($Ce_{0.4}Mg_{0.6}$ alloy) with the lower melting temperature was melted on top of the block ($Ce_{0.333}Al_{0.667}$ alloy) with the higher melting temperature in an arc-melting furnace. The prepared samples were also annealed at 673 K for four weeks. The annealed alloys were well grinded and polished before EPMA analysis. The starting materials were pure metals: La foil (50mm*50mm*1.0mm, 99.9% (REO)), Ce ingot (99.8 % (REO)), Al ingot (99.999 wt. %) and Mg ingot (99.8 wt. %).

It is desirable to combine the diffusion couple technique with subsequent investigation of the selected equilibrated alloys so that the precision and reliability of the information obtained could be guaranteed. Using equilibrated alloys to determine the phase diagram is a traditional and widely-used method. The phase equilibria obtained are important input data for the thermodynamic optimization. In the present study, two equilibrated alloys of Mg rich–Al–La alloys and two of Mg rich–Al–Ce alloys were arc–melted with a water-cooled copper crucible under argon atmosphere to avoid extensive evaporation of Mg and Al. Four ternary equilibrated alloys for Al–Mg–Pr system were prepared by melting stoichiometric amounts of the constituent elements in an induction furnace under the protective argon atmosphere. Three equilibrated alloys for Al–Mg–Nd system were melted by the arc-melting furnace in the water-cooled copper crucible under the protective argon atmosphere. The prepared samples were annealed in the resistance furnace at 673 K for four weeks before quenching in the cold water. All the samples were grinded up to 1200 grit using SiC paper and polished up to 1 mm using diamond paste. EPMA (JEOL-JXA-8900) was employed to detect the phases and determine their compositions with a 2 μm probe diameter, 15 kV accelerating voltage and 20 nA probe current. The Phi-Rho-Z (PRZ) matrix corrections (modified ZAF) were applied during the composition analysis (Zhang, 2010). The starting materials were pure metals: Pr ingot (99.9 % (REO)), Nd ingot (99.8 % (REO)), Al ingot (99.999 wt. %) and Mg ingot (99.8 wt. %).

The measurement error of EPMA is estimated to be 1-2 wt.%. The morphology, suface features and grain size can affect the accurability of analysis.

3.5 Estimation Techniques Based on Systematic Analysis

The various physical properties of rare earth metals have been summarized by Gschneidner (Gschneidner, 1990a) based on published data of rare earth properties. The systematics of the enthalpies of formation of rare earth compounds with most of the elements in the periodic table (*i.e.* RM$_x$) was reviewed by Gschneidner (Gschneidner, 1990b). The lanthanide metals have the crystal structure sequence hcp ➧ Sm-type ➧ dhcp ➧ fcc This sequence is realized both as a function of decreasing atomic numbers going from lutetium to lanthanum and as a function of pressure. For example, if pressure is applied to Dy (hcp), Dy (fcc) structure could eventually be

obtained. Johansson and Rosengren (Johansson & Rosengren, 1975) constructed the generalized phase diagram for the lanthanide metals using the observed regularity in the crystal structures. In this study, the properties which are of particular interest in phase diagram studies (crystal structure, metallic radius, atomic volume, density, transition temperatures, enthalpies of transformation of rare earth metals) were taken from Gschneidner (Gschneidner, 1990a) and listed in Appendix 1 together with the electron configurations of rare earth elements. The similar electronic configurations of rare earth elements are the main reason for their similarity.

The atomic volumes (and metallic radii) of the lanthanide metals are very similar and tend to decrease slowly with atomic number, while the melting points slightly increase with atomic number. Two divalent lanthanide metals, Eu and Yb are exceptions to the above generalizations; they have larger atomic volumes, lower melting points and display cubic structures at lower temperatures. The lanthanide contraction occurs due to the following reason: although each increase in nuclear charge is balanced by a simultaneous increase in electronic charge, the directional characteristics of the 4f orbitals cause the $4f^n$ electrons to shield themselves and other electrons from the nuclear charge only imperfectly. Consequently, each unit increase in nuclear charge leads to a net increase in attraction for the whole extra nuclear electron charge cloud and each ion shrinks slightly in comparison to the previous element (Ferro & Saccone, 2008). On the other hand, although a similar overall reduction is seen in the metal radii, Eu and Yb are very irregular. The reason is that most of the metals are composed of a lattice of Ln^{3+} ions with a $4f^n$ configuration and 3 valence electrons. However, metallic Eu and Yb, are composed predominantly of the larger Ln^{2+} ions with $4f^{n+1}$ configurations and only 2 valence electrons. The smaller and opposite irregularity for metallic Ce is due to the presence of ions in a +4 oxidation state. Similar discontinuities are found in other properties of the metals, particularly at Eu and Yb. Figure 3.1 shows the trends of ionic radius for Ln^{3+} and Ln elements (here, Ln represents a rare earth element). Figures 3.2 and 3.3 show the trends for melting points of rare earths and enthalpy of formation of $REAl_2$, respectively.
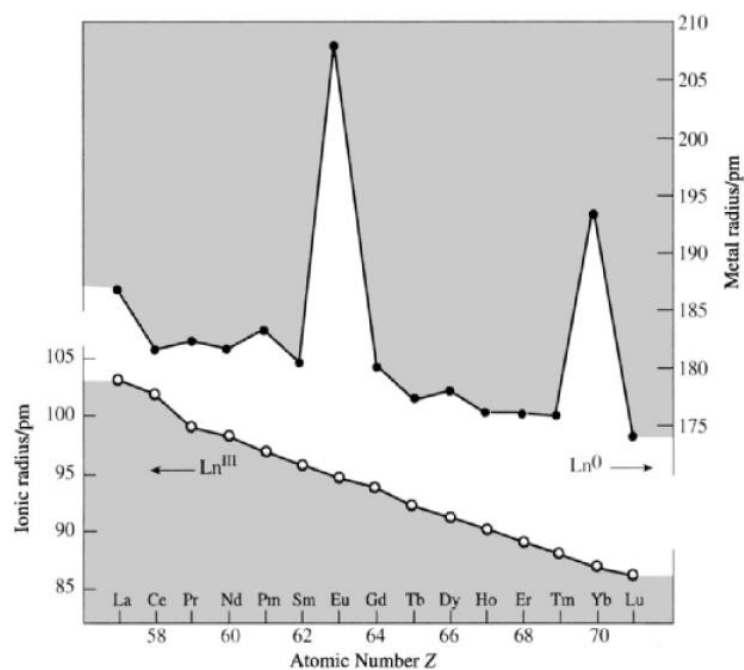
Figure 3.1 Ionic radius for Ln^{3+} and Ln elements (Greenwood & Earnshaw, 1998)
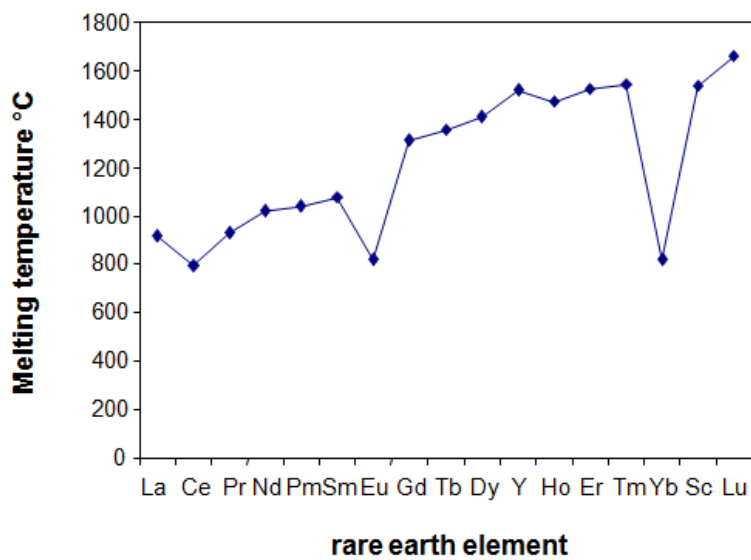
Figure 3.2 Melting point of rare earth elements
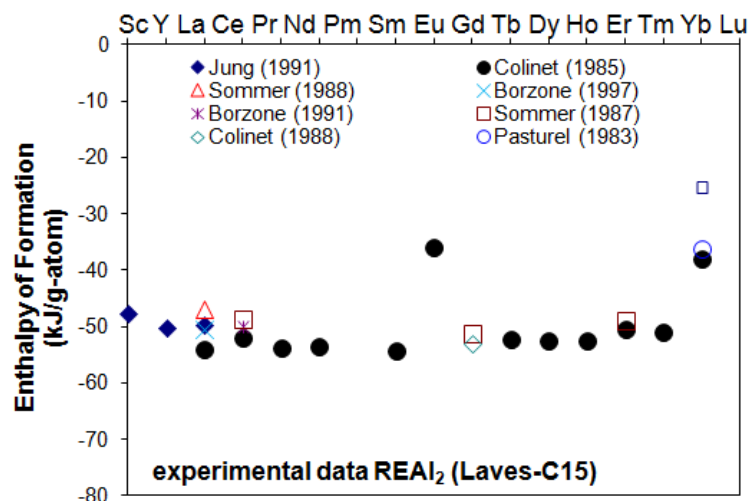
Figure 3.3 Enthalpy of formation of $REAl_2$ (Borzone et al., 1991; Borzone et al., 1997; Colinet et al., 1985, 1988; Jung et al., 1991; Pasturel et al., 1983; Sommer & Keita, 1987; Sommer et al., 1988)

As is seen in Figures 3.2 and 3.3, Eu and Yb show abnormalities. These could be explained by their special electronic configurations. Eu has a half-filled $4f$ orbital and Yb has completely filled $4f$ orbital. Both are very stable configurations of low energy. Alloying with aluminum to form intermetallic compounds disturbs these stable electronic configurations through charge transfer or chemical bonding (Gao et al., 2007).

To predict the trends of the enthalpies of formation for lanthanide alloys, it was suggested by Gschneider (Gschneidner, 1969; Gschneidner, 1990b) that these should be related to the relative molar volumes and reduced temperatures. He also indicated that these quantities should reflect the characteristics of lanthanide contraction in the compounds compared to the contraction of the pure metals. For example if the lanthanide contraction in the compounds from La to Lu become greater than that in the corresponding pure metals, then the enthalpies of formation are predicted to become more exothermic in the same sequence. In this scheme the reduced temperature [the ratio of the melting point of the compound to the melting point of the lanthanide element, see Eq. (3.19)] and the ratio of the molar volumes of the compound to the atomic volume of the pure element normalized with respect to the first member of the series [for example La, see Eq.

(3.20)] were used as indicators for predicting the systematic behavior of the stability of the alloys (Meschel & Kleppa, 2001).

According to Gschneider's proposal, the reduced temperature is expressed by:

$$r_{temp} = \frac{T_m(RE_{1-x}M_x)}{T_m(RE)}$$
(3.19)

where T_m is the melting (or transformation) temperature expressed in Kelvin. RE is a rare earth element, and M denotes any other element.

The volume ratio relative to a selected rare earth (La), also known as the relative molar volume, is expressed by:

$$r_{vol} = \frac{V(RE_{1-x}M_x)}{V(La_{1-x}M_x)} \cdot \frac{V_{La}}{V_{RE}}$$
(3.20)

where V is the volume of one mole of the stated compound or element. The r_{vol} ratio gives some indication of the relative degree of the lanthanide contraction and of the volume contraction in the synthesis of a certain family of compounds.

Figures 3.4 and 3.5 show the trends of relative molar volume and reduced temperature of $REAl_2$ across the lanthanide series.

Tables 3.1 and 3.2 summarize the crystal structures of different phases in the Al–RE and Mg–RE binary systems. The choice of thermodynamic model used in the present work is based on the crystal structures of phases.
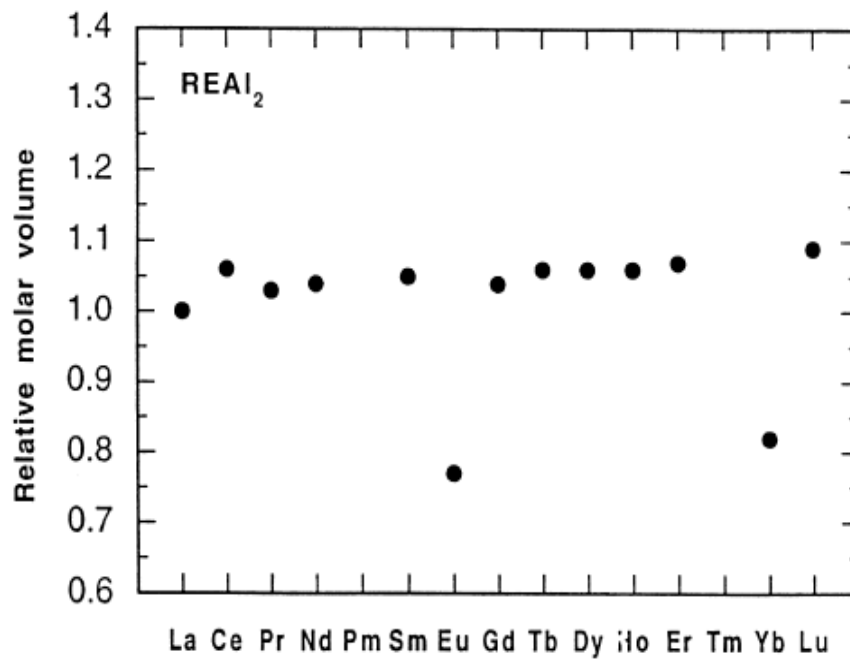
Figure 3.4 Relative molar volume of REAl$_2$ (Meschel & Kleppa, 2001)
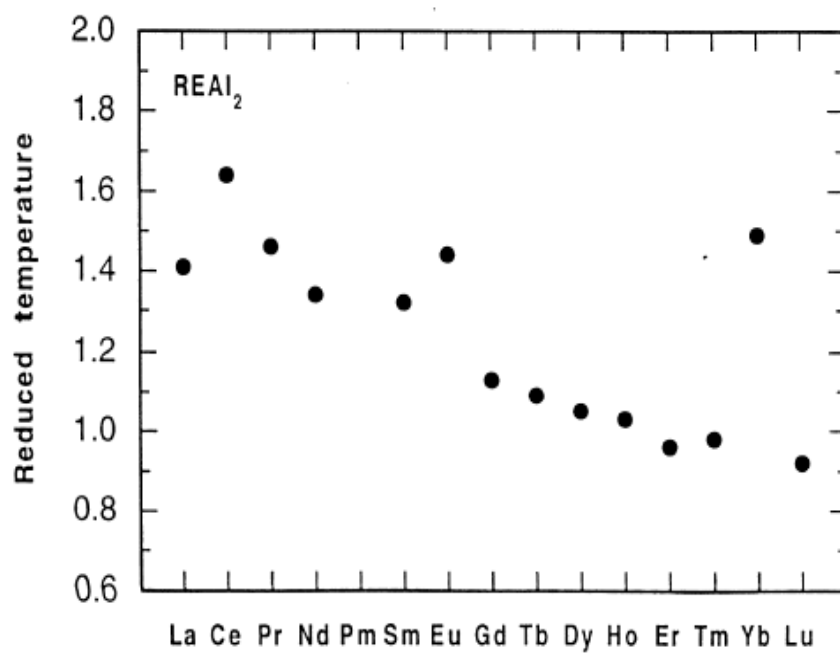
Figure 3.5 Reduced temperature of REAl$_2$ (Meschel & Kleppa, 2001)

Table 3.1 Crystal Structures of the Different Phases in the Al–RE Binary Systems

Stoichiometry		Sc	Y	La	Ce	Pr	Nd	Pm	Sm	Eu	Gd	Tb	Dy	Ho	Er	Tm	Yb	Lu	Structural Types
R₃Al	LT			+	+	+	+												+hP8-Ni₃Sn
	HT				*	*													*cP4-AuCu₃
R₂Al		*	+			+	+		+		+	+	+	+	+			×	+oP12-Co₂Si *hP6-Ni₂In
R₃Al₂			+								+	+	+	+	+	+		+	+tP20-Zr₃Al₂
RAl	LT	#	Δ	&	&	+	+		+	■	+	+	+	+	+	+	×	+	+oP16-ErAl ΔoC8-CrB
	HT					&													■oP20-EuAl
																			#cP2-CsCl &oC16-CeAl
RAl₂			+	+	+	+	+		+	+	+	+	+	+	+	+	+	+	+ cF24-MgCu₂
R₂₂Al₅₃				+															+ hP3-AlB₂
RAl₃	LT	#	+	+	+	+	+		+		+	&	Δ	■	#	#	#	#	+hP8-Ni₃Sn #cP4-AuCu₃
	HT		&										■						■hR60-HoAl₃ &hR36-BaPb₃ ΔhP16-Ni₃Ti
R₃Al₁₁	LT			#	#	#	#												+ tI10-BaAl₄ (Al deficient)
	HT			+	+	+	+		#										#oI28-αLa₃Al₁₁
RAl₄										+									+tI10-BaAl₄
R=		**Sc**	**Y**	**La**	**Ce**	**Pr**	**Nd**	**Pm**	**Sm**	**Eu**	**Gd**	**Tb**	**Dy**	**Ho**	**Er**	**Tm**	**Yb**	**Lu**	

Gd: for GdAl₄, there is some disagreement on its existence (i.e. stability);

        for Gd₂Al₁₇ no other investigators reported this except (Pop et al., 1979)

Er: for RAl₃, This structure is stabilized by the presence of small amounts of Si according to (Meyer, 1970)

Tm: for R₃Al₂, this intermetallic compound is not reported by (Gschneidner & Calderwood, 1989a)

Yb: for RAl, only reported by (Vengrenovich & Psarev, 1969). (Palenzona, 1972) confirmed that it does not exist, and not reported by (Gschneidner & Calderwood, 1989b)

Lu: for Lu₂Al, only reported by (Kuzma et al., 1992)

Table 3.2 Crystal Structures of the Different Phases in the Mg–RE Binary Systems

Stoichiometry	Sc	Y	La	Ce	Pr	Nd	Pm	Sm	Eu	Gd	Tb	Dy	Ho	Er	Tm	Yb	Lu	Structural Types
≈R_2Mg													+	+	+			+ cI2-W
RMg	+	+	+	+	+	+		+	+	+	+	+	+	+	+		+	+ cP2-CsCl
RMg_2		+	Δ	Δ	Δ	Δ		Δ	+	Δ	+	+	+	+	+	+	+	+ hp12-$MgZn_2$ Δ cF24-Cu_2Mg
RMg_3			+	+	+	+		+		+	+	+						+ cF16-BiF_3
RMg_4									+									+ hP94-$Mg_{38}Sr_9$
R_5Mg_{24}		+									+	+	+	+	+		+	+ cI58-αMn
RMg_5								+	Δ	+								+cF448-$GdMg_5$ ΔhP36-$ErZn_5$
R_5Mg_{41}				+	+	+		+										+ tI92-Ce_5Mg_{41}
R_2Mg_{17}			+	+					+									+ hP38-Th_2Ni_{17}
RMg_{12}			+	+														+oI338-$CeMg_{12}$
				Δ	Δ													Δ tI26-$ThMn_{12}$
R=	**Sc**	**Y**	**La**	**Ce**	**Pr**	**Nd**	**Pm**	**Sm**	**Eu**	**Gd**	**Tb**	**Dy**	**Ho**	**Er**	**Tm**	**Yb**	**Lu**	

Ce: for $CeMg_{12}$ (*oI*338) orthorhombic structure is reported by Johnson *et al.*(Johnson et al., 1964)

Pr: $PrMg_3$, the prototype is $BiLi_3$ reported by Nayeb-Hashemi and Clark (Nayeb-Hashemi & Clark, 1988e)

Nd: $NdMg_{12}$ is metastable, and it is observed in samples quenched from the liquid state (Gorsse et al., 2005)

Sm: $Sm_2Mg_{13,}$ reported by Zheng *et al.* (Zheng et al., 1986), but Saccone (Saccone et al., 1989) suggested $SmMg_5$ and Sm_5Mg_{41} instead of Sm_2Mg_{13}

Dy: for Dy_2Mg, concluded in (Ferro et al., 1993), but not in (Du et al., 2004)

Ho: for Ho_2Mg, concluded in (Ferro et al., 1993), but not in (Saccone et al., 1993)

Tm: β phase≈Tm_2Mg (cubic) reported by (Saccone et al., 1995)

Figure 6 and 7 show the similarities of the Al-RE and Mg-RE systems. For the Al-RE systems, it is noted that each system (including the Al-Eu and Al-Yb systems) has an $REAl_2$ compound, which is the most stable intermetallic phase. They have the highest melting points in the phase diagrams and have the Laves_C15 ($cF24$-Cu_2Mg) crystal structure. There is a $REAl_3$ phase for each Al-RE system (except Al-Eu). For rare earth metals with large metallic radii (La, Ce, Pr, Nd, Sm and Gd) and Y, the hexagonal ($hP8$-Ni_3Sn) type is observed, while for rare earth metals with small metallic radii (Er, Tm, Yb, Lu and Sc), the cubic structure ($cP4$-$AuCu_3$) is found. For the rare earth metals in between (Tb, Dy, Ho), the structures ($hR36$-$BaPb_3$ for $TbAl_3$, $hR60$-$HoAl_3$ for $\beta DyAl_3$ and $HoAl_3$, $hP16$-Ni_3Ti for $\alpha DyAl_3$) have large unit cells in which both cubic and hexagonal stacking are mixed in an ordered way (Buschow & Van Vucht, 1967). It was also pointed out by Buschow and Van Vucht (Buschow & Van Vucht, 1967) that $BaPb_3$ type has 33.33% cubic character, while Ni_3Ti type 50% and $HoAl_3$ type 60%. For La, Ce, Pr, Nd and Sm, the Al-richest compound is RE_3Al_{11} while for Gd, Tb, Dy, Ho, Er, Tm, Yb and Lu, the Al-richest compound is $REAl_3$. For Eu, the Al-richest compound is Al_4Eu. The metallic radius of Eu, when in the divalent state, lies between that of calcium and strontium and the occurrence of Al_4Ca and Al_4Sr compounds (Al-richest compounds) has been observed in Al-Ca and Al-Sr systems.

For the Mg-RE systems, a $REMg_2$ compound is observed for each system (including the Al-Eu and Al-Yb systems). For rare earth metals with large metallic radii (La, Ce, Pr, Nd, Sm and Gd), cubic Laves_C15 ($cF24$-Cu_2Mg) crystal structure is found while for rare earth metals with small metallic radii (Eu, Tb, Dy, Ho, Er, Tm, Yb, Lu and Y), hexagonal Laves_C14 ($hp12$-$MgZn_2$) is reported. A REMg compound with cubic ($cP2$-CsCl) structure is observed in all the Mg-RE systems except Mg-Yb, while REAl with crystal structure other than $cP2$-CsCl structure is found in all the Al-RE systems. The Mg-richest compound shifts to the RE side across the lanthanides. For La, Ce, and Pr, the Mg-richest compound is $REMg_{12}$; for Nd and Sm, the Mg-richest compound is RE_5Mg_{41}; for Tb, Dy, Ho, Er Tm, Lu, and Y, the Mg-richest compound is RE_5Mg_{24}.
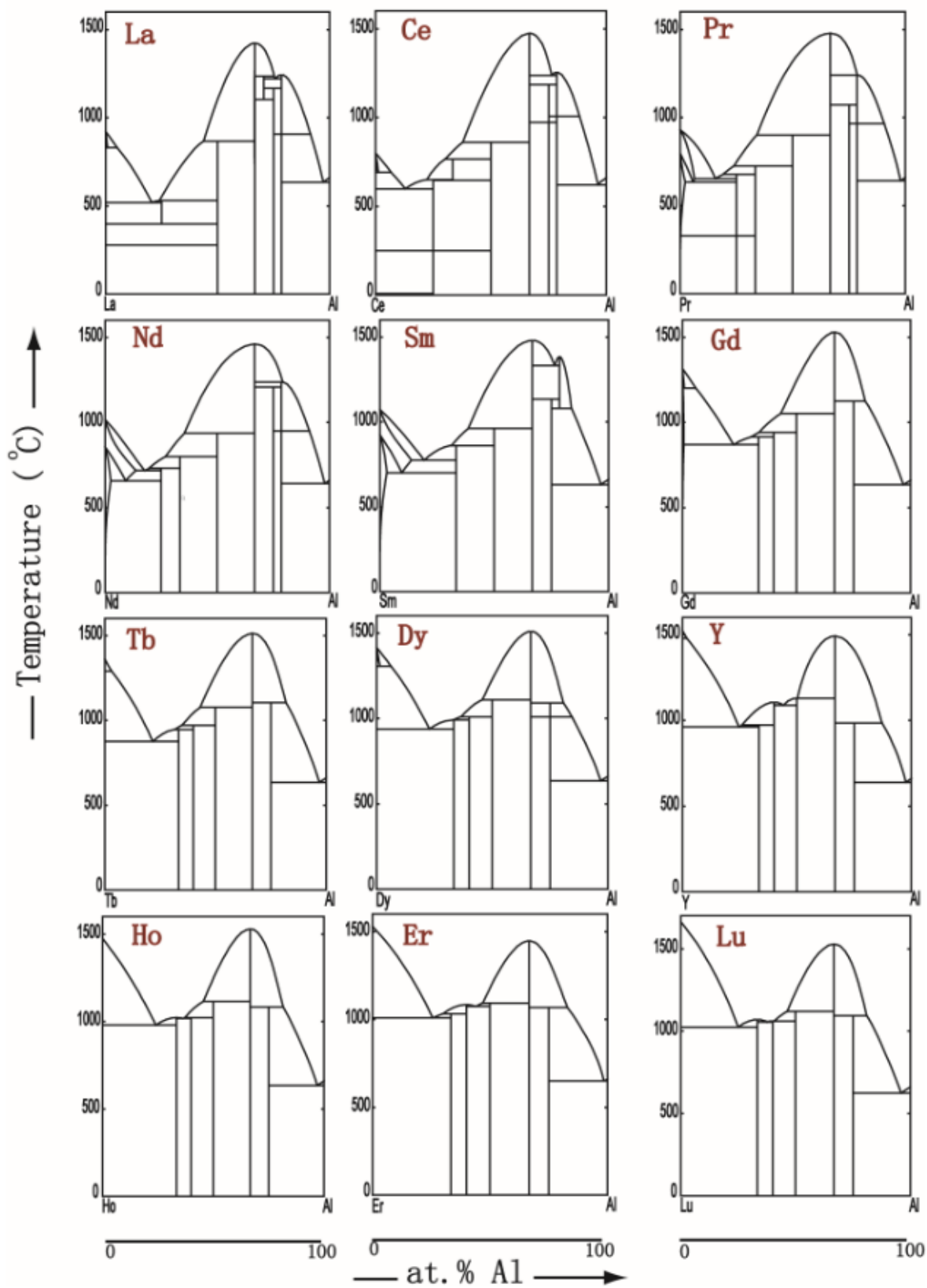
Figure 3.6 Similarities and trends in Al–RE phase diagrams
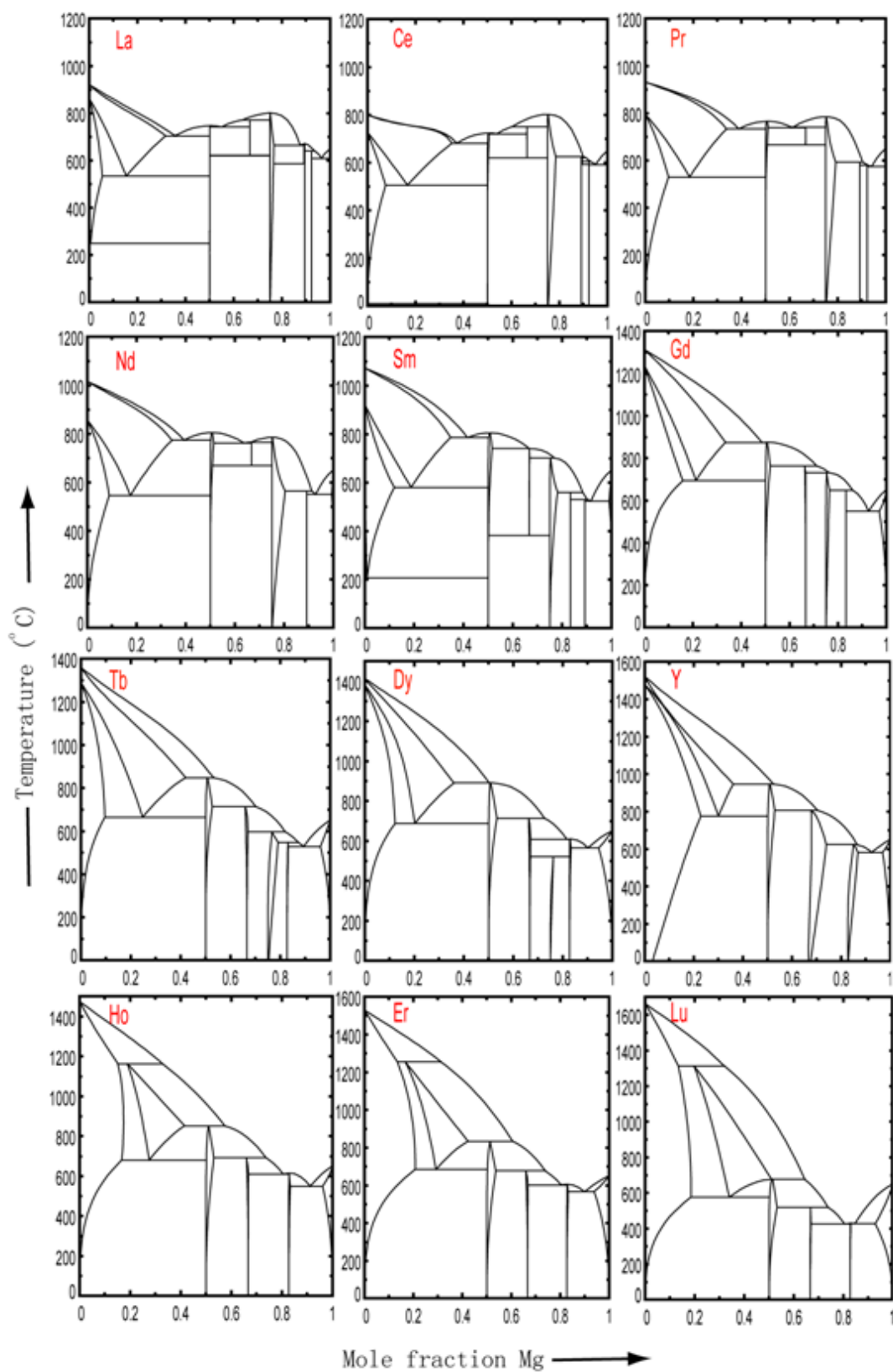
Figure 3.7 Similarities and trends in Mg–RE phase diagrams

The differences of enthalpies of formation at 298 K between the metastable phases $LaMg_3$, $CeMg_3$, $PrMg_3$, $NdMg_3$ and $SmMg_3$ in the Ni_3Sn-hP8 structure and the stable phases ($LaMg_3$, $CeMg_3$, $PrMg_3$, $NdMg_3$ and $SmMg_3$ in the BiF_3-cF16 structure) were taken from the results of ab-initio calculations by Tao [56; 57]. The entropies of formation at 298 K for these metastable phases are assumed to be the same as the ones calculated from their respective stable phases. The enthalpies of formation of metastable phases ($NdMg_{12\ (tI26)}$ and $SmMg_{12\ (tI26)}$) were extrapolated from the optimized values of $LaMg_{12\ (tI26)}$, $CeMg_{12\ (tI26)}$, $PrMg_{12\ (tI26)}$ stable phases, assuming the same linear relationship as that of the calculated enthalpy of formation of $LaMg_{12\ (tI26)}$, $CeMg_{12\ (tI26)}$, $PrMg_{12\ (tI26)}$, $NdMg_{12\ (tI26)}$ and $SmMg_{12\ (tI26)}$ phases from First-Principles with increasing atomic numbers of rare earth elements.

CHAPTER 4   **ORGNIZATION OF THE ARTICLES**

The results obtained in this work were presented in the following articles published or submitted to the journals. It was necessary to repeat model descriptions in each article.

The first article presented in Chapter 5 is entitled "Thermodynamic evaluation and optimization of Al–La, Al–Ce, Al–Pr, Al–Nd and Al–Sm systems using the Modified Quasichemical Model for liquids". It was published in the journal CALPHAD: Computer Coupling of Phase Diagrams and Thermochemistry (Jin et al., 2011). This article contains a thorough literature review and the thermodynamic optimizations of these five binary systems of Al–light rare earths (La, Ce, Pr, Nd and Sm). The optimization procedure was biased by putting strong emphasis on the observed trends in the thermodynamic properties of Al–RE phases. The systematic trends were shown for the enthalpies and entropies of mixing in the liquids and enthalpies and entropies of formation for the compounds. Optimized model parameters of the Gibbs energies for all phases, which reproduced satisfactorily all the reliable experimental data, have been obtained. The entropy of mixing in the liquid is better controlled and optimized systematically in the present study compared to the irregular entropy of mixing from independent optimizations of Al–RE systems in the litterature.

The second article presented in Chapter 6 is entitled "Thermodynamic evaluation and optimization of Al–Gd, Al–Tb, Al–Dy, Al–Ho and Al–Er systems using a Modified Quasichemical Model for the liquid". It was published in the journal of CALPHAD: Computer Coupling of Phase Diagrams and Thermochemistry (Jin et al., 2010). This article contains a literature review and the thermodynamic optimizations of these five binary systems of Al–heavy rare earths (Gd, Tb, Dy, Ho and Er). The same optimization technique was used as in chapter 4. The Modified Quasichemical Model, which takes short–range ordering into account, was used for the liquid phase and the Compound Energy Formalism was used for the solid solutions in the binary systems. It was shown that the Modified Quasichemical Model used for the liquid alloys

enables determination of entropies of mixing that are more reliable than those based on the Bragg – Williams random mixing model, which does not take short–range ordering into account.

The third article presented in Chapter 7 is entitled "Thermodynamic evaluations and optimizations of binary Mg–light Rare Earth (La, Ce, Pr, Nd, Sm) systems". It was published in the journal CALPHAD: Computer Coupling of Phase Diagrams and Thermochemistry (Kang et al., 2012). The solid solubility of RE (La, Ce, Pr, Nd and Sm) in Mg-HCP solutions were critically reviewed and optimized, as part of a complete thermodynamic re-optimization of the Mg–La, Mg–Ce, Mg–Nd, Mg–Pr and Mg–Sm systems combined with First-Principles and Miedema model. The experimental data of solid solubilities of RE in Mg–HCP from Rokhlin (Rokhlin, 1995) were preferred in the present study based on the combination of new solid solubility data for Mg–Nd system from Kopp using atom probe tomography (Kopp et al., 2011), the analysis of the solid solubility data on the $\ln x_{RE}^{HCP}$ versus $1/T$ relationship and the recent experimental enthalpy of formation data in the Mg–La system from Berche (Berche et al., 2010). It may be noteworthy that all the Mg–light Rare Earth binary systems show quite similar thermodynamic properties, and a similar behaviour is expected in the Mg–heavy rare earth binary systems too. It should be pointed out that the independent optimizations from Guo and Du (Guo & Du, 2004, 2005) for Mg–La and Mg–Pr systems, from Gorsse *et al.* (Gorsse et al., 2005) for Mg–Nd system, and from Jia *et al*. (Jia et al., 2008) seem not to have the similar entropies of mixing in the liquid. In the present study, the combination of systematic techniques, Miedema model, First-Principles, and the CALPHAD method would be helpful in developing Mg–Al–RE thermodynamic database, in particular when the experimental data of enthalpy of formation were either scarce or of unacceptable uncertainty.

The fourth article presented in Chapter 8 is entitled "Thermodynamic evaluation and optimizations of Al–Mg–RE (RE= La, Ce, Pr, Nd, Sm) systems coupled with equilibrated alloy experiments and Miedema's model", which was submitted to the Journal of Chemical Thermodynamics. The enthalpies of formation of the ternary compounds $Al_{40}Mg_{17}La_3$, $Al_{13}Mg_6Ce$, $Al_{50}Mg_{22}Pr_3$, and $Al_{50}Mg_{22}Nd_3$ were estimated by the Miedema model. Arc-melted key alloys were annealed at 673 K for four weeks and the phases were analyzed with electron

probe micro-analysis (EPMA). Optimized model parameters have been obtained for the Gibbs energy functions of all stable phases in the Al–Mg–RE (RE= La, Ce, Pr, Nd, Sm) systems.

Chapter 9 is entitled "Thermodynamic evaluation and optimizations of Al–Mg–RE (RE= Gd, Tb, Dy, Ho, Er) systems", which will be published in a future article. By using the Miedema model, the enthalpies of formation of the ternary compounds Al_4GdMg, Al_4TbMg, $Al_{10}Dy_2Mg_3$, $Al_{10}Ho_2Mg_3$ and $Al_{20}Er_3Mg_7$ were estimated. Systematical thermodynamic evaluations and optimizations of the Al–Mg–Sm, Al–Mg–Gd, Al–Mg–Dy, Al–Mg–Ho and Al–Mg–Er systems have been presented on the basis of literature information.

No ternary parameters were used for all the Al–Mg–RE ternary systems, which indicates that the Gibbs energy data sets of the binary phases were described accurately and that the extrapolation from the binary data produced a satisfactory agreement with the ternary experimental data. Ten ternary systems studied show similar characteristics.

Chapter 10 is a general discussion of present study. Some examples on the application of the resulting thermodynamic database are given.

Some physical properties of the rare earths from the literature are listed in Appendix 1. Appendix 2 is an article published in the Magnesium Conference, 2012 for the thermodynamic properties of Al–RE and Mg–RE systems; some industrial application examples are given. The thermodynamic properties and phase equilibria of RE'–RE" and Al–RE'–RE" (RE', RE" =La, Ce, Pr, and Nd) systems using the modified quasi-chemical model for the liquid, are presented in Appendix 3.

CHAPTER 5   ARTICLE 1: THERMODYNAMIC EVALUATION AND OPTIMIZATION OF AL–LA, AL–CE, AL–PR, AL–ND AND AL–SM SYSTEMS USING THE MODIFIED QUASICHEMICAL MODEL FOR LIQUIDS

Published in CALPHAD, 35(2011), 30-41.

Liling Jin [a], Youn-Bae Kang [a], Patrice Chartrand [a,*], and Carlton D. Fuerst [b]

[a] Center for Research in Computational Thermochemistry (CRCT), Dept. of Chemical Engineering, Ecole polytechnique de Montréal, Montréal, Québec, Canada

[b] General Motors, Warren, MI, USA

[*] Corresponding author. Centre de Recherche en Calcul Thermochimique (CRCT), École Polytechnique de Montréal, Montréal, QC, CANADA, H3C 3A7. Tel : +1 514 3404711 ext. 4089; fax : +1 514 3405840. E-mail address: Patrice.Chartrand @polymtl.ca

Abstract: The Al–La, Al–Ce, Al–Pr, Al–Nd and Al–Sm (Al–light rare earth) binary systems have been systematically assessed and optimized based on the available experimental data and ab–initio data using the FactSage thermodynamic software. Optimized model parameters of the Gibbs energies for all phases which reproduced all the reliable experimental data to satisfaction have been obtained. The optimization procedure was biased by putting a strong emphasis on the observed trends in the thermodynamic properties of Al–RE phases. The Modified Quasichemical Model, which takes short-range ordering into account, is used for the liquid phase and the Compound Energy Formalism is used for the solid solutions in the binary systems. It is shown that the Modified Quasichemical Model used for the liquid alloys permits us to obtain entropies of mixing that are more reliable than that based on the Bragg – Williams random mixing model which does not take short–range ordering into account.

Keywords: Aluminum – Rare Earth Alloys, Modified Quasichemical Model, Thermodynamic Modeling, Phase Diagram

5.1 Introduction

Adding rare earth metals (RE = Y, Sc, La, Ce, Pr, Nd, Pm, Sm, Eu, Gd, Tb, Dy, Ho, Er, Tm, Yb, and Lu) to aluminum and Al–transition metal alloys can result in increased mechanical properties of the materials, such as tensile strength, heat resistance, corrosion resistance, vibration resistance, and extrudability [1-3]. Moreover, Mg–based alloys with rare earth metals show several interesting applications in the automotive and aeronautical industries because of their low density and potentially high strength/weight ratios. Most commercial magnesium alloys are based on the Mg–Al system, with some additions of other alloying elements, such as Mn, Zn, Ca, and rare–earth metals, to reach certain application requirements [4]. It is an important task for alloy design to develop a better thermodynamic understanding of novel aluminum and magnesium alloy systems with additions of rare earth elements.

La, Ce, Pr and Nd are the main components of mischmetal, which is a mixture of rare earth elements. Rare earth elements form very stable intermetallic compounds with aluminum. Therefore, adding a little rare earth elements to magnesium alloys will have significant effects on the properties of alloys since Al–RE compounds are readily precipitated when Al is present.

Rare earth elements are often divided into two subgroups: the light rare earths (from La to Sm) and the heavy rare earths (from Gd to Lu, except Yb). It has been well known that rare earths show certain trends and similar regularities across the lanthanide series (from La to Lu all of which form trivalent rare earth ions upon oxidation, except Eu and Yb which form divalent ions upon oxidation). Such similarity and trends of the physical and chemical properties are shown in lanthanides with another common metal (like Ag [5], Al[6-8], Mg [8], In [9], Sn [10], Tl [11]) and non-metal (like lanthanide oxides [12], Lanthanide trihalides [13], Lanthanide carbides, Lanthanide silicides [14]). In the thermodynamic evaluation and modeling of Al–rare earth (RE) binary systems, this trend shown in Al–RE systems may give some hints when the experimental data is missing for some systems.

As part of ongoing projects in our laboratory to develop thermodynamic databases for multi-component Mg– and Al– based alloys, we have systematically assessed the binary Al–La, Al–Ce, Al–Pr, Al–Nd, Al–Sm, Al–Gd, Al–Tb, Al–Dy, Al–Ho, Al–Er, Al–Tm, and Al–Lu, Al–Y, and Al–Sc systems. The Al–Ce, Al–Y, and Al–Sc systems were previously optimized by Kang et al [15]. In the current paper, thermodynamic evaluation and modeling of the Al–La, Al–Ce, Al–Pr, Al–Nd, and Al–Sm (Al–light lanthanides) systems will be examined (Al–Ce system was reoptimized in order to keep consistency with other systems regarding thermodynamic parameters) while the Al–Gd, Al–Tb, Al–Dy, Al–Ho, and Al–Er systems (Al–heavy lanthanides) will be presented in a next paper. Thermodynamic predictions of Al–Tm and Al–Lu systems will be discussed in another paper together with the systematic study of thermodynamic properties and phase equilibria across the lanthanides, since there is little experimental data available for the Al–Tm and Al–Lu systems. Moreover, the trends of thermodynamic properties shown in Al–light rare earth systems are the same as those shown in Al–heavy rare earth systems.

5.2   Thermodynamic models and optimization strategies

All the present optimizations have been carried out by means of the FactSage thermodynamic software [16, 17]. The thermodynamic properties of pure Al and light rare earth (La, Ce, Pr, Nd and Sm) are taken from SGTE database [18], except the Pr and Sm in the FCC–structure, together with La, Pr, Nd and Sm in the HCP– structure taken from Kang et al. [19]. A list of all phases appeared in the five binary systems considered in present study is given in Table 5.1.

Table 5.1 Crystallographic structures of all phases in the Al–La, Al–Ce, Al–Pr, Al–Nd, and Al–Sm systems

Phases	Struktur-bericht	Prototype	Pearson Symbol	Space Group	Model	Stable end-members
liquid	-	-	-	-	MQM	
FCC	A1	Cu	cF4	$Fm\bar{3}m$	CEF	Al, La, Ce
BCC	A2	W	cI2	$Im\bar{3}m$	CEF	La, Ce, Pr, Nd,
HCP	A3	Mg	hP2	$P6_3/mmc$	CEF	Sm,
DHCP	A3´	αLa	hP4	$P6_3/mmc$	CEF	La,Ce,Pr,Nd
(αSm)	-	αSm	hR3	$R\bar{3}m$	CEF	Sm
Laves-C15	C15	Cu_2Mg	cF24	$Fd\bar{3}m$	CEF	Al_2La, Al_2Ce, Al_2Pr Al_2Nd, Al_2Sm
αLa_3Al_{11}	-	αLa_3Al_{11}	oI28	Immm	ST	
βLa_3Al_{11}	$D1_3$	Al_4Ba	tI10	I4/mmc	ST	
$D0_{19}$	$D0_{19}$	Ni_3Sn	hP8	$P6_3/mmc$	CEF	
$La_{22}Al_{53}$	-	AlB_2	hP3	-	ST	
LaAl	-	AlCe	oC16	Cmcm	ST	
αCe_3Al_{11}	-	αLa_3Al_{11}	oI28	Immm	ST	
βCe_3Al_{11}	$D1_3$	Al_4Ba	tI10	I4/mmc	ST	
$\alpha CeAl_3$	$D0_{19}$	Ni_3Sn	hP8	$P6_3/mmc$	ST	
$\beta CeAl_3$	-	-	-	-	ST	
CeAl	-	AlCe	oC16	Cmcm	ST	
Ce_2Al	-	-	-	-	ST	
αCe_3Al	$D0_{19}$	Ni_3Sn	hP8	$P6_3/mmc$	ST	
βCe_3Al	$L1_2$	$AuCu_3$	cP4	$Pm\bar{3}m$	ST	
αPr_3Al_{11}	-	αLa_3Al_{11}	oI28	Immm	ST	
βPr_3Al_{11}	$D1_3$	Al_4Ba	tI10	I4/mmc	ST	

αPr_3Al	$D0_{19}$	Ni_3Sn	hP8	$P6_3/mmc$	ST	
βPr_3Al	$L1_2$	$AuCu_3$	cP4	$Pm\bar{3}m$	ST	
Pr_2Al	C23	Co_2Si	oP12	Pnma	ST	
PrAl	---	ErAl	oP16	Pmma	ST	
$PrAl_3$	$D0_{19}$	Ni_3Sn	hP8	$P6_3/mmc$	ST	
αNd_3Al_{11}	-	αLa_3Al_{11}	oI28	Immm	ST	
βNd_3Al_{11}	$D1_3$	Al_4Ba	tI10	I4/mmc	ST	
$NdAl_3$	$D0_{19}$	Ni_3Sn	hP8	$P6_3/mmc$	ST	
NdAl	-	ErAl	oP16	Pmma	ST	
Nd_2Al	C23	Co_2Si	oP12	Pnma	ST	
Nd_3Al	$D0_{19}$	Ni_3Sn	hP8	$P6_3/mmc$	ST	
Sm_2Al	C23	Co_2Si	oP12	Pnma	ST	
SmAl	---	ErAl	oP16	Pmma	ST	
$SmAl_3$	$D0_{19}$	Ni_3Zn	hP8	$P6_3/mmc$	ST	
Sm_3Al_{11}	$D1_3$	Al_4Ba	tI10	I4/mmm	ST	

MQM = Modified Quasichemical Model, CEF = Compound Energy Formalism, ST =

5.2.1 Modified Quasichemical Model (MQM) for the liquid phase

The MQM in the pair approximation [20] was used to model the thermodynamic properties of the liquid solution in the present study. A detailed description of the MQM and its associated notation is given by Pelton et al. [20]. The same notation is used in the present article. The MQM has been successfully applied to alloy solutions [21, 22], molten oxides [23, 24], molten salts [25, 26], and molten sulphides [27]. A brief summary of this model is given below. The following pair exchange reaction between atoms A and B distributing over the sites of a quasilattice is considered in the MQM:

$$(A - A)_{pair} + (B - B)_{pair} = 2\ (A - B)_{pair}\ , \qquad \Delta g_{AB} \tag{5.1}$$

Where $(i-j)_{pair}$ represents a first-nearest-neighbor pair of atom. The Gibbs energy change for the formation of 1 mole of (A − B) pairs is $\Delta g_{AB}/2$. Let n_A and n_B be the number of moles of A and B, n_{AA}, n_{BB}, and n_{AB} be the number of moles of (A − A), (B − B), and (A − B) pairs. And Z_A and Z_B are the coordination numbers of A and B. The Gibbs energy of the solution is given by:

$$G = (n_A g^o_A + n_B g^o_B) - T\Delta S^{config} + (n_{AB}/2)\Delta g_{AB} , \tag{5.2}$$

where g^o_A and g^o_B are the molar Gibbs energies of the pure component A and B, and ΔS^{config} is the configurational entropy of mixing given by randomly distributing the (A − A), (B − B) and (A − B) pairs in the one − dimensional Ising approximation [20]:

$$\Delta S^{config} = -R\ (n_A \ln X_A + n_B \ln X_B) - R\ (n_{AA}\ln\frac{X_{AA}}{Y_A^2} + n_{BB}\ln\frac{X_{BB}}{Y_B^2} + n_{AB}\ln\frac{X_{AB}}{2Y_A Y_B}) \tag{5.3}$$

Where X_{AA}, X_{BB} and X_{AB} are pair fractions of (A − A), (B − B) and (A − B) pairs; Y_A, and Y_B are equivalent fractions of A and B:

$$X_{ij} = \frac{n_{ij}}{n_{AA}+n_{BB}+n_{AB}} \qquad (i, j\ = A\ or\ B) \tag{5.4}$$

$$Y_i = \frac{Z_i n_i}{Z_A n_A + Z_B n_B} \qquad (i = A\ or\ B) \tag{5.5}$$

Moreover, the following equation can be written:

$$Z_A n_A = 2n_{AA} + n_{AB} \tag{5.6}$$

$$Z_B n_B = 2n_{BB} + n_{AB} \tag{5.7}$$

It may be noted that there is no exact expression for the configurational entropy in three dimensions. Although Eq. (3) is only an approximate expression in three dimensions, it is exact one-dimensionally (when $Z = 2$) [20]. As explained in Pelton et al. [20], one is forced by the approximate nature of Eq. (3) to use nonphysical values of the coordination numbers in order to yield good fits between the experimental data and calculated ones. The mathematical approximation of one-dimensional Ising model of Eq. (3) can be partially compensated by selecting values of Z_A and Z_B which are smaller than the experimental values [15]. As is known, the MQM model is sensitive to the ratio of coordination numbers, but less sensitive to their absolute values. From practical standpoint for the development of large thermodynamic databases, values of Z_A and Z_B of the order of 6 have been found necessary for the solutions with a small or medium degree of ordering (*i.e.* alloy solutions). The MQM has been successfully applied in many alloy systems [15, 21, 22, 28-32].

Δg_{AB} is expanded in terms of the pair fractions X_{AA} and X_{BB}:

$$\Delta g_{AB} = \Delta g_{AB}^0 + \sum_{i \geq 1} g_{AB}^{i0} X_{AA}^i + \sum_{j \geq 1} g_{AB}^{0j} X_{BB}^j \,, \tag{5.8}$$

Where Δg_{AB}^0, g_{AB}^{i0}, g_{AB}^{0j} are the parameters of the model which can be functions of temperature. The equilibrium state of the system is obtained by minimizing the total Gibbs energy at constant composition, temperature and pressure. The equilibrium pair distribution is calculated by setting

$$\left(\frac{\partial G}{\partial n_{AB}}\right)_{n_A, n_B} = 0, \tag{5.9}$$

This gives the "equilibrium constant" for the "quasichemical pair reaction" of Eq. (1):

$$\frac{X_{AB}^2}{X_{AA}X_{BB}} = 4\exp\left(-\frac{\Delta G_{AB}}{RT}\right). \tag{5.10}$$

Moreover, the model permits Z_A and Z_B to vary with compositions as follows [20]:

$$\frac{1}{Z_A} = \frac{1}{Z_{AA}^A}\left(\frac{2n_{AA}}{2n_{AA}+n_{AB}}\right) + \frac{1}{Z_{AB}^A}\left(\frac{n_{AB}}{2n_{AA}+n_{AB}}\right) \tag{5.11}$$

$$\frac{1}{Z_B} = \frac{1}{Z_{BB}^B}\left(\frac{2n_{BB}}{2n_{BB}+n_{AB}}\right) + \frac{1}{Z_{BA}^B}\left(\frac{n_{AB}}{2n_{BB}+n_{AB}}\right), \tag{5.12}$$

Where Z_{AA}^A and Z_{AB}^A are the values of Z_A when all nearest neighbours of an A are As, and when all nearest neighbours of an A are Bs, and where Z_{BB}^B and Z_{BA}^B are defined similarly.

The composition of maximum short–range ordering (SRO) is determined by the ratio of the coordination numbers Z_{AB}^A / Z_{AB}^B. The values of the coordination numbers chosen in the present study are listed in Table 5.2, and the same values of the coordination numbers are chosen for the Al–heavy rare earth systems.

Table 5.2 Optimized model parameters of the MQM for the liquid in Al–La, Al–Ce, Al–Pr, Al–Nd and Al–Sm phases with the format of $\Delta g_{AlRE} = (a_{00} + b_{00}T) + (a_{10} + b_{10}T)X_{AlAl} + (a_{01})X_{RERE}$.

Coordination numbers				Gibbs energies of pair exchange reactions
i	j	Z_{ij}^i	Z_{ij}^j	
Al	La	3	6	Δg_{AlLa}= -48,116 +4.60T + (-11,088 -1.674T)X_{AlAl} -15,732X_{LaLa}
Al	Ce	3	6	Δg_{AlCe}= -46,024 +5.65T + (-17,364 -1.13T)X_{AlAl} -10,460X_{CeCe}
Al	Pr	3	6	Δg_{AlPr}= -40,587 +4.87T + (-13,809 -5.65T)X_{AlAl} -17,398X_{PrPr}
Al	Nd	3	6	Δg_{AlNd}= -39,622 +5.40T + (-12,970 -4.00T)X_{AlAl} -18,828X_{NdNd}
Al	Sm	3	6	Δg_{AlSm}= -44,267 +5.65T + (-8,786 -3.77T)X_{AlAl} -16,318X_{SmSm}

5.2.2 Compound Energy Formalism for solid solutions

The compound energy formalism was introduced by Hillert [33] to describe the Gibbs energy of solid phases with sub–lattices. Ideal mixing on each sub–lattice is assumed. The same notation for the model parameters is used as those in Kang et al. [15].

5.2.3 Optimization Strategies

Unlike the previous optimizations of Al–light rare earth systems [15, 34-39], all of which used the Bragg–Williams random mixing approximation for the liquid except one using MQM by the co-authors [15] and one using associate model by Zhou and Napolitano [36], all the present optimizations have been carried out by employing the MQM for the liquid to take into account the high degree of short–range ordering which is evidenced by the very negative enthalpy of mixing curve in the liquid for all the Al–RE binary systems.

Based on the similarities mentioned above for the Al–RE systems, thermodynamic evaluations and systematic optimizations were performed in the present study for Al–La, Al–Pr, Al–Nd, and Al–Sm systems. Moreover, Al–Ce system was re-optimized in order to keep consistency with other Al–RE systems.

In order to account for the short–range ordering (SRO) around the composition $X_{RE} = 1/3$, the coordination numbers Z_{Al} and Z_{RE} are calculated using the following functions (13) and (14):

$$\frac{1}{Z_{Al}} = \frac{1}{6}(\frac{2n_{AlAl}}{2n_{AlAl}+n_{AlRE}}) + \frac{1}{3}(\frac{n_{AlRE}}{2n_{AlAl}+n_{AlRE}}) \tag{5.13}$$

$$\frac{1}{Z_{RE}} = \frac{1}{6}(\frac{2n_{RERE}}{2n_{RERE}+n_{AlRE}}) + \frac{1}{6}(\frac{n_{AlRE}}{2n_{RERE}+n_{AlRE}}) \ . \tag{5.14}$$

Furthermore, for the pair exchange reaction in the Al–RE systems

$$(Al - Al)_{pair} + (RE - RE)_{pair} = 2 \ (Al - RE)_{pair} \ , \qquad \Delta g_{AlRE} \qquad\qquad (5.15)$$

Δg_{AlRE} is constrained to the following expression (16):

$$\Delta g_{AlRE} = (a_{00} + b_{00}T) + (a_{10} + b_{10}T)X_{AlAl} + (a_{01})X_{RERE} \ , \qquad\qquad (5.16)$$

where a_{00}, b_{00}, a_{10}, b_{10} and a_{01} were optimized parameters which are independent of temperature and composition. The optimized values for a_{00} are in the range of -40 ~ -48 (-44 ~ -48 for Al–heavy rare earth systems); the optimized values for b_{00} are in the range of 4.60 ~ 5.65 (4.20 ~ 5.50 for Al–heavy rare earth systems from [40]); the optimized values for a_{10} are in the range of -9 ~ -17 (0 ~ -5 for Al–heavy rare earth systems from [40]); the optimized values for b_{10} are in the range of -1.13 ~ -5.65 (-1.67 ~ -2.09 for Al–heavy rare earth systems from [40]), and the optimized values for a_{01} are in the range of -10 ~ -17 (-7 ~ -14.5 for the Al–heavy rare earth systems from [40]). All the parameters for Δg_{AlRE} in each binary liquid alloy are given in Table 5.2. The same optimization strategy is used for the Al–heavy RE systems (Al–Gd, Al–Tb, Al–Dy, Al–Ho, and Al–Er systems) [40], and similar trends are obtained.

5.3 Thermodynamic assessment of binary systems

5.3.1 The Al–La system

The thermodynamic assessment of Al–La system is based on the experimental investigations of Buschow et al. [41], Saccone et al. [42] on the La–rich part, and Kononenko and Golubev [43] on Al–rich region. This system has been

thermodynamically optimized by Yin et al. [34], Cacciamani et al. [35] and Zhou et al. [44]. According to the compilation by Gschneidner et al. [45] and Okamoto [46, 47], there are five intermetallic compounds, and one of them, La_3Al_{11}, has two allotropic forms (αLa_3Al_{11}, βLa_3Al_{11}, $LaAl_3$, $LaAl_X$, $LaAl$, and La_3Al), $LaAl_X$ was previously reported as $La_{22}Al_{53}$ which was accepted in this paper. $LaAl_2$ is considered as a Laves–C15 phase. The stability range of the La_3Al phase is controversial. Kober et al. [48] observed seven plateaus in the potential-time curve by using the concentration cell $Al(La)/KCl–LiCl + 5$ wt %$LaCl_3$ /La–Bi in the temperature range of 400-600 ℃. It was pointed out that these seven plateaus corresponded to the potentials of La, Al, and 5 intermetallic compounds (La_3Al, $LaAl$, $LaAl_2$, $LaAl_3$ and $LaAl_4$). Unfortunately, their investigation did not give any indication or confirmation that the $AlLa_3$ is stable all way to zero temperature. Sommer et al. [49] indicated $AlLa_3$ is a stable phase up to room temperature by preparing $AlLa_3$ sample for the drop calorimeter measurement. According to their investigation, the chemical compositions of the intermetallic phases ($Al_{11}La_3$, Al_2La and $AlLa_3$) after preparation and subsequent heat treatment were confirmed by X–ray fluorescence analysis. However, the detailed preparation process of samples and heat treatment were not given. Later on, Saccone et al. [42] studied the La–rich region of the La–Al system by usig DTA, metallographic analysis, EPMA, and XRD. It was observed that the samples in which the $AlLa_3$ phase was formed, subjected to annealing at 400 ℃ for 7 days and then quenched, showed the complete eutectoid decomposition of the phase into La and LaAl. It was evidenced by the microstructure analysis for the complete decomposition of the La_3Al phase. Furthermore, the temperature range of the compound $AlLa_3$ was suggested to be about 400-520 ℃. Subsequently, Borzone et al. [50] measured the standard molar enthalpies of formation for the different La–Al alloys by means of direct calorimetry. The heats of formation were reported for the LaAl, $LaAl_2$, $LaAl_3$, and La_3Al_{11} intermetallic compounds (no La_3Al compound), and several La-Al alloys including the alloy composition of 25 at. % Al. It was demonstrated by their optical micrograph that it was difficult to reach equilibrium state in calorimetric samples up to 32 at. % Al, which suggested indirectly that La_3Al phase reported in Sommer et al. [49] was probably a metastable phase at room temperature. As a matter of fact, it was mentioned that La_3Al was only stable in the temperature range of about 400–520 ℃ in the discussion

part of Borzone et al. [50]. Zhou and Napolitano [44] performed First-Principles calculations on $LaAl_2$ (prototype Cu_2Mg), $LaAl_3$ (prototype Ni_3Sn), La_3Al (prototype Ni_3Sn) and $LaAl_4$ (prototype Al_4Ba) compounds. The stability for the La_3Al–$D0_{19}$ phase was extended to 0 K according to their First-Principles results (see Figure 5.4), which were greatly differed from the results of Cacciamani et al. [35]. Since the stability of La_3Al–$D0_{19}$ phase is controversial, it is preferred that La_3Al–$D0_{19}$ phase is stable in the temperature range of about 400-520 ℃ in the present study, which is evidenced by the recent experimental work from Saccone et al. [42, 50]. It is noted that La_3Al–$D0_{19}$ phase and $LaAl_3$–$D0_{19}$ phase have the same structure, and are treated as a solid solution $D0_{19}$ phase. All the phases considered for this system are shown in Table 5.1.

The previous thermodynamic optimizations [34, 35] employing Bragg–Williams (BW) random mixing of atoms in the liquid solution reproduced the phase diagram quite well. The partial enthalpies of mixing measured by Lee and Sommer [51] and Sommer et al. [49] in the liquid were well reproduced by the BW models [34, 35], as shown in Figure 5.1. However, the shape of the partial enthalpies of mixing curve reproduced by BW models did not reflect the strong short–range ordering around the composition $X_{RE} = 1/3$, which is one of the common thermodynamic characteristics in Al–light rare earth systems. The calculated curve for the enthalpy of mixing of the liquid at 1200 K is compared with experimental data [49, 52, 53] and other calculations using BW model shown in Figure 5.2. It may be noted that the enthalpy of mixing measured by Kononenko [52] using a Knudsen effusion method, and the partial enthalpy of mixing of La in aluminum–rich liquid measured by Lebedev et al [54] were inconsistent with other data measured by calorimetry. As discussed by Pelton and Kang [55], the use of the MQM for the liquid phase render better estimations of the thermodynamic properties in the multi–component systems.
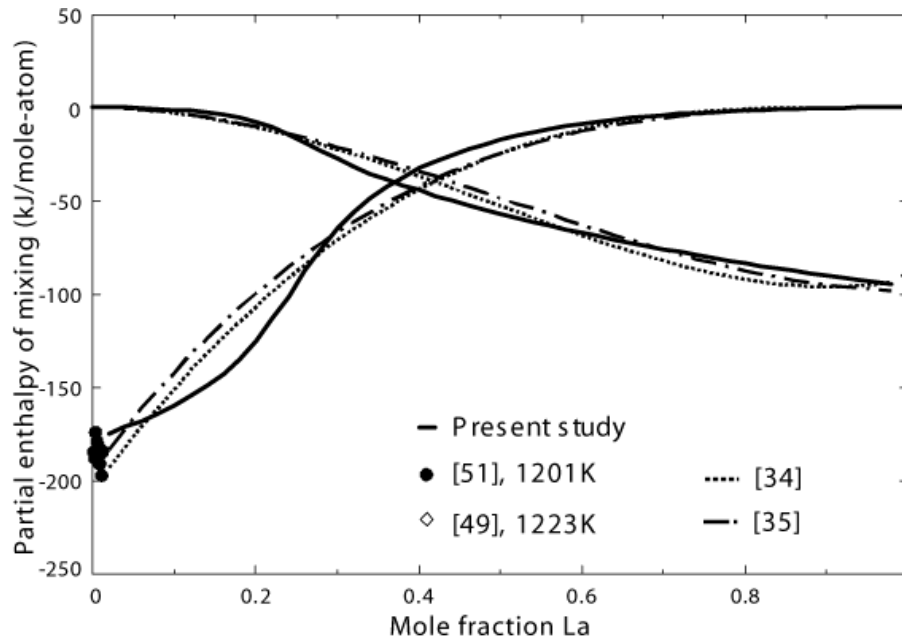
Figure 5.1 Calculated partial enthalpies of mixing of Al and La in liquid Al–La alloy at 1200 K. Comparison of experimental data from [49, 51] with calculations from present study and from [34, 35]'s sets of parameters.
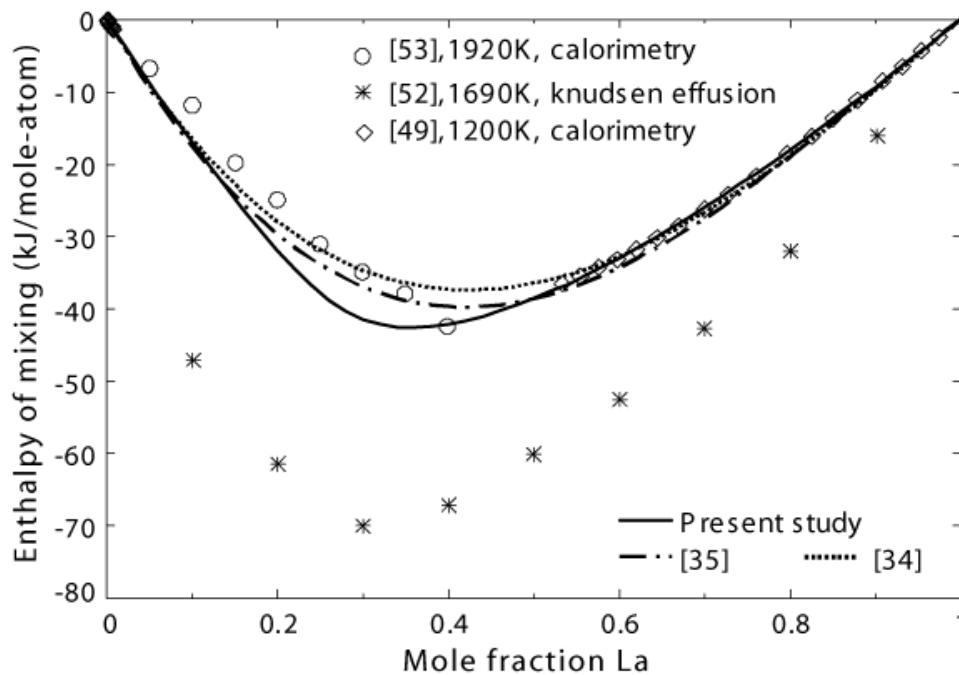
Figure 5.2 Calculated enthalpy of mixing of Al and La in liquid Al–La alloy at 1200 K. Comparison of experimental data [49, 52, 53] and calculations from present study and from [34, 35].

The calculated curve for the entropy of mixing in liquid Al–La alloys at 1873 K is presented in Figure 5.3 showing a minimum value near $X_{La} = 1/3$ and compared with the calculation from [34, 35]. The calculated entropy of mixing in the present study seems to be more reasonable than one calculated from Cacciamani et al.'s [35] set of parameters, as their minimum value is lower than -14 J/mol-K. The entropy of mixing calculated from Yin et al.'s [34] set of parameters has a much more reasonable value than the one calculated from Cacciamani et al.'s [35] set of parameters, but suffers from a minimum value at a composition rich in La, where there is no evidence that SRO occurs.

Figure 5.3 Calculated entropy of mixing of Al and La in liquid Al–La alloy at 1873 K. Comparison of calculation from present study with the ones calculated from [34, 35] 's sets of parameters.

The calculated enthalpy of formation for the stable intermetallic compounds in the Al–La system at 298 K is shown in Figure 5.4, as compared with experimental data and ab-initio data [44, 48-50, 56, 57]. The enthalpy of formation of Kober et al. [48] is derived from their electromotive force (e. m. f) measurements and is inconsistent with other calorimetrical data [49, 50, 56, 57].
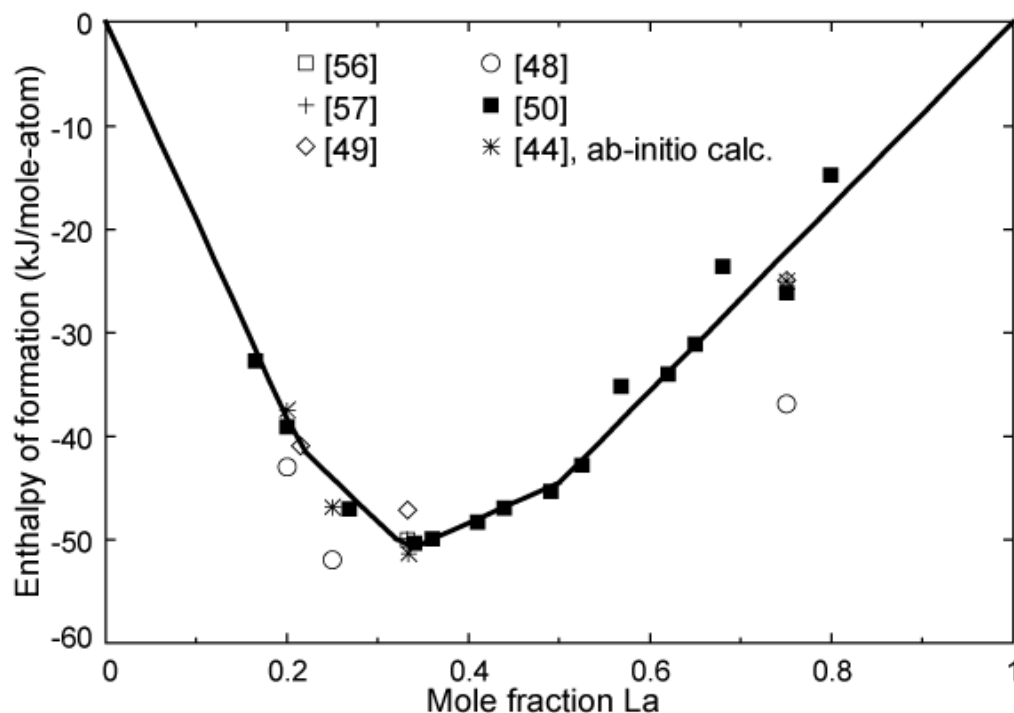
Figure 5.4 Calculated enthalpy of formation for the stable intermetallic compounds in the Al–La system at 298 K. Present calculation compared to the experimental data from [44, 48-50, 56, 57].

The calculated phase diagram of the Al–La system shown in Figure 5.5 is compared with the experimental data [41-43, 58]. The solubility of La in Al–FCC phase was reported to be 0.002 at.% at 873 K and 0.006 at.% at 893 K by Drits et al. [58] who employed microstructure examination, hardness and electrical resistivity measurement. The solubility of La in Al–FCC phase was not detected by X–ray method performed by Buschow [41]. The peritectic formation of La₃Al was also reported by Buschow [41], while a peritectoidic formation of this intermetallic compound was found by Saccone et al [42]. Since the experimental investigation in La–rich region is difficult due to the chemical reactivity of the La rare earth element, it was considered not necessary to use complex thermodynamic functions to fit the disputable experimental data. The calculated non–stoichiometry of the LaAl₂ Laves–C15 phase is negligible. The optimized model parameters of the present study are shown in Tables 5.2-5.4.
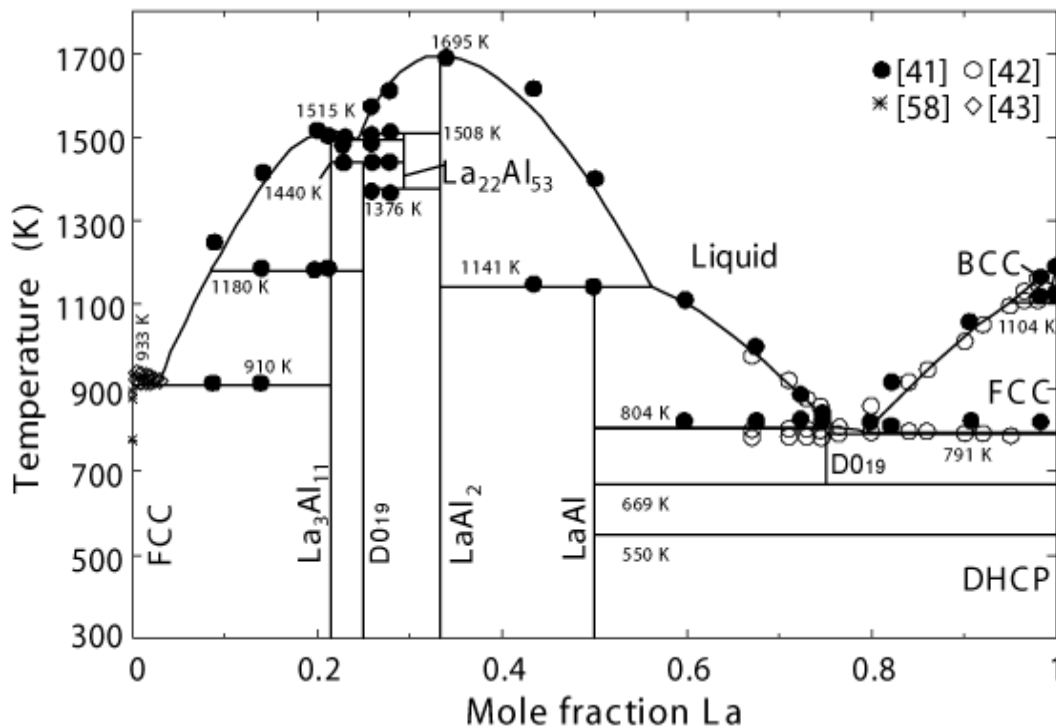
Figure 5.5 Calculated phase diagram of the Al–La system compared to the experimental data from [41-43, 58].

Table 5.3 Optimized CEF model parameters of solid solutions for the Al-La, Al-Ce, Al-Pr, Al-Nd and Al-Sm binary systems.

Laves-C15 (Cu₂Mg type): (Al, La, Ce, Pr, Nd, Sm)₂[Al, La, Ce, Pr, Nd, Sm]	
$G_{Al:Al}$ = 3**GHSERAL** + 41,840	$G_{Al:La}$ = 2**GHSERAL** + **GHSERLA** − 153,000 + 4.2T
$G_{La:La}$ = 3**GHSERLA** + 62,760	$G_{Al:Ce}$ = 2**GHSERAL** + **GHSERCE** − 153,000 + 8.1T
$G_{Ce:Ce}$ = 3**GHSERCE** + 62,760	$G_{Al:Pr}$ = 2**GHSERAL** + **GHSERPR** − 161,900 + 16.24T
$G_{Pr:Pr}$ = 3**GHSERPR** + 62,760	$G_{Al:Nd}$ = 2**GHSERAL** + **GHSERND** − 164,700 + 22.18T
$G_{Nd:Nd}$ = 3**GHSERND** + 62,760	$G_{Al:Sm}$ = 2**GHSERAL** + **GHSERSM** − 165,000 + 18.2T
$G_{Sm:Sm}$ = 3**GHSERSM** + 62,760	$G_{Pr:Al}$ = 2**GHSERPR** + **GHSERAL** + 41,840
$G_{La:Al}$ = 2**GHSERLA** + **GHSERAL** + 41,840	$G_{Nd:Al}$ = 2**GHSERND** + **GHSERAL** + 41,840
$G_{Ce:Al}$ = 2**GHSERCE** + **GHSERAL** + 41,840	$G_{Sm:Al}$ = 2**GHSERSM** + **GHSERAL** + 41,840

FCC: (Al, La, Ce, Pr, Nd, Sm)	
G(Pr, FCC) = **GHSERPR** + 900 − 0.5439T *	G(Sm, FCC) = **GHSERSM** + 1,500 *
HCP: (Al, La, Pr, Nd, Sm)	
G(La, HCP) = **GHSERLA** + 2,500	G(Sm, HCP) = **GHSERSM** + 2,900 *
G(Pr, HCP) = **GHSERPR** + 2,800 *	G(Nd, HCP) = **GHSERND** + 2,500 *
L(Al, Sm) = -66,944	
BCC: (Al, La, Ce, Pr, Nd, Sm)	
L(Al, La) = -76,149	L(Al, Nd) = -113,805 − 41,840 (X_{Al}-X_{Nd})
L(Al, Ce) = -67,362	L(Al, Sm) = -116,315 − 41,840 (X_{Al}-X_{Sm})
L(Al, Pr) = -77,822	
DHCP: (Al, Pr, Nd)	
L(Al, Pr) = -64,852	L(Al, Nd) = -65,689
D0$_{19}$: (Al, La)$_3$[Al, La]	
$G_{La:La}$= 4**GHSERLA** + 4,184	$G_{Al:La}$ =3**GHSERAL** + **GHSERLA** − 176,552 + 3.54T
$G_{Al:Al}$ = 4**GHSERAL** + 21,924-7.2T	$G_{La:Al}$ =3**GHSERLA** + **GHSERAL** − 77,300 − 12T
L(La : Al, La) = 28,870	

*from Kang *et al*. [19]

Table 5.4 Optimized model parameters of stoichiometric compounds in the Al–La, Al–Ce, Al–Pr, Al–Nd and Al–Sm binary systems.

Compound	ΔH°_{298K} (J/mol)	S°_{298K} (J/mol-K)	ΔS°_{298K} (J/mole-atom-K)
αLa$_3$Al$_{11}$	-575000	473.41	-0.61
βLa$_3$Al$_{11}$ *	-574000	474.26	-0.55
La$_{22}$Al$_{53}$ *	-3510000	2714.62	-0.50
LaAl	-89000	79.51	-2.85
αCe$_3$Al$_{11}$	-610000	480.61	-2.79
βCe$_3$Al$_{11}$ *	-600000	488.43	-2.23
αCeAl$_3$	-184800	142.29	-3.02
βCeAl$_3$ *	-183800	143.09	-2.82

CeAl	-91880	84.84	-6.46
Ce$_2$Al *	-67500	183.58	5.46
αCe$_3$Al	-101800	216.8	-4.97
βCe$_3$Al *	-99800	220.62	-4.01
αPr$_3$Al$_{11}$	-614974	474.05	-4.22
βPr$_3$Al$_{11}$ *	-613974	474.86	-4.16
αPr$_3$Al	-102000	231.19	-4.73
βPr$_3$Al *	-101000	232.85	-4.31
Pr$_2$Al	-97500	161.06	-5.03
PrAl	-93500	87.71	-7.26
PrAl$_3$	-187760	140.54	-4.57
αNd$_3$Al$_{11}$	-575000	471.07	-3.82
βNd$_3$Al$_{11}$ *	-574000	471.89	-3.76
NdAl$_3$	-181100	136.30	-4.92
NdAl	-95000	82.40	-8.49
Nd$_2$Al	-991600	154.30	-5.39
Nd$_3$Al	-98660	227.66	-3.47
Sm$_2$Al	-103000	152.13	-5.05
SmAl	97000	81.80	-7.90
SmAl$_3$	-197000	124.50	-8.58
Sm$_3$Al$_{11}$ *	-334800	635.20	8.43

Note : * High-temperature stable compounds

5.3.2   The Al–Pr system

The Al–Pr system has mainly been investigated by Kober et al. [59] using emf method, by Canneri [60] with thermal analysis, by Buschow et al. [6, 61] using thermal analysis, X–ray diffraction techniques, and metallography, and by Saccone et al. [42] on the Pr–rich side. This system has been thermodynamically optimized by Yin et al. [62]. According to the review of Okamoto [63], there are five intermetallic compounds, while

Pr_3Al_{11}, PrAl and Pr_3Al have two allotropes (αPr_3Al_{11}, βPr_3Al_{11}, $PrAl_3$, $\alpha PrAl$, $\beta PrAl$, Pr_2Al, and αPr_3Al, βPr_3Al). In the present study, the phase transformation between $\alpha PrAl$ and $\beta PrAl$ was not considered due to insufficient experimental data. $PrAl_2$ is considered as a Laves–C15 phase. All phases considered for this system are presented in Table 5.1. The enthalpy of mixing for the liquid was measured at 1250 K and 1550 K by Zviadadze et al. [64] using high temperature calorimetry. Like the Al–La system, the Al–Pr system exhibits very stable intermetallic compounds, one of which is Al_2Pr with highest melting temperature of 1751 K. From similarities with other Al–RE systems, the same modelling strategy was used with similar model parameters for the liquid Al–Pr alloy and the same maximum SRO composition around $X_{Pr} = 1/3$. The calculated enthalpy of mixing in the Al–Pr liquid at 1550 K is shown in Figure 5.6 with the experimental data [64], compared with the calculation of Yin et al. [62].
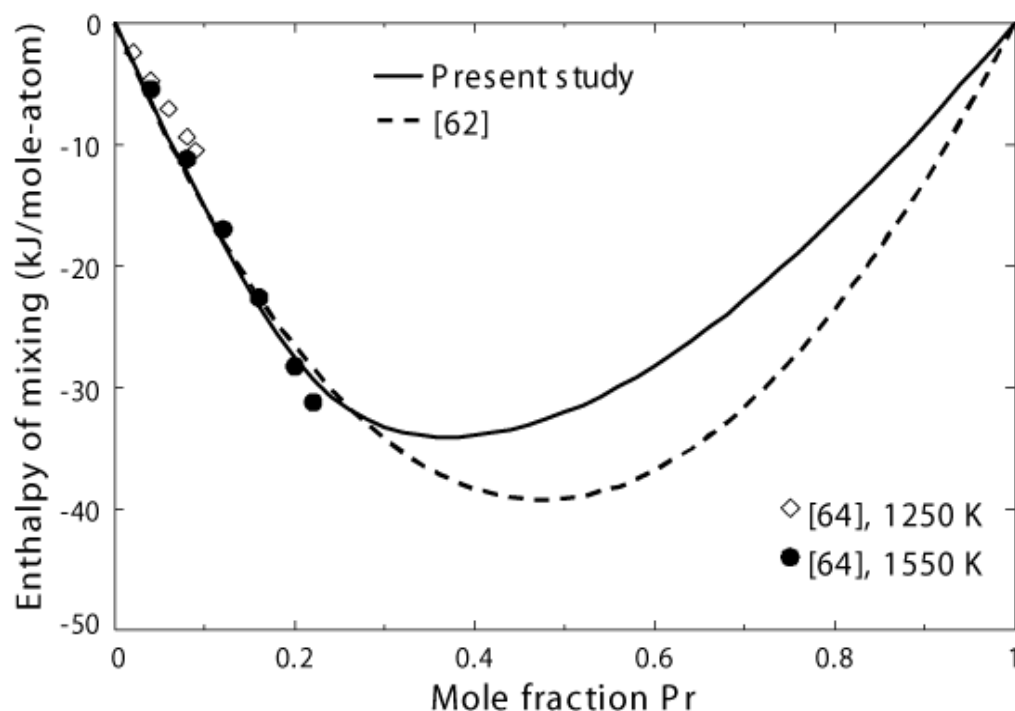
Figure 5.6 Calculated enthalpy of mixing of Al and Pr in the liquid Al–Pr alloy at 1550 K Comparison of experimental data [64] with calculations from present study and from [62].

The calculated curve for the entropy of mixing of the liquid at 1873 K in the present study is shown in Figure 5.7 with the minimum value near $X_{Pr} = 1/3$. The calculated

entropy of mixing in the present study seems to be more reasonable than the one calculated from Yin et al.'s [62] set of parameters, as their minimum value is lower than -12 J/mol-K.
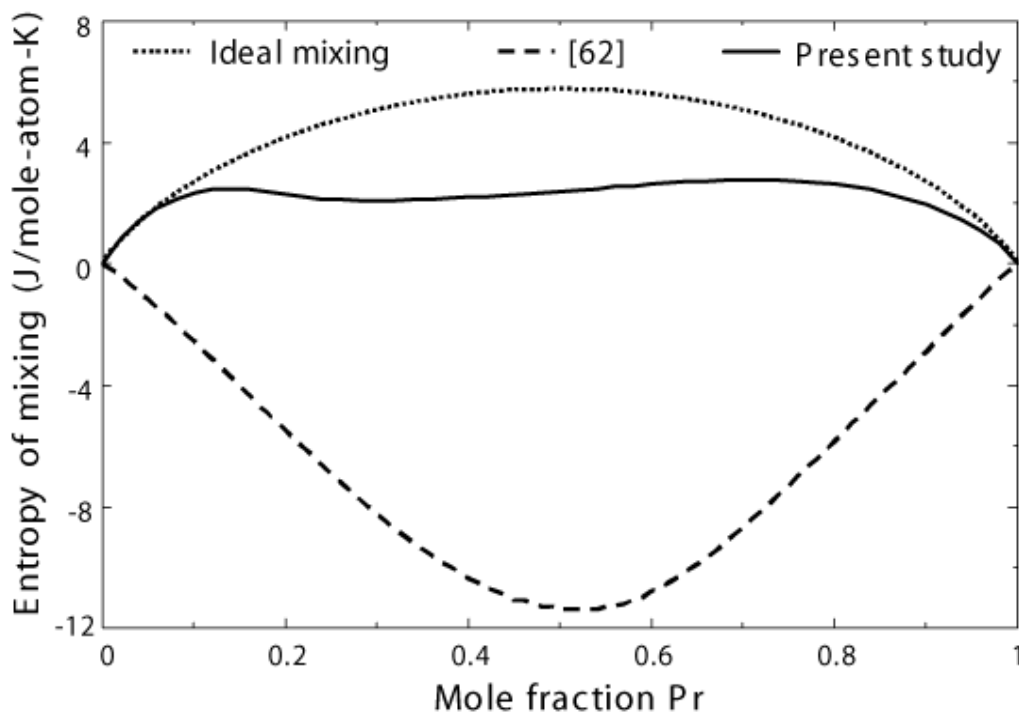
Figure 5.7 Calculated entropy of mixing of Al and Pr in the liquid Al–Pr alloy at 1873 K. Comparison of calculations from present study with the one calculated from [62]'s set of parameters.

The calculated enthalpy of formation for the stable intermetallic compounds at 298 K is shown in Figure 5.8, compared with the experimental data and ab–initio theoretical data [60, 65-67]. It can be seen from Figure 5.8 that the ab–initio data is likely more positive than the experimental data, but the trends are usually well predicted.
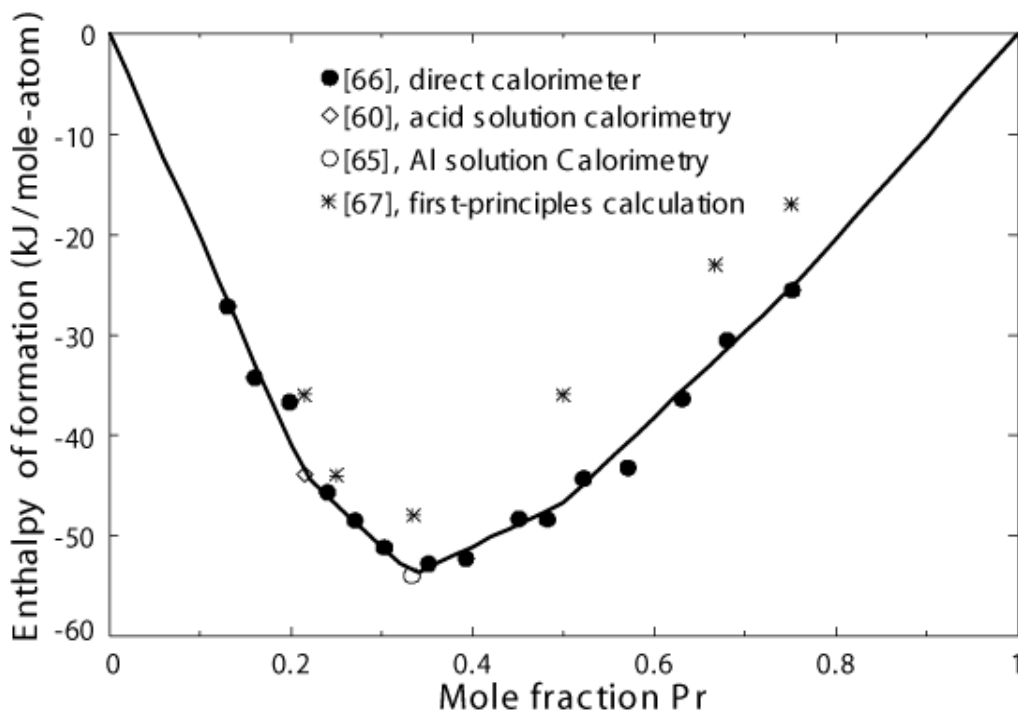
Figure 5.8 Calculated enthalpy of formation for the stable intermetallic compounds in the Al–Pr system at 298 K. Present calculation compared to the experimental data and ab–initio theoretical data from [60, 65-67].

The calculated phase diagram of the Al–Pr system shown in Figure 5.9 is compared with the experimental data [42, 58, 61]. The solubility of Pr in Al was reported to be 0.004 at.% at 873 K and 0.008 at.% at 893 K by Drits et al. [58] who employed microstructure examination and micro–hardness and electrical resistivity measurement, while it was reported to be insignificant according to Rolla et al. [68]. The peritectic formation of Pr_3Al was confirmed by Saccone et al. [42], although it was previously suggested by Buschow and Van Vucht [61] to be a peritectoid formation for this compound at 903 K. The allotropic transformation of the Pr_3Al intermetallic compound was also confirmed by Saccone et al. [42], with the transformation temperature around 603 K. The solubility of Pr in Al–FCC phase is small, while there is an extensive solid solubility of Al in Pr–BCC phase, as shown in Figure 5.9. The calculated non–stoichiometry of the $PrAl_2$ Laves–C15 phase is negligible. The optimized model parameters are presented in Tables 5.2-5.4.
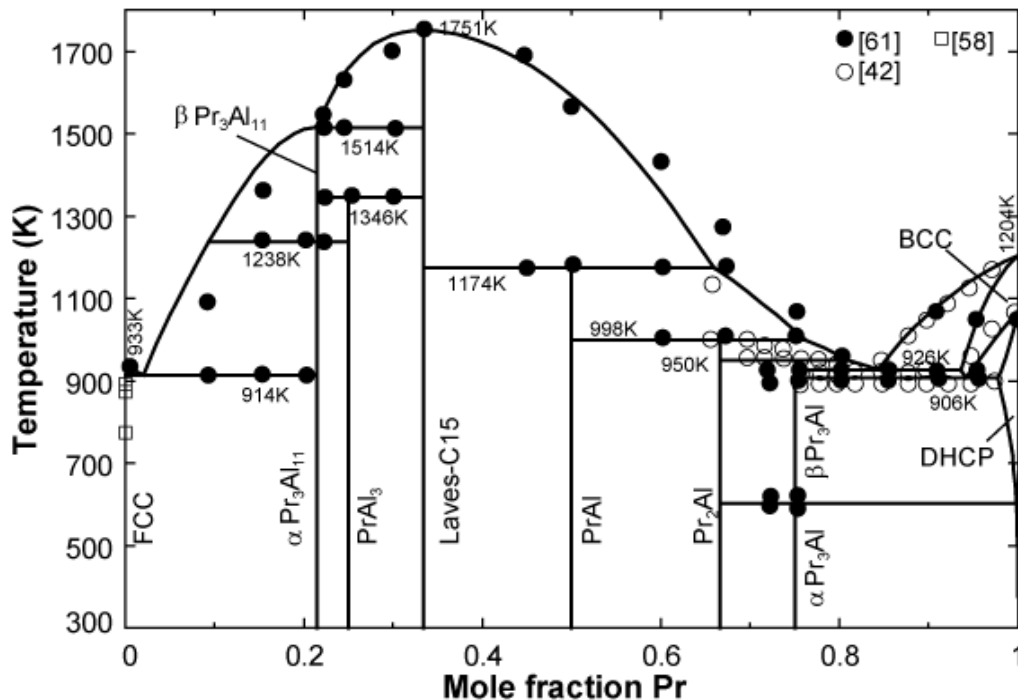
Figure 5.9 Calculated phase diagram of the Al–Pr system compared to the experimental data from [42, 58, 61].

5.3.3 The Al–Nd system

The Al–Nd system was investigated by many researchers. Buschow [69] investigated the phase diagram in the whole composition range; Gschneidner and Calderwood [70] reported eutectic reaction between αNd_3Al_{11} and aluminium at 913 K, whereas later Kononenko and Golubev [43] examined the Al–rich region up to 6 at. % Nd and suggested the eutectic compostion of 2.5% Nd at 905 K; Kale et al. [71] proposed the solubility of Nd in Al to be 2.12 at. %Nd, while Drits et al. [58] reported a small solubility of Nd in Al; Saccone et al. [42] studied the Nd–rich side up to 30 at% Al. Although Savitskii et al. [72] investigated in the composition range of 57 to 100 at. % Al, it is not considered in the present work due to a noticeable discrepancy from other experimental data [69]. This system was thermodynamically optimized by Wang [38], Clavaguera and Du [37], and Cacciamani and Ferro [35]. Later, the Al–Nd system was reassessed by Gao *et al.* [39] who showed that there are five intermetallic compounds

(αNd$_3$Al$_{11}$, βNd$_3$Al$_{11}$ or NdAl$_4$, NdAl$_3$, NdAl, Nd$_2$Al, and Nd$_3$Al) in the system by their own experiment. Nd$_3$Al$_{11}$ phase transformation is considered in the present work. NdAl$_2$ is considered as a Laves–C15 phase. All phases of this system are shown in Table 5.1.

The enthalpy of mixing for the liquid at 1250 K and 1550 K were measured by Zviadadze et al. [64] using high temperature calorimetry. Like the Al–La and Al–Pr system, the system exhibits very stable intermetallic compounds, one of which is Al$_2$Nd with highest melting temperature of 1733 K. It was used the same modelling strategy with similar model parameters for the liquid Al–Nd alloy and the same maximum SRO composition around X_{Nd} = 1/3. The calculated enthalpy of mixing is shown in Figure 5.10, as compared with the experimental data [64] and previous optimizations [35, 37]. The calculated curve for the entropy of mixing of the liquid is presented in Figure 5.11 showing the minimum value near X_{Nd} = 1/3 due to the short range ordering around this composition. The calculated entropy of mixing in the present study seems to be more reasonable than the ones calculated from Clavaguera and Du 's [37] and Cacciamani and Ferro 's [35] set of parameters, as both of their minimum values are lower than -10 J/mol-K.
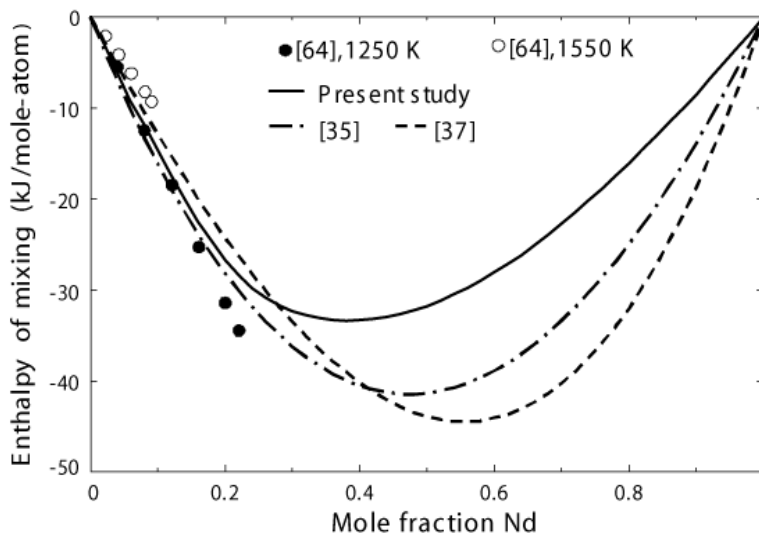
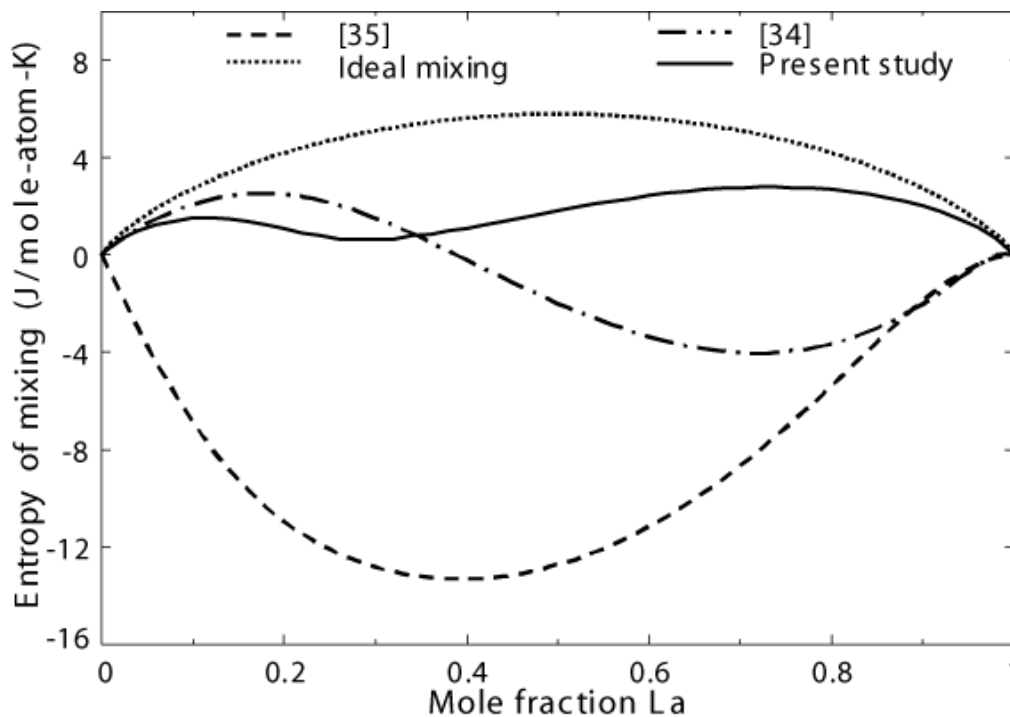
Figure 5.10 Calculated enthalpies of mixing of Al and Nd in liquid Al–Nd alloy at 1250 K. Comparison of experimental data [64] with calculations from present study and from [35, 37].
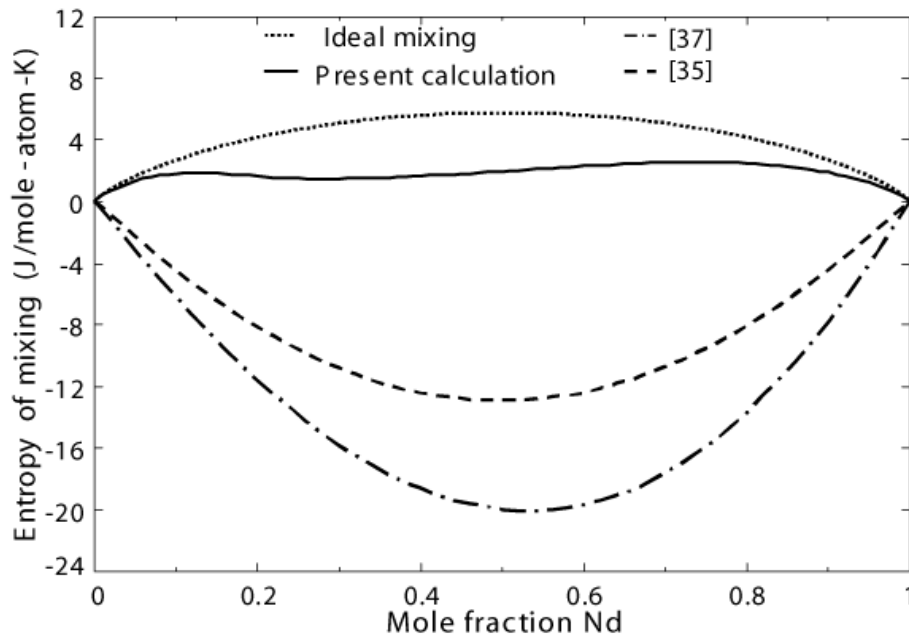
Figure 5.11 Calculated entropy of mixing of Al and Nd in liquid Al–Nd alloy at 1873 K. Comparison of calculations from present study with the ones calculated from [35, 37] 's sets of parameters.

The calculated curve of enthalpy of formation for the stable intermetallic compounds at 298 K is shown in Figure 5.12, along with the experimental data [65, 67, 73, 74]. The calculated enthalpies of transformation for Nd_3Al_{11} are 1 kJ/mole at 1223 K. The calculated phase diagram of the Al–Nd system shown in Figure 5.13 is compared with the experimental data [42, 43, 58, 69, 71]. The calculated non–stoichiometry of the Al_2Nd Laves–C15 phase is negligible. The calculated phase diagram is in good agreement with the experimental data, and the optimized model parameters are presented in Tables 5.2-5.4.
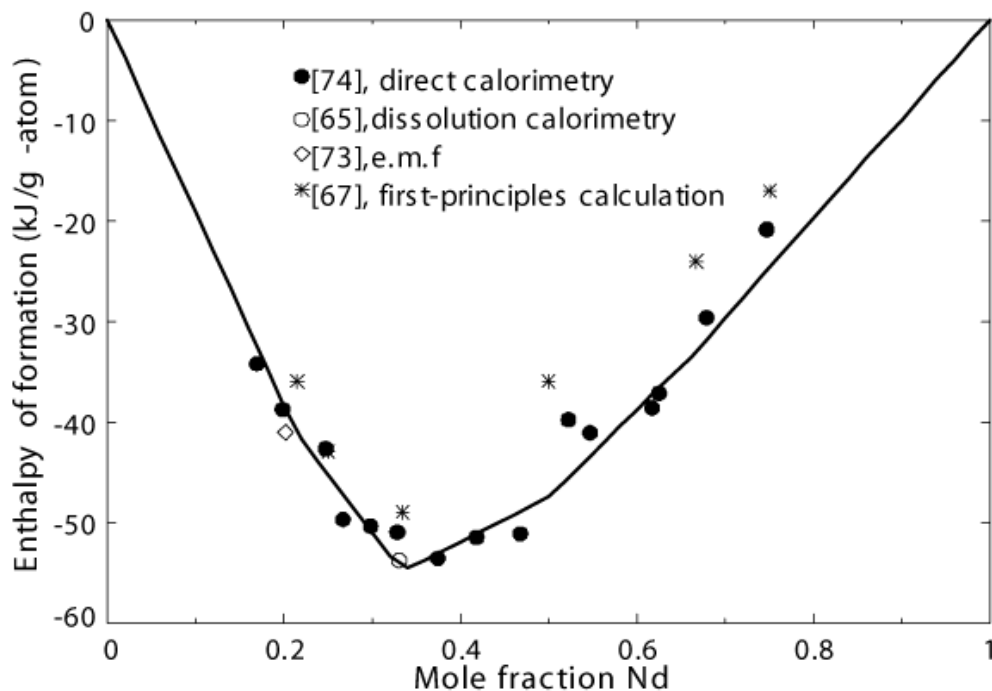
Figure 5.12 Calculated enthalpy of formation for the stable intermetallic compounds in the Al–Nd system at 298 K. Present calculation compared to the experimental data and ab–initio data from [65, 67, 73, 74].
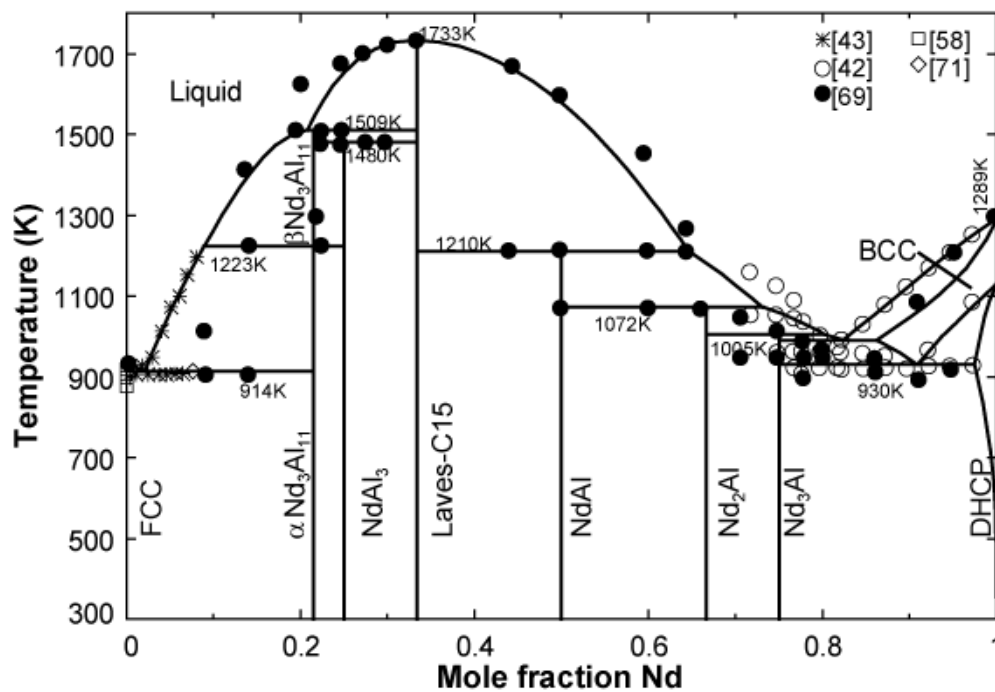
Figure 5.13 Calculated phase diagram of the Al–Nd system compared to the experimental data from [42, 43, 58, 69, 71].

5.3.4 The Al–Sm System

The Al–Sm system was first investigated by Casteels and Buschow for Al–rich part of the Al–Sm system *via* thermal, micrographic, x–ray methods, and microprobe analysis [75-77]. However, they have not determined the liquidus curve in the Sm–rich region, because of the experimental difficulty due to the low boiling point and high vapour pressure of Sm metal. They proposed Sm_3Al_{11} compound to melt congruently, and followed by a catatectic reaction around 1343 K, unlike the other RE_3Al_{11} (La_3Al_{11}, Pr_3Al_{11}, and Nd_3Al_{11}) phases which have two allotropic forms in the solid state. Phase diagrams in the Al–rich part were constructed by Kononenko and Golubev [43] using DTA, metallography, and X–ray method. More recently, Saccone et al. [7] studied the whole Al–Sm system using thermal analysis, micrographic examination, microprobe and X–ray diffraction method. It was suggested by Saccone et al. [7] that the solid–state transformation for Sm_3Al_{11} compound occurred around 1343 K. Recently, Zhou and Napolitano [78] investigated the controversial Sm_3Al_{11} phase by microstructural, microchemical, and X–ray diffraction method, together with First-Principles approach using VASP code [79], and proposed that Sm_3Al_{11} phase is stable from 1655 K to 1343 K. The melting temperature and transition temperatures for Sm was reported by Gschneidner et al. [80]; the Laves–C15 type structure for Al_2Sm was determined by Wernick and Geller [81]; Ni_2Si–type structure for Sm_2Al was obtained by Buschow and Van der Goot [82]. Buschow et al. [77] found out five intermetallic compounds Sm_2Al, $SmAl$, $SmAl_2$, $SmAl_3$, and $SmAl_4$. The existence of Sm_3Al_{11} instead of $SmAl_4$ compound has been confirmed by Saccone et al. [7] and Delsante et al. [83]. According to the compilation of Gschneidner et al [84] and Raghavan [85], there are four intermetallic compounds in this system: Sm_2Al, $SmAl$, $SmAl_3$, and Sm_3Al_{11}. $SmAl_2$ is considered as a Laves–C15 solid solution. This system has been assessed by Saccone et al. [7], by Jia et al. [86] and by Zhou and Napolitano [36] recently. However, Jia et al. [86] used the liquid model parameter from [7]. Associate model for the liquid phase was employed by Zhou and Napolitano [36] with the chemical associate formulation ($SmAl_2$). The temperature for the invariant reaction Liq.$\rightarrow$ FCC+ Al_3Sm was 919.5 K from their modeling result, much higher than the experimental data 903K from [77]. All phases considered for this system in present paper are shown in Table 5.1.

The same modelling strategy with similar model parameters using Eq. (5.16) and the same maximum SRO composition around $X_{Sm} = 1/3$ is assumed for the liquid Al–Sm system due to the similar chemical properties and similar electronic configuration among rare earth metals. Moreover, Zhou and Napolitano [36] noted that the ratio $\Delta H_{mixing}^{liquid} / \Delta H_{formation}^{Al_2RE}$ (for X_{RE}=0.3333) is roughly constant. It is found that this ratio is approximately equal to 0.62 according to Al–Pr and Al–Nd systems in present study. Assuming the same radio, the $\Delta H_{mixing}^{liquid}$ for the X_{Sm}= 0.333 in the liquid is estimated to around -34 kJ/mol based on the experimental data $\Delta H_{formation}^{Al_2Sm}$= -55kJ/mol. The model parameters for the liquid in the Al–Sm system are shown in Table 5.2. The enthalpy of mixing of the liquid at 1873 K is shown in Figure 5.14 and the entropy of mixing of the liquid at 1873 K is presented in Figure 5.15, together with those from the previous optimizations [7, 36]. Zhou and Napolitano [36] employed associate model for the liquid assuming that the chemical associate formulation (SmAl₂) was formed in the liquid phase.
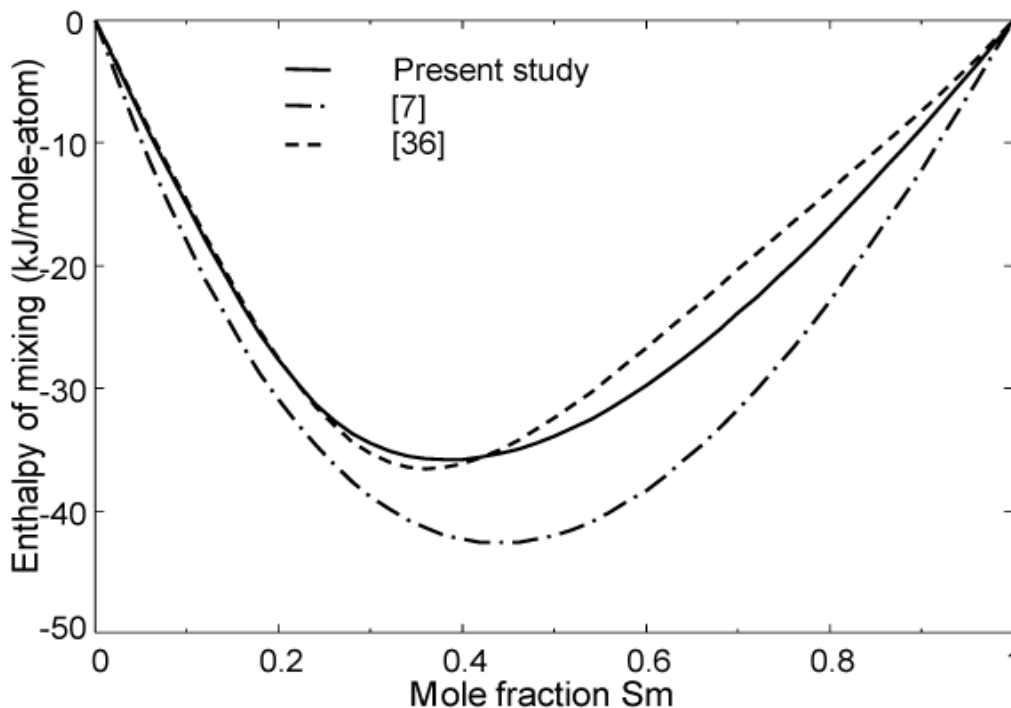
Figure 5.14 Calculated enthalpy of mixing of Al and Sm in the liquid Al–Sm alloy at 1873 K. Comparison of calculations from present study with the calculations from [7, 36].
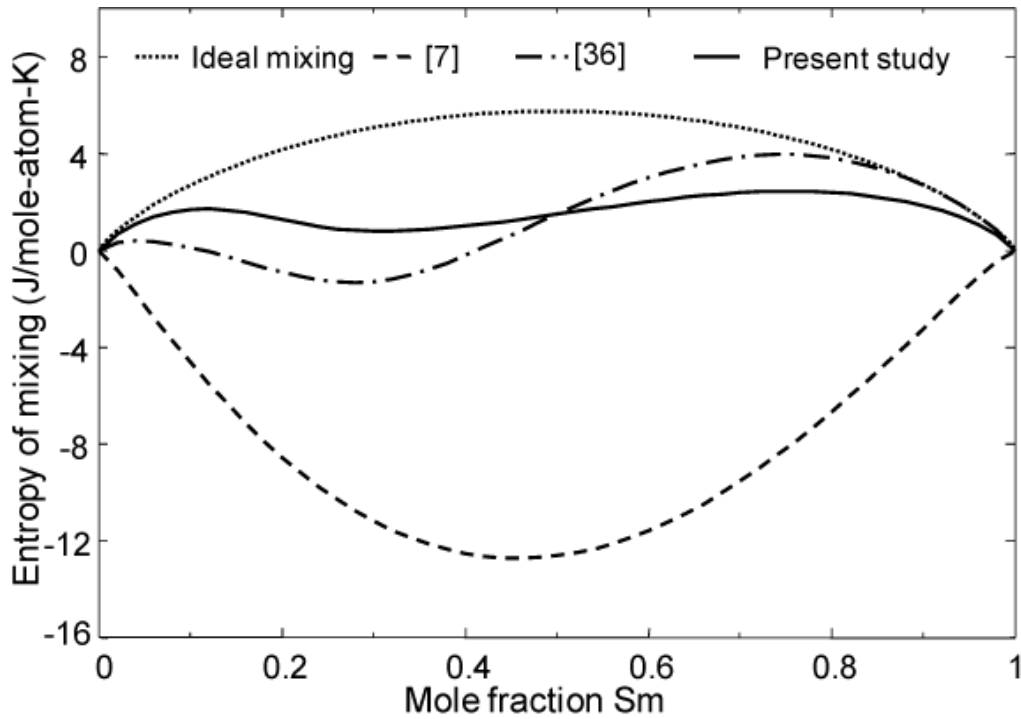
Figure 5.15 Calculated entropy of mixing of Al and Sm in the liquid Al–Sm alloy at 1873 K. Comparison of calculations from present study with those calculated from [7, 36]'s set of parameters.

The calculated enthalpy of formation for the stable intermetallic compounds was shown in Figure 5.16 along with the experimental data by Borzone et al. [87], Colinet et al. [65], Kober et al. [88], and First–Principles data by Gao et al. [67].
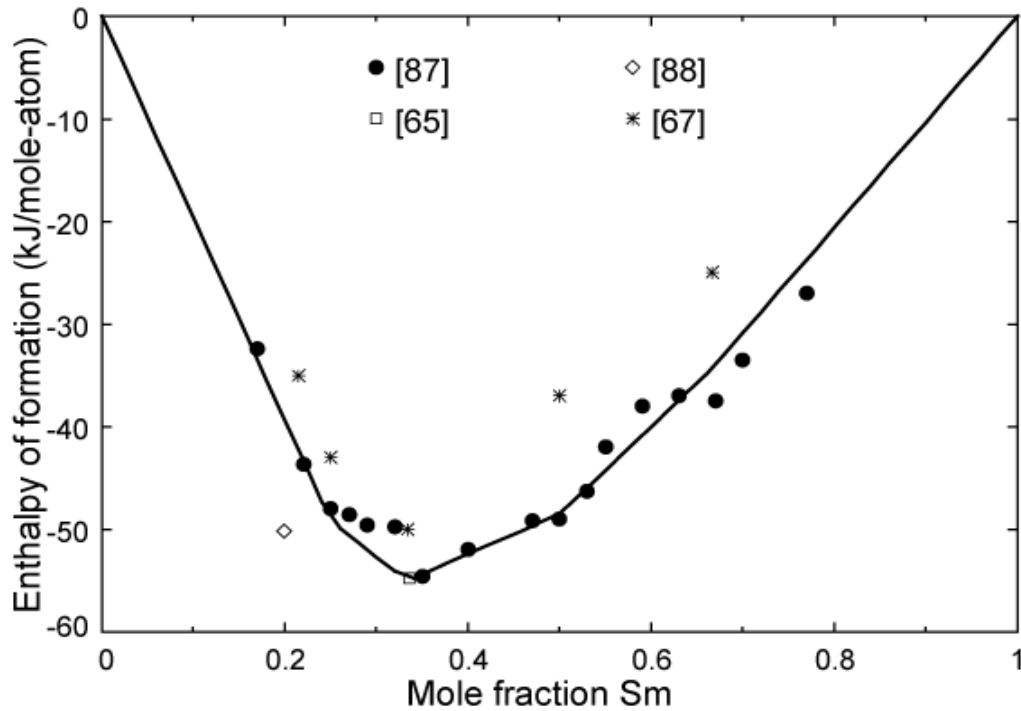
Figure 5.16 Calculated enthalpy of formation for the stable intermetallic compounds in the Al–Sm system at 298 K. Present calculation compared to the experimental data from [65, 87, 88], and First–Principles data from [67].

The calculated phase diagram of the Al–Sm system shown in Figure 5.17 is compared with the experimental data [7, 43, 75], and all optimized model parameters are presented in Tables 5.2-5.4.
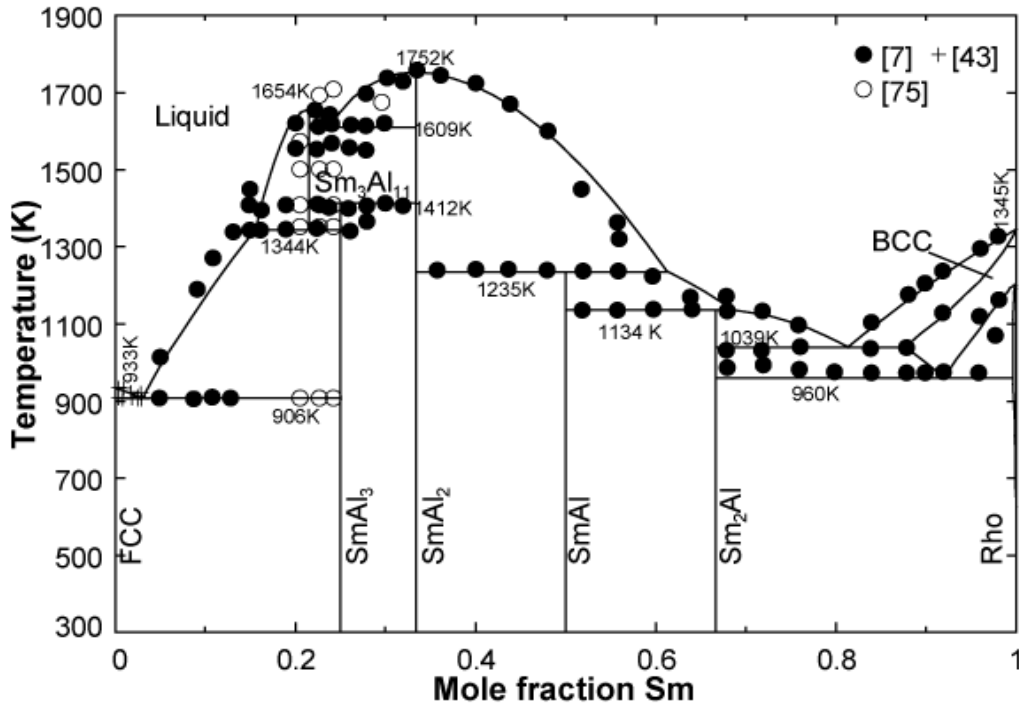
Figure 5.17 Calculated phase diagram of the Al–Sm system compared to the experimental data from [7, 43, 75].

5.3.5 Al–Ce System

This system has been optimized previously by Cacciamani et al. [35, 89] and Gao et al. [39] using Bragg–William model for the liquid, and by the co-authors Kang et al. [15] using the MQM for the liquid. In order to keep the consistency with other Al–RE systems optimized in the present study, the Al–Ce system was reoptimized. The literature review and detailed evaluation of the Al–Ce system was omitted in the present study, due to the extensive assessment already given in the paper of co-authors Kang et al. [15]. The calculated phase diagram looks only a little different. The βCe_3Al_{11} phase [35, 90] was considered in the present study instead of the $CeAl_4$ high–temperature phase [39], more experiments are required in order to clarify its stoichiometry.

The same modelling strategy with similar model parameters and the same maximum SRO composition around $X_{Ce} = 1/3$ is used for the liquid Al–Ce system. although this system

has been optimized several times, the re–calculated thermodynamic properties of the liquid in the present study are only compared with the optimization done by Kang et al. [15], since the same model (MQM) for the liquid is used in both studies. The calculated partial enthalpy of mixing in the present study is shown in Figure 5.18 along with the experimental data [91, 92] and the calculation of Kang et al. [15] of the liquid phase at 1600 ℃, The calculated enthalpy of mixing of the liquid phase at 1873 K with the experimental data [91, 93], entropy of mixing compared with the calculation from Kang et al. [15], enthalpy of formation of solid phases at 25 ℃ with the experimental data [65, 94-98], and phase diagram with experimental data [39, 42, 61, 92] are shown in Figure 5.19 ~ Figure 5.22 respectively. It is seen that the calorimetric data points for the enthalpy of mixing of Al in Ce-rich solutions (at $X_{Ce} > 0.8$ in Figure 5.19) are not reproduced by the model. As explained in Kang et al. [15] , these data points are almost certainly in error. If they were correct, a liquid–liquid immiscibility gap would occur according to the resultant experimental integral enthalpy of mixing curve. However, no such gap is observed.
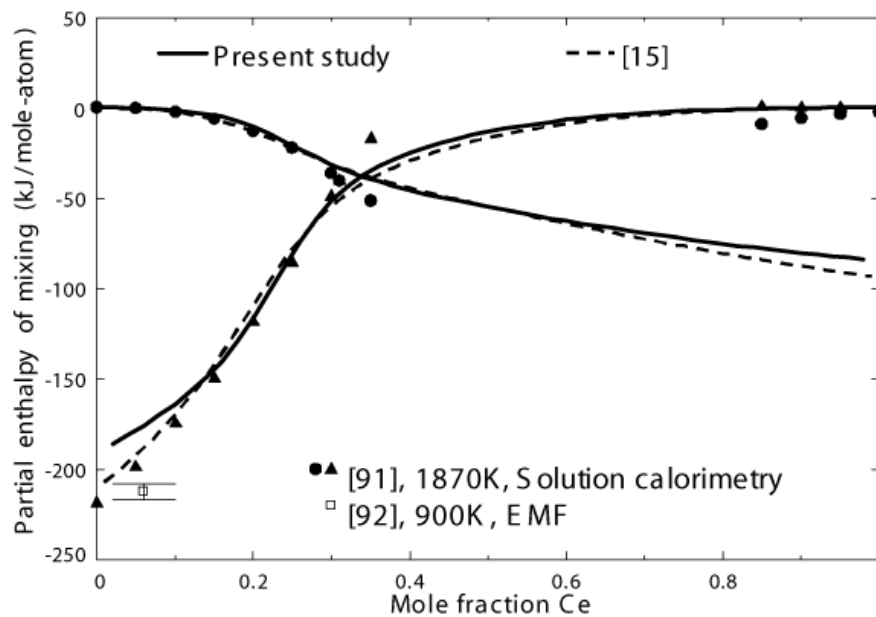
Figure 5.18 Calculated partial enthalpy of mixing of Al and Ce in the liquid Al–Ce alloy at 1873 K. Comparison of the experimental data [91, 92] with calculations from present study and from [15].
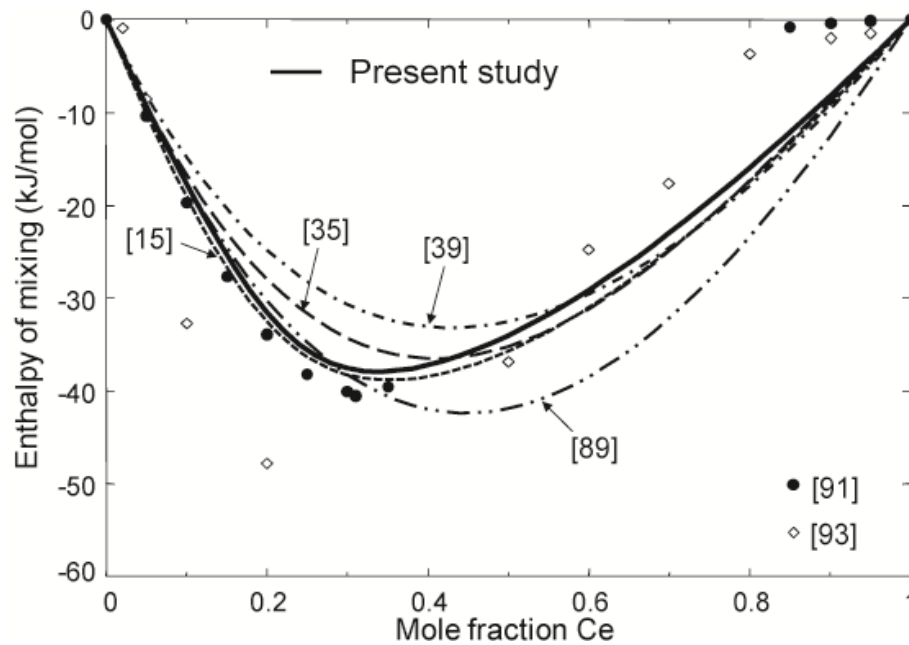
Figure 5.19 Calculated enthalpy of mixing of Al and Ce in the liquid Al–Ce alloy at 1873 K. Comparison of the experimental data [91, 93] with calculations from present study and from [15, 35, 39, 89].
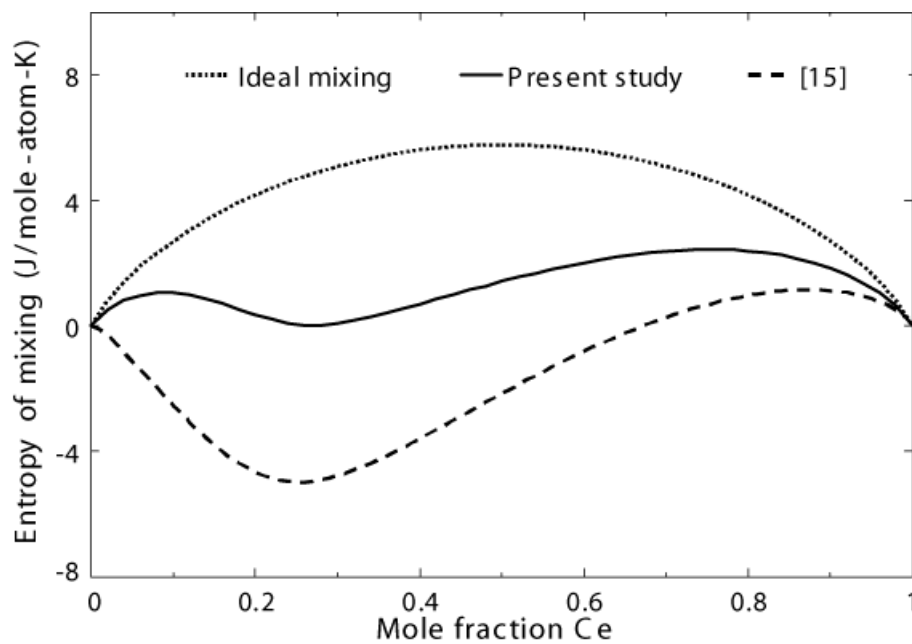

Figure 5.20 Calculated entropy of mixing in liquid Al–Ce alloy at 1873 K. Comparison of calculations from present study with the one from [15].
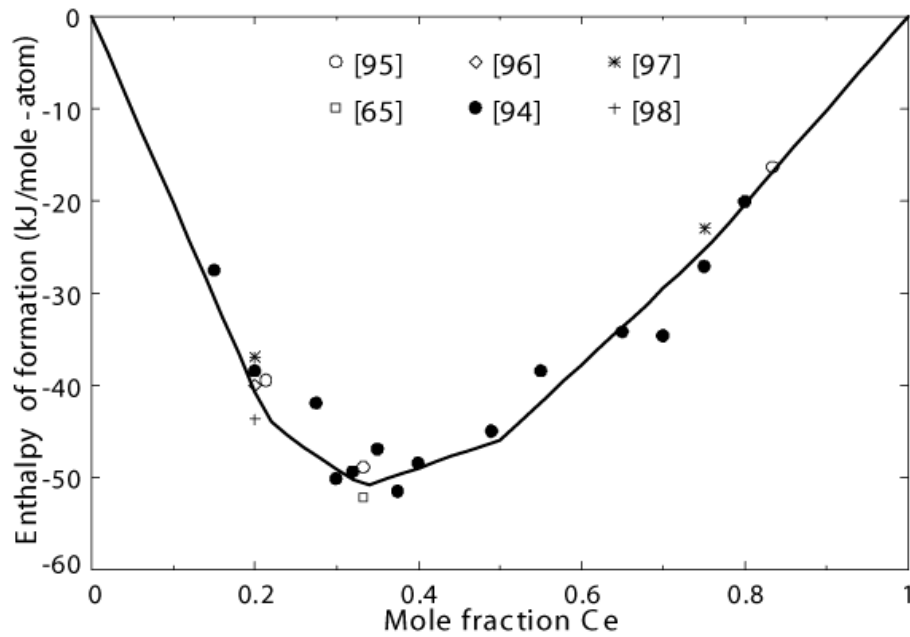
Figure 5.21 Calculated enthalpy of formation for the stable intermetallic compounds in the Al–Ce system at 298 K. Present calculation compared to the experimental data from [65, 94-98].
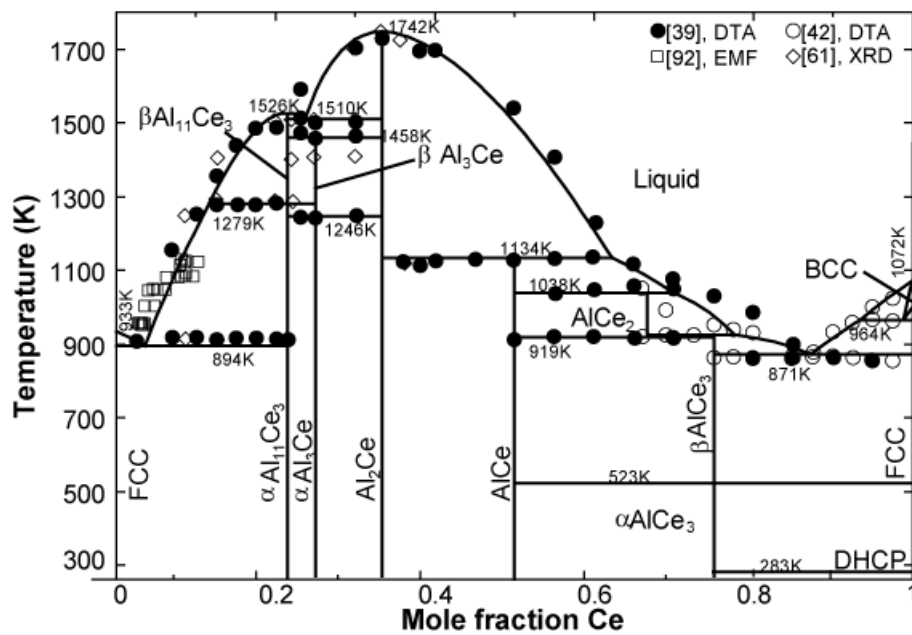
Figure 5.22 Calculated phase diagram of the Al–Ce system compared to the experimental data from [39, 42, 61, 92].

The calculated entropy of mixing in the present study seems to be more reasonable than the one calculated by Kang et al. [15] and it is also consistent with other Al–RE systems. The optimized model parameters are presented in Tables 5.2-5.4.

5.4 Discussion and Systematic Analysis

It has been shown that MQM for the liquid phase reproduced the experimentally thermodynamic and phase equilibria data well, and the value of the "m–shaped" integral entropy of mixing seems to be more realistic, unlike the very negative entropy of mixing in the previous optimizations when the Bragg–Williams random mixing approximation was used. Moreover, the calculated partial enthalpy of mixing curve of the liquid reflects the strong SRO, as the experimental data indicated.

As it has been well known that rare earths show similar regularities across the Al–rare earth series, the enthalpy of mixing of the binary liquids at 1873 K, the entropy of mixing of the binary liquids at 1873 K, the enthalpy of formation of solid at 298 K and the entropy of formation of solid at 298 K is superimposed respectively in Figures 5.23-5.26 for the Al–light rare earth systems. The minimum values of the enthalpy of mixing and the entropy of mixing of the binary liquids at 1873 K are at a composition around $X_{RE} = 1/3$ and in the range of -40 ~ -33 kJ/mole of atoms (-39 ~ -35 kJ/mole of atoms for the Al-heavy rare earth systems from [40]) and 0 ~ 2 J/mole-atom-K (0 ~ 1 J/mole-atom-K for the Al-heavy rare earth systems from [40]) respectively. The enthalpy of formation at 298 K shows the minimum at a composition $X_{RE} = 1/3$, in the range of -55 ~ -51 kJ/mole of atoms (-53 ~ -50 kJ/mole of atoms for the Al-heavy rare earth systems from [40]), while the enthalpy of formation at 298 K for the RE_3Al_{11}, and REAl are in the range of -44 ~ -41 kJ/mole of atoms and -49 ~ -45 kJ/mole of atoms respectively. The compound in equilibrium with Al–FCC phase is RE_3Al_{11} (except Sm) while the compound in equilibrium with RE–DHCP phase is RE_3Al for all the Al–light rare earth systems. More systematic analysis will be presented in a next paper in this series.
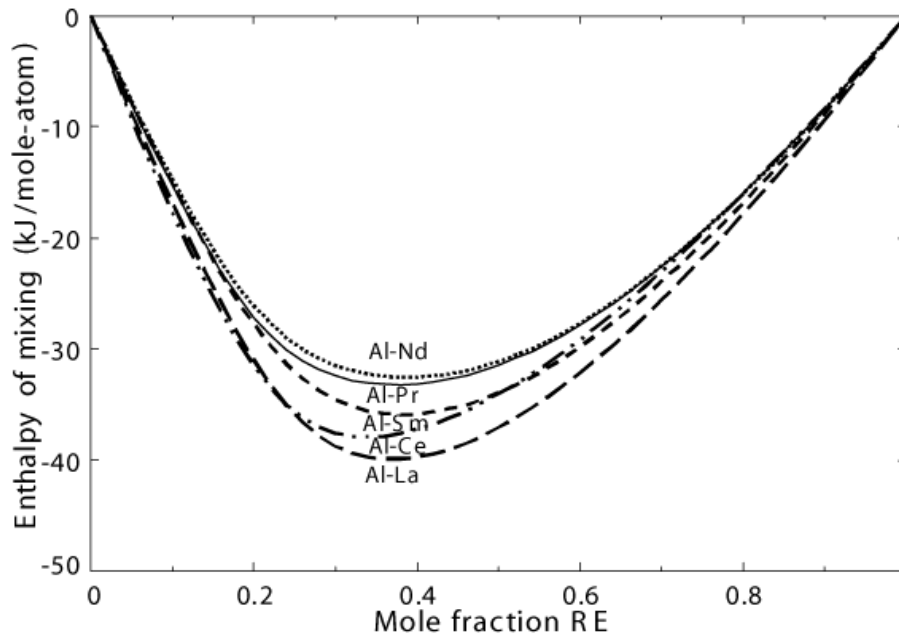
Figure 5.23 Calculated enthalpies of mixing of Al and RE in liquid Al-light RE alloys at 1873 K. (RE is La, Ce, Pr, Nd and Sm; ↕ represents the range of minimum enthalpies of mixing of liquid at 1873 K at around $X_{RE} = 1/3$ in Al–heavy rare earth systems).
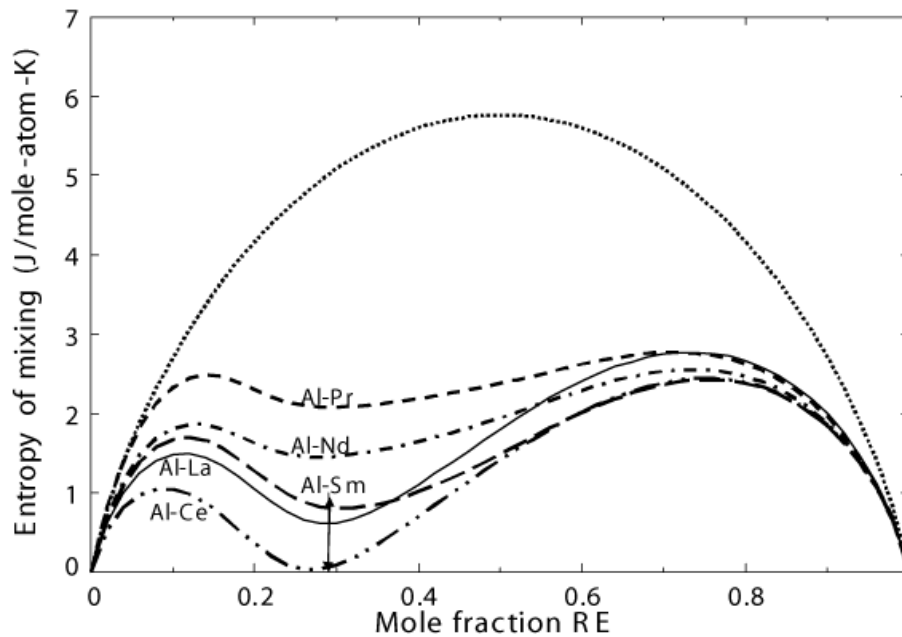
Figure 5.24 Calculated entropies of mixing of Al and RE in liquid Al–light RE alloys at 1873 K. (RE is La, Ce, Pr, Nd and Sm; ↕ represents the range of minimum entropies of mixing of liquid at 1873 K at around $X_{RE} = 0.3$ in Al–heavy rare earth systems).
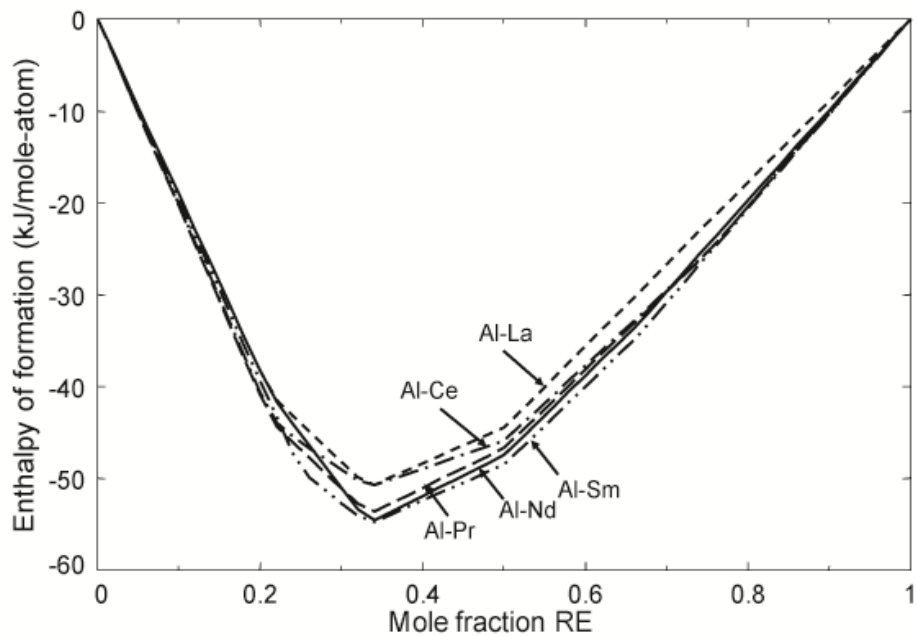
Figure 5.25 Calculated curve of enthalpy of formation for the stable intermetallic compounds at 298 K in the Al-RE systems (RE is La, Ce, Pr, Nd and Sm).
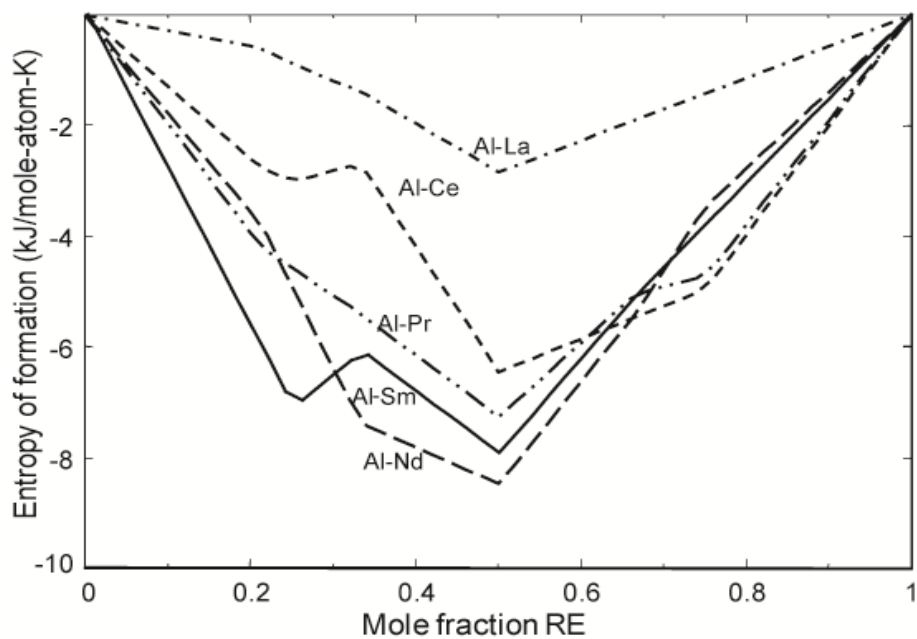
Figure 5.26 Calculated curve of entropy of formation for the stable intermetallic compounds in the Al–light RE alloys at 298 K (RE is La, Ce, Pr, Nd and Sm).

5.5 Conclusions

Systematically thermodynamic evaluations and optimizations of the Al–La, Al–Ce, Al–Pr, Al–Nd and Al–Sm systems have been presented on the basis of the literature information. Optimized model parameters of the Gibbs energies for all phases which reproduce the experimental data very well were obtained in the present study. It may be noteworthy that all the Al–rare earth binary systems exhibit a very large degree of short–range ordering (SRO) in the liquid and show the similar thermodynamic properties. The Modified Quasichemical Model (MQM) for the liquid phases which takes the SRO into account fitted the experimental data very well, and the value of the "m–shaped" integral entropy of mixing seems to be more realistic, unlike the very negative entropy of mixing in the previous optimizations when the Bragg–Williams random mixing approximation was used. It should be noteworthy that the large negative entropy of mixing results in a spurious inverted miscibility gap at high temperatures. Moreover, the shape of partial enthalpy of mixing curve was well reproduced as the experimental data indicated using MQM for the liquid.

As it has been well known that rare earths show similar regularities across the Al–rare earth series, similar regularities for the thermodynamic properties, like the enthalpies of mixing of binary liquids at 1873 K, the entropies of mixing of binary liquids at 1873 K, the enthalpies of formation for the stable intermetallic compounds at 298 K and the entropies of formation for the solid phase at 298 K were presented and compared across the Al–light rare earth series. Furthermore, the same optimization strategy is adopted in the Al–heavy rare earth series (Al–Gd, Al–Tb, Al–Dy, Al–Ho and Al–Er systems), and similar regularities for the thermodynamic properties is also shown. Importantly, it indicates that it should be interesting and very important to evaluate and optimize the series of lanthanides instead of assessing them independently.

It would be expected that MQM for the liquid gives better extrapolations into multicomponent systems based on parameters in the binary and ternary systems. These better predictions and estimations of phase equilibria will help to develop and design novel magnesium alloys.

5.6 Acknowledgements

5.7 References

[1]   R. Lundin and J. R. Wilson, Advanced Materials & Processes, 158(2000), 52-55.

[2]   D. Ping, K. Hono, and A. Inoue, Metallurgical and Materials Transactions A, 31(2000), 607-614.

[3]   K. A. Gschneidner, Jr., L. Eyring, and Editors, Handbook on the Physics and Chemistry of Rare Earths, Volume 25. 1998, 83.

[4]   H. Cao and M. Wessen, Metallurgical and Materials Transactions A: Physical Metallurgy and Materials Science, 35A(2003), 309-319.

[5]   R. Ferro and S. Delfino, J. Less-Common Met. , 68(1979), 23-29.

[6]   K. H. J. Buschow and J. H. N. Van Vucht, Philips Research Reports, 22(1967), 233-245.

[7]   A. Saccone, G. Cacciamani, D. Maccio, G. Borzone, and R. Ferro, Intermetallics, 6(1998), 201-215.

[8]   R. Ferro, S. Delfino, G. Borzone, A. Saccone, and G. Cacciamani, Journal of Phase Equilibria, 14(1993), 273-279.

[9]   S. Delfino, A. Saccone, and R. Ferro, J. Less-Common Met., 102(1984), 289-310.

[10] G. Borzone, A. Borsese, and R. Ferro, Zeitschrift fuer Anorganische und Allgemeine Chemie, 501(1983), 199-208.

[11] A. Saccone, S. Delfino, and R. Ferro, J. Less-Common Met., 143(1988), 1-23.

[12] E. H. P. Cordfunke and R. J. M. Konings, Thermochimica Acta, 375(2001), 65-79.

[13] E. H. P. Cordfunke and R. J. M. Konings, Thermochimica Acta, 375(2001), 17-50.

[14] S. V. Meschel and O. J. Kleppa, Journal of Alloys and Compounds, 321(2001), 183-200.

[15] Y.-B. Kang, A. D. Pelton, P. Chartrand, and C. D. Fuerst, Calphad, 32(2008), 413-422.

[16] C. W. Bale, P. Chartrand, S. A. Degterov, G. Eriksson, K. Hack, R. Ben Mahfoud, J. Melancon, A. D. Pelton, and S. Petersen, CALPHAD: Computer Coupling of Phase Diagrams and Thermochemistry, 26(2002), 189-228.

[17] C. Bale, A. Pelton, and W. Thompson, Factsage thermochemical software and databases, http://www.crct.polymtl.ca/

[18] A. T. Dinsdale, Calphad, 15(1991), 317-425.

[19] Y.-B. Kang, L.-L. Jin, P. Chartrand, and A. D. Pelton, unpublished work., Ecole polytechnique de Montréal, Quebéc, Canada(2007).

[20] A. D. Pelton, S. A. Degterov, G. Eriksson, C. Robelin, and Y. Dessureault, Metallurgical and Materials Transactions B: Process Metallurgy and Materials Processing Science, 31B(2000), 651-659.

[21]   Y.-B. Kang, A. D. Pelton, P. Chartrand, P. Spencer, and C. D. Fuerst, Metallurgical and Materials Transactions A: Physical Metallurgy and Materials Science, 38(2007), 1231-1243.

[22]   Y.-B. Kang, A. D. Pelton, P. Chartrand, P. Spencer, and C. D. Fuerst, Journal of Phase Equilibria and Diffusion, 28(2007), 342-354.

[23]   Y.-B. Kang, I.-H. Jung, S. A. Decterov, A. D. Pelton, and H.-G. Lee, ISIJ International, 44(2004), 975-983.

[24]   I.-H. Jung, S. A. Decterov, and A. D. Pelton, Journal of the European Ceramic Society, 25(2005), 313-333.

[25]   A. Pelton and P. Chartrand, Metallurgical and Materials Transactions A, 32(2001), 1361-1383.

[26]   P. Chartrand and A. Pelton, Metallurgical and Materials Transactions A, 32(2001), 1385-1396.

[27]   P. Waldner and A. D. Pelton, Metall. Mater. Trans. B 35B(2004), 897-907.

[28]   A. Shukla, Y.-B. Kang, and A. D. Pelton, Int. J. Mater. Res., 100(2009), 208-217.

[29]   A. Shukla, Y.-B. Kang, and A. D. Pelton, CALPHAD: Comput. Coupling Phase Diagrams Thermochem. FIELD Full Journal Title:CALPHAD: Computer Coupling of Phase Diagrams and Thermochemistry, 32(2008), 470-477.

[30]   P. J. Spencer, A. D. Pelton, Y.-B. Kang, P. Chartrand, and C. D. Fuerst, CALPHAD: Comput. Coupling Phase Diagrams Thermochem., 32(2008), 423-431.

[31]   S. Wasiur-Rahman and M. Medraj, Intermetallics FIELD Full Journal Title:Intermetallics, 17(2009), 847-864.

[32]   M. Aljarrah and M. Medraj, CALPHAD: Comput. Coupling Phase Diagrams Thermochem. FIELD Full Journal Title:CALPHAD: Computer Coupling of Phase Diagrams and Thermochemistry, 32(2008), 240-251.

[33]   M. Hillert, Journal of Alloys and Compounds, 320(2001), 161-176.

[34] F. Yin, X. Su, Z. Li, M. Huang, and Y. Shi, Journal of Alloys and Compounds, 302(2000), 169-172.

[35] G. Cacciamani and R. Ferro, Calphad: Computer Coupling of Phase Diagrams and Thermochemistry, 25(2001), 583-597.

[36] S. H. Zhou and R. E. Napolitano, Metall. Mater. Trans. A, 39A(2008), 502-512.

[37] N. Clavaguera and Y. Du, Journal of Phase Equilibria, 17(1996), 107-111.

[38] J. Wang, CALPHAD: Computer Coupling of Phase Diagrams and Thermochemistry, 20(1996), 135-138.

[39] M. C. Gao, N. Ünlü, G. J. Shiflet, M. Mihalkovic, and M. Widom, Metallurgical and Materials Transactions A: Physical Metallurgy and Materials Science, 36A(2005), 3269-3279.

[40] L.-L. Jin, P. Chartrand, Y.-B. Kang, and C. D. Fuerst, Calphad, (2010), submitted.

[41] K. H. J. Buschow, Philips Res. Rept., 20(1965), 337-348.

[42] A. Saccone, A. M. Cardinale, S. Delfino, and R. Ferro, Zeitschrift fuer Metallkunde, 87(1996), 82-87.

[43] V. I. Kononenko and S. V. Golubev, Izvestiya Akademii Nauk SSSR, Metally, (1990), 197-199.

[44] S. H. Zhou and R. E. Napolitano, Acta Materialia, 54(2006), 831-840.

[45] K. Gschneidner and F. Calderwood, Journal of Phase Equilibria, 9(1988), 686-689.

[46] H. Okamoto, Journal of Phase Equilibria and Diffusion, 28(2007), 581.

[47] H. Okamoto, Journal of Phase Equilibria, 21(2000), 205.

[48] V. I. Kober, I. F. Nichkov, S. P. Raspopin, and V. A. Nauman, Izvestiya Vysshikh Uchebnykh Zavedenii, Tsvetnaya Metallurgiya, (1977), 83-86.

[49] F. Sommer, M. Keita, H. G. Krull, B. Predel, and J. J. Lee, Journal of the Less-Common Metals, 137(1988), 267-275.

[50]   G. Borzone, A. M. Cardinale, N. Parodi, and G. Cacciamani, Journal of Alloys and Compounds, 247(1997), 141-147.

[51]   J.-J. Lee and F. Sommer, Z. Metallkunde, 76(1985), 750-753.

[52]   V. I. Kononenko, V. G. Shevchenko, and A. L. Sukhman, Tezisy Nauchn. Soobshch. Vses. Konf. Str. Svoistvam Met. Shlakovykh Rasplavov, 3rd, 2(1978), 406-410.

[53]   Y. O. Esin, S. P. Kolesnikov, V. M. Baev, M. S. Petrushevskii, and P. V. Gel'd, Zhurnal Fizicheskoi Khimii, 55(1981), 1587-1588.

[54]   V. A. Lebedev, V. I. Kober, I. F. Nichkov, S. P. Raspopin, and A. A. Kalinovskii, Izvestiya Akademii Nauk SSSR, Metally, (1972), 91-95.

[55]   A. D. Pelton and Y.-B. Kang, International Journal of Materials Research, 98(2007), 907-917.

[56]   G. Canneri and A. Rossi, Gazzetta Chimica Italiana, 62(1932), 202-211.

[57]   W. G. Jung, O. J. Kleppa, and L. Topor, Journal of Alloys and Compounds, 176(1991), 309-318.

[58]   M. E. Drits, E. S. Kadaner, and C. Nguyen Dinh, Izvestiya Akademii Nauk SSSR, Metally, (1969), 219-223.

[59]   V. I. Kober, I. F. Nichkov, S. P. Raspopin, and A. A. Bogdanov, Izvestiya Vysshikh Uchebnykh Zavedenii, Tsvetnaya Metallurgiya, (1983), 58-60.

[60]   G. Canneri, Alluminio, 2(1933), 87-89.

[61]   K. H. J. Buschow and J. H. N. van Vucht, Zeitschrift fuer Metallkunde, 57(1966), 162-166.

[62]   F. Yin, X. Su, Z. Li, and P. Zhang, Zeitschrift fuer Metallkunde, 92(2001), 447-450.

[63]   H. Okamoto, Journal of Phase Equilibria, 23(2002), 381.

[64]   G. N. Zviadadze, L. A. Chkhikvadze, and M. V. Kereselidze, Soobshcheniya Akademii Nauk Gruzinskoi SSR, 81(1976), 149-152.

[65]   C. Colinet, A. Pasturel, and K. H. J. Buschow, Journal of Chemical Thermodynamics, 17(1985), 1133-1139.

[66]   R. Ferro, G. Borzone, N. Parodi, and G. Cacciamani, Journal of Phase Equilibria, 15(1994), 317-329.

[67]   M. C. Gao, A. D. Rollett, and M. Widom, Physical Review B: Condensed Matter and Materials Physics, 75(2007), 174120/174121-174120/174116.

[68]   L. Rolla, A. Iandelli, G. Canneri, and R. Vogel, Z. Metallkd. , 35(1943), 29-42.

[69]   K. H. J. Buschow, Journal of the Less-Common Metals, 9(1965), 452-456.

[70]   K. A. Gschneidner, Jr. and F. W. Calderwood, Bulletin of Alloy Phase Diagrams, 10(1989), 28-30, 81-22.

[71]   G. B. Kale, A. Biswas, and I. G. Sharma, Scripta Materialia, 37(1997), 999-1003.

[72]   E. M. Savitskii, E. S. Stepanov, and V. F. Terekhova, Izvestiya Akademii Nauk SSSR, Otdelenie Tekhnicheskikh Nauk, Metallurgiya i Toplivo, (1960), 73-78.

[73]   V. I. Kober, I. F. Nichkov, S. P. Raspopin, and V. I. Kuz'minykh, Termodin. Svoistva Met. Rasplavov, Mater. Vses. Soveshch. Termodin. Met. Splavov (Rasplavy), 4th, 2(1979), 72-76.

[74]   G. Borzone, A. M. Cardinale, G. Cacciamani, and R. Ferro, Zeitschrift fuer Metallkunde, 84(1993), 635-640.

[75]   F. Casteels, Journal of the Less-Common Metals, 12(1967), 210-220.

[76]   K. H. J. Buschow and J. H. N. Van Vucht, Journal of the Less-Common Metals, 13(1967), 369-370.

[77]   K. H. J. Buschow and J. H. V. van Vucht, Philips Res. Repts., 20(1965), 15-22.

[78]   S. H. Zhou and R. E. Napolitano, Metallurgical and Materials Transactions A, 38(2007), 1145-1151.

[79]   VASP package, http://cms.mpi.univie.ac.at/vasp/vasp/vasp.html

[80]   K. A. Gschneidner, Jr., L. Eyring, and Editors, Handbook on the Physics and Chemistry of Rare Earths, Vol. 8. 1986, 382 pp.

[81]   J. H. Wernick and S. Geller, Transactions of the Metallurgical Society of AIME*,* 218(1960), 866-868.

[82]   K. H. J. Buschow and A. S. Van der Goot, Journal of the Less-Common Metals*,* 24(1971), 117-120.

[83]   S. Delsante, R. Raggio, G. Borzone, and R. Ferro, Journal of Phase Equilibria and Diffusion*,* 28(2007), 240-242.

[84]   K. A. Gschneidner, Jr. and F. W. Calderwood, Bulletin of Alloy Phase Diagrams*,* 10(1989), 37-39, 87-38.

[85]   V. Raghavan, J. Phase Equilib. Diffus.*,* 30(2009), 69-70.

[86]   B. R. Jia, L. B. Liu, D. Q. Yi, Z. P. Jin, and J. F. Nie, Journal of Alloys and Compounds*,* 459(2008), 267-273.

[87]   G. Borzone, A. M. Cardinale, A. Saccone, and R. Ferro, Journal of Alloys and Compounds*,* 220(1995), 122-125.

[88]   V. I. Kober, I. F. Nichkov, and S. P. Raspopin, Izvestiya Vysshikh Uchebnykh Zavedenii, Tsvetnaya Metallurgiya*,* (1987), 116-118.

[89]   G. Cacciamani, G. Borzone, and R. Ferro, *in* COST507-Thermochemical Databases for Light Metal Alloys, (2) 1998, 20-22.

[90]   H. Okamoto, Journal of Phase Equilibria*,* 19(1998), 396.

[91]   Y. O. Esin, G. M. Ryss, and P. V. Gel'd, *in* Termodin. Svoistva Met. Rasplavov, Mater. Vses. Soveshch. Termodin. Met. Splavov, Vol. 2, p. 53-56, 1979.

[92]   V. I. Kober, V. A. Lebedev, I. F. Nichkov, S. P. Raspopin, and L. F. Yamshchikov, Izv. Akad. Nauk SSSR, Metal. *,* (1973), 217-220.

[93]   V. G. Shevchenko, V. I. Kononenko, and A. L. Sukhman, Zhurnal Fizicheskoi Khimii*,* 53(1979), 1351.

[94]   G. Borzone, G. Cacciamani, and R. Ferro, Metallurgical Transactions A: Physical Metallurgy and Materials Science*,* 22A(1991), 2119-2123.

[95]   F. Sommer and M. Keita, Journal of the Less-Common Metals*,* 136(1987), 95-99.

[96]   V. I. Kober, I. F. Nichkov, S. P. Raspopin, and A. S. Kondratov, Izvestiya Vysshikh Uchebnykh Zavedenii, Tsvetnaya Metallurgiya, (1982), 101-102.

[97]   W. Biltz and H. Pieper, Z. Anorg. Allg. Chem., 134(1924), 13-24.

[98]   L. F. Yamshchikov, V. A. Lebedev, V. I. Kober, I. F. Nichkov, and S. P. Raspopin, Izv. Akad. Nauk SSSR, Met., (1977), 90.

CHAPTER 6   ARTICLE 2: THERMODYNAMIC EVALUATION AND OPTIMIZATION OF AL–GD, AL–TB, AL–DY, AL–HO AND AL–ER SYSTEMS USING A MODIFIED QUASICHEMICAL MODEL FOR THE LIQUID

Published in Calphad, 34(2010), 456-466

Liling Jin [a], Youn-Bae Kang [a], Patrice Chartrand [a,*], and Carlton D. Fuerst [b]

[a] Center for Research in Computational Thermochemistry (CRCT), Dept. of Chemical Engineering, Ecole polytechnique de Montréal, Montréal, Québec, Canada

[b] General Motors, Warren, MI, USA

[*] Corresponding author. Centre de Recherche en Calcul Thermochimique (CRCT), École Polytechnique de Montréal, Montréal, QC, CANADA, H3C 3A7. Tel : +1 514 3404711 ext. 4089; fax : +1 514 3405840. E-mail address: Patrice.Chartrand @polymtl.ca

Abstract: The Al–Gd, Al–Tb, Al–Dy, Al–Ho and Al–Er (Al–heavy rare earths) binary systems have been systematically assessed and optimized based on the available experimental data and ab–initio data using the FactSage thermodynamic software. A systematic technique (reduced melting temperature proposed by Gschneidner) was used for estimating the Al-Tb phase diagram due to lack of experimental data. Optimized model parameters of the Gibbs energies for all phases which reproduced all the reliable experimental data to satisfaction have been obtained. The optimization procedure was biased by putting a strong emphasis on the observed trends in the thermodynamic properties of Al–RE phases. The Modified Quasichemical Model, which takes short–range ordering into account, is used for the liquid phase and the Compound Energy Formalism is used for the solid solutions in the binary systems. It is shown that the Modified Quasichemical Model used for the liquid alloys permits one to obtain entropies of mixing that are more reliable than that based on the Bragg – Williams random mixing model which does not take short–range ordering into account.

Keywords: Aluminum – Rare Earth Alloys, Modified Quasichemical Model, Thermodynamic Modeling, Phase Diagram.

6.1 Introduction

Adding rare earth metals (RE = Y, Sc, La, Ce, Pr, Nd, Pm, Sm, Eu, Gd, Tb, Dy, Ho, Er, Tm, Yb, and Lu) to aluminum and Al-transition metal alloys can result in increased mechanical properties of the materials, such as tensile strength, heat resistance, corrosion resistance, vibration resistance, and extrudability [1-3]. Moreover, Mg–based alloys with rare earth metals show several interesting applications in the automotive and aeronautical industries because of their low density and potentially high strength/weight ratios. Most commercial magnesium alloys are based on the Mg–Al system, with some additions of other alloying elements, such as Mn, Zn, Ca, and rare–earth metals, to reach certain application requirements[4]. It is an important task for alloy design to develop a better thermodynamic understanding of novel aluminum and magnesium alloy systems with additions of rare earth elements.

La, Ce, Pr and Nd are the main components of mischmetal, which is a mixture of rare earth elements. Rare earth elements form very stable intermetallic compounds with aluminum. Therefore, adding small amounts of rare earth elements to magnesium alloys will have significant effects on the properties of magnesium alloys since Al–RE compounds are readily precipitated when Al is present.

Rare earth elements are often divided into two subgroups: the light rare earths (from La to Sm) and the heavy rare earths (from Gd to Lu, except Yb). It has been well known that rare earths show certain trends and similar regularities across the lanthanide series (from La to Lu all of which form trivalent rare earth ions upon oxidation, except Eu and Yb which form divalent ions upon oxidation). Such similarity and trends of the physical and chemical properties are shown in lanthanides with another common metal (like Ag [5], Al[6-8], Mg [8], In [9], Sn [10], Tl [11]) and non-metals (like lanthanide oxides [12], Lanthanide trihalides [13], Lanthanide carbides, Lanthanide silicides [14]). In the thermodynamic evaluation and modelling of Al–rare earth (RE) binary systems, this trend

shown in Al–RE systems may give some hints when the experimental data is missing for some systems.

As part of ongoing projects in our laboratory to develop thermodynamic databases for multi-component Mg– and Al– based alloys, we have systematically assessed the binary Al–La, Al–Ce, Al–Pr, Al–Nd, Al–Sm, Al–Gd, Al–Tb, Al–Dy, Al–Ho, Al–Er, Al–Tm, and Al–Lu, Al–Y, and Al–Sc systems. The Al–Ce, Al–Y, and Al–Sc systems were previously optimized by Kang et al. [15]; In a previous paper [16], the Al–La, Al–Ce, Al–Pr, Al–Nd, and Al–Sm (Al–light lanthanides) binary systems have been examined systematically (Al–Ce system was reoptimized in order to keep consistency with other systems regarding thermodynamic parameters). In the current study, the Al–Gd, Al–Tb, Al–Dy, Al–Ho, and Al–Er systems (Al–heavy lanthanides) will be investigated systematically. Thermodynamic predictions of Al–Tm and Al–Lu systems will be discussed in another paper [17] together with the systematic study of thermodynamic properties and phase equilibria across the lanthanides, since there is little experimental data available for the Al–Tm and Al–Lu systems. The trends of thermodynamic properties shown in present study are the same as those from [16].

6.2 Thermodynamic models and optimization strategies

The thermodynamic properties of pure Al and heavy rare earths (Gd, Tb, Dy, Ho, and Er) are taken from SGTE database [18], except the Gd, Dy, Ho, and Er in the FCC–structure and Ho and Er in BCC–structure taken from Kang et al. [19]. All the present optimizations have been carried out by means of the FactSage thermodynamic software [20, 21]. A list of all phases appeared in the five binary systems considered in present study is given in Table 6.1.

Table 6.1 Crystallographic structures of all phases in the Al-Gd, Al-Tb, Al-Dy, Al-Ho and Al-Er systems

Phases	Struktur-bericht	Prototype	Pearson Symbol	Space Group	Model	Stable end-members
liquid	-	-	-	-	MQM	
FCC	A1	Cu	cF4	$Fm\bar{3}m$	CEF	Al
BCC	A2	W	cI2	$Im\bar{3}m$	CEF	Gd, Tb, Dy
HCP	A3	Mg	hP2	$P6_3/mmc$	CEF	Gd, Tb, Dy,Ho, Er
Laves-C15	C15	Cu_2Mg	cF24	$Fd\bar{3}m$	CEF	Al_2Gd, Al_2Tb, Al_2Dy, Al_2Ho, Al_2Er
Gd_2Al	C23	Co_2Si	oP12	Pnma	ST	
Gd_3Al_2	-	Al_2Zr_3	tP20	$P4_2/mnm$	ST	
GdAl	-	ErAl	oP16	Pmma	ST	
$GdAl_3$	$D0_{19}$	Ni_3Sn	hP8	$P6_3/mmc$	ST	
Tb_2Al	C23	Co_2Si	oP12	Pnma	ST	
Tb_3Al_2	-	Al_2Zr_3	tP20	$P4_2/mnm$	ST	
TbAl	-	ErAl	oP16	Pmma	ST	
$TbAl_3$	-	$BaPb_3$	hR12	$R\bar{3}m$	ST	
Dy_2Al	C23	Co_2Si	oP12	Pnma	ST	
Dy_3Al_2	-	Al_2Zr_3	tP20	$P4_2/mnm$	ST	
DyAl	-	ErAl	oP16	Pmma	ST	
$\alpha DyAl_3$	$D0_{24}$	Ni_3Ti	hP16	$P6_3/mmc$	ST	
$\beta DyAl_3$	-	Al_3Ho	hR20	$R\bar{3}m$	ST	

Ho$_2$Al	C23	Co$_2$Si	oP12	Pnma	ST	
Ho$_3$Al$_2$	-	Al$_2$Zr$_3$	tP20	P4$_2$/mnm	ST	
HoAl	-	ErAl	oP16	Pmma	ST	
HoAl$_3$	-	Al$_3$Ho	hR20	R$\bar{3}$m	ST	
Er$_2$Al	C23	Co$_2$Si	oP12	Pnma	ST	
Er$_3$Al$_2$	-	Al$_2$Zr$_3$	tP20	P4$_2$/mnm	ST	
ErAl	-	ErAl	oP16	Pmma	ST	
ErAl$_3$	L1$_2$	AuCu$_3$	cP4	Pm$\bar{3}$m	ST	

MQM = Modified Quasichemical Model, CEF = Compound Energy Formalism, ST = Stoichiometric

6.2.1 Modified Quasichemical Model (MQM) for the liquid phase

The MQM in the pair approximation [22] was used to model the thermodynamic properties of the liquid solution. A detailed description of the MQM and its associated notation are given by Pelton et al. [22]. The same notation is used in the present article. As a brief introduction to this model, the reader is referred to the paper [16] for Al–light rare earth systems. The composition of maximum short–range ordering (SRO) is determined by the ratio of the coordination numbers Z_{ij}^i / Z_{ij}^j. The values of the coordination numbers chosen in the present study, which are the same as those for Al–light rare earth systems [16] are listed in Table 6.2.

Table 6.2 Optimized model parameters of the MQM for the liquid in Al–Gd, Al–Tb, Al–Dy,   Al–Ho   and   Al–Er   phases   with   the   format   of $\Delta g_{AlRE} = (a_{00} + b_{00}T) + (a_{10} + b_{10}T)X_{AlAl} + (a_{01})X_{RERE}$ (see equation (6.4) in the text).

Coordination numbers				Gibbs energies of pair exchange reactions
i	j	Z_{ij}^i	Z_{ij}^j	
Al	Gd	3	6	Δg_{AlGd}= -48,116 +5.02T + (-3,264 -1.80T)X$_{AlAl}$ -7,113X$_{GdGd}$

Al	Tb	3	6	Δg_{AlTb}= -44,350 +4.60T + (-5,230 -2.09T)X_{AlAl} -13,389X_{TbTb}
Al	Dy	3	6	Δg_{AlDy}= -47,279 +4.18T + (-3,347 -1.67T)X_{AlAl} -8,786X_{DyDy}
Al	Ho	3	6	Δg_{AlHo}= -46,944 +4.18T + (-3,766 -2.09T)X_{AlAl} -11,715X_{HoHo}
Al	Er	3	6	Δg_{AlEr}= -46,861 +4.18T + (-1.67T)X_{AlAl} -14,519X_{ErEr}

The MQM has been successfully applied to alloy solutions [23, 24], molten oxides [25, 26], molten salts [27-29], and molten sulphides [30]. Generally, as discussed by Pelton and Kang [31], the use of the MQM for the liquid phase render better estimations of the thermodynamic properties in the multi–component systems.

6.2.2 Compound Energy Formalism for solid solutions

The compound energy formalism was introduced by Hillert [32] to describe the Gibbs energy of solid solution phases with sub–lattices. Ideal mixing on each sub–lattice is assumed. The same notation for the model is used as described in Kang et al. [15].

6.2.3 Optimization Strategies

Unlike the previous optimizations of Al–RE systems, all of which used the Bragg–Williams random mixing approximation with the Redlich-Kister/Muggianu expansion of the excess terms for the liquid (except the previous studies from our group using MQM for the liquid [15, 16] for Al–RE systems (RE=Sc, Y, La, Ce, Pr, Nd, and Sm) and one from Zhou et al. [33] using association model for the liquid in Al–La system), all the optimizations in current study employ the MQM for the liquid to take into account the high degree of short–range ordering which is evidenced by the very negative enthalpy of mixing curve in the liquid for all the Al–RE binary systems.

Based on the similarities mentioned before for the Al–RE systems, the same optimization strategy [16] is used in the present study for Al–heavy rare earth systems (Al–Gd, Al–Tb,

Al–Dy, Al–Ho and Al–Er systems, and these systems are evaluated and assessed systematically. Moreover, the same trends are observed across all the Al–RE systems (Al–light rare earth systems and Al–heavy rare earth systems).

In order to account for the short–range ordering (SRO) around the composition $X_{RE} = 1/3$, Z_{AlRE}^{Al} was set to 3, Z_{AlRE}^{RE} was set to 6 ($Z_{AlRE}^{Al} / Z_{AlRE}^{RE} = 1/2$), $Z_{AlAl}^{Al} = Z_{RERE}^{RE} = 6$. Moreover, the coordination numbers Z_{Al} and Z_{RE} were permitted to vary with the composition as following functions (6.1) and (6.2):

$$\frac{1}{Z_{Al}} = \frac{1}{6} \left(\frac{2n_{AlAl}}{2n_{AlAl} + n_{AlRE}} \right) + \frac{1}{3} \left(\frac{n_{AlRE}}{2n_{AlAl} + n_{AlRE}} \right) , \tag{6.1}$$

$$\frac{1}{Z_{RE}} = \frac{1}{6} \left(\frac{2n_{RERE}}{2n_{RERE} + n_{AlRE}} \right) + \frac{1}{6} \left(\frac{n_{AlRE}}{2n_{RERE} + n_{AlRE}} \right) . \tag{6.2}$$

Furthermore, for the pair exchange reaction in the Al–RE systems

$$(Al - Al)_{pair} + (RE - RE)_{pair} = 2 \, (Al - RE)_{pair} , \qquad \Delta g_{AlRE} \tag{6.3}$$
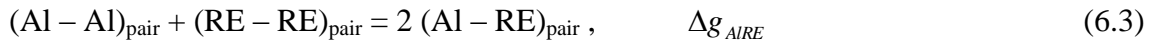
Where $(Al - Al)_{pair}$, $(RE - RE)_{pair}$, and $(Al - RE)_{pair}$ represents a first–nearest–neighbour pair of atom. Δg_{AlRE} is the nonconfigurational Gibbs energy change for the formation of two moles of $(Al - RE)$ pairs since one mole of (Al-Al) pairs and one mole of (RE-RE) pairs produce two moles of $(Al - RE)$ pairs.

Δg_{AlRE} is constrained to the following expression (6.4):

$$\Delta g_{AlRE} = (a_{00} + b_{00}T) + (a_{10} + b_{10}T)X_{AlAl} + (a_{01})X_{RERE} ,$$
(6.4)

Where a_{00}, b_{00}, a_{10}, b_{10} and a_{01} were optimized parameters which are independent of temperature and composition. This proposed function keeps the consistency with Al–light rare earth systems. Most importantly, it is judged not necessary to introduce extra modeling parameters in order to have a good fit between the calculated data and experimental data. All the parameters for Δg_{AlRE} in each binary liquid alloy are given in Table 6.2.

6.3 Thermodynamic assessment of binary systems

6.3.1 The Al–Gd system

The Al–Gd system has been critically assessed by Gschneidner and Calderwood [34]. The Al–rich region has been investigated by Runnalls and Boucher [35], the Gd–rich part by Copeland and Kato [36] and the entire region by Buschow [37]. More recently, the phase equilibria in the 0 to 66.7 at. % Al composition range has been studied by Saccone et al. [38]. According to the review of De Negri et al. [39] and Cacciamani et al. [40], there are four intermetallic compounds: Gd_2Al, Gd_3Al_2, GdAl, and $GdAl_3$. $GdAl_2$ is considered as a Laves–C15 solid solution. $GdAl_4$ has been reported by Runnalls and Boucher [35], but not by Buschow [37]. Gd_3Al has been found by Copeland and Kato [36], but it was suggested by Buschow and Van Vucht [6] that Gd_3Al may be stabilized by impurities. All the phases of this system considered in current paper are shown in Table 6.1.

The previous thermodynamic optimizations by Gröbner et al. [41] and Cacciamani et al. [40] assuming Bragg–Williams (BW) random mixing of atoms in the liquid solution reproduced the phase diagram quite well (the thermodynamic model parameters were not shown in the paper of Gröbner et al. [41]). However, the enthalpies of mixing of the

liquid measured later on by Kanibolotsky et al. [42] were not well reproduced by the BW models, as shown in Figure 6.1. The calculated partial enthalpy of mixing of the liquid is compared with experimental data [42, 43] and shown in Figure 6.2.
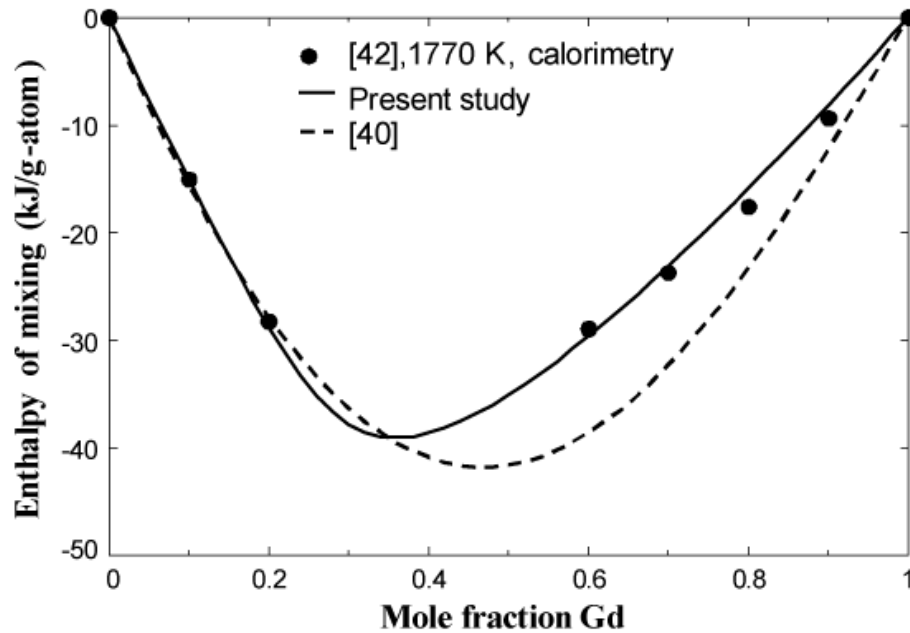
Figure 6.1 Calculated enthalpies of mixing of Al and Gd in liquid Al–Gd alloy at 1770 K. Comparison of experimental data [42] with calculations from present study and from [40].
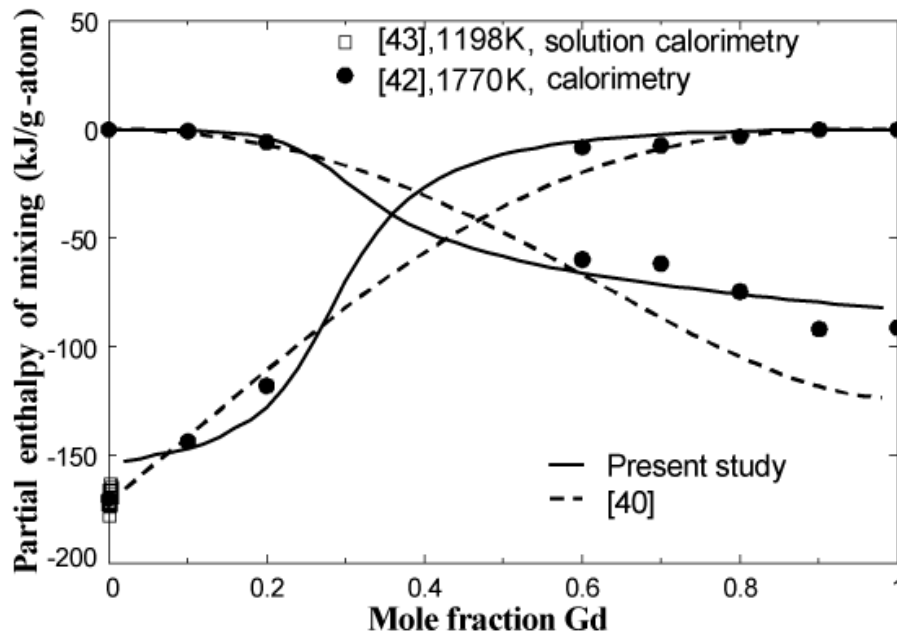
Figure 6.2 Calculated partial enthalpy of mixing of Al and Gd in liquid Al–Gd alloy at 1770 K. Comparison of experimental data [42, 43] with calculations from present study and from [40]'s sets of parameters.

The calculated entropy of mixing in liquid Al–Gd alloys at 1873 K is presented in Figure 6.3 showing a minimum value near $X_{Gd} = 1/3$ and compared with previous optimization [40]. The calculated entropy of mixing in the present study seems to be more reasonable than one calculated from Cacciamani et al.'s [40] set of parameters, as their minimum value is around -8 J/mol-K. It is worth noting that the large negative value of the entropy of mixing in the model of Cacciamani et al. [40] results in a spurious liquid–liquid miscibility gap at high temperatures [15, 44].
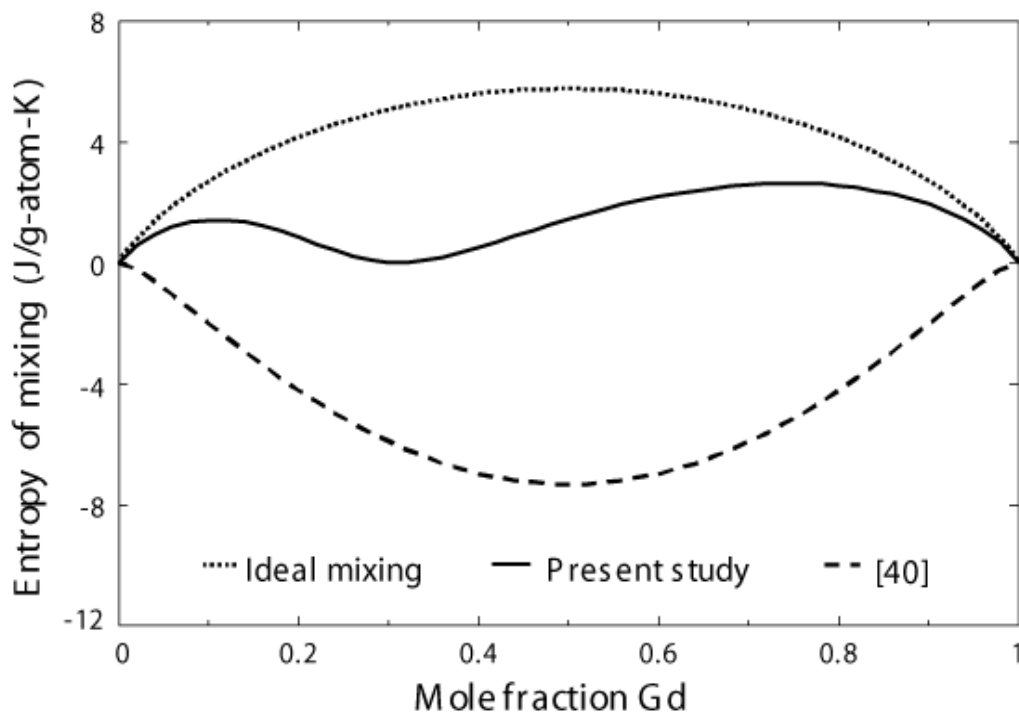
Figure 6.3 The calculated entropy of mixing in liquid Al–Gd alloys at 1873 K.
Comparison of calculations from present study with the one calculated from [40]'s sets of
parameters.

The calculated enthalpy of formation for the stable intermetallic compounds at 298 K in
the Al–Gd system is shown in Figure 6.4, as compared with experimental data and ab-
initio data [45-47]. It may be pointed out that the enthalpy of formation measured by
Kober et al. [48] was derived from their electromotive force (e. m. f) measurements and
was inconsistent with other calorimetrical data, thus it was not shown in present study.
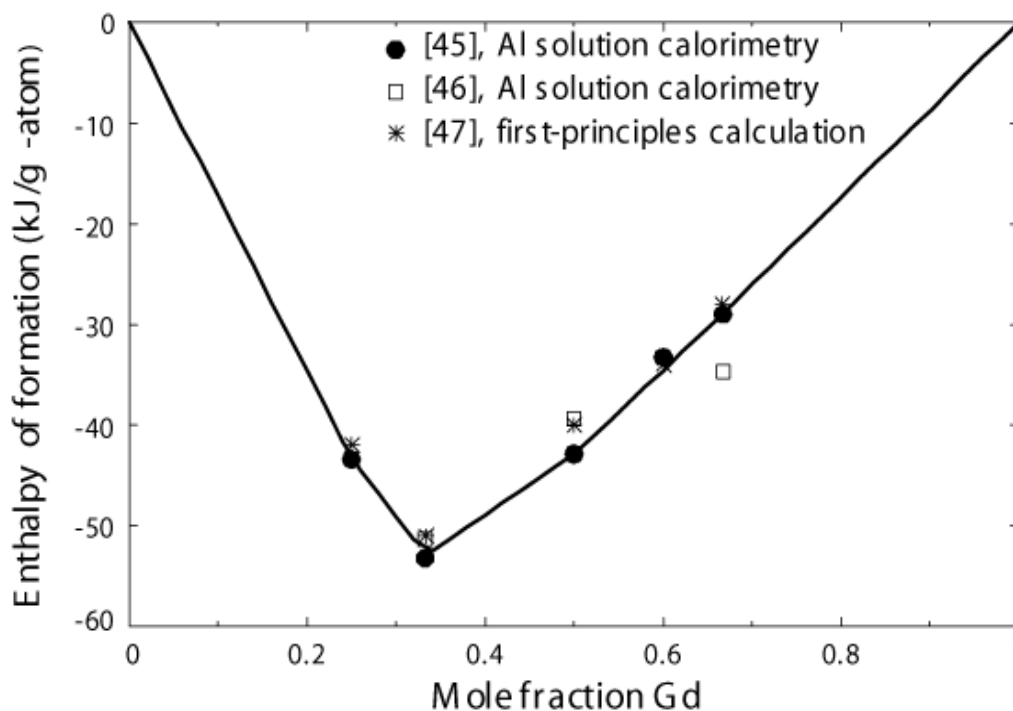
Figure 6.4 The calculated enthalpy of formation for the stable intermetallic compounds in the Al–Gd system at 298 K. Present calculation compared to the experimental data and ab-initio data [45-47].

The calculated phase diagram of the Al–Gd system shown in Figure 6.5 is compared with the experimental data [37, 38, 49]. There are no data available on the solubility of Gd in Al–FCC phase. The calculated limiting liquidus slope at $X_{Al} = 1.0$ is consistent with the one calculated by the Van't Hoff equation when solid solubility is negligible. Therefore, no solid solubility of Gd in Al–FCC phase was assumed. The calculated non–stoichiometry of the GdAl$_2$ Laves–C15 phase is negligible. The optimized model parameters of the present study are shown in Tables 6.2-6.4.

Table 6.3 Optimized CEF model parameters of solid solutions for the Al-Gd, Al-Tb, Al-Dy, Al-Ho and Al-Er binary systems (kJ/mol).

Laves-C15 (Cu₂Mg type): (Al, Gd, Tb, Dy, Ho, Er)₂[Al, Gd, Tb, Dy, Ho, Er]	
$G_{Al:Al}$ = 3**GHSERAL** + 43,959 + 62.76T *	$G_{Al:Gd}$ = 2**GHSERAL** + **GHSERGD** – 159,000 + 10.6T
$G_{Gd:Gd}$ = 3**GHSERGD** + 125,520	$G_{Al:Tb}$ = 2**GHSERAL** + **GHSERTB** – 158,000 + 14.6T
$G_{Tb:Tb}$ = 3**GHSERTB** + 125,520	$G_{Al:Dy}$ = 2**GHSERAL** + **GHSERDY** – 158,300 + 11.5T
$G_{Dy:Dy}$ = 3**GHSERDY** + 125,520	$G_{Al:Ho}$ = 2**GHSERAL** + **GHSERHO** – 157,500 + 10.8T
$G_{Ho:Ho}$ = 3**GHSERHO** + 125,520	$G_{Al:Er}$ = 2**GHSERAL** + **GHSERER** – 151,500 + 2.4T
$G_{Er:Er}$ = 3**GHSERER** + 125,520	$G_{Gd:Al}$ = 2**GHSERGD** + **GHSERAL** + 41,840
$G_{Ho:Al}$ = 2**GHSERHO** + **GHSERAL** + 41,840	$G_{Tb:Al}$ = 2**GHSERTB** + **GHSERAL** + 41,840
$G_{Er:Al}$ = 2**GHSERER** + **GHSERAL** + 41,840	$G_{Dy:Al}$ = 2**GHSERDY** + **GHSERAL** + 41,840
FCC: (Al, Gd, Tb, Dy, Ho, Er)	
G(Gd, FCC) = **GHSERGD** + 1,000 *	G(Ho, FCC) = **GHSERHO** + 1,600 *
G(Dy, FCC) = **GHSERDY** + 900 *	G(Er, FCC) = **GHSERER** + 2,300 *
HCP: (Al, Gd)	
L(Al, Gd) = -37,656	
BCC: (Al, Gd, Tb, Dy, Ho, Er)	
G(Ho, BCC) = **GHSERHO** + 4,380 – 2.5T *	G(Er, BCC) = **GHSERER** + 4,600 – 2.5T *
L(Al, Gd) = -55,647	L(Al, Dy) = -64,015

Note: * from [31]

Table 6.4 Optimized model parameters of stoichiometric compounds in the Al–Gd, Al–Tb, Al–Dy, Al–Ho and Al–Er binary systems.

Compound	$\Delta H^o_{25°C}$ (J/mol)	$S^o_{25°C}$ (J/mol-K)	C_p (J/mol-K)
Gd_2Al	-87,000	162.98	$C_p=2C_p$ (Gd, HCP–A3) + C_p(Al,FCC–A1)
Gd_3Al_2	-173,000	254.91	$C_p=3C_p$ (Gd, HCP–A3) + $2C_p$(Al,FCC–A1)
GdAl	-85,800	91.39	$C_p=C_p$ (Gd, HCP–A3) + C_p(Al,FCC–A1)
$GdAl_3$	-173,600	141.73	$C_p=C_p$ (Gd, HCP–A3) + $3C_p$(Al,FCC–A1)
Tb_2Al	-88,300	170.21	$C_p=2C_p$ (Tb, HCP–A3) + C_p(Al,FCC–A1)
Tb_3Al_2	-174,000	265.37	$C_p=3C_p$ (Tb, HCP–A3) + $2C_p$(Al,FCC–A1)
TbAl	-85,300	94.70	$C_p=C_p$ (Tb, HCP–A3) + C_p(Al,FCC–A1)
$TbAl_3$	-173,700	141.09	$C_p=C_p$ (Tb, HCP–A3) + $3C_p$(Al,FCC–A1)
Dy_2Al	-89,600	173.94	$C_p=2C_p$ (Dy, HCP–A3) + C_p(Al,FCC–A1)
Dy_3Al_2	-175,700	272.16	$C_p=3C_p$ (Dy, HCP–A3) + $2C_p$(Al,FCC–A1)
DyAl	-84,600	98.66	$C_p=C_p$ (Dy, HCP–A3) + C_p(Al,FCC–A1)
$\alpha DyAl_3$	-175,100	145.07	$C_p=C_p$ (Dy, HCP–A3) + $3C_p$(Al,FCC–A1)
$\beta DyAl_3$*	-174,100	145.85	$C_p=C_p$ (Dy, HCP–A3) + $3C_p$(Al,FCC–A1)
Ho_2Al	-89,500	174.91	$C_p=2C_p$ (Ho, HCP–A3) + C_p(Al,FCC–A1)
Ho_3Al_2	-173,300	274.64	$C_p=3C_p$ (Ho, HCP–A3) + $2C_p$(Al,FCC–A1)
HoAl	-83,000	100.03	$C_p=C_p$ (Ho, HCP–A3) + C_p(Al,FCC–A1)
$HoAl_3$	-173,000	146.42	$C_p=C_p$ (Ho, HCP–A3) + $3C_p$(Al,FCC–A1)
Er_2Al	-91,000	173.53	$C_p=2C_p$ (Er, HCP–A3) + C_p(Al,FCC–A1) - 4.5
Er_3Al_2	-180,000	273.75	$C_p=3C_p$ (Er, HCP–A3) + $2C_p$(Al,FCC–A1) - 9
ErAl	-84,000	100.06	$C_p=C_p$ (Er, HCP–A3) + C_p(Al,FCC–A1) - 4.5
$ErAl_3$	-160,000	156.31	$C_p=C_p$ (Er, HCP–A3) + $3C_p$(Al,FCC–A1) - 9

note : * High-temperature stable compounds
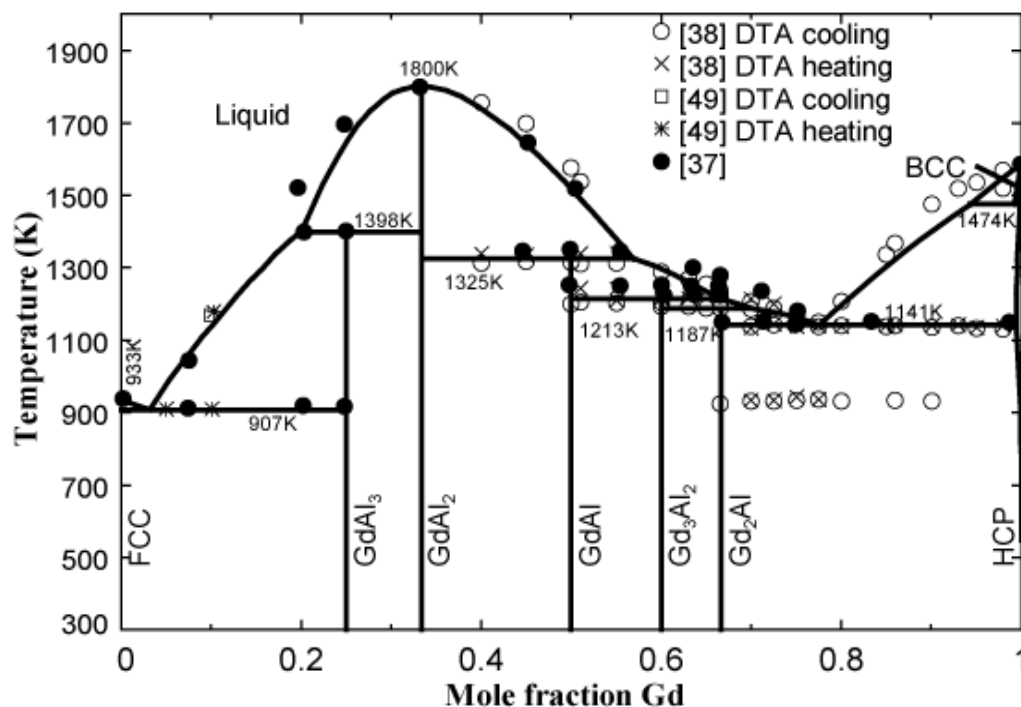
Figure 6.5 The calculated phase diagram of the Al–Gd system compared with the experimental data [37, 38, 49].

6.3.2 The Al–Dy system

The Al–Dy system has been reviewed by Gschneidner and Calderwood [50] for the Al–rich part, by Okamoto [51] and by Franke and Neuschütz [52] for the whole region. This system has been thermodynamically optimized by Cacciamani et al. [40] based on the experimental data. The Al–rich part of the Al–Dy system has been investigated by Casteels [53] and by Copeland and Kato [36], while recently this binary system has been studied by Saccone et al. [38] in the region of 0 to 66.7 at. % Al. Casteels [53] verified the existence of the allotropic transformation for $DyAl_3$ intermetallic compound, although the crystal structure type was disputable [6, 54]. According to the recent review of Franke and Neuschütz [52], there are four intermetallic compounds, while $DyAl_3$, have two allotropes (Dy_2Al, Dy_3Al_2, $DyAl$, $\alpha DyAl_3$ and $\beta DyAl_3$). $DyAl_2$ is considered as a Laves–C15 phase. All phases of this system considered in current study are presented in Table 6.1.

The calculated enthalpy of mixing for the liquid at 1873 K is shown in Figure 6.6 and compared with the optimization of Cacciamani et al. [40], although there is no experimental data available. Like the Al–Gd system, the Al–Dy system exhibits very stable intermetallic compounds, one of which is $DyAl_2$ with highest melting temperature of 1763 K. The same modelling strategy and similar model parameters for the liquid Al–Dy alloy were used based on the similarities among rare earth elements and alloys with other Al–RE systems. Taken SRO into account for the liquid, the composition of maximum SRO was set around $X_{Dy} = 1/3$. The calculated minimum of enthalpy of mixing in the Al–Dy liquid is close to that in the Al–Gd system.
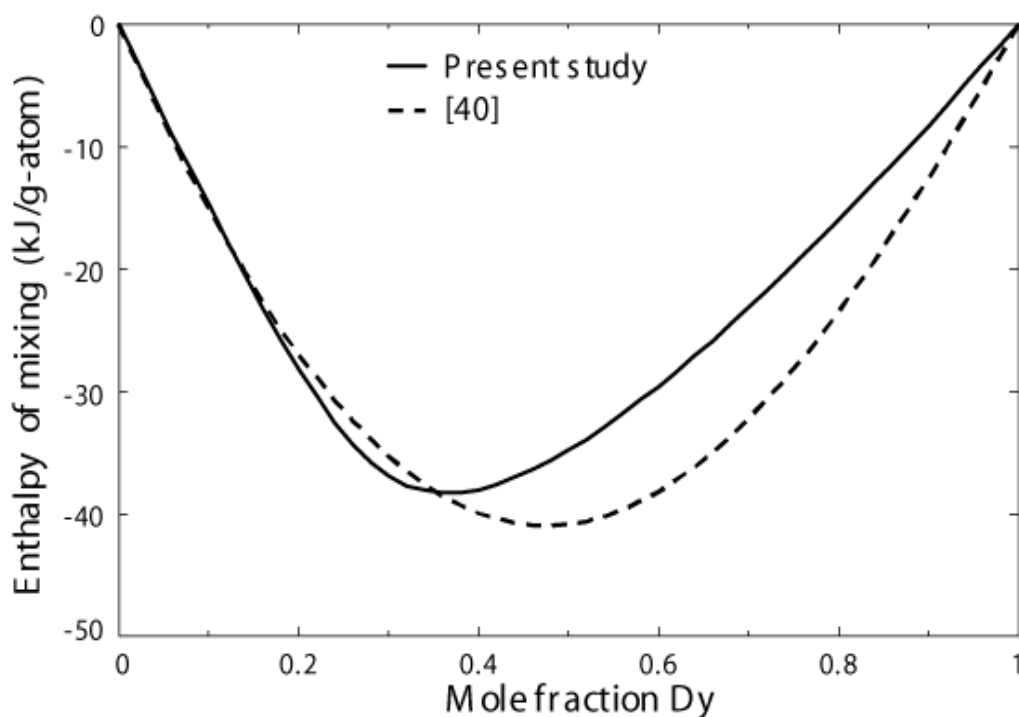
Figure 6.6 The calculated enthalpy of mixing of Al and Dy in Al–Dy liquid at 1873 K. Comparison of calculations from present study and from [40].

The calculated entropy of mixing of the liquid at 1873 K is shown in Figure 6.7 with the minimum value near $X_{Dy} = 1/3$. The calculated entropy of mixing of the liquid in present study seems to be more reasonable than the one calculated from Cacciamani et al. [40]'s

set of parameters, as their minimum value is around -10 J/mol-K and it causes a spurious liquid–liquid miscibility gap at high temperatures [15, 44].
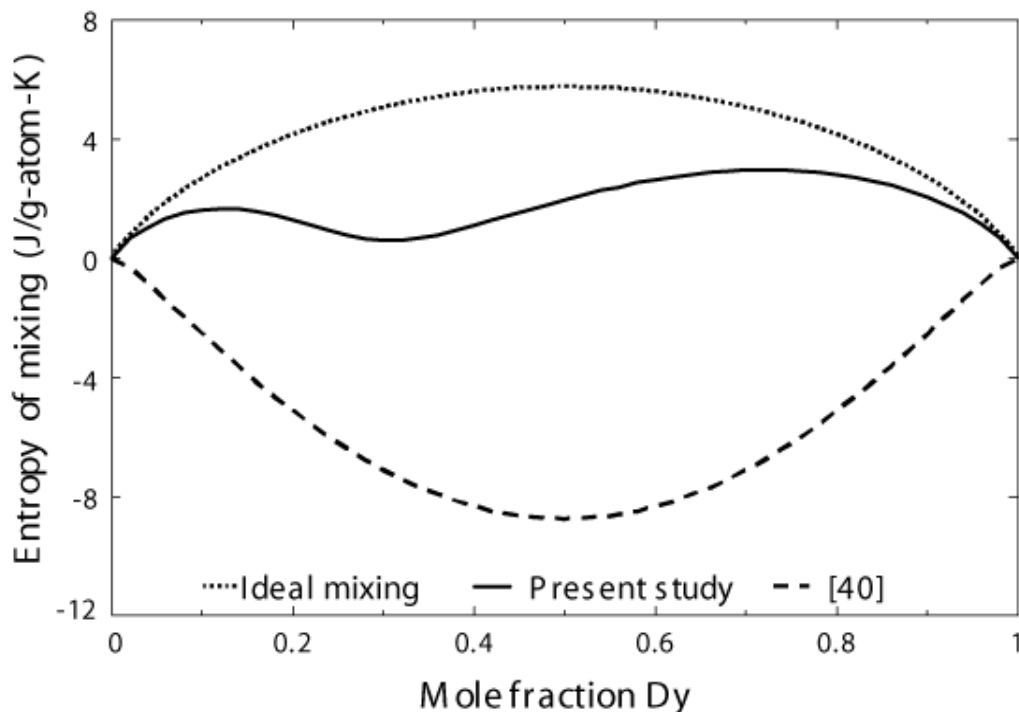
Figure 6.7 The calculated entropy of mixing in liquid Al–Dy alloys at 1873 K. Comparison of calculations from present study with the one calculated from [40]'s sets of parameters.

The calculated enthalpy of formation for the stable intermetallic compounds at 298 K is shown in Figure 6.8, and compared with the experimental data and ab–initio theoretical data [47, 55]. There are no other experimental data available for the intermetallic compounds. It can be seen from Figure 6.8 that the ab–initio data is likely more positive than the experimental data, but the trends are usually in agreement with the experimental data [47].
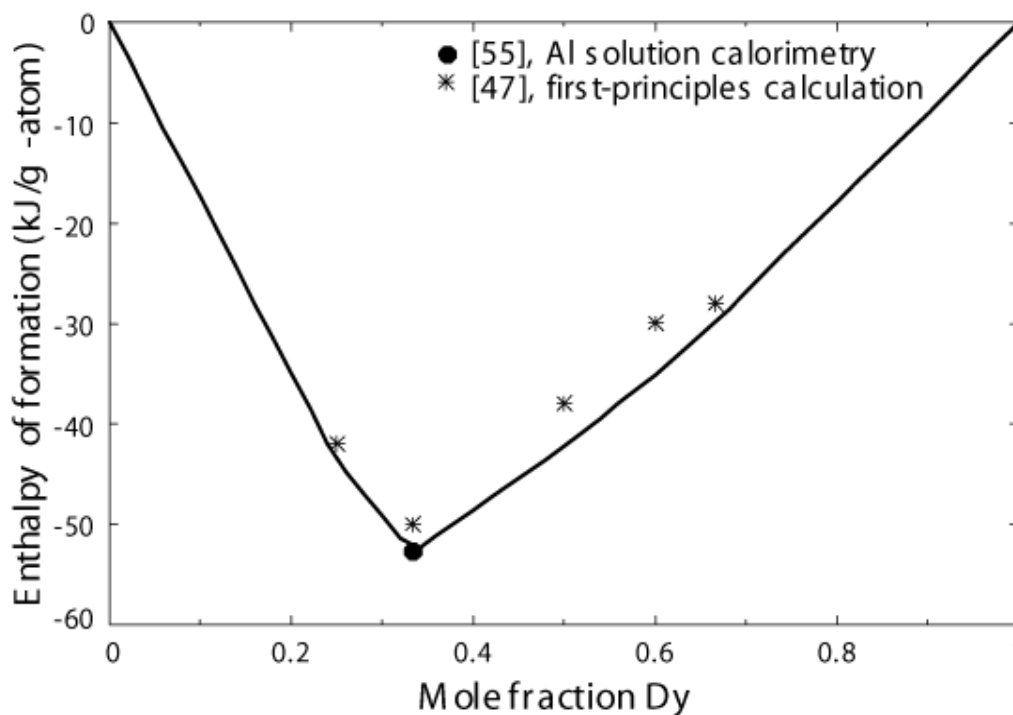
Figure 6.8 The calculated enthalpy of formation for the stable intermetallic compounds in the Al–Dy system at 298 K. Present calculation compared to the experimental data and ab–initio data from [47, 55].

The calculated phase diagram of the Al–Dy system shown in Figure 6.9 is compared with the experimental data [38, 53]. There are no data available on the solubility of Dy in Al–FCC phase. Therefore, no solid solubility of Gd in Al–FCC phase was assumed, since the calculated limiting liquidus slope at $X_{Al} = 1.0$ is consistent with the one calculated by Van't Hoff equation when solid solubility is negligible. No solid solubility of Al in Dy–HCP phase was assumed due to the lack of data. Saccone et al. [38] detected the small thermal effect around 993 K in the range of 5 to 30 at. % Al, it was suggested that it might be the metastable or impurity stabilised phase, or the allotropic transformation of the Dy_2Al intermetallic compound. Allotropic transformation of Dy_2Al was not considered in the present study in analogy with Al–Gd system. The calculated non–stoichiometry of the $DyAl_2$ Laves–C15 phase is negligible. The optimized model parameters of the present study are shown in Tables 6.2-6.4.
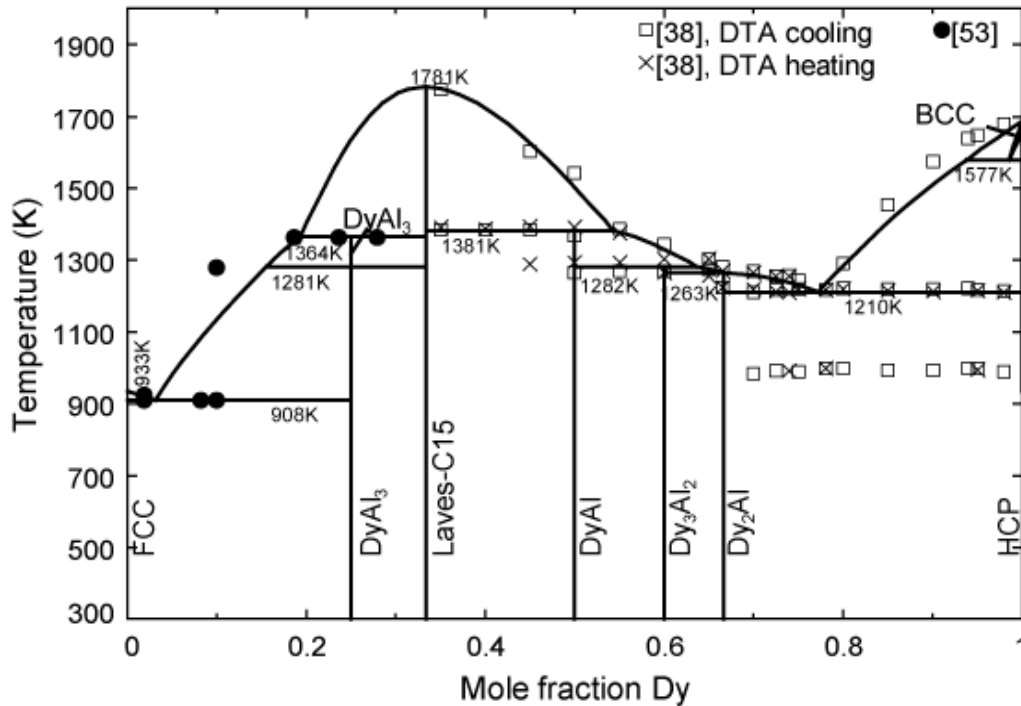
Figure 6.9 The calculated phase diagram of the Al–Dy system compared to the experimental data [38, 53].

6.3.3 The Al–Ho system

The Al–Ho system has been reviewed by Gschneidner and Calderwood [56] and by Franke and Neusch ütz [57]. It has been investigated by Meyer [58] in the composition range of 0 to 85 at. % Ho. This system has been thermodynamically optimized by Cacciamani et al. based on the experimental data. According to the recent review of Franke and Neusch ütz. [57], there are four intermetallic compounds as follows: Ho_2Al, Ho_3Al_2, $HoAl$, and $HoAl_3$. $HoAl_2$ is considered as a Laves–C15 phase. Unlike the Al–Dy system, there is no allotropic transformation for the $HoAl_3$ intermetallic compound, which was confirmed by Buschow and Van Vucht [6]. The crystal structure types of these phases were reported in the literature [59-61]. All phases of this system considered in the current study are shown in Table 6.1.

The calculated enthalpy of mixing of the liquid at 1873 K is shown in Figure 6.10, as compared with previous optimization of Cacciamani et al. [40], although there is no experimental data available. Similar to the Al–Gd and Al–Dy systems, the Al–Ho system exhibits very stable intermetallic compounds, one of which is Al_2Ho with highest melting temperature of 1802 K. The same modelling strategy was used with similar model parameters for the liquid Al–Ho alloy and the composition of maximum SRO is set around $X_{Ho} = 1/3$. The calculated minimum of enthalpy of mixing is close to that in the Al–Gd and Al–Dy systems.
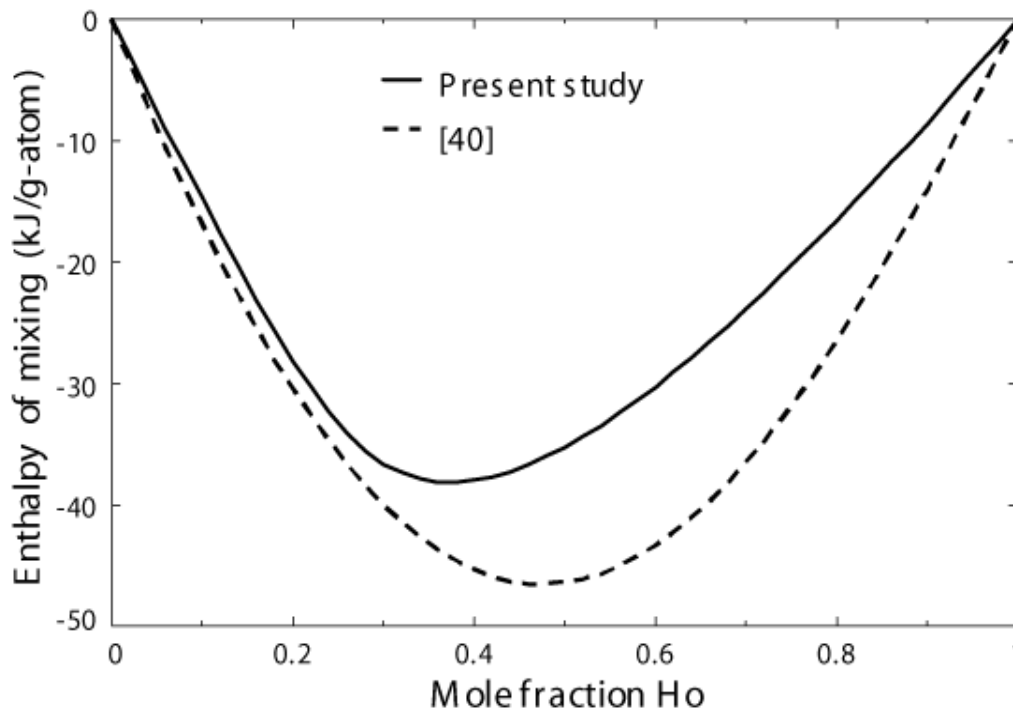
Figure 6.10 The calculated enthalpy of mixing of Al and Ho in Al–Ho liquid at 1873 K. Comparison of calculations from present study and from [40].

The calculated entropy of mixing of the liquid at 1873 K is shown in Figure 6.11 with the minimum value near $X_{Ho} = 1/3$. The calculated entropy of mixing in the present study may be more reasonable than the one calculated from Cacciamani et al.'s [40] set of parameters, as its minimum value for the entropy of mixing is around -10 J/mol-K. This large negative entropy of mixing will cause a spurious inverted miscibility gap at high temperatures [15, 44].
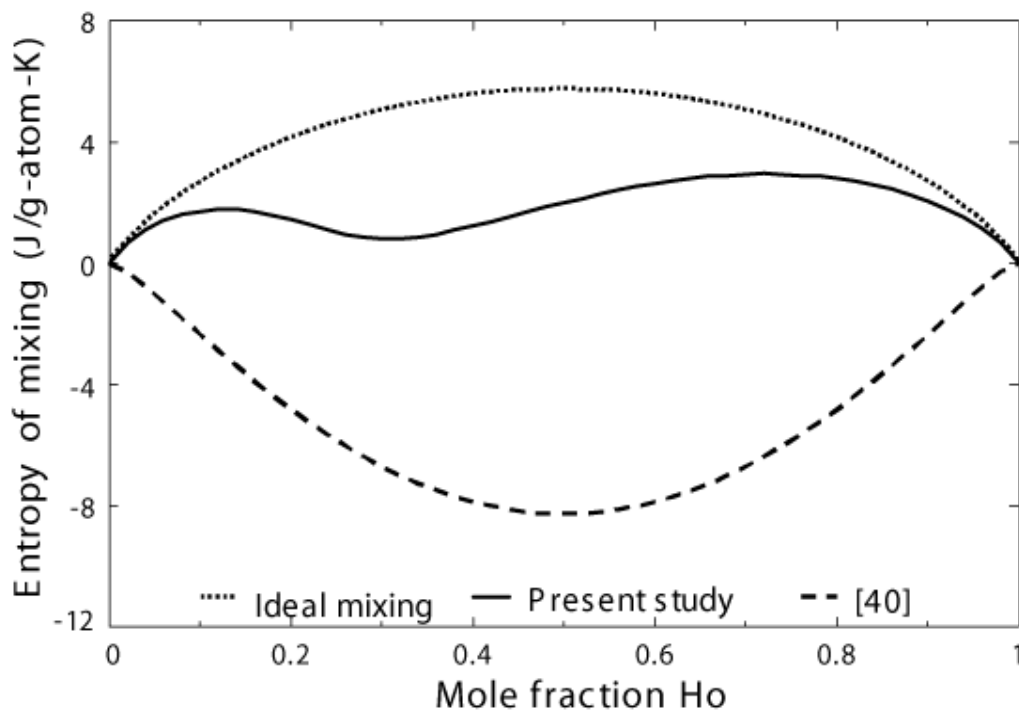
Figure 6.11 The calculated entropy of mixing in liquid Al–Ho alloy at 1873 K. Comparison of calculations from present study with the one calculated from Cacciamani et al.'s [40] set of parameters.

The calculated curve of enthalpy of formation for the stable intermetallic compounds in the Al–Ho system at 298 K is shown in Figure 6.12, and compared with the experimental data and ab–inito data [47, 55]. There are no other experimental data available for the intermetallic compounds.
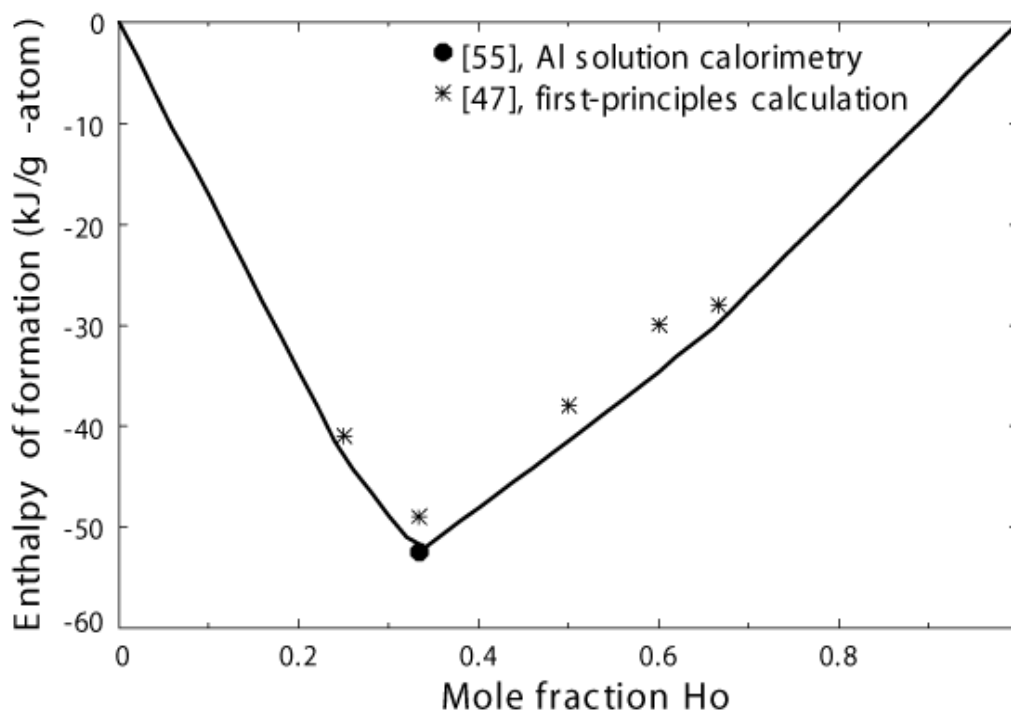
Figure 6.12 The calculated enthalpy of formation for the stable intermetallic compounds in the Al–Ho system at 298 K. Present calculation compared to the experimental data and ab–inito data [47, 55].

The calculated phase diagram of the Al–Ho system shown in Figure 6.13 is compared with the experimental data [58]. There are no data available on the solubility of Ho in Al–FCC phase. Therefore, no solid solubility of Ho in Al–FCC and of Al in Ho–HCP phase was assumed. Moreover, the calculated limiting liquidus slope at $X_{Al} = 1.0$ is consistent with the one calculated by the Van't Hoff equation when solid solubility is negligible. The calculated non–stoichiometry of the Al_2Ho Laves–C15 phase is negligible. It may be noted that the experimental data for the liquidus of Al_2Ho Laves–C15 phase is very "sharp" and very asymmetric, which is an unlikely case. It is known that Al and rare earth metals are prone to oxidize at high temperatures during the experiments. It is very difficult to criticize the experimental data of Meyer [58] since no other experimental data is available. Moreover, these data are not consistent with the similarity observed in all other Al − rare earth systems [16]. Therefore, it is decided to use similar modeling parameters in order to keep consistency with other Al − rare earth systems instead of

fitting the questionable experimental data, *i.e.* Al–Gd system where the experimental data obtained by different authors have a small scatter in Al–rich side.
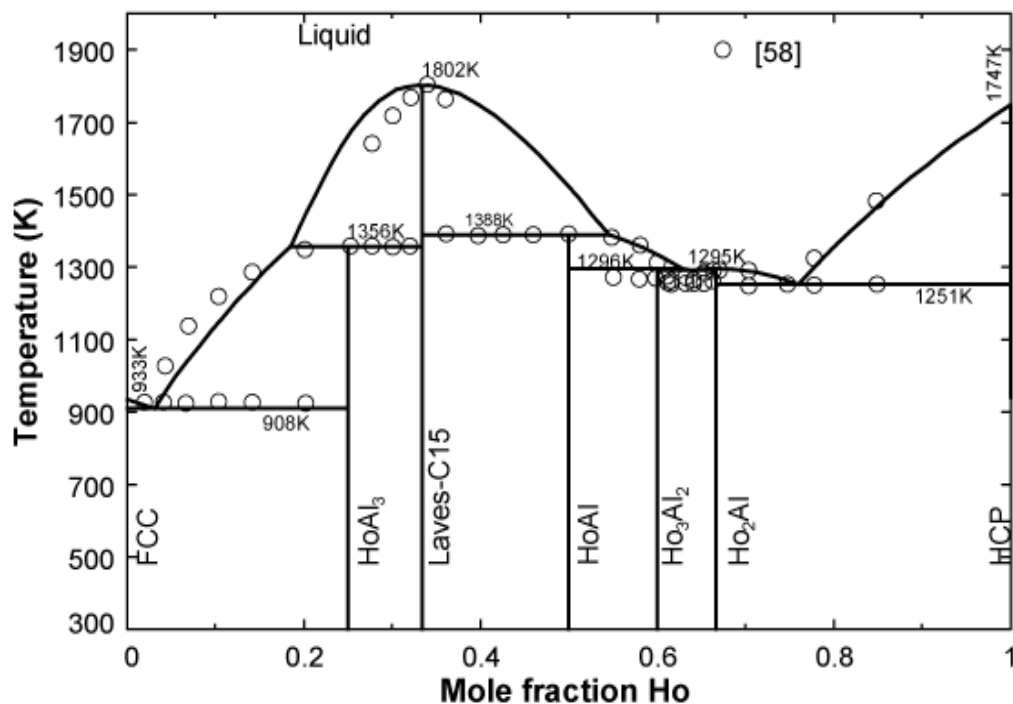
Figure 6.13 The calculated phase diagram of the Al–Ho system compared to the experimental data from [58].

The optimized model parameters in current study are presented in Tables 6.2-6.4.

6.3.4 The Al–Er System

The Al–Er system was reviewed by Gschneidner and Calderwood [62] and by Okamoto [63]. The phase diagram from Gschneidner and Calderwood [62] is mainly based on the thermodynamic investigation of Buschow [64]. Cacciamani et al. [65] optimized this system mainly based on the data of Buschow [64] and their own reinvestigations in the range of 50 to 80 at. % Er [66]. According to the compilation of Okamoto [63], there are four intermetallic compounds in the Al–Er system: Er_2Al, Er_3Al_2, $ErAl$, and $ErAl_3$. $ErAl_2$

is considered as a Laves–C15 solid solution. All phases considered for this system in present study are shown in Table 6.1.

Due to the similarities among rare earth elements and Al–RE binary systems, the same modelling strategy is used with similar model parameters for the liquid Al–Er system and the composition of maximum SRO is set around $X_{Er} = 1/3$. The enthalpy of mixing of the liquid at 1873 K is shown in Figure 6.14 compared with the previous optimization [65]. The entropy of mixing of the liquid at 1873 K is presented in Figure 6.15, together with the one calculated from Cacciamani et al.'s [65] set of parameters. As its minimum value for the entropy of mixing is around -10 J/mol-K, it will cause a spurious inverted miscibility gap at high temperatures.
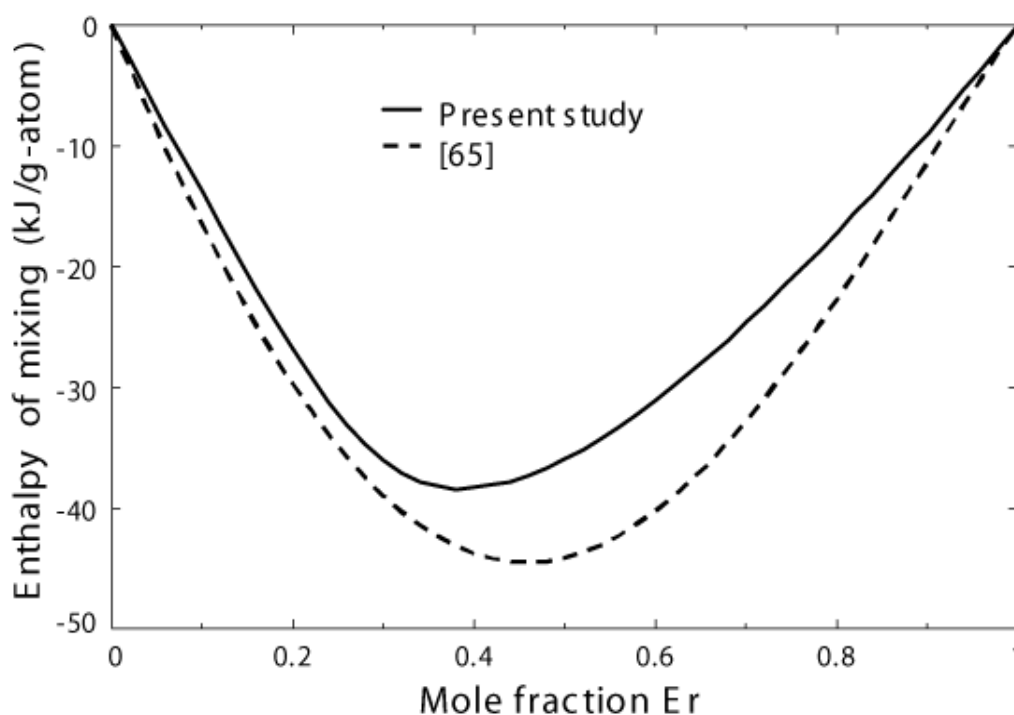
Figure 6.14 The calculated enthalpy of mixing of Al and Er in liquid Al–Er alloy at 1873 K. Present calculation compared to the calculation from [65].
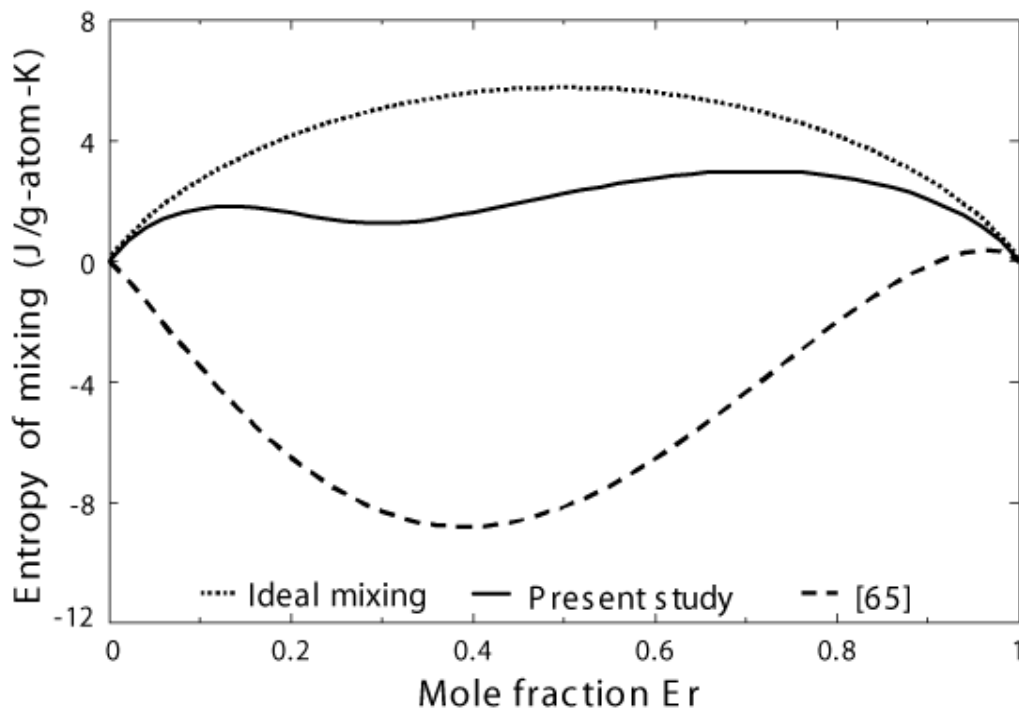
Figure 6.15 The calculated entropy of mixing in liquid Al–Er alloy at 1873 K. Comparison of calculations from present study with the one calculated from [65] 's set of parameters.

The values of $(h_T\text{-}h_{273K})$ for Al$_2$Er were reported by Merlo [67]. With these data, the difference of heat capacity (ΔCp) of ErAl$_2$ from the Kopp–Neumann rule was estimated using the same method as Kang et al. [15] employed. The other intermetallic compounds were linearly interpolated between pure Al and ErAl$_2$ or pure Er and ErAl$_2$ shown in Figure 6.16. The calculated enthalpy of formation for the stable intermetallic compounds at 298 K was shown in Figure 6.17 along with the experimental data by Colinet et al. [55], Sommer and Keita [46], and First–Principles data by Gao et al. [47].
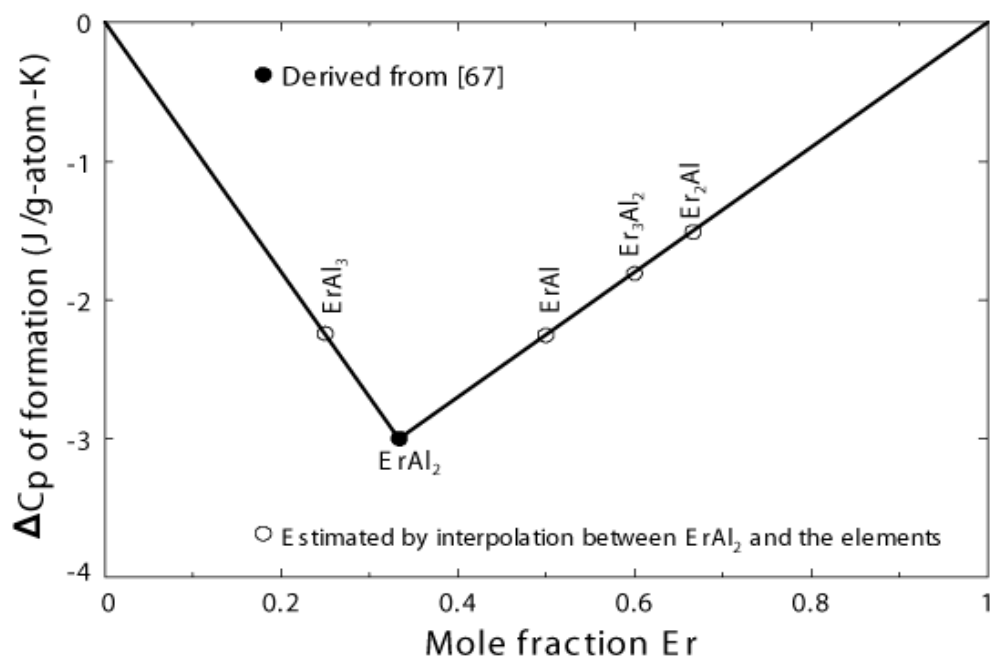
Figure 6.16 ΔC_p of formation of intermetallic compounds from Al (FCC) and Er (HCP) in Al–Er system according to the experimental data from [67].
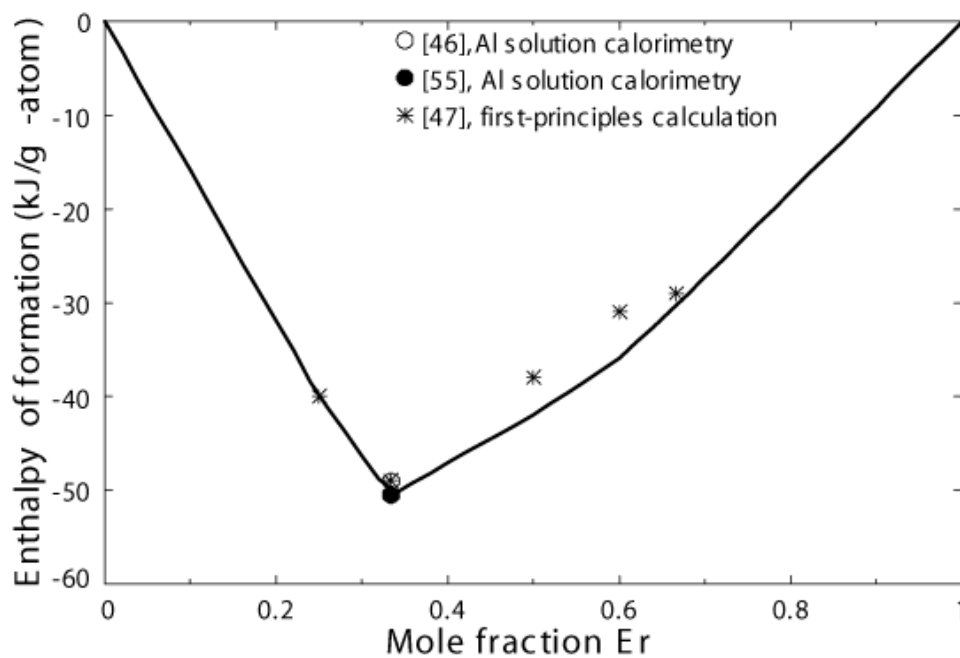
Figure 6.17 Calculated enthalpy of formation for the stable intermetallic compounds in Al–Er system at 298 K. Present calculation compared to the experimental data from [46, 55], and First–Principles data from [47].

The calculated phase diagram of the Al–Er system shown in Figure 6.18 is compared with the experimental data [64, 66]. The optimized phase diagram is in good agreement with the experimental data, and all optimized model parameters are presented in Tables 6.2-6.4.
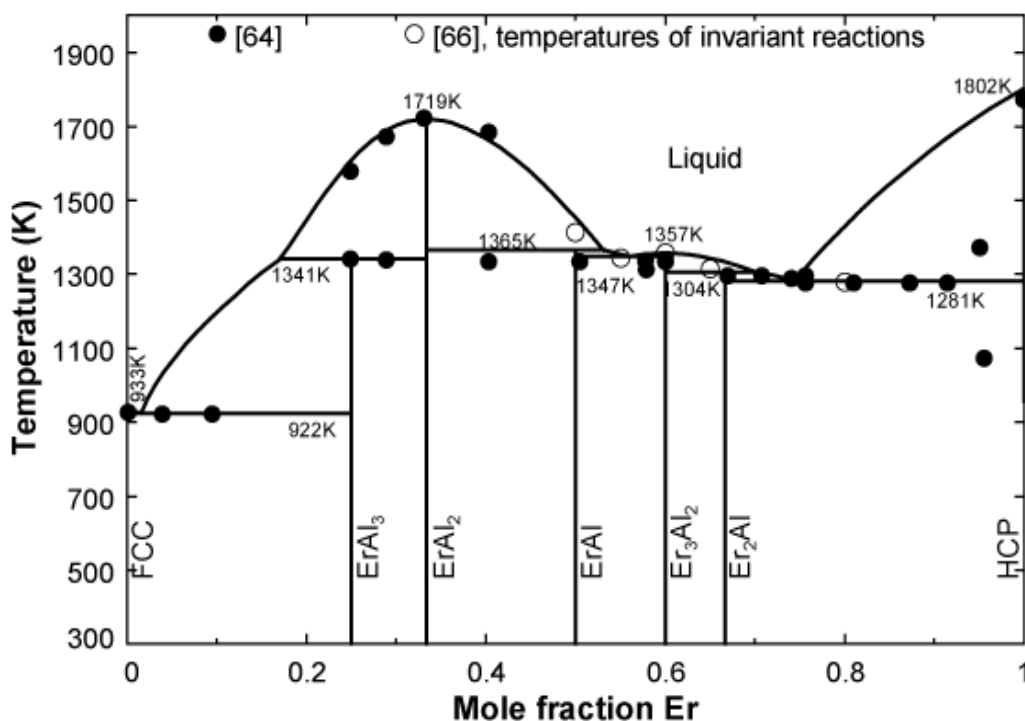
Figure 6.18 Calculated phase diagram of the Al–Er system compared to the experimental data from [64, 66].

6.3.5 Al–Tb System

The Al–Tb system was reviewed by Gschneidner and Calderwood [68] and by Predel [69]. Unfortunately, little thermodynamic information is available for the Al–Tb system. Drits et al. [70] and Runnalls and Boucher [35] have studied the Al–rich region. Runnalls and Boucher [35] reported a eutectic reaction around the composition of 10 wt. % Tb at 917 K and TbAl$_4$ compound. However, TbAl$_3$ was reported to be the Al–richest compound by Drits et al. [70]. According to the compilation of Gschneidner and

Calderwood [68], there are four intermetallic compounds: Tb_2Al, Tb_3Al_2, $TbAl$, and $TbAl_3$. $TbAl_2$ is considered as a Laves–C15 solid solution. All phases considered for this system in present study are shown in Table 6.1.

Due to the lack of the thermodynamic properties and phase equilibria for the Al–Tb system, the regular trends obtained by convenient normalization criteria were used in present study. For example, the reduced melting temperature proposed by Gschneidner [71] has been employed in order to show the trends across the lanthanides.

$$r_{temp} = \frac{T_m(RE_{1-x}Al_x)}{T_m(RE)} \ ,$$

(6.5)

where $T_m(RE_{1-x}Al_x)$ is the melting temperature of intermetallic compound $RE_{1-x}Al_x$, in Kelvin. RE is the rare earth element. $T_m(RE)$ is the melting temperature of rare earth RE.

Such a trend is summarised in the paper of Jin et al. [17]. The melting temperatures of intermetallic compounds in the Al–Tb system can be interpolated linearly according to this trend. Assuming the similarities between the Al–Gd and Al–Dy system, the Al–Tb phase diagram can be estimated. The enthalpy of mixing and entropy of mixing in the liquid at 1873 K are shown in Figure 6.19 and Figure 6.20 respectively. Like all other Al–RE systems, it should be noteworthy that the entropy of mixing seems to be reasonable. The calculated enthalpy of formation for the stable intermetallic compounds in the Al–Tb system at 298 K is shown in Figure 6.21 along with the experimental data by Colinet et al. [55], and First–Principles data by Gao et al. [47].
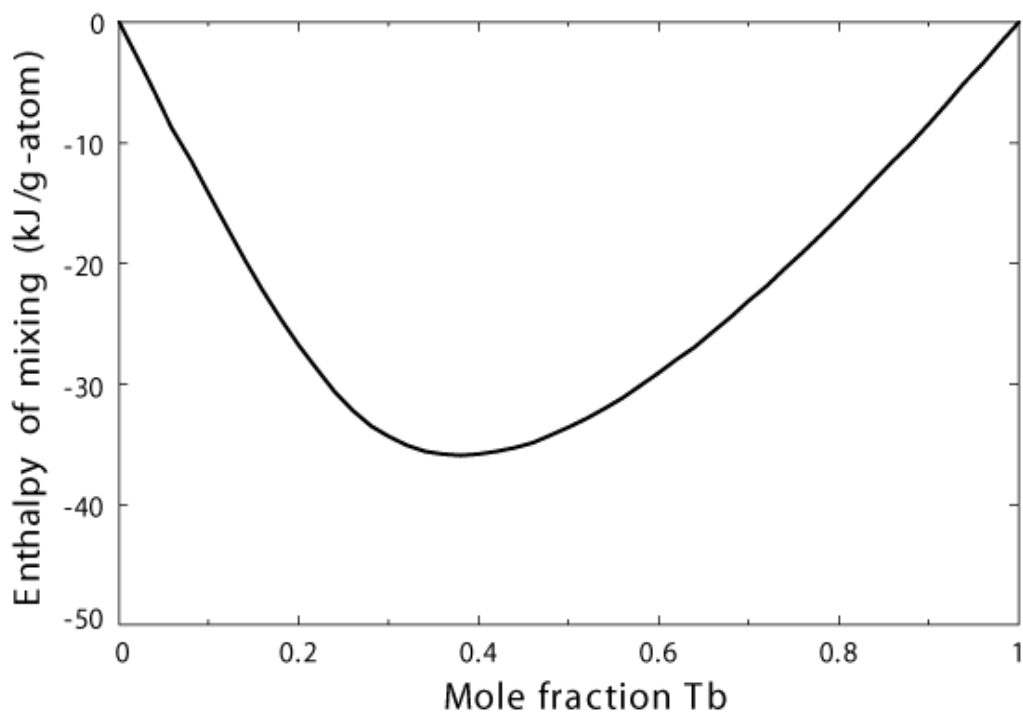
Figure 6.19 The calculated enthalpy of mixing of Al and Tb in liquid Al–Tb alloy at 1873 K.
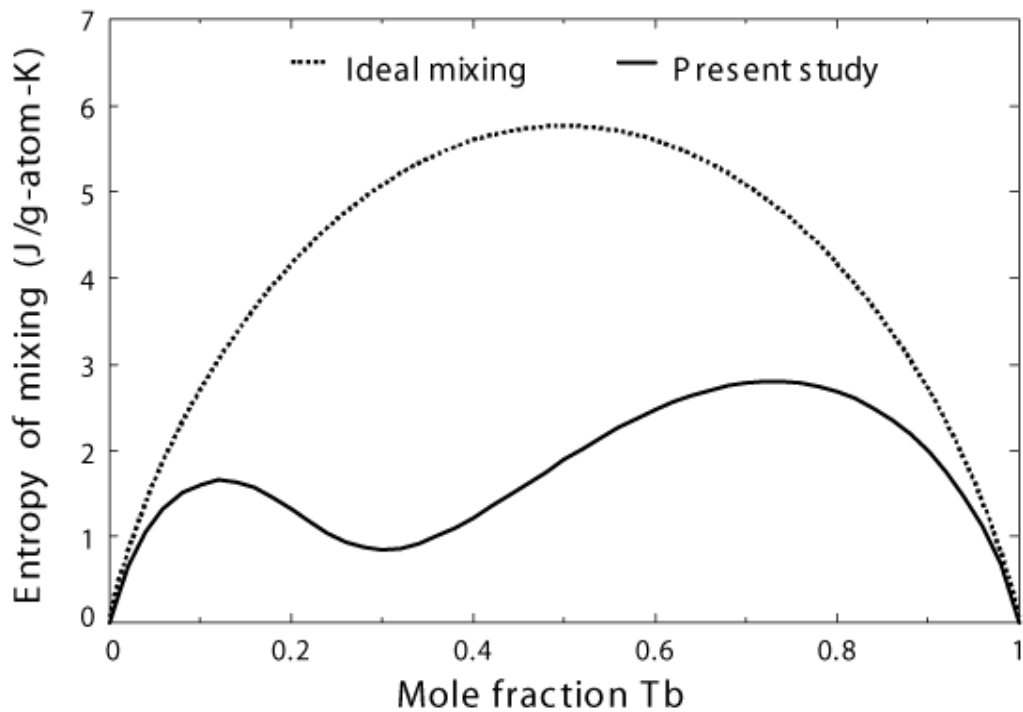
Figure 6.20 The calculated entropy of mixing in liquid Al–Tb alloy at 1873 K.
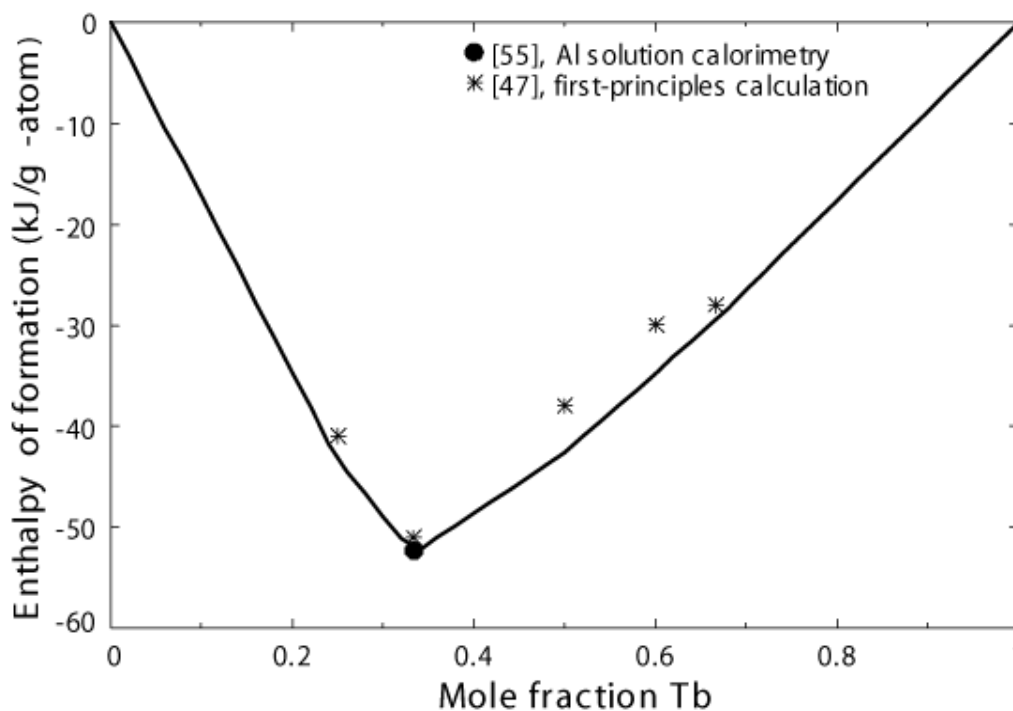
Figure 6.21 The calculated enthalpy of formation for the stable intermetallic compounds in the Al–Tb system at 298 K. Present calculation compared to the experimental data from [55] and First–Principles data from [47].

The calculated phase diagram of the Al–Tb system is presented in Figure 6.22 together with the experimental data in the Al–rich region [70]. No solid solubility of Tb in the Al–FCC phase or of Al in the Tb–HCP phase is assumed due to the lack of data. Furthermore, the calculated limiting liquidus slope at $X_{Al} =1.0$ is consistent with the one calculated by the Van't Hoff equation when solid solubility is negligible. The calculated non–stoichiometry of the $TbAl_2$ Laves–C15 phase is very small. The optimized model parameters are presented in Tables 6.2-6.4.
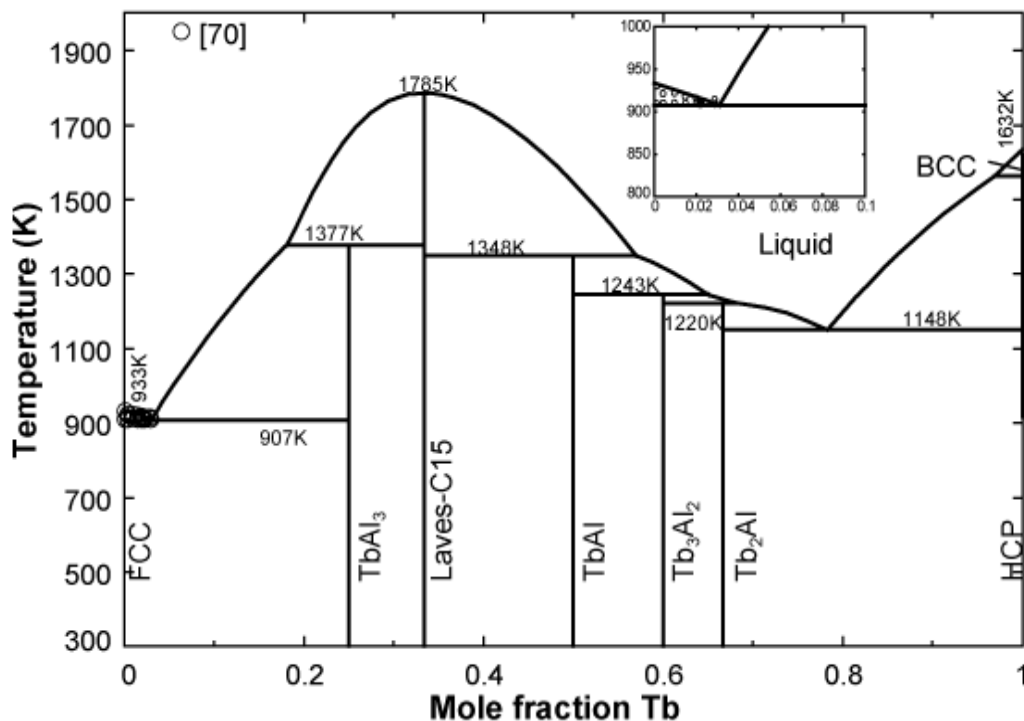
Figure 6.22 The calculated phase diagram of the Al–Tb system with the experimental data in Al–rich region from [70].

6.4 Discussions and Systematic Analysis

It has been shown in the present study that the MQM for the liquid phase reproduced the experimentally thermodynamic and phase equilibrium data well, and the value of the "m–shaped" integral entropy of mixing seems to be more realistic, unlike the very negative entropies of mixing in the previous optimizations [40, 65], which cause a spurious inverted liquid-liquid miscibility gaps. These liquid-liquid miscibility gaps in Al-heavy rare earth systems are shown in Figure 6.23 which are calculated from the liquid model proposed in [40, 65]. Moreover, the calculated partial enthalpy of mixing of the liquid in the current study reflects the strong SRO, as the experimental data indicated.
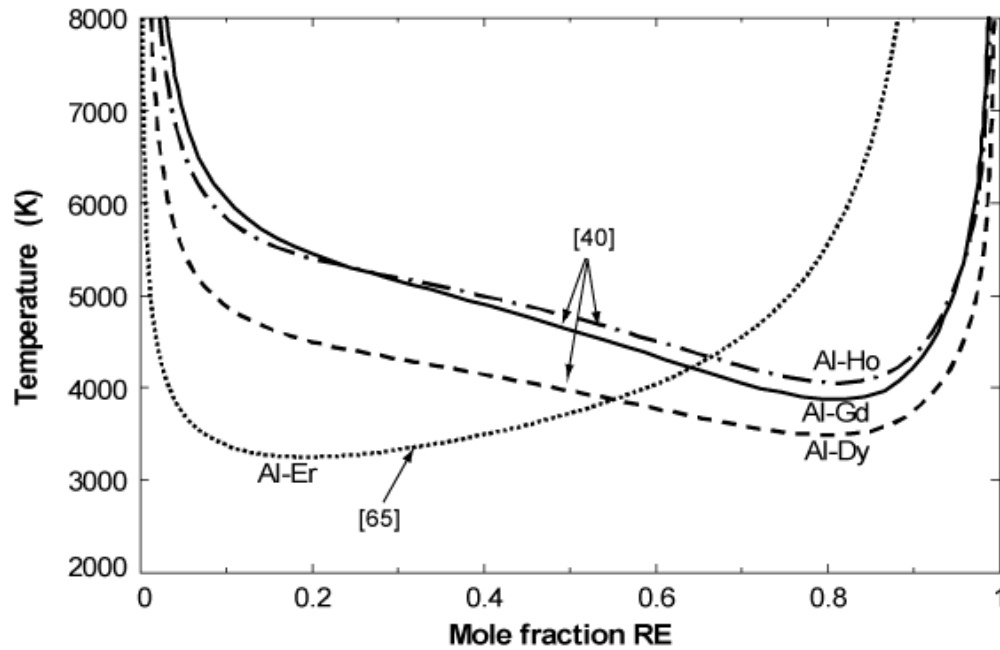
Figure 6.23 Liquid-liquid miscibility gaps in Al-heavy rare earth systems calculated from the liquid model proposed in [40, 65].
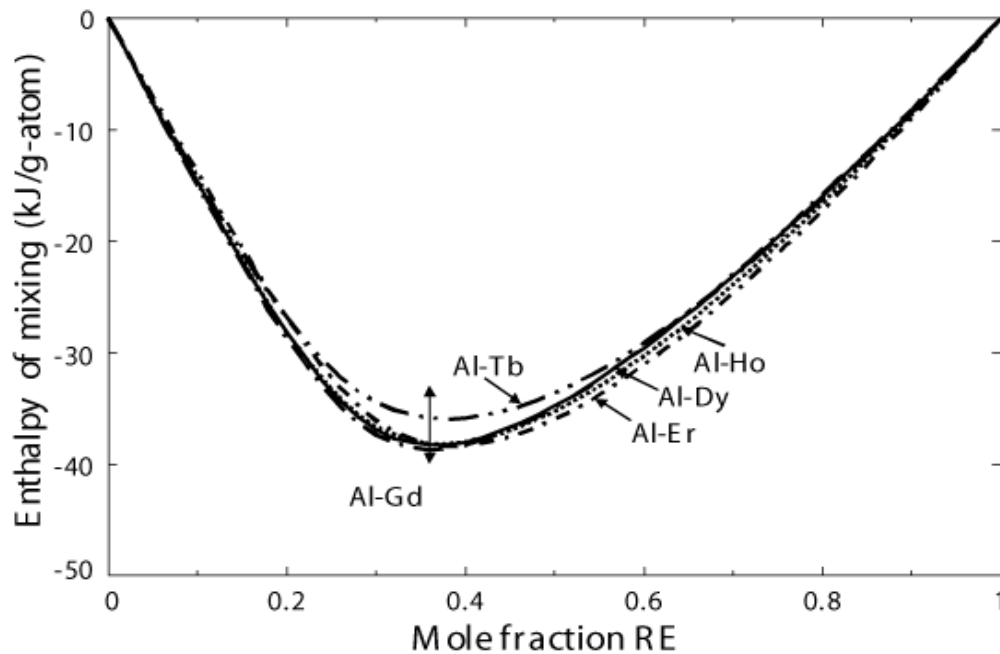
Figure 6.24 Calculated enthalpies of mixing of Al and RE in liquid Al–RE alloys at 1873 K (RE is Gd, Dy, Ho, Er and Tb; ↕ represents the range of minimum enthalpies of mixing of liquid at around $X_{RE} = 0.36$ in Al–light rare earth systems at 1873 K).
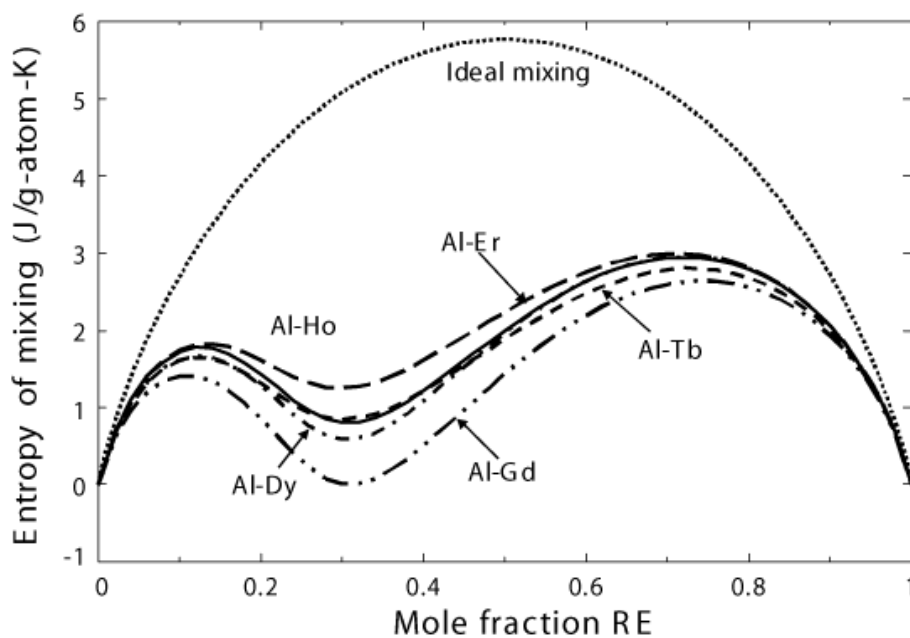
Figure 6.25 Calculated entropies of mixing of Al and RE in liquid Al–RE alloys at 1873 K (RE is Gd, Dy, Ho, Er and Tb).
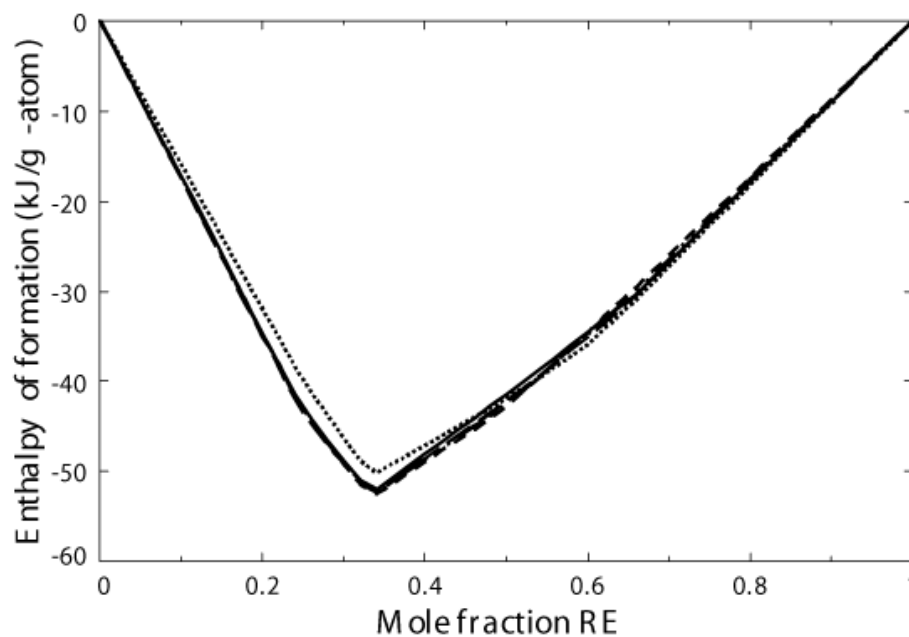
Figure 6.26(a) Calculated enthalpies of formation for the stable intermetalllic compounds in the Al–RE systems at 298 K (RE is Gd, Dy, Ho, Er and Tb; ↕ represents the range of minimum enthalpies of formation at around $X_{RE} = 0.33$ in Al–light rare earth systems at 298 K).
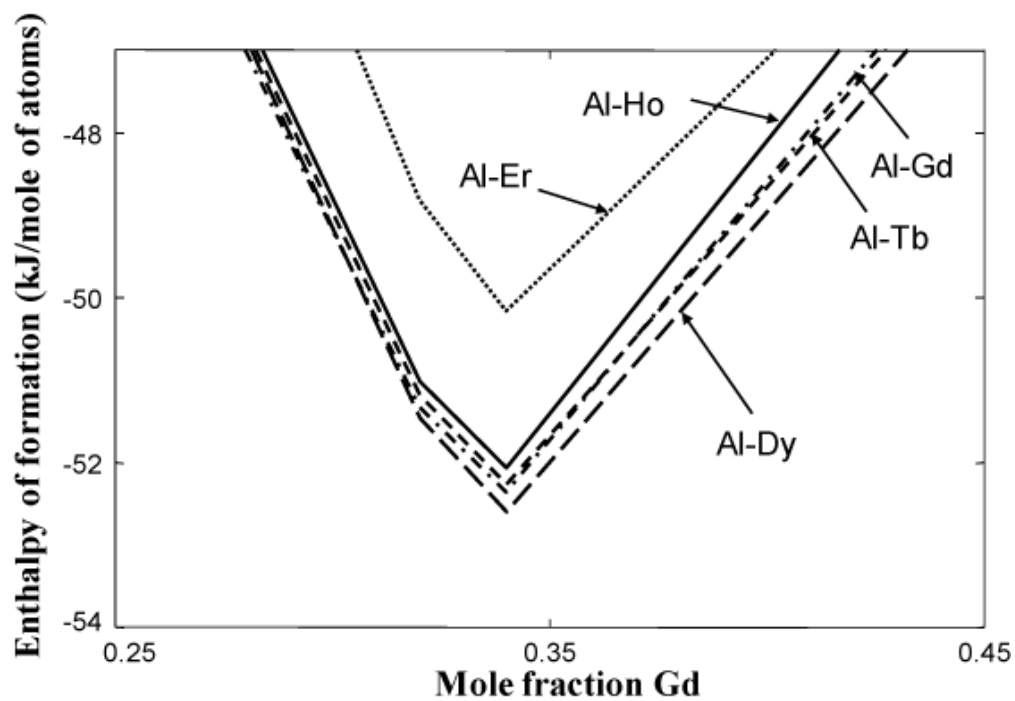
Figure 6.27(b) Local enlargement of calculated enthalpies of formation for the stable
intermetalllic compounds in the Al–RE systems at 298 K.
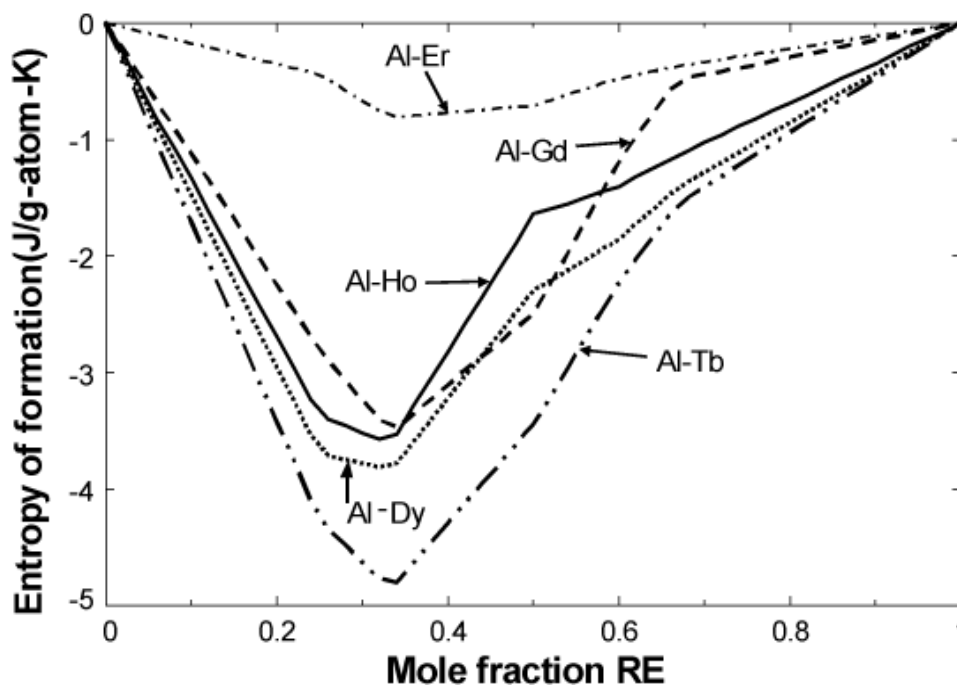
Figure 6.28 Calculated curve of entropy of formation for the stable intermetallic
compounds in the Al–RE systems at 298 K (RE is Gd, Dy, Ho, Er and Tb).

As it has been well-known that rare earths show similar regularities across the Al–RE series, the optimized values for the Δg_{AlRE} are expected to be similar too. The optimized values for a_{00} are in the range of -44 ~ -48 (-40 ~ -48 for Al–light rare earth systems from [16]); the optimized values for b_{00} are in the range of 4.20 ~ 5.50 (4.60 ~ 5.65 for Al–light rare earth systems from [16]); the optimized values for a_{10} are in the range of 0 ~ -5 (-9 ~ -17 for Al–light rare earth systems from [16]); the optimized values for b_{10} are in the range of -1.67 ~ -2.09 (-1.13 ~ -5.65 for Al–light rare earth systems from [16]), and the optimized values for a_{01} are in the range of -7 ~ -14.5 (-10 ~ -17 for the Al–light rare earth systems from [16]). The enthalpies of mixing of binary liquids at 1873 K, the entropies of mixing of binary liquids at 1873 K, the enthalpies of formation of solid at 298 K and the entropies of formation of solid at 298 K are superimposed respectively in Figure 6.24, Figure 6.25, Figure 6.26(a), Figure 6.26(b), and Figure 6.27 for the Al–heavy rare earth systems. The minimum values of the enthalpies of mixing of binary liquids at 1873 K are at a composition around X_{RE}=0.36 and in the range of -39 ~ -35 kJ/g-atom (-40 ~ -33 kJ/g-atom for Al–light rare earth systems from [16]). The minimum values of the entropies of mixing of binary liquids at 1873 K are at a composition around X_{RE}=0.3 and in the range of 0 ~ 1 J/g-atom-K (0 ~ 2 J/g-atom-K for Al–light rare earth systems from [16]). The enthalpies of formation for the stable intermetallic compounds at 298 K show minimum values at a composition around X_{RE}=1/3 and are in the range of -53 ~ -50 kJ/g-atom (-55 ~ -51 kJ/g-atom for Al–light rare earth systems from [16]), while the enthalpies of formation at 298 K for the Al_3RE, and AlRE are in the range of -44 ~ -40 kJ/g-atom (-48 ~ -44 kJ/g-atom for Al–light rare earth systems from [16]), and -43 ~ -40 kJ/ g-atom (-49 ~ -45 kJ/ g-atom for Al–light rare earth systems from [16]) respectively. The compound in equilibrium with the Al–FCC phase is Al_3RE while the compound in equilibrium with the RE–HCP phase is $AlRE_2$ for all the Al–heavy rare earth systems. More systematic analysis will be presented in a next paper [17] in this series.

6.5 Conclusion

Systematic thermodynamic evaluations and optimizations of the Al–Gd, Al–Dy, Al–Ho, and Al–Er systems have been presented on the basis of the literature information. Moreover, thermodynamic properties of Al–Tb system have been predicted with the help of systematic analysis (reduced melting temperature), as it is known that rare earths show certain trends and regularities across the lanthanide series. Optimized model parameters of the Gibbs energies for all phases which reproduced the experimental data to satisfaction are obtained in the present study. It may be noteworthy that all the Al–rare earth binary systems exhibit a very large degree of short–range ordering (SRO) in the liquid and show the similar thermodynamic properties. The Modified Quasichemical Model (MQM) for the liquid phases which takes the SRO into account fits the experimental data very well, and the value of the "m–shaped" integral entropy of mixing seems to be more realistic, unlike the very negative entropy of mixing in the previous optimizations when the Bragg–Williams random mixing approximation was used. The large negative entropy of mixing results in a spurious inverted miscibility gap at high temperatures. Moreover, the shape of partial enthalpy of mixing curve is reproduced well as the experimental data indicated using MQM for the liquid.

As it has been well known that rare earths show similar regularities across the Al–RE series, similar regularities for the thermodynamic properties, like the enthalpies of mixing of binary liquids at 1873 K, the entropies of mixing of binary liquids at 1873 K, the enthalpies of formation of the stable compounds at 298 K and the entropies of formation of solid at 298 K are presented and compared across the Al–heavy rare earth series. Furthermore, the same optimization strategy is used across the whole lanthanide series (the Al–light rare earth systems were assessed in a previous paper [16]) and the similar regularities for the thermodynamic properties are also shown. Importantly, it indicates that it should be interesting and very important to evaluate and optimize the series of lanthanides instead of assessing them independently, as is usually the case in the CALPHAD approach.

It would be expected that MQM for the liquid gives better extrapolations into multicomponent systems based on parameters in the binary and ternary systems. These better predictions and estimations of phase equilibria will help to develop and design novel magnesium and aluminum alloys.

6.6 Acknowledgements

6.7 References

[1]   R. Lundin and J. R. Wilson, Advanced Materials & Processes, 158(2000), 52-55.

[2]   D. Ping, K. Hono, and A. Inoue, Metallurgical and Materials Transactions A, 31(2000), 607-614.

[3]   K. A. Gschneidner, Jr., L. Eyring, and Editors, Handbook on the Physics and Chemistry of Rare Earths, Volume 25. 1998, 83.

[4]   H. Cao and M. Wessen, Metallurgical and Materials Transactions A: Physical Metallurgy and Materials Science, 35A(2003), 309-319.

[5]   R. Ferro and S. Delfino, J. Less-Common Met. , 68(1979), 23-29.

[6]   K. H. J. Buschow and J. H. N. Van Vucht, Philips Research Reports, 22(1967), 233-245.

[7]   A. Saccone, G. Cacciamani, D. Maccio, G. Borzone, and R. Ferro, Intermetallics, 6(1998), 201-215.

[8]   R. Ferro, S. Delfino, G. Borzone, A. Saccone, and G. Cacciamani, Journal of Phase Equilibria, 14(1993), 273-279.

[9]   S. Delfino, A. Saccone, and R. Ferro, J. Less-Common Met., 102(1984), 289-310.

[10]   G. Borzone, A. Borsese, and R. Ferro, Zeitschrift fuer Anorganische und Allgemeine Chemie, 501(1983), 199-208.

[11]   A. Saccone, S. Delfino, and R. Ferro, J. Less-Common Met., 143(1988), 1-23.

[12]   E. H. P. Cordfunke and R. J. M. Konings, Thermochimica Acta, 375(2001), 65-79.

[13]   E. H. P. Cordfunke and R. J. M. Konings, Thermochimica Acta, 375(2001), 17-50.

[14]   S. V. Meschel and O. J. Kleppa, Journal of Alloys and Compounds, 321(2001), 183-200.

[15]   Y.-B. Kang, A. D. Pelton, P. Chartrand, and C. D. Fuerst, Calphad, 32(2008), 413-422.

[16]   L.-L. Jin, Y.-B. Kang, P. Chartrand, and C. D. Fuerst, Calphad 35 (2011): 30-41.

[17]   L.-L. Jin, P. Chartrand, and Y.-B. Kang, (2009), in preparation.

[18]   A. T. Dinsdale, Calphad, 15(1991), 317-425.

[19]   Y.-B. Kang, L.-L. Jin, P. Chartrand, and A. D. Pelton, unpublished work., Ecole polytechnique de Montréal, Quebéc, Canada(2007).

[20]   C. W. Bale, P. Chartrand, S. A. Degterov, G. Eriksson, K. Hack, R. Ben Mahfoud, J. Melancon, A. D. Pelton, and S. Petersen, CALPHAD: Computer Coupling of Phase Diagrams and Thermochemistry, 26(2002), 189-228.

[21]   C. Bale, A. Pelton, and W. Thompson, Factsage thermochemical software and databases, http://www.crct.polymtl.ca/

[22]   A. D. Pelton, S. A. Degterov, G. Eriksson, C. Robelin, and Y. Dessureault, Metallurgical and Materials Transactions B: Process Metallurgy and Materials Processing Science, 31B(2000), 651-659.

[23]   Y.-B. Kang, A. D. Pelton, P. Chartrand, P. Spencer, and C. D. Fuerst, Metallurgical and Materials Transactions A: Physical Metallurgy and Materials Science, 38(2007), 1231-1243.

[24]   Y.-B. Kang, A. D. Pelton, P. Chartrand, P. Spencer, and C. D. Fuerst, Journal of Phase Equilibria and Diffusion, 28(2007), 342-354.

[25]   Y.-B. Kang, I.-H. Jung, S. A. Decterov, A. D. Pelton, and H.-G. Lee, ISIJ International, 44(2004), 975-983.

[26]   I.-H. Jung, S. A. Decterov, and A. D. Pelton, Journal of the European Ceramic Society, 25(2005), 313-333.

[27]   A. Pelton and P. Chartrand, Metallurgical and Materials Transactions A, 32(2001), 1361-1383.

[28]   P. Chartrand and A. Pelton, Metallurgical and Materials Transactions A, 32(2001), 1417-1430.

[29]   P. Chartrand and A. Pelton, Metallurgical and Materials Transactions A, 32(2001), 1385-1396.

[30]   P. Waldner and A. D. Pelton, Metall. Mater. Trans. B 35B(2004), 897-907.

[31]   A. D. Pelton and Y.-B. Kang, International Journal of Materials Research, 98(2007), 907-917.

[32]   M. Hillert, Journal of Alloys and Compounds, 320(2001), 161-176.

[33]   S. H. Zhou and R. E. Napolitano, Acta Materialia, 54(2006), 831-840.

[34]   K. Gschneidner and F. Calderwood, Journal of Phase Equilibria, 9(1988), 680-683.

[35]   O. J. C. Runnalls and R. R. Boucher, Journal of the Less-Common Metals, 13(1967), 431-442.

[36]   M. I. Copeland and H. Kato, Proc. Symp. Phys. Mater. Probl. Reactor Control Rods, Vienna, (1964), 295-316.

[37]   K. H. J. Buschow, Journal of the Less-Common Metals, 9(1965), 452-456.

[38]   A. Saccone, A. M. Cardinale, S. Delfino, and R. Ferro, Zeitschrift fuer Metallkunde, 91(2000), 17-23.

[39]   S. De Negri, A. Saccone, G. Cacciamani, and R. Ferro, Intermetallics, 11(2003), 1125-1134.

[40]   G. Cacciamani, S. De Negri, A. Saccone, and R. Ferro, Intermetallics, 11(2003), 1135-1151.

[41]   J. Gröbner, D. Kevorkov, and R. Schmid-Fetzer, Zeitschrift fuer Metallkunde, 92(2001), 22-27.

[42]   D. S. Kanibolotsky, N. V. Golovataya, and V. V. Lisnyak, Journal of Thermal Analysis and Calorimetry, 76(2004), 323-327.

[43]   J.-J. Lee and F. Sommer, Z. Metallkunde, 76(1985), 750-753.

[44]   G. Cacciamani and R. Ferro, Calphad: Computer Coupling of Phase Diagrams and Thermochemistry, 25(2001), 583-597.

[45]   C. Colinet, A. Pasturel, and K. H. J. Buschow, Physica B+C, 150(1988), 397-403.

[46]   F. Sommer and M. Keita, Journal of the Less-Common Metals, 136(1987), 95-99.

[47]   M. C. Gao, A. D. Rollett, and M. Widom, Physical Review B: Condensed Matter and Materials Physics, 75(2007), 174120/174121-174120/174116.

[48]   V. I. Kober, I. F. Nichkov, S. P. Raspopin, and V. A. Nauman, Izvestiya Vysshikh Uchebnykh Zavedenii, Tsvetnaya Metallurgiya, (1977), 83-86.

[49]   R. E. Hackenberg, M. C. Gao, L. Kaufman, and G. J. Shiflet, Acta Materialia, 50(2002), 2245-2258.

[50]   K. Gschneidner and F. Calderwood, Journal of Phase Equilibria, 9(1988), 673-675.

[51]   H. Okamoto, Journal of Phase Equilibria, 21(2000), 569.

[52] P. Franke and D. Neuschütz, (eds.), Al - Dy (Aluminium - Dysprosium). *in* SpringerMaterials - The Landolt-Börnstein Database (http://www. springermaterials.com), Springer-Verlag. (5a) 2007, DOI: 10.1007/978-3-540-45280-5_20.

[53] F. Casteels, Journal of the Less-Common Metals, 12(1967), 210-220.

[54] K. H. J. Buschow and J. H. N. Van Vucht, Journal of the Less-Common Metals, 13(1967), 369-370.

[55] C. Colinet, A. Pasturel, and K. H. J. Buschow, Journal of Chemical Thermodynamics, 17(1985), 1133-1139.

[56] K. Gschneidner and F. Calderwood, Journal of Phase Equilibria, 9(1988), 684-686.

[57] P. Franke and D. Neuschütz, (eds.), Al-Ho (Aluminium - Holmium). *in* SpringerMaterials - The Landolt-Börnstein Database (http://www. springermaterials.com). Springer-Verlag. , (5a) 2007, DOI: 10.1007/978-3-540-45280-5_22.

[58] A. Meyer, Journal of the Less-Common Metals, 10(1966), 121-129.

[59] K. H. J. Buschow, Journal of the Less-Common Metals, 8(1965), 209-212.

[60] A. Meyer, Naturwissenschaften, 51(1964), 189-190.

[61] J. H. N. van Vucht and K. H. J. Buschow, Philips Res. Rept., 19(1964), 319-322.

[62] K. Gschneidner and F. Calderwood, Journal of Phase Equilibria, 9(1988), 676-678.

[63] H. Okamoto, Journal of Phase Equilibria, 24(2003), 277.

[64] K. H. J. Buschow, Z. Metallkunde, 56(1965), 9-13.

[65] G. Cacciamani, A. Saccone, S. De Negri, and R. Ferro, Journal of Phase Equilibria, 23(2002), 38-50.

[66] A. Saccone, G. Cacciamani, S. De Negri, and R. Ferro, Journal of Phase Equilibria, 23(2002), 29-37.

[67] F. Merlo, Thermochimica Acta, 64(1983), 115-122.

[68] K. A. Gschneidner, Jr. and F. W. Calderwood, Bulletin of Alloy Phase Diagrams, 10(1989), 40-42.

[69] B. Predel, *in* Al-Tb (Aluminum - Terbium), 2006, 1-1.

[70] M. E. Drits, E. S. Kadaner, N. I. Turkina, and V. I. Kuz'mina, Izvestiya Vysshikh Uchebnykh Zavedenii, Tsvetnaya Metallurgiya, (1978), 157-158.

[71] K. A. Gschneidner, Jr., J. Less-Common Metals, 17(1969), 1-12.

CHAPTER 7 ARTICLE 3: THERMODYNAMIC EVALUATIONS AND OPTIMIZATIONS OF BINARY MG – LIGHT RARE EARTH (LA, CE, PR, ND, SM) SYSTEMS

Published in Calphad 38 (2012) 100-116

Youn-Bae Kang [a], Liling Jin [b,*], Patrice Chartrand [b], Aïmen E. Gheribi [b], Kewu Bai [c], Ping Wu [c]

[a] Graduate Institute of Ferrous Technology (GIFT), Pohang University of Science and Technology, Pohang, Korea, 790-784

[b] Centre de Recherche en Calcul Thermochimique (CRCT), École Polytechnique de Montréal, Montréal, QC, CANADA, H3C 3A7

[c] Institute of High Performance Computing, 1 Fusionopolis Way, #16-16 Connexis, *Singapore* 138632

* Corresponding author. Centre de Recherche en Calcul Thermochimique (CRCT), École Polytechnique de Montréal, Montréal, QC, CANADA, H3C 3A7. Tel : +1 514 3404711 ext. 2483; fax : +1 514 3405840. E-mail address: liling.jin@polymtl.ca

Abstract: Mg-light rare earth element (RE: La, Ce, Pr, Nd and Sm) binary systems have been systematically assessed and optimized based on the available experimental data and estimated data by first-principles and Miedema's model. The optimization procedure was biased by putting an emphasis on the observed trends in the thermodynamic properties of Mg–RE phases. The Modified Quasichemical Model, which takes short-range ordering into account, is used for the liquid phase, and the Compound Energy Formalism is used for the solid solutions. Optimized model parameters have been obtained for the Gibbs energy functions of all stable phases, and the model reproduce most critically assessed experimental data. It is shown that the Modified Quasichemical Model used for the liquid alloys permits us to obtain entropies of mixing that are more reliable than those based on the Bragg–Williams random mixing model which does not take short–range ordering into account.

Keywords: Magnesium–Rare Earth Alloys, Thermodynamic modelling, First-Principles calculations, Miedema's Model, Modified Quasichemical Model

7.1 Introduction

Adding Rare Earth elements (RE = Y, Sc, La, Ce, Pr, Nd, Pm, Sm, Eu, Gd, Tb, Dy, Ho, Er, Tm, Yb, and Lu) to Mg–based alloys show several interesting applications in the automotive and aeronautical industries because of their low density and potentially high strength/weight ratios. Much attention has been paid to the solid solubility of the rare-earth metals in solid Mg in the investigations because of its positive effect on the strength properties and plasticity of the magnesium alloys. It was confirmed from the recent study of Hantzsche *et al.* [1] that magnesium sheets with weak textures, which promise improved sheet formability [2], can be obtained by adding small amounts of alloying elements such as Nd, Ce and Y. It was worth noting that the amount of the RE addition required for sufficient texture weakening is connected with the solid solubility of the respective element in the (Mg)–HCP phase. Hence, it is important to have reliable values of the solid solubility of rare earth elements in the (Mg)–HCP phase and a proper model to predict it in binary and higher order systems. The solubility of elements in a disordered terminal solid solution like (Mg)–HCP can be calculated by the CALPHAD method after a critical evaluation and optimization of the thermodynamic functions of the relevant phases in equilibrium with (Mg)–HCP and the Gibbs energy of mixing of Mg–RE in the HCP (A3) structure. The properties of rare-earth elements and their related compounds usually vary in a relatively monotonous way within the light and the heavy rare-earths respectively. As the Gibbs energy of mixing of the HCP solution and the Gibbs energy of formation of RE_yMg_x compounds in equilibrium with (Mg)–HCP enable the calculation of the solubility of rare-earth elements in (Mg)–HCP, a thermodynamic assessment of binary Mg–RE systems should take into account that a general trend be respected among the light Rare-Earth elements and the heavy Rare-Earth elements.

The Mg–RE systems may be categorized into three sub-groups: (1) Mg-light RE (RE = La, Ce, Pr, Nd, Pm, Sm) binary systems, (2) Mg-heavy RE (RE = Gd, Tb, Dy, Ho, Er, Tm) binary systems which look very similar to the Mg–Y binary system, and (3) other two systems which do not share any similarities with other systems, Mg–Eu and Mg–Yb binary systems. In the present paper, thermodynamic evaluation and modeling of the Mg–La, Mg–Ce, Mg–Pr, Mg–Nd, and Mg–Sm (Mg-light lanthanides) systems will be performed using the CALPHAD method and by

also adding estimation from the Miedema's model and first-principles calculations, while the Mg–Gd, Mg–Tb, Mg–Dy, Mg–Ho, Mg–Er, Mg-Tm (Mg–heavy lanthanides) together with Mg–Eu and Mg–Yb systems will be presented in a future paper. Mg–Pm system is not considered in the present study since Pm element is radioactive and no experimentally thermodynamic data on Mg–Pm system is available in the literature. The present work is a part of our ongoing projects to develop thermodynamic databases for multi-component Mg- and Al- based alloys with RE. The Al–RE (La, Ce, Pr, Nd, Sm, Gd, Tb, Dy, Ho, Er) systems and Al–Mg system have been optimized [3-5], while optimizations of the ternary Al–Mg–RE systems will be presented in a future paper.

In the present study, first-principles calculations were performed to study the dilute enthalpy of mixing of RE elements in the (Mg)–HCP solid solutions, and the enthalpy of formation of $LaMg_{12(tI26)}$, $CeMg_{12(tI26)}$, $PrMg_{12(tI26)}$, and $Nd_5Mg_{41(tI92)}$ which are the four binary stable compounds in equilibrium with (Mg)–HCP related to the four most abundant rare-earth elements (La, Ce, Pr, Nd) in mischmetal. Other first-principles calculations were also made for the enthalpy of formation of the stable compounds $LaMg_{2(cF24)}$, $La_5Mg_{41(tI92)}$ (stable at high temperature), $CeMg_{2(cF24)}$, $Ce_5Mg_{41(tI92)}$, $Pr_5Mg_{41(tI92)}$, $Nd_5Mg_{41(tI92)}$, $SmMg_{(cP2)}$, $SmMg_{2(cF24)}$, $SmMg_{3(cF16)}$ and $Sm_5Mg_{41(tI92)}$.

The semi-empirical Miedema's model was employed to estimate the enthalpy of formation of compounds and the enthalpy of mixing for the HCP solution in the Mg–RE binary systems. The calculated results were compared with the available experimental data and the data from first-principles calculations.

7.2 Optimization strategies

Kang *et al*. [6] reported the thermodynamic optimization of the Mg–Ce binary system which is typical of Mg-light rare earth binary systems. Experimental information such as the enthalpy of

mixing of the liquid, the enthalpy of formation of the solid phases, vapor pressure measurements, and phase diagram data were critically assessed to obtain model parameters [6].

The enthalpy of mixing of the liquid and/or the enthalpy of formation of some of the solid phases are of great importance to obtain physically meaningful Gibbs energy expressions ($G = H - TS$) for the phases concerned during the optimization. Then the absolute entropy of those phases (including the mixing entropy for solutions) can be estimated from experimental data such as phase diagram, vapor pressure or activity measurements. Calorimetric data on the solid phases of Mg-light rare earth systems are scarce [7-9]. Although first-principles calculations based on Density Functional Theory (FP-DFT) may not accurately predict the enthalpy of mixing and enthalpy of formation at high temperature in rare-earth systems, FP-DFT can generally give reasonable estimations when RE elements are involved as discussed by Gao *et al*. [10]. These estimations can also be compared with the estimations from the Miedema's model. Moreover, in the Miedema's model, the enthalpy of formation of solid phases and the enthalpy of mixing of the disordered HCP solution for the Mg–rare earth binary systems can be estimated with reasonable accuracy using well-chosen model parameters (chemical potential and electronic density) for the rare-earth elements.

In the present study, systematic approaches were carried out based on the similarities shown in the rare-earth elements and Al–RE binary systems [3, 4]. It was assumed that the enthalpy of mixing of the Mg–Ce binary liquid solution could be used as a prototype for the enthalpy of mixing of the Mg–Nd, MgcPr and Mg–Sm binary liquid solutions, for which no experimentally data have been reported. Enthalpy of mixing data is available for the Mg–La liquid solution, and they were used in our evaluation. In the light of similarities of the stoichiometry of intermetallic phases (REMg$_{12(tI26)}$, RE$_5$Mg$_{41(tI92)}$, REMg$_{3(cF16)}$ and REMg$_{(BCC–B2)}$, all with the same crystal structure respectively), and considering the fact that all light pure RE have the DHCP–A3' structure at 298.15K, except Sm which has a rhombohedral structure at 298.15K, and Ce which has a FCC–A1 structure at 298.15 K but transforms into DHCP–A3' below 283.15 K, the entropy of formation of intermetallic phases having the same stoichiometry were assumed to be similar (a deviation of less than ± 2 J/mol-atom-K was judged acceptable). The enthalpies of formation of

those intermetallic phases were optimized using the experimental calorimetric data or estimations (FP-DFT or Miedema's model).

In the thermodynamic optimizations, a high priority has been given to the solid solubility limits of RE elements in (Mg)–HCP. The solid solubility limits of RE in (Mg)–HCP are dependent on the Gibbs energy of the (Mg)–HCP and the Gibbs energy of the phase which is in equilibrium with it. In a Mg–RE binary system, the solid solution (Mg)–HCP is in equilibrium with a solid phase $Mg_mRE_n(\theta)$. The thermodynamic equilibrium can be computed using:

$$m(Mg)_{HCP} + n(RE)_{HCP} \leftrightarrow Mg_mRE_n, \quad \Delta G = 0 \tag{7.1}$$

when the solid solubility of RE elements in (Mg)–HCP is very small, and when the θ phase is assumed to be pure, then

$$\Delta G \cong \Delta G^0 + RT \ln \frac{1}{(x_{RE}^{HCP} \gamma_{RE}^{HCP})^n} = 0 \tag{7.2}$$

$$\Delta G^0 = G^{Mg_mRE_n} - m\,^0G_{Mg}^{HCP} - n\,^0G_{RE}^{HCP} \tag{7.3}$$

where Mg in HCP solution is chosen as the standard state of Mg and RE in HCP solution is chosen as the standard state of RE.

Finally, we obtain

$$\ln x_{RE}^{HCP} = \frac{\Delta G^0}{nRT} - \ln \gamma_{RE}^{HCP} \tag{7.4}$$

from the above equation, it is found that $\ln x_{RE}^{HCP}$ has a linear relationship with $1/T$ when $\ln x_{RE}^{HCP}$ is very small, provided that γ_{RE}^{HCP} is only dependant on $1/T$ as is the case for regular or sub-regular solutions with no excess entropy terms. This criterion is used in our assessment of the

experimental data of the solid solubility of RE elements in (Mg)–HCP. The reported solubility data in (Mg)–HCP are usually considerably scattered, therefore the above relation (linearity of logarithm scale of solubility limit to the reciprocal of temperature) is used as a diagnostic tool to check trends between the solubility limits of the different light rare-earth elements.

7.3 Methodology used in the present optimization

7.3.1 First-principles calculations

All electronic structure calculations have been performed using the ab initio total-energy and molecular-dynamics program VASP (Vienna ab initio simulation program) developed at the Institute für Materialphysik of the Universität Wien [11-14]. The Kohn–Sham equations were solved using the projector augmented plane wave (PAW) method [15, 16] with the generalized gradient approximation (GGA). Perdew–Burke–Ernzerhof (PBE) gradient approximation was chosen to describe the exchange-correlation interaction. The interaction between ions and electrons were described by the standard frozen-core potentials which combines the accuracy of augmented plane wave method and the flexibility of pseudopotentials approach. For La, Ce, Pr and Nd elements, 5s, 5p, 6s, 5d electrons were treated within the valence band while the other electrons were kept frozen in the core. Spin polarization with collinear magnetization were not considered in the calculations, since no significant magnetic contribution to the total energy was found after our comparison studies. It was also pointed out by Gao *et al*. [10] that the magnetic contribution to the total energy is zero or negligible when the trivalent potentials for La, Ce, Pr and Nd elements are used. The plane wave cut-off energy (E_{cut}) in the magnitude of 300 eV was set up after the convergence test. The total energy was converged to within 2 meV/atom. For the Brilloin zone integration, the Monkhort–Pack grid [17] and Gamma-centered grid (for hexagonal structures) were used. Reciprocal space (k-point) meshes were increased until the total energy was converged to within 2 meV/atom.

The actual first-principles total energy calculations are performed in a self-consistent iteration. We first estimate the initial charge density function. By solving Schrödinger's equations, a new

charge density is obtained. This iteration step commences until the charge density (or the total energy) does not change within the desired accuracy. In practice, the nuclei also have to be relaxed into their equilibrium positions so that the quantum-mechanical forces acting on each of them vanish. Such structural relaxations are usually performed using a conjugate-gradient or a quasi-Newton scheme. The final obtained total energies can be used to extract the formation enthalpies of stable, metastable or even unstable structures at T=0K using the following equation:

$$\Delta H(RE_m Me_n) = \frac{E(RE_m Me_n) - m \cdot E(RE) - n \cdot E(Me)}{m + n} \tag{7.5}$$

where E's are the first-principles calculated total energies of $RE_m Me_n$ and pure elements RE and Me using their standard reference states, each fully relaxed to their equilibrium (zero-pressure) geometries, respectively. The standard reference states for Al, Mg, La, Ce, Pr, Nd, and Sm are $cF4$-Cu, $hP2$-Mg, $hP4$-La, $cF4$-Cu, $hP4$-La, $hP4$-La and $hR3$-Sm, respectively. $\Delta H(RE_m Me_n)$ is the enthalpy of formation for the $RE_m Me_n$ compound.

The supercell method was employed for (Mg)–HCP solid solution with the volume conservation. The mixing energies in dilute region are determined by relaxations for a single RE-substituted atom in a 96-atom Mg supercell ($4 \times 4 \times 3$). The atomic positions are relaxed until the total energy is converged to within 5 meV/atom. The dilute enthalpy of mixing in (Mg)–HCP phase can be calculated by the following equation:

$$\Delta H_{Mg}(RE) = \frac{1}{96} \cdot [E(RE \text{ in Mg supercell})\text{-}1 \cdot E(RE)\text{-}95 \cdot E(Mg)] \tag{7.6}$$

where $\Delta H_{Mg}(RE)$ is the dilute enthalpy of mixing in (Mg)–HCP phase. $E(RE$ in Mg supercell) is the energy with one Mg atom substituted by RE atom (RE: La, Ce, Pr and Nd). $E(RE)$ and $E(Mg)$ are the energies of pure elements RE and Mg, respectively.

7.3.2 Miedema's model for binary alloys

Although it may not be as accurate as ab initio techniques, the semi-empirical Miedema's model can provide a good initial guess for the enthalpy of formation of compounds and the enthalpy of

mixing for solutions for thermodynamic optimizations without high computing cost. Proposed by Miedema *et al.* [18-20] more than thirty years ago, it is still widely used to estimate the glass formability, alloying behavior and phase stabilities for binary and ternary systems [21-28]. In the present study, calculations from semi-empirical Miedema's model are compared to first-principles calculations.

The enthalpy of mixing [20, 29] for a A–B disordered solution estimated using the Miedema's model can be expressed by:

$$\Delta H_{AB} = f_{AB} \frac{x_A (1 + \mu_A x_B (\phi_A - \phi_B)) x_B (1 + \mu_B x_A (\phi_B - \phi_A))}{x_A V_A^{2/3}[1 + \mu_A x_B (\phi_A - \phi_B)] + x_B V_B^{2/3}[1 + \mu_B x_A (\phi_B - \phi_A)]} \tag{7.7}$$

For an ordered stoichiometric compound, the expression for the enthalpy of formation is:

$$(\Delta H_{AB})_{order} = \Delta H_{AB} \left[1 + \gamma \left(\frac{V_A^{2/3} V_B^{2/3} \Delta H_{AB}}{f_{AB} \left\{ x_A V_A^{2/3}[1 + \mu_A x_B (\phi_A - \phi_B)] + x_B V_B^{2/3}[1 + \mu_B x_A (\phi_B - \phi_A)] \right\}} \right)^2 \right] \tag{7.8}$$

$$f_{AB} = \frac{2P V_A^{2/3} V_B^{2/3}}{\frac{1}{n_{WS_A}^{1/3}} + \frac{1}{n_{WS_B}^{1/3}}} \cdot [-(\phi_B^* - \phi_A^*)^2 + \frac{Q}{P}(n_{WS_A}^{1/3} - n_{WS_B}^{1/3})^2 - a \times \frac{R}{P}] \tag{7.9}$$

where x_i, ϕ_i, V_i, n_{WS_i} are, respectively, the mole fraction, chemical potential (or work function), molar volume, and the electronic density at the Winger–Seitz cell boundary of component *i*. *a*, *P*, $\frac{R}{P}$, $\frac{Q}{P}$, μ_i, and γ are the semi-empirical parameters evaluated and reported by Miedema [20]. The empirical parameter *P* assumes different values according to whether *A* and *B* are both transition, both non-transition or transition and non-transition elements; *Q/P* is assumed to be constant (equal to 9.4) [20].

The formation enthalpy of a crystalline solid solution can be described by:

$$\Delta H^{cryst} = \Delta H^{chem} + \Delta H^{elastic} + \Delta H^{struct} \tag{7.10}$$

where ΔH^{chem} is the chemical contribution due to the mixing of two components given by eq. (7.7); $\Delta H^{elastic}$ is the elastic contribution due to the atom-size mismatch effect; ΔH^{struct} is the structure contribution due to the valence and crystal structure difference of the two components.

$$\Delta H^{elastic} = x_A \cdot x_B (x_A \Delta H^{elastic}_{BinA} + x_B \Delta H^{elastic}_{AinB}) \tag{7.11}$$

where $\Delta H^{elastic}_{BinA}$ and $\Delta H^{elastic}_{AinB}$ are the atom-size mismatch contribution to the solution enthalpy in a binary system. It can be evaluated by:

$$\Delta H^{elastic}_{AinB} = \frac{2G_B(V_A^* - V_B^*)^2}{3V_B^* + 4G_B K_A V_A^*} \tag{7.12}$$

$$(V_i^*)^{2/3} = V_i^{2/3}(1 + \mu_i(\varphi_i - \varphi_j)) \quad (i, j = A, B) \tag{7.13}$$

where G_B is the shear modulus of the solvent; K_A is the compressibility of the solute and V_i^* ($i = A, B$) are the molar volumes of the solute or the solvent.

The contribution of formation enthalpy from two different structures has minimal effect; then, it can be neglected [30].

$$\Delta H^{struct} \approx 0. \tag{7.14}$$

The model parameters of ϕ_i, V_i, n_{WS_i} used in the present calculations were taken from Shubin and Shunya'ev [31] and are shown in Table 7.2. Note that they are different from those described by Boer $et\ al.$ [20].

7.3.3 Thermodynamic models

All the present optimizations have been carried out by means of the FactSage^{TM} thermodynamic software [32, 33]. The thermodynamic properties of the pure phases of Mg and light rare earth (La, Ce, Pr, Nd and Sm) are taken directly from the SGTE database [34]. The standard element reference phases (SER) of the pure elements Mg, La, Ce, Pr, Nd and Sm are HCP−A3, DHCP− A3', FCC−A1, DHCP−A3', DHCP−A3', and rhombohedral phases at 25 ℃, respectively. For the Pr and Sm in the FCC−A1 structure, together with La, Pr, Nd and Sm in the HCP−A3 structure, and Sm in DHCP−A3' structure, which are not available in the SGTE database, Kang *et al*. [35] assumed the same lattice stability with respect to their respective standard state as those calculated from first-principles by Gao *et al*. at zero Kelvin [10]. The Gibbs energies of Ce in the HCP−A3 and DHCP−A3' structures were optimized by Kang *et al.* [6] and used in the present study. The Gibbs energy of Mg in the FCC−A1 structure was optimized to fit the solid solubility of FCC solid solution in Mg−Al system [5]. The Gibbs energy of Mg in the DHCP−A3' structure was optimized to fit the DHCP solid solution in Mg−Nd (Pr) system.

7.3.3.1   Modified quasichemical model (MQM) for the liquid phase

The MQM in the pair approximation [36] was used to model the thermodynamic properties of the liquid solution in the present study. A brief summary of MQM is given in Jin *et al*. [3, 4]. It refers to Pelton *et al*. [36] for the detailed description of the MQM and its associated notation. The same notation is used in the present article. The MQM has been successfully applied to alloy liquid solutions [6, 37], molten oxides [38, 39], molten salts [40, 41], and molten metal-sulphides systems [42]. As was shown by Kang *et al*. [6], liquid Mg–RE alloys usually exhibits a strong short-range ordering near $X_{RE} = 0.25 - 0.33$. Such short-range ordering in binary liquid alloy becomes more evident in several binary Al–RE systems as discussed by Jin *et al*. [3, 4]. In order to treat short-range ordering effectively, the modified quasichemical model in the pair approximation has been used in the present study.

7.3.3.2 Compound energy formalism for solid solutions

The compound energy formalism was introduced by Hillert [43] to describe the Gibbs energies of solid phases on distinctive sub–lattices. When there is only one lattice for the mixing, then the model reduces to a simple random mixing model as is the case for the terminal solid solutions (HCP–A3, BCC–A2, FCC–A1, DHCP–A3') The same notation for the model parameters is used as those in Kang *et al*. [44].

Table 7.1 Crystal structures of the solid phases in Mg-light RE systems.

Prototype	$Mn_{12}Th$	$Ni_{17}Th_2$	$Mg_{41}Ce_5$	Mg_5Gd	BiF_3	Cu_2Mg	CsCl	W	Cu	La	Mg	α-Sm
Pearson symbol	tI26	hP38	tI92	cF448	cF16	cF24	cP2	cI2	cF4	hP4	hP2	hR9
Mg-La	$LaMg_{12}$	La_2Mg_{17}	La_5Mg_{41}	✻	$LaMg_3$	$LaMg_2$	LaMg	BCC	FCC	DHCP	HCP	✻
Mg-Ce	$CeMg_{12}$	Ce_2Mg_{17}	Ce_5Mg_{41}	✻	$CeMg_3$	$CeMg_2$	CeMg	BCC	FCC	DHCP	HCP	✻
Mg-Pr	$PrMg_{12}$	✻	Pr_5Mg_{41}	✻	$PrMg_3$	$PrMg_2$	PrMg	BCC	✻	DHCP	HCP	✻
Mg-Nd	✻	✻	Nd_5Mg_{41}	✻	$NdMg_3$	$NdMg_2$	NdMg	BCC	✻	DHCP	HCP	✻
Mg-Sm	✻	✻	Sm_5Mg_{41}	$SmMg_5$	$SmMg_3$	$SmMg_2$	SmMg	BCC	✻	✻	HCP	RHOM

✻: the phase is not a stable phase

Table 7.2 The empirical parameters used for Miedema's model from Shubin and Shunya'ev [31].

element	$V^{2/3}$ (cm^2)	$Nws^{1/3}$ (d.u.)	Φ^* (V)	G_i(GPa)	K_i(1/GPa)
Al	4.6	1.39	4.2	26.2	0.01385
La	7.98	1.09	3.05	14.9	0.04120
Ce	7.54	1.07	3.02	13.5	0.04180
Pr	7.57	1.08	3.03	13.54	0.03270
Nd	7.51	1.11	3.04	14.52	0.03060
Sm	7.36	1.10	3.10	12.65	0.03400
Mg	5.81	1.17	3.45	17.36	0.02822

The crystal structure of the different solid phases is shown in Table 7.1. All Mg–RE binary systems, except for the Mg–Yb binary system, contain the ordered $MgRE_{(BCC–B2)}$ phase. This phase may be modeled using two sub-lattice compound energy formalism in order to describe

order/disorder transition, which occurs at a temperature higher than the melting point for all rare-earth elements. This approach requires to consider Mg and all the RE elements to be occupied in both sub-lattices, e.g., $(Mg,La)_1(Mg,La)_1$. However, the observed order/disorder transition in the Mg–RE binary systems is 1st order transition, not 2nd order transition usually observed in Fe–Si, Fe–Al binary alloys. Such 1st order phase transition may be described by treating the two bcc phases (BCC–A2 and BCC–B2) as separate phases. In the present study, the BCC–B2 phase was simply modeled using two sub-lattice CEF with $(Mg)(Mg, La, Ce, …, Sm)$ formula.

All the Mg-light Rare-Earth binary systems contain the $Mg_2RE_{(cF24)}$ phase, which is a Laves-C15 phase. Since $Mg_2RE_{(cF24)}$ phases are almost stoichiometric compounds, they can actually be considered as the stoichiometric compounds or as a A_2B_1 two sub-lattice solution where there are no anti-site atoms for each sub-lattice in the binary systems. However, for the purpose of developing a general multi-component light alloy database, the $Mg_2RE_{(cF24)}$ phase was modeled with a two sub-lattice CEF with $(Mg, La, Ce,…, Sm)_2(Mg, La, Ce,…, Sm)$ formula, as was done for the Mg_2Ce binary phase [6]. The Gibbs energy of the pure end-members $G_{Mg:RE}$ are directly taken from the corresponding stoichiometric compounds, while the Gibbs energies of remaining end-members were either taken from Kang *et al.* [6] or were arbitrarily set to high positive values (Table 7.4) so that the resulting non-stoichiometry be negligible.

In the previous optimization of the Mg–Ce binary system by Kang *et al.* [6], the $Mg_3Ce_{(cF16)}$ phase was treated as a stoichiometric phase since no non-stoichiometry was reported. Considerable solubility of Mg in $Mg_3Pr_{(cF16)}$ was reported by Saccone *et al.* [45] using a Smith thermal analysis technique. In order to model this solubility in the Mg_3Pr, this phase was modeled using a two sub-lattice CEF with the $(Mg)_3(Mg,Pr)$ formula. A similar approach was applied for all $Mg_3RE_{(cF16)}$ phases, therefore final formula of the two sub-lattice CEF becomes $(Mg)_3(Mg, La, Ce, Pr, Nd, Sm)$.

All other binary intermetallic phases were treated as stoichiometric phases. However, due to similarities of their stoichiometry and crystal structure, the Rare-Earth elements are assumed to

mix ideally on one sub-lattice in every ordered solid solution, e.g., $(Mg)_{41}(La, Ce, Pr, Nd, Sm)_5$ for the $Mg_{41}RE_{5(tI92)}$ phase.

Table 7.3 Crystal structures of compounds: Strukturbericht designation, prototype, Pearson symbol, and space group and lattice parameter from this work and from Pauling file [46].

Compound	Struktur-bericht	Proto-type	Pearson symbol	Space Group	Lattice parameter a,b,c in Å	
					This work (FPC)	Reference[45]
Mg	A3	Mg	$hP2$	P6$_3$/mmc	3.194,3.194,5.185	3.210, 3.210, 5.211
La	A3'	αLa	$hP4$	P6$_3$/mmc	3.723,3.723,12.46	3.773,3.773,12.16
Ce	A1	Cu	$cF4$	Fm$\bar{3}$m	5.320(a=b=c)	5.161(a=b=c)
Pr	A3'	αLa	$hP4$	P6$_3$/mmc	3.714,3.714,12.34	3.671,3.671,11.83
Nd	A3'	αLa	$hP4$	P6$_3$/mmc	3.695,3.695,12.15	3.655,3.655,11.80
Sm	C19	αSm	$hR3$	R$\bar{3}$m	3.661,3.661,8.792	3.628,3.628,8.73
LaMg$_2$	C15	MgCu$_2$	$cF24$	Fd$\bar{3}$m	8.775 (a=b=c)	8.787 (a=b=c)
LaMg$_{12}$		ThMn$_{12}$	$tI26$	I4/mmm	10.279,10.279,5.899	10.33,10.33,5.96
La$_5$Mg$_{41}$		Ce$_5$Mg$_{41}$	$tI92$	I4/m	14.791,14.791,10.408	14.82,14.82,10.47
CeMg$_2$	C15	MgCu$_2$	$cF24$	Fd$\bar{3}$m	8.738 (a=b=c)	8.731(a=b=c)
CeMg$_{12}$		ThMn$_{12}$	$tI26$	I4/mmm	10.386,10.386, 5.823	10.33, 10.33,5.96
Ce$_5$Mg$_{41}$		Ce$_5$Mg$_{41}$	$tI92$	I4/m	14.751,14.751,10.418	14.78,14.78,10.43
PrMg$_{12}$		ThMn$_{12}$	$tI26$	I4/mmm	10.357, 10.357, 5.836	10.34,10.34,5.98

Pr$_5$Mg$_{41}$		Ce$_5$Mg$_{41}$	*tI*92	I4/m	14.726,14.726,10.391	14.75,14.75,10.41
NdMg$_{12}$		ThMn$_{12}$	*tI*26	I4/mmm	10.274,10.274,5.914	-
Nd$_5$Mg$_{41}$		Ce$_5$Mg$_{41}$	*tI*92	I4/m	14.741,14.741,10.396	14.575,14.575,10.45
SmMg	B2	CsCl	cP2	Pm$\bar{3}$m	3.848(a=b=c)	3.81(a=b=c)
SmMg$_2$	C15	MgCu$_2$	*cF*24	Fd$\bar{3}$m	8.621(a=b=c)	8.622(a=b=c)
SmMg$_3$	D0$_3$	BiF$_3$	cF16	Fm$\bar{3}$m	7.371(a=b=c)	7.371(a=b=c)
Sm$_5$Mg$_{41}$		Ce$_5$Mg$_{41}$	*tI*92	I4/m	14.693,14.693,10.292	14.77,14.77,10.32

7.4 Results and discussion on the thermodynamic assessment of binary systems

The crystal structural data of the compounds calculated from our first-principles (FPC) are shown in the Table 7.3 together with the crystal structure data from the Pauling File [46]. The calculated results of the enthalpy of formation of pure phases and the enthalpy of mixing of the HCP solution in the Mg–RE systems from Miedema's model, and the estimations of the enthalpy of mixing and the enthalpy of formation from first-principles calculations were embodied in the related figures (Figures 7.2, 7.8, 7.15, 7.21 and 7.31-7.33). It should be pointed out that the first-principles calculations for the Mg–RE systems from Tao's dissertation [47], which were published in Tao *et al*. [48], were also included in Figures 7.2, 7.8, 7.15 and 7.21 for the purpose of comparison. These first-principles calculations were also performed by using VASP with GGA-PAW and Perdew–Wang parameterization (PW91) (PBE in the present study) was employed for the GGA exchange-correlation function. The plane-wave cut-off energy was set to be constant (350 ev) for all the Mg$_x$RE$_y$ compounds in Tao *et al*. [48], while the convergence test is made for cut-off energy in the present study. In general, the difference between the results of Tao *et al*. [48] and of present study is within 2 kJ/g-atom, except that the difference is 2.9 kJ/g-

atom for Mg_2La compound where the calculated value by Tao *et al*. [48] is –12 kJ/g-atom and the present calculated result is –14.9 kJ/g-atom. Considering the source of errors from the first-principle calculation and the assumption that the *f* electrons are kept frozen in the core for the rare earth elements, this difference is considered acceptable. In the present study, the similarity between the rare earth elements is considered and a systematic approach is used for the thermodynamic optimization of Mg–La, Mg–Ce, Mg–Pr, Mg–Nd and Mg–Sm systems. Table 7.4 shows the optimized model parameters of binary phases in the Mg–RE (La, Ce, Pr, Nd and Sm) systems. The model parameters of the MQM for the liquid in Mg–RE systems are shown in Table 7.5.

Table 7.4 Optimized model parameters of binary phases in the Mg–RE (La, Ce, Pr, Nd, Sm) systems (J/mole).

Laves_C15 (Cu₂Mg-type): (Mg, La, Ce, Pr, Nd, Sm)₂(Mg, La, Ce, Pr, Nd, Sm)
Gibbs energies of end members and parameters
G(Mg:Mg) $= 3\textbf{\textit{GHSERMG}} + 15{,}000$ [a]
G(Mg:Ce) $= 2\textbf{\textit{GHSERMG}} + \textbf{\textit{GHSERCE}} - 47{,}449 + 10.35T$ [a]
G(Ce:Ce) $= 3\textbf{\textit{GHSERCE}} + 62{,}760$ [a]
G(Ce:Mg) $= 2\textbf{\textit{GHSERCE}} + \textbf{\textit{GHSERMG}} + 41{,}840$ [a]
G(Mg:La) $= 2\textbf{\textit{GHSERMG}} + \textbf{\textit{GHSERLA}} - 46{,}670 + 8.63T$
G(La:La) $= 3\textbf{\textit{GHSERLA}} + 188{,}280$
G(La:Mg) $= 2\textbf{\textit{GHSERLA}} + \textbf{\textit{GHSERMG}} + 41{,}840$
G(Mg:Pr) $= 2\textbf{\textit{GHSERMG}} + \textbf{\textit{GHSERPR}} - 50{,}388 + 14.66T$
G(Pr:Pr) $= 3\textbf{\textit{GHSERPR}} + 188{,}280$
G(Pr:Mg) $= 2\textbf{\textit{GHSERPR}} + \textbf{\textit{GHSERMG}} + 41{,}840$
G(Mg:Nd) $= 2\textbf{\textit{GHSERMG}} + \textbf{\textit{GHSERND}} - 47{,}699 + 11.83T$
G(Nd:Nd) $= 3\textbf{\textit{GHSERND}} + 188{,}280$
G(Nd:Mg) $= 2\textbf{\textit{GHSERND}} + \textbf{\textit{GHSERMG}} + 41{,}840$
G(Mg:Sm) $= 2\textbf{\textit{GHSERMG}} + \textbf{\textit{GHSERSM}} - 44{,}550 + 10.36T$
G(Sm:Sm) $= 3\textbf{\textit{GHSERSM}} + 188{,}280$

G(Sm:Mg)	= 2*GHSERSM* + *GHSERMG* + 41,840
BCC_B2 (CsCl-type): ((Mg)(Mg, La, Ce, Pr, Nd, Sm)	
Gibbs energies of end members and parameters	
G(Mg:Mg)	= 2*GHSERMG* +8,368 [a]
G(Mg:Ce)	= *GHSERMG* + *GHSERCE* – 28,600 + 5.08T [a]
G(Mg:La)	= *GHSERMG* + *GHSERLA* – 28,990 + 5.08T
G(Mg:Pr)	= *GHSERMG* + *GHSERPR* – 28,800 + 5.08T
G(Mg:Nd)	= *GHSERMG* + *GHSERND* – 29,291 + 5.08T
G(Mg:Sm)	= *GHSERMG* + *GHSERSM* – 28,600 + 5.08T
[Mg]$_{12}$(La,Ce,Pr, Nd, Sm)	
Gibbs energies of end members and parameters	
G(Ce:Mg)	= *GHSERCE* + 12*GHSERMG* -74,057 + 11.6T
G(La:Mg)	= *GHSERLA* + 12*GHSERMG* -77,781+ 4.9T
G(Pr:Mg)	= *GHSERPR* + 12*GHSERMG* -72,802+ 14.9T
[Mg]$_{41}$(La,Ce, Pr, Nd, Sm)$_5$	
Gibbs energies of end members and parameters	
G(Mg:Ce)	= 41*GHSERMG* +5*GHSERCE* -371,961 + 71.72T
G(Mg:La)	= 41*GHSERMG* +5*GHSERLA* -373,500 + 29,09T
G(Mg:Pr)	= 41*GHSERMG* +5*GHSERPR* -365,682 + 86.19T
G(Mg:Nd)	= 41*GHSERMG* +5*GHSERND* -376,560 + 115.53T
G(Mg:Sm)	= 41*GHSERMG* +5*GHSERSM* -380,744 + 151.35T
[Mg]$_3$(Mg, La, Ce, Pr, Nd, Sm)	
Gibbs energies of end members and parameters	
G(Mg:Mg)	= 4*GHSERMG* +8,368
G(Mg:La)	= 3*GHSERMG* +*GHSERLA* -75,600+ 24.8T
G(Mg:Ce)	= 3*GHSERMG* +*GHSERCE* -76,000+ 26.5T
G(Mg:Pr)	= 3*GHSERMG* +*GHSERPR* -74,000+ 26.5T
G(Mg:Nd)	= 3*GHSERMG* +*GHSERND* -73,500+ 26.5T
G(Mg:Sm)	= 3*GHSERMG* +*GHSERSM* -67,500+ 26.5T

$Mg_{17}RE_2$ ($Ni_{17}Th_2$-type) : $(Mg)_{17}(La,Ce)_2$
Gibbs energies of end members and parameters
G(Mg:La) = 17***GHSERMG*** + 2***GHSERLA*** - 151,461 + 12.03T
G(Mg:Ce) = 17***GHSERMG*** + 2***GHSERCE*** -137,453 + 15.22T
HCP_A3 (Mg, La, Ce, Pr, Nd, Sm)
Gibbs energies of end members and parameters
G(Ce, HCP_A3) =***GHSERCE*** +5,230 [a]
G(La, HCP_A3) =***GHSERLA*** +2,500 [b]
G(Pr, HCP_A3) =***GHSERPR*** +2,800 [b]
G(Nd, HCP_A3) =***GHSERND*** +2,500 [b]
G(Sm, HCP_A3) =***GHSERSM*** +70-0.07T [b]
$L_{Mg, La}$ = -19,665
$L_{Mg, Ce}$ = -20,920
$L_{Mg, Pr}$ = -21,757
$L_{Mg, Nd}$ = -24,686
$L_{Mg, Sm}$ = -14,518- 7,113(X_{Mg}-X_{Sm})
FCC_A1 (Mg, La, Ce, Pr, Nd, Sm)
Gibbs energies of end members and parameters
G(Pr, FCC_A1) =***GHSERPR*** +900 -0.544T [b, c]
G(Sm, FCC_A1) =***GHSERSM*** +1,500 [b]
G(Mg, FCC_A1) =***GHSERMG*** +1,220 +2.3T [d]
DHCP_A3' (Mg, La, Ce, Pr, Nd, Sm)
Gibbs energies of end members and parameters
G(Ce, DHCP_A3') =***GHSERCE*** -1,200 + 4.2T [a]
G(Sm, DHCP_A3') =***GHSERLA*** + 600 [b]
G(Mg, DHCP_A3') =***GHSERMG*** +2,188 [b]

[a] taken from Kang *et al.* [6];   [b] taken from Kang *et al.* [35]. [c] taken from Jin *et al.* [3]. [d] taken from Chartrand [5].

Table 7.5 Optimized model parameters of the MQM for the liquid in Mg–RE (RE= La, Ce, Pr, Nd, Sm) systems.

Coordination numbers				Gibbs energies of pair exchange reactions
i	j	Z^i_{ij}	Z^j_{ij}	
Mg	La	2	6	$\Delta g_{MgLa} = -14{,}435 + 5.75T + (-13{,}807 + 4.6T))X_{MgMg} - 8{,}368 X_{LaLa}$
Mg	Ce	2	6	$\Delta g_{MgCe} = -15{,}899 + 7.43T + (-9{,}623 + 2.51T))X_{MgMg} - 8{,}368 X_{CeCe}$ [a]
Mg	Pr	2	6	$\Delta g_{MgPr} = -15{,}899 + 7.43T + (-9{,}623 + 2.51T))X_{MgMg} - 8{,}368 X_{PrPr}$
Mg	Nd	2	6	$\Delta g_{MgNd} = -15{,}899 + 7.43T + (-9{,}623 + 2.51T))X_{MgMg} - 8{,}368 X_{NdNd}$
Mg	Sm	2	6	$\Delta g_{MgSm} = -15{,}899 + 7.43T + (-9{,}623 + 2.51T))X_{MgMg} - 8{,}368 X_{SmSm}$

[a] Taken from Kang *et al.* [6].

7.4.1 Mg–Ce system

This binary system has been previously thermodynamically optimized by Kang *et al.* [6] using the MQM for the liquid phase, by Guo *et al.* [49, 50] using a Bragg–William model for the liquid phase and by Cacciamani *et al.* [51]. A detailed literature review of the Mg–Ce system is given in Kang *et al.* [6] and omitted here. The following phases are considered as stable phases: liquid, (Mg)–HCP, $Mg_{12}Ce$, $Mg_{17}Ce_2$, $Mg_{41}Ce_5$, Mg_3Ce, Mg_2Ce (Laves-C15), MgCe (BCC–B2), (Ce)–BCC, (Ce)–FCC, and (Ce)–DHCP. It is noted that the $Mg_{10.3}Ce$ phase with $Ni_{17}Th_2$ type ($Mg_{17}Ce_2$ in the present work) was considered in Nayeb-Hashemi and Clark [52] and Saccone [53]. In the present study, the liquid properties of the Mg-Ce system and the properties of the solid solutions (Laves–C15, BCC–B2, BCC–A2, DHCP–A3') were kept the same as that of Kang *et al.* [6]. Due to its importance, the solid solubility of Ce in (Mg)–HCP is re-examined in the view of the procedure mentioned previously. Three modifications were made on the Mg-rich side.

First, in the work of Kang *et al.* [6], the CeMg$_3$ phase was treated as a stoichiometric phase. As discussed previously, in order to keep a consistency with other REMg$_3$ phases, in particular with PrMg$_3$ exhibiting excess Mg solubility from the stoichiometric composition, the CeMg$_3$ phase is now treated as a solid solution having non-stoichiometry toward the Mg side. As no solution is reported in Mg$_3$Ce, the parameters were adjusted to minimize it.

Second, the solid solubility of Ce in (Mg)–HCP is reported to be small, but the disparity of the available experimental data is large. The experimental data from Rokhlin [54], Park and Wyman [55], from Dow Chemical Co. Ltd. [56], Crosby and Fowler [57] and Weibke and Schmidt [58] were not consistent with each other. Based on the criterion of the linear relationship of ln $x_{Ce} \propto$ 1/T, as shown in Figure 7.1, the slopes of each set of experimental data are almost the same except that of Park and Wyman [55]. Kang *et al.* [6] favored the work of Park and Wyman [55]. The experimental data of Rokhlin [54] had been criticized in previous reviews [59, 60]: first, it was argued, for all the Mg–RE systems, that the samples from Rokhlin [54] could be contaminated by alumina crucibles which were used to melt the alloys; second, the methods used to determine the solid solubility are different, the X-ray method used in the work of Park and Wyman [55] was believed to be more reliable than the electrical resistivity measurements used by Rokhlin [54]. Rokhlin [61], later defending their experimental data, confirmed by several techniques that the contamination did not happen to significant levels: photometry, spectrographic analyses and atomic absorption. It was also pointed out by Rokhlin [61] that the X-ray method used for the solid solubility measurement by Park and Wyman [55] is not more reliable than the resistivity method they used. As a matter of fact, for very small solubility limits, the change of resistivity is more significant than the change in the lattice parameters.
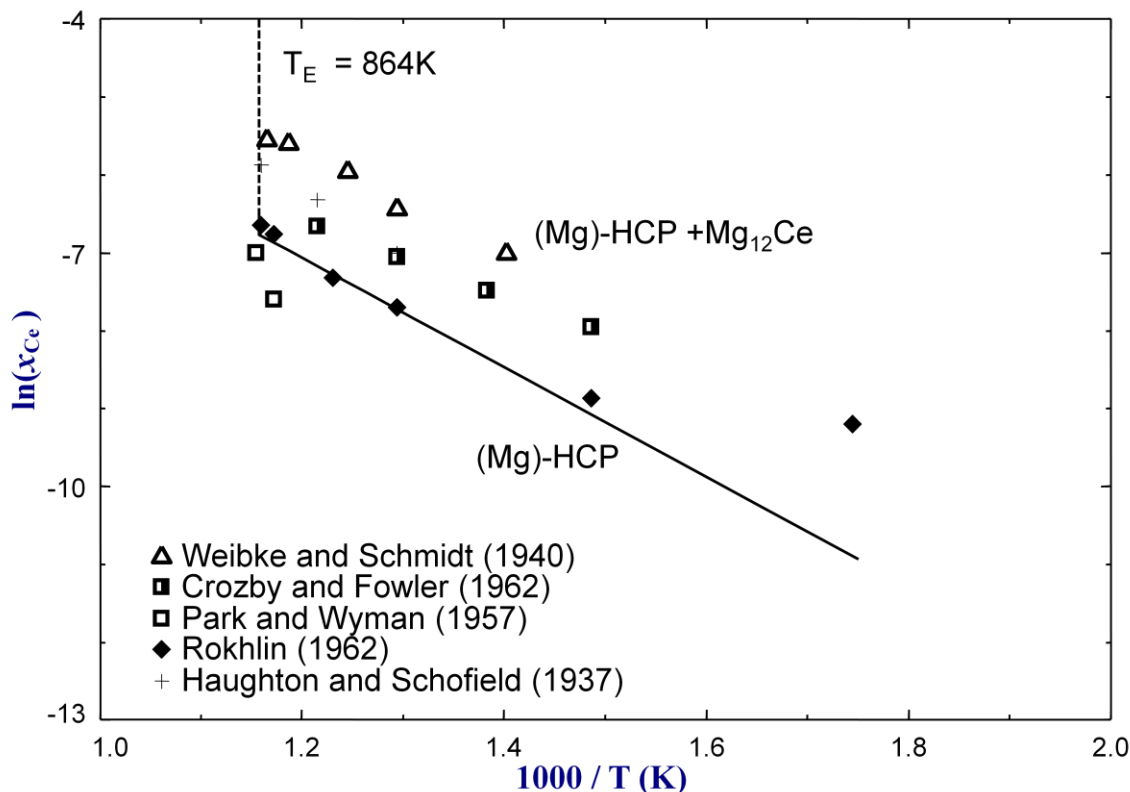
Figure 7.1 The calculated solubility of Ce in (Mg)–HCP with the experimental data from [54-58].

Finally, the enthalpy of formation of LaMg$_{12}$, CeMg$_{12}$ and PrMg$_{12}$ should be of similar magnitude. The enthalpy of formation of LaMg$_{12}$ from the recent experimental work (–4.9 kJ/mole of atoms) by Berche *et al*. [8] is more positive than the optimized value of CeMg$_{12}$ (–10.76 kJ/mole of atoms) from Kang *et al.* [6]. The enthalpy of formation for CeMg$_{12}$ estimated by the Miedema model (–5.2 kJ/mole of atoms) and the First-Principles calculations (–5.9 kJ/mole of atoms) suggest that the enthalpy of formation of the CeMg$_{12}$ should be modified. In the present optimization, the value is –5.7 kJ/mole of atoms, which reproduces well the solubility slope shown in Figure 7.1 where the data from Rokhlin [54] were preferred. The calculated enthalpy of formation of the stable intermetallic compounds of the Mg–Ce system is presented in Figure 7.2 with the experimental data from Biltz and Pieper [9], Nagarajan and Sommer [62], Pahlman and Smith [63], Ogren *et al*. [64] and the *ab-initio* data from Tao [47, 48] together with our estimated values from Miedema's model and first-principles calculations. A revised

calculated phase diagram of the Mg–Ce system is shown in Figure 7.3 with the experimental data from Flandorfer *et al.* [65], Haughton and Schofield [66], Vogel and Heumann [67], Joseph and Gschneidner [68], Wood and Cramer [69], Gschneidner [70] and Saccone *et al.* [53] (Smith Thermal Analysis (STA)).
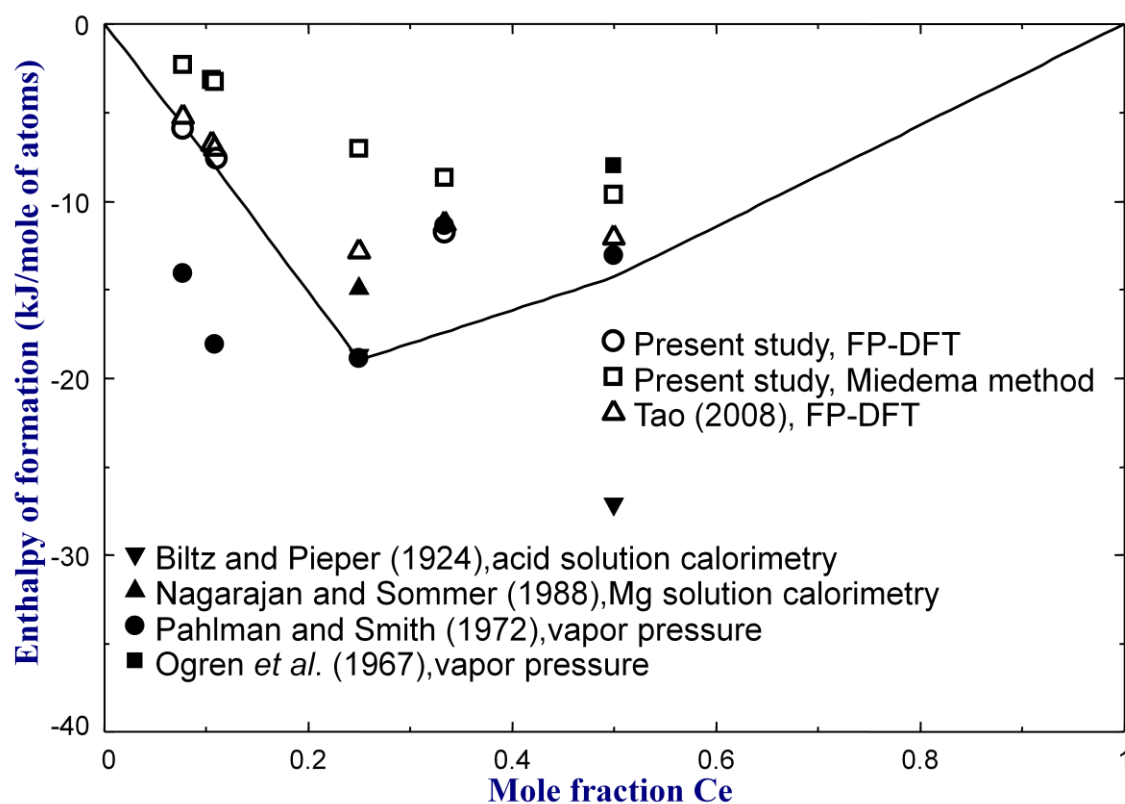
Figure 7.2 The calculated enthalpy of formation of stable intermetallic compounds in the Mg-Ce system at 298 K, with the experimental data from [9, 62-64], *ab-initio* data from Tao [47, 48] and our calculated values from Miedema's model and first-principles.
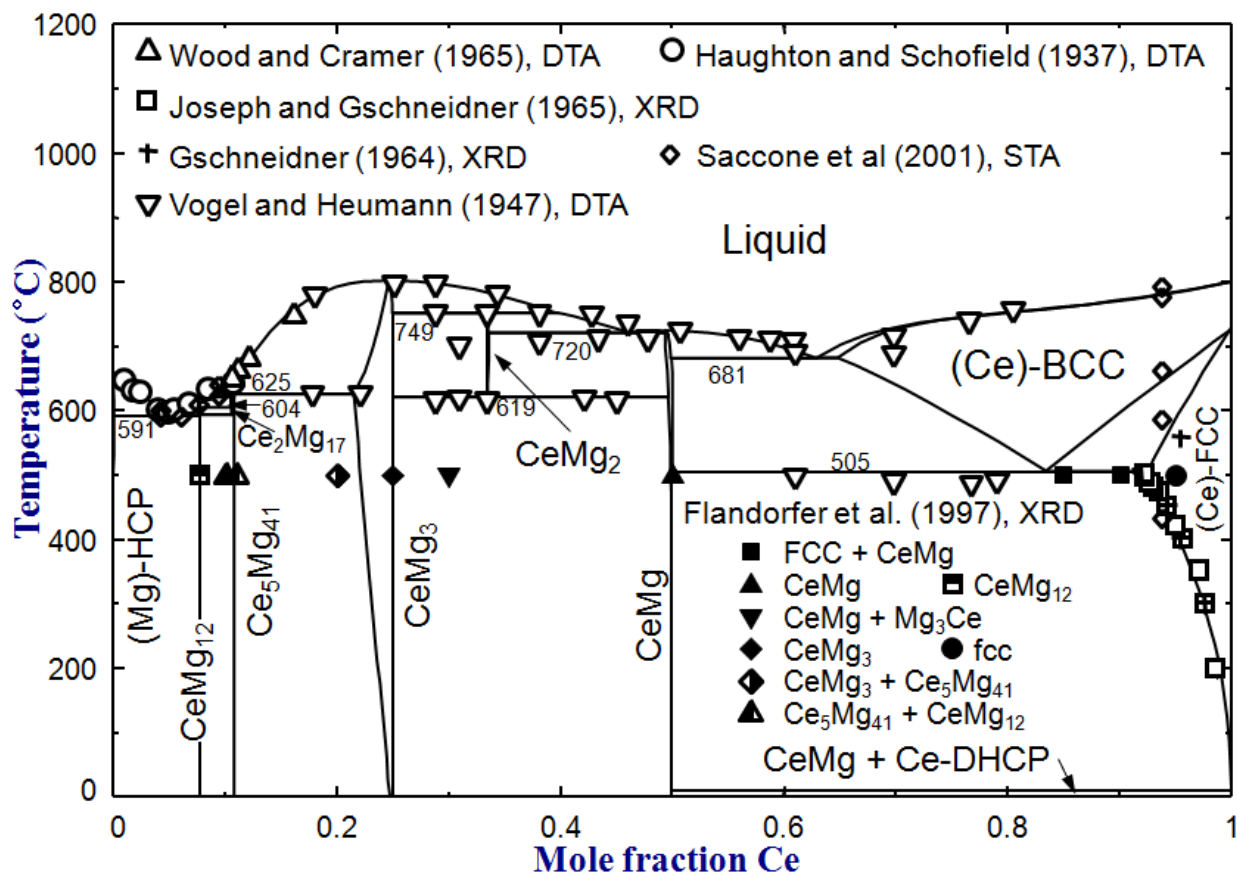
Figure 7.3 The calculated Mg-Ce phase diagram with the experimental data from [53, 65-70].

7.4.2 The Mg–La System

This system was extensively reviewed by Nayeb-Hashemi and Clark [60] and Franke *et al.* [71]. It was thermodynamically optimized by Guo and Du [72]. The following phases were reported as stable phases: liquid, (Mg)–HCP, $LaMg_{12}$, La_5Mg_{41}, $LaMg_3$, $LaMg_2$, $LaMg$, (La)–BCC, (La)–FCC, and (La)–DHCP.

Nayeb-Hashemi and Clark [60] followed by Guo and Du [72] reported that $Mg_{17}La_2$ is stable down to room temperature, instead of $Mg_{41}La_5$. In the homologous Mg–Ce binary system, both phases are known to be stable but Ce_2Mg_{17} is stable only in a very limited temperature range. No other Mg–RE system has a stable RE_2Mg_{17} phase. It was suggested by Giovannini *et al.* [73]

through their experimental results that $Mg_{17}La_2$ was more stable at lower temperature than La_5Mg_{41}. The recent experiment from Berche *et al.* [74] confirms the stability of La_2Mg_{17} to room temperature, and that La_5Mg_{41} is stable only at high temperature. Wróbel *et al.* [75] also suggested that the La_2Mg_{17} phase is metastable at 0 K from their ab initio calculation. Therefore, in the present study, it was considered that La_5Mg_{41} is only stable at high temperature while La_2Mg_{17} phase is stable down to room temperature.

Guo and Du [72] used several enthalpies of formation of intermetallic phases estimated by Miedema model [76] in order to obtain model parameters for the Mg–La intermetallic phases. A Bragg–Williams random mixing model was used to model the liquid phase. $LaMg_{12}$ and $LaMg_3$ were treated to be non-stoichiometric phase using two sub-lattice CEF. Du *et al.* [77] re-optimized the Mg–La system using Bragg-William random mixing model for the liquid while the optimized model parameters were presented in Guo *et al.* [49]. Recently, Berche *et al.* [78] optimized the Mg–La system with consideration of their experimental data [8, 74] using the substitutional model with Redlich–Kister formalism for the liquid. In the present work, the experimental data from Berche *et al.* [8, 74] was preferred and short-range ordering in the liquid was considered by using MQM for the liquid.
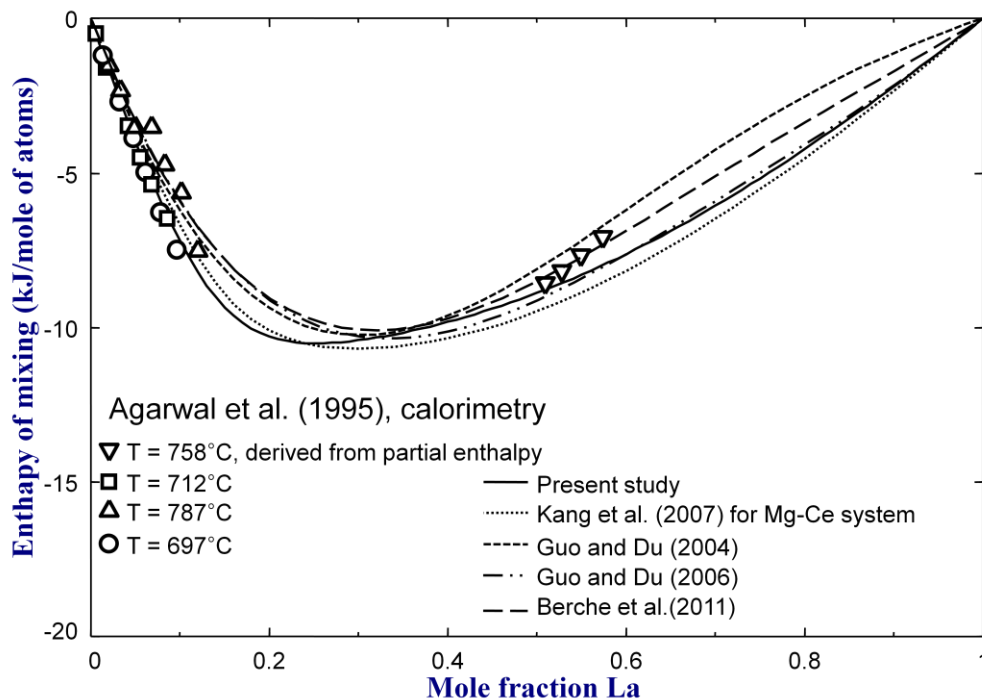
Figure 7.4 The calculated integral enthalpy of mixing of Mg–La liquid alloys at several temperatures.
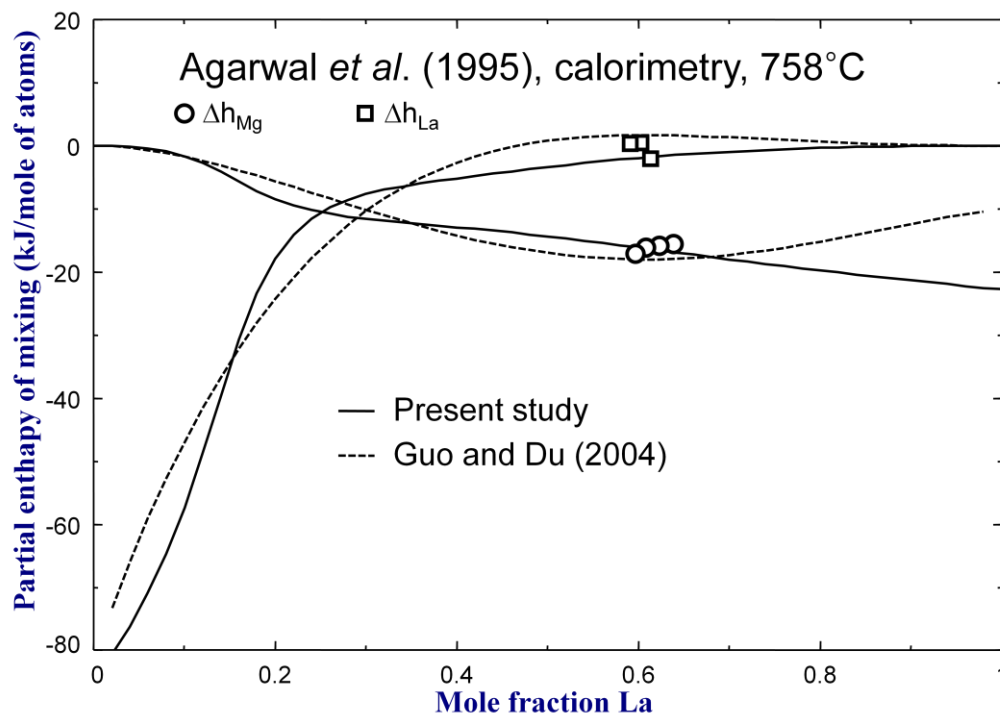
Figure 7.5 The calculated partial enthalpy of mixing at 758 ℃ in Mg–La liquid alloys.
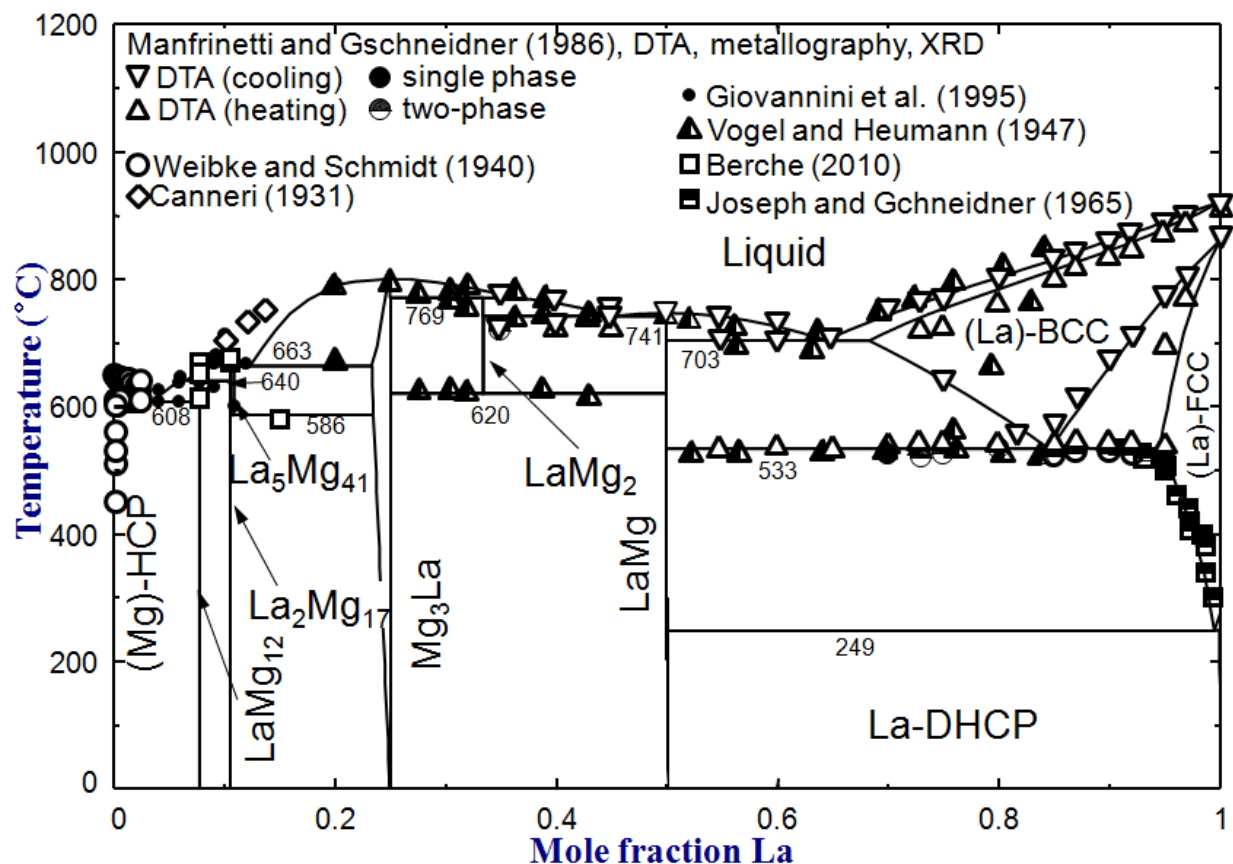
Figure 7.6 The calculated Mg-La phase diagram along with experimental data [58, 67, 68, 73, 80].

Figure 7.4 shows the calculated integral enthalpy of mixing of liquid Mg-La alloys at 758 ℃. The dotted curve is the calculated (optimized) integral enthalpy of mixing in the Mg–Ce binary liquid phase from Kang *et al*. [6] for the comparison purpose. The calculated integral enthalpy of mixing of liquid Mg–La alloys from Guo and Du [72], Du *et al*. [77] and Berche *et al*. [78] are also compared. Figure 7.5 shows the calculated partial enthalpy of mixing of Mg and of La at 758 ℃, with the measurements of Agarwal *et al*.[79]. Figure 7.6 shows the calculated phase diagram of the Mg–La binary system along with experimental data [58, 67, 68, 73, 80]. Most experimental data agree well each other, and also agree to the calculation made in the present study except for the liquidus of Mg₃La on the Mg-rich side. It was very difficult to reproduce this liquidus without causing an inverted liquid immiscibility at high temperature. The relationship between the solid solubility of La in the (Mg)–HCP and temperature is presented in Figure 7.7 compared with

available experimental data [55, 56, 58, 81]. As discussed for the Mg–Ce system, among several experimental data sets, Rokhlin [81] was chosen in the present optimization. Figure 7.8 shows the optimized enthalpy of formation of solid phases, along with the experimental data [7, 8] and FP-DFT estimations [47, 82] and with our estimated data from Miedema's model and first-principles calculations. The optimized values are close to those measured by Berche *et al.* [8] and also to our calculated data from Miedema's model and first-principles. Figure 7.9 and Figure 7.10 show the calculated vapor pressure (essentially $Mg_{(g)}$) over LaMg–(La)–FCC alloy and the experimental data by Ogren *et al.* using a Knudsen effusion cell [64], and the calculated activity of Mg in the liquid alloy with the derived data from the vapor pressure measurements by Afanas'yev *et al.* [83], respectively. Finally, the calculated entropy of mixing in the liquid Mg–La alloy at 707 ℃ is shown in Figure 7.11 (solid curve), with the calculated curve from Guo and Du (dashed curve) [72].
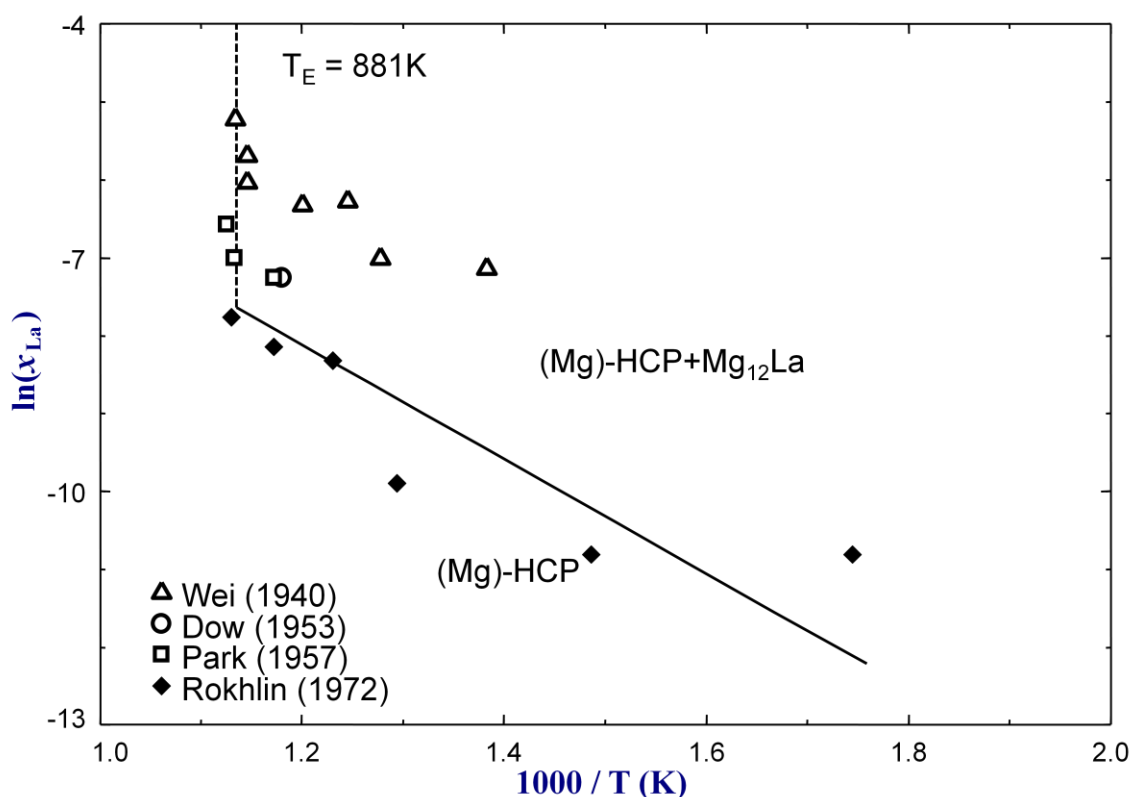
Figure 7.7 The calculated solubility of La in (Mg)–HCP with the experimental data from [55, 56, 58, 81].
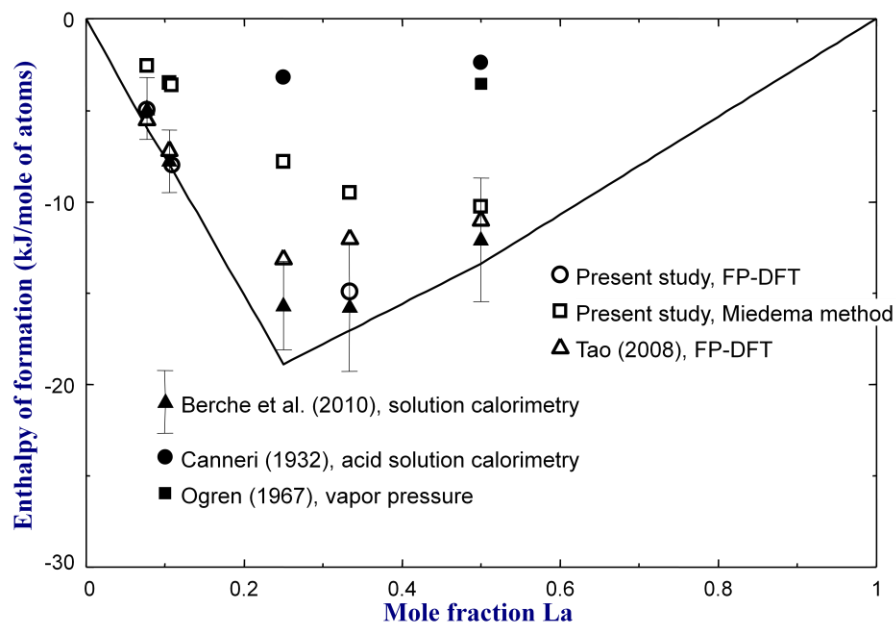
Figure 7.8 The optimized enthalpy of formation of solid phases in the Mg–La system compared with data from [7, 8, 47, 82], with our calculated data from Miedema's model and with First-Principles estimations.
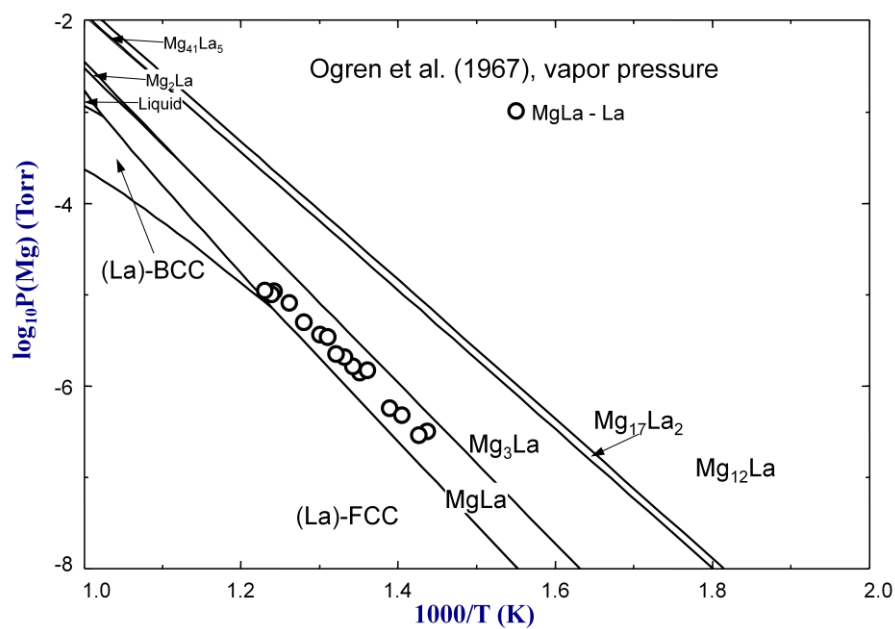
Figure 7.9 The calculated vapor pressure over MgLa– (La)–FCC alloy.
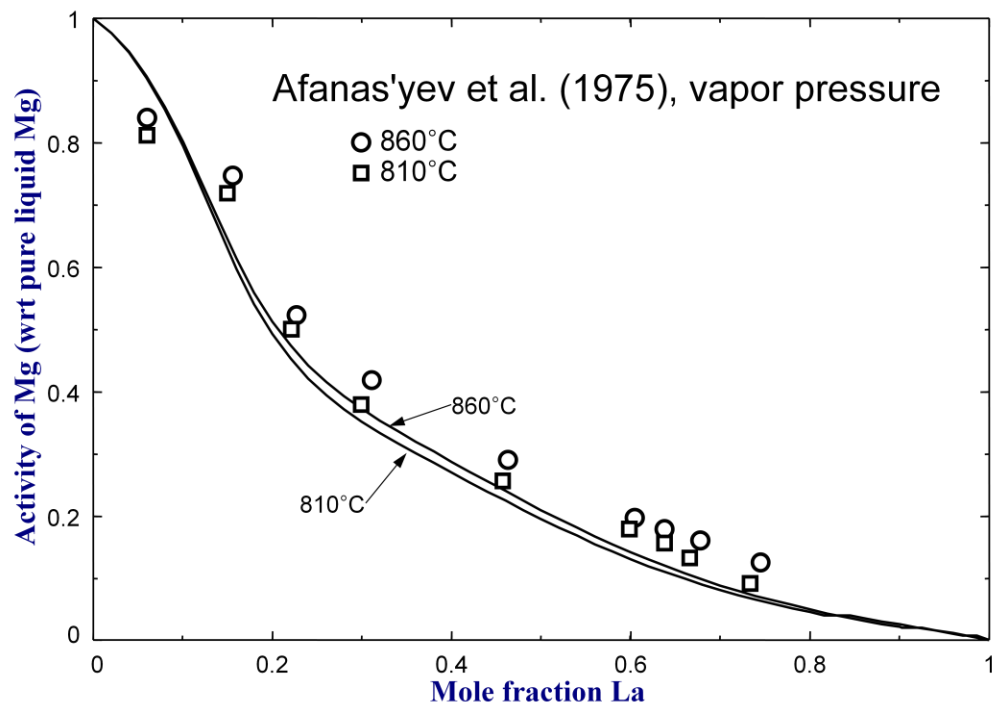
Figure 7.10 The calculated activity of Mg in liquid alloy.
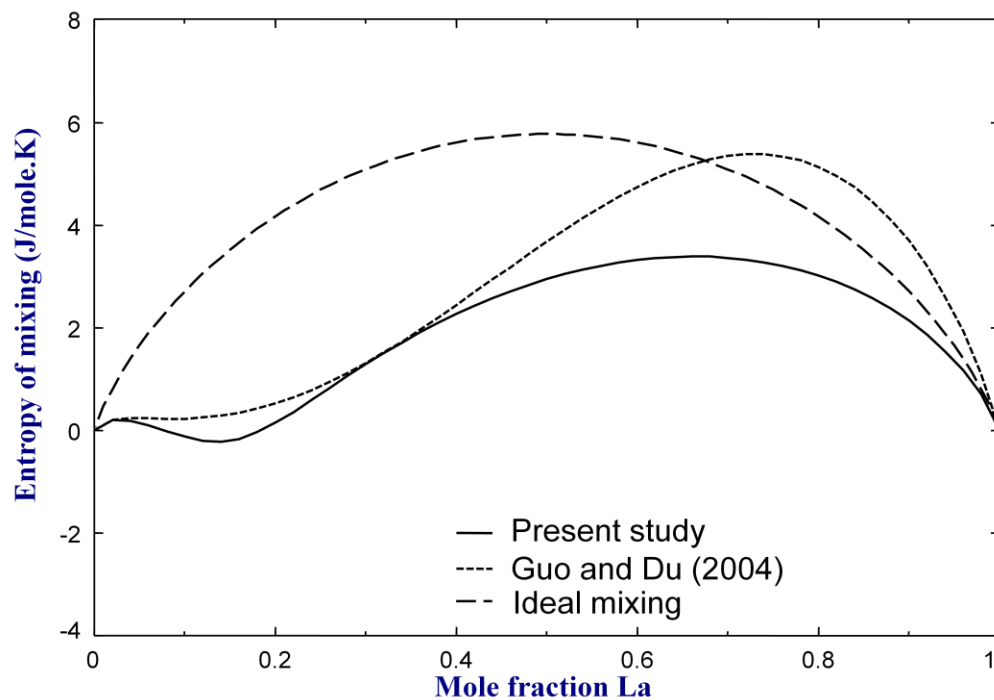
Figure 7.11 The calculated entropy of mixing in the liquid Mg–La alloy (solid curve: present study; dashed curve: Guo and Du [72]).

7.4.3 The Mg–Pr System

This system was extensively reviewed by Nayeb-Hashemi and Clark [84] and was thermodynamically optimized by Guo and Du [85], who later revised their assessment [86]. The following phases were reported as stable phases: liquid, (Mg)–HCP, $Mg_{12}Pr$, $Mg_{41}Pr_5$, Mg_3Pr, Mg_2Pr (Laves–C15), MgPr (BCC–B2), (Pr)–BCC, and (Pr)–DHCP.

The earlier optimization by Guo and Du [85] used the enthalpy of formation of several intermetallic phases (estimated by Miedema's model [76]) in order to obtain model parameters for these phases. Acid solution calorimetry conducted by Canneri and Rossi [87] were also taken into account. A Bragg–Williams random mixing model was used to model the liquid phase. $Mg_{41}Pr_5$, Mg_3Pr, and MgPr were treated to be non-stoichiometric phases using a two sub-lattice CEF [43]. The thermodynamic assessment of Mg–Pr system was revised later by Guo *et al.* [86] based on the same experimental information [45, 76, 87] and taking into account the Mg–Pr–Y ternary phase equilibria data [73].

Figure 7.12 The calculated integral enthalpy of mixing in the liquid Mg–Pr alloys at 707 ℃.
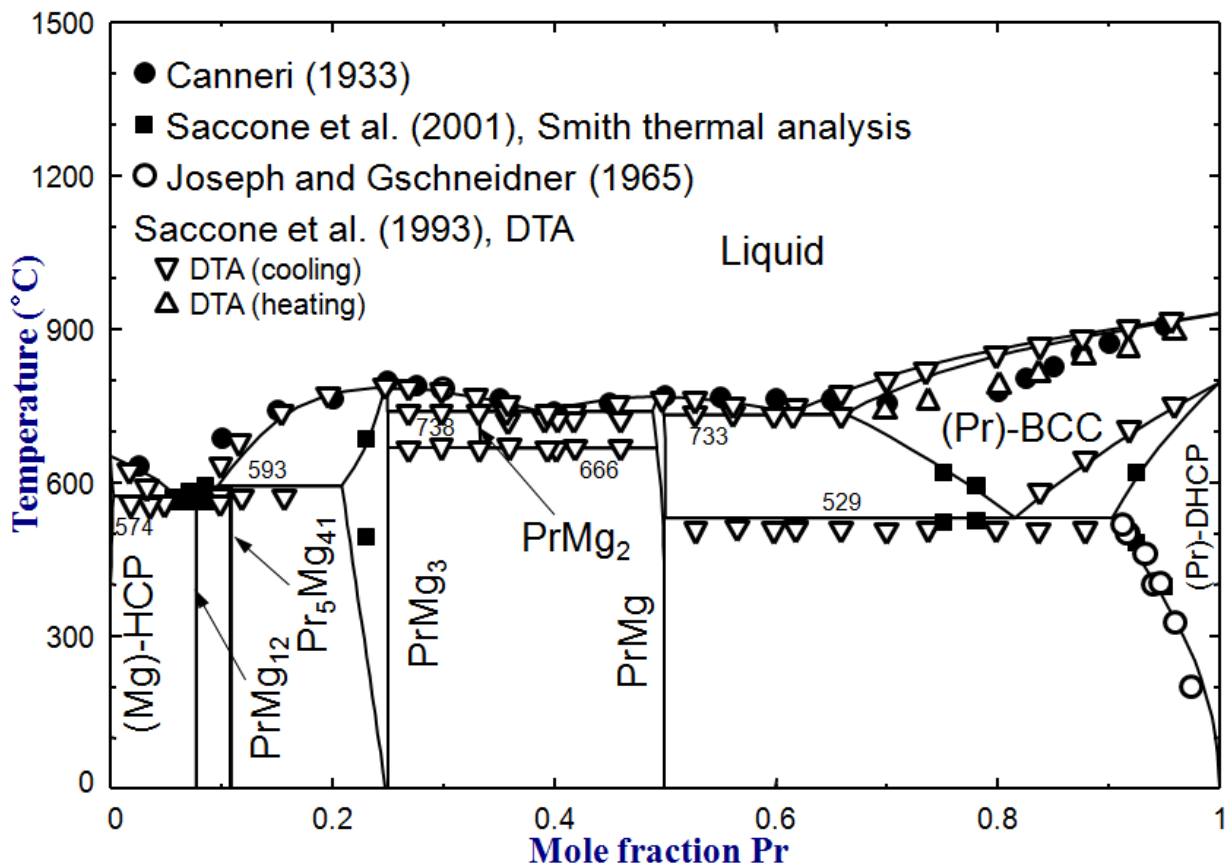
Figure 7.13 The calculated phase diagram of the Mg–Pr binary system along with experimental data [45, 68, 87, 88].

Figure 7.12 shows our calculated integral enthalpy of mixing in the liquid Mg–Pr alloys at 707 ℃. The solid curve is the calculated integral enthalpy of mixing in the present study at 707 ℃ and the dashed curve is the calculated integral enthalpy of mixing by Guo and Du [85]. No calorimetric measurements were reported. Therefore, it was assumed that the Gibbs energy of mixing of the Mg–Pr liquid alloy is the same as the Mg–Ce liquid alloy (same parameters for the mixing part of the Gibbs energy model of the liquid solution with $Z_{MgPr}^{Mg}/Z_{MgPr}^{Pr} = 1/3$). Figure 7.13 shows the calculated phase diagram of the Mg–Pr binary system along with reported experimental data [45, 68, 87, 88]. Most experimental data agree well with each other, and also agree to our calculations except for the solidus of (Pr)–BCC. The calculated solid solubility of Pr in (Mg)–HCP is shown in Figure 7.14 with the experimental data [45, 55, 61, 89, 90]. The solid solubility data from Rokhlin [61] were preferred in the present optimization.
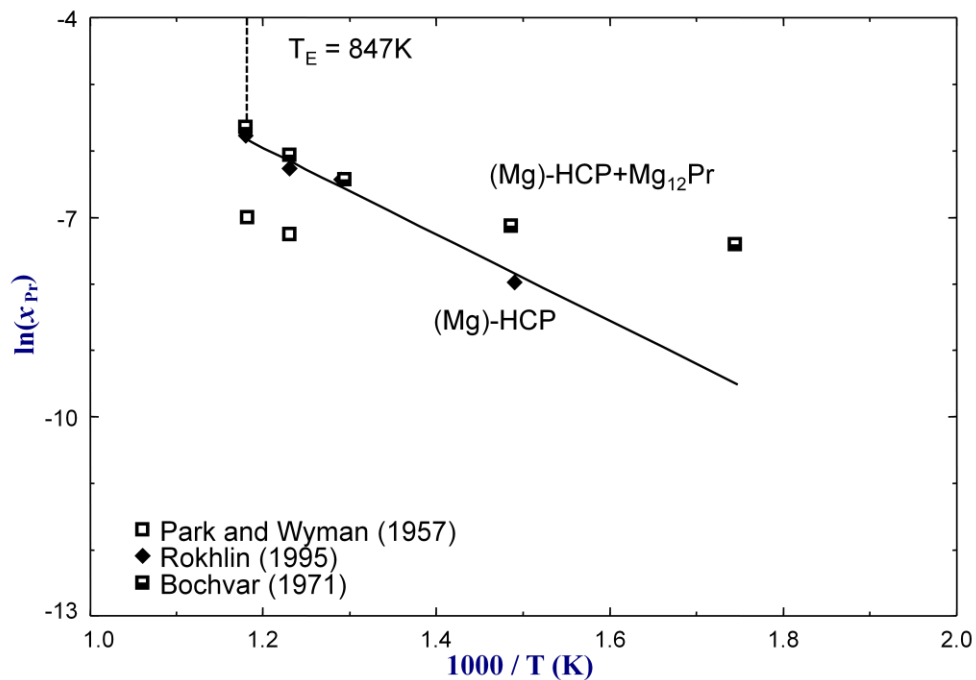
Figure 7.14 The calculated solubility of Pr in (Mg)–HCP with the experimental data from [45, 55, 61, 89, 90].
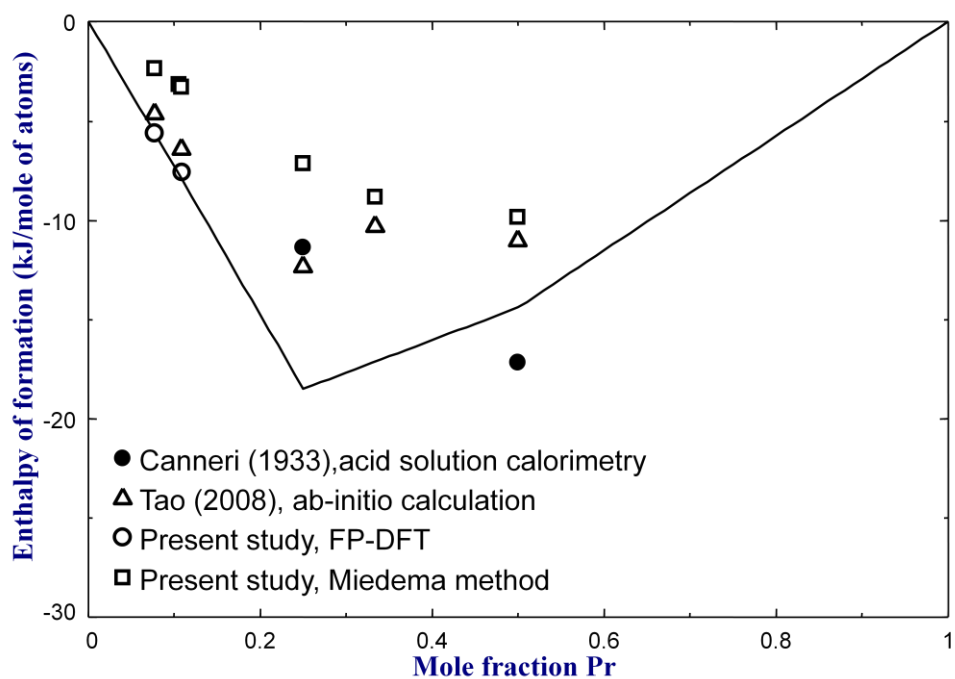
Figure 7.15 The optimized enthalpy of formation of solid phases with experimental data from Canneri and Rossi [91], ab-initio data from Tao [47] and our calculated data.

Figure 7.15 shows the optimized enthalpy of formation of solid phases, along with available data (acid solution calorimetric data by Canneri and Rossi [91], and ab initio data from Tao [47]) and our calculated data from Miedema's model and first-principles. Since the enthalpy data obtained by acid solution calorimetry is usually less reliable, the data were not used in the optimization. Figure 7.16 shows the calculated total vapor pressure over MgPr–(Pr)–DHCP alloys and the data reported by Ogren *et al.* using Knudsen effusion cell [64]. Finally, the calculated entropy of mixing in the liquid Mg–Pr alloy is shown in Figure 7.17 (solid curve) compared with the calculated curve by Guo and Du (dashed curve) [85].
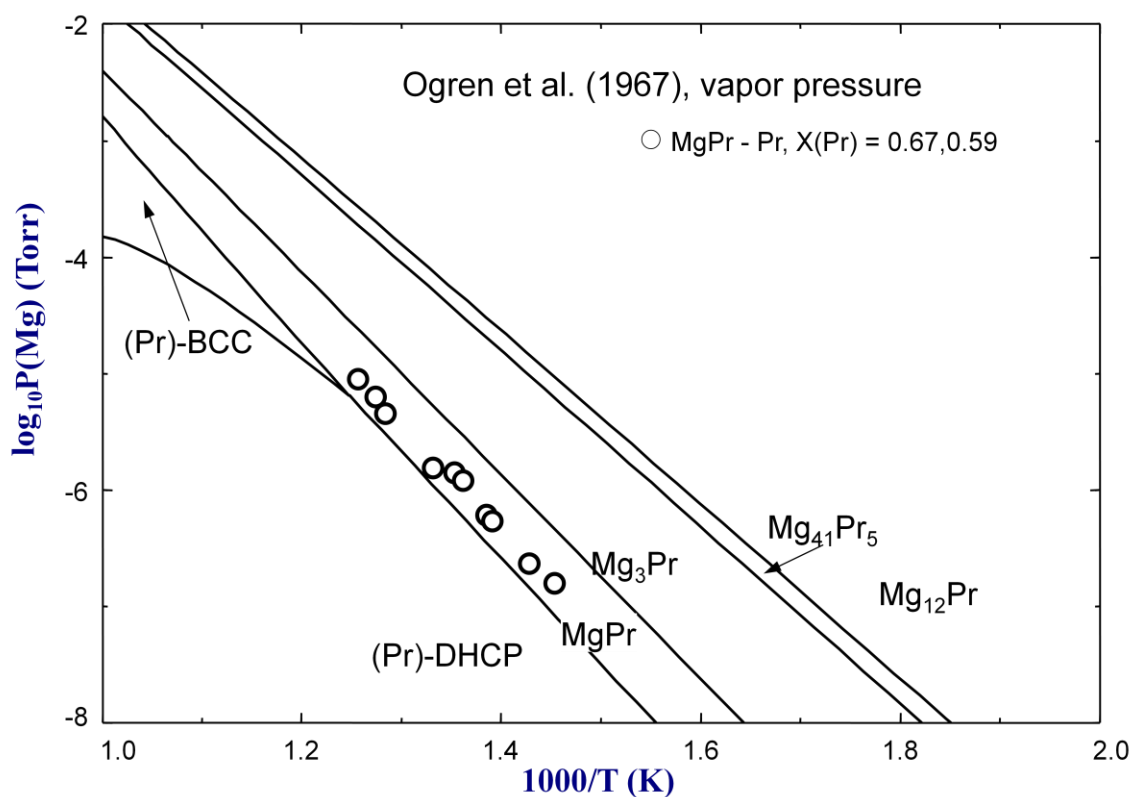
Figure 7.16 The vapor pressure over MgPr – (Pr) –DHCP alloy by Ogren *et al.* [64].
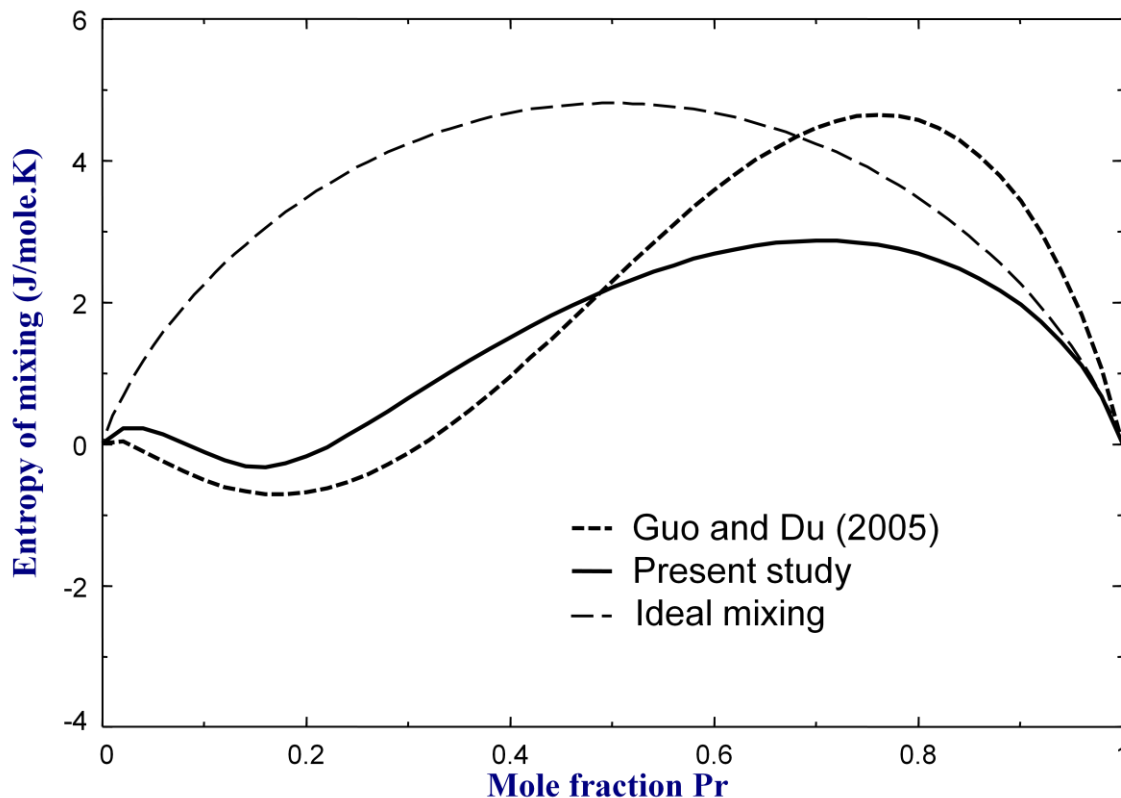
Figure 7.17 The calculated entropy of mixing in the liquid Mg–Pr alloy (solid curve: the present study; dashed curve : Guo and Du [85].

7.4.4 The Mg–Nd System

This system was extensively reviewed by Nayeb-Hashemi and Clark [59] and was thermodynamically optimized by Gorsee *et al*. [92], Meng *et al*. [93] and Guo *et al*. [50, 94]. The following phases were reported to be stable phases: liquid, (Mg)–HCP, Nd_5Mg_{41}, $NdMg_3$, $NdMg_2$, $NdMg$, (Nd)–BCC, and (Nd)–DHCP. The $NdMg_{12}$ is reported by [95] to be metastable, and it is present as precipitates only in quenched samples.

No calorimetric data for intermetallic phases have been reported. The earlier optimization by Gorsee *et al*. [92], Meng *et al*. [93] and Guo *et al*. [50] used the estimated enthalpy of formation from Miedema's model [76] or estimated from vapor pressure measurements [63] in order to

obtain model parameters for intermetallic phases. NdMg$_3$, and NdMg were treated to be non-stoichiometric phase using the two sub-lattice CEF in the assessments by Meng *et al*. [93] and Guo *et al*. [50], while those phases were treated as line compounds in the assessment of Gorsee *et al*. [92]. In all these assessments, a Bragg–Williams random mixing model was used to model the liquid phase. In addition, Gorsee *et al*. [92] also tried to use the associate model assuming the existence of a "NdMg$_3$" complex along with free "Mg" and "Nd", and they concluded that the associate model describes better the binary Mg–Nd liquid solution that the BW random mixing model does, supporting that some short-range order is present in the liquid phase.
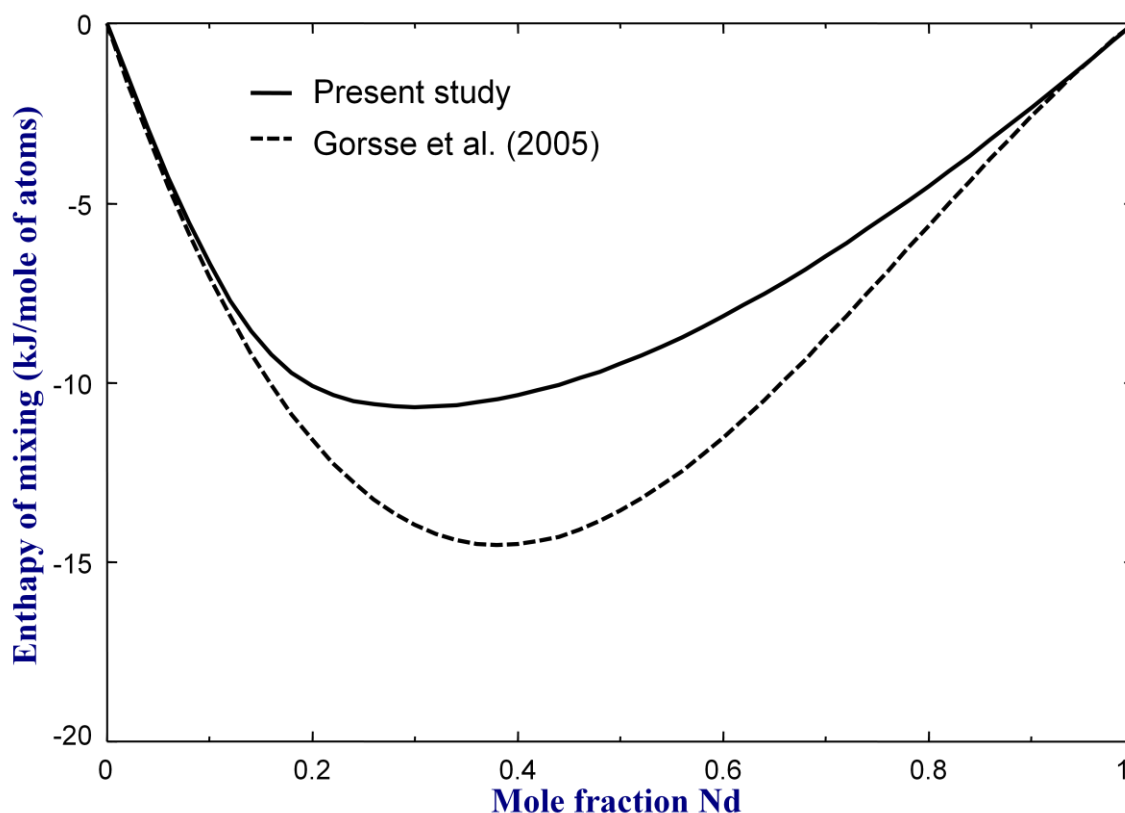
**Figure 7.18** The calculated integral enthalpy of mixing in the liquid Mg–Nd alloys at 707 ℃.

Figure 7.18 shows the calculated integral enthalpy of mixing in the liquid Mg–Nd alloys at 707 ℃. The solid curve is the calculated integral enthalpy of mixing of the liquid in the present study at 707 ℃ while the dashed curve is the calculated value by Gorsse *et al*. [92] using a BW random mixing model. No calorimetric measurements of the enthalpy of mixing in the binary Mg–Nd alloys were reported. Therefore, it was assumed that the Gibbs energy of mixing of the Mg–Nd

liquid alloy is the same as the Mg–Ce liquid alloy (same parameters for the mixing part of the Gibbs energy model of the liquid solution with $Z_{MgNd}^{Mg}/Z_{MgNd}^{Nd}=1/3$). Figure 7.19 shows the calculated phase diagram of the Mg–Nd binary system along with the experimental data [68, 95]. Most reported experimental data agree well with each other, and also agree to the estimation made in the present study. The relationship between the solid solubility of Nd in the (Mg)–HCP and temperature is presented in Figure 7.20 with the experimental data [54, 55, 96, 97]. From the same reason as that of the Mg–Ce system, among several experimental data, that of Rokhlin [54] was chosen in the present optimization. Furthermore, the recent study from Kopp *et al*. [97] by atom probe tomography confirms that the solid solubility of Nd in (Mg)–HCP is closer to that of Rokhlin [54] and much higher than that of Park and Wyman [55].
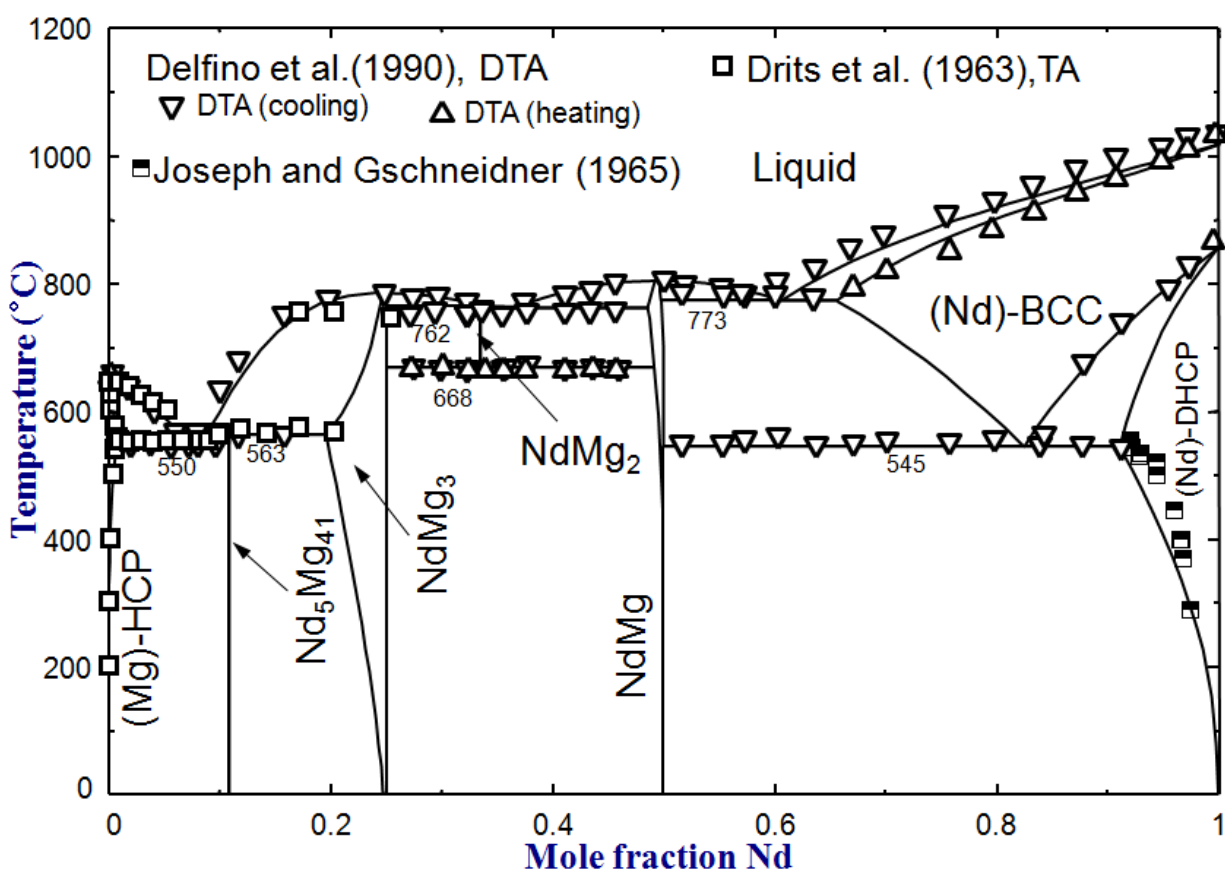
Figure 7.19 The calculated phase diagram of the Mg–Nd binary system along with experimental data [68, 95].
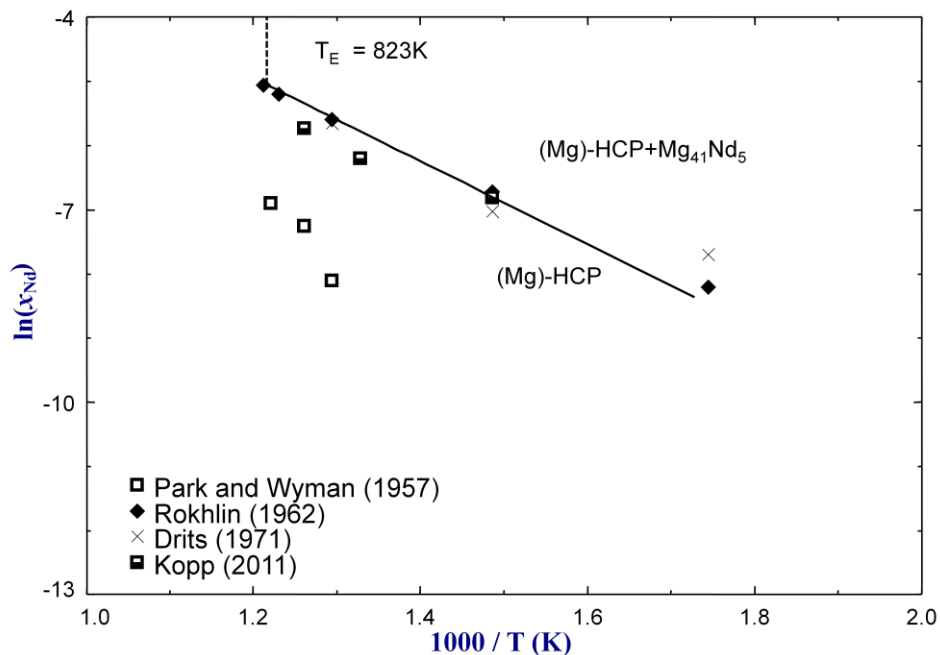
Figure 7.20 The calculated solubility of Nd in (Mg)–HCP with the experimental data from [54, 55, 96, 97].
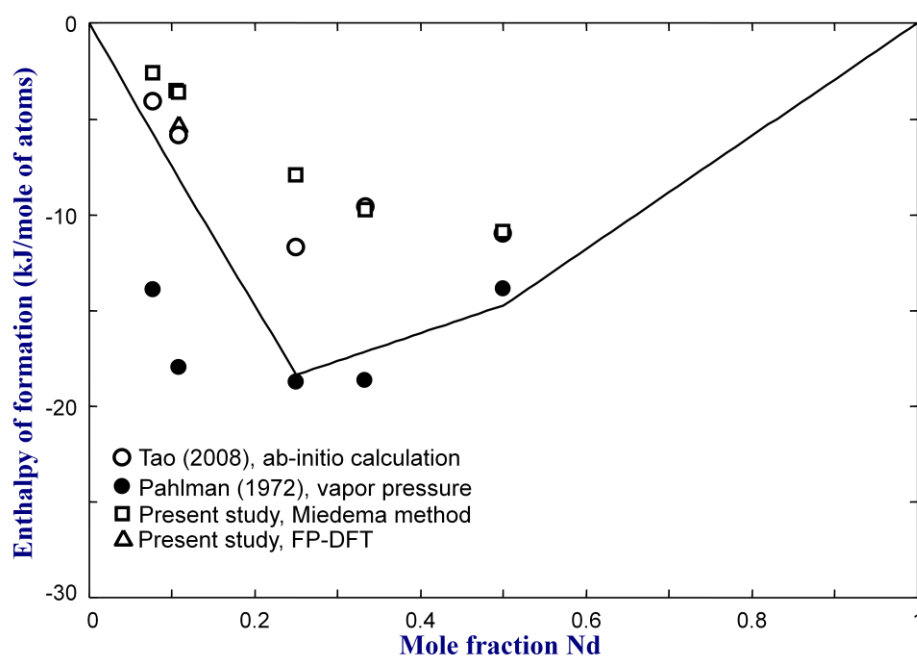
Figure 7.21 The optimized enthalpy of formation of solid phases of Mg–Nd system with estimated data from vapor pressure measurement [63], ab-initio data from Tao [47] and our calculated data from Miedema's model and first-principles.

Figure 7.21 shows the optimized enthalpy of formation of solid phases, along with estimated data from vapor pressure measurement [63], ab initio data from Tao [47] and our calculated data from Miedema's model and FP-DFT. The optimized enthalpies of formation are generally located between the calculations (FP-DFT and Miedema method) and the experimental data (derived values from vapor pressure measurement). Figure 7.22 shows the calculated vapor pressure over several alloy compositions used by Ogren *et al*. [64] and Pahlman and Smith [63]. The calculated curve is generally in reasonable agreement with the experimental points. Finally, the calculated entropy of mixing in the liquid Mg–Nd alloy at 707 ℃ is shown in Figure 7.23, and the calculation in the present study (solid curve) is compared with that of BW random mixing model by Gorsse *et al*. (dashed curve) [92].
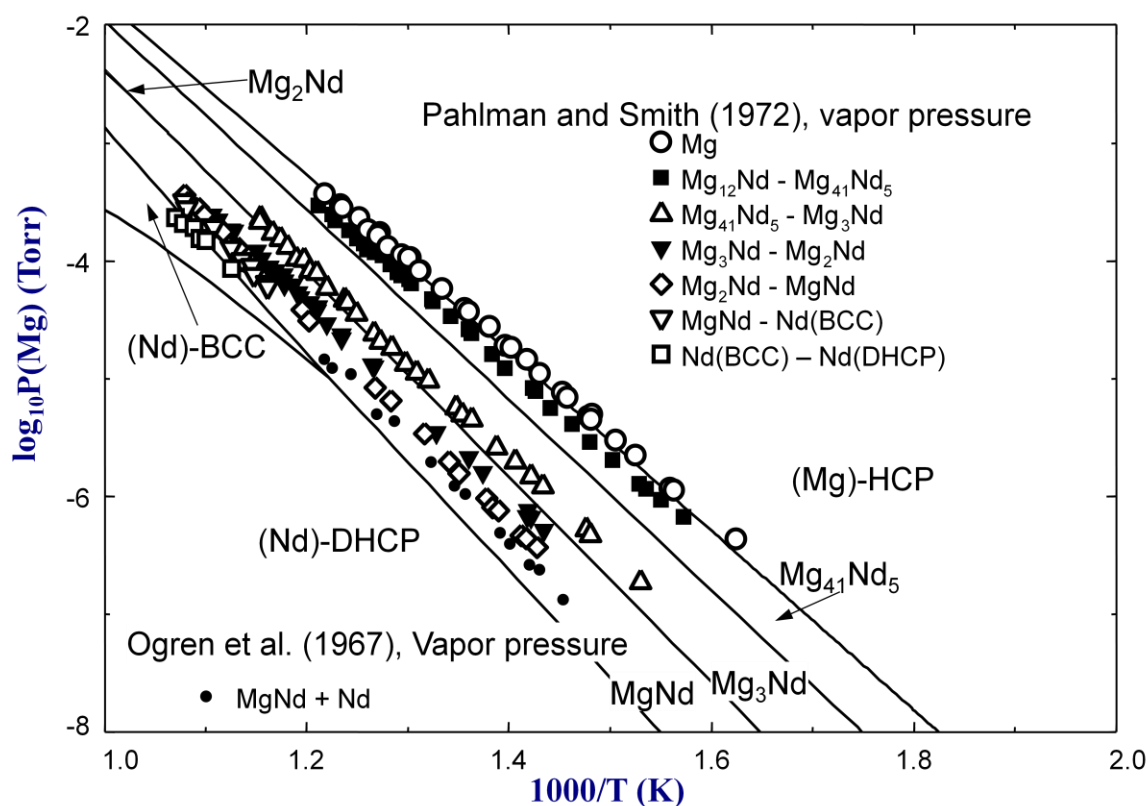
Figure 7.22 The vapor pressure over several alloys in the Mg–Nd system by Ogren *et al*. [64] and Pahlman and Smith [63].
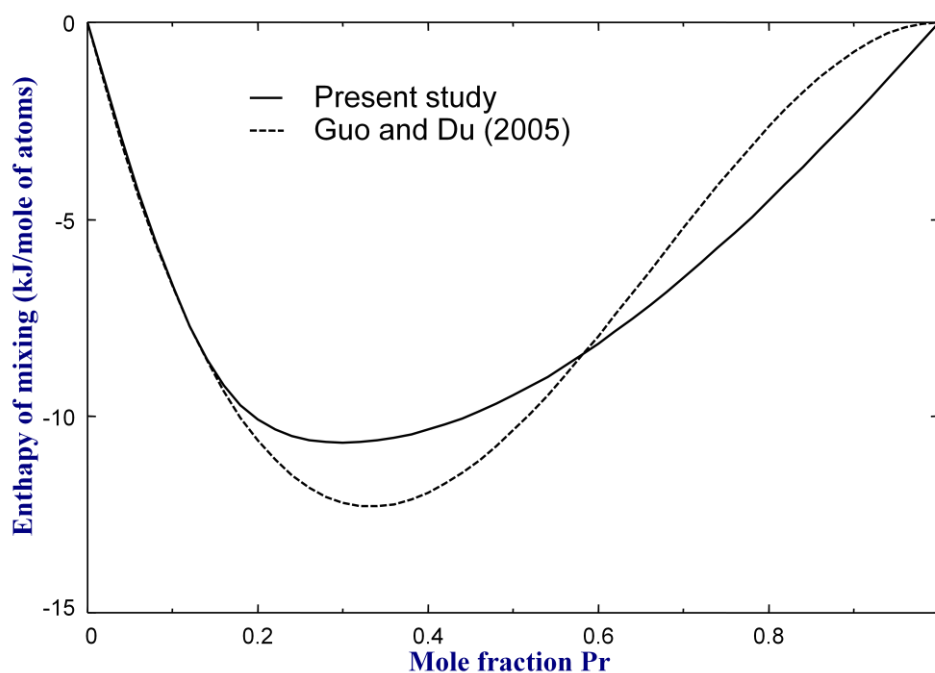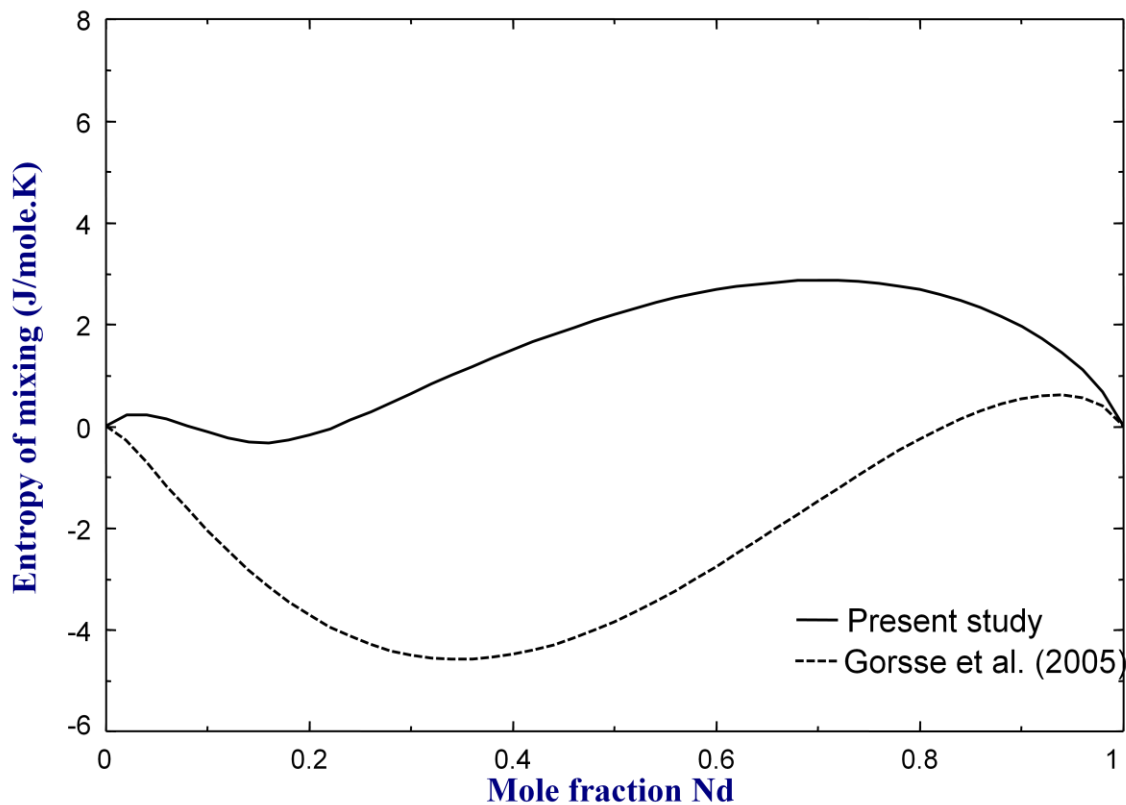
Figure 7.23 The calculated entropy of mixing in the liquid Mg–Nd alloy (solid curve: the present study; dashed curve: Gorsee *et al*. [92].

7.4.5 The Mg–Sm System

This system was extensively reviewed by Nayeb-Hashemi and Clark [98] and Okamoto [99]. It was thermodynamically optimized by Jia *et al*. [100]. The following phases were considered as stable phases: liquid, (Mg)–HCP, Sm_5Mg_{41}, $SmMg_5$, $SmMg_3$, $SmMg_2$ (Laves–C15), SmMg (BCC–B2), (Sm)–BCC, (Sm)–HCP, Sm–rhombohedral.

For this system, a "preliminary" calorimetric data for intermetallic phases have been reported by Cacciamani *et al*. [101]. However, this calorimetric data has not been utilized in the earlier optimization by Jia *et al*. [100]. In their assessment, all intermetallic phases were treated to be the

stoichiometric phases. A Bragg–Williams random mixing model was used to model the liquid phase. They seemed to only rely on phase diagram data during the course of the assessment.
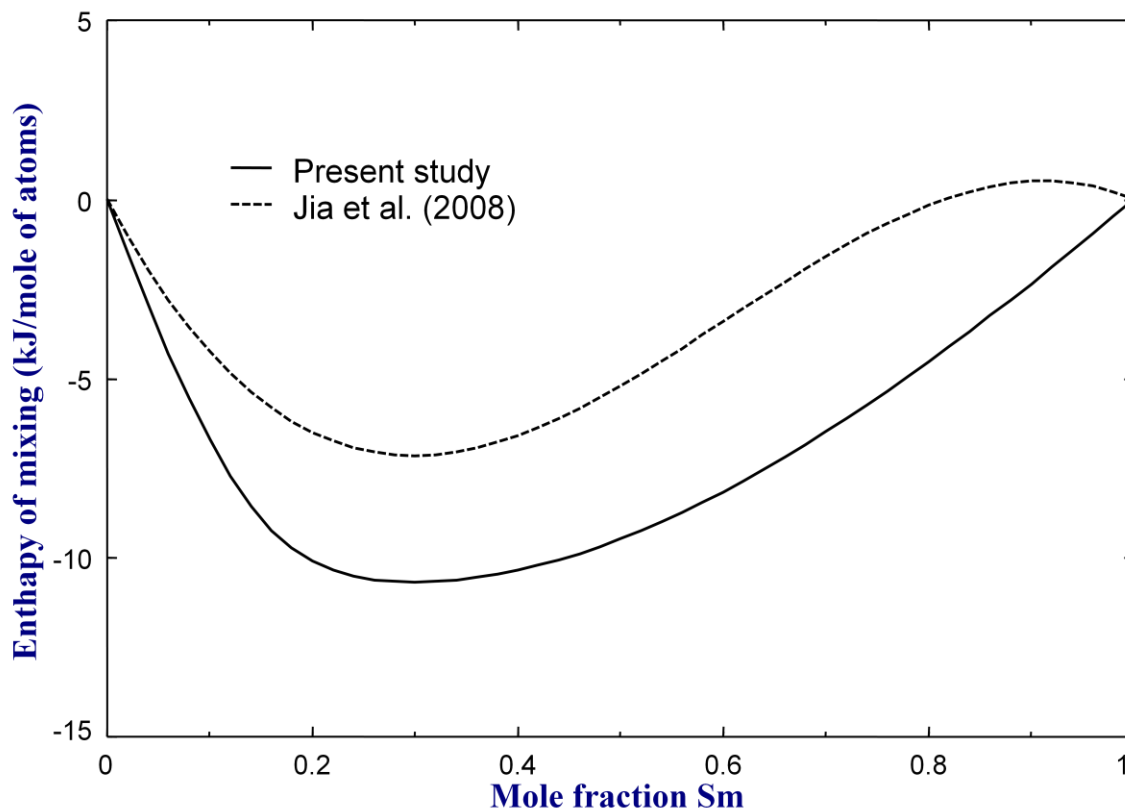
Figure 7.24 The calculated integral enthalpy of mixing in the liquid Mg–Sm alloys at 707 ℃ (Solid curve: the present study; Dashed curve: calculated from the Jia *et al*. [100] using BW random mixing model).
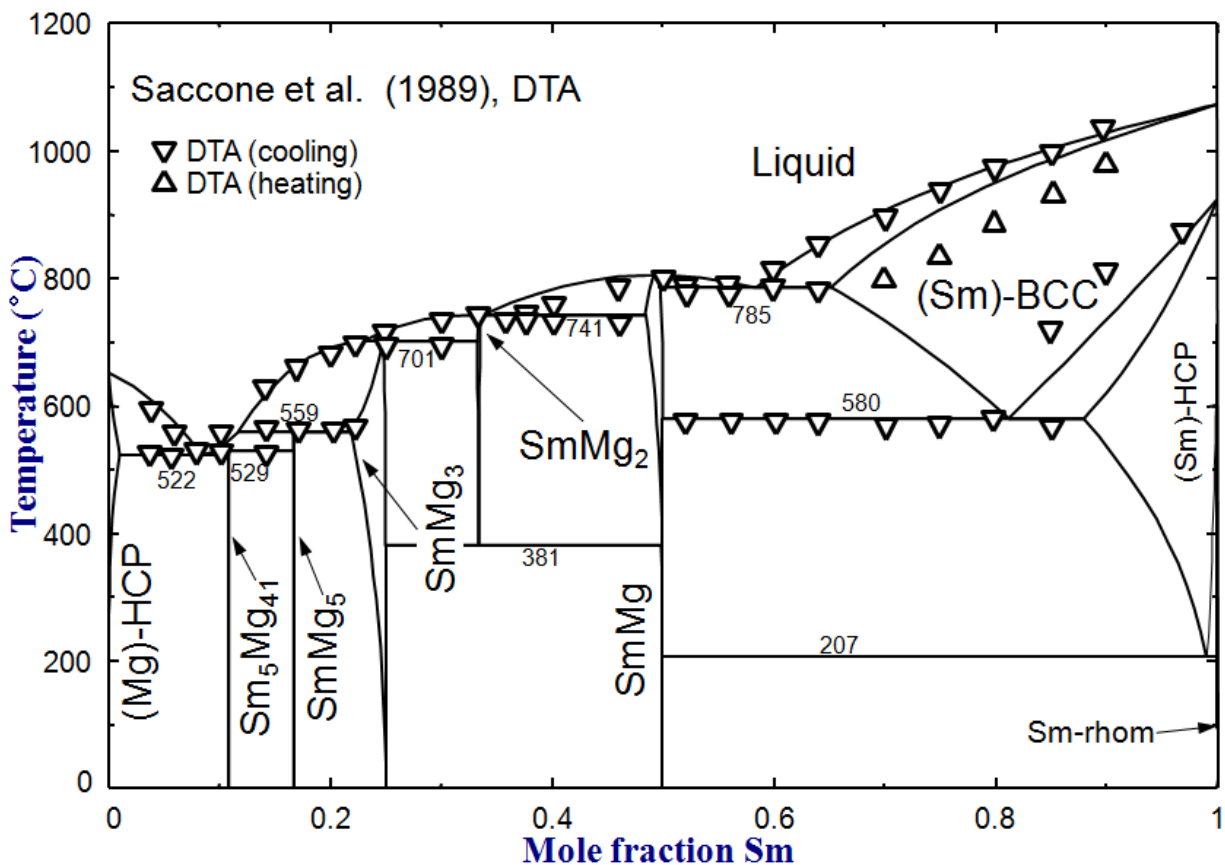
Figure 7.25 The calculated phase diagram of the Mg–Sm binary system along with experimental data from [102].

Figure 7.24 shows the calculated integral enthalpy of mixing in the liquid Mg–Sm alloys at 707 ℃. The solid curve is the calculated integral enthalpy of mixing in the present study at 707 ℃, while the dashed curve is a calculated integral enthalpy of mixing by Jia *et al.* [100] using BW random mixing model. There has been no calorimetric measurement on the enthalpy of mixing in the binary Mg–Sm alloys. Therefore, as mentioned before, it was assumed that Gibbs energy of mixing of the Mg–Sm liquid alloy is the same as that of the Mg–Ce liquid alloy. As was done for other Mg–light RE binary liquid alloy, the MQM with $Z_{MgSm}^{Mg}/Z_{MgSm}^{Sm}=1/3$ was used. Figure 7.25 shows a calculated phase diagram of the Mg–Sm binary system along with the experimental data [102]. Most experimental data agree to the calculation made in the present study, except for the solidus of (Sm)–BCC. The relationship between the solid solubility of Sm in the (Mg)–HCP and temperature is presented in Figure 7.26 with the experimental data from Rokhlin *et al.* [103]. It is

similar to those of previous mentioned Mg–RE (RE: La, Ce, Pr and Nd) systems, although the compound which is in equilibrium with (Mg)–HCP is $Mg_{41}Sm_5$ instead. From the same reason as that of Mg–Ce system, the experimental data of Rokhlin *et al.* [103] was considered to be reliable and it was used in the present optimization. It was found by Rokhlin [104] that the solubility of the RE of the lanthanide series in Mg successively increase with increasing the atomic number, with the consequence of decreasing the metallic atomic radius of RE (known as lanthanide shortening, except Eu and Yb).
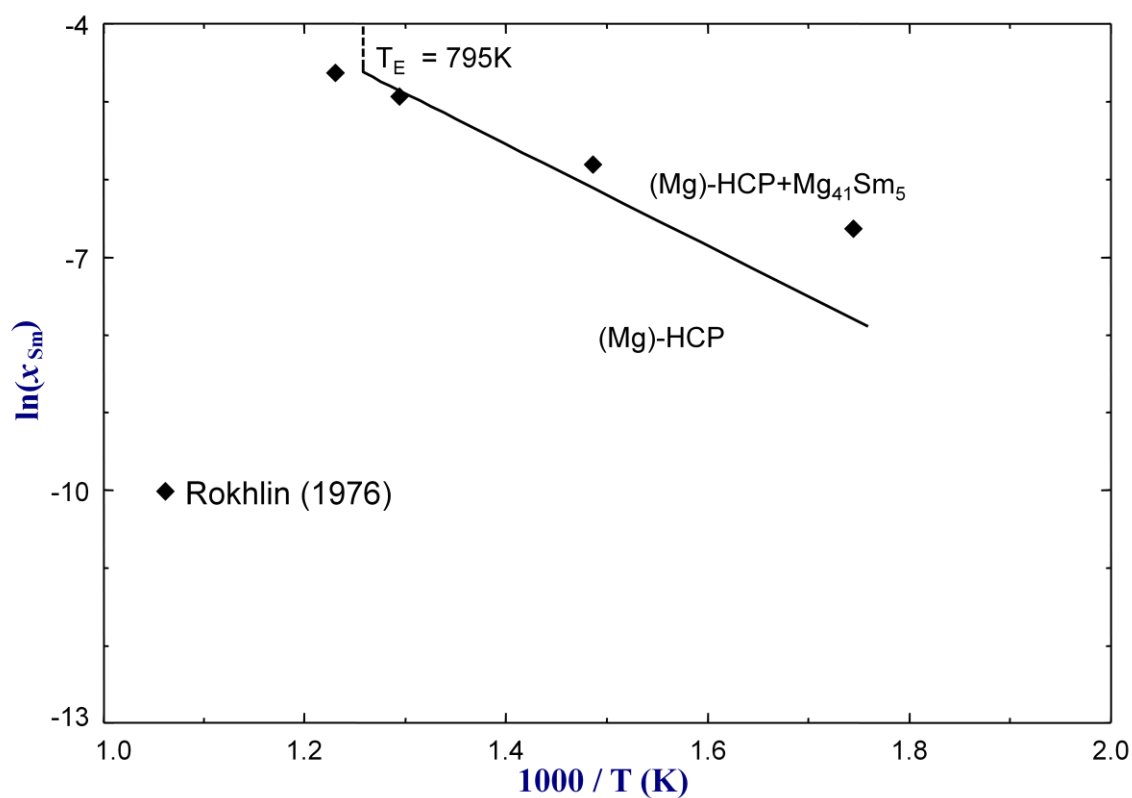
Figure 7.26 The calculated solubility of Sm in (Mg)–HCP with experimental data from [103].
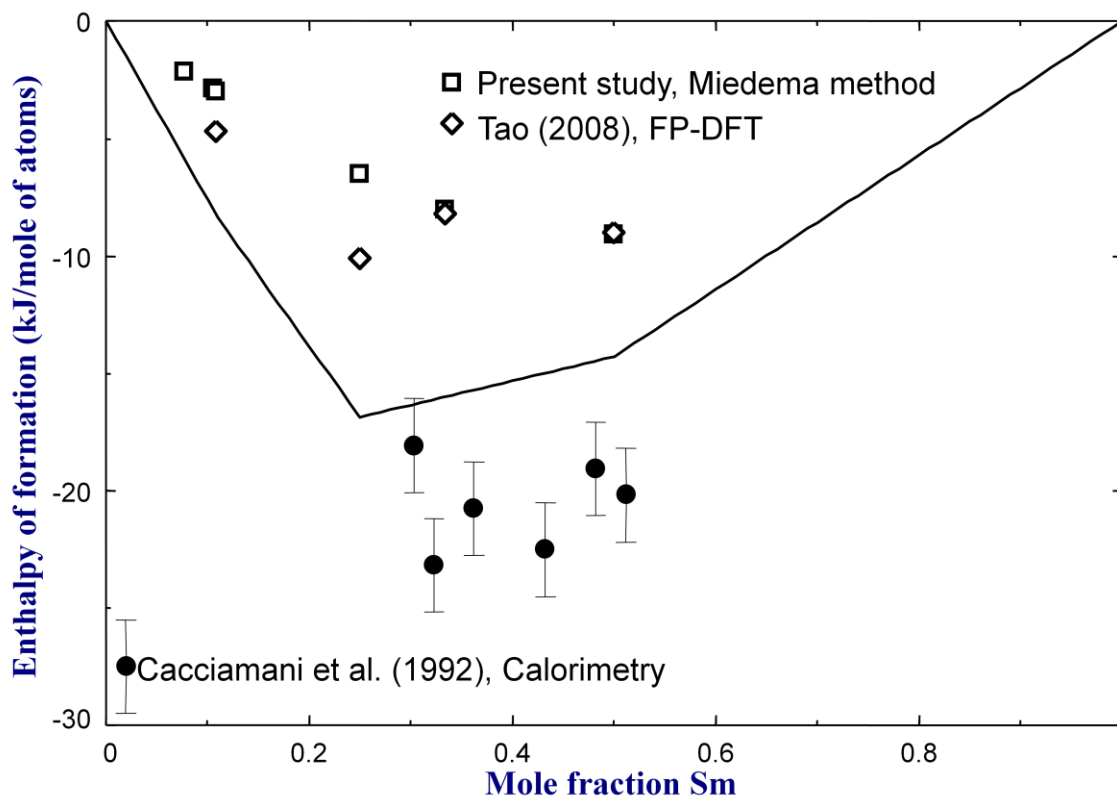
Figure 7.27 The optimized enthalpy of formation of solid phases, along with the calorimetric data by Cacciamani *et al*. [101].

Figure 7.27 shows the optimized enthalpy of formation of the solid phases, along with the calorimetric data by Cacciamani *et al.* [101]. The optimized enthalpies of formation (keeping the same entropy of formation from corresponding binary intermetallic phases in Mg–Ce system) are slightly less negative than those measured by Cacciamani *et al*. [101]. However, during the course of the present optimization, it was found that reproducing the calorimetric data [101] results in much wider liquidus of MgSm phase. Therefore, it was not attempted to reproduce those data [101] in the optimization. Figure 7.28 shows vapor pressure over MgSm – (Sm)–HCP alloys by Ogren *et al*. [64]. The calculated curve is also shown in the Figure 7.28, showing generally reasonable agreement. Finally, the calculated entropy of mixing in the liquid Mg–Sm alloy at 707 ℃ is shown in Figure 7.29, and the calculation in the present study (solid curve) is compared with that of BW random mixing model by Jia *et al*. (dashed curve) [100]. It may be noteworthy that all the Mg-light rare earth binary systems show quite similar thermodynamic

properties. However, the independent optimizations from Guo and Du [72, 85] for Mg–La and Mg–Pr systems, from Gorsse *et al.* [92] for Mg–Nd system, and from Jia *et al.* [100] did not demonstrate the similar entropy of mixing in the liquid shown in Figs 11, 17, 23 and 29.
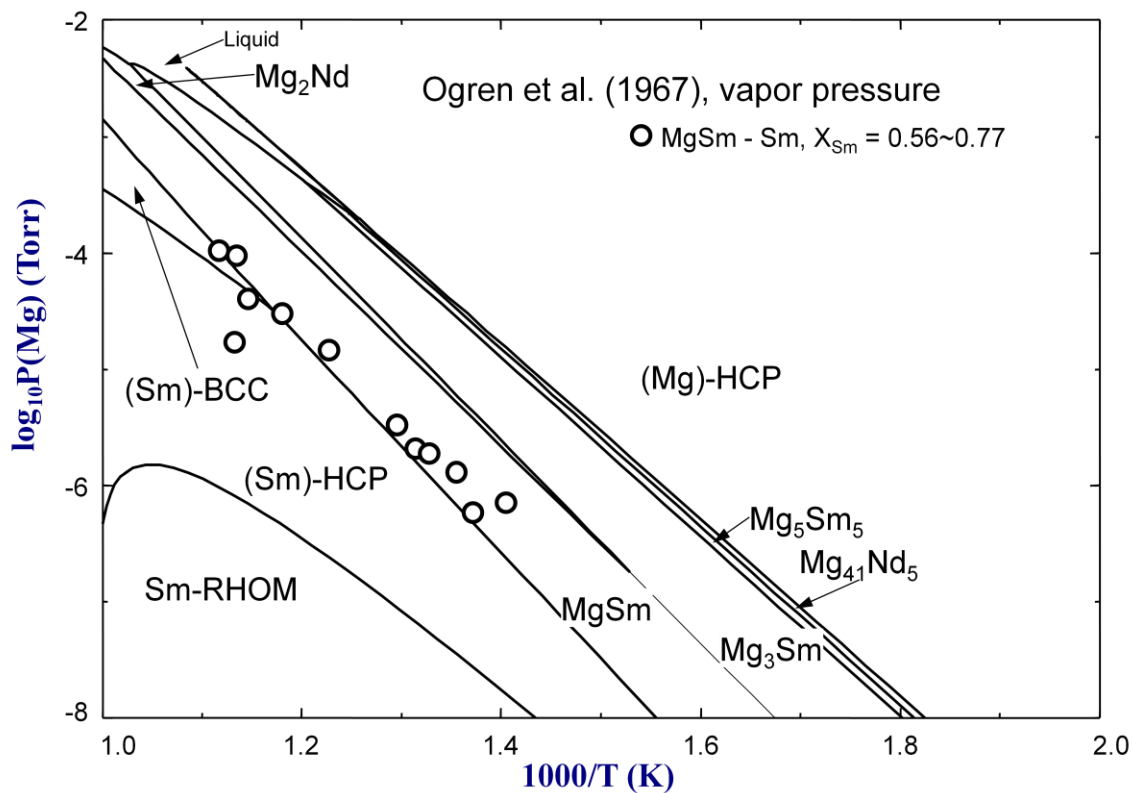
Figure 7.28 The vapor pressure over MgSm – (Sm) –HCP alloys by Ogren *et al.* [64].
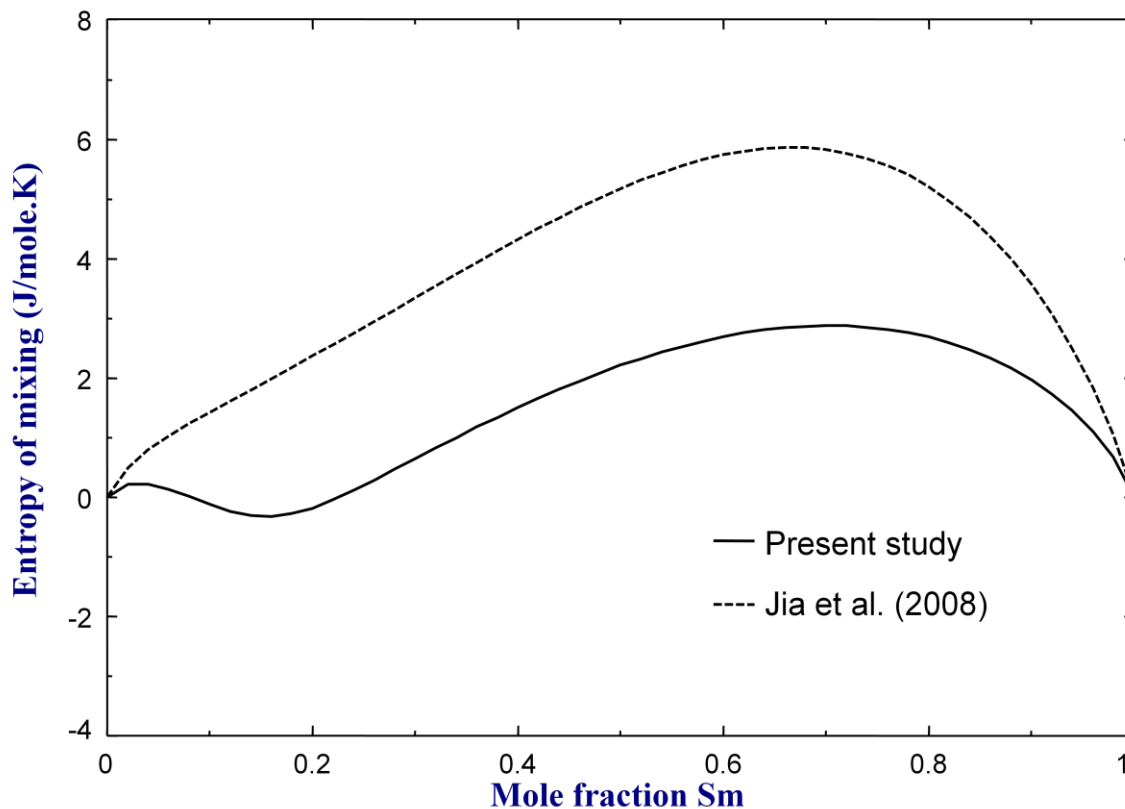
Figure 7.29 The calculated entropy of mixing in the liquid Mg–Sm alloy (solid curve : the present study; dashed curve: that of BW random mixing model by Jia *et al*. [100]).

7.4.6 Solid solubility of light RE (La, Ce, Pr, Nd and Sm) in (Mg)–HCP phase

Figure 7.30 shows the solid solubility of light RE (La, Ce, Pr, Nd and Sm) in (Mg)–HCP in terms of the relationship between $\ln x_{RE}^{HCP}$ and $1/T$. The solid solubility from Rokhlin [54, 61, 103] is preferred in the course of the thermodynamic optimization of Mg–RE (La, Ce, Pr, Nd and Sm) systems. However, it is worth noting that the solid solubility of light RE (La, Ce, Pr, Nd and Sm) at the lowest temperature of 573K from the experimental work of Rokhlin [54, 61, 103], is much higher than the one from the thermodynamic optimizations. It may be due to the slow diffusion process of rare earth elements in the solid state at the lowest temperature of 573K. As shown in Figure 7.30, the slope of each linear relationship is similar, and an increasing trend for the solid solubility of RE (La, Ce, Pr, Nd and Sm) in (Mg)–HCP phase with the increasing atomic number

of rare earth elements can be clearly seen, which is also observed by Rokhlin [61]. It is believed that the solid solubility of RE (La, Ce, Pr, Nd and Sm) in (Mg)–HCP phase is well evaluated taking into account the new solid solubility data for Mg–Nd system from Kopp using atom probe tomography [97], which favors the data from Rokhlin [54], the trend shown in Figure 7.30 and the recent experimental enthalpy of formation data in Mg–La system from Berche [8], which influences, to a great extent, the slope of the linear relationship $\ln x_{RE}^{HCP}$ versus $1/T$.
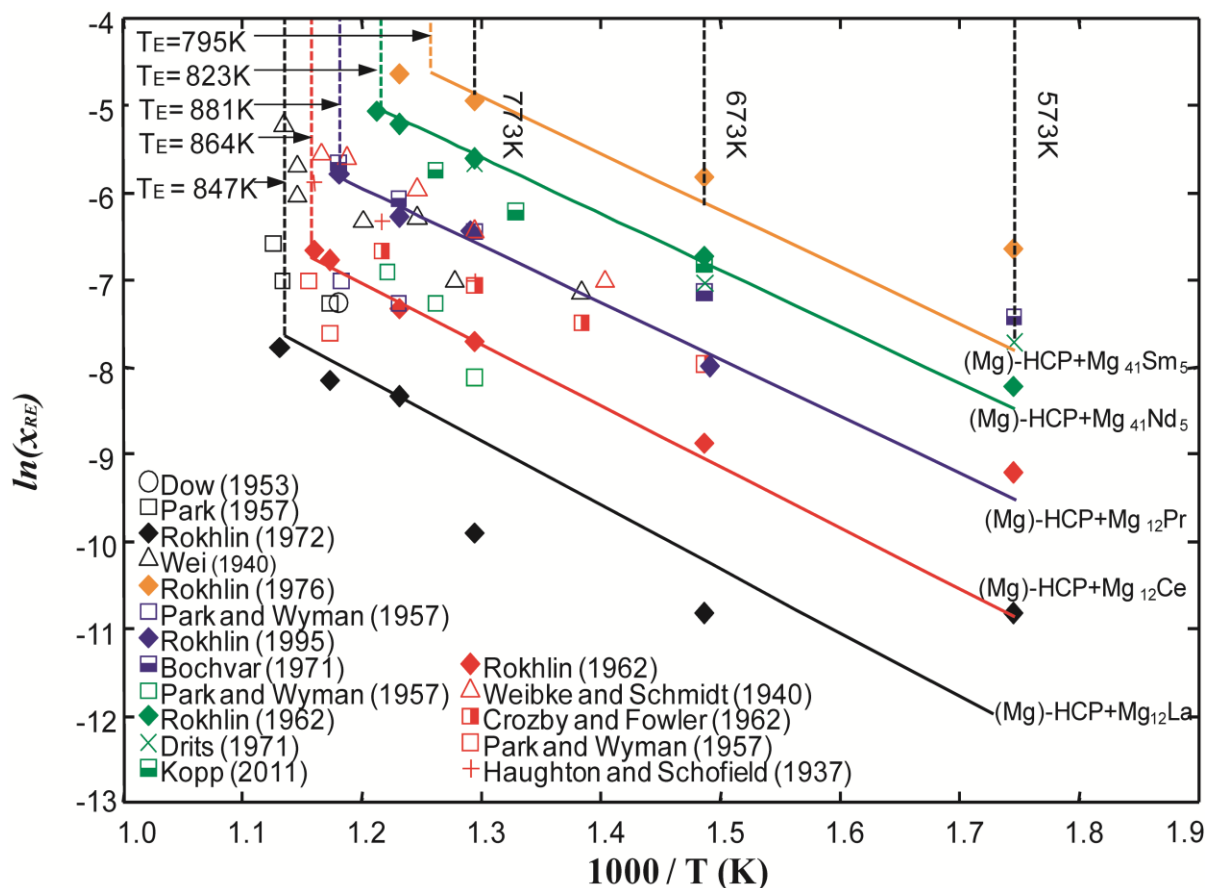
Figure 7.30 The relationship between the solid solubility of RE (La, Ce, Pr, Nd, Sm) in the (Mg)–HCP and temperature (black: Mg–La system with the experimental data from [55, 56, 58, 81], red: Mg–Ce system with the experimental data from [54-58], blue: Mg–Pr system with the experimental data from [45, 55, 61, 89, 90], green: Mg–Nd system with the experimental data from [54, 55, 96]; orange: Mg–Sm system with experimental data from [102]).

7.4.7 Enthalpy of mixing of the HCP solid solution in the Mg–RE (La, Ce, Pr, Nd and Sm) systems

The optimized enthalpy of mixing in the HCP solid solution was compared with the calculated data from Miedema's model and FP-DFT using supercell technique, and with the optimized enthalpy of mixing in the liquid at 1500K. Figures 7.31-7.35 show the enthalpies of mixing of the HCP solid solution in the Mg–RE (La, Ce, Pr, Nd and Sm) systems, respectively. Generally, the agreement on the calculated enthalpy of mixing by Miedema's model and by FP-DFT was obtained. It was judged to be unnecessary to lower the enthalpies of mixing of the HCP solid solution in order to fit the results of Miedema's model, which would be at the expense of additional excess entropy term for the HCP solid solution in the Mg–RE (La, Ce, Pr, Nd and Sm) systems. No excess entropies of mixing of the HCP solid solution in the Mg–RE (La, Ce, Pr, Nd and Sm) systems were reported. The enthalpy of mixing of the (Mg)–HCP solid solution in the whole region of Mg–RE systems can be calculated by special quasirandom structure (SQS) calculations through density functional theory.
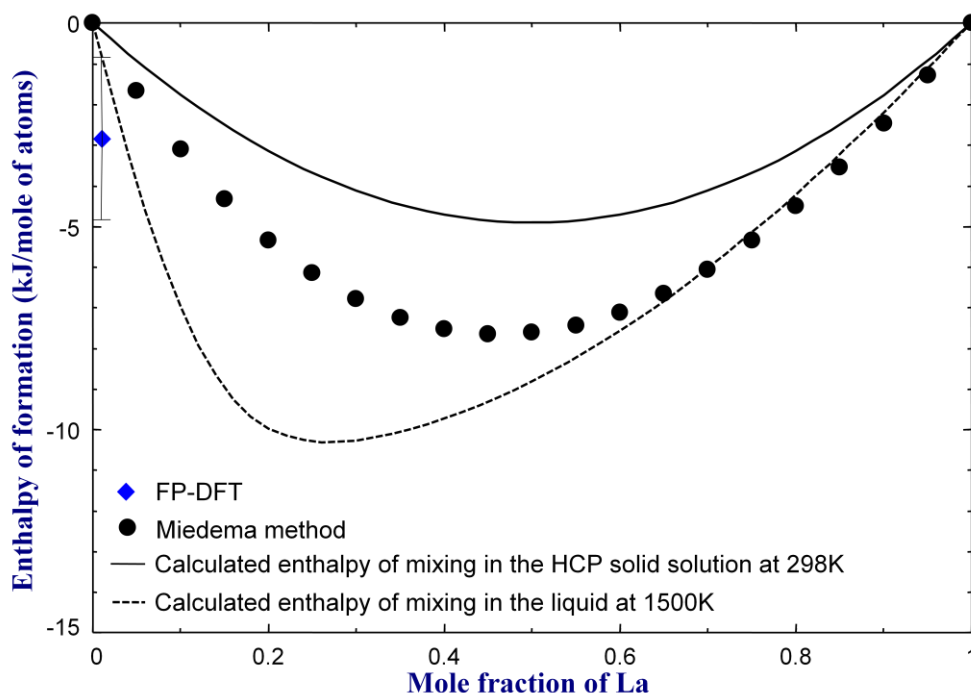
Figure 7.31 The calculated enthalpy of mixing of the Mg–La HCP solid solution.
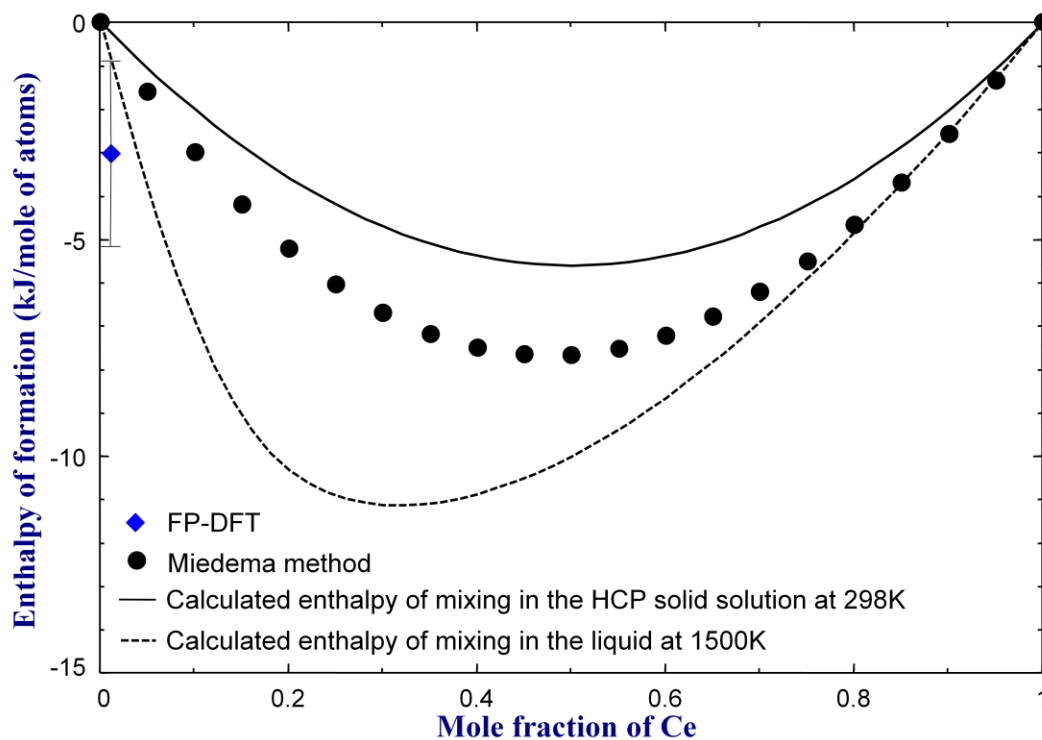
Figure 7.32 The calculated enthalpy of mixing of the HCP solid solution in the Mg–Ce system.
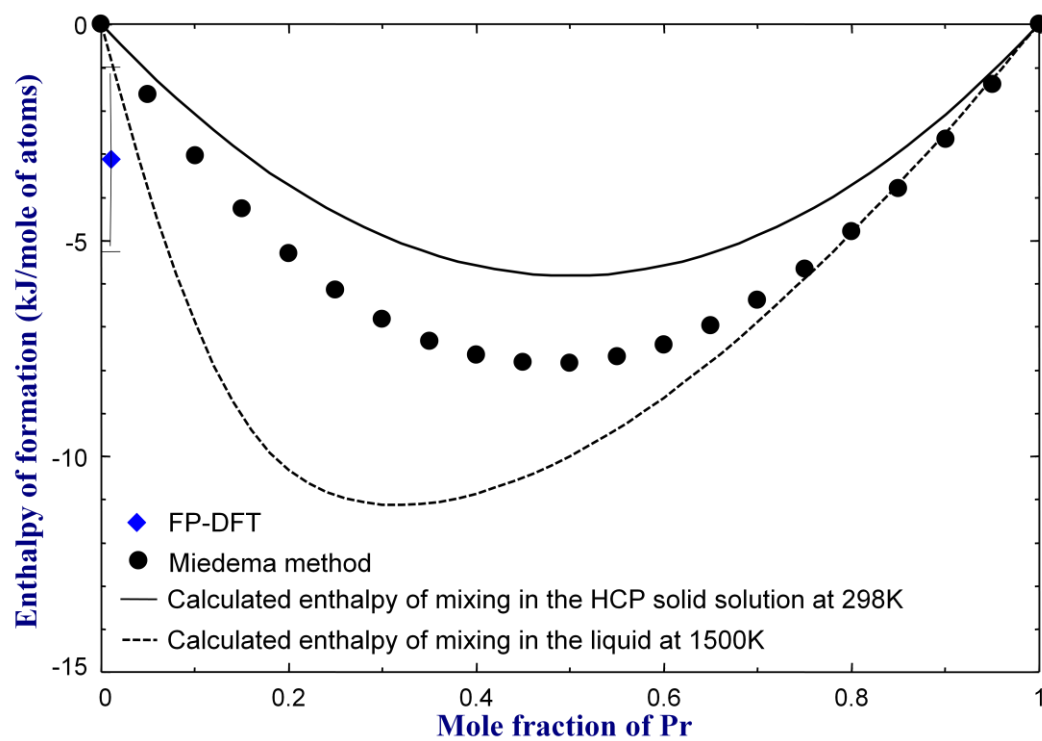
Figure 7.33 The calculated enthalpy of mixing of the HCP solid solution in the Mg–Pr system.
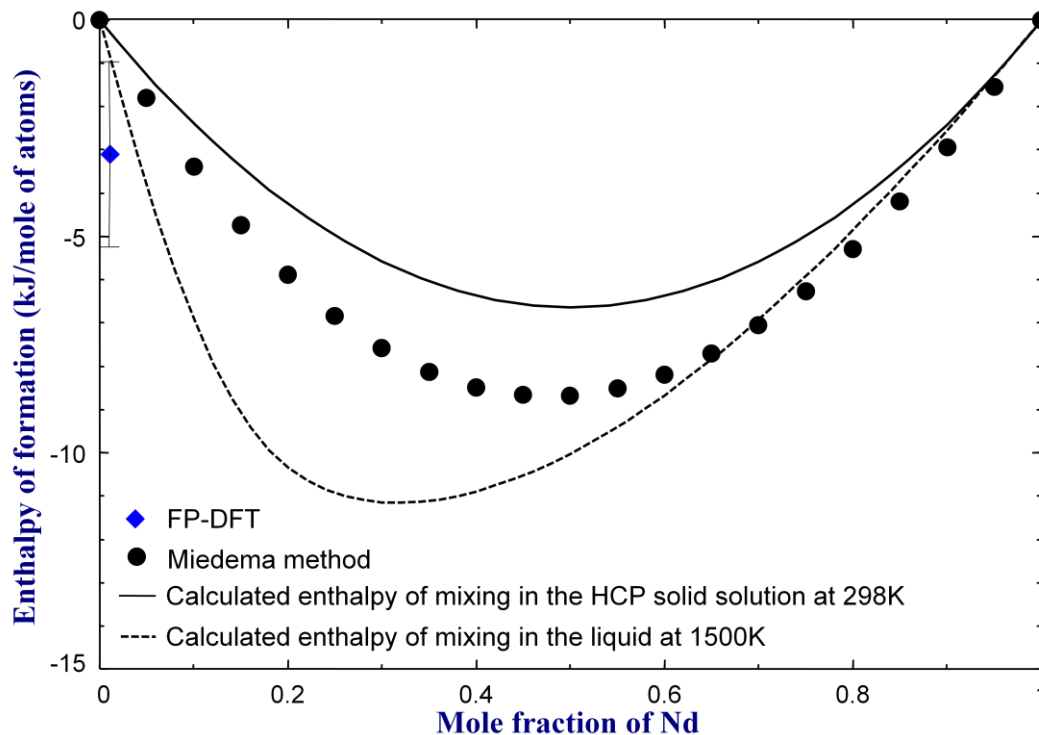
Figure 7.34 The calculated enthalpy of mixing of the HCP solid solution in the Mg–Nd system.
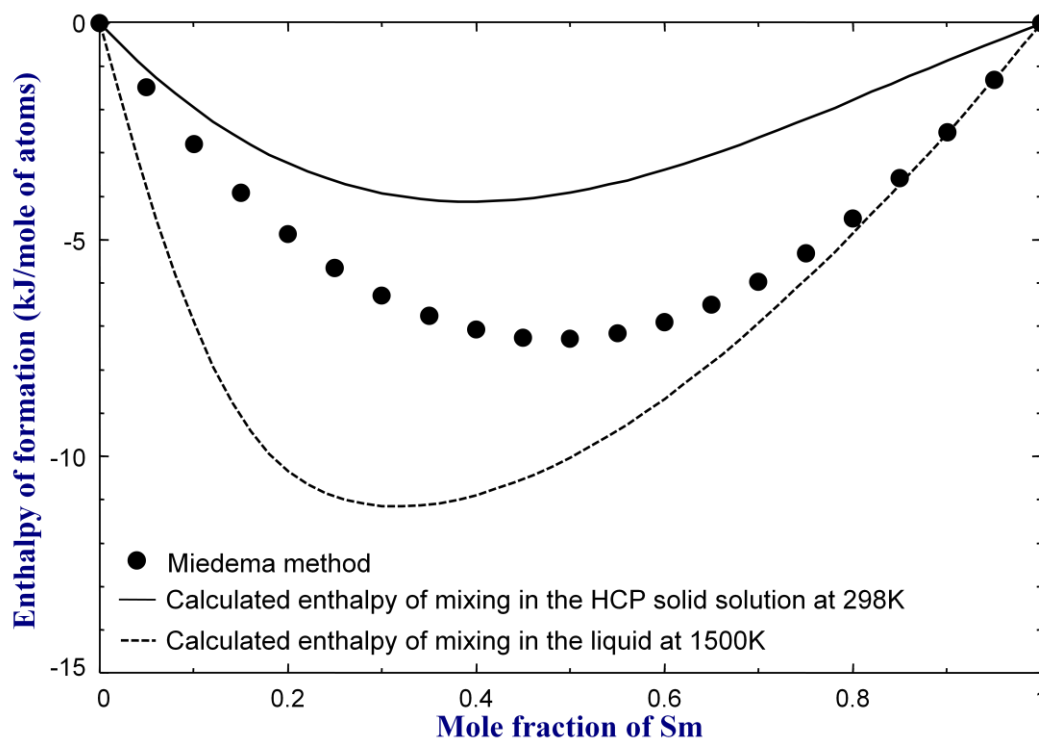
Figure 7.35 The calculated enthalpy of mixing of the HCP solid solution in the Mg–Sm system.

7.4.8 Relative stability of Mg$_{12}$RE $_{(tI26)}$ and Mg$_{41}$RE$_5$ $_{(tI92)}$ (RE' =La, Ce, Pr; RE'' =Nd, Sm) in Mg–RE'–RE'' ternary systems

Rare earth mischmetal (a mixture of rare earth elements) is widely used as an alloying source instead of the pure RE elements. In Mg-light RE systems, the equilibrium phase that saturates (Mg)–HCP is REMg$_{12(tI26)}$ for La, Ce and Pr, while it is RE$_5$Mg$_{41(tI92)}$ for Nd and Sm. However, NdMg$_{12(tI26)}$ is only observed in the quenched Mg–Nd samples [95], and is considered a metastable phase in the present study. The molar ratios of Nd+Sm over La+Ce+Pr in the mischmetal source will affect which of the REMg$_{12(tI26)}$ or RE$_5$Mg$_{41(tI92)}$ solution phase will be stable during an annealing treatment. Therefore, the Gibbs energy of formation of NdMg$_{12(tI26)}$ and SmMg$_{12(tI26)}$ phases have been estimated assuming that the entropy of formation of NdMg$_{12(tI26)}$ and SmMg$_{12(tI26)}$ phases are the same as that of PrMg$_{12(tI26)}$, and that the enthalpy of formation of NdMg$_{12(tI26)}$ and SmMg$_{12(tI26)}$ phases are extrapolated from the linear relationship of the estimated enthalpy of formation of LaMg$_{12(tI26)}$, CeMg$_{12(tI26)}$, PrMg$_{12(tI26)}$ NdMg$_{12(tI26)}$ and SmMg$_{12(tI26)}$ phases from Tao [47] with increasing atomic numbers of rare earth elements.
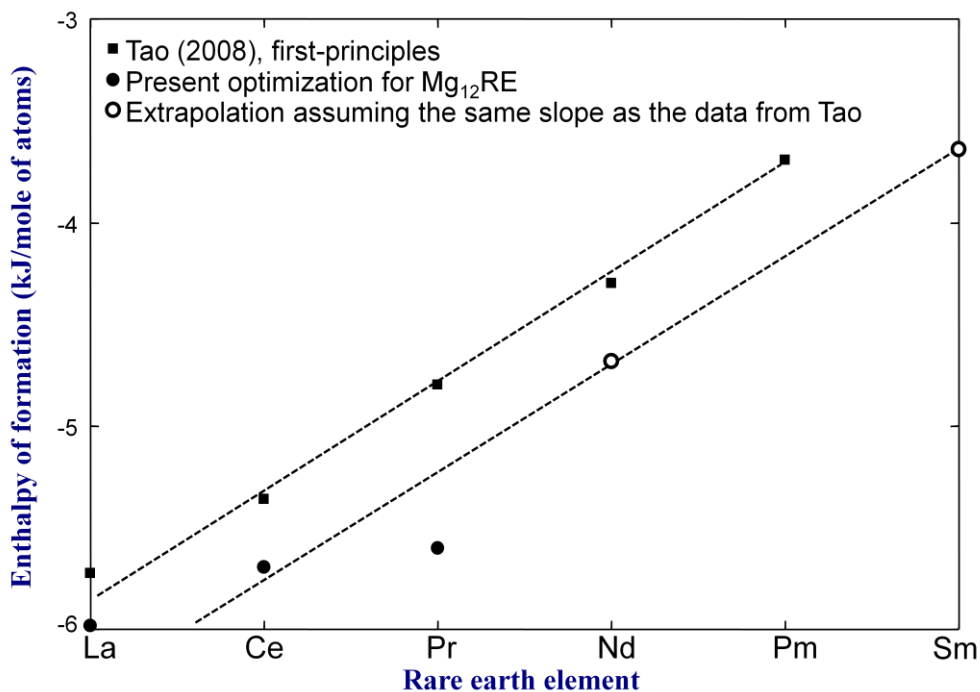
Figure 7.36 The extrapolated enthalpy of formation for the Mg$_{12}$Nd$_{(tI26)}$ and Mg$_{12}$Sm$_{(tI26)}$ phases.

The average value of the optimized enthalpy of formation of $LaMg_{12(tI26)}$, $CeMg_{12(tI26)}$, $PrMg_{12(tI26)}$ was used to determine the intercept of this linear line shown in Figure 7.36. Ideal mixing of the rare-earth elements on their sub-lattice in the $REMg_{12}$ and RE_5Mg_{41} solutions is assumed. Figures 7.37-7.42 show the effect of the Rare Earth atomic ratios $\dfrac{Nd}{Nd+La}$, $\dfrac{Nd}{Nd+Ce}$, $\dfrac{Nd}{Nd+Pr}$, $\dfrac{Sm}{Sm+La}$, $\dfrac{Sm}{Sm+Ce}$ and $\dfrac{Sm}{Sm+Pr}$ on the stability of $REMg_{12(tI26)}$ and $RE_5Mg_{41(tI92)}$ phases for a Mg/RE molar ratio of 14 (*i.e.*, at 93.33 at% Mg) respectively. Note that these diagrams are quite insensitive to the Mg/RE molar ratio as long as it lies within the (Mg)–HCP + $Mg_{12}RE$ region.
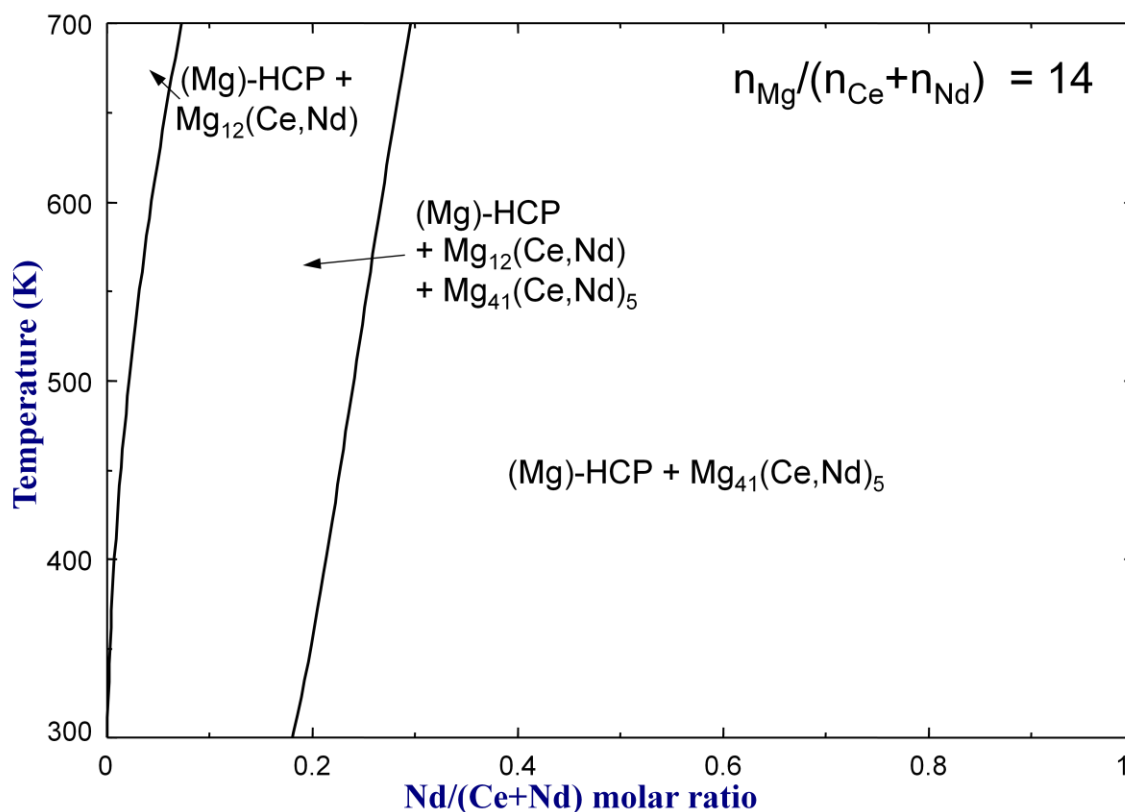
Figure 7.37 The calculated relative stability of $Mg_{12}RE_{(tI26)}$ and $Mg_{41}RE_{5\ (tI92)}$ as a function of the $\left(\dfrac{Nd}{Nd+La}\right)$ molar ratio at $\dfrac{Mg}{Nd+La}=14$ (molar ratio).
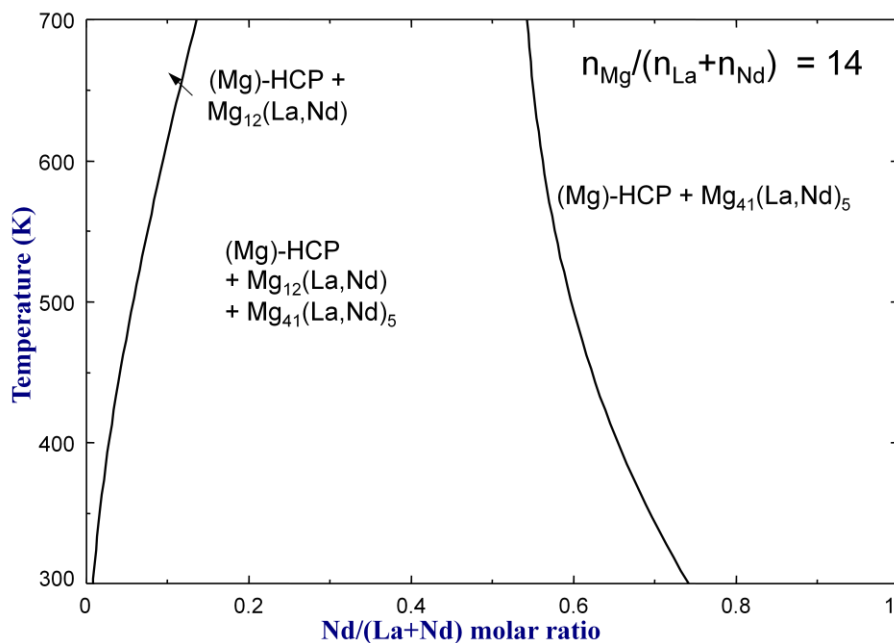
Figure 7.38 The calculated relative stability of $Mg_{12}RE$ $_{(tI26)}$ and $Mg_{41}RE_5$ $_{(tI92)}$ as a function of

the ($\dfrac{Nd}{Nd + Ce}$) molar ratio at $\dfrac{Mg}{Nd + Ce} = 14$ (molar ratio).
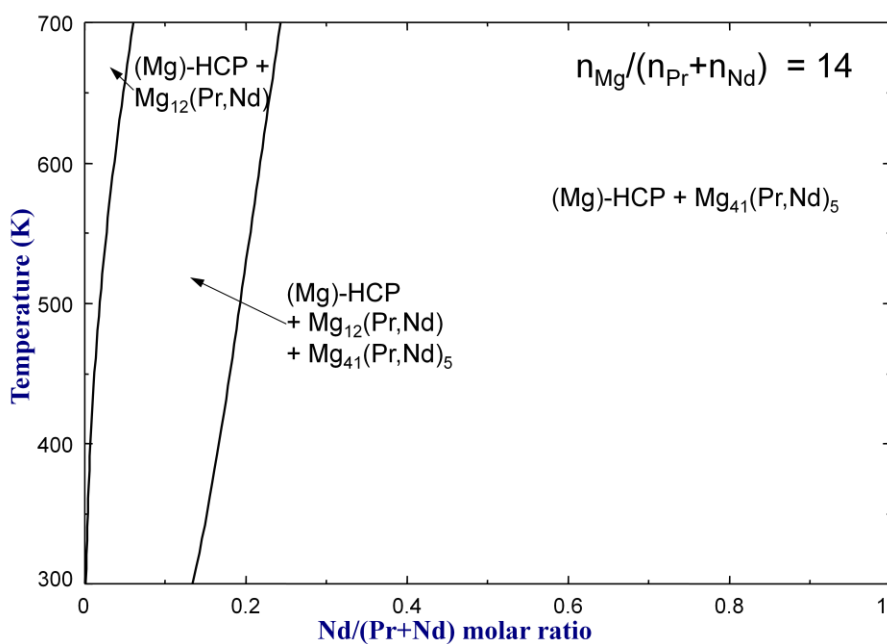
Figure 7.39 The calculated relative stability of $Mg_{12}RE$ $_{(tI26)}$ and $Mg_{41}RE_5$ $_{(tI92)}$ as a function of

the ($\dfrac{Nd}{Nd + Pr}$) molar ratio at $\dfrac{Mg}{Nd + Pr} = 14$ (molar ratio).
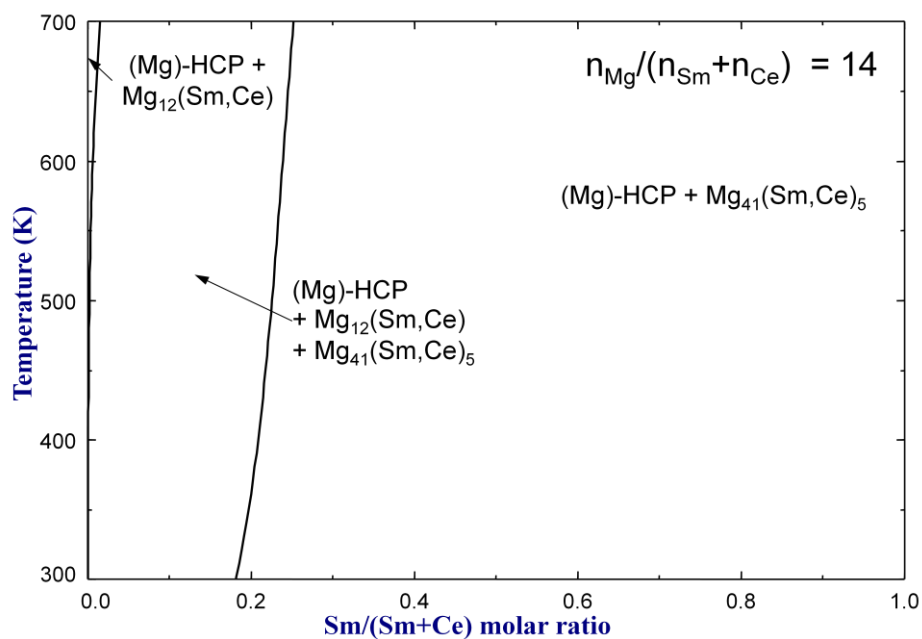
Figure 7.40 The calculated relative stability of Mg$_{12}$RE $_{(tI26)}$ and Mg$_{41}$RE$_5$ $_{(tI92)}$ as a function of

$$\text{the }(\frac{Sm}{Sm+La})\text{ molar ratio at }\frac{Mg}{Sm+La}=14\text{ (molar ratio).}$$
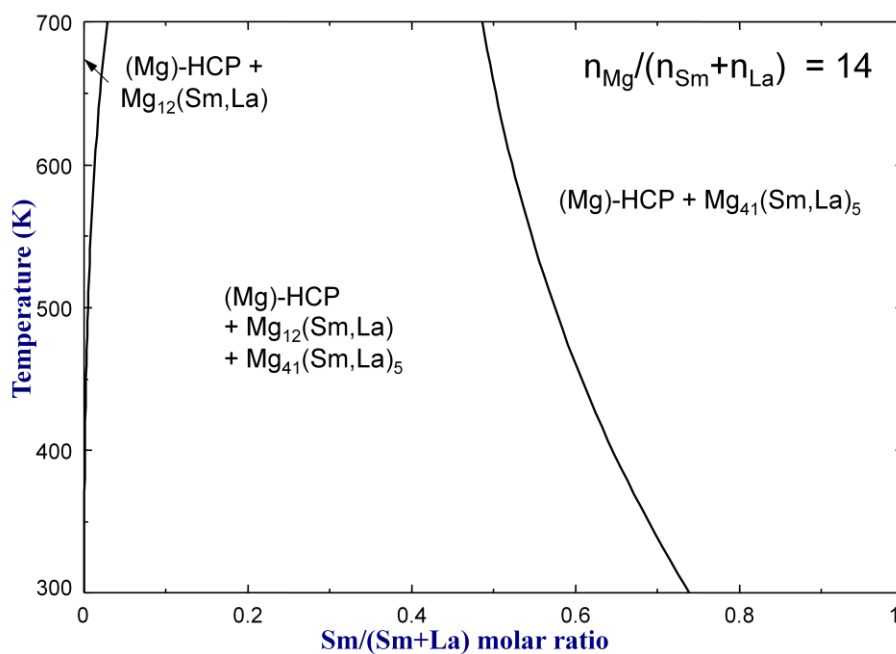
Figure 7.41 The calculated relative stability of Mg$_{12}$RE $_{(tI26)}$ and Mg$_{41}$RE$_5$ $_{(tI92)}$ as a function of

$$\text{the }(\frac{Sm}{Sm+Ce})\text{ molar ratio at }\frac{Mg}{Sm+Ce}=14\text{ (molar ratio).}$$
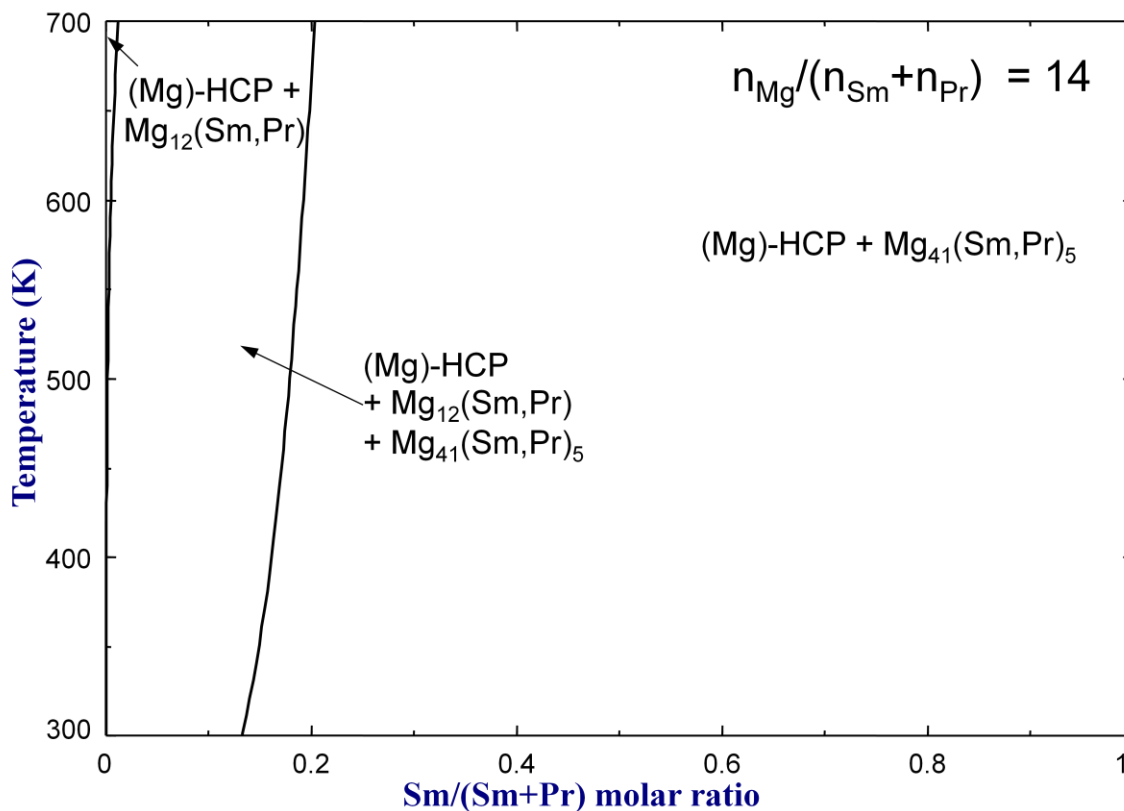
Figure 7.42 The calculated relative stability of $Mg_{12}RE_{(tI26)}$ and $Mg_{41}RE_{5\,(tI92)}$ as a function of

the ($\dfrac{Sm}{Sm+\text{Pr}}$) molar ratio at $\dfrac{Mg}{Sm+\text{Pr}}=14$ (molar ratio).

7.5 Conclusions

The solid solubility of RE (La, Ce, Pr, Nd and Sm) in Mg–HCP solutions are critically reviewed and optimized, as part of a complete thermodynamic re-optimization of the Mg–La, Mg–Ce, Mg–Nd, Mg–Pr and Mg–Sm systems. The experimental data from Rokhlin [61] were preferred in the present study based on the combination of new solid solubility data for Mg–Nd system from Kopp using atom probe tomography [97], the analysis of the solid solubility data on the $\ln x_{RE}^{HCP}$ versus $1/T$ relationship and the recent experimental enthalpy of formation data in Mg–La system from Berche [8], which determined, to a great extent, the slope of the linear relationship $\ln x_{RE}^{HCP}$ versus $1/T$. The combination of the Miedema's model, first-principles, and CALPHAD method

would be helpful in particular when the experimental data of enthalpy of formation were either scarce or of great uncertainty.

Systematic thermodynamic evaluations and optimizations of the Mg–La, Mg–Ce, Mg–Pr, Mg–Nd and Mg–Sm systems have been presented on the basis of the literature data and calculated data from Miedema's model and FP-DFT. It should be pointed out that the calculated results from ab initio and from Miedema's model are comparable. Optimized model parameters of the Gibbs energies for all phases which reproduce the experimental data very well were obtained in the present study. It may be noteworthy that all the Mg-light rare earth binary systems show quite similar thermodynamic properties, and a similar behaviour is expected in the Mg-heavy rare earth binary systems too. However, the independent optimizations from Guo and Du [72, 85] for Mg–La and Mg–Pr systems, from Gorsse *et al.* [92] for Mg–Nd system, and from Jia *et al.* [100] seems not having the similar entropy of mixing in the liquid shown in Figs 11, 17, 23 and 29. The Modified Quasichemical Model (MQM) for the liquid phases which takes the SRO into account fitted the experimental data very well. It would be expected that MQM for liquid solutions gives better extrapolations into multi-component systems (Mg–Al–RE, Mg–Zn–RE for example) based on parameters in the binary and ternary systems. These better predictions and estimations of phase equilibria will help to develop and design novel magnesium alloys.

7.6 Acknowledgments

7.7 References

[1]   K. Hantzsche, J. Bohlen, J. Wendt, K. U. Kainer, S. B. Yi and D. Letzig, Effect of rare earth additions on microstructure and texture development of magnesium alloy sheets, Scri. Mater. 63 (2010): 725-730.

[2]   S. Yi, J. Bohlen, F. Heinemann and D. Letzig, Mechanical anisotropy and deep drawing behaviour of AZ31 and ZE10 magnesium alloy sheets, Acta Mater. 58 (2010): 592-605.

[3]   L.-L. Jin, Y.-B. Kang, P. Chartrand and C. D. Fuerst. Thermodynamic evaluation and optimization of Al–La,Al–Ce, Al–Pr, Al–Nd and Al–Sm systems using Modified Quasichemical Model for the liquid, Calphad 35 (2011): 30-41.

[4]   L.-L. Jin, P. Chartrand, Y.-B. Kang and C. D. Fuerst, Thermodynamic evaluation and optimization of Al–Gd, Al–Tb, Al–Dy, Al–Ho, and Al–Er systems using Modified Quasichemical Model for the liquid, Calphad 34 (2010): 456-466.

[5]   P. Chartrand, Thermodynamic optimization of the Al–Mg system, École Polytechnique de Montréal, Canada (2006): unpublished research.

[6]   Y.-B. Kang, A. D. Pelton, P. Chartrand, P. Spencer and C. D. Fuerst, Critical evaluation and thermodynamic optimization of the binary systems in the Mg–Ce–Mn–Y system, J. Phase Equilib. Diff. 28 (2007): 342-354.

[7]   G. Canneri and A. Rossi, The heat of formation of compounds of lanthanum and magnesium and of lanthanum and aluminum, Gazz. Chim. Ital. 62 (1932): 202-211.

[8]   A. Berche, F. Marinelli, J. Rogez and M. C. Record, Enthalpy of formation of the La–Mg intermediate phases, Thermochim. Acta 499 (2010): 65-70.

[9]   W. Biltz and H. Pieper, Contributions to the systematic affinity principle. XXVII. The heats of formation of intermetallic compounds. IV. Cerium alloys, Z. Anorg. Allg. Chem. 134 (1924): 13-24.

[10]   M. C. Gao, A. D. Rollett and M. Widom, Lattice stability of aluminum–rare earth binary systems: a first-principles approach, Phys. Rev. B: Condens. Matter Mater. Phys. 75 (2007): 174120/1-/16.

[11] VASP package. Retrieved from http://cms.mpi.univie.ac.at/vasp/vasp/vasp.html.

[12] G. Kresse and J. Hafner, Ab initio molecular dynamics for liquid metals. Phys. Rev. B 47 (1993): 558.

[13] G. Kresse and J. Furthmüller, Efficiency of ab initio total energy calculations for metals and semiconductors using a plane-wave basis set, Comput. Mater. Sci. 6 (1996): 15-50.

[14] G. Kresse and J. Furthmüller, Efficient iterative schemes for ab initio total-energy calculations using a plane-wave basis set, Phys. Rev. B 54 (1996): 11169-11186.

[15] P. E. Blochl, Projector augmented-wave method. Phys. Rev. B 50 (1994): 17953.

[16] G. Kresse and D. Joubert, From ultrasoft pseudopotentials to the projector augmented-wave method, Phys. Rev. B 59 (1999): 1758.

[17] H. J. Monkhorst and J. D. Pack, Special points for Brillouin-zone integrations, Phys. Rev. B 13 (1976): 5188.

[18] A. R. Miedema, F. R. de Boer and R. Boom, Model predictions for the enthalpy of formation of transition metal alloys. Calphad 1 (1977): 341-359.

[19] A. R. Miedema, P. F. De Chatel and F. R. De Boer, Cohesion in alloys − fundamentals of a semiempirical model, Physica B+C: Phys. Condens. Matter + Atom. Mol. Plasma Phys. Opt. (Amsterdam) 100 (1980): 1-28.

[20] F. R. D. Boer, R. Boom, W. C. M. Mattens, A. R. Miedema and A. K. Niessen, Cohesion In Metals: Transition Metal Alloys, New York, North-Holland(1988).

[21] S. Ghosh, J. Basu, D. Ramachandran, E. Mohandas and M. Vijayalakshmi, A unified approach to phase and microstructural stability for Fe–ETM alloys through Miedema's model, Intermetallics 23 (2012): 148-157.

[22] Z.-w. Chen, C.-y. Ma and P. Chen, Eutectic modification of A356 alloy with Li addition through DSC and Miedema model, Trans. Nonferrous Met. Soc. China 22 (2012): 42-46.

[23] A. Takeuchi and A. Inoue, Mixing enthalpy of liquid phase calculated by miedema's scheme and approximated with sub-regular solution model for assessing forming ability of amorphous and glassy alloys, Intermetallics 18 (2010): 1779-1789.

[24]   P. K. Ray, M. Akinc and M. J. Kramer, Applications of an extended Miedema's model for ternary alloys, J. Alloys Compd. 489 (2010): 357-361.

[25]   R. Hojvat de Tendler, M. R. Soriano, M. E. Pepe, J. A. Kovacs, E. E. Vicente and J. A. Alonso, Calculation of metastable free-energy diagrams and glass formation in the Mg–Cu–Y alloy and its boundary binaries using the Miedema model, Intermetallics 14 (2006): 297-307.

[26]   J. Basu, B. S. Murty and S. Ranganathan, Glass forming ability: Miedema approach to (Zr, Ti, Hf) – (Cu, Ni) binary and ternary alloys, J. Alloys Compd. 465 (2008): 163-172.

[27]   S. P. Sun, D. Q. Yi, Y. Jiang, B. Zang, C. H. Xu and Y. Li, An improved atomic size factor used in Miedema's model for binary transition metal systems, Chem. Phys. Lett. 513 (2011): 149-153.

[28]   X. Shi and J. Luo, Developing grain boundary diagrams as a materials science tool: A case study of nickel-doped molybdenum, Phys. Rev. B 84 (2011): 014105.

[29]   H. Bakker, Enthalpies in alloys. Miedema's semi-empirical model, Mater. Sci. Found. 1 (1998): i-ii, v, vii-x, 1-78.

[30]   S. P. Sun, D. Q. Yi, H. Q. Liu, B. Zang and Y. Jiang, Calculation of glass forming ranges in Al-Ni-RE (Ce, La, Y) ternary alloys and their sub-binaries based on Miedema's model, J. Alloys Compd. 506 (2010): 377-387.

[31]   A. B. Shubin and K. Y. Shunyaev, Enthalpies of mixing of rare earth metal – aluminum alloys: model calculations, Rasplavy (2010): 44-50.

[32]   C. W. Bale, P. Chartrand, S. A. Degterov, G. Eriksson, K. Hack, R. Ben Mahfoud, *et al.,* FactSage thermochemical software and databases, CALPHAD 26 (2002): 189-228.

[33]   C. Bale, A. Pelton and W. Thompson (2008). Factsage Thermochemical Software and Databases. Retrieved from http://www.crct.polymtl.ca/.

[34]   A. T. Dinsdale, SGTE data for pure elements. Calphad 15 (1991): 317-425.

[35]   Y.-B. Kang, L.-L. Jin, P. Chartrand and A. D. Pelton, unpublished work. Ecole polytechnique de Montréal, Quebéc, Canada (2007).

[36]   A. D. Pelton, S. A. Degterov, G. Eriksson, C. Robelin and Y. Dessureault, The modified quasichemical model I – binary solutions, Metall. Mater. Trans. B 31B (2000): 651-659.

[37]   Y.-B. Kang, A. D. Pelton, P. Chartrand, P. Spencer and C. D. Fuerst, Thermodynamic database development of the Mg–Ce–Mn–Y system for Mg alloy design, Metall. Mater. Trans. A 38 (2007): 1231-1243.

[38]   Y.-B. Kang, I.-H. Jung, S. A. Decterov, A. D. Pelton and H.-G. Lee, Phase equilibria and thermodynamic properties of the CaO–MnO–Al_2O_3–SiO_2 system by critical evaluation, modeling and experiment, ISIJ Int. 44 (2004): 975-983.

[39]   I.-H. Jung, S. A. Decterov and A. D. Pelton, Critical thermodynamic evaluation and optimization of the CaO-MgO-SiO_2 system, J. Eur. Ceram. Soc. 25 (2005): 313-333.

[40]   A. Pelton and P. Chartrand, Thermodynamic evaluation and optimization of the LiCl-NaCl-KCl-RbCl-CsCl-$MgCl_2$-$CaCl_2$ system using the modified quasi-chemical model, Metall. Mater. Trans. A 32 (2001): 1361-1383.

[41]   P. Chartrand and A. Pelton, Thermodynamic evaluation and optimization of the LiF-NaF-KF-MgF_2-CaF_2 system using the modified quasi-chemical model, Metall. Mater. Trans. A 32 (2001): 1385-1396.

[42]   P. Waldner and A. D. Pelton, Critical thermodynamic assessment and modeling of the Fe-Ni-S system, Metall. Mater. Trans. B 35B (2004): 897-907.

[43]   M. Hillert. The compound energy formalism, J. Alloys Compd. 320 (2001): 161-176.

[44]   Y.-B. Kang, A. D. Pelton, P. Chartrand and C. D. Fuerst, Critical evaluation and thermodynamic optimization of the Al–Ce, Al–Y, Al–Sc and Mg–Sc binary systems, Calphad 32 (2008): 413-422.

[45]   A. Saccone, D. Macciò, J. A. J. Robinson, F. H. Hayes and R. Ferro. Smith thermal analysis of selected Pr–Mg alloys, J. Alloys Compd. 317-318 (2001): 497-502.

[46]   P. Villars, M. Berndt, K. Brandenburg, K. Cenzual, J. Daams, F. Hulliger, *et al.,* The Pauling File, Binaries Edition, J. Alloys Compd. 367 (2004): 293-297.

[47] X. Tao, First-Principles Calculations on the Thermodynamic Properties of Al-Rare Earth and Mg-Rare Earth Alloys, Central South University.Changsha, China,Ph. D. Thesis, in Chinese (2008).

[48] X. Tao, Y. Ouyang, H. Liu, Y. Feng, Y. Du, Y. He, *et al,* Phase stability of magnesium-rare earth binary systems from first-principles calculations, J. Alloys Compd. 509 (2011): 6899-6907.

[49] C. Guo, Z. Du and C. Li, A thermodynamic description of the Ce–La–Mg system, Int. J. Mater. Res. 101 (2010): 1424-1431.

[50] C. Guo, Z. Du and C. Li, Thermodynamic description of the Ce–Mg–Y and Mg–Nd–Y systems, Int. J. Mater. Res. 99 (2008): 650-668.

[51] G. Cacciamani, A. Saccone and R. Ferro, I. Ansara, et al., Ed. The Ce–Mg system in: COST 507: Thermochemical Database for Light Metal Alloys, Luxembourg, 2 (1998): 137-140.

[52] A. A. Nayeb-Hashemi and J. B. Clark, The Ce−Mg (cerium–magnesium) system, J. Phase Equilib. 9 (1988): 162-172.

[53] A. Saccone, D. Maccio, S. Delfino, F. H. Hayes and R. Ferro, Mg-Ce alloys experimental investigation by Smith thermal analysis, J. Therm. Anal. Calorim. 66 (2001): 47-57.

[54] L. L. Rokhlin, Solubility of neodymium and cerium in magnesium in the solid state, Izv. Akad. Nauk SSSR, Otd. Tekh. Nauk, Metall. Topl. (1962): 126-130.

[55] J. J. Park and L. L. Wyman, Phase relations in magnesium alloys, Natl. Bur. of Standards. WADC-TR-57-504(1957): 33.

[56] D. C. Company, Contract DA-11-022-ORD-1645,Project TB4-15, Summary report, Part I. 1955).

[57] R. L. Crosby and K. A. Fowler, Studies of magnesium alloys for use at moderate temperatures, U.S. Bur. Mines, Rep. Invest. No.6078 (1962): 28.

[58] F. Weibke and W. Schmidt, The solubility of lanthanum in aluminum, magnesium and in alloys of magnesium and aluminum, Z. Elektrochem. Angew. Phys. Chem. 46 (1940): 357-364.

[59] A. A. Nayeb-Hashemi and J. B. Clark, Ed. "Mg–Nd (magnesium–neodymium)" in: Phase Diagrams of Binary Magnesium Alloys Metals Park, Ohio, ASM International (1988): 213-218.

[60] A. A. Nayeb-Hashemi and J. B. Clark, "The La–Mg (lathanium–magnesium)", Bull. Alloy Phase Diagr. 9 (1988): 172-178.

[61] L. L. Rokhlin, Regularities of the Mg sides of the Mg–RE (magnesium–rare earth metal) phase diagrams: comments on evaluations, J. Phase Equilib. 16 (1995): 504-507.

[62] K. Nagarajan and F. Sommer, Calorimetric investigations of cerium-magnesium liquid alloys, J. Less-Common Met. 142 (1988): 319-328.

[63] J. E. Pahlman and J. F. Smith, Thermodynamics of formation of compounds in the cerium–magnesium, neodymium–magnesium, gadolinium–magnesium, dysprosium–magnesium, erbium–magnesium, and lutetium–magnesium binary systems in the temperature range 650 deg. to 930 deg.K, Metall. Trans. 3 (1972): 2423-2432.

[64] J. Ogren, N. Magnani and J. Smith, Thermodynamics of formation of binary rare earth–magnesium phases with CsCl-type structure, Trans Soc AIME 239 (1967): 766–771.

[65] H. Flandorfer, M. Giovannini, A. Saccone, R. Rogi and R. Ferro, The Ce–Mg–Y system, Metall. Mater. Trans. A 28 (1997): 265-276.

[66] J. L. Haughton and T. H. Schofield, Alloys of magnesium, Part V. —the constitution of the magnesium rich alloys of magnesium and cerium, J. Inst. Met. 60 (1937): 339-344.

[67] R. Vogel and T. Heumann, On the cerium–magnesium and lanthanum–magnesium Systems, Z. Metallkd. 38 (1947): 1-8.

[68] R. R. Joseph and K. A. Gschneidner, Solid solubility of Mg in some lanthanide metals, Trans. Met. Soc. AIME 233 (1965): 2063-2069.

[69] D. H. Wood and E. M. Cramer, Phase relations in the magnesium-rich portion of the cerium–magnesium system, J. Less-Common Met. 9 (1965): 321-337.

[70] J. Karl A. Gschneidner. Rare Earth Research II, Proc. Third Conf. K. S. Vorres. New York, Gordon and Breach Science Publishers (1964).

[71] P. Franke, D. Neuschütz and Scientific Group Thermodata Europe, Ed. La–Mg (lanthanum–magnesium) in: Binary Systems. Part 5: Binary Systems Supplement 1. (2007): 1-4.

[72] C. Guo and Z. Du, Thermodynamic assessment of the La–Mg system, J. Alloys Compd. 385 (2004): 109-113.

[73] M. Giovannini, A. Saccone, R. Marazza and R. Ferro, The isothermal section at 500 ℃ of the Y–La–Mg ternary system, Metall. Mater. Trans. A 26 (1995): 5-10.

[74] A. Berche, P. Benigni, J. Rogez and M.-C. Record, Re-investigation of the La–Mg phase diagram, J. Therm. Anal. Calorim. (2011): 1-11.

[75] J. Wróbel, L. G. Hector Jr, W. Wolf, S. L. Shang, Z. K. Liu and K. J. Kurzydłowski, Thermodynamic and mechanical properties of lanthanum–magnesium phases from density functional theory, J. Alloys Compd. 512 (2012): 296-310.

[76] A. K. Niessen, F. R. De Boer, R. Boom, P. F. De Chatel, W. C. M. Mattens and A. R. Miedema, Model predictions for the enthalpy of formation of transition metal alloys. II. CALPHAD 7 (1983): 51-70.

[77] Z. Du, C. Guo, C. Li and W. Zhang, Thermodynamic modeling of the La–Mg–Y system and Mg-based alloys database, Rare Met. 25 (2006): 492-500.

[78] A. Berche, P. Benigni, J. Rogez and M.-C. Record. Thermodynamic assessment of the La–Mg system, Calphad 35 (2011): 580-587.

[79] R. Agarwal, H. Feufel and F. Sommer, Calorimetric measurements of liquid La–Mg, Mg–Yb and Mg–Y alloys, J. Alloys Compd. 217 (1995): 59-64.

[80] P. Manfrinetti and K. A. Gschneidner, Jr, Phase equilibrium in the lanthanum–magnesium (0-65 at% Mg) and gadolinium–magnesium systems, J. Less-Common Met. 123 (1986): 267-275.

[81] L. L. Rokhlin and N. R. Bochvar, Magnesium–lanthanum–cerium phase diagram, Izv. Akad. Nauk SSSR, Met. (1972): 193-197.

[82]   Y.-F. Wang, W.-B. Zhang, Z.-Z. Wang, Y.-H. Deng, N. Yu, B.-Y. Tang, *et al,* First-principles study of structural stabilities and electronic characteristics of Mg–La intermetallic compounds, Comput. Mater. Sci. 41 (2007): 78-85.

[83]   Y. A. Afanas'ev, A. P. Bayanov and Y. A. Frolov, Thermodynamic properties of liquid lanthanum-magnesium alloys, Izv. Akad. Nauk SSSR, Met. (1975): 186-90.

[84]   A. A. Nayeb-Hashemi and J. B. Clark, Ed. "Mg–Pr (magnesium–praseodymium)" in: Phase diagrams of binary magnesium alloys Metals Park, Ohio, ASM International (1988): 252-256.

[85]   C. Guo and Z. Du, Thermodynamic assessment of the Mg–Pr system, J. Alloys Compd. 399 (2005): 183-8.

[86]   C. Guo, Z. Du and C. Li, A thermodynamic description of the Mg–Pr–Y system, Calphad 32 (2008): 177-187.

[87]   G. Canneri, Alloys of praseodymium and magnesium. Metall. Ital. 25 (1933): 250-252.

[88]   A. Saccone, S. Delfino, D. Macció and R. Ferro, Magnesium-rare earth phase diagrams: experimental investigation of the Ho-Mg system, J. Phase Equilib. 14 (1993): 280-287.

[89]   A. Saccone, A. M. Cardinale, S. Delfino and R. Ferro, A contribution to the rare earth intermetallic chemistry: praseodymium-magnesium alloy system, Intermetallics 1 (1993): 151-158.

[90]   N. R. Bochvar, A. M. Korol′kov, Ed. Structure and Properties of Light Alloys in., (1971): 21-23.

[91]   G. Canneri and A. Rossi, The heat of formation of compounds of praseodymium with magnesium and of praseodymium with aluminum, Gazz. Chim. Ital. 63 (1933): 182-185.

[92]   S. Gorsse, C. R. Hutchinson, B. Chevalier and J. F. Nie, A thermodynamic assessment of the Mg–Nd binary system using random solution and associate models for the liquid phase, J. Alloys Compd. 392 (2005): 253-262.

[93]   F.-g. Meng, H.-s. Liu, L.-b. Liu and Z.-p. Jin, Thermodynamic optimization of Mg–Nd system, Trans. Nonferrous Met. Soc. China (English Edition) 17 (2007): 77-81.

[94]   C. Guo and Z. Du, Thermodynamic assessment of the Mg–Nd system, Int. J. Mater. Res. 97 (2006): 130-135.

[95]   S. Delfino, A. Saccone and R. Ferro. Phase relationships in the neodymium–magnesium alloy system, Metall. Trans. A 21A (1990): 2109-2114.

[96]   M. E. Drits, E. M. Padezhnova and N. V. Miklina, The combined solubility of neodymium and zinc in solid magnesium, Russ. Metall. 1 (1971): 143-146.

[97]   V. Kopp, W. Lefebvre and C. Pareige, Determination of the Mg-rich phase boundary of the binary Mg-Nd phase diagram by means of atom probe tomography, J. Phase Equilib. Diff. 32 (2011): 298-301.

[98]   A. A. Nayeb-Hashemi and J. B. Clark, Ed. "Mg–Sm (magnesium–samarium)" in: Phase Diagrams of Binary Magnesium Alloys Metals Park, Ohio, ASM International (1988): 289-292.

[99]   H. Okamoto, Mg–Sm (magnesium–samarium), J. Phase Equilib. Diff. 30 (2009): 299.

[100] B. R. Jia, L. B. Liu, D. Q. Yi, Z. P. Jin and J. F. Nie. Thermodynamic assessment of the Al–Mg–Sm system, J. Alloys Compd. 459 (2008): 267-273.

[101] G. Cacciamani, A. Saccone, G. Borzone, S. Delfino and R. Ferro, Computer coupling of thermodynamics and phase diagrams: the gadolinium–magnesium system as an example, Thermochim. Acta 199 (1992): 17-24.

[102] A. Saccone, S. Delfino, G. Borzone and R. Ferro, The samarium–magnesium system: a phase diagram, J. Less-Common Met. 154 (1989): 47-60.

[103] L. L. Rokhlin, E. M. Padezhnova and L. S. Guzei, Study of the solubility of samarium in a magnesium-based solid solution, Izv. Akad. Nauk SSSR, Met. (1976): 204-208.

[104] L. L. Rokhlin, The regularities in the Mg-rich parts of the phase diagrams, phase transformations and mechanical properties of magnesium alloys with individual rare earth metals, Arch. Metall. Mater. 52 (2007): 5-11.

CHAPTER 8   ARTICLE 4: AL–MG–RE (RE: LA, CE, PR, ND, SM) SYSTEMS: THERMODYNAMIC EVALUATIONS AND OPTIMIZATIONS COUPLED WITH KEY EXPERIMENTS AND MIEDEMA'S MODEL ESTIMATIONS

Submitted to the Journal of Chemical Thermodynamics, 2012

Liling Jin [a,*], Dmytro Kevorkov [b], Mamoun Medraj [b], Patrice Chartrand [a]

[a] Centre de Recherche en Calcul Thermochimique (CRCT), Département de génie chimique, École Polytechnique, Montréal, QC, Canada

[b] Dept. of Mechanical Engineering, Concordia University, Montréal, QC, Canada

[*] Corresponding author. CRCT, Département de génie chimique, École Polytechnique, Montréal, QC, CANADA, H3C 3A7. Tel: +1 514 3404711 ext. 2483; fax: +1 514 3405840. E-mail address: liling.jin@polymtl.ca

Abstract: The solid solubilities of Al in $Mg_{12}La$, $Mg_{12}Ce$, $Mg_{12}Pr$, $Mg_{41}Nd_5$ phases were investigated by key experiments. The enthalpy of formation of the ternary compounds was estimated using Miedema's model. The systematically thermodynamic evaluation and optimizations of ternary Al–Mg–RE (RE: La, Ce, Pr, Nd, Sm) systems were based on the available experimental data and current investigation. The Al–Mg–Pr and Al–Mg–Nd systems were optimized for the first time using a systematic approach. Arc-melted key alloys were annealed at 673 K for four weeks and the phases were analyzed with electron probe micro-analysis (EPMA). The $Mg_{12}La$ intermetallic phase was confirmed by the present investigation. Optimized model parameters have been obtained for the Gibbs energy functions of all stable phases, and the model reproduces most critically assessed experimental data. The Modified Quasichemical Model, which takes short–range ordering into account, is used for the liquid phase and the Compound Energy Formalism (CEF) is used for the solid solutions in the binary and ternary systems. Kohler–type extrapolation from binary systems was employed, where no ternary parameters were used for the liquid phase.

Keywords: Thermodynamics; Aluminum – Magnesium – Rare Earth Alloys; Modified Quasichemical Model; electron probe micro-analysis

8.1 Introduction

Magnesium – aluminum – based alloys are widely used because of their low density, high strength-to-weight ratio, specific rigidity, satisfactory salt-spray corrosion resistance and good ductility [1]. Special automobile applications, like engine blocks or powertrain components require sufficient creep resistance at elevated temperature. Lanthanum and Cerium are two dominating constituents of the mischmetal, which is a mixture of rare earth elements (mostly light rare earths) with typical composition ranges of La (25-34%), Ce (48-55%), Pr (4-7%) and Nd (11-17%) [2]. These elements are important alloying additives for the development of magnesium alloys since adding rare earth (RE= La, Ce, Pr, Nd, Sm, Gd, Tb, Dy, Ho, Er, Tm, Lu, Y, and Sc) elements in Mg–Al alloys improve the creep resistance [3] and strength at elevated temperatures. This is attributed to the precipitation of intermetallic phases (such as $Al_{11}RE_3$ and Al_2RE phases), and the suppression of the formation of the detrimental $Mg_{17}Al_{12}$ phase in the interdendritic or grain boundary region. To estimate the nature of precipitating phases, precipitation sequences and the relative amounts of secondary phases, it is necessary to know thermodynamic properties and the phase diagram of the ternary Al–Mg–RE systems which requires a self-consistent thermodynamic database of Mg alloys containing rare earth elements.

Furthermore, it is worth noting the importance of the solid solubility of rare-earth metals in solid (Mg)-HCP phase in the multi-component alloy systems, including the influence of Al, because of the positive effect of this solubility on the mechanical properties and plasticity of magnesium alloys. It was confirmed from the recent study of Hantzsche *et al.* [4] that magnesium sheets with weak textures, which promise improved sheet formability [5], can be obtained by adding alloying elements such as Nd, Ce and Y. It was also pointed out that the amount of the RE addition required for sufficient texture weakening depends on the solid solubility of the respective element in magnesium matrix.

Generally, the phase equilibria and thermodynamic properties in the systems of the rare earth elements show smooth and regular variations when passing from one rare earth element to the next along the lanthanide light rare earth series. Similarities among all the Mg–Al–RE ternary

systems are also expected. The Al–Mg–La, Al–Mg–Ce and Al–Mg–Sm ternary systems were optimized independently by Hosseinifar and Malakhov [6], Grobner *et al.* [7] and Jia *et al.* [8], respectively. No thermodynamic optimization on the Al–Mg–Pr or Al–Mg–Nd system could be found in the literature. It is of great importance to study the Al–Mg–RE (RE: La, Ce, Pr, Nd, Sm) ternary systems in a systematic and consistent way especially as estimation techniques must be used for the mixing properties of intermetallic solutions.

As part of ongoing projects in our laboratory to develop thermodynamic databases for multi-component Mg– and Al– based alloys, the Al–Mg–light RE (La, Ce, Pr, Nd and Sm) were systematically evaluated and optimized based on 1) binary Al–Mg [9], Al–RE [10] and Mg–RE [11] thermodynamic and phase equilibria optimizations, 2) a critical literature review, 3) new experimental results from this work and 4) estimations from Miedema's model carried out in the present study. Key experiments were performed to verify the phase relationship and solid solubility limits in the ternary systems. The binary Al–RE systems have been assessed previously by our group [10; 12; 13]. The trends in the thermodynamic properties (such as the enthalpy of mixing for the liquid, the entropy of mixing for the liquid, and the enthalpy of formation for the intermetallic compounds) of Al–RE systems were also discussed in Jin *et al.* [10; 13]. The binary thermodynamic parameters of Al –light RE (light RE= La, Ce, Pr, Nd, Sm) were taken from Jin *et al*. [10] , whereas the Mg – light RE binary systems were from Kang *et al*. [14]. The thermodynamic evaluation and modeling of Al–Mg–heavy RE (heavy RE: Gd, Tb, Dy, Ho, Er) systems will be presented in a future article.

8.2 Experimental information in the literature

For the Mg–Al–La system, Rogl [15] reported the experimental information published prior to the year 1988, while Raghavan [16] reviewed the experimental investigations published up to the year 2008. Zarechnyuk *et al.* [17] studied the partial isothermal section at 400 ℃ for La concentration up to 33.3 at.%. According to these authors, no ternary intermetallic compound was found and a limited solubility of Al in La_2Mg_{17} and in $LaMg_3$ was reported. Odinaev *et al.* [18] prepared 115 alloys with an arc melting furnace using Al, Mg, and La as starting materials with

99.995, 99.95 and 98.48 wt. % purity, respectively. They annealed the alloys at 400 ℃ for 480 hours. Phase equilibria in this isothermal section were then investigated by metallography and X–ray powder diffraction (XRD). Extensive solid solutions were observed. It was reported that $LaMg_2$ (prototype: $MgCu_2$) and $LaAl_2$ (prototype: $MgCu_2$) formed a continuous Laves_C15 solid solution at 673K with a miscibility gap (20 ~ 37 at.% Mg) and LaMg (prototype: CsCl) formed an extensive BCC_B2 solid solution with LaAl (prototype: CeAl) up to ~ 29 at.% Al. Moreover, a ternary compound $Al_2Mg_{0.85}La_{0.15}$ of unknown structure was found to be stable at this temperature. Odinaev et al. [19] studied the phase equilibria in the Al–Mg–$LaAl_2$ sub-system by metallography, DTA, and XRD. The liquidus projection and four pseudobinary sections were constructed in this region. The existence of $LaMg_{12}$ phase remained unclear according to Raghavan [16], although the $LaMg_{12}$ phase was considered in the thermodynamic optimization of the La–Mg system by Guo and Du [20] based on the investigation of Darriet et al. [21]. Zheng et al. [22] investigated the liquidus surface in the Al-rich corner of the Al–Mg–La system and reported a eutectic reaction Liquid $\leftrightarrow$ αLa_3Al_{11} + Al_3Mg_2 + Al at 718K. Noting that Odinaev et al. investigated the Al–La–Mg [18], and Al–Ce–Mg [23] systems using the same experimental technique (DTA) to determine the liquidus temperatures and that the experimental work from Grobner et al. [7] suggested the liquidus temperatures in Al–Ce–Mg system were much higher than those from Odinaev et al. [23], Hosseinifar and Malakhov [6] recently studied two key alloys in the Al–Mg–La system (Al 60 wt. %, La 20.1 wt. %, Mg 19.9 wt. % and Al 70 wt. %, La 15.07 wt. %, Mg 14.93 wt. % respectively), by differential scanning calorimeter (DSC) to verify the liquidus temperatures and thermal arrests during the solidification process. They also reported an optimized Al–Mg–La ternary system.

For the Mg–Al–Ce system, Zarechnyuk and Kripyakevich [24] prepared 16 binary and 57 ternary alloys and determined a partial isothermal section at 673K for Ce compositions up to 33.3 at. %. A ternary compound $Al_{67}Ce_5Mg_{28}$ was reported with a structure of the $MgZn_2$ type (hexagonal Laves_C14 phase with a = 0.552 nm and c = 0.889 nm). Two ternary compounds, $Al_{23}CeMg_9$ and Al_4CeMg_4 were reported by Cui and Wu [25] from their metallographic analysis on sixty arc-melted samples, which were annealed at 673K for 608 hours. The crystal structure of these two ternary compounds was not reported. However, these two compounds were not confirmed in a later study by Odinaev et al. [23] who reported a ternary compound $Al_2Ce_{0.2}Mg_{0.8}$ with the $MgZn_2$ type structure. This compound was most likely the same compound observed by

Zarechnyuk and Kripyakevich [24]. In a later investigation, the same authors [26], using DTA, examined a number of pseudo–binary sections in the Al–Mg–Ce ternary system. It was reported that the ternary compound $Al_2Ce_{0.2}Mg_{0.8}$ (or $Al_2Ce_{0.15}Mg_{0.85}$) melts congruently at 908 K. Extensive solid solutions were observed by Odinaev *et al*. [23] from microstructural and X–ray examinations. They reported that $CeMg_2$ and $CeAl_2$ form a continuous solid solution at 673K with a miscibility gap (5 ~ 20 at% Mg) and CeMg forms an extensive solid solution with CeAl up to ~ 30 at. % Al. Moreover, a limited solubility of Al in $CeMg_{12}$ was found [24]. Zheng *et al*. [27] measured a eutectic temperature at 719K involving liquid–Al–Ce_3Al_{11}–$Al_{140}Mg_{89}$ by thermal analysis.

Recently, Grobner *et al*. [7] prepared four key experiments by arc melting under purified argon, sealed them in silica tubes and annealed them at 673K for 500 hours. According to their DTA and XRD studies, Grobner *et al*. [7] suggested that the ternary compound $Al_{13}CeMg_6$ (referred to $Al_{67}Ce_5Mg_{28}$ [24], $Al_2Ce_{0.2}Mg_{0.8}$ or $Al_2Ce_{0.15}Mg_{0.85}$ [23; 26]) melted incongruently around 728K. It was also claimed that solid solutions of the BCC_B2, Laves_C15, and $Ce(Mg,Al)_{12}$ phases were formed in the Al–Mg–Ce ternary system and an optimized Al–Mg–Ce ternary system was obtained [7].

For the Al–Mg–Pr ternary system, no optimized ternary phase diagram could be found in the literature. This ternary system has been reviewed by Raghavan [28]. Odinaev *et al*.[29] prepared about 150 alloys with arc melting furnace and annealed them at 673K for 480 hours with the starting metals of 99.995% Al, 99.95% Mg and 99.78% Pr. Phase equilibria in this isothermal section were investigated by metallography and XRD techniques. Extensive solid solutions were observed. They found that $PrMg_2$ (prototype: $MgCu_2$) and $PrAl_2$ (prototype: $MgCu_2$) form a continuous Laves_C15 solid solution at 673K with a miscibility gap (5 ~ 27 at% Mg), and PrMg (prototype: CsCl) forms an extensive BCC_B2 solid solution with PrAl up to ~ 30 at. % Al. Also, a ternary compound $Al_2Mg_{0.88}Pr_{0.12}$ of $MgZn_2$-type structure (Laves_C14) was found to be stable at this temperature. Odinaev *et al*. [30] prepared 153 alloys in the Al–Mg–$PrAl_2$ region with the same starting metals as used in their previous paper [29]. Phase equilibria were studied by metallography, DTA, and XRD techniques. The liquidus projection and four pseudobinary sections were constructed in this region.

For the Mg–Al–Nd system, no optimized ternary phase diagram could be found in the literature. The Al–Mg–Nd ternary system has been reviewed by Raghavan [31]. Zarechnyuk *et al* [17] studied a partial isothermal section at 673K for Nd composition up to 33.3 at.%. No ternary intermetallic compound was reported and a limited solubility of Al in $NdMg_{12}$ and in $NdMg_3$ was found. Odinaev *et al.* [32] prepared 87 alloys with arc melting furnace and annealed them at 673K for 480 hours with the starting metals of 99.995% Al, 99.95% Mg, and 99.98% Nd purity. Phase equilibria in this isothermal section were investigated by metallography and XRD techniques. Extensive solid solutions were also observed. According to their investigation [32], $NdMg_2$ (prototype: $MgCu_2$) and $NdAl_2$ (prototype: $MgCu_2$) form a continuous Laves_C15 solid solution at 673K with a miscibility gap (3 ~ 30 at% Mg) and NdMg (prototype: CsCl) forms an extensive BCC_B2 solid solution with NdAl up to ~ 40 at. % Al. Also, a ternary compound $Al_2Mg_{0.88}Nd_{0.12}$ of $MgZn_2$-type structure (Laves_C14) was stable at this temperature. Odinaev *et al*. [33] prepared 60 alloys in the Al–Mg–$NdAl_2$ region with the same starting metals as used in their previous paper [32]. Phase equilibria were studied by metallography, DTA, and XRD techniques. The liquidus projection and several pseudobinary sections were constructed in this region.

The Al – Mg – Sm ternary system has been reviewed by Raghavan [34]. Zheng *et al.* [35] reported 15 single phase regions, 27 two-phase regions, and 13 three-phase regions for the isothermal section at 673K studied by X-ray, metallographic and chemical analysis, and no ternary compound was found. Jia *et al.* [8] optimized this ternary phase diagram based on the investigation by Zheng *et al.* [35]. No ternary interaction parameters were used and the ternary phase diagram was merely extrapolated from the three binary sub-systems.

8.3 Methodology

8.3.1 Experimental methods

A solid–solid diffusion couple for the Al–Mg–La system was prepared from two blocks of Mg and Al alloys with a La foil in the middle, like a sandwich. The blocks' facing surfaces and the

La foil were pre-grinded up to 1200 grit using SiC paper and polished using 1 μm water-based diamond suspension. The blocks were pressed together using a hydraulic press, placed in a Ta container and then sealed in a quartz tube under protective argon atmosphere. The prepared samples were annealed at 673 K for four weeks before quenching in cold water. The annealed samples were grinded and polished before being analyzed by electron probe microscopy analysis (EPMA) using point and line scans. However, no intermediate layers in the Al–Mg–La solid–solid diffusion couple were observed, probably due to the small diffusion coefficient at 673K or poor surface contact. Therefore, two key samples were arc–melted in a water-cooled copper crucible under protective argon atmosphere in order to avoid extensive oxidation of Mg and Al. The starting materials are: La foil (50mm*50mm*1.0mm, 99.9% (REO)), Al ingot (99.999 wt. %) and Mg ingot (99.8 wt. %).

A solid–liquid diffusion couple in the Al–Mg–Ce system was prepared using $Ce_{0.333}Mg_{0.667}$ and $Ce_{0.333}Al_{0.667}$ alloys. The block with lower liquidus temperature ($Ce_{0.333}Mg_{0.667}$ alloy) was melted on top of the block with higher melting temperature ($Ce_{0.333}Al_{0.667}$ alloy) in an arc-melting furnace. Furthermore, two additional key samples of Al–Mg–Ce alloys were prepared. The prepared samples were also annealed at 673 K for four weeks. The annealed alloys were grinded and polished before EPMA analysis. The starting materials are: Ce ingot (99.8 % (REO)), Al ingot (99.999 wt. %) and Mg ingot (99.8 wt. %).

Four ternary alloys in the Al–Mg–Pr system were prepared by melting stoichiometric amounts of the constituent elements in an induction furnace under a protective argon atmosphere. Two alloys for the Al–Mg–Nd system were melted in an arc-melting furnace in a water-cooled copper crucible under a protective argon atmosphere. The prepared samples were annealed in a resistance furnace at 673 K for four weeks before quenching in cold water. All the samples were grinded up to 1200 grit using SiC paper and polished using 1 μm water-based diamond suspension. Electron probe microscopy analysis (EPMA) was employed to detect the phases and determine their compositions. The starting materials were: Pr ingot (99.9 % (REO)), Nd ingot (99.8 % (REO)), Al ingot (99.999 wt. %) and Mg ingot (99.8 wt. %).

8.3.2 Miedema's model estimations for binary and ternary thermodynamic data

The enthalpy of mixing [36; 37] for a A–B disordered solution is estimated using Miedema's model with the following expression:

$$\Delta H_{AB} = f_{AB} \frac{x_A(1+\mu_A x_B(\phi_A - \phi_B))x_B(1+\mu_B x_A(\phi_B - \phi_A))}{x_A V_A^{2/3}[1+\mu_A x_B(\phi_A - \phi_B)] + x_B V_B^{2/3}[1+\mu_B x_A(\phi_B - \phi_A)]} \tag{8.1}$$

For an ordered stoichiometric compound, enthalpy of formation is given by the following expression:

$$(\Delta H_{AB})_{order} = \Delta H_{AB}\left[1+\gamma\left(\frac{V_A^{2/3}V_B^{2/3}\Delta H_{AB}}{f_{AB}\left\{x_A V_A^{2/3}[1+\mu_A x_B(\varphi_A - \varphi_B)] + x_B V_B^{2/3}[1+\mu_B x_A(\varphi_B - \varphi_A)]\right\}}\right)^2\right] \tag{8.2}$$

$$f_{AB} = \frac{2PV_A^{2/3}V_B^{2/3}}{\dfrac{1}{n_{WS_A}^{1/3}} + \dfrac{1}{n_{WS_B}^{1/3}}} \cdot [-(\phi_B^* - \phi_A^*)^2 + \frac{Q}{P}(n_{WS_A}^{1/3} - n_{WS_B}^{1/3})^2 - a \times \frac{R}{P}] \tag{8.3}$$

In Eqs (8.1-8.3), x_i, ϕ_i, V_i, n_{WS_i} are the mole fraction, chemical potential (or work function), molar volume, and the electronic density at the Winger-Seitz cell boundary of component i, respectively. a, P, $\frac{R}{P}$, $\frac{Q}{P}$, μ_i, and γ are semi-empirical parameters evaluated and reported in Miedema [36]. The empirical parameter P assumes different values depending if A and B are both transition, both non-transition, or transition and non-transition elements; Q/P is assumed to be a constant that equals 9.4 [36].

The formation enthalpy of a crystalline solid solution can be described as [38]:

$$\Delta H^{cryst} = \Delta H^{chem} + \Delta H^{elastic} + \Delta H^{struct} \tag{8.4}$$

where

ΔH^{chem}: chemical contribution due to the mixing of two components given by Eq. (8.1).

$\Delta H^{elastic}$: elastic contribution due to the atom-size mismatch effect.

ΔH^{struct}: structural contribution due to the valence and crystal structure difference of the two components.

$$\Delta H^{elastic} = x_A \cdot x_B (x_A \Delta H^{elastic}_{BinA} + x_B \Delta H^{elastic}_{AinB}) \tag{8.5}$$

where $\Delta H^{elastic}_{BinA}$ and $\Delta H^{elastic}_{AinB}$ are the atom-size mismatch contribution to the solution enthalpy in a binary system. It can be evaluated by the following expression:

$$\Delta H^{elastic}_{AinB} = \frac{2G_B(V_A^* - V_B^*)^2}{3V_B^* + 4G_B K_A V_A^*} \tag{8.6}$$

$$(V_i^*)^{2/3} = V_i^{2/3}(1 + \mu_i(\varphi_i - \varphi_j)) \quad (i,j = A, B) \tag{8.7}$$

where G_B is the shear modulus of the solvent; K_A is the compressibility of the solute and V_i^* (i= A, B) are the molar volumes of the solute or the solvent.

The structural contribution to the enthalpy is difficult to obtain without the use of ab-initio calculations. It is argued that this contribution has a minor effect compared to the chemical and elastic contribution to the total enthalpy [39]. In the present study, the structural contribution is neglected.

$$\Delta H^{struct} \approx 0 . \tag{8.8}$$

The enthalpy of formation of a ternary alloy is assumed to be the sum of contribution from the three binary sub-systems. For a ternary system, there are a few simple and reliable interpolation models such as Kohler, Muggianu and Toop models to estimate the thermodynamic properties from binary sub-systems. A general interpolation technique of the thermodynamic model for the multicomponent systems is given by Pelton [40]. The choice of the interpolation model should be made according to the thermodynamic properties of three sub-binary alloys. In the current study, the thermodynamic properties (e.g. enthalpy of mixing in the liquid) of three binary systems Al–

Mg, Al–RE and Mg–RE are quite different from each other. The Kohler model is chosen in the present study, and the enthalpy of formation for the ternary compound can be expressed as:

$$\Delta H_{ijk}{}^{cryst} = (1-x_i)\Delta H_{jk}^{cryst}(\frac{x_j}{x_j+x_k},\frac{x_k}{x_j+x_k}) + (1-x_j)\Delta H_{ik}^{cryst}(\frac{x_i}{x_i+x_k},\frac{x_k}{x_i+x_k})$$
$$+(1-x_k)\Delta H_{ij}^{cryst}(\frac{x_i}{x_i+x_j},\frac{x_j}{x_i+x_j})$$

(8.9)

where i, j, k are the three components in a ternary system, x_i, x_j or x_k is the mole fraction of each component, ΔH_{ij}^{cryst}, ΔH_{jk}^{cryst}, ΔH_{ik}^{cryst} and ΔH_{ijk}^{cryst} are the contributions (chemical, elastic and structural contributions) of three sub-binary systems and ternary system, respectively. The chemical and elastic enthalpies of ternary alloys can be extrapolated similarly from those of sub-binary systems by the Eq. (8.9).

The model parameters of ϕ_i, V_i, and n_{WS_i} from Shubin and Shunya'ev [41] are preferred in the present calculations. The estimations of the enthalpy of formation using the model parameters from Shubin and Shunya'ev [41] give better agreement with the available experimental data than those calculated from the model parameters of Boer *et al.* [36].

8.3.3 Thermodynamic models used in the present study

All the present optimizations have been carried out using FactSage thermodynamic software [42; 43]. The thermodynamic properties of pure Mg and light rare earths (La, Ce, Pr, Nd and Sm) are taken from the SGTE database [44], except the Pr and Sm in the FCC–structure, together with La, Pr, Nd and Sm in the HCP– structure which are taken from Kang *et al.* [11]. The present study is based on thermodynamic and phase equilirium modeling of Al–Mg, Al–RE and Mg–RE (RE: La, Ce, Pr, Nd and Sm) binary systems [9; 10; 11], in which the Modified Quasichemical Model (MQM) was used for the liquid phase with a consistent set of coordination numbers for the elements ensuring compatibility with our previous database.

8.3.3.1 Modified Quasichemical Model (MQM) for the liquid phase

The detailed description of the MQM can be found in Pelton *et al.* [45]. A brief summary of MQM is given in Jin *et al.* [10; 13]. The same notation is used in the present article. The MQM has been successfully applied to alloy liquid solutions [46; 47], molten oxides [48; 49], molten salts [50; 51], and molten metal-sulphides systems [52]. As was shown by Kang *et al.* [47], liquid Mg–RE alloys usually exhibits a strong short-range ordering near $X_{RE} = 0.25 - 0.33$. Such short-range ordering in binary liquid alloy becomes more evident in several binary Al–RE systems as discussed by Jin *et al.* [10; 13]. In order to treat short-range ordering effectively in the Mg–Al–RE ternary systems, the Modified Quasichemical Model in the pair approximation has been used in the present study. The Kholer method [40] was used to estimate the excess Gibbs energy in ternary liquid in the present study.

8.3.3.2 Compound Energy Formalism (CEF) for solid solutions

The compound energy formalism was introduced by Hillert [53] to describe the Gibbs energy of solid phases with sub–lattices. Ideal mixing of species on each sub–lattice is assumed. The sub-lattice stoichiometry depends on the base crystal structure. The same notation for the model parameters is used as those in Kang *et al.* [12].

Table 8.1 shows the reported crystal structures of the stable binary and ternary phases of the studied systems. In the present work, it is assumed that Mg and Al can potentially substitute each other on their respective sublattices for all solid solutions. As shown in Table 8.1, the ternary phases ($Al_{40}Mg_{17}La_3$, $Al_{13}Mg_6Ce$, $Al_{50}Mg_{22}Pr_3$, and $Al_{50}Mg_{22}Nd_3$) are considered to be stoichiometric phases, although a narrow homogeneity range of their existence could not be excluded. The CEF is used for all solid solutions in the present study, and the sublattices species for each one is given in Table 8.1. For each intermetallic phase in the Mg–light RE (MgRE, Mg_3RE, $Mg_{12}RE$, $Mg_{41}RE_5$, and $Mg_{17}RE_2$ phases) and Al–light RE (Al_2RE, Al_3RE, and $Al_{11}RE_3$ phases) sub-systems, a solid solution with the corresponding crystal structure is constructed, where a substitution of the RE elements by another light RE is permitted. For the Mg_3RE solid solution, the same model is used as the one from Kang *et al.* [11] except that Mg and Al substitute each other on the first sub-lattice. Mg is introduced in the second sub-lattice [11] since

considerable solubility of Mg in $PrMg_{3 (cF16)}$ was reported by Saccone *et al*. [54] using a Smith thermal analysis technique.

Table 8.1 The solid phases in the Al-Mg-RE (RE = La, Ce, Pr, Nd, Sm) ternary systems.

Phase symbol	Phase description	Prototype	Pearson symbol
BCC_B2	(Mg, Al)(Mg, La, Ce, Pr, Nd, Sm)	CsCl	cP2
Laves_C15	(Mg, Al, La, Ce, Pr, Nd, Sm)$_2$(Mg, Al, La, Ce, Pr, Nd, Sm)	Cu$_2$Mg	cF24
REMg3	(Mg, La, Ce, Pr, Nd, Sm)(Mg, Al)$_3$	BiF$_3$	cF16
REAl3	(La, Ce, Pr, Nd, Sm)(Mg, Al)$_3$	Ni$_3$Sn	hP8
RE3Al11	(La, Ce, Pr, Nd, Sm)$_3$(Mg, Al)$_{11}$	αLa$_3$Al$_{11}$	oI28
REMg12	(La, Ce, Pr, Nd, Sm)(Mg, Al)$_{12}$	CeMg$_{12}$	oI338
RE5Mg41	(La, Ce, Pr, Nd, Sm)$_5$(Mg, Al)$_{41}$	Ce$_5$Mg$_{41}$	tI92
RE2Mg17	(La, Ce, Pr, Nd, Sm)$_2$(Mg, Al)$_{17}$	Ni$_{17}$Th$_2$	hP38
BCC_A2	(Al, Mg, La, Ce, Pr, Nd, Sm)	W	cI2
FCC_A1	(Al, Mg, La, Ce, Pr, Nd, Sm)	Cu	cF4
HCP_A3	(Al, Mg, La, Ce, Pr, Nd, Sm)	Mg	hP2
DHCP_A3'	(Al, Mg, La, Ce, Pr, Nd, Sm)	La	hP4
Al$_{40}$Mg$_{17}$La$_3$	Stoichiometric	-	-
Al$_{13}$Mg$_6$Ce	Stoichiometric	MgZn$_2$	*hP*12
Al$_{50}$Mg$_{22}$Pr$_3$	Stoichiometric	MgZn$_2$	*hP*12
Al$_{50}$Mg$_{22}$Nd$_3$	Stoichiometric	MgZn$_2$	*hP*12

For the BCC_B2 phase, as is known, all Mg–RE binary systems, except for the Mg–Yb binary system, contain the BCC_B2 phase (prototype CsCl) while all AlRE phases in the Al–RE binary systems do not have this CsCl structure. The initial guess of Gibbs energy of the metastable AlRE-BCC_B2 phases is based on the assumption that the difference of energy between two different structures (stable AlRE strucutre and AlRE-BCC_B2 structure) are the same as the one calculated by Gao *et al*. [55] using first-principles and the entropy of formation of metastable AlRE-BCC_B2 phases was assumed to be the same as the one from the corresponding stable phase. Then, the Gibbs energy of the metastable AlRE-BCC_B2 phases is optimized to fit the available ternary experimental data. In the present study, the BCC_B2 phase was modeled using two sub-lattice CEF with (Mg, Al)(Mg, La, Ce, …, Sm) formula.

For the Laves_C15 phase, all studied Al–RE and Mg–RE (RE: La, Ce, Pr, Nd, Sm) binary systems contain the Laves_C15 phase ($cF24$, prototype Cu_2Mg). A two sub-lattice CEF with (Al, Mg, La, Ce, Pr, Nd, Sm)$_2$(Al, Mg, La, Ce, Pr, Nd, Sm) formula was employed to model the Laves_C15 phase.

For other solid solutions (Al_3RE, $Al_{11}RE_3$, $Mg_{12}RE$, $Mg_{41}RE_5$, and $Mg_{17}RE_2$), Al and Mg atoms were introduced in the first sub-lattice, while the rare earth elements are assumed to mix ideally on the second sub-lattice in each one of these solid solutions, e.g., (Al, Mg)$_3$(La, Ce, Pr, Nd, Sm) for the $Al_3RE_{(hP8)}$ phase.

8.3.4 Estimations on Gibbs energy of metastable end-members in solid solutions

The difference in enthalpy of formation at 298 K between the metastable phases $LaMg_3$, $CeMg_3$, $PrMg_3$, $NdMg_3$ and $SmMg_3$ in the Ni_3Sn-hP8 structure and the stable phases ($LaMg_3$, $CeMg_3$, $PrMg_3$, $NdMg_3$ and $SmMg_3$ in the BiF_3-cF16 structure) was taken from the results of ab-initio calculations by Tao [56; 57], while the entropy of formation at 298K for these metastable phases are assumed to be the same as the ones calculated from their respective stable phases. The RE_3Mg_{11} phase in the αLa_3Al_{11}-oI28 structure, the $REAl_{12}$ phase in the $CeMg_{12}$-oI338 structure, the RE_2Al_{17} in the Th_2Ni_{17}-hP38 structure, and the RE_5Al_{41} phase (RE= La, Ce, Pr, Nd, Sm) in the Ce_5Mg_{41}-tI92 structure are calculated using the Miedema model and the results are shown in

Table 8.2. The entropy of formation at 298 K of the RE_3Mg_{11} phases in the αLa_3Al_{11}-oI28 structure is linearly interpolated between the entropy of the stable $REMg_3$ and RE_5Mg_{41} (RE= La, Ce, Pr, Nd) phases or between the entropy of the stable $SmMg_3$ and $SmAl_5$ compound at 298 K. The entropy of formation at 298 K of the $REAl_{12}$ phases in the $CeMg_{12}$-oI338 structure, the RE_2Al_{17} phases in the Th_2Ni_{17}-hP38 structure, and the RE_5Al_{41} phases (RE= La, Ce, Pr, Nd, Sm) in the Ce_5Mg_{41}-tI92 structure is linearly interpolated between the entropy of Al and the entropy of the Al-richest stable compound (that is RE_3Al_{11} where RE is La, Ce, Pr and Nd, $SmAl_3$ where RE is Sm) at 298 K.

Table 8.2 The enthalpies of formation of several Al-RE, Mg-RE and Al-Mg-RE compounds calculated by the Miedema model

Compounds	Enthalpies of formation (kJ/mole of atoms)
$LaAl_{12}$	-11.70
$CeAl_{12}$	-11.39
$PrAl_{12}$	-11.30
$NdAl_{12}$	-12.56
$SmAl_{12}$	-11.18
La_2Al_{17}	-15.72
Ce_2Al_{17}	-15.41
Pr_2Al_{17}	-15.26
Nd_2Al_{17}	-16.98
Sm_2Al_{17}	-15.13
La_5Al_{41}	-16.20
Ce_5Al_{41}	-15.89
Pr_5Al_{41}	-15.73

Nd_5Al_{41}	-17.51
Sm_5Al_{41}	-15.61
La_3Mg_{11}	-4.10
Ce_3Mg_{11}	-5.21
Pr_3Mg_{11}	-5.07
Nd_3Mg_{11}	-5.92
Sm_3Mg_{11}	-5.06
$Al_{13}Mg_6Ce$ ($Al_2Mg_{0.8}Ce_{0.2}$)	-12.67
$Al_{40}Mg_{17}La_3$ ($Al_2Mg_{0.85}La_{0.15}$)	-10.49
$Al_{50}Mg_{22}Pr_3$ ($Al_2Mg_{0.88}Pr_{0.12}$)	-7.60
$Al_{50}Mg_{22}Nd_3$ ($Al_2Mg_{0.88}Nd_{0.12}$)	-8.35

8.4 Results and discussions

8.4.1 Experimental results

The experimental results of microanalysis on ten key alloys (A1, A2… A10) are listed in Table 8.3. Backscattered electron images of two key alloys (A1, A2) in the Al–Mg–La system annealed at 673 K for four weeks are shown in Figures 8.1 and 8.2. The compositions of the detected phases have been measured by EPMA (Table 8.3). The stability of the $LaMg_{12}$ phase at 673 K was confirmed and the solid solubility of Al in this phase is found to be small. Shown in Figure 8.2 is a microphotograph of sample A2, where three phases ((Al), La_3Al_{11}, ternary phase (noted as τ1)) are in equilibrium at 673 K. The composition of the ternary τ1 phase in the A2 sample is close to the stoichiometry $Al_{40}Mg_{17}La_3$, which is used in the present optimization. This ternary phase corresponds to the $Al_2Mg_{0.85}La_{0.15}$ proposed by Odinaev $et\ al$. [18].
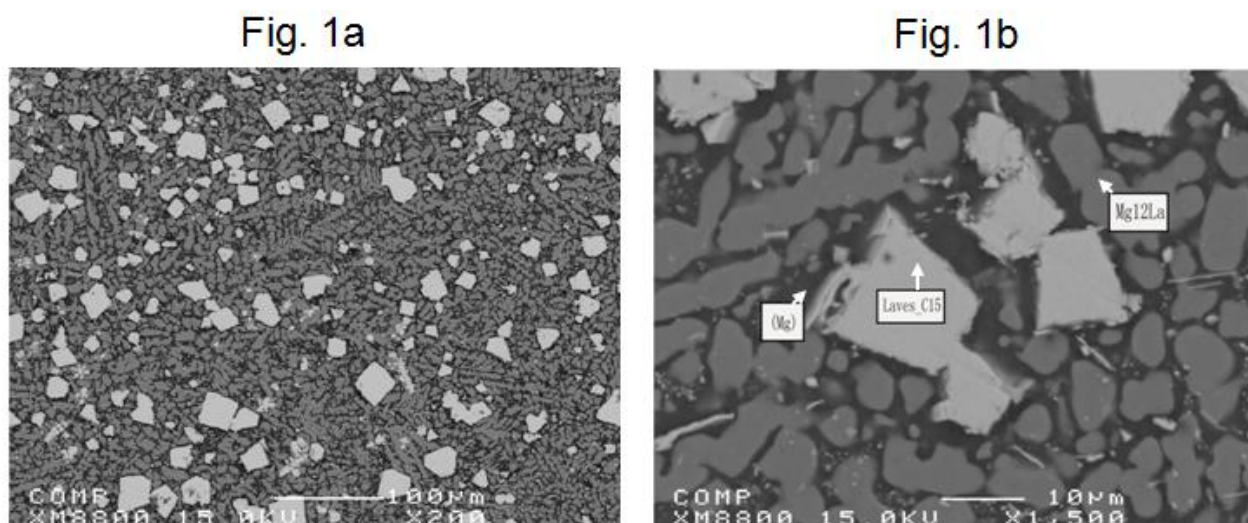
Figure 8.1 Backscattered electron images of A1 alloy annealed at 673 K for four weeks.

Table 8.3 Composition and microanalysis data of the studied alloys.

Sample	Ternary system	Alloy composition (at.%)	Observed Phases	EPMA analysis (at.%)		
				Al	Mg	RE
A1	Al-Mg-La	$Al_{10}Mg_{82}La_8$	(Mg)	0.3	99.4	0.3
			$La(Al_xMg_{1-x})_2$	58.9	8.4	32.7
			$La(Al_xMg_{1-x})_{12}$	1.3	91.2	7.5
A2	Al-Mg-La	$Al_{80}Mg_{12.5}La_{7.5}$	$La_3(Al_xMg_{1-x})_{11}$	78.4	1.5	20.1
			(Al)	90.7	9.1	0.2
			Ternary phase $\tau 1$	69.0	23.9	7.1
A3	Al-Mg-Ce	$Al_{76}Mg_{16}Ce_8$	(Al)	89.4	10.5	0.1
			$Ce_3(Al_xMg_{1-x})_{11}$	77.4	0.3	22.3
			Ternary phase $\tau 2$	66.0	26.7	7.3
A4	Al-Mg-Ce	$Al_8Mg_{57}Ce_{35}$	$Ce(Al_xMg_{1-x})$	42.2	7.7	50.1
			$Ce(Al_xMg_{1-x})_2$	9.2	56.4	34.4

A5	Al-Mg-Pr	$Al_{10.6}Mg_{79.4}Pr_{10}$	(Mg)	0.0	99.9	0.1
			$Pr(Al_xMg_{1-x})_2$	61.0	4.8	34.2
			$Pr(Al_xMg_{1-x})_{12}$	0.3	91.9	7.8
A6	Al-Mg-Pr	$Al_{56.2}Mg_{22.4}Pr_{21.4}$	(Mg)	2.0	98.0	0.0
			$Pr(Al_xMg_{1-x})_2$	64.5	1.5	34.0
			$Pr(Al_xMg_{1-x})_3$	71.2	3.7	25.1
A7	Al-Mg-Pr	$Al_{34}Mg_{63}Pr_3$	(Mg)	8.6	91.4	0.0
			$Pr_3(Al_xMg_{1-x})_{11}$	73.6	3.3	23.1
			Gamma	37.3	60.9	1.8
A8	Al-Mg-Pr	$Al_{78}Mg_{15}Pr_7$	(Al)	92.2	7.8	0.0
			$Pr_3(Al_xMg_{1-x})_{11}$	76.2	0.2	23.6
			Ternary phase $\tau3$	66.9	27.0	6.1
A9	Al-Mg-Nd	$Al_{26.9}Mg_{70.3}Nd_{2.8}$	(Mg)	10.3	89.6	0.1
			$Nd_3(Al_xMg_{1-x})_{11}$	76.1	1.8	22.1
			Gamma	38.3	60.5	1.2
A10	Al-Mg-Nd	$Al_{10.6}Mg_{79.4}Nd_{10}$	(Mg)	0.2	99.3	0.5
			$Nd(Al_xMg_{1-x})_2$	61.6	4.3	34.1
			$Nd_5(Al_xMg_{1-x})_{41}$	0.2	89.9	9.9
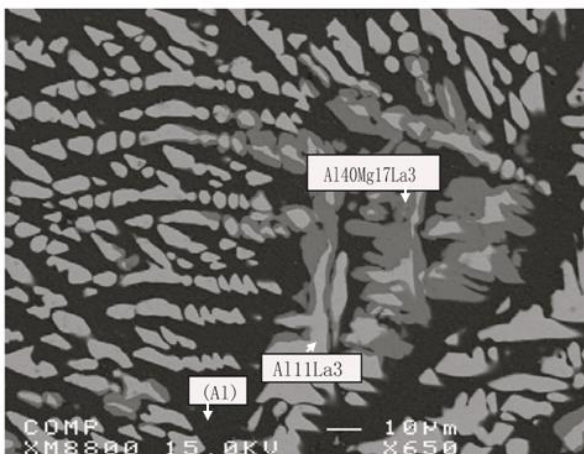
Figure 8.3 Backscattered electron images of A2 alloy annealed at 673K for four weeks.
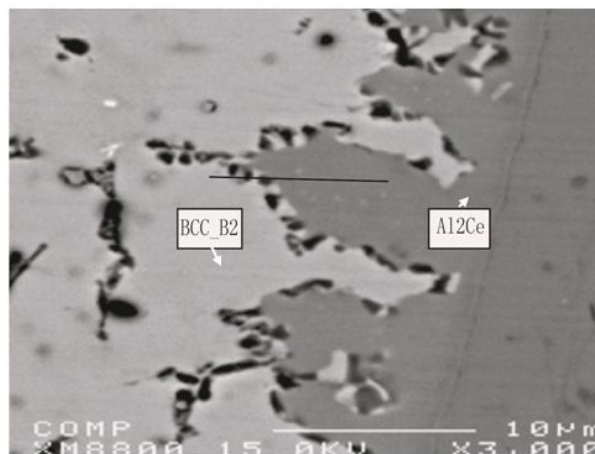
Figure 8.2 Backscattered electron image of the solid-solid Al_2Ce-MgCe diffusion couple annealed at 673K for ten weeks.

A backscattered electron image of the solid-solid $CeAl_2$–CeMg diffusion couple annealed at 673 K for ten weeks is shown in Figure 8.3. Unfortunately, some phases (probably Mg_3Ce and Ce_5Mg_{41} intermetallic compounds) in the solid-solid $CeAl_2$–CeMg diffusion couple were chipped out during the quenching process probably due to their brittleness. The composition profiles from the result of EPMA 26 μm line scan in the diffusion couple are shown in Figure 8.4. Three phases were identified: BCC_B2, Laves_C15 and the $CeAl_2$ compound. One tie-line between BCC_B2 and Laves_C15 is established. Backscattered electron images of two key alloys (A3, A4) in the Al–Mg–Ce system annealed at 673 K for four weeks were shown in Figures 8.5(a), 8.5(b) and Figure 8.6, respectively. The identified phases and microanalysis data are listed in Table 8.3. Three phases (Al-FCC solid solution, a ternary phase (noted as τ2) and the Ce_3Al_{11} compound) are in equilibrium at 673 K as shown in Figure 8.5. The composition of the ternary phase (τ2) is close to $Al_{13}Mg_6Ce$ proposed by Gröbner *et al*. [7], which corresponds to the $Al_2Mg_{0.8}Ce_{0.2}$ reported by Odinaev *et al.* [23]. One tie-line was constructed between BCC_B2 and Laves_C15 from Figure 9.6, which is also consistent with the results of Gröbner *et al*. [7].
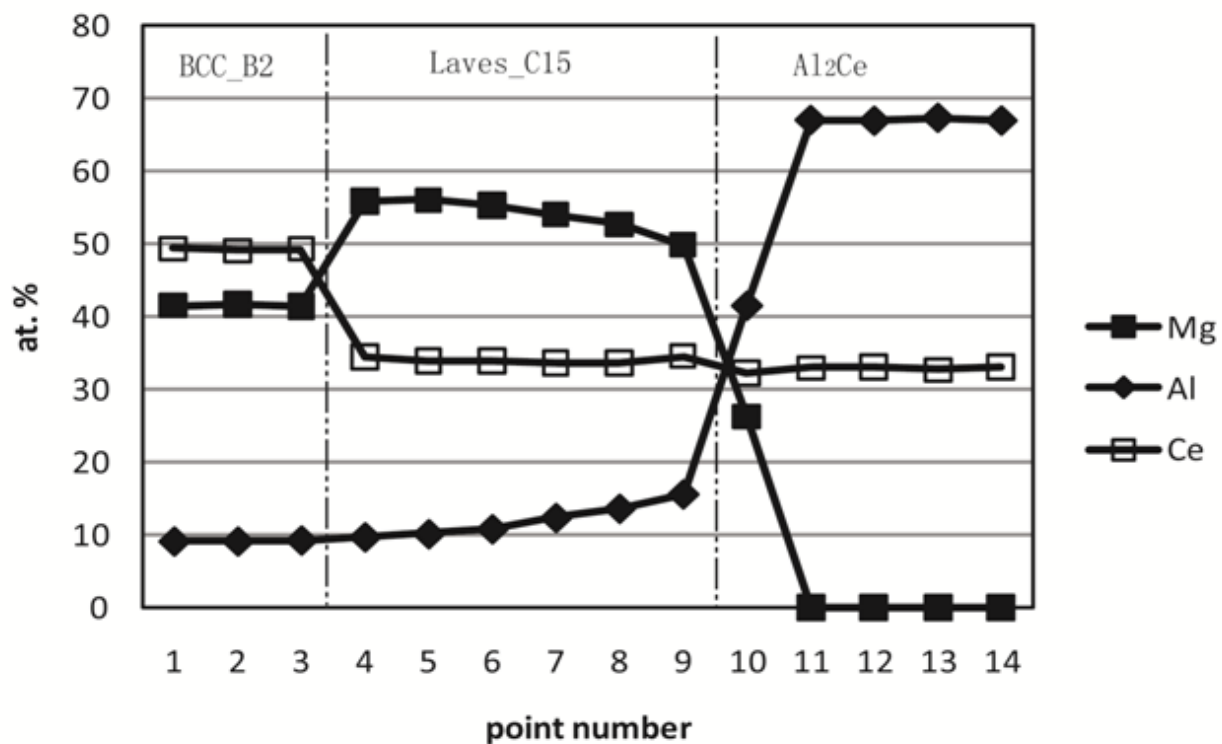
Figure 8.4 The composition profiles from the line scan of the $CeAl_2$-CeMg diffusion couple.
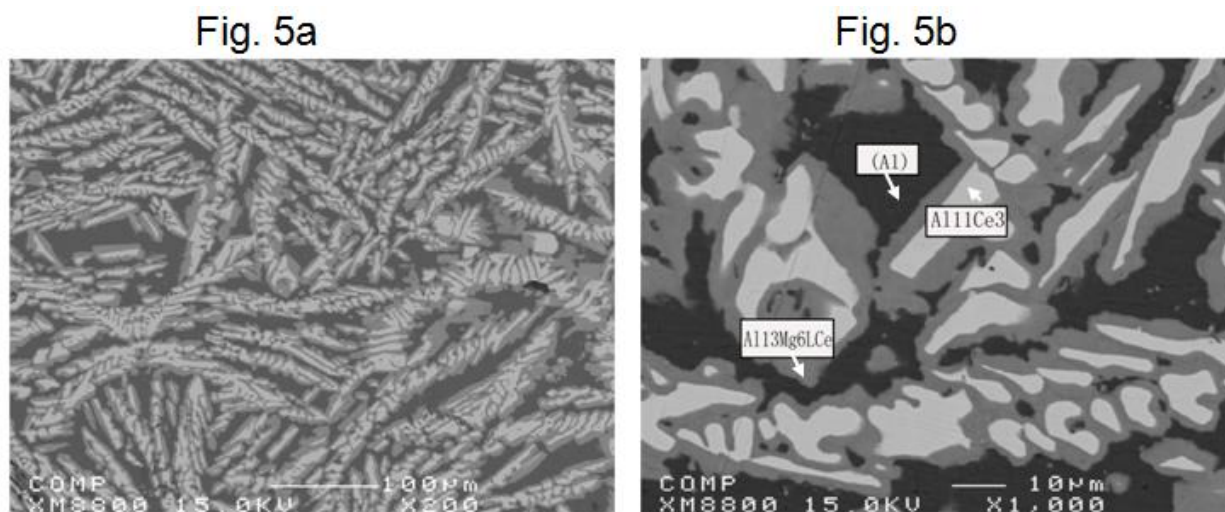
Figure 8.5 Backscattered electron images of A3 alloy annealed at 673 K for four weeks.
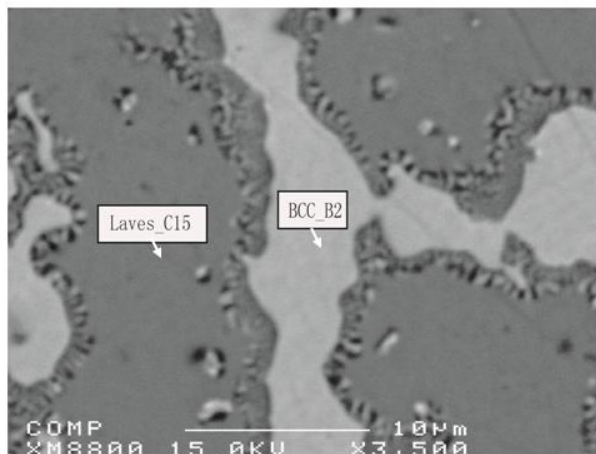
Figure 8.6 Backscattered electron images of A4 alloy annealed at 673 K for four weeks.
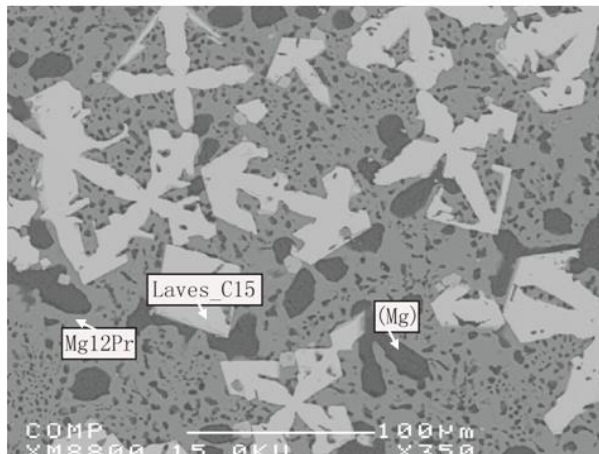
Figure 8.7 Backscattered electron images of A5 alloy annealed at 673 K for four weeks.

For the Al–Mg–Pr system, backscattered electron images of four key alloys (A5, A6, A7, and A8) annealed at 673 K for four weeks are shown in Figures 8.7 to 8.10 respectively. Their microanalysis data are listed in Table 8.3. The solid solubility of Al in $PrMg_{12}$ phase is negligible, unlike in $LaMg_{12}$ and $CeMg_{12}$. This is consistent with the phase equilibria determined by Odinaev *et al.* [29]. Small amount of Mg in $Pr(Mg,Al)_3$ solid solution is detected and used in the present optimization. This characteristic is similar to the $La(Mg,Al)_3$ phase. The microstructure of the sample A8, which is in a three-phase field, is shown in Figure 8.10, where the presence of a ternary phase ($\tau3$) in the Al-rich region is highlighted. The average composition of this ternary phase is close to the stoichiometry $Al_2Mg_{0.88}Pr_{0.12}$ [28], which is labelled as $Al_{50}Mg_{22}Pr_3$ in the present study.
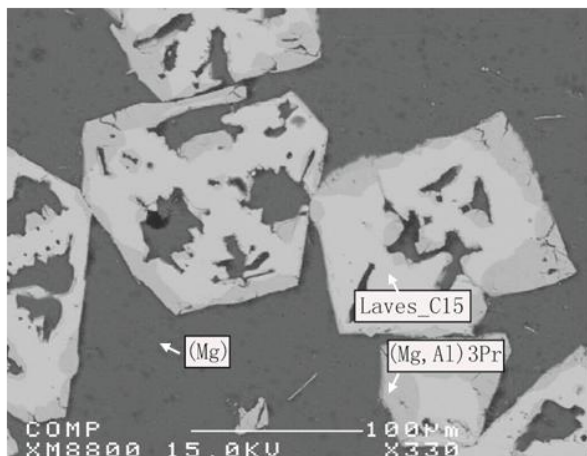
Figure 8.8 Backscattered electron images of A6 alloy annealed at 673 K for four weeks.
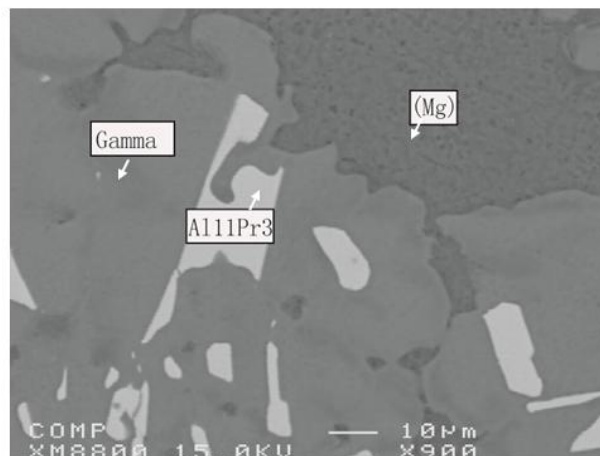
Figure 8.9 Backscattered electron images of A7 alloy annealed at 673 K for four weeks.
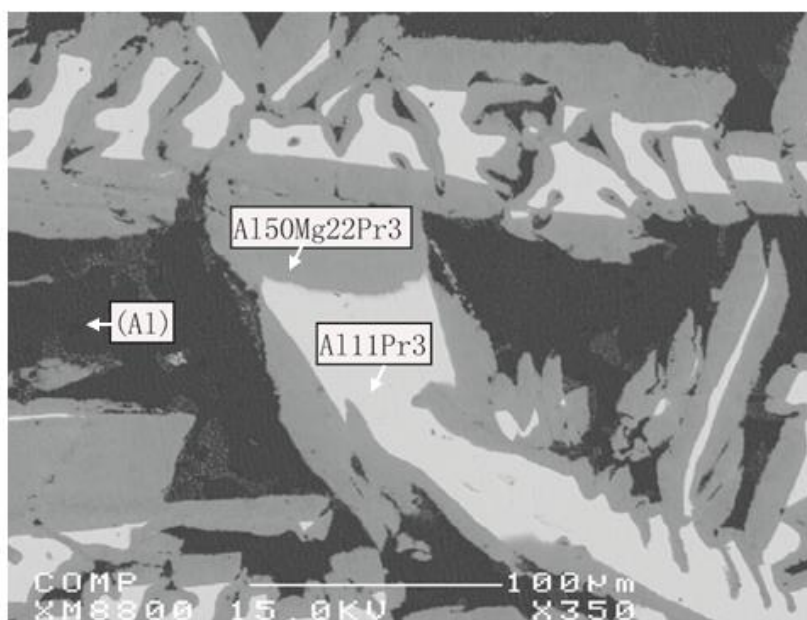
Figure 8.10 Backscattered electron images of A8 alloy annealed at 673 K for four weeks.
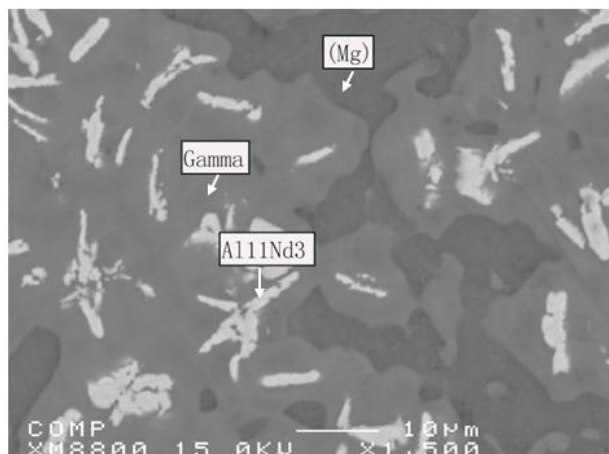
Figure 8.11 Backscattered electron images of A9 alloy annealed at 673 K for four weeks.
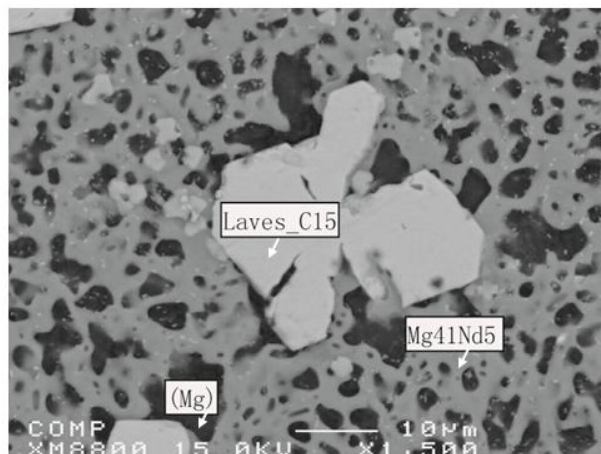
Figure 8.12 Backscattered electron images of A10 alloy annealed at 673 K for four weeks.

For the Al–Mg–Nd system, backscattered electron images of two key alloys (A9, A10) annealed at 673 K for four weeks are shown in Figures 8.11 and 8.12 respectively. The solid solubility of Nd in the gamma phase is negligible. A small solubility of Mg in Nd(Mg,Al)$_3$ is observed (see Table 8.3). Negligible solid solubility of Al in Nd$_5$Mg$_{41}$ phase is detected.

All the observed phases and their compositions are considered in the present optimization.

8.4.2 Thermodynamic optimizations of Al–Mg–RE (La, Ce, Pr, Nd, Sm) ternary systems

Table 8.2 shows the estimated enthalpies of formation of the stable ternary compounds (Al$_{40}$Mg$_{17}$La$_3$, Al$_{13}$Mg$_6$Ce, Al$_{50}$Mg$_{22}$Pr$_3$ and Al$_{50}$Mg$_{22}$Nd$_3$) from Miedema's model, which are used as initial guesses for the thermodynamic optimizations. The entropies of formation of these four ternary compounds are estimated from the contribution of RE$_3$Al$_{11}$ and Mg$_x$Al$_y$ alloy (x, y is calculated by mass balance) in Mg-Al-RE$_3$Al$_{11}$ system. The enthalpies of formation of these ternary phases were later optimized (Table 8.7) in order to obtain satisfactory results for phase equilibria. As is seen in Table 8.2, the hypothetical phases (LaAl$_{12}$, CeAl$_{12}$, PrAl$_{12}$, NdAl$_{12}$ and

SmAl$_{12}$) in the CeMg$_{12}$-oI338 structure, which are the end-members of the (La, Ce, Pr, Nd, Sm)(Mg, Al)$_{12}$ solid solution (CeMg$_{12}$-oI338), are also estimated from the Miedema model together with other hypothetical phases, such as RE$_3$Mg$_{11}$ phase in the αLa$_3$Al$_{11}$-oI28 structure and RE$_5$Al$_{41}$ phase in the *tI*92-Ce$_5$Mg$_{41}$ structure.

Due to great importance of the HCP_A3 solid solution in Mg alloys, the enthalpy of mixing of the HCP_A3 solution in the Al–RE (RE= La, Ce, Pr, Nd, Sm) subsystems are also estimated using Miedema's model. The Gibbs energy of the HCP_A3 solution, which is supposed to be less stable than the DHCP solution in the Al-RE systems, has to be evaluated although it is not stable in the Al–RE (RE= La, Ce, Pr, Nd, Sm) phase diagrams. Figures 8.13-8.17 show the optimized enthalpies of mixing of HCP_A3 solution in the Al–RE (RE= La, Ce, Pr, Nd, Sm) respectively, compared with the enthalpies of mixing of the liquid at 1500 K in the Al–RE systems and the estimated enthalpies of mixing from the Miedema model.
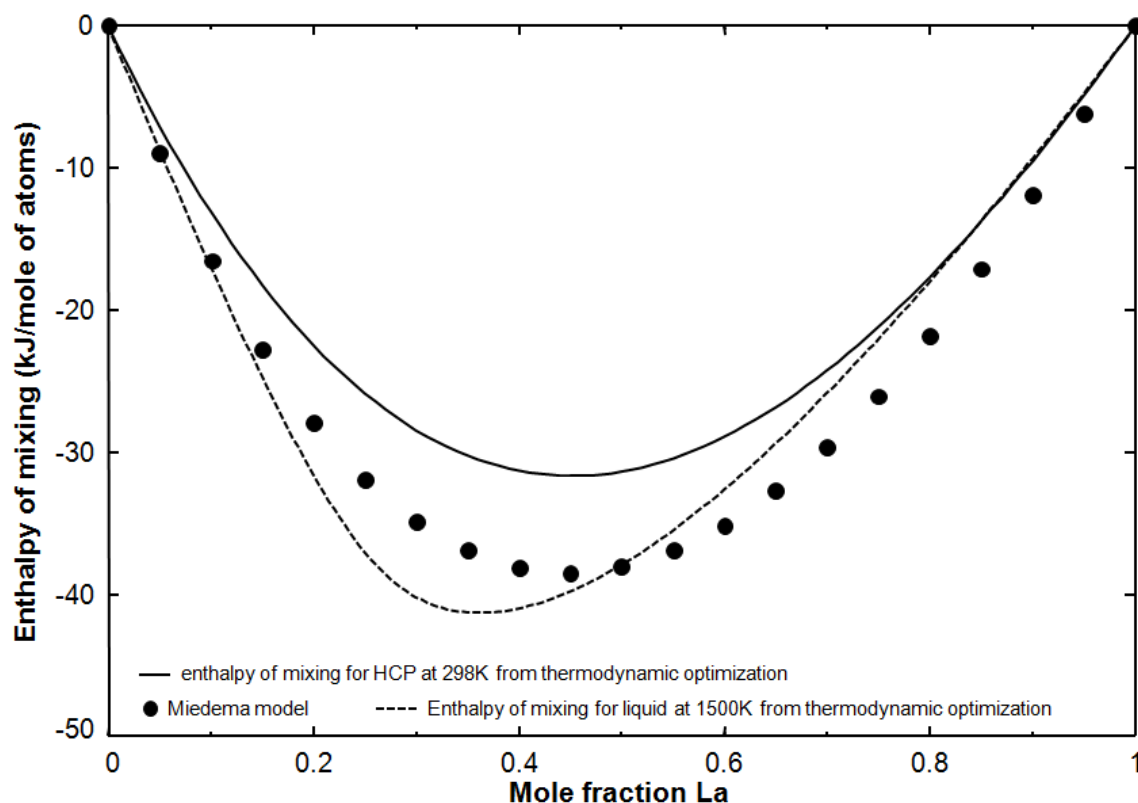
Figure 8.13 The enthalpy of mixing of the HCP solid solution in the Al-La system.
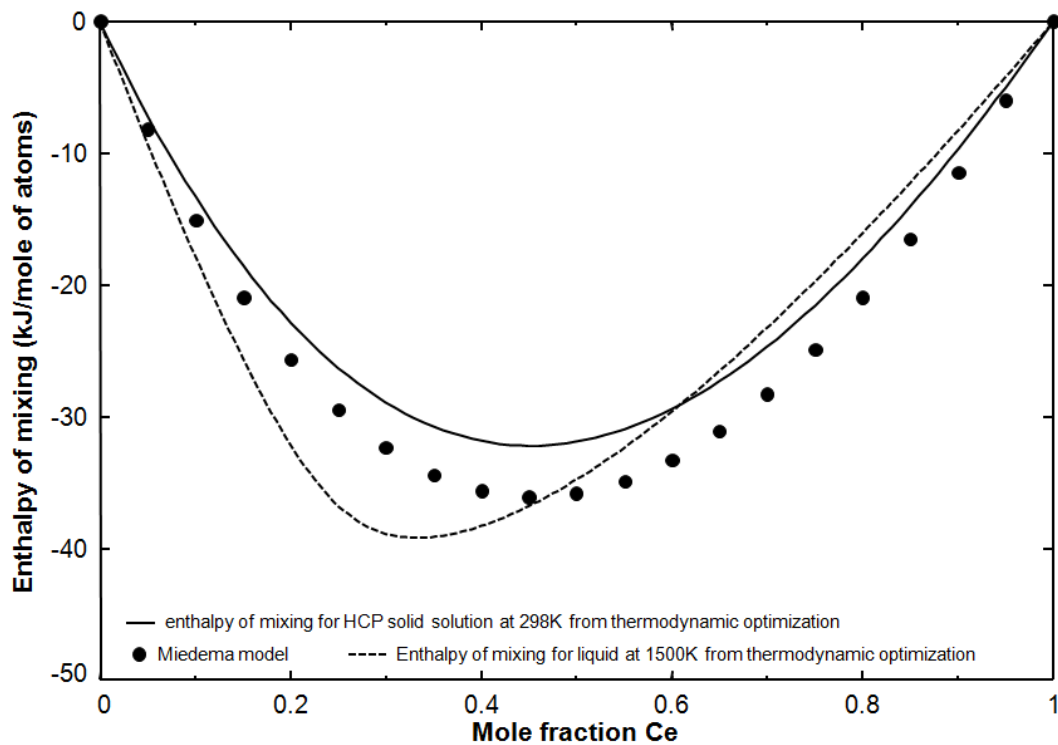
Figure 8.14 The enthalpy of mixing of the HCP solid solution in the Al-Ce system.
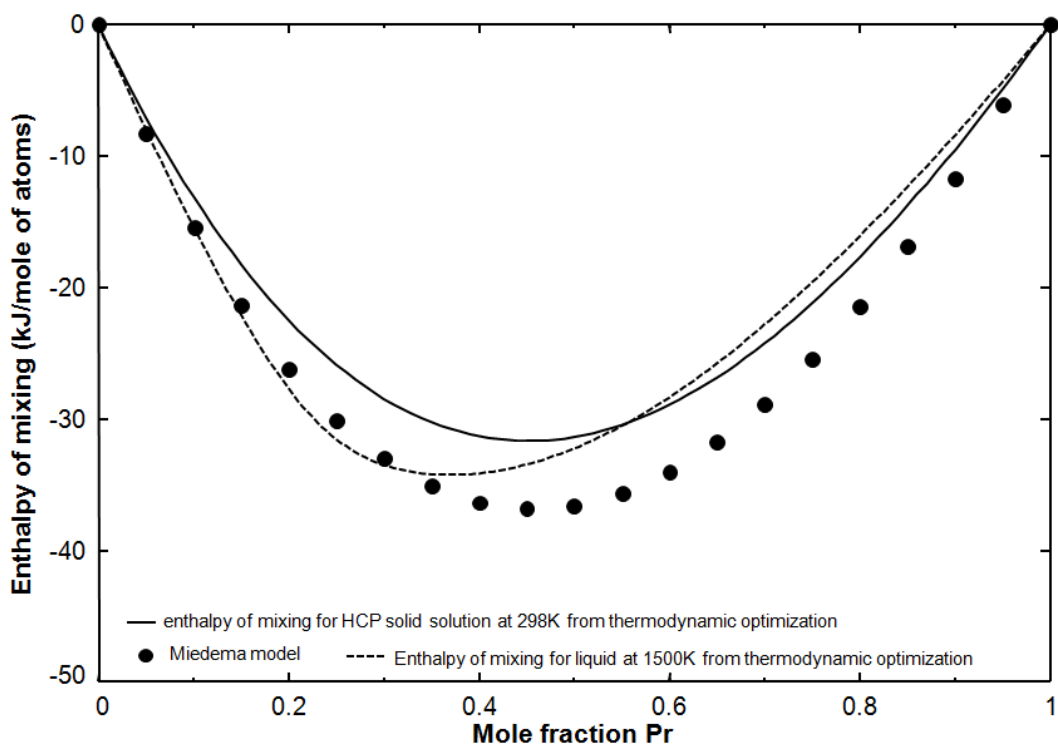
Figure 8.15 The enthalpy of mixing of the HCP solid solution in the Al-Pr system.
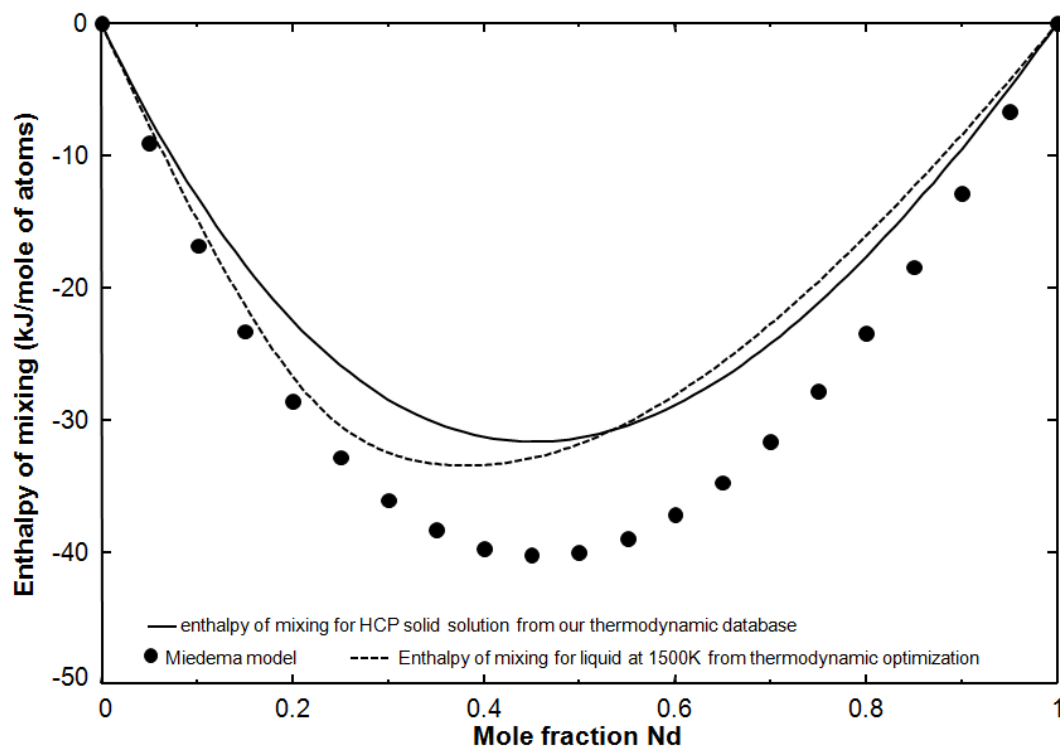
Figure 8.16 The enthalpy of mixing of the HCP solid solution in the Al-Nd system.
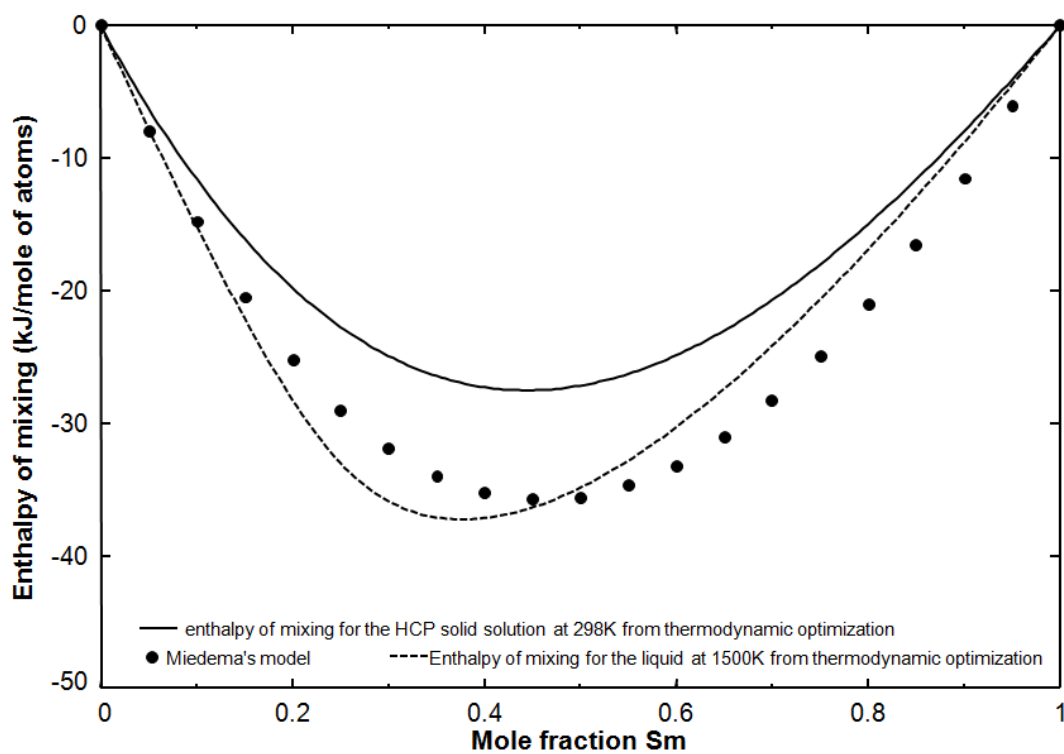
Figure 8.17 The enthalpy of mixing of the HCP solid solution in the Al-Sm system.

Since new optimizations of the Al – RE (RE= La, Ce, Pr, Nd, Sm) [10] and Mg – RE [11] binary systems are carried out using the Modified Quasichemical Model for the liquid, the thermodynamic properties and phase diagram of the Mg–Al–RE system are calculated by combining our two new optimizations with the previous optimization for the Al–Mg system by Chartrand [9]. In the Al–Mg system by Chartrand [9], there are liquid, FCC, HCP, Gamma ($Al_{12}Mg_{17}$), Beta ($Al_{140}Mg_{89}$), and Epsilon ($Al_{30}Mg_{23}$) phases. As shown in Table 8.1, two sublattices were used for all the solid solution phases involved in the present study.

Laves_C15 and BCC_B2 phases appears in all the Mg-Al-RE (RE= La, Ce, Pr, Nd, Sm) isothermal sections at 673 K. For the Laves_C15 phase, two optimized interaction parameters for the Al and Mg mixing in the first sub–lattice were required in order to reproduce the observed miscibility gap by Odinaev *et al.* [18] at 673K. The Laves phases observed in the binary systems $REAl_2$ and $REMg_2$ are expected to show negligible deviations from stoichiometry. In other words, the phases can be described as stoichiometric compounds in the binary systems. Therefore, $G^0_{Al_2RE}$ and $G^0_{Mg_2RE}$ were set equal to the Gibbs energy of the corresponding stoichiometric compounds Al_2RE and Mg_2RE; the Gibbs energies of other end members were taken either from the SGTE database [58], or were set to arbitrarily large values (Table 8.6). For the BCC_B2 phase, G^0_{AlRE} was used as a model parameter to reproduce the Al solubility measured by Odinaev *et al.* [18]; other Gibbs energies were either taken from the binary optimization in the RE–Mg system [11] or were set to arbitrarily large values. One interaction parameter was necessary to reproduce the 2–phase equilibria between the BCC_B2 and pure RE phases at 673K (Table 8.6).

It is worth noting that liquidus experimental data are available only for the Al-Mg-$REAl_2$ systems. In the present study, thermodynamic properties in the region of $X_{RE} > 1/3$ are estimated. Only invariant reactions of the Al-Mg-RE system for $X_{RE} < 1/3$ are listed (Tables 8.4, 8.5-8.11).

8.4.2.1 **The Al – Mg – La system**

The Al – Mg – La ternary system has been reviewed by Raghavan [16]. Recently, Hosseinifar and Malakhov [6] thermodynamically optimized this system to conduct a feasibility study to produce a new material containing a ductile FCC matrix with LaMg (BCC_B2) intermetallic via casting. In their study, they partially revised the Mg–La system and optimized the Al–Mg–La ternary system based on the optimized Al–Mg system from Liang *et al*. [59], the optimized Mg–La system from Guo and Du [20] using substitional solution model with Redlich-Kister formalism to describe the excess Gibbs energy for Al–Mg and Mg–La liquid solutions, and the optimized Al–La system from Zhou and Napolitano [60] using an associate model for the liquid with Al, La and Al_2La as mixing species. They used Muggianu method [40] for the evaluation of the Al–Mg–La ternary liquid [6].

The ternary compound, $Al_{40}Mg_{17}La_3$ (noted as $Al_2Mg_{0.85}La_{0.15}$ in [18]), was assumed to be a stoichiometric compound.

Table 8.4 Some invariant reactions of the Al-Mg-La system for $X_{La} < 1/3$

Reaction	T (K)		Type[†]	Composition (at%)			
	Exp.*	Calc.		Phase	Calc.		
					Al	La	Mg
L + $Al_{53}La_{22}$ ↔ Laves_C15 + LaAl$_3$	-	1468	U	L	73.0	23.9	3.1
L ↔ HCP + Laves_C15 + La(Mg,Al)$_{12}$	-	873	E	L	2.2	3.8	94.0
L ↔ FCC + La$_3$Al$_{40}$Mg$_{17}$ + Beta	706,719[a]	724	E	L	62.8	0. 2	37.0

L ↔ Gamma + La₃Al₄₀Mg₁₇ + Beta	709	724	E	L	60.1	0. 2	39.7
L + α-Al₁₁La₃ +FCC ↔ Al₄₀La₃Mg₁₇	-	739	P	L	65.5	0. 3	34.2
L + La₂Mg₁₇ ↔ Laves_C15 + La(Mg,Al)₁₂	-	903	U	L	2.3	8.7	89.0
L ↔ HCP + Gamma + α-Al₁₁La₃	705	711	E	L	30	0. 1	69.9
L + α-Al₁₁La₃+La₃Al₄₀Mg₁₇ ↔ Gamma	-	730	P	L	54.6	0. 2	45.2
L + La₂Mg₁₇ + La₅Mg₄₁↔ Laves_C15	-	920	P	L	2.3	13.1	84.6

† P: peritectic, U: quasiperitectic, E: eutectic

* Experimental data were taken from Odinaev *et al*. [19] unless another reference is given.

ᵃ Experimental data were taken from Hosseinifar and Malakhov[6].

The invariant reactions for $X_{La}<1/3$ are listed in Table 8.4 and compared with the available experimental data [19]. The Gibbs energy of the liquid phase was calculated using the symmetric Kohler–like approximation with no ternary interaction parameters. The optimized model parameters are summarized in Tables 8.5 to 8.7.

Table 8.5 Model parameters of the Modified Quasichemical Model used for liquid alloys

Coordination Numbers				References
i	*j*	Z_{ij}^{i}	Z_{ij}^{j}	
Al	Al	6	6	[10]
Ce	Ce	6	6	[10]
La	La	6	6	[10]

Pr	Pr	6	6	[10]
Nd	Nd	6	6	[10]
Sm	Sm	6	6	[10]
Mg	Mg	6	6	[11]
Al	Ce	3	6	[10]
Al	La	3	6	[10]
Al	Pr	3	6	[10]
Al	Nd	3	6	[10]
Al	Sm	3	6	[10]
Mg	Ce	2	6	[11]
Mg	La	2	6	[11]
Mg	Pr	2	6	[11]
Mg	Nd	2	6	[11]
Mg	Sm	2	6	[11]

For the $Mg_{12}RE$ solid solution, $G^o_{Al_{12}La}$ and a binary parameter (Table 8.6) for the mixing of Al and Mg in one sublattice is used to fit the experimental data on the solid solubility of Al. For all solution phases, no ternary parameters were required. The Gibbs energy of the $Al_{40}Mg_{17}La_3$ compound, formed with a peritectic reaction as can be seen in Figure 8.2, was optimized to reproduce the measured phase equilibria at 673 K. In general, the optimization was directed mainly towards reproducing the phase equilibrium data at 673 K measured by Odinaev *et al*. [18].

A calculated isothermal section of the Mg–Al–La ternary system at 673K is shown in Figure 8.18 along with the experimental data of Odinaev *et al*. [18]. LaMg and LaAl are only partially miscible because they have different crystal structures (CsCl and AlCe type, respectively). On the other hand, both $LaMg_2$ and $LaAl_2$ have the Cu_2Mg type structure and they form a Laves_C15 solid solution with a miscibility gap at low temperature. The miscibility gap in the Laves_C15 solution measured by Odinaev *et al*. [18] compares favorably with the present thermodynamic

calculation. Most experimental data were well reproduced by present calculations and the agreement between the calculated and experimental sections are satisfactory.
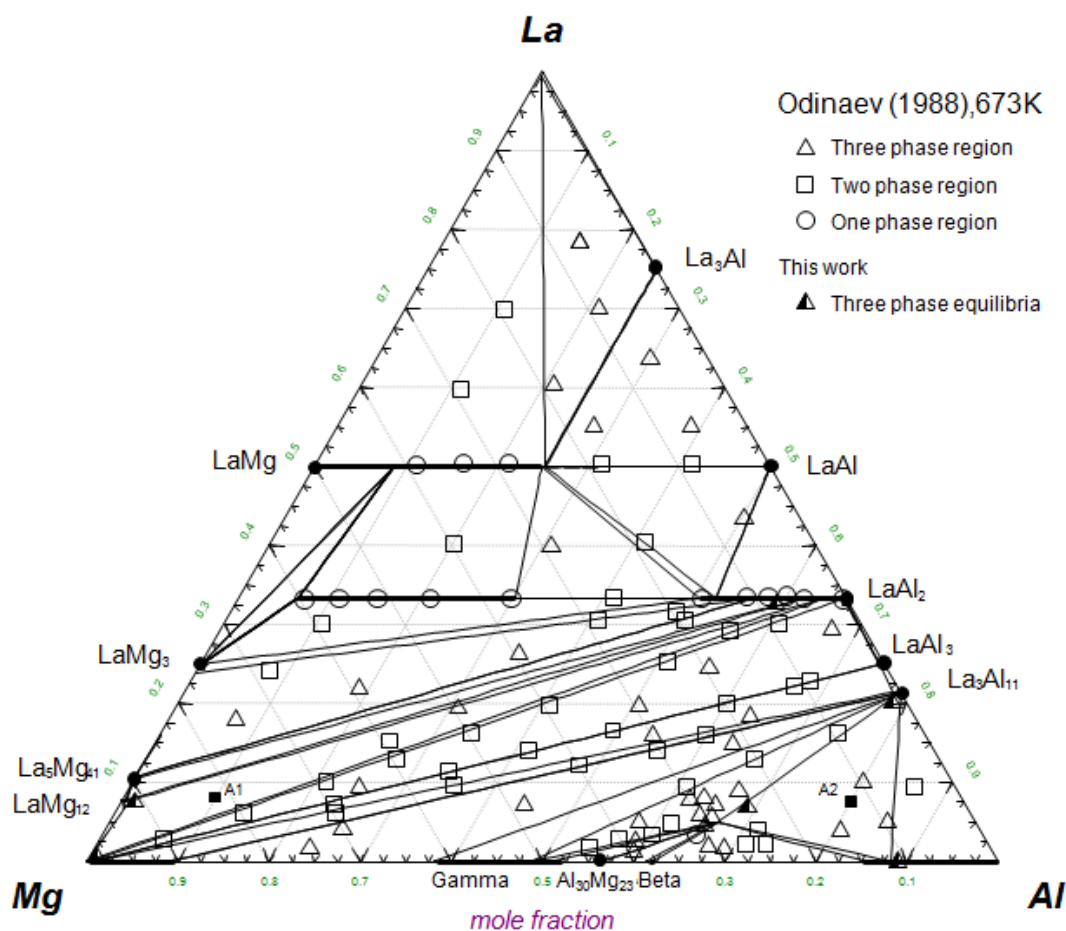
Figure 8.18 The calculated isothermal section of the Mg–Al–La ternary system at 673K compared with experimental data of Odinaev *et al*. [18].

However, there are a few discrepancies between the study of Odinaev *et al*. [18] and the current study. Similar differences were also encountered by Hosseinifar and Malakhov [6]. The LaMg$_2$ phase is unstable at 673 K in the present study. According to Odinaev *et al*. [18], LaMg$_2$ is stable at 673 K. This contradicts the result of Vogel and Heumann [61] who reported that LaMg$_2$ decomposes into LaMg$_3$ and LaMg near 887 K. However, it is stabilized over a wide temperature range as LaAl$_2$ dissolves into it. Kang *et al*. [11] and Guo and Du [20] considered that the LaMg$_2$ phase is unstable at 673 K. Secondly, the LaMg$_{12}$ and Al$_{30}$Mg$_{23}$ phases were considered in the current investigation, which were overlooked by Odinaev *et al*. [18]. Finally, the LaAl$_2$ and LaAl two-phase equilibrium is only reported in the Al–La binary system by Odinaev *et al*. [18].

However, it is probable that Mg dissolves in LaAl$_2$ phase, the reason of which is stated above. Then the LaAl$_2$ and LaAl two-phase equilibrium could extend into the ternary region. Moreover, the present interpretation of the microstructure of the anneal alloy Al$_{0.5}$Mg$_{0.06}$La$_{0.44}$ did not contradict the observed three-phase field in Odinaev *et al*. [18]. There are two differences between the present calculations and the optimized phase diagram of Hosseinifar and Malakhov [6]. Firstly, the solid solubility of Al in LaMg$_{12}$ was considered in the present study which was evidenced by the experimental data of Gröbner *et al.* [7]. This modification might be of practical importance to Mg alloys design, since the LaMg$_{12}$ phase could precipitate from the primary Mg phase during the solidification process, the amount of which could affect the mechanical properties of Mg alloy very much. Secondly, the La$_5$Mg$_{41}$ phase was taken into consideration in the present study.

Table 8.6 Optimized model parameters for solid solutions in the studied ternary systems (J/mol)

Laves_C15 (Cu$_2$Mg-type): (Al,Mg,La,Ce,Pr,Nd,Sm)$_2$[Al,Mg,La,Ce,Pr,Nd,Sm]	
Gibbs energies of end members and parameters	References
G(Al:Al) $= 3$***GHSERAL*** $+ 41{,}840$	Al-Mg[9]
G(Al:Mg) $= 2$***GHSERAL*** $+$ ***GHSERMG*** $+ 30{,}000 + 4T$	Al-Mg[9]
G(Mg:Al) $= 2$***GHSERMG*** $+$ ***GHSERAL*** $+ 104{,}971 - 16.46T$	Al-Mg[9]
G(Mg:Mg) $= 3$***GHSERMG*** $+ 15{,}000$	Al-Mg[9]
G(Ce:Ce) $= 3$***GHSERCE*** $+ 62{,}760$	Mg-RE[11]
G(Ce:Mg) $= 2$***GHSERCE*** $+$ ***GHSERMG*** $+ 41{,}840$	Mg-RE[11]
G(La:La) $= 3$***GHSERLA*** $+ 62{,}760$	Mg-RE[11]
G(La:Mg) $= 2$***GHSERLA*** $+$ ***GHSERMG*** $+ 41{,}840$	Mg-RE[11]
G(Pr:Pr) $= 3$***GHSERPR*** $+ 62{,}760$	Mg-RE[11]
G(Pr:Mg) $= 2$***GHSERPR*** $+$ ***GHSERMG*** $+ 41{,}840$	Mg-RE[11]
G(Nd:Nd) $= 3$***GHSERND*** $+ 62{,}760$	Mg-RE[11]
G(Nd:Mg) $= 2$***GHSERND*** $+$ ***GHSERMG*** $+ 41{,}840$	Mg-RE[11]
G(Sm:Sm) $= 3$***GHSERSM*** $+ 62{,}760$	Mg-RE[11]
G(Sm:Mg) $= 2$***GHSERSM*** $+$ ***GHSERMG*** $+ 41{,}840$	Mg-RE[11]
G(Ce:Al) $= 2$***GHSERCE*** $+$ ***GHSERAL*** $+ 41{,}840$	This work

G(La:Al)	= 2*GHSERLA* + *GHSERAL*+ 41,840	This work
G(Pr:Al)	= 2*GHSERPR* + *GHSERAL*+ 41,840	This work
G(Nd:Al)	= 2*GHSERND* + *GHSERAL*+ 41,840	This work
G(Sm:Al)	= 2*GHSERSM* + *GHSERAL*+ 41,840	This work
L(Al,Mg:La)	= 20,920$(Y_{Al}-Y_{Mg})$- 20,083$(Y_{Al}-Y_{Mg})^2$	This work
L(Al,Mg:Ce)	= -20,920 + 33,890$(Y_{Al}-Y_{Mg})$	This work
L(Al,Mg:Pr)	= -4,184+ 27,196$(Y_{Al}-Y_{Mg})$	This work
L(Al,Mg:Nd)	= -8,368+ 33,054$(Y_{Al}-Y_{Mg})$	This work
L(Al,Mg:Sm)	= 29,288	This work
BCC_B2 (CsCl-type): (Al,Mg)[Mg,Ce,La,Pr,Nd,Sm]		
Gibbs energies of end members and parameters		references
G(Al:La)	= *GHSERAL* + *GHSERLA*− 79,000 + 5.70*T*	Al-RE[10]
G(Al:Ce)	= *GHSERAL* + *GHSERCE* − 82,217 + 12.91*T*	Al-RE[10]
G(Al:Pr)	= *GHSERAL* + *GHSERPR* − 83,496 + 10.34*T*	Al-RE[10]
G(Al:Nd)	= *GHSERAL* + *GHSERND* − 89,092 + 12.81*T*	Al-RE[10]
G(Al:Sm)	= *GHSERAL* + *GHSERSM* − 91,000 + 16.00*T*	Al-RE[10]
G(Mg:La)	= *GHSERMG* + *GHSERLA* − 28,990 + 5.08*T*	Mg-RE[11]
G(Mg:Ce)	= *GHSERMG* + *GHSERCE* − 28,600 + 5.08*T*	Mg-RE[11]
G(Mg:Pr)	= *GHSERMG* + *GHSERPR*− 28,800 + 5.08*T*	Mg-RE[11]
G(Mg:Nd)	= *GHSERMG* + *GHSERND* − 29,291 + 5.08*T*	Mg-RE[11]
G(Mg:Sm)	= *GHSERMG* + *GHSERSM* − 28,600 + 5.08*T*	Mg-RE[11]
L(Al,Mg:La) = -25,104		This work
L(Al,Mg:Ce) = -41,840		This work
L(Al,Mg:Pr) = -24,686		This work
L(Al,Mg:Nd) = -23,430		This work
L(Al,Mg:Sm) = -12,552		This work
(La,Ce,Pr,Nd,Sm)[Al,Mg]$_{12}$		
Gibbs energies of end members and parameters		references
G(Ce:Mg)	= *GHSERCE* + 12*GHSERMG* -74,057 + 11.6*T*	Mg-RE[11]

G(La:Mg)	= *GHSERLA* + 12*GHSERMG* -77,781+ 4.9*T*	Mg-RE[11]
G(Pr:Mg)	= *GHSERPR* + 12*GHSERMG* -72,802+ 14.9*T*	Mg-RE[11]
G(Nd:Mg)	= *GHSERND* + 12*GHSERMG* -59,200+ 14.9*T*	This work
G(Sm:Mg)	= *GHSERSM* + 12*GHSERMG* -45,800+ 14.9*T*	This work
G(Ce:Al)	= *GHSERCE* + 12*GHSERAL*– 168,000+11.6T	This work
G(La:Al)	= *GHSERLA* + 12*GHSERAL*– 186,000+6.64T	This work
G(Pr:Al)	= *GHSERPR* + 12*GHSERAL*– 171,000+14.9T	This work
G(Nd:Al)	= *GHSERND* + 12*GHSERAL*– 164,000+14.9T	This work
G(Sm:Al)	= *GHSERSM* + 12*GHSERAL*– 151,000+14.9T	This work
L(Ce:Al,Mg) = -167,360		This work
L(La:Al,Mg) = -41,840		This work
Al₃RE (Ni₃Sn) : (Al,Mg)₃[La,Ce,Pr,Nd,Sm]		
Gibbs energies of end members and parameters		references
G(Mg:La)	= 3*GHSERMG* + *GHSERLA* − 36,400 + 5.51*T*	This work
G(Mg:Ce)	= 3*GHSERMG* + *GHSERCE* − 40,800 + 12.6*T*	This work
G(Mg:Pr)	= 3*GHSERMG* + *GHSERPR*– 39,600 + 19.1*T*	This work
G(Mg:Nd)	= 3*GHSERMG* + *GHSERND* − 38,400 + 20.6*T*	This work
G(Mg:Sm)	= 3*GHSERMG* + *GHSERSM* − 34,000 + 20.6*T*	This work
L(Al,Mg:La) = 16,736		This work
L(Al,Mg:Ce) = 16,736		This work
Al₁₁RE₃ (αAl₁₁La₃) : (Al,Mg)₁₁[La,Ce,Pr,Nd,Sm]₃		
Gibbs energies of end members and parameters		references
G(Al:La)	= 11*GHSERAL* + 3*GHSERLA* − 575,000 + 8.6T	Al-RE [10]
G(Al:Ce)	= 11*GHSERAL* + 3*GHSERCE* − 610,000 + 39.0*T*	Al-RE [10]
G(Al:Pr)	= 11*GHSERAL* + 3*GHSERPR*– 615,000 + 59.1*T*	Al-RE [10]
G(Al:Nd)	= 11*GHSERAL* + 3*GHSERND* − 575,000 + 53.5*T*	Al-RE [10]
G(Al:Sm)	= 11*GHSERAL* + 3*GHSERSM* − 527,000 + 53.5*T*	Al-RE [10]
G(Mg:La)	= 11*GHSERMG* + 3*GHSERLA* − 84,626 + 8.6*T*	This work
G(Mg:Ce)	= 11*GHSERMG* + 3*GHSERCE* − 69,550 + 39.0*T*	This work

G(Mg:Pr)	= 11**GHSERMG** + 3**GHSERPR** − 58,800 + 53.5T	This work
G(Mg:Nd)	= 11**GHSERMG** + 3**GHSERND** − 48,700 + 53.5T	This work
G(Mg:Sm)	= 11**GHSERMG** + 3**GHSERSM** − 38,885 + 53.5T	This work
Al$_{17}$RE$_2$ (Ni$_{17}$Th$_2$) **: (Al,Mg)$_{17}$[La,Ce,Pr,Nd,Sm]$_2$**		
Gibbs energies of end members and parameters		references
G(Al:La)	= 17**GHSERAL** + 2**GHSERLA** -298,692+ 5.7T	This work
G(Al:Ce)	= 17**GHSERAL** + 2**GHSERCE** -292,732+ 26.0T	This work
G(Al:Pr)	= 17**GHSERAL** + 2**GHSERPR** -289,945+ 39.4T	This work
G(Al:Nd)	= 17**GHSERAL** + 2**GHSERND** -322,546+ 35.7T	This work
G(Al:Sm)	= 17**GHSERAL** + 2**GHSERSM** -287,564+ 59.8T	This work

It is worth noting that a miscibility gap occurred within Laves_C15 phase at 673K. This is a common phenomenon for Laves_C15 phases, which was also found in the Al–Mg–Ce, Al–Mg–Pr and Al–Mg–Nd systems.

Figures 8.19 to 8.26 show several calculated sections compared with the experimental DTA data by Odinaev *et al*. [19]. It is observed that the reported liquidus temperatures of Odinaev *et al*. [19] are far below those from present calculation. Hosseinifar and Malakhov [6] did calorimetric investigation on two alloys (Al$_{61.3}$La$_{18.7}$Mg$_{20}$ and Al$_{70.6}$La$_{14}$Mg$_{15.4}$ by wt%) to check liquidus temperature in Al-Mg-La system and their measured values were much higher than those of Odinaev *et al*. [19]. Grobner *et al*. [7] investigated the liquidus temperature in the Mg–Al–Ce system using DTA and concluded that the low liquidus temperature of Odinaev *et al*. [26] could not be accepted. They pointed out that the reliable DTA data at high temperature can only be obtained by using hermetically sealed inert crucible to avoid evaporation, oxidation and side reactions. Although the experimental details were not given by Odinaev *et al*. [18], their liquidus temperature might be in error due to the oxidation of the rare earth elements, high evaporation of Mg metal and experimental difficulties at high temperature.
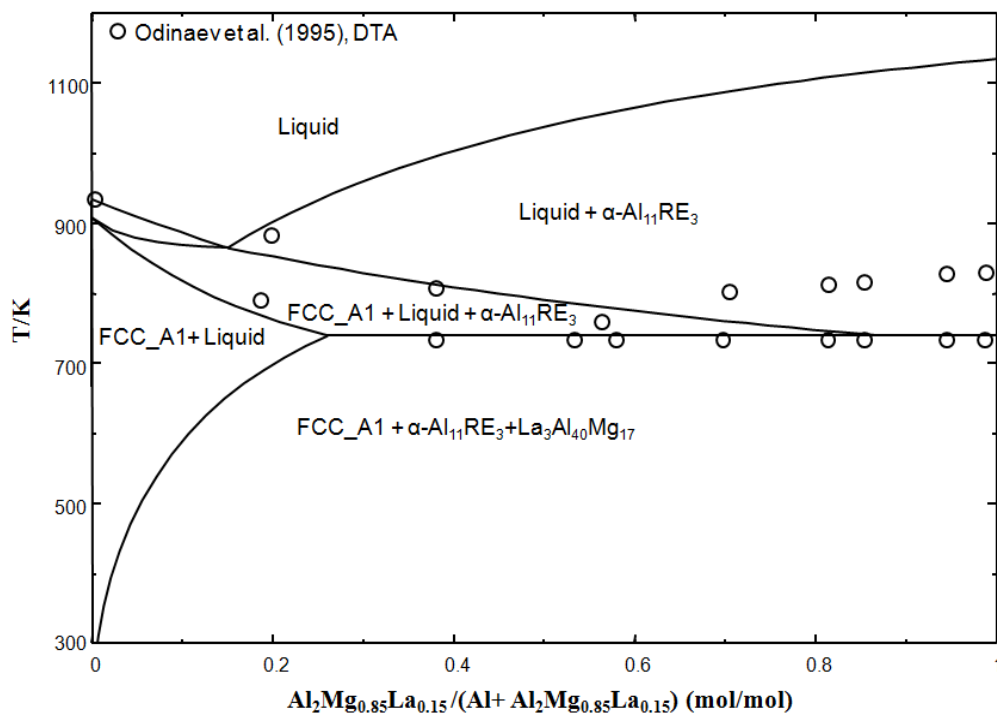
Figure 8.19 Calculated Al-Al$_2$Mg$_{0.85}$La$_{0.15}$ section compared with experimental data of Odinaev *et al*. [19].
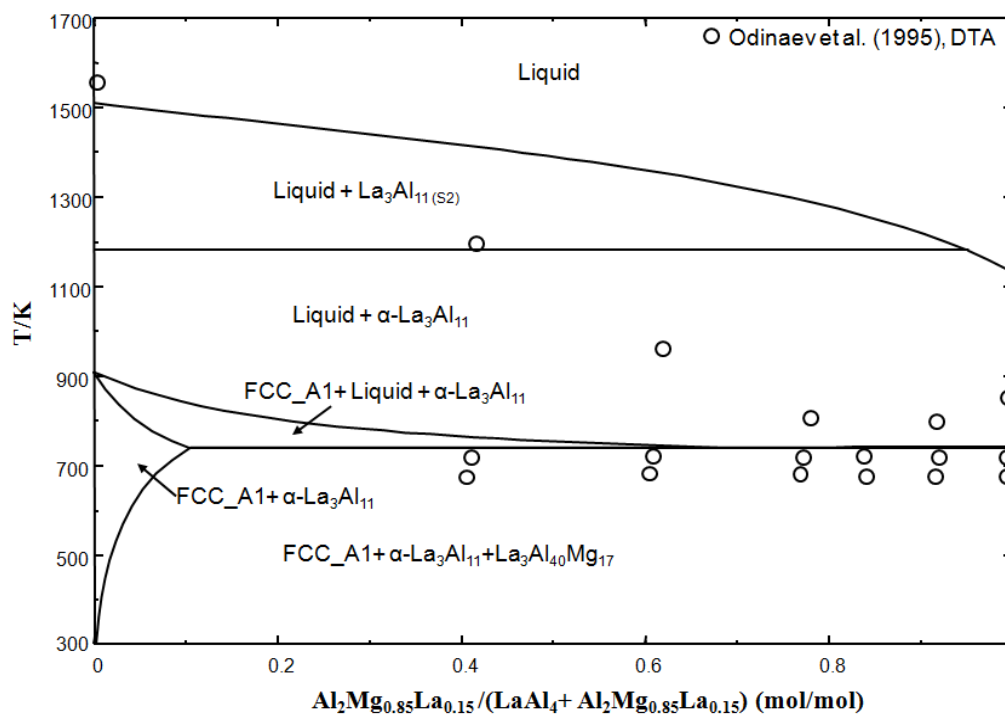
Figure 8.20 Calculated LaAl$_4$-Al$_2$Mg$_{0.85}$La$_{0.15}$ section compared with experimental data of Odinaev *et al*. [19].
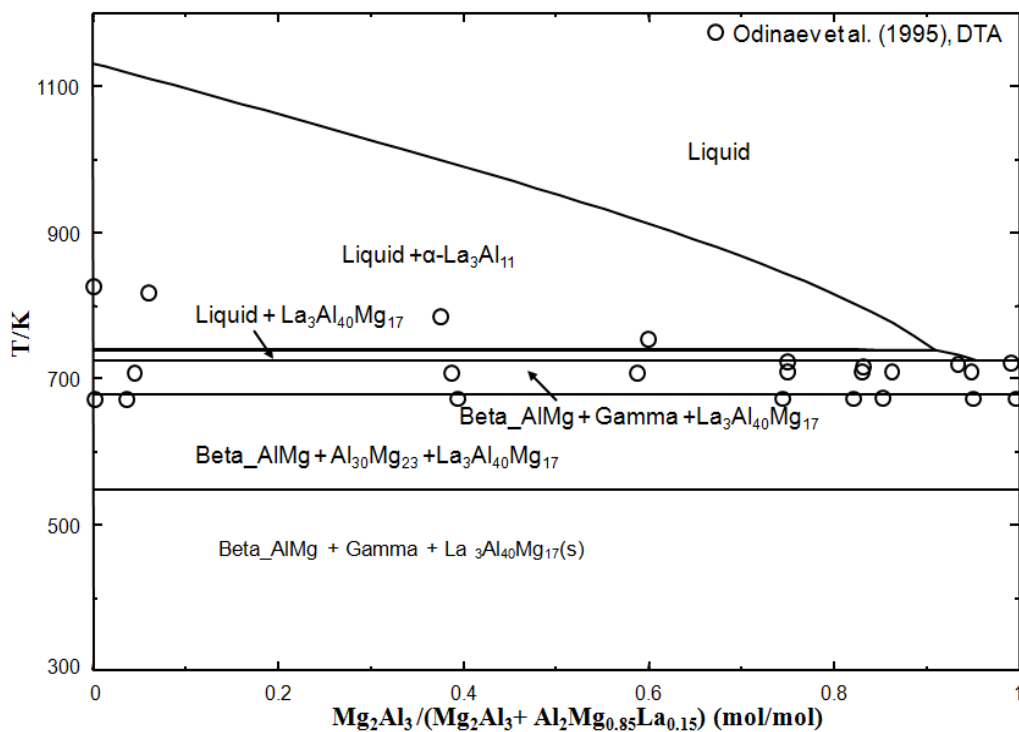
Figure 8.21 Calculated Mg_2Al_3-$Al_2Mg_{0.85}La_{0.15}$ section compared with experimental data of Odinaev *et al*. [19].
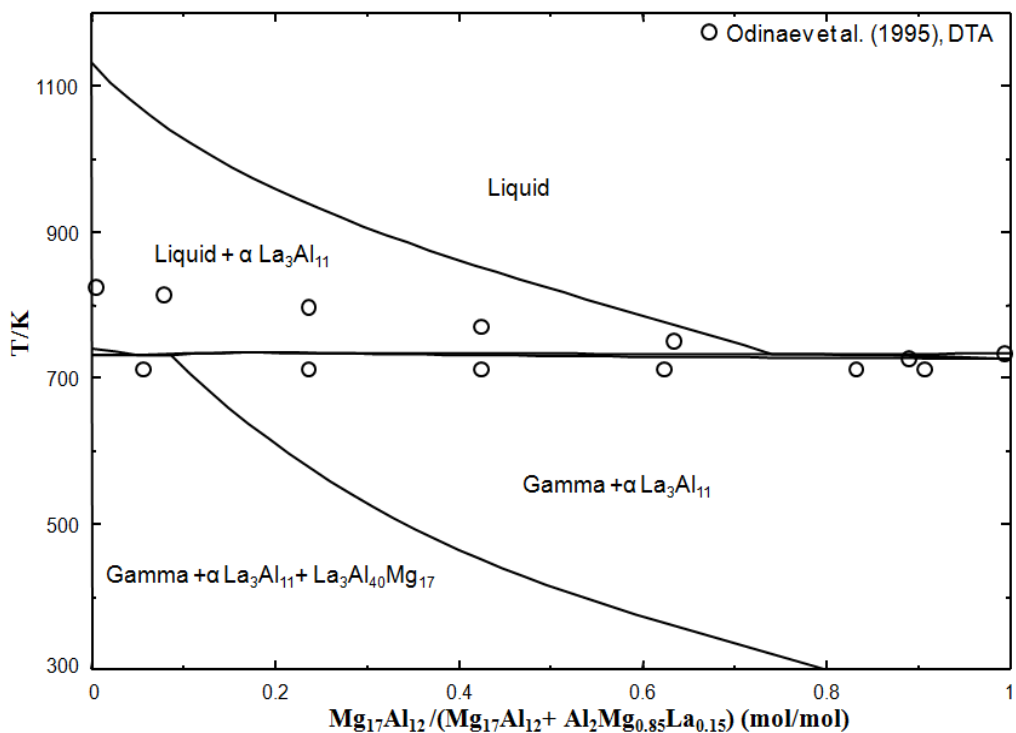
Figure 8.22 Calculated $Mg_{17}Al_{12}$-$Al_2Mg_{0.85}La_{0.15}$ section compared with experimental data of Odinaev *et al*. [19].
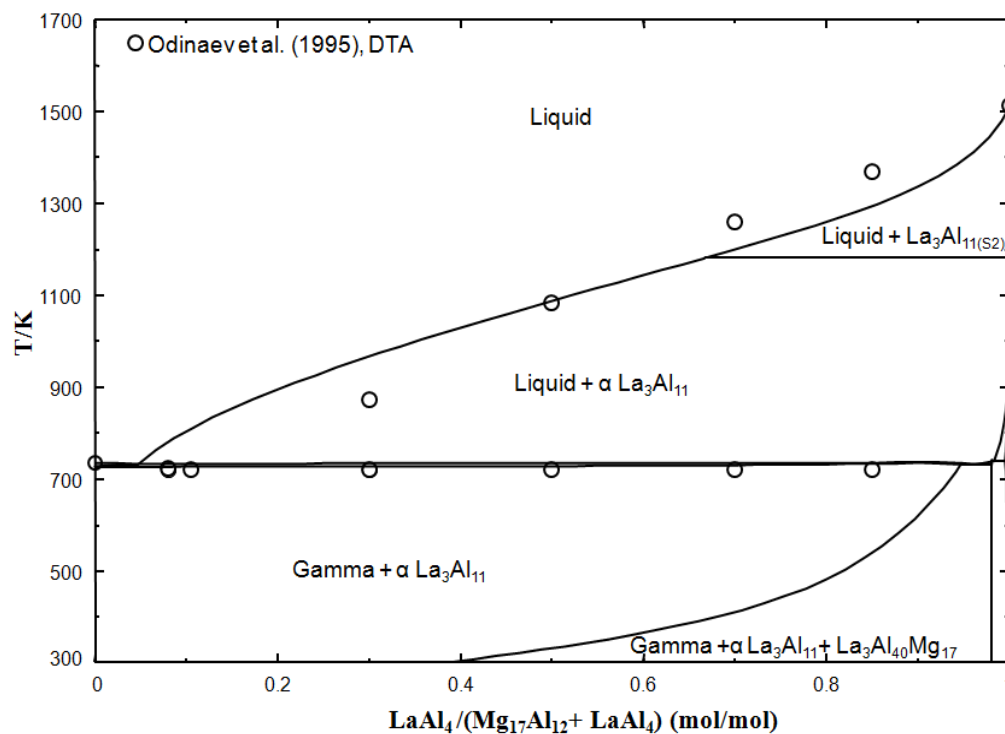
Figure 8.23 Calculated LaAl$_4$ - Mg$_{17}$Al$_{12}$ section compared with experimental data of Odinaev *et al*. [19].
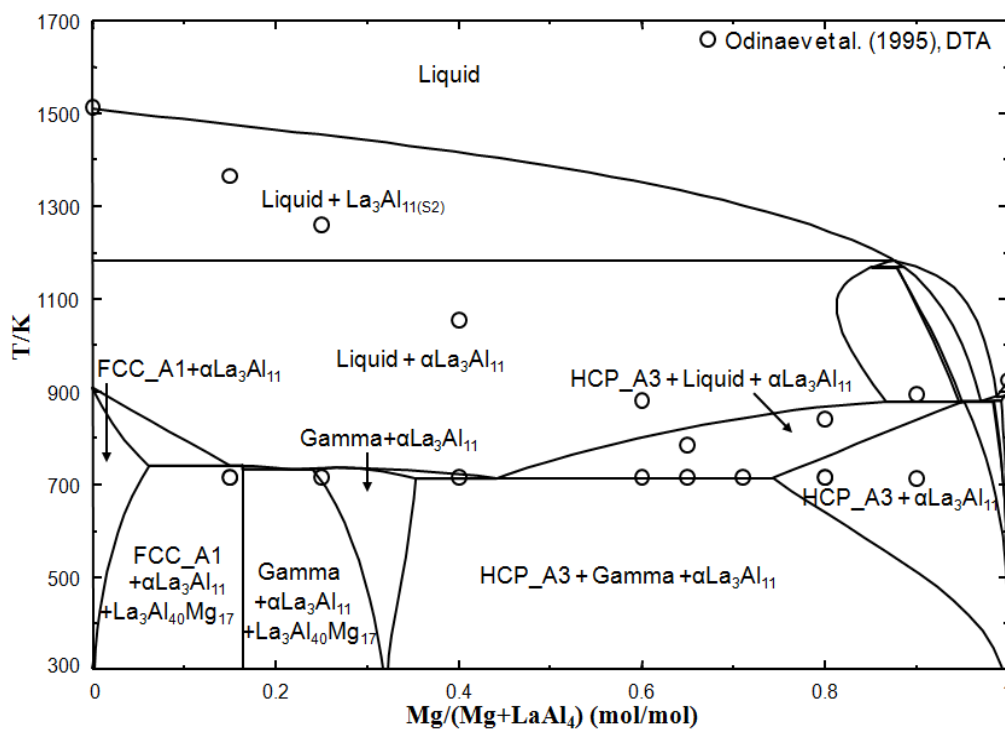
Figure 8.24 Calculated LaAl$_4$ - Mg section compared with experimental data of Odinaev *et al*. [19].
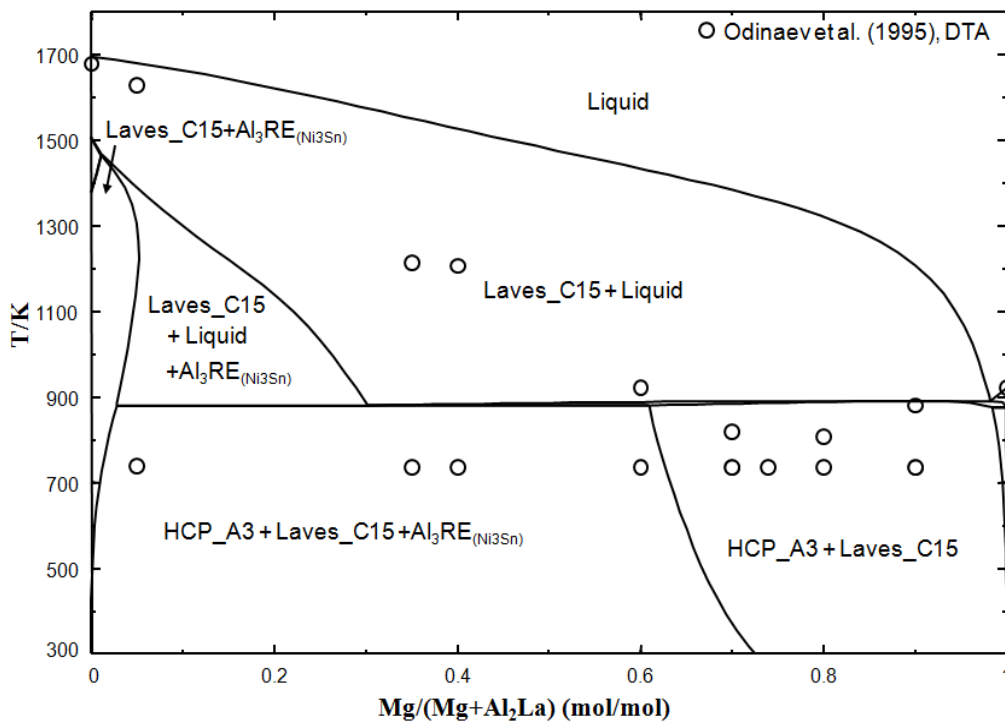
Figure 8.25 Calculated LaAl$_2$ - Mg section compared with experimental data of Odinaev *et al*. [19].
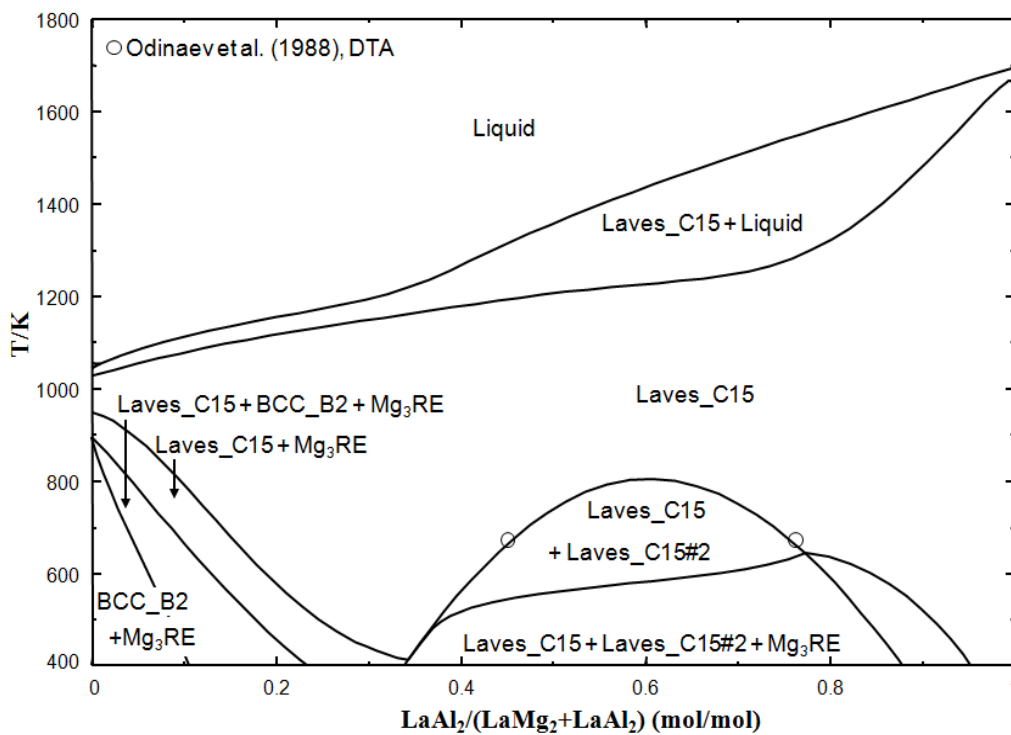
Figure 8.26 Calculated LaAl$_2$ – LaMg$_2$ section compared with experimental data of Odinaev *et al*. [19].

Figure 8.27 shows the calculated liquidus surface in the Mg–Al–La system with the experimental data from Hosseinifar and Malakhov [6]. It can be seen that the calculated liquidus temperature agrees well with the experimental data [6]. The liquidus surface is dominated by the Laves_C15 (almost pure Al$_2$La) and Al$_{11}$RE$_3$ phases, which have high melting temperatures and very negative enthalpies of formations. The primary phase regions of these phases intersect that of Mg (HCP_A3). Therefore, these phases are likely to precipitate in the HCP phase during Mg alloy solidification process. The ternary phase Al$_{40}$Mg$_{17}$La$_3$ is formed peritectically (Table 8.4), which is in agreement with our experiment as can be seen in Figure 8.2.
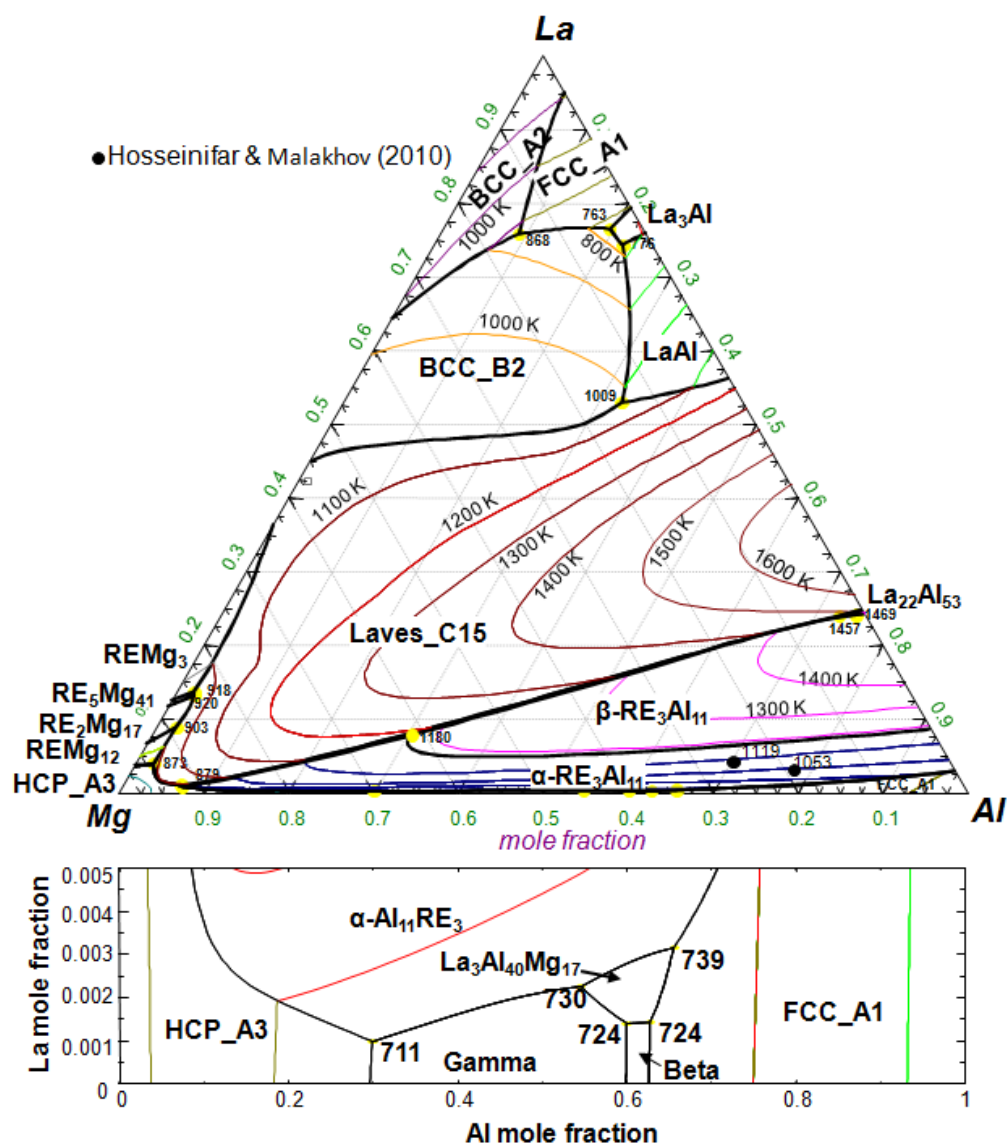
Figure 8.27 The liquidus projection of Al-Mg-La system with experimental data of Hosseinifar and Malakhov [6].

8.4.2.2 **The Al–Mg–Ce system**

The Al–Mg–Ce system has been thermodynamically optimized by Grobner *et al*. [7] without ternary interaction parameters for the liquid phase using a substitutional solution model for the liquid with Muggianu interpolation from three binary sub-systems. Unfortunately, the short-range ordering effect was not considered in the substitutional solution model of their liquid phase. In the present study, MQM is employed for the ternary liquid taking into account the short-range ordering effect and Kohler-type interpolation is used. The ternary compound $Al_{13}CeMg_6$ has a $MgZn_2$ type structure, which is the same as that of the Laves_C14 phase. However, it was assumed to be a stoichiometric (line) compound because no solid solubility has been observed experimentally.

The invariant reactions for $X_{Ce}<1/3$ are listed in Table 8.8. The Gibbs energy of the liquid phase was calculated using the symmetric Kohler–like approximation [40] with no ternary interaction parameters. The transformation temperature from pure FCC(Ce) to pure DHCP(Ce) was changed by Kang *et al.* [12] from 334 K (the current value in the COST–507 database [58]) to 283 K reported in [62]. The optimized model parameters are summarized in Tables 8.5 to 8.7.

Table 8.7 Optimized model parameters for stoichiometric compounds.

Compound	$\Delta H\,^{\circ}_{298}$(J/mol)	$S\,^{\circ}_{298}$(J/mol-K)	C_p (J/mol-K)
$LaAl_{12}$	-152,100	393.63	$C_p = C_p$(La, DHCP) + 12C_p(Al,FCC_A1)
$CeAl_{12}$	-148,070	396.03	$C_p = C_p$(Ce,FCC_A1) + 12C_p(Al,FCC_A1)
$PrAl_{12}$	-146,900	393.85	$C_p = C_p$(Pr, DHCP) + 12C_p(Al,FCC_A1)
$NdAl_{12}$	-163,280	392.86	$C_p = C_p$(Nd, DHCP) + 12C_p(Al,FCC_A1)
$SmAl_{12}$	-145,340	379.20	$C_p = C_p$(Sm, Rhom) + 12C_p(Al,FCC_A1)
La_2Al_{17}	-298,680	589.17	$C_p = 2C_p$(La, DHCP) + 17C_p(Al,FCC_A1)
Ce_2Al_{17}	-292,790	593.98	$C_p = 2C_p$(Ce,FCC_A1) + 17C_p(Al,FCC_A1)

Pr_2Al_{17}	-289,940	589.60	$C_p = 2C_p(Pr, DHCP) + 17C_p(Al,FCC\_A1)$
Nd_2Al_{17}	-322,620	587.61	$C_p = 2C_p(Nd, DHCP) + 17C_p(Al,FCC\_A1)$
Sm_2Al_{17}	-287,470	560.29	$C_p = 2C_p(Sm, Rhom) + 17C_p(Al,FCC\_A1)$
La_5Al_{41}	-745,200	1430.48	$C_p = 5C_p(La, DHCP) + 41C_p(Al,FCC\_A1)$
Ce_5Al_{41}	-730,940	1442.49	$C_p = 5C_p(Ce,FCC\_A1) + 41C_p(Al,FCC\_A1)$
Pr_5Al_{41}	-723,580	1431.56	$C_p = 5C_p(Pr, DHCP) + 41C_p(Al,FCC\_A1)$
Nd_5Al_{41}	-805,460	1426.58	$C_p = 5C_p(Nd, DHCP) + 41C_p(Al,FCC\_A1)$
Sm_5Al_{41}	-718,060	1358.27	$C_p = 5C_p(Sm, Rhom) + 41C_p(Al,FCC\_A1)$
La_3Mg_{11}	-57,400	463.21	$C_p = 3C_p(La, DHCP) + 11C_p(Mg, HCP\_A3)$
Ce_3Mg_{11}	-72,940	494.52	$C_p = 3C_p(Ce,FCC\_A1) + 11C_p(Mg, HCP\_A3)$
Pr_3Mg_{11}	-70,980	507.01	$C_p = 3C_p(Pr, DHCP) + 11C_p(Mg, HCP\_A3)$
Nd_3Mg_{11}	-82,880	496.02	$C_p = 3C_p(Nd, DHCP) + 11C_p(Mg, HCP\_A3)$
Sm_3Mg_{11}	-70,840	488.91	$C_p = 3C_p(Sm, Rhom) + 11C_p(Mg, HCP\_A3)$
$Al_{13}CeMg_6$	-248,368.0	627.48	$C_p = 13C_p(Al,FCC\_A1) + C_p(Ce,FCC\_A1)$ $+ 6C_p(Mg,HCP\_A3)$
$Al_{40}Mg_{17}La_3$	-701,000.0	1878.07	$C_p = 40C_p(Al,FCC\_A1) + 17C_p(Mg,HCP\_A3)$ $+ 3C_p(La,DHCP)$
$Al_{50}Mg_{22}Pr_3$	-776,101.6	2325.97	$C_p = 50C_p(Al,FCC\_A1) + 22C_p(Mg,HCP\_A3)$ $+ 3C_p(Pr,DHCP)$
$Al_{50}Mg_{22}Nd_3$	-738,772.0	2322.99	$C_p = 50C_p(Al,FCC\_A1) + 22C_p(Mg,HCP\_A3)$ $+ 3C_p(Nd,DHCP)$

Table 8.8 Some invariant reactions of the Al-Mg-Ce system for $X_{Ce} < 1/3$

Reaction	T (K)		Type[†]	Composition (at%)			
	Exp.*	Calc.		Phase	Calc.		
					Al	Ce	Mg
L + Laves_C15 $\leftrightarrow$ HCP + Al$_3$Ce	-	892	U	L	4.6	1.0	94.4
L + Al$_3$Ce $\leftrightarrow$ α-Al$_{11}$Ce$_3$ + HCP	-	890	U	L	5.2	0.8	94.0
L + HCP $\leftrightarrow$ Laves_C15 + Ce(Mg,Al)$_{12}$	-	875	U	L	2.1	3.3	94.6
L + FCC $\leftrightarrow$ Al$_{13}$CeMg$_6$ + Beta	714 719[27][§]	723	U	L	63.0	0.3	36.7
L $\leftrightarrow$ Gamma + Al$_{11}$CeMg$_6$ + Beta	715	723	E	L	60.1	0.3	39.6
L + α-Al$_{11}$Ce$_3$ $\leftrightarrow$ FCC + Al$_{13}$CeMg$_6$	718 728[7]	734	U	L	65.4	0.6	34.0
L + Ce$_5$Mg$_{41}$ $\leftrightarrow$ Laves_C15 + Ce(Mg,Al)$_{12}$	-	881	U	L	0.8	8.6	90.6
L $\leftrightarrow$ HCP + Gamma + α-Al$_{11}$Ce$_3$	-	711	E	L	30.1	0.1	69.8
L + α-Al$_{11}$Ce$_3$ + Al$_{13}$CeMg$_6$ $\leftrightarrow$ Gamma	-	730	P	L	53.9	0.4	45.7
L + CeMg$_3$ $\leftrightarrow$ Laves_C15 + Ce$_5$Mg$_{41}$	-	893	U	L	4.6	1.0	94.4

† P: peritectic, U: quasiperitectic, E: eutectic

* Experimental data were taken from Odinaev *et al*. [26] unless another reference is given.

§ Reported reaction is L $\leftrightarrow$ (Al) + Al$_4$Ce + Al$_8$Mg$_5$ from Zheng *et al*. [27].

In order to reproduce the observed miscibility gap for the Laves_C15 phase [23], two optimized interaction parameters were required ($L^0_{Al,Mg:Ce}, L^1_{Al,Mg:Ce}$). One interaction parameter was necessary to reproduce the 2–phase equilibria between the BCC_B2 and the FCC_A1 (Ce) phases. For the Ce(Al,Mg)$_{12}$ phase, the Gibbs energy of hypothetical CeAl$_{12}$ and one interaction parameter were optimized in order to reproduce the experimental data. For the other solution phases, no ternary parameters were required. The Gibbs energy of the Al$_{13}$CeMg$_6$ compound was optimized to reproduce the measured peritectic melting temperature [7] and phase equilibria at 673 K [23].
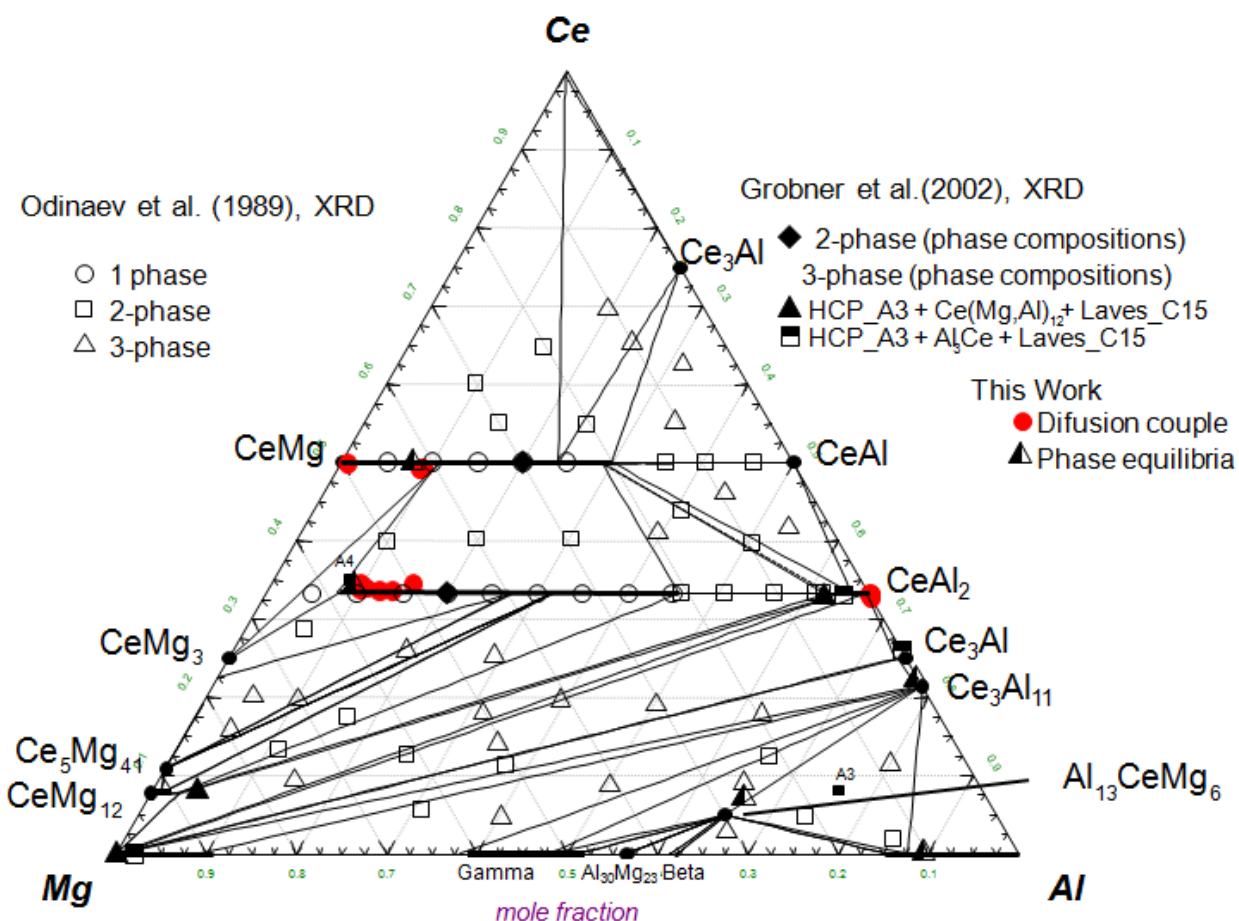
Figure 8.28 The calculated isothermal section of the Mg–Al–Ce ternary system at 673K compared with experimental data of Odinaev *et al*. [23] and Grobner *et al*. [7].

In Figure 8.28, a calculated isothermal section of the Mg–Al–Ce ternary system at 673K is shown along with the experimental data of Odinaev *et al*. [23] and Grobner *et al*. [7]. CeMg and CeAl

are only partially miscible since they have different crystal structures (CsCl and CeAl type, respectively). However, CeMg$_2$ and CeAl$_2$ form a Laves_C15 solid solution because they have the same structure (Cu$_2$Mg type) with a miscibility gap at low temperature. For the isothermal section of the Mg–Al–Ce ternary system at 673 K, most experimental data are well reproduced by current calculations. According to Odinaev *et al.* [23], CeMg$_2$ is stable and forms a solid solution at 673 K. However, this contradicts the result of Vogel and Heumann [61] who reported that CeMg$_2$ decomposes into CeMg$_3$ and CeMg near ~ 888 K. This can be also seen in Figure 8.29, in which the calculated CeMg$_2$–CeAl$_2$ is shown. CeMg$_2$ is only stable over a limited temperature range (891 K ~ 1023 K). However, it is stabilized over a wide temperature range as CeAl$_2$ dissolves into it. The miscibility gap in the Laves_C15 solution measured by Odinaev *et al.* [23] compares favorably with the present thermodynamic calculation.
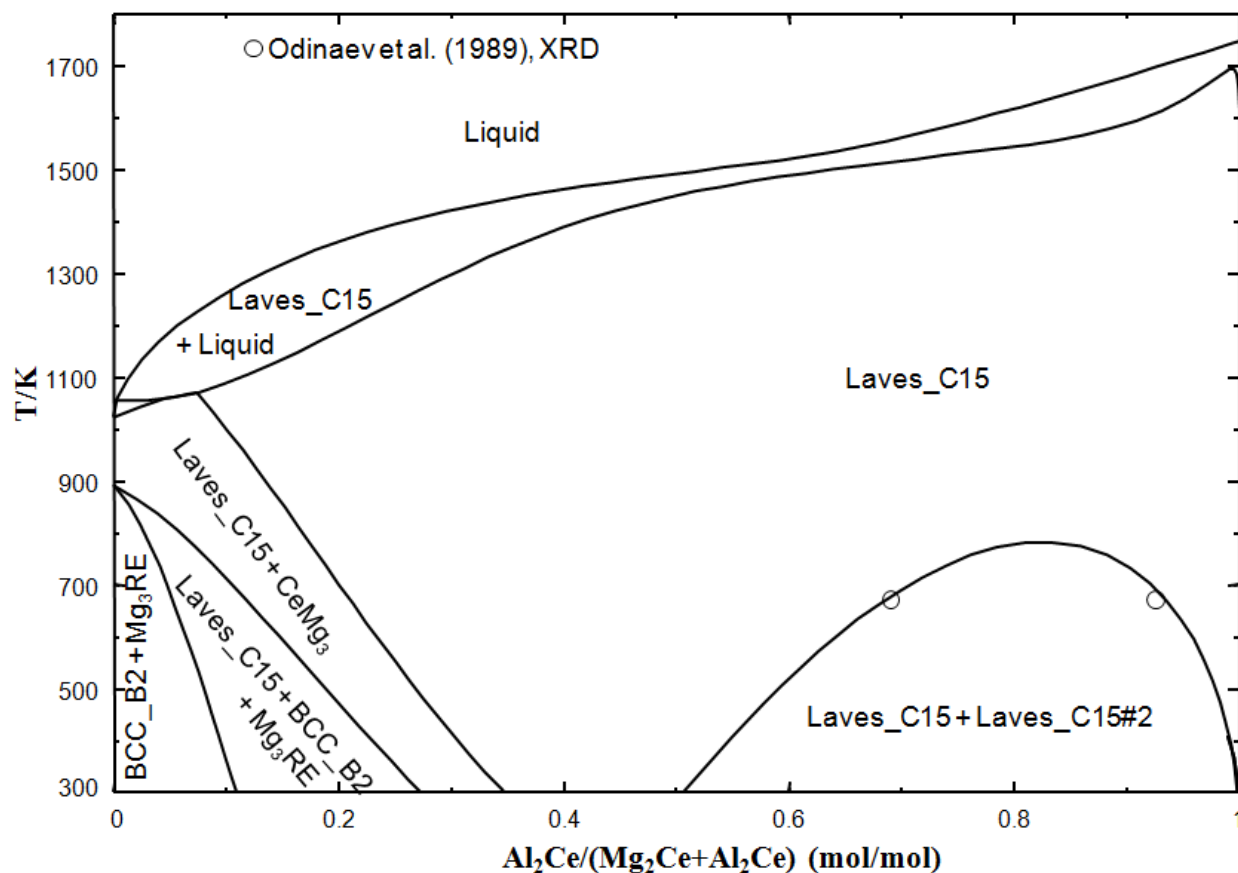
Figure 8.29 Calculated Al$_2$Ce-Mg$_2$Ce section compared with experimental data of Odinaev *et al.* [23].

Figures 8.30 to 8.33 show several calculated sections compared with the experimental DTA data by Odinaev *et al.* [26] and Gröbner *et al.* [7]. In all these figures it can be observed that the thermodynamic calculations reproduce the temperatures where liquid alloys first form, through either eutectic or peritectic reactions, very closely. However, the reported liquidus temperatures of Odinaev *et al.* [26] are far below the present calculations. Similar discrepancies were also observed in the calculations of the Mg–Al–La and Mg–Al–Y systems, in which experimental DTA data are also available from Odinaev *et al.* [63].
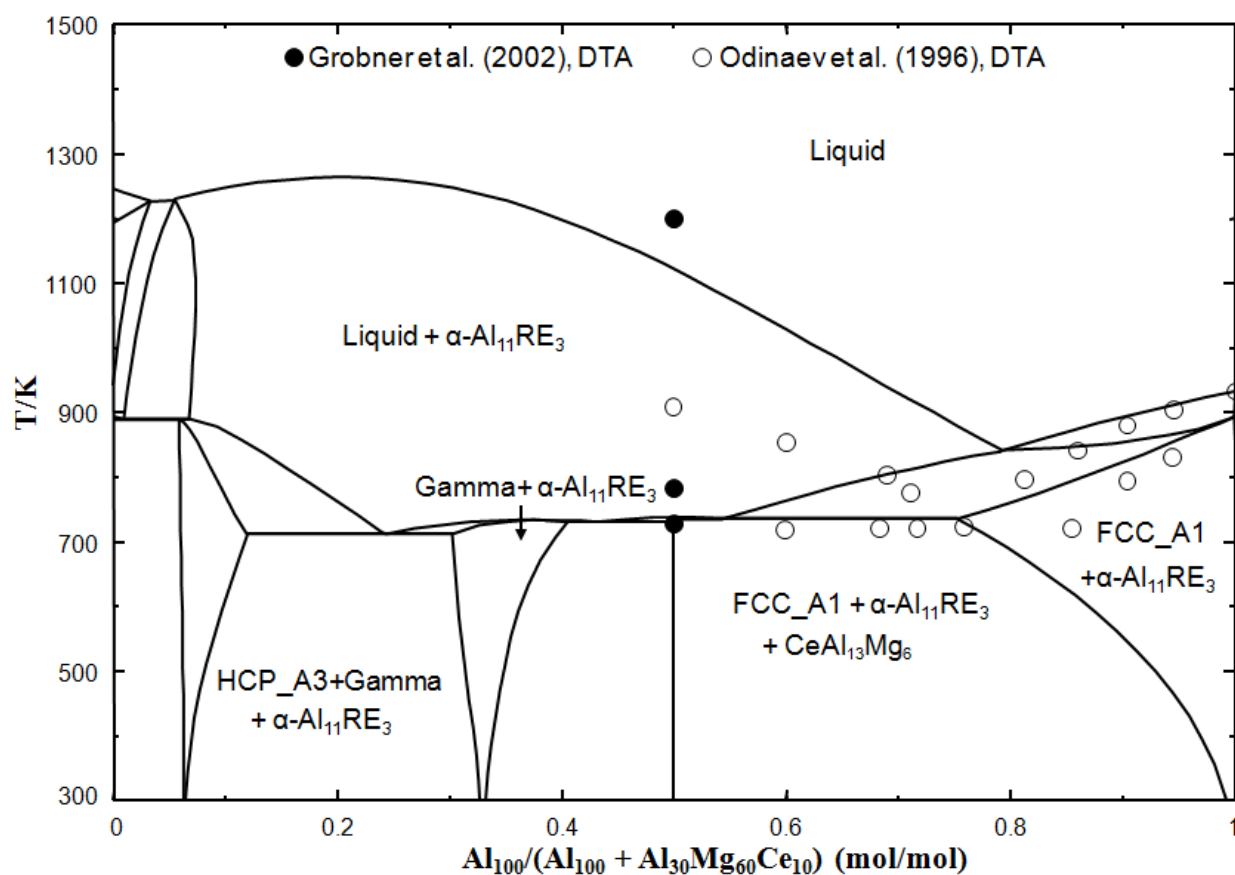
Figure 8.30 Calculated Al_{100}-$Al_{30}Mg_{60}Ce_{10}$ section compared with experimental data of Odinaev *et al.* [26] and Grobner *et al.* [7].

In connection with this, Grobner *et al.* [7] claimed that the reported liquidus temperatures by Odinaev *et al.* [26] might be in error due to experimental difficulties at high temperature, although the experimental details were not given. Grobner *et al.* [7] used sealed Ta crucibles in

their DTA experiment to measure the liquidus temperature, which we believe is to be more accurate than that of Odinaev *et al.* [26]. As seen in Figure 8.30, the measured liquidus temperatures from two different studies show considerable discrepancy (~290 K). The calculated liquidus temperature in the present study is closer to the temperature reported by Gröbner *et al.* [7]. Clearly, further experimental work to measure liquidus temperatures is required.
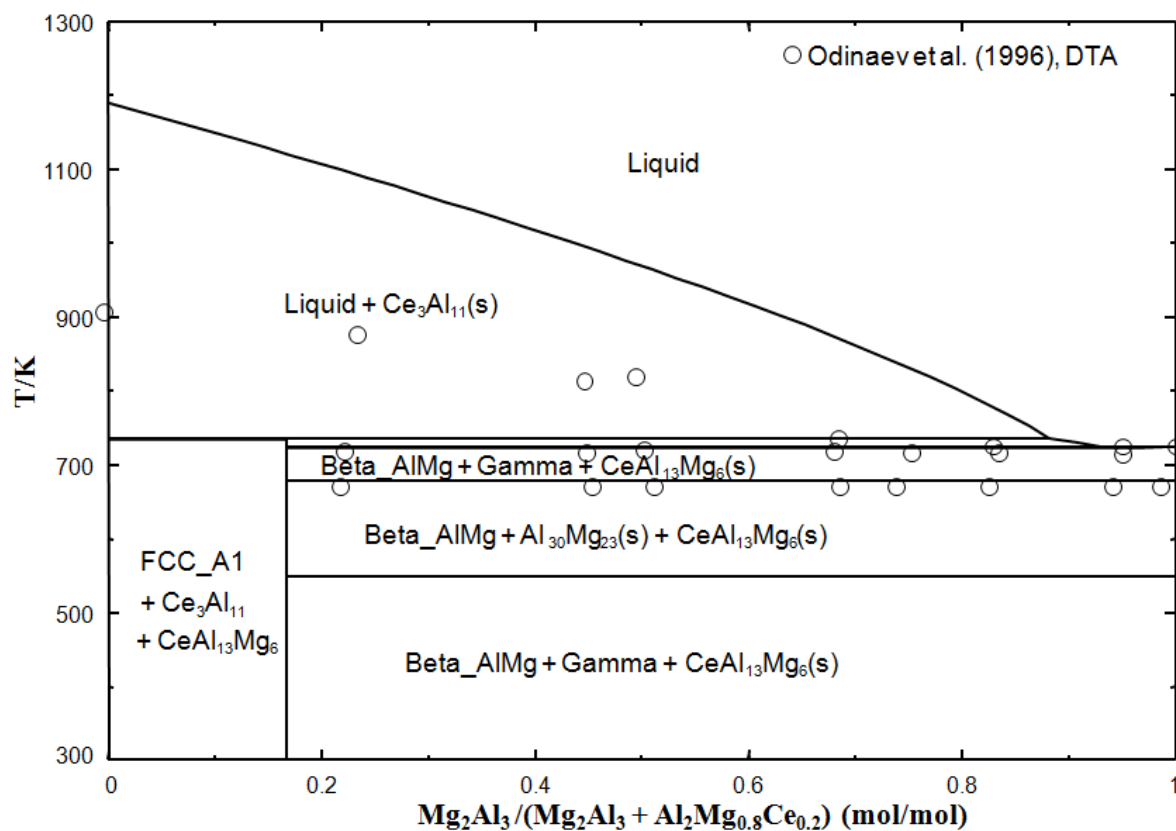
Figure 8.31 Calculated Mg_2Al_3-$Al_2Mg_{0.8}Ce_{0.2}$ section compared with experimental data of Odinaev *et al.* [26].
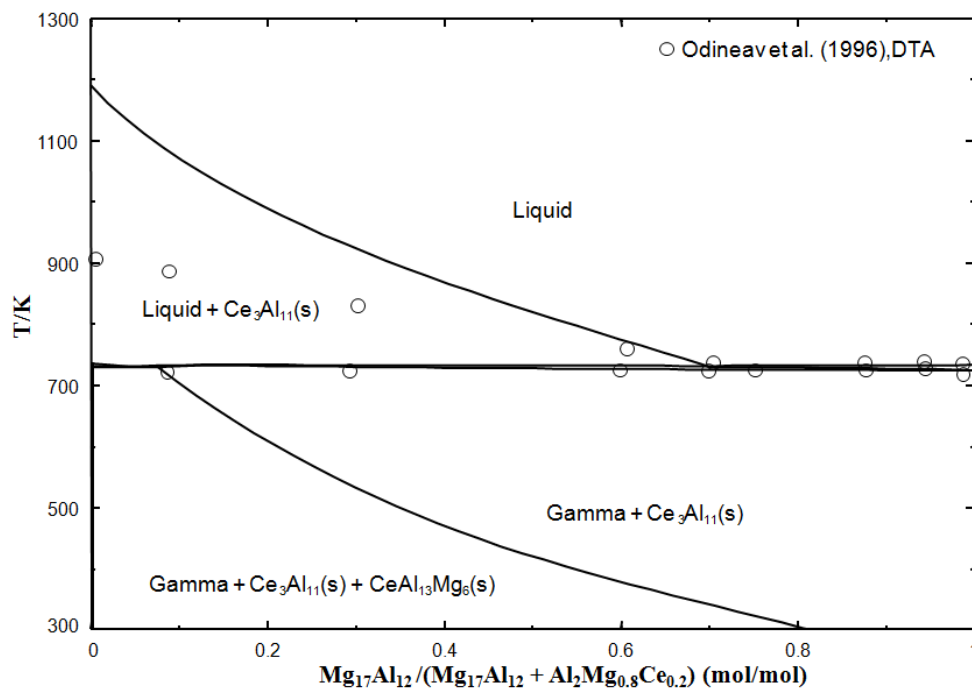
Figure 8.32 Calculated $Mg_{17}Al_{12}$-$Al_2Mg_{0.8}Ce_{0.2}$ section compared with experimental data of Odinaev *et al*. [26].
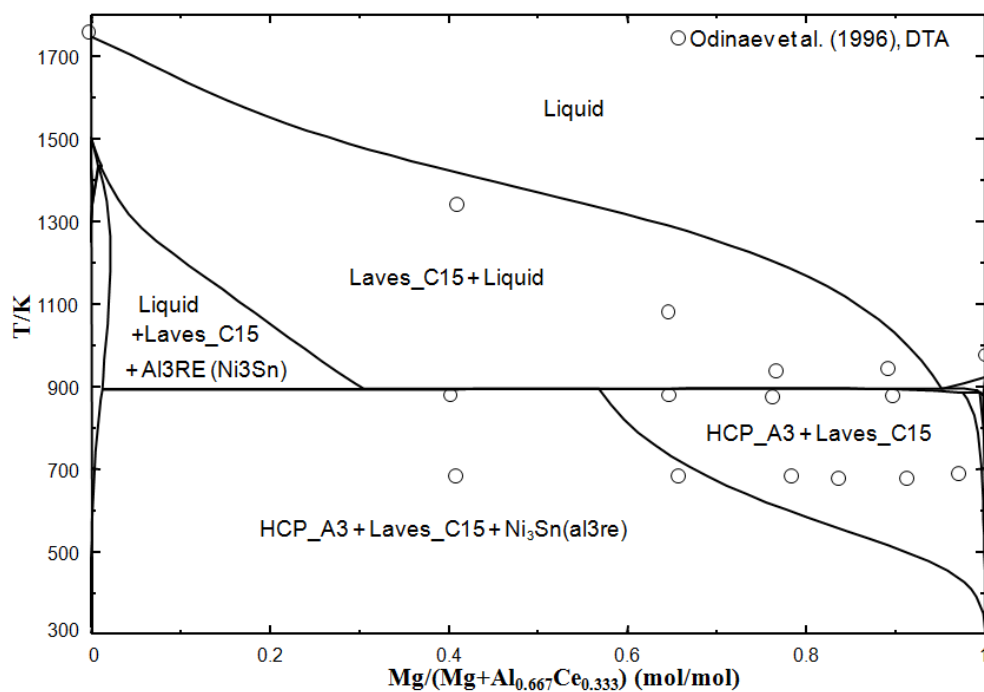
Figure 8.33 Calculated Mg-$Al_{0.667}Ce_{0.333}$ section compared with experimental data of Odinaev *et al*. [26].
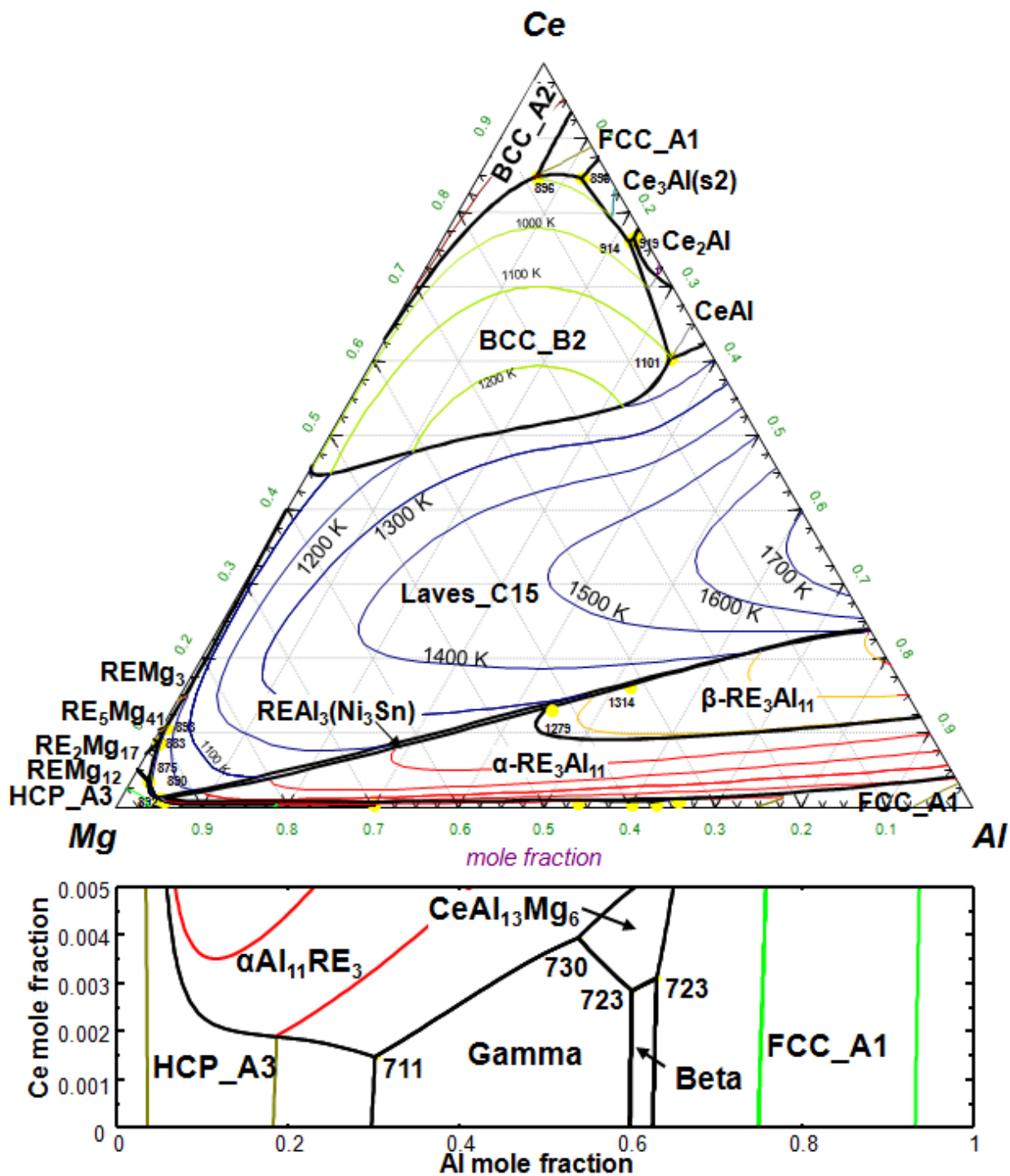
Figure 8.34 The liquidus projection of Al-Mg-Ce system.

Figure 8.34 shows the calculated liquidus surface in the Mg–Al–Ce system. The liquidus surface is dominated by the Laves_C15 (almost pure CeAl$_2$) and Ce$_3$Al$_{11}$ phases, which have high melting temperatures and very negative enthalpies of formations. The primary phase regions of

these phases intersect that of Mg (HCP_A3). Therefore, these phases are likely to precipitate in the HCP phase during Mg alloy production. The peritectially formed ternary phase $Al_{13}Mg_6Ce$ is in agreement with our experiment (Figure 8.4).

In general, the thermodynamic calculation results in the present study give very similar or superior results when compared to the calculations by Gröbner *et al.*[7].

8.4.2.3 The Al – Mg – Pr system

The Gibbs energy of the liquid phase was calculated using the symmetric Kohler approximation [40] with no ternary interaction parameters for the liquid phase. The invariant reactions for Al–Mg–Pr system are listed in Table 8.9. The optimized model parameters for the solid solutions are summarized in Tables 8.5 to 8.7.

Table 8.9 Some invariant reactions of the Al-Mg-Pr system for $X_{Pr} < 1/3$

Reaction	T (K)		Type[†]	Composition (at%)			
	Exp.*	Calc.		Phase	Calc.		
					Al	Pr	Mg
L + Pr_5Mg_{41} ↔ Laves_C15 + $PrMg_3$	-	861	U	L	0.7	10.1	89.2
L ↔ HCP + Laves_C15 + $Pr(Mg,Al)_{12}$	-	843	E	L	0.8	6.1	93.1
L + Pr_5Mg_{41} ↔ Laves_C15 + $Pr(Mg,Al)_{12}$	-	847	U	L	0.8	8.2	91.0
L ↔ Gamma +Beta+ $Pr_3Al_{50}Mg_{22}$	709	724	E	L	59.98	0.05	39.97

|							
L+ Pr$_3$Al$_{11}$ +FCC $\leftrightarrow$ Pr$_3$Al$_{50}$Mg$_{22}$	-	730	P	L	0.639	0.001	0.36
L $\leftrightarrow$ Gamma +HCP_A3+ Pr$_3$Al$_{11}$	708	712	E	L	29.77	0.03	70.2
L+ FCC$\leftrightarrow$ Beta+ Pr$_3$Al$_{50}$Mg$_{22}$	-	724	U	L	62.64	0.06	37.3
L + Pr$_3$Al$_{50}$Mg$_{22}$ + Pr$_3$Al$_{11}$$\leftrightarrow$ Gamma	-	726	P	L	58.83	0.07	41.1

† P: peritectic, U: quasiperitectic, E: eutectic

* Experimental data were taken from Odinaev *et al*. [30] unless another reference is given.

For Pr(Mg,Al)$_{12}$, the similarity among the La, Ce, Pr and Nd was considered although no data for the solid solubility of Al in PrMg$_{12}$ phase was reported. The enthalpy of formation of PrAl$_{12}$ compound was calculated by the Miedema's model in the present study. Similar to Al–Mg–La and Al–Mg–Ce systems, nine ternary solid solutions (Laves_C15, BCC_B2, Pr(Mg, Al)$_3$, Pr$_3$(Mg, Al)$_{11}$, Pr(Mg, Al)$_{12}$), HCP_A3, FCC_A1, BCC_A2 and Gamma) were considered in the present study. For the Laves_C15 phase, two optimized interaction parameters for the first sub-lattice were required in order to reproduce the observed miscibility gap by Odinaev *et al.* [18] at 673K. One interaction parameter was necessary to reproduce the 2-phase equilibria between the BCC_B2 and the DHCP_A3' (Pr) phases. For the Pr(Al,Mg)$_{12}$ phase, the Gibbs energy of hypothetical PrAl$_{12}$ and one interaction parameter were optimized in order to reproduce our experimental data. The ternary compound, Al$_{50}$Mg$_{22}$Pr$_3$ (noted as Al$_2$Mg$_{0.88}$Pr$_{0.12}$ in [29]), was assumed to be a stoichiometric (line) compound in the present study because no solid solubility has been reported. The Gibbs energy of the Al$_{50}$Mg$_{22}$Pr$_3$ compound was optimized to reproduce phase equilibria at 673 K.
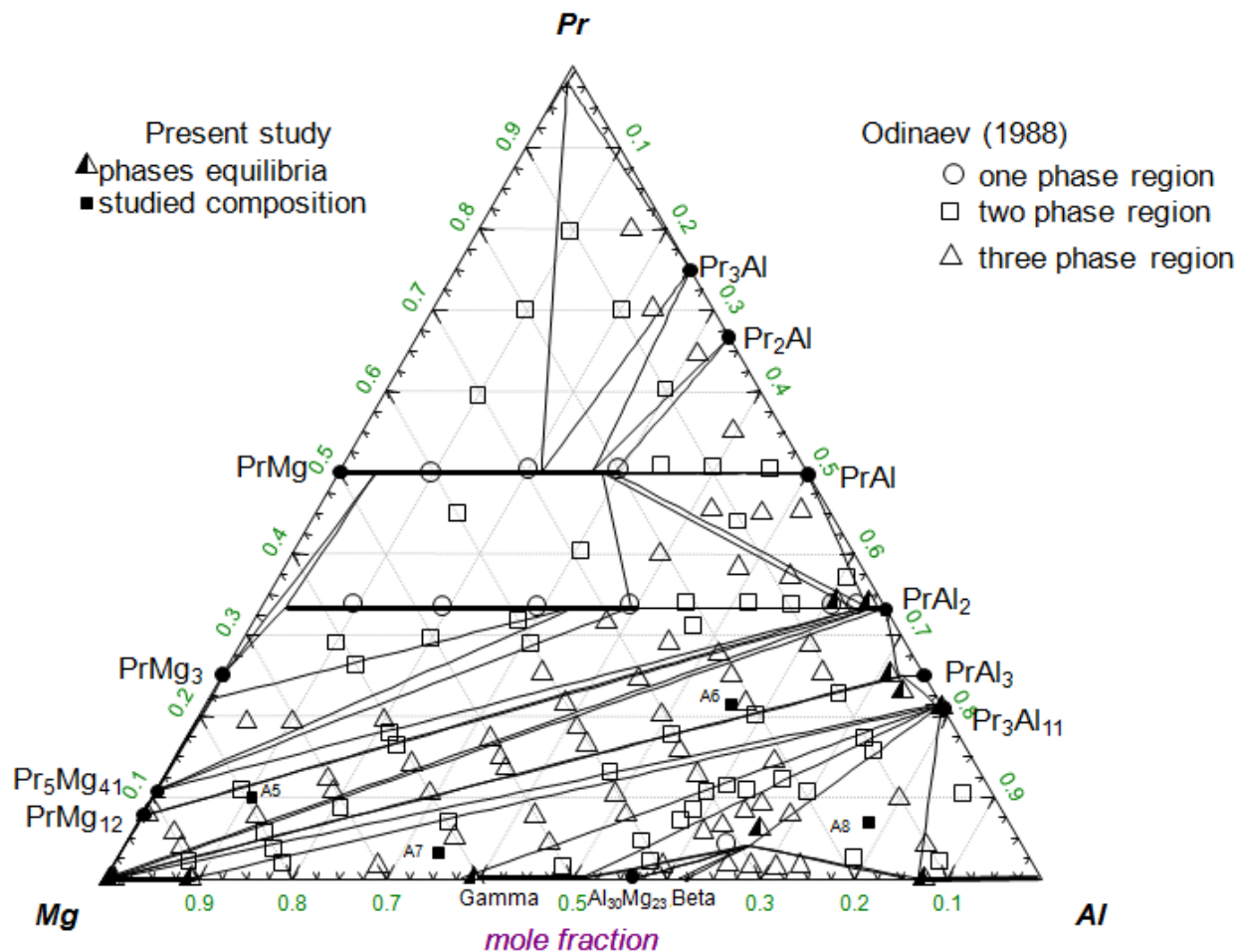
Figure 8.35 The calculated isothermal section of the Mg–Al–Pr ternary system at 673 K compared with experimental data of Odinaev *et al*. [29].

The calculated isothermal section of the Mg–Al–Pr ternary system at 673 K is shown in Figure 8.35 along with the experimental data of Odinaev *et al*. [29]. PrMg and PrAl are only partially miscible because they have different crystal structures (CsCl and AlEr type, respectively). On the other hand, both $PrMg_2$ and $PrAl_2$ have the Cu_2Mg type structure and they form a Laves_C15 solid solution with a miscibility gap at low temperature. Most experimental data are well reproduced by the calculations. According to Odinaev *et al*. [29], $PrMg_2$ is stable and forms a solid solution at 673 K. However, this contradicts the result of Saccone *et al*. [64] who reported that $PrMg_2$ decomposes into $PrMg_3$ and PrMg near 943 K. $PrMg_2$ is only stable over a limited temperature range (943 K ~ 1013 K). However, it is stabilized over a wide temperature range as

PrAl$_2$ dissolves into it. The miscibility gap in the Laves_C15 solution measured by Odinaev *et al.* [29] compares favorably with the present thermodynamic calculation.
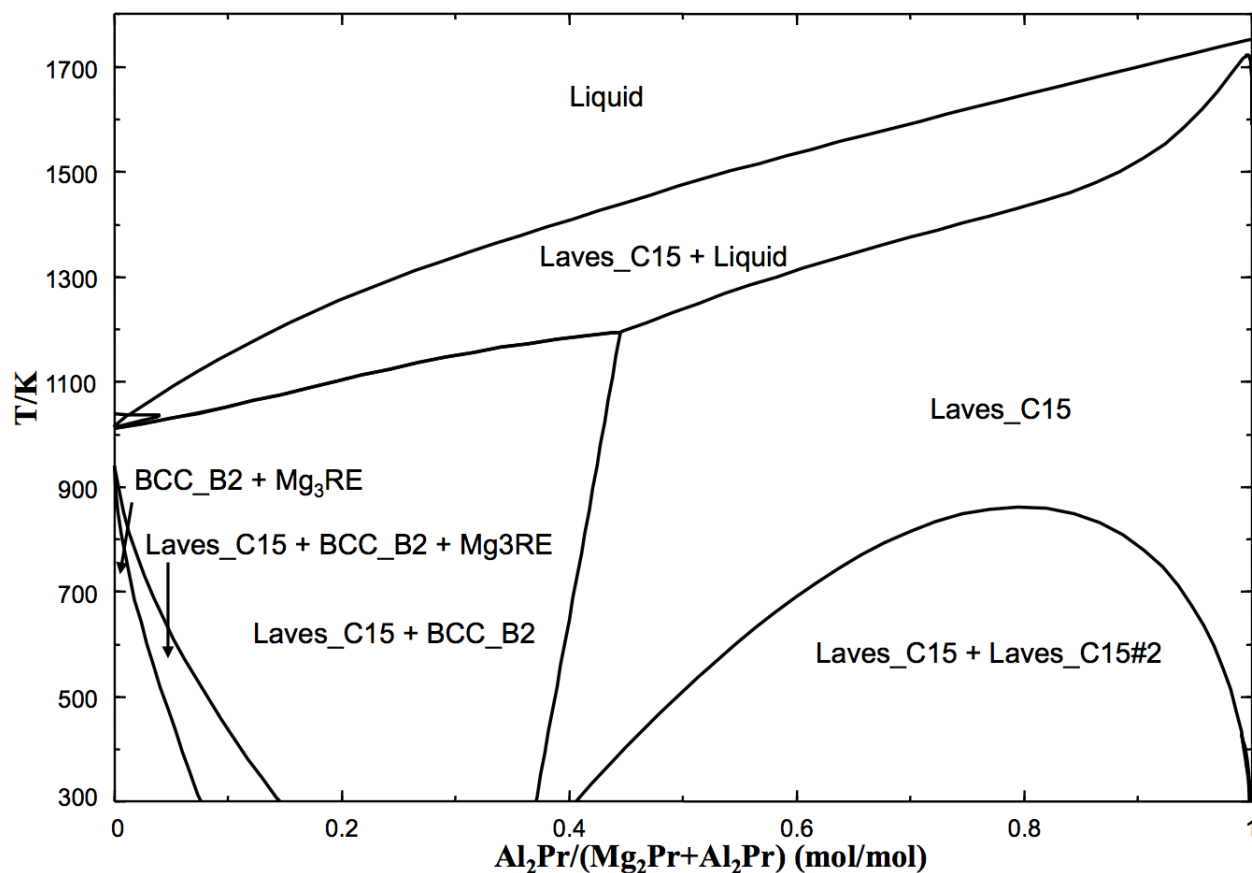
Figure 8.36 The calculated Al$_2$Pr-Mg$_2$Pr section.

Figures 8.36 to 8.39 show several calculated sections compared with the experimental DTA data by Odinaev *et al.* [30]. In all these figures it can be observed that the thermodynamic calculations reproduce the temperatures where liquid alloys first form, through either eutectic or peritectic reactions, very closely. However, the reported liquidus temperatures of Odinaev *et al.* [29] are far below the present calculations. Similar discrepancies were also observed in calculations of the Mg–Al–La and Mg–Al–Ce system in the present study, in which experimental DTA data are also available from the work of Odinaev *et al.* [18; 26]. It might be in error due to experimental difficulties at high temperature, although the experimental details were not given.
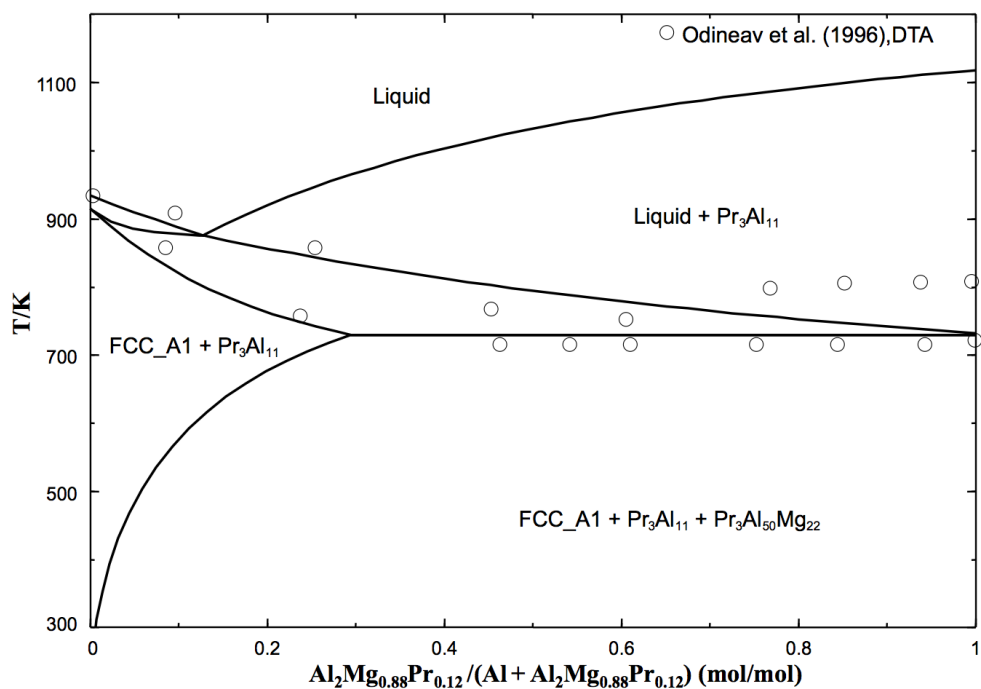
Figure 8.37 Calculated Al-Al$_2$Mg$_{0.88}$Pr$_{0.12}$ section compared with experimental data of Odinaev *et al*. [30].
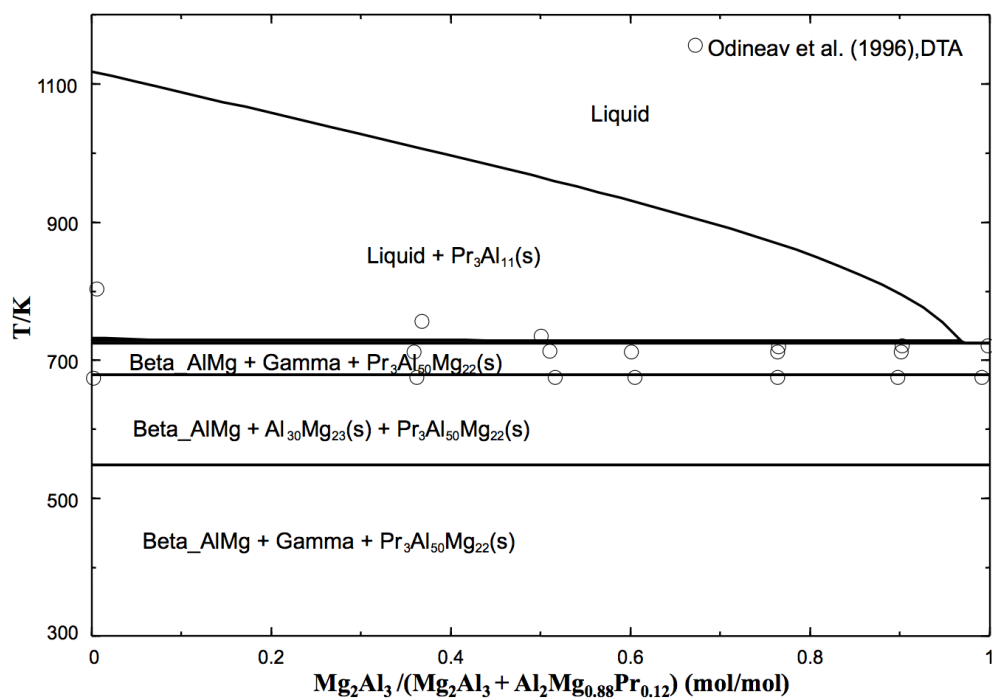
Figure 8.38 Calculated Mg$_2$Al$_3$-Al$_2$Mg$_{0.88}$Pr$_{0.12}$ section compared with experimental data of Odinaev *et al*. [30].
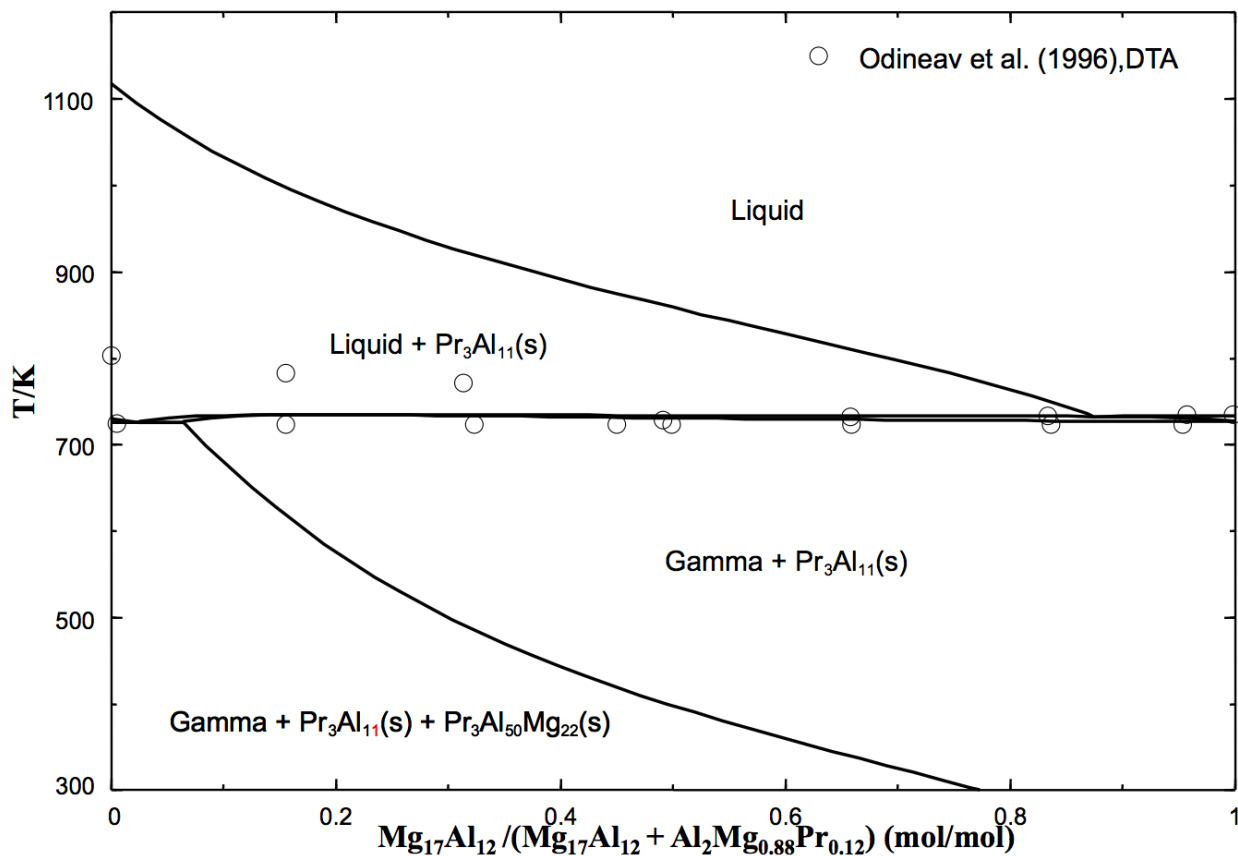
Figure 8.39 Calculated $Mg_{17}Al_{12}$-$Al_2Mg_{0.88}Pr_{0.12}$ section compared with experimental data of Odinaev *et al.* [30].

Figure 8.40 shows the calculated liquidus surface for the Al–Mg–Pr system. The liquidus surface is dominated by the Laves_C15 (almost pure $PrAl_2$) and Pr_3Al_{11} phases, which have high melting temperatures and very negative enthalpies of formations. The primary phase regions of these phases intersect that of Mg (HCP_A3). Therefore, these phases are likely to precipitate in the HCP phase during Mg alloy solidification process. The peritectically formed ternary phase $Al_{50}Mg_{22}Pr_3$ is confirmed by our experiment (see Figure 8.10).
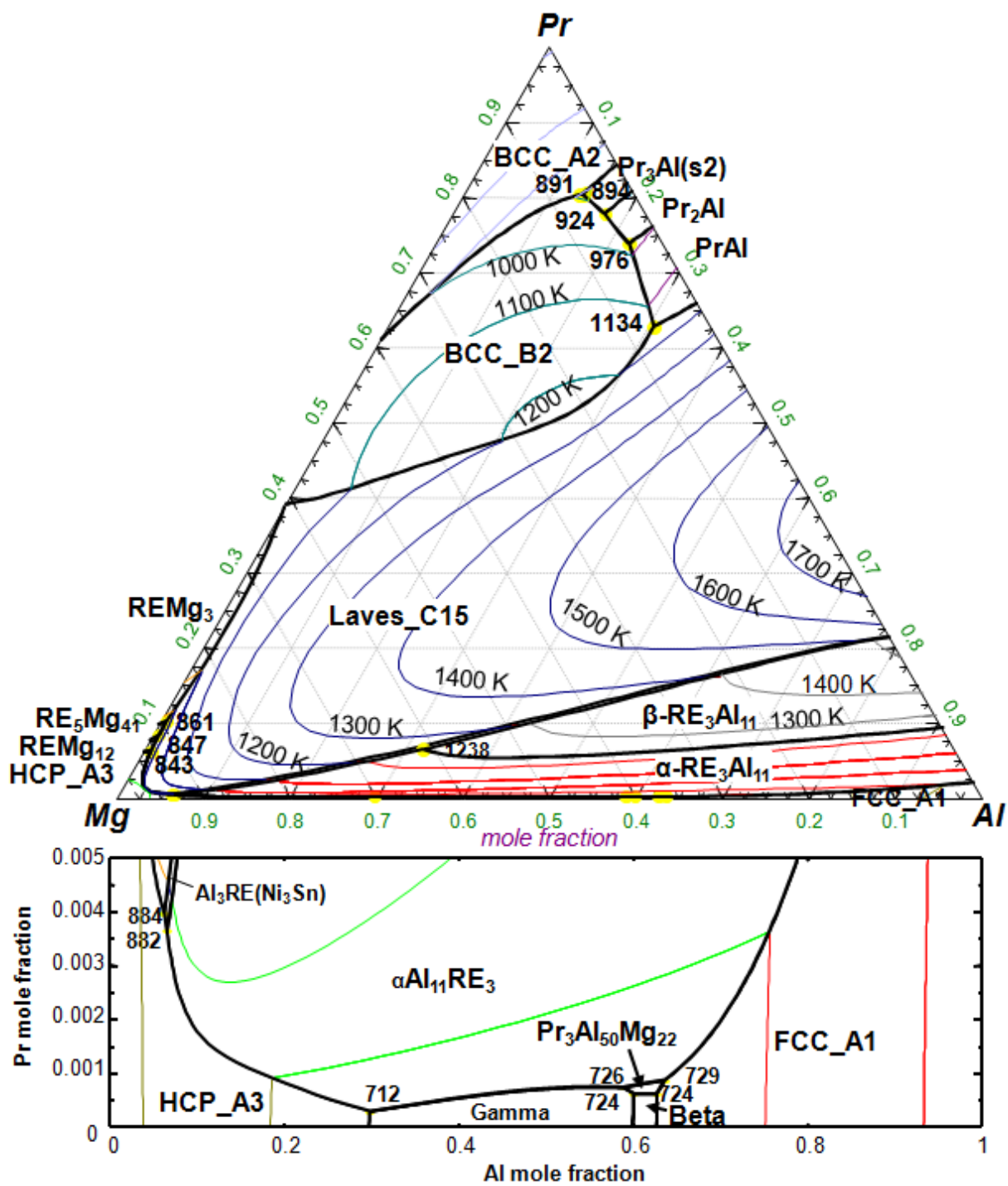
Figure 8.40 The liquidus projection of Al-Mg-Pr system.

8.4.2.4 The Al–Mg–Nd system

The invariant reactions for the Al–Mg–Nd system are listed in Table 8.10. The Gibbs energy of the liquid phase was calculated using the symmetric Kohler-like approximation [40] with no ternary interaction parameters. The optimized model parameters are summarized in Tables 8.5 to 8.7.

Table 8.10 Invariant reactions of the Al-Mg-Nd system for $X_{Nd} < 1/3$

Reaction	T (K)		Type[†]	Composition (at%)			
	Exp.*	Calc.		Phase	Calc.		
					Al	Nd	Mg
L $\leftrightarrow$ Laves_C15 + Nd$_5$Mg$_{41}$+ HCP_A3	-	820	E	L	0.6	7.4	92.0
L+ NdMg$_3$ $\leftrightarrow$ Laves_C15 + Nd$_5$Mg$_{41}$	-	833	U	L	0.5	9.1	90.4
L+Al$_3$Nd $\leftrightarrow$ HCP_A3+ Nd$_3$Al$_{11}$	-	845	U	L	11.9	0.3	87.8
L $\leftrightarrow$ Gamma +Beta+ Nd$_3$Al$_{50}$Mg$_{22}$	708	724	E	L	62.63	0.07	37.3
L $\leftrightarrow$ Gamma +HCP_A3+ Nd$_3$Al$_{11}$	708	712	E	L	29.81	0.05	70.14
L $\leftrightarrow$ Beta +Gamma+ Nd$_3$Al$_{50}$Mg$_{22}$	709	724	E	L	59.98	0.07	39.95
L + Nd$_3$Al$_{11}$ +FCC_A1$\leftrightarrow$ Nd$_3$Al$_{50}$Mg$_{22}$		734	U	L	64.43	0.13	35.44

† P: peritectic, U: quasiperitectic, E: eutectic

* Experimental data were taken from Odinaev *et al*. [33] unless another reference is given.

For Nd(Mg,Al)$_{12}$, the similarity among the La, Ce, Pr and Nd was considered although no data for the solid solubility of Al in PrMg$_{12}$ phase was reported. The enthalpy of formation of NdAl$_{12}$ compound was calculated by the Miedema's model. Similar to Al–Mg–La, Al–Mg–Ce and Al–Mg–Pr systems, nine ternary solid solutions (Laves_C15, BCC_B2, Nd(Mg, Al)$_3$, Nd$_3$(Mg, Al)$_{11}$, Nd(Mg, Al)$_{12}$), HCP_A3, FCC_A1, BCC_A2 and Gamma) were considered in the present study. For the Laves_C15 phase, like Al–Mg–Pr system, two optimized interaction parameters for the first sub-lattice were required in order to reproduce the observed miscibility gap at 673 K by Odinaev *et al.* [32]. One interaction parameter was necessary to reproduce the 2-phase equilibria between the BCC_B2 and the DHCP_A3' (Nd) phases. The ternary compound, Al$_{50}$Mg$_{22}$Nd$_3$ (noted as Al$_2$Mg$_{0.88}$Nd$_{0.12}$ in [32]), was assumed to be a stoichiometric (line) compound in the present study because no solid solubility has been reported. The Gibbs energy of the Al$_{50}$Mg$_{22}$Nd$_3$ compound was optimized to reproduce phase equilibria at 673 K. In general, the optimization was directed mainly towards reproducing the phase equilibrium data at 673 K measured by Odinaev *et al.* [32].

A calculated isothermal section of the Mg–Al–Nd ternary system at 673 K is shown in Figure 8.41 along with the experimental data of Odinaev *et al.* [32]. NdMg and NdAl are only partially miscible because they have different crystal structures (CsCl and AlEr type, respectively). On the other hand, both NdMg$_2$ and NdAl$_2$ have the Cu$_2$Mg type structure and they form a Laves_C15 solid solution with a miscibility gap at low temperature. Most experimental data are well reproduced by the calculations. According to Odinaev *et al.* [32], NdMg$_2$ is stable and forms a solid solution at 673 K. However, this contradicts the result of Delfino *et al.* [65] who reported that NdMg$_2$ decomposes into NdMg$_3$ and NdMg near 949 K. NdMg$_2$ is only stable over a limited temperature range (949 K ~ 1034 K). However, it is stabilized over a wide temperature range as NdAl$_2$ dissolves into it. The miscibility gap in the Laves_C15 solution measured by Odinaev *et al.* [32] compares favorably with the present thermodynamic calculation.
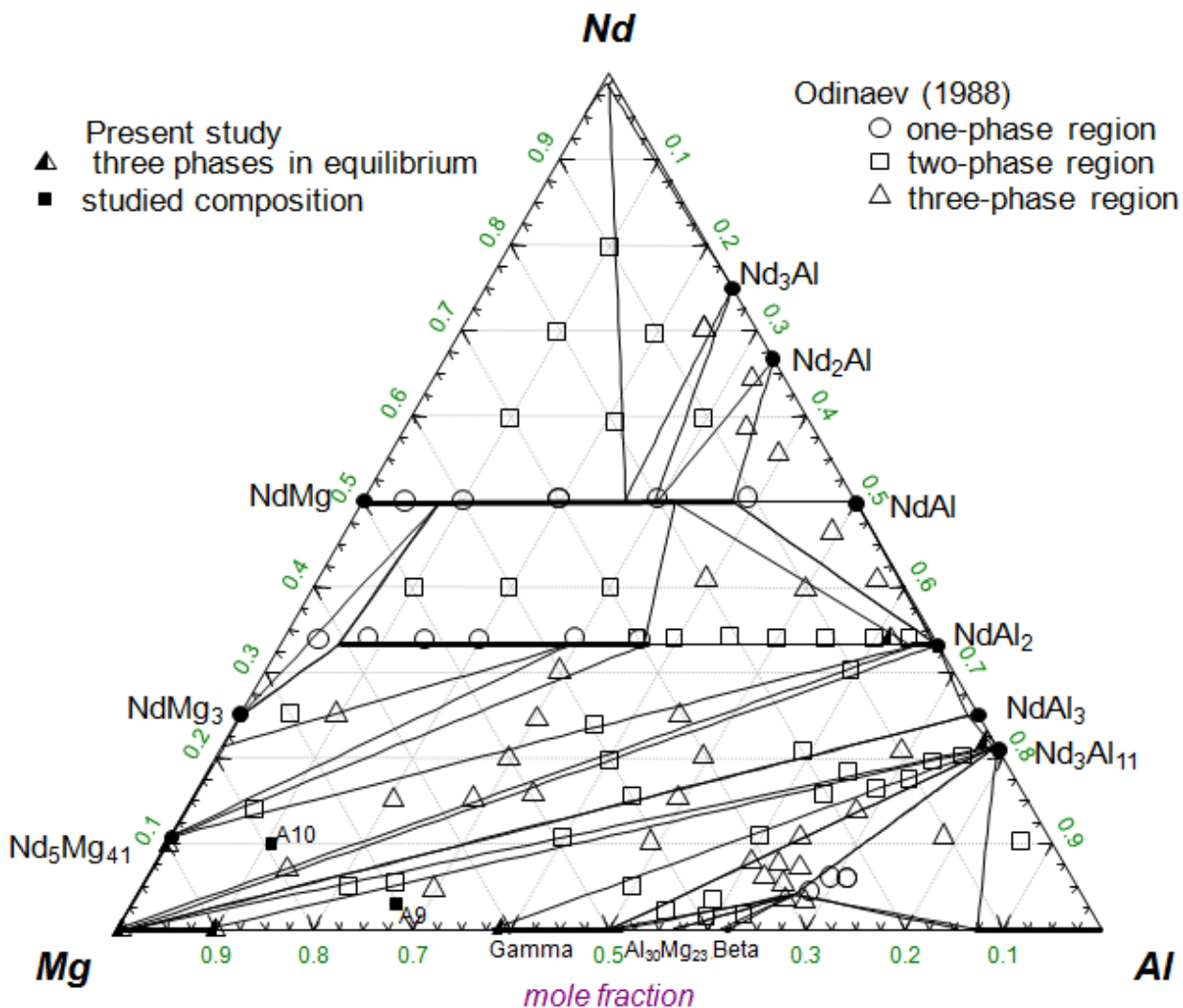
Figure 8.41 The calculated isothermal section of the Mg–Al–Nd ternary system at 673 K compared with experimental data of Odinaev *et al*. [32].

Figures 8.42 to 8.45 show several calculated sections compared with the experimental DTA data by Odinaev *et al*.[33]. In all these figures it can be observed that the thermodynamic calculations reproduce the temperatures where liquid alloys first form, through either eutectic or peritectic reactions, very closely. However, the reported liquidus temperatures of Odinaev *et al*. [19] are far below the present calculations. Similar discrepancies were also observed in calculations of the Mg–Al–La, Mg–Al–Ce and Mg–Al–Pr systems. It might be in error due to experimental difficulties at high temperature, although the experimental details were not given.
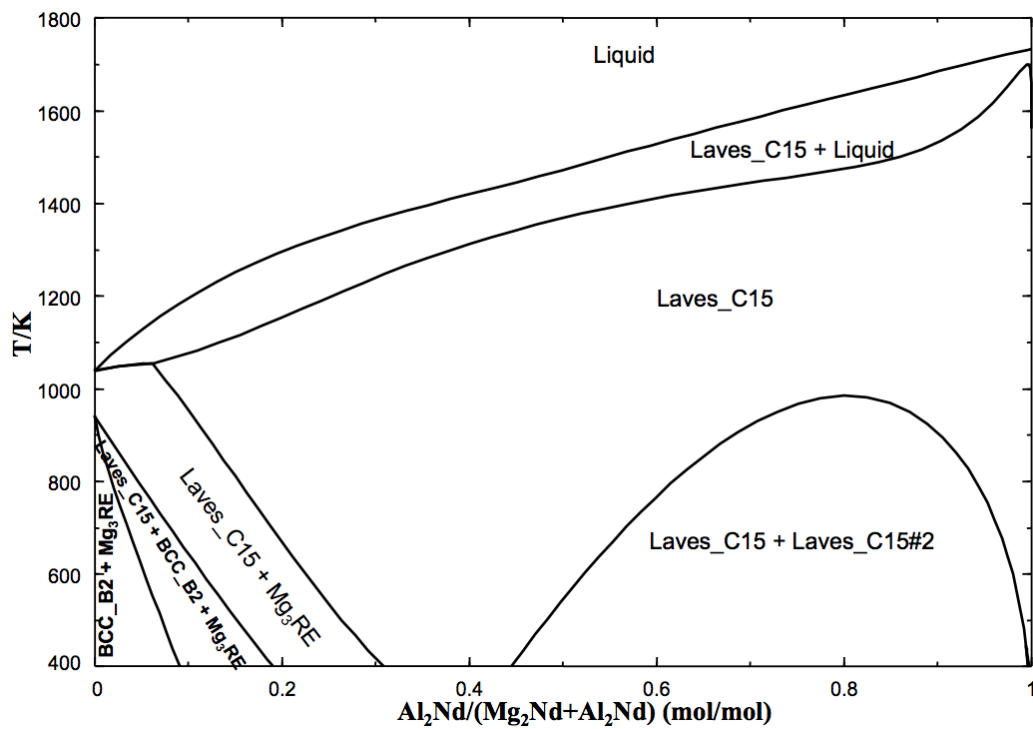
Figure 8.42 Calculated Al$_2$Nd-Mg$_2$Nd section.
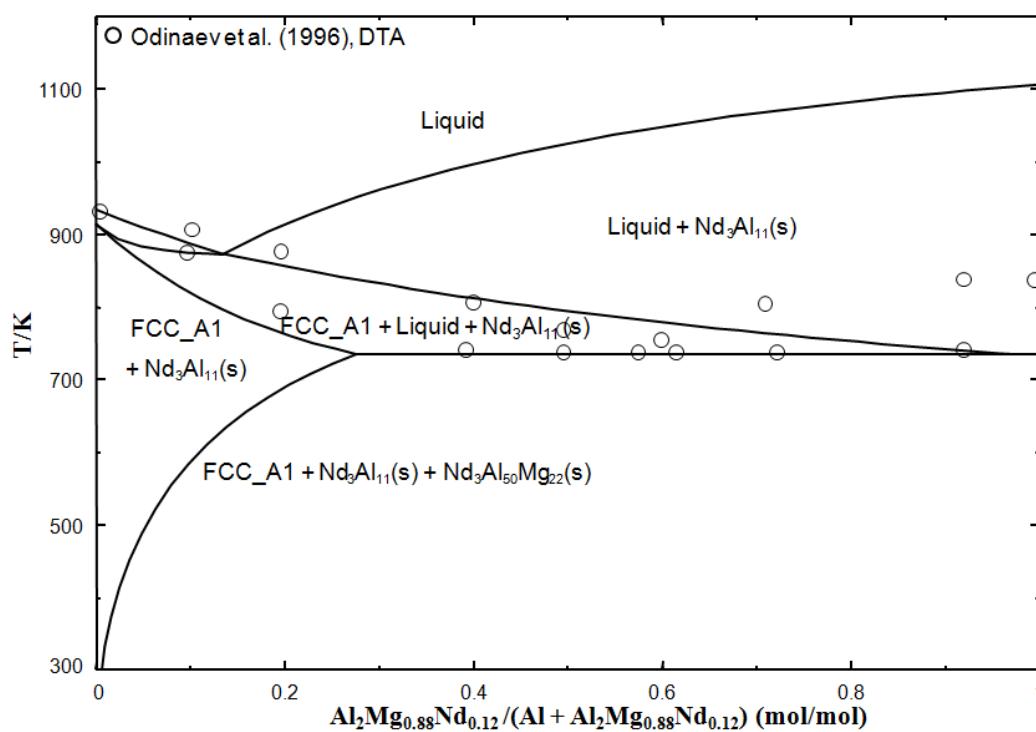
Figure 8.43 Calculated Al-Al$_2$Mg$_{0.88}$Nd$_{0.12}$ section compared with experimental data of Odinaev *et al*.[33].
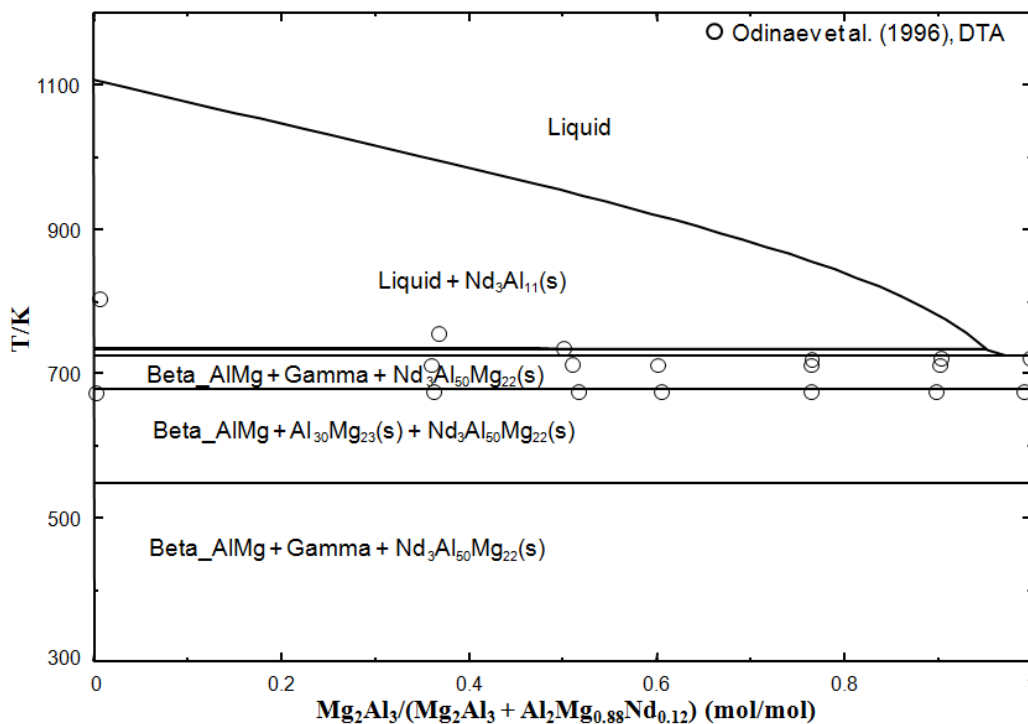
Figure 8.44 Calculated Mg_2Al_3-$Al_2Mg_{0.88}Nd_{0.12}$ section compared with experimental data of Odinaev *et al*.[33].
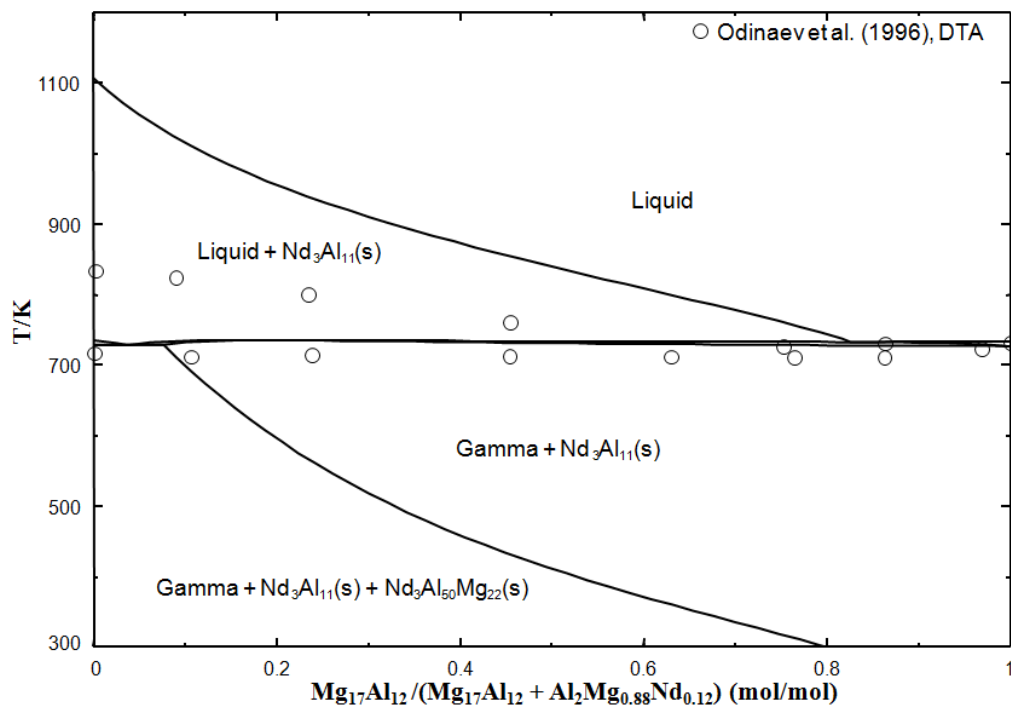
Figure 8.45 Calculated $Mg_{17}Al_{12}$-$Al_2Mg_{0.88}Nd_{0.12}$ section compared with experimental data of Odinaev *et al*.[33].
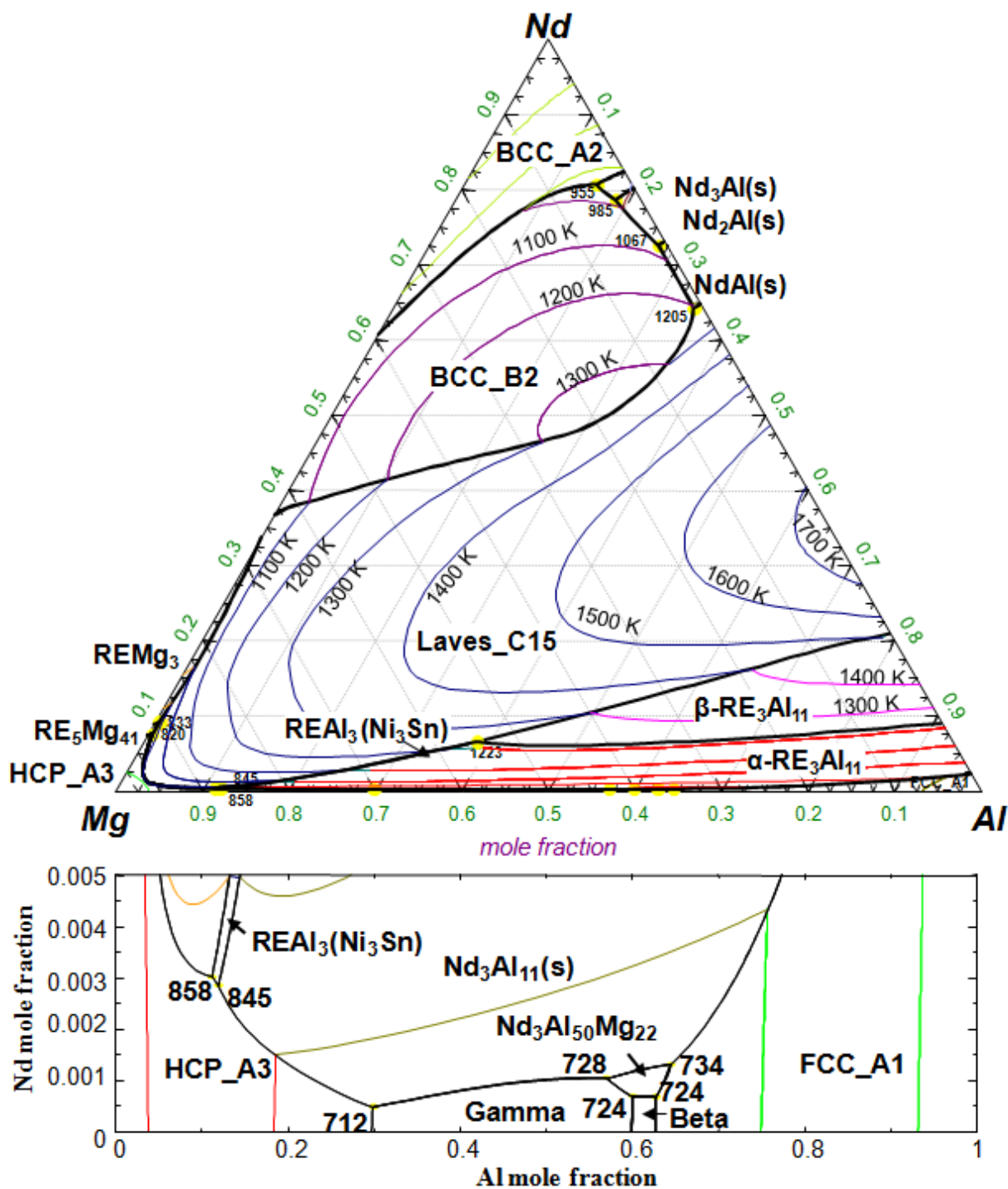
Figure 8.46 The liquidus projection of Al-Mg-Nd system.

Figure 8.46 shows the calculated liquidus surface in the Mg–Al–Nd system. The liquidus surface is dominated by the Laves_C15 (almost pure $NdAl_2$) and Nd_3Al_{11} phases, which have high

melting temperatures and very negative enthalpies of formations. The primary phase regions of these phases intersect that of Mg (HCP_A3). Therefore, these phases are likely to precipitate in the HCP phase during Mg alloy solidification process.

8.4.2.5   The Al – Mg – Sm system

The calculated isothermal section is illustrated in Figure 8.47 with the experimental data at 673 K by Zheng *et al.* [35]. Despite the fact that intermetallic compound phases Al_4Sm and $AlSm_3$ have not been taken into consideration in this work due to the contradiction with the optimized Al–Sm [10] binary phase diagram whereas $SmMg_5$ and Sm_5Mg_{41} exist in recently optimized Mg–Sm [11] binary phase diagram, the calculated isothermal section have reproduced the experimental data to satisfaction. It is worth noting a few differences in the optimization between Jia *et al.* [8] and the current study. First of all, there is a modification of Sm_3Al_{11} phase. In the present study, Sm_3Al_{11} phase exists only at high-temperature range from 1351 K to 1684 K [10], which was mainly based on the investigation of Delsante *et al.* [66]. Secondly, the Mg_2Sm phase was considered to be stable at high-temperature range from 653 K to 1015 K [11] and decomposed to $SmMg_3$ and SmMg phases at 653 K, which was similar to $LaMg_2$, $CeMg_2$, $PrMg_2$ and $NdMg_2$ phases. Thirdly, it was assumed that there is certain solid solubility of Al in SmMg (BCC_B2) phase, which was believed to be reasonable by considering the similarities among Al–Mg–La, Al–Mg–Ce, Al–Mg–Pr, Al–Mg–Nd, Al–Mg–Gd, Al–Mg–Dy, Al–Mg–Ho, Al–Mg–Er [67] and Al–Mg–Sm systems. Thirdly, it was believed that $SmMg_2$ and $SmAl_2$ could form Laves_C15 solid solution since both of them have the same crystal structure (C15, $MgCu_2$-type). Finally, unlike the investigation of Zheng *et al.* [35], $SmAl_4$ and Sm_3Al were not considered in Al–Sm and Al–Mg–Sm systems; Sm_2Mg_{13} was described as Sm_5Mg_{41} and $SmMg_5$ exists in Mg–Sm and Al–Mg–Sm systems [34], Al_3Mg_2 phase was considered as $Al_{30}Mg_{23}$. The Gibbs energy of the liquid phase was calculated using the symmetric Kohler approximation with no ternary interaction parameters.
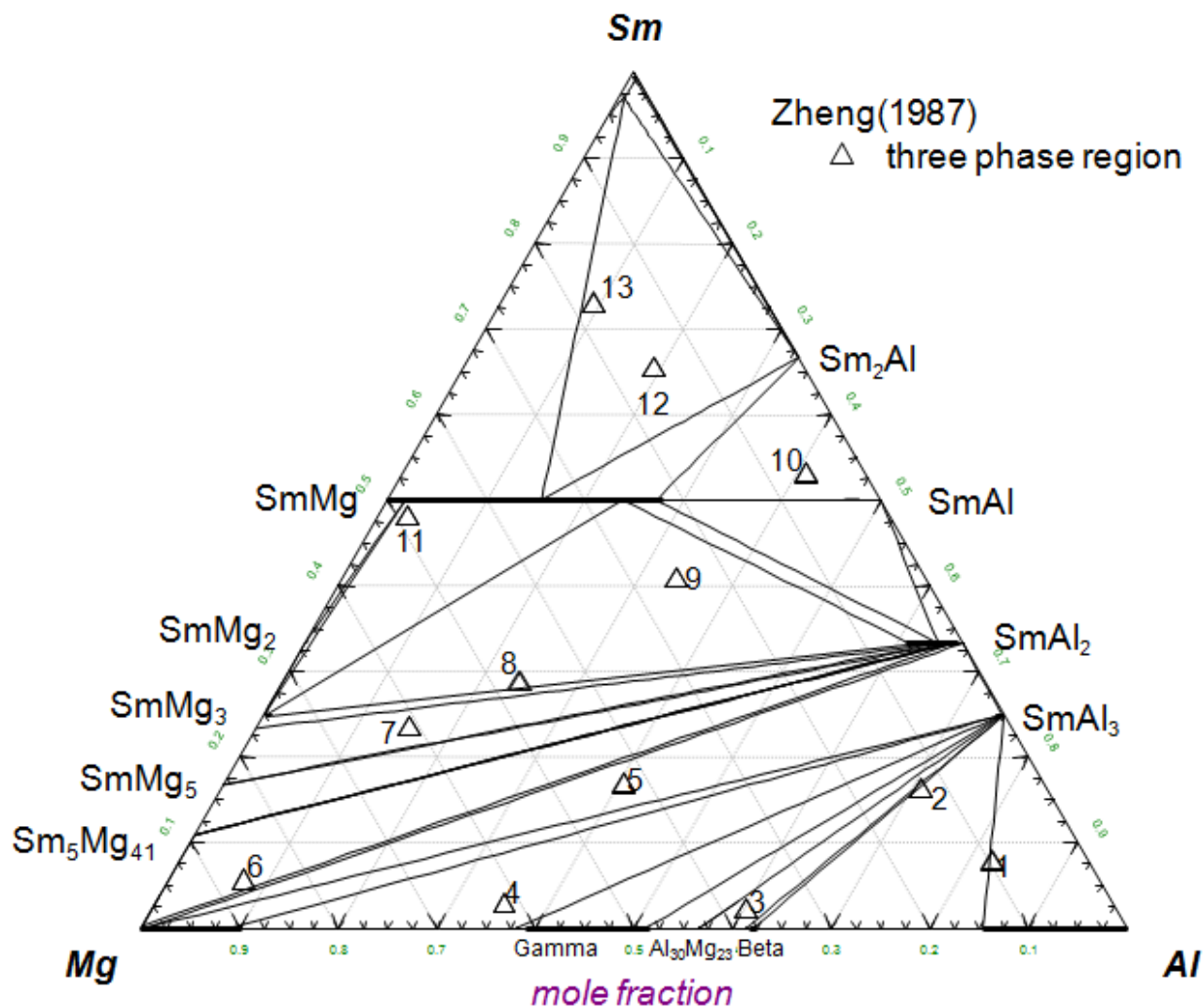
Figure 8.47 The calculated isothermal section of the Mg–Al–Sm ternary system at 673K compared with experimental data of Zheng *et al.* [35].

For the Laves_C15 and BCC_B2 phases, the excess Gibbs energies were similar to those in Al–Mg–Pr and Al–Mg–Nd systems.

The liquidus projection with the univariant points was presented in Figure 8.48. The liquidus surface is dominated by the Laves_C15 (almost pure SmAl$_2$) and Ni$_3$Sn (SmAl$_3$) phases, which have high melting temperatures and very negative enthalpies of formations. The primary phase

regions of these phases intersect that of Mg (HCP_A3). Therefore, these phases are likely to precipitate in the HCP phase during Mg alloy solidification process.
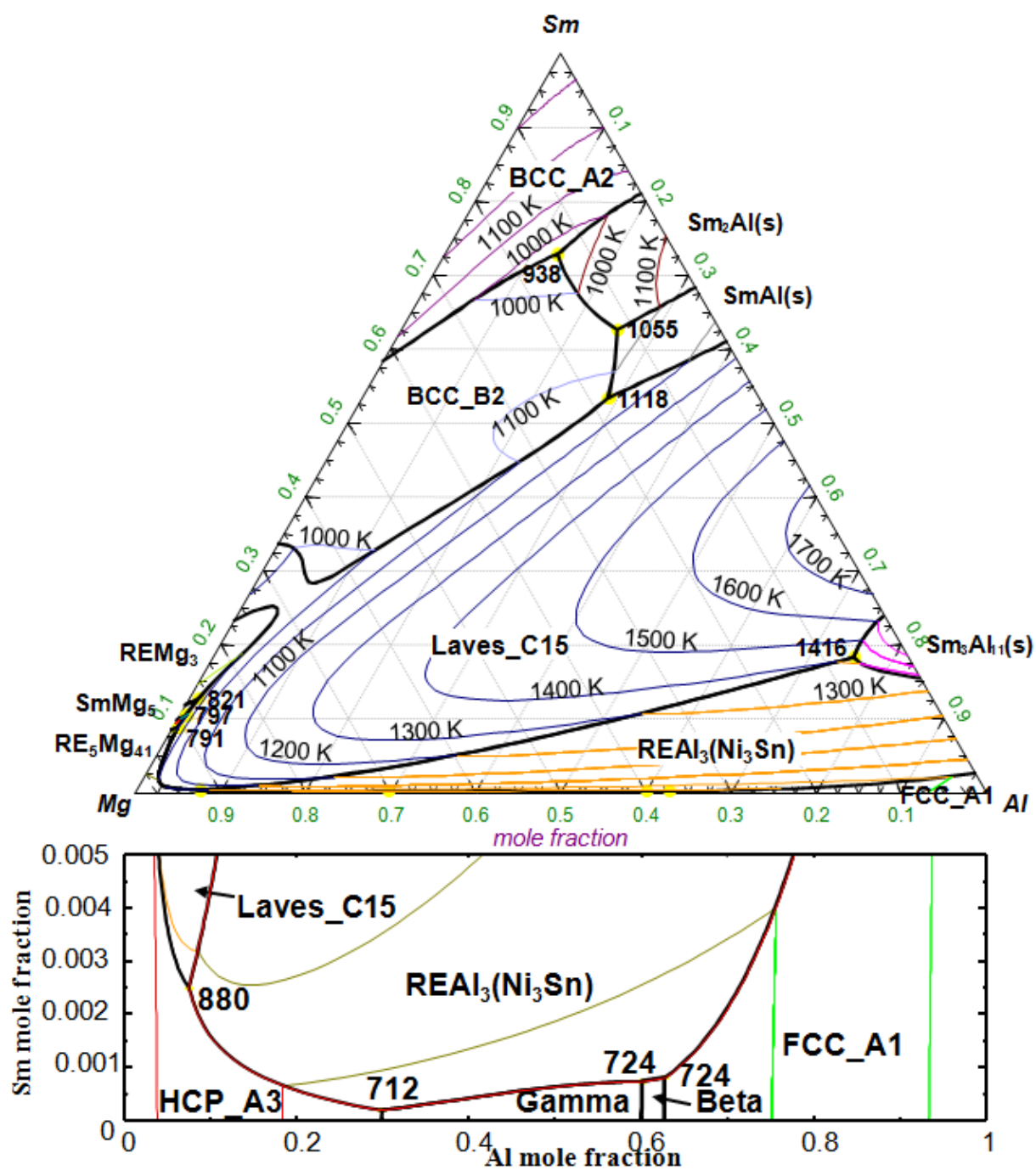
Figure 8.48 The liquidus projection of Al-Mg-Sm system.

The calculated invariant reactions in Al–Mg–Sm system are listed in Table 8.11 compared with the calculated results from Jia *et al.* [8]. The optimized model parameters are summarized in Tables 8.5 - 8.7.

Table 8.11 Invariant reactions of the phase diagram for $X_{Sm} < 1/3$.

Reaction	T (K)		Type[†]	Composition (at%)			
	Exp.	Calc.		Phase	Calc.		
					Al	Sm	Mg
L ↔ Laves_C15 + Sm$_5$Mg$_{41}$+ HCP_A3	-	791	E	L	0.6	8.8	90.6
L + SmMg$_5$↔ Laves_C15 + Sm$_5$Mg$_{41}$	-	797	E	L	0.8	10.4	88.8
L+ SmMg$_3$ ↔ Laves_C15 + SmMg$_5$	-	821	U	L	1.2	12.6	86.2
L +Sm$_3$Al$_{11}$ + Laves_C15 ↔SmAl$_3$	-	1416	P	L	75.3	18.3	6.4
L ↔ HCP_A3+ Gamma+SmAl$_3$	-	712	E	L	29.78	0.02	70.2
L + FCC↔ Beta+SmAl$_3$	-	724	U	L	62.68	0.08	37.24
L + Beta ↔Gamma+SmAl$_3$	-	724	U	L	59.99	0.07	39.94
L ↔ HCP_A3+ Laves_C15+SmAl$_3$	-	880	E	L	7.4	0.3	92.3

† P: peritectic, U: quasiperitectic, E: eutectic

Compared to Al–Mg–La, Al–Mg–Ce, Al–Mg–Pr and Al–Mg–Nd systems, Al–Mg–Sm system exhibits three dissimilarities. Firstly, no ternary compound was reported for the Al–Mg–Sm system, while one ternary compound with similar composition in the Al-rich part was reported for the Al–Mg–La, Al–Mg–Ce, Al–Mg–Pr and Al–Mg–Nd systems. It is worth noting that Sm (rhombohedral) has a different structure from La, Ce, Pr and Nd elements, all of which have a double hexagonal close-packed structure at low temperature. Secondly, there was almost no solid solubility of Mg in Laves_C15 (almost pure Al_2Sm) phase, contrary to Al–Mg–La, Al–Mg–Ce, Al–Mg–Pr and Al–Mg–Nd systems, where a miscibility gap would occur in Laves_C15 phase at low temperature (< 800 K). Although the topology of the Al–Mg–Sm isothermal section at 673 K is different between the present study and Jia *et al.* [8], there is no contradiction to the reported three-phase equilibira of Zheng *et al.* [35] for the alloys labeled as 8 and 9 in the Figure 8.47. Finally, Sm_3Al_{11} exist only at high temperature, different from La_3Al_{11}, Ce_3Al_{11}, Pr_3Al_{11} and Nd_3Al_{11}, which are stable down to room temperature.

Generally, the calculated isothermal section at 673 K shows satisfactory agreement with the experimental data of Zheng *et al.* [35].

8.5   Conclusions

Thermodynamic evaluations and optimizations of the Al–Mg–RE (RE= La, Ce, Pr, Nd, Sm) systems have been systematically carried out on the basis of the literature information and new experimental results from this work. The Al–Mg–Pr and Al–Mg–Nd systems were optimized for the first time using a systematic approach. Similar model parameters were used for these five ternary systems. It was pointed out that previous thermal analysis data interpreted as liquidus temperature by Odinaev *et al.* [19; 26; 30; 33] are much lower than the experimental data from [6; 7] which is preferred in the present study. The Miedema's model was used to calculate enthalpies of formation for the ternary compounds and metastable phases $REAl_{12}$ ($CeMg_{12}$-oI338), RE_2Al_{17} ($Ni_{17}Th_2$-hP38), and RE_5Al_{41} (Ce_5Mg_{41}-tI92). The entropies of formation of these metastable phases are interpolated between Al and stable RE_3Al_{11} phases. The difference in enthalpy of formation for Mg_3RE phase between two different strucutures (metastable Ni_3Sn-hP8

and stable BiF_3-cF16) was assumed to be the same as those from First-Principles by Tao *et al*. [57]. The calculated phase equilibria in the designated equilibrated-alloys agree well with the experiments carried out in the present investigation. The optimized phase diagrams agreed well with our key experiments. No ternary parameters were used for the ternary systems. The extrapolation from the binary systems produced a satisfactory agreement with the ternary experimental data, thus indicating accurate Gibbs energy data sets of binary phases.

8.6 Acknowledgments

8.7 References

[1]   Z. Yang, J.P. Li, J.X. Zhang, G.W. Lorimer, J. Robson, Acta Metall. Sin.(Engl. Lett.) 21 (2008) 313-328.

[2]   J. Gnobner, R. Schmid-Fetzer, Scr. Mater. 63 (2010) 674-679.

[3]   G. Pettersen, H. Westengen, R. Hoier, O. Lohne, Materials Science and Engineering A 207 (1996) 115-120.

[4]   K. Hantzsche, J. Bohlen, J. Wendt, K.U. Kainer, S.B. Yi, D. Letzig, Scr. Mater. 63 (2010) 725-730.

[5]   S. Yi, J. Bohlen, F. Heinemann, D. Letzig, Acta Mater. 58 (2010) 592-605.

[6]   M. Hosseinifar, D.V. Malakhov, J. Alloys Compd. 505 (2010) 459-466.

[7]   J. Grobner, D. Kevorkov, R. Schmid-Fetzer, Intermetallics 10 (2002) 415-422.

[8]   B.R. Jia, L.B. Liu, D.Q. Yi, Z.P. Jin, J.F. Nie, J. Alloys Compd. 459 (2008) 267-273.

[9]   P. Chartrand, École Polytechnique de Montréal, Canada (2006) unpublished research.

[10]   L.-L. Jin, Y.-B. Kang, P. Chartrand, C.D. Fuerst, Calphad 35 (2011) 30-41.

[11]   Y.B. Kang, L. Jin, P. Chartrand, A. Gheribi, K. Bai, P. Wu, Calphad (2012) In press.

[12]   Y.-B. Kang, A.D. Pelton, P. Chartrand, C.D. Fuerst, Calphad 32 (2008) 413-422.

[13]   L.-L. Jin, P. Chartrand, Y.-B. Kang, C.D. Fuerst, Calphad 34 (2010) 456-466.

[14]   Y.-B. Kang, École polytechnique de Montréal, Canada (2008) unpublished work.

[15]   P. Rogl, Ternary Alloys: a comprehensive compendium of evaluated constitutional data and phase diagrams. in: G.Petzow, G. Effenberg, (Eds.), Weinheim, New York, 1988.

[16]   V. Raghavan, J. Phase Equilib. Diffus. 29 (2008) 270-271.

[17]   O.S. Zarechnyuk, V.V. Kinzhibalo, A.T. Tyvanchuk, R.M. Rykhal, Izvestiya Akademii Nauk SSSR, Metally (1981) 221-223.

[18]   K.O. Odinaev, I.N. Ganiev, V.V. Kinzhibalo, A.T. Tyvanchuk, Izv. Vyssh. Uchebn. Zaved., Tsvetn. Metall. (1988) 81-85.

[19]   K.O. Odinaev, I.N. Ganiev, Metally (1995) 161-166.

[20]   C. Guo, Z. Du, J. Alloys Compd. 385 (2004) 109-113.

[21]   B. Darriet, M. Pezat, A. Hbika, P. Hagenmuller, Mater. Res. Bull. 14 (1979) 377-385.

[22]   C. Zheng, Y. Xing, J. Qian, Y. Ye, Jinshu Xuebao 19 (1983) A515-A520.

[23]   K.O. Odinaev, I.N. Ganiev, V.V. Kinzhibalo, K.K. Kurbanov, Izv. Vyssh. Uchebn. Zaved., Tsvetn. Metall. (1989) 75-77.

[24]   O.S. Zarechnyuk, P.I. Kripyakevich, Izvestiya Akademii Nauk SSSR, Metally (1967) 188-190.

[25]   Z. Cui, R. Wu, Jinshu Xuebao 20 (1984) B323-B331.

[26]   K.O. Odinaev, I.N. Ganiev, A.Z. Ikromov, Metally (1996) 165-169.

[27]   C. Zheng, Y. Wu, J. Qian, Y. Ye, Jinshu Xuebao 22 (1986) B63-B67.

[28]   V. Raghavan, J. Phase Equilib. Diffus. 29 (2008) 275-277.

[29]   K.O. Odinaev, I.N. Ganiev, V.V. Kinzhibalo, Izv. Vyssh. Uchebn. Zaved., Tsvetn. Metall. (1988) 91-94.

[30]   K.O. Odinaev, I.N. Ganiev, A.Z. Ikromov, Metally (1996) 170-173.

[31]   V. Raghavan, J. Phase Equilib. Diffus. 29 (2008) 272-274.

[32]   K.O. Odinaev, I.N. Ganiev, V.V. Kinzhibalo, A.T. Tyvanchuk, Izv. Vyssh. Uchebn. Zaved., Tsvetn. Metall. (1988) 94-97.

[33]   K.O. Odinaev, I.N. Ganiev, A.Z. Ikromov, Metally (1996) 168-172.

[34]   V. Raghavan, J. Phase Equilib. Diffus. 30 (2009) 69-70.

[35]   C. Zheng, L. Chen, Y. Ye, Jinshu Xuebao 23 (1987) B117-B120.

[36]   F.R.D. Boer, R. Boom, W.C.M. Mattens, A.R. Miedema, A.K. Niessen, Cohesion In Metals: Transition Metal Alloys, North-Holland, New York, 1988.

[37]   H. Bakker, Mater. Sci. Found. 1 (1998) i-ii, v, vii-x, 1-78.

[38]   S.P. Sun, D.Q. Yi, H.Q. Liu, B. Zang, Y. Jiang, J. Alloys Compd. 506 (2010) 377-387.

[39]   J. Basu, B.S. Murty, S. Ranganathan, J. Alloys Compd. 465 (2008) 163-172.

[40]   A.D. Pelton, Calphad 25 (2001) 319-328.

[41]   A.B. Shubin, K.Y. Shunyaev, Rasplavy (2010) 44-50.

[42]   C.W. Bale, P. Chartrand, S.A. Degterov, G. Eriksson, K. Hack, R. Ben Mahfoud, J. Melancon, A.D. Pelton, S. Petersen, CALPHAD: Comput. Coupling Phase Diagrams Thermochem. 26 (2002) 189-228.

[43]   C. Bale, A. Pelton, W. Thompson, Factsage thermochemical software and databases, 2008.

[44]   A.T. Dinsdale, Calphad 15 (1991) 317-425.

[45]   A.D. Pelton, S.A. Degterov, G. Eriksson, C. Robelin, Y. Dessureault, Metall. Mater. Trans. B 31B (2000) 651-659.

[46]   Y.-B. Kang, A.D. Pelton, P. Chartrand, P. Spencer, C.D. Fuerst, Metall. Mater. Trans. A 38 (2007) 1231-1243.

[47]   Y.-B. Kang, A.D. Pelton, P. Chartrand, P. Spencer, C.D. Fuerst, J. Phase Equilib. Diffus. 28 (2007) 342-354.

[48]   Y.-B. Kang, I.-H. Jung, S.A. Decterov, A.D. Pelton, H.-G. Lee, ISIJ Int. 44 (2004) 975-983.

[49]   I.-H. Jung, S.A. Decterov, A.D. Pelton, J. Eur. Ceram. Soc. 25 (2005) 313-333.

[50]   A. Pelton, P. Chartrand, Metall. Mater. Trans. A 32 (2001) 1361-1383.

[51]   P. Chartrand, A. Pelton, Metall. Mater. Trans. A 32 (2001) 1385-1396.

[52]   P. Waldner, A.D. Pelton, Metall. Mater. Trans. B 35B (2004) 897-907.

[53]   M. Hillert, J. Alloys Compd. 320 (2001) 161-176.

[54]   A. Saccone, D. Macciò, J.A.J. Robinson, F.H. Hayes, R. Ferro, J. Alloys Compd. 317-318 (2001) 497-502.

[55]   M.C. Gao, A.D. Rollett, M. Widom, Phys. Rev. B: Condens. Matter Mater. Phys. 75 (2007) 174120/174121-174120/174116.

[56]   X. Tao, First-principles calculations on the thermodynamic properties of Al-Rare Earth and Mg-Rare Earth alloys, materials science, Central south university, Changsha, China, 2008, pp. 133.

[57]   X. Tao, Y. Ouyang, H. Liu, Y. Feng, Y. Du, Y. He, Z. Jin, J. Alloys Compd. 509 (2011) 6899-6907.

[58]   I. Ansara, A.T. Dinsdale, M.H.Rand, (Eds.), COST 507: Thermochemical Database for Light Metal Alloys, Luxembourg, 1998.

[59]   P. Liang, H.-L. Su, P. Donnadieu, M.G. Harmelin, A. Quivy, P. Ochin, G. Effenberg, H.J. Seifert, H.L. Lukas, F. Aldinger, Z. Metallkd. 89 (1998) 536-540.

[60]   S.H. Zhou, R.E. Napolitano, Acta Mater. 54 (2006) 831-840.

[61]   R. Vogel, T. Heumann, Z. Metallkd. 38 (1947) 1-8.

[62]   K.A. Gschneidner, V.K. Pecharsky, J. Cho, S.W. Martin, Scr. Mater. 34 (1996) 1717-1722.

[63]   K.O. Odinaev, I.N. Ganiev, Izv. Vyssh. Uchebn. Zaved., Tsvetn. Metall. (1990) 90-95.

[64]   A. Saccone, A.M. Cardinale, S. Delfino, R. Ferro, Intermetallics 1 (1993) 151-158.

[65]   S. Delfino, A. Saccone, R. Ferro, Metall. Trans. A 21A (1990) 2109-2114.

[66]   S. Delsante, R. Raggio, G. Borzone, R. Ferro, J. Phase Equilib. Diffus. 28 (2007) 240-242.

[67]   L.-L. Jin, P. Chartrand, in preparation (2012).

CHAPTER 9   **THERMODYNAMIC EVALUATIONS AND OPTIMIZATIONS OF AL–MG–RE (RE: GD, DY, HO, ER, TB) SYSTEMS**

Similar to the Al–Mg–light rare earth systems, which were optimized systematically in Chapter 8, the parameters of the thermodynamic models for the phases in the Al–Mg–RE (RE= Gd, Tb, Dy, Ho and Er) ternary systems were optimized in a systematic and similar approach. The similarity between all the Mg–Al–RE ternary systems is expected.

The thermodynamic evaluations and modeling of Al–Mg–heavy RE (heavy RE= Gd, Tb, Dy, Ho, Er) were made in the present study. The enthalpies of formation for the ternary compounds were estimated using the Miedema model. A detailed description of the Miedema model is given in the paper of Jin *et al*. (Jin et al., 2012).

9.1 Literature data on the Al–Mg–RE (Gd, Dy, Ho, Er, Tb) systems

The Al–RE (RE= Gd, Dy, Ho, Er, Tb) binary systems have been studied by several researchers (Cacciamani et al., 2003b; Franke & Neuschütz, 2007; Gröbner et al., 2001; Jin et al., 2010; Jin et al., 2011; Zhou & Napolitano, 2008). The recent thermodynamic optimizations on the Al–RE binary systems by our research group (Jin et al., 2010), where the modified quasi-chemical model has been used for the liquid solution, have been adopted in the present study. The detailed literature reviews on Al–RE systems are omitted here. However, it was necessary to re-optimize slightly the binary parameters for the REAl$_2$ and REAl$_3$ phases in order to reproduce the experimentally determined ternary phase equilibria in the Al–Mg–RE (RE= Gd, Dy, Ho, Er, Tb) systems. Consequently, the parameters for the liquid in the Al–rich side have been slightly adjusted to fit the binary eutectic temperatures determined by experiments. The Mg–RE (RE= Gd, Dy, Ho, Er, Tb) binary systems have been reviewed by Nayeb-Hashemi and J.B. Clark (Nayeb-Hashemi & Clark, 1988a, 1988b, 1988c, 1988d, 1988f). The thermodynamic

optimizations of Mg–RE systems from Kang *et al.* (Kang, 2008) are adopted in the present study. The crystallographic structures and phases in the Mg–RE systems are shown in Table 9.1; the corresponding information for the Al–RE systems are given in Jin *et al.* (Jin et al., 2010).

Table 9.1 Crystallographic structures of phases in the Mg–Gd, Mg–Tb, Mg–Dy, Mg–Ho and Mg–Er systems (Kang, 2008)

Systems	Phases	Struktur-	Prototype	Pearson	Space
Mg–Gd	$GdMg_5$	-	$GdMg_5$	cF448	-
	$GdMg_3$	$D0_3$	BiF_3	cF16	$Fm\overline{3}m$
	$GdMg_2$	C15	$MgCu_2$	cF24	$Fd\overline{3}m$
	GdMg	B2	CsCl	cP2	$Pm\overline{3}m$
Mg–Tb	Tb_5Mg_{24}	A12	αMn	cI58	$I\overline{4}3m$
	$TbMg_3$	$D0_3$	BiF_3	cF16	$Fm\overline{3}m$
	$TbMg_2$	C14	$MgZn_2$	hP12	$P6_3/mmc$
	TbMg	B2	CsCl	cP2	$Pm\overline{3}m$
Mg–Dy	Dy_5Mg_{24}	A12	αMn	cI58	$I\overline{4}3m$
	$DyMg_3$	$D0_3$	BiF_3	cF16	$Fm\overline{3}m$
	$DyMg_2$	C14	$MgZn_2$	hP12	$P6_3/mmc$
	DyMg	B2	CsCl	cP2	$Pm\overline{3}m$
Mg–Ho	Ho_5Mg_{24}	A12	αMn	cI58	$I\overline{4}3m$
	$HoMg_2$	C14	$MgZn_2$	hP12	$P6_3/mmc$
	HoMg	B2	CsCl	cP2	$Pm\overline{3}m$
Mg–Er	Er_5Mg_{24}	A12	αMn	cI58	$I\overline{4}3m$
	$ErMg_2$	C14	$MgZn_2$	hP12	$P6_3/mmc$
	ErMg	B2	CsCl	cP2	$Pm\overline{3}m$

The Al–Mg–Gd system was previously investigated by Rokhlin *et al.* (Rokhlin et al., 1996, 1997). Sixty alloys, with starting materials of 99.99% Al, 99.85% Gd and 99.96% Mg, were investigated by optical microscopy, scanning electron microscopy and X-ray diffraction techniques. The phase relationships were established in the Al–Mg–GdMg$_5$–GdAl$_2$–Al fields at 673 K. One ternary compound Al$_4$GdMg [noted as Al$_2$Gd$_{0.5}$Mg$_{0.5}$ in (Rokhlin et al., 1996)], indexed as Laves_C14 (MgZn$_2$-type), was reported. Three vertical sections were constructed respectively at constant Al compositions of 50 wt%, 70 wt% and along the Mg–GdAl$_2$ join. Subsequently, the Al–Mg–Gd system was studied by three key experiments with arc-melted samples and thermodynamically optimized by Gröbner *et al.* (Gröbner et al., 2000; Gröbner et al., 2001) using the Bragg-Williams approximation for the mixing entropy of the liquid phase. This investigation was mainly based on the experimental data of Rokhlin *et al.* (Rokhlin et al., 1996, 1997). It was claimed (Gröbner et al., 2001) that no solid solubility was detected by measurement of d-values of the binary GdMg, GdMg$_5$, GdAl$_2$, GdAl$_3$ and ternary Al$_4$GdMg phases. The melting temperature of this ternary phase was assumed to be approximately 1073 K. Four vertical sections at constant compositions of 9 wt% Mg, 50 wt% Al, 70 wt% Al and along the Mg–GdAl$_2$ join were calculated together with the liquidus projection and the isothermal section at 673 K (Gröbner et al., 2001). Recently, De Negri *et al.* (De Negri et al., 2003) prepared five induction-melted alloys and investigated them by optical microscopy, X-ray diffraction and electron probe microanalysis. It was found that the BCC_B2 Gd(Al,Mg) solid solution has been extended to the ternary field up to 33-34 at.% Al, while the Laves_C15 (Al, Mg)$_2$Gd solid solution contains up to 9 at.% Mg. This differs from the findings of Gröbner *et al.* (Gröbner et al., 2001). The ternary phase Al$_4$GdMg has been indexed as a hP24-MgNi$_2$ (Laves_C36) phase, and the computed formation temperature for the ternary phase Al$_4$GdMg is approximately 723 K, about 350 K lower than the calculated value from Gröbner *et al.* (Gröbner et al., 2001). The Al–Mg–Gd system was re-optimized by Cacciamani *et al.*(Cacciamani et al., 2003b) based on the experimental results from De Negri *et al.* (De Negri et al., 2003), using the Bragg-Williams approximation for the mixing entropy of the liquid phase.

In the Al–Mg–Dy system, no experimental information is available except the results of De Negri *et al.* (De Negri et al., 2003). They induction-melted eight ternary alloys with starting metals of 99.999 wt.% Al, 99.99 wt.% Mg and 99.9 wt.% Dy. The samples were annealed at 673 K for five

weeks and then quenched in cold water. They were characterized by the optical and electron microscopy, X-ray powder diffraction and electron probe microanalysis. One ternary compound $Al_2Dy_{0.36}Mg_{0.64}$ (Laves_C36, $MgNi_2$-type) was reported at this annealing temperature 673 K and the peritectic formation at about 803 K for this ternary phase was reported according to their DTA experiments. The BCC_B2 (mainly DyMg) solid solution dissolves up to 35 at. % Al, and the Laves_C15 (mainly $DyAl_2$) solid solution extends up to 15 at. % Mg. The other binary phases, Dy_5Mg_{24}, DyAl, Dy_3Al_2, Dy_2Al showed very small solid solubilities for the third element Al or Mg. Moreover, a few phase equilibria at 673 K were established by experiments with their equilibrated alloys.

Like the Al–Mg–Dy system, no experimental information is available for the Al–Mg–Ho system except experimental data from De Negri *et al.* (De Negri et al., 2003). The same experimental procedure (De Negri et al., 2003) was employed for the Al–Mg–Ho system. They induction-melted seven ternary alloys with starting metals of 99.999 wt. % Al, 99.99 wt. % Mg and 99.9 wt. % Ho. The samples were annealed at 673 K for five weeks and then quenched in cold water. This was followed by optical and electron microscopy, X-ray powder diffraction and electron probe microanalysis. Differential thermal analysis was also performed. One ternary compound $Al_2Ho_{0.39}Mg_{0.61}$ (Laves_C36, $MgNi_2$-type) was reported at this annealing temperature 673 K and the peritectic formation at about 723 K for this ternary phase was suggested by their DTA experiments and results of microstructural analysis. The BCC_B2 (mainly HoMg) solid solution dissolves up to 35 at. % Al, and the Laves_C15 (mainly $HoAl_2$) solid solution extends up to 10 at. % Mg. A few auxiliary phase equilibria were established.

As for the Al–Mg–Er system, no information is available except experimental data from Saccone *et al.* (Saccone et al., 2002), the same research group who investigated the Al–Mg–Dy and Al–Mg–Ho systems. Saccone *et al.* (Saccone et al., 2002) induction-melted 33 ternary alloys with starting metals of 99.999 wt.% Al, 99.9 wt.% Mg and 99.9 wt.% Er. The samples were annealed at 673 K for 500-850 h and then quenched in cold water. This was followed by optical and electron microscopy, X-ray powder diffraction and electron probe microanalysis. Differential thermal analysis was also performed. One ternary compound at the composition of

$Al_{66.7}Er_{10}Mg_{23.3}$ (Laves_C14, $MgZn_2$-type) was reported at this annealing temperature 673 K and the peritectic formation at 803 K for this ternary phase was shown by their DTA experiments and microstructural analysis. The BCC_B2 (mainly ErMg) solid solution dissolves up to 39 at. % Al, and the Laves_C15 (mainly $ErAl_2$) solid solution extends up to 10 at. % Mg.

For the Al–Mg–Tb system, no experimental information is available except results from Strucheva and Novozhenov (Strucheva & Novozhenov, 2009) who studied the Al and Mg corners of the Al–Mg–Tb system by X-ray diffraction and differential thermal analysis (DTA). The presence of the $Tb(Mg_{0.15}Al_{0.85})_2$ solid solution was established.

9.2 Thermodynamic assessments and discussion

All the present optimizations have been carried out by means of FactSage^{TM} thermodynamic software (Bale et al., 2002; C. Bale et al., 2008). The thermodynamic properties of pure Al and rare earths (Gd, Dy, Ho and Er) were taken from the SGTE database (Dinsdale, 1991) and Kang *et al.* (Kang et al., 2008a). The Kohler interpolation method (Pelton, 2001) was employed and no ternary interaction parameter was used for the Al–Mg–Gd, Al–Mg–Dy, Al–Mg–Ho, Al–Mg–Er and Al–Mg–Tb systems. Table 9.2 shows the reported crystal structures and selected thermodynamic models for the ternary phases in the systems studied. The ternary phases (Al_4GdMg, Al_4TbMg, $Al_{10}Dy_2Mg_3$ ($Al_2Dy_{0.36}Mg_{0.64}$ in (De Negri et al., 2003)), $Al_{10}Ho_2Mg_3$ ($Al_2Ho_{0.39}Mg_{0.61}$ in (De Negri et al., 2003)) and $Al_{20}Er_3Mg_7$ ($Al_{66.7}Er_{10}Mg_{23.3}$ in (Saccone et al., 2002))) are considered to be stoichiometric, although a narrow homogeneity range of their existence could not be ruled out. The CEF is used for all the solid solutions, and the sublattices species for each one is given in Table 9.2.

Table 9.2 Thermodynamic models for phases in the Mg–Al–RE systems (RE= Gd, Tb, Dy, Ho, Er)

Phase	Struktur-bericht	Prototype	Pearson symbol	Model*
Liquid	-	-	-	QC
Laves_C15	$C15$	Cu_2Mg	$cF24$	$(Al, Mg, RE)(Al, Mg, RE)_2$,
BCC_B2	$B2$	CsCl	$cP2$	$(Mg, RE)(Al, Mg)$, CEF
Gamma	A12	αMn	$cI58$	$(Mg, RE)_{10}(Al, Mg)_{24}(Al, Mg)_{24}$
REAl	-	ErAl	$oP16$	$(RE)(Al)$, CEF
RE3Al2	-	Zr_3Al_2	$tP20$	$(RE)_3(Al)_2$, CEF
RE2Al	C23	Co_2Si	$oP12$	$(RE)_2(Al)$, CEF
REMg3	$D0_3$	BiF_3	$cF16$	$(RE)(Mg)_3$, CEF
REAl3	-	Al_3Ho	$hR60$	$(Dy, Ho)(Al)_3$, CEF
Al_4GdMg	C36	$MgNi_2$	$hP24$	ST
Al_4TbMg	-	-	-	ST
$Al_{10}Dy_2Mg_3$	C36	$MgNi_2$	$hP24$	ST
$Al_{10}Ho_2Mg_3$	C36	$MgNi_2$	$hP24$	ST
$Al_{20}Er_3Mg_7$	C14	$MgZn_2$	$hP12$	ST

*QC = Modified Quasichemical Model, ST = Stoichiometric compound, CEF = Compound Energy Formalism

It is worth noting that Mg-heavy RE binary systems contain the "RE5Mg24" phase (RE = Tb, Dy, Ho, Er, Tm, Lu, Y) with the cI58-αMn structure. In the Mg–Y system studied by Kang *et al*. (Kang et al., 2007b), this phase was modeled using a three sub-lattice CEF with the

$(Mg)_{24}(Mg,Y)_4(Y)_1$ formula after study of the site occupations by Fabrichnaya *et al*. (Fabrichnaya et al., 2003). However, the crystal structure (cI58-αMn) of this phase is identical to that of the Gamma ($Al_{12}Mg_{17}$) phase in Mg–Al binary system. Since the present study is a part of a wider research program to develop a consistent thermodynamic database of Mg–Al–RE systems, both the "RE5Mg24" phase and the "Gamma ($Al_{12}Mg_{17}$)" phase appear at the same time in the Mg–Al–RE ternary systems. It is necessary to combine these two phases using a single model equation which has also been emphasized by Ansara *et al*. (Ansara et al., 1997). Therefore, in the present study, it was decided that the "RE5Mg24" phase and Gamma ($Al_{12}Mg_{17}$) phase were to be modeled as one single phase (Gamma) using a three sub-lattice CEF with the $(Mg, RE)_{10}(Al, Mg)_{24}(Al, Mg)_{24}$ formula, after Ansara *et al*. (Ansara et al., 1997).

For the BCC_B2 phase, the CEF model with the (Mg, Al)(Mg, Gd, Tb, Dy, Ho, Er) formula as used in the Al–Mg–light rare earth systems (Jin & Chartrand, 2011a) is adopted in the present study. For the other solid solutions (REAl, RE3Al2, RE2Al, REAl3), it is assumed that RE elements mix ideally on one sub-lattice, e.g., (Gd, Tb, Dy, Ho, Er)(Al) in the "REAl" phase (ErAl-*oP*16).

For the REMg$_3$ (BiF$_3$-*cF*16) phase, the enthalpies of formation of HoMg$_3$ and ErMg$_3$ were assumed to be those calculated by Tao *et al*. (Tao et al., 2011) using First-Principles. The entropies of formation were interpolated between the stable Laves_C14 (REMg$_2$) and Gamma (RE$_5$Mg$_{24}$) phases; this was the same strategy used for the metastable end-members in the Al–Mg–light rare earth systems (Jin et al., 2012).

Shown in Table 9.3 are the optimized enthalpies of formation of the ternary phases together with calculations from the Miedema model, which was described in detail by Jin *et al*. (Jin & Chartrand, 2011a). These calculated results were used in the course of the thermodynamic optimizations. The entropies of formation of these ternary phases at 298 K were assumed to be the contributions from the Al-richest compound REAl$_3$ (RE= Gd, Tb, Dy, Ho, Er) and Mg_xAl_{1-x} mixture since the ternary phases are in the Mg–Al–REAl$_3$ field.

Table 9.3 Optimized model parameters for the ternary compounds at 298 K (ΔH_f from the present optimizations and from the Miedema model).

Compounds	ΔH_{298} (kJ/mole of atoms)		S_{298} (J/g-atom-K)	Cp (J/mol-K)
	Optimized	Miedema		
Al_4GdMg	-28.4	-30.1	209.4	$C_p= 4C_p(Al,FCC–A1)+ C_p (Gd, HCP–A3)+ C_p (Mg, HCP–A3)$
Al_4TbMg	-29.2	-32.2	205.9	$C_p= 4C_p(Al,FCC–A1)+ C_p (Tb, HCP–A3)+ C_p (Mg, HCP–A3)$
$Al_{10}Dy_2Mg_3$ $(Al_2Dy_{0.36}Mg_{0.64})$	-23.8	-23.6	518.1	$C_p= 10C_p(Al,FCC–A1)+ 2C_p (Dy, HCP–A3)+ 3C_p (Mg, HCP–A3)$
$Al_{10}Ho_2Mg_3$ $(Al_2Ho_{0.39}Mg_{0.61})$	-23.6	-26.8	517.8	$C_p= 10C_p(Al,FCC–A1)+ 2C_p (Ho, HCP–A3)+ 3C_p (Mg, HCP–A3)$
$Al_{20}Er_3Mg_7$ $(Al_2Er_{0.3}Mg_{0.7})$	-18.1	-21.6	1013.4	$C_p= 20C_p(Al,FCC–A1)+ 3C_p (Er, HCP–A3)+ 7C_p (Mg, HCP–A3)$

For the Al–RE (RE= Gd, Tb, Dy, Ho, Er) systems, the stability of the $REAl_3$ and $REAl_2$ compounds (RE= Gd, Tb, Dy, Ho, Er) were slightly re-optimized from our previous optimizations (Jin et al., 2010) within 2 kJ/g-atom in order to fit three-phase equilibria Mg+Gamma+$REAl_2$ at 673 K in the respective ternary systems. Accordingly, the model parameters of the REAl phase and the liquid solution in the Al-rich side were slightly adjusted to fit the reported binary experimental data [found in (Jin et al., 2010)], if necessary. The modified phase diagrams of the Al–RE systems were shown in Appendix 4. The experimental data shown are from Buschow (Buschow, 1965b), Hackenberg *et al.* (Hackenberg et al., 2002) and Saccone *et al.* (Saccone et al., 2000) for the Al–Gd system, Drits *et al.* (Drits et al., 1978) for the Al–Tb system, Saccone *et al.* (Saccone et al., 2000) and Casteels (Casteels, 1967) for the Al–Dy system, Meyer (Meyer, 1966) for the Al–Ho system, Buschow (Buschow, 1965a) and Saccone *et al.* (Saccone et al., 2002) for the Al–Er system. Only the re-optimized thermodynamic model parameters of the binary systems are presented in Appendix 4. The thermodynamic model

parameters of binary systems studied, which are not listed in Appendix 4, are the same as those from Jin *et al*. (Jin et al., 2010).

The thermodynamic properties and phase diagrams of the Al–Mg–RE systems were optimized by combining the present study results and optimizations of the Al–RE systems (Jin et al., 2010) and Mg–RE systems (Kang, 2008) with the optimization results of the Al–Mg system by Chartrand (Chartrand, 2006). The parameters are given in Appendix 4. Short-range ordering was considered in these binary subsystems through use of the MQM for the liquid. The Gibbs energies of certain end members of the Laves_C14 phase were set to arbitrarily large values in order to ensure negligible solid solubility in the Al–Tb–Mg, Al–Dy–Mg, Al–Ho–Mg, Al–Er–Mg ternary systems. For other solid solutions, the Gibbs energies of the end members were taken either from the SGTE database (Dinsdale, 1991), or from our binary optimizations for the Al–RE (Jin et al., 2010) and Mg–RE (Kang, 2008) systems, or from estimation techniques. The model parameters used or optimized in the present study are shown in Table 9.4.

In general, the results of present optimized Al–Mg–Gd, Al–Mg–Dy, Al–Mg–Ho, and Al–Mg–Er systems are in good agreement with the experimental data from De Negri *et al.*(De Negri et al., 2003) and Saccone *et al.* (Saccone et al., 2002).

Table 9.4 Optimized model parameters for solid solutions (J/mole)

Laves_C15: (Al, Mg, Gd, Tb, Dy, Ho, Er)$_2$[Al, Mg, Gd, Tb, Dy, Ho, Er]
Gibbs energies of end members and parameters
G(Al:Al)　　= 3*GHSERAL* + 43,959 + 62.76T[a]
G(Mg:Mg)　= 3*GHSERMG* + 22,740[a]
G(Al:Mg)　= 2*GHSERAL* + *GHSERMG* −4,803 + 4.184T[a]
G(Mg:Al)　= 2*GHSERMG* + *GHSERAL* + 64,170[a]
G(Mg:Gd)　= 2*GHSERMG* + *GHSERGD* −43,630+10.9T[b]

G(Mg:Tb)	$= 2GHSERMG + GHSERTB -39{,}120+10.9T$
G(Mg:Dy)	$= 2GHSERMG + GHSERDY -34{,}826+10.9T$
G(Mg:Ho)	$= 2GHSERMG + GHSERHO -31{,}840+10.9T$
G(Mg:Er)	$= 2GHSERMG + GHSERER - 29{,}410+10.9T$
G(Al:Gd)	$= 2GHSERAL + GHSERGD -163{,}631+14.9T$
G(Al:Tb)	$= 2GHSERAL + GHSERTB -164{,}013+17.9T$
G(Al:Dy)	$= 2GHSERAL + GHSERDY -162{,}339+14.2T$
G(Al:Ho)	$= 2GHSERAL + GHSERHO -162{,}758+13.8T$
G(Al:Er)	$= 2GHSERAL + GHSERER -156{,}482+5.3T-9TlnT$
G(Gd:Al)	$=2GHSERGD + GHSERAL+15{,}000$
G(Tb:Al)	$=2GHSERTB + GHSERAL+15{,}000$
G(Dy:Al)	$=2GHSERGD + GHSERAL+15{,}000$
G(Ho:Al)	$=2GHSERHO + GHSERAL+15{,}000$
G(Er:Al)	$=2GHSERER + GHSERAL+15{,}000$
G(Gd:Mg)	$=2GHSERGD + GHSERMG+15{,}000$
G(Tb:Mg)	$=2GHSERTB + GHSERMG+15{,}000$
G(Dy:Mg)	$=2GHSERDY + GHSERMG+15{,}000$
G(Ho:Mg)	$=2GHSERHO + GHSERMG+15{,}000$
G(Er:Mg)	$=2GHSERER + GHSERMG+15{,}000$
L(Al,Mg:Gd) = +28,451; L(Al:Mg,Gd) = +12,552	
L(Al,Mg:Tb) = +27,196; L(Al:Mg,Tb) = +12,552	
L(Al,Mg:Dy) = 20,083; L(Al:Mg,Dy) = +12,552	
L(Al,Mg:Ho) = 22,175; L(Al:Mg,Ho) = +12,552	

L(Al,Mg:Er) = 22,594; L(Al:Mg,Er) = +12,552
Laves_C14: (Al, Mg, Gd, Tb, Dy, Ho, Er)$_2$[Al, Mg, Gd, Tb, Dy, Ho, Er]
Gibbs energies of end members and parameters
G(Al:Al)   = 3*GHSERAL* + 43,959 + 62.76T[(c)]
G(Mg:Mg) = 3*GHSERMG* + 23,373[(c)]
G(Al:Mg)   = 2*GHSERAL* + *GHSERMG* −6,039 + 46[(c)]
G(Mg:Al)   = 2*GHSERMG* + *GHSERAL* + 66,705[(c)]
G(Mg:Gd)   = 2*GHSERMG* + *GHSERGD* −41,840+14.6*T*
G(Mg:Tb)   = 2*GHSERMG* + *GHSERTB* −41,631+12.6*T*
G(Mg:Dy)   = 2*GHSERMG* + *GHSERDY* −38,174+9.1*T*
G(Mg:Ho)   = 2*GHSERMG* + *GHSERHO* −33,472+6.6*T*
G(Mg:Er)   = 2*GHSERMG* + *GHSERER* − 31,000+6.6*T*
G(Al:Gd)   = 2*GHSERAL* + *GHSERGD* −125,665+14.9*T*
G(Al:Tb)   = 2*GHSERAL* + *GHSERTB* −116,160+17.9*T*
G(Al:Dy)   = 2*GHSERAL* + *GHSERDY* −125,665+14.2*T*
G(Al:Ho)   = 2*GHSERAL* + *GHSERHO* −94,740+13.8*T*
G(Al:Er)   = 2*GHSERAL* + *GHSERER* −122,212+5.3*T-9TlnT*
G(Gd:Al)   =2*GHSERGD* + *GHSERAL*+15,000
G(Tb:Al)   =2*GHSERTB* + *GHSERAL*+15,000
G(Dy:Al)   =2*GHSERGD* + *GHSERAL*+15,000
G(Ho:Al)   =2*GHSERHO* + *GHSERAL*+15,000
G(Er:Al)   =2*GHSERER* + *GHSERAL*+15,000
G(Gd:Mg)   =2*GHSERGD* + *GHSERMG*+15,000

G(Tb:Mg)	$= 2GHSERTB + GHSERMG + 15{,}000$
G(Dy:Mg)	$= 2GHSERDY + GHSERMG + 15{,}000$
G(Ho:Mg)	$= 2GHSERHO + GHSERMG + 15{,}000$
G(Er:Mg)	$= 2GHSERER + GHSERMG + 15{,}000$
BCC_B2 (CsCl-type): (Al,Mg)[Mg, Gd, Tb, Dy, Ho, Er]	
G(Al:Gd)	$= GHSERAL + GHSERGD - 81{,}800 + 5.0T$
G(Al:Ho)	$= GHSERAL + GHSERHO - 79{,}000 + 3.3T$
G(Al:Er)	$= GHSERAL + GHSERER - 80{,}000 + 1.4T - 4.5\,TlnT$
G(Mg:Gd)	$= GHSERMG + GHSERGD - 30{,}000 + 7.3T$ [b]
G(Mg:Tb)	$= GHSERMG + GHSERTB - 27{,}196 + 6.1T$ [b]
G(Mg:Dy)	$= GHSERMG + GHSERDY - 27{,}900 + 6.1T$ [b]
G(Mg:Ho)	$= GHSERMG + GHSERHO - 25{,}732 + 6.1T$ [b]
G(Mg:Er)	$= GHSERMG + GHSERER - 24{,}058 + 6.1T$ [b]
G(Al:Mg)	$= GHSERAL + GHSERMG + 41{,}840$ [a]
G(Mg:Mg)	$= 2GHSERMG + 8{,}368$ [a]
L(Al,Mg:Gd) = -12,552	
L(Al,Mg:Tb) = -22,594	
L(Al,Mg:Dy) = -22,594	
L(Al,Mg:Ho) = -12,552	
L(Al,Mg:Er) = -12,552	
AlRE (ErAl-type) : (Al)[Gd, Tb, Dy, Ho, Er]	
G(Al:Gd)	$= GHSERAL + GHSERGD - 86{,}548 + 6.9T$ [d]
G(Al:Er)	$= GHSERAL + GHSERER - 84{,}000 + 1.4T - 4.5TlnT$ [d]

Al2RE3 (Al$_2$Zr$_3$-type): (Al)$_2$[Gd,Tb, Dy, Ho, Er]$_3$	
G(Al:Gd)	= 2$GHSERAL$ + 3$GHSERGD$-175,245+12.1T
G(Al:Er)	= 2$GHSERAL$ + 3$GHSERER$-180,000+2.4T-$9TlnT$[d]
AlRE2 (Co$_2$Si-type): (Al)[Gd,Tb, Dy, Ho, Er]$_2$	
G(Al:Gd)	= $GHSERAL$ + 2$GHSERGD$-88,496+5.6T[d]
G(Al:Er)	= $GHSERAL$ + 2$GHSERER$-91,000+1.1T-4.5$TlnT$[d]
Al3RE (Al$_3$Ho-type): (Al)$_3$[Dy, Ho]	
G(Al:Dy)	= 3$GHSERAL$ + $GHSERDY$ -163,488+6.4T
Mg3RE (BiF$_3$-type): (Mg)$_3$[Gd,Tb, Dy, Ho, Er]	
G(Mg:Gd)	= 3$GHSERMg$ + $GHSERGD$-55,140+14.7T[b]
G(Mg:Ho)	= 3$GHSERMg$ + $GHSERHO$ -24,800+6.9T
G(Mg:Er)	= 3$GHSERMg$ + $GHSERER$ -21,200+6.9T
[a] taken from Jin *et al.* (Jin et al. 2011),[b] taken from Kang *et al.* (Kang, 2008), [c] taken from Kang *et al.* (Kang, 2007), [d] taken from Jin *et al.* (Jin, 2010).	

9.2.1 The Al–Mg–Gd system

The Al–Mg–Gd system has been thermodynamically optimized by Grobner *et al.*(Gröbner et al., 2001) using no ternary interaction parameter for the liquid phase. No short-range ordering was considered and the Muggianu-type extrapolation (Pelton, 2001) was used for the ternary system. It was suggested (Gröbner et al., 2001) that the ternary compound Al$_4$MgGd is formed in a peritectic reaction at 1034 K; the experimental phase equilibria data in the range 0%-66.7 at.% Al in the Al–Gd system from Saccone *et al.* (Saccone et al., 2000) were not taken into consideration. Cacciamani *et al.*(Cacciamani et al., 2003b) optimized this system using their own experimental data with ternary interaction parameters for the liquid. In their study, the sublattice model was

used for the solution phases, no short-range ordering was considered in the model for the liquid and the Muggianu interpolation method was used for the ternary system.

In this work, a Kohler interpolation method (Pelton, 2001) was used for the ternary system. Two sublattices were used for the Laves_C15 phase and the BCC_B2 phase (solid solution of GdMg with extensive solubility of GdAl). The ternary compound Al_4GdMg has a $MgNi_2$ type structure (De Negri et al., 2003). It was assumed to be a stoichiometric (line) compound in the present study. The optimized model parameters are summarized in Table 9.4. The calculated invariant reactions in the Al–Gd–Mg system are listed in Table 9.5.

Table 9.5 Calculated invariant reactions in the Al–Mg–Gd system

Reaction	T (K)	Type[†]		Composition (at%)		
					Calc	
	Calc		Phase			
				Al	Gd	Mg
L + Laves_C15 ↔ AlGd + BCC_B2	1291	U	L	39.0	56.7	4.3
L + AlGd ↔ Al_2Gd_3+ BCC_B2	1191	U	L	31.2	66.0	2.8
L + Al_2Gd_3↔ $AlGd_2$+ BCC_B2	1160	U	L	27.4	69.1	3.5
L+ $AlGd_2$ ↔ HCP_A3+ BCC_B2	1110	U	L	20.7	74.1	5.2
L + HCP_A3+ BCC_A2 ↔ BCC_B2	1155	P	L	13.9	71.3	14.8
L + $GdMg_3$↔ Laves_C15 + $GdMg_5$	909	U	L	1.7	14.8	83.5
L ↔ Laves_C15 + $GdMg_5$ + HCP_A3	817	U	L	0.6	7.7	91.7
L ↔ FCC_A1+$GdAl_3$ + $GdAl_4Mg$	726	E	L	63.3	0.3	36.4
L ↔ FCC_A1+Beta + $GdAl_4Mg$	723	E	L	62.9	0.2	36.9

L ↔ Gamma+ Beta + GdAl₄Mg	723	E	L	60.1	0.2	39.7
L ↔ Gamma+ HCP_A3 + GdAl₄Mg	712	E	L	29.8	0.1	70.1

† P: peritectic, U: quasiperitectic, E: eutectic, D: degenerate

The Gibbs energy of the Al_4GdMg compound was optimized to reproduce the measured formation temperature around 723 K by De Negri et al. (De Negri et al., 2003) and phase equilibria at 673 K (De Negri et al., 2003; Gröbner et al., 2001; Rokhlin et al., 1997).

The calculated isothermal section of the Al–Gd–Mg ternary system at 673K is shown in Figure 9.1. The ternary phase Al_4GdMg (τ1) can be part of 2-phase equilibria and 3-phase equilibria with the following phases: (Al), Gamma ($Al_{12}Mg_{17}$), $Al_{30}Mg_{23}$, Beta (Al_3Mg_2), Laves_C15 (Al_2Gd), and Al_3Gd. It is in good agreement with the experimental data of Rokhlin et al. (Rokhlin et al., 1996) and De Negri et al.(De Negri et al., 2003), expect for the $Al_{30}Mg_{23}$ phase, which was not considered in the investigation of Rokhlin et al. (Rokhlin et al., 1996).
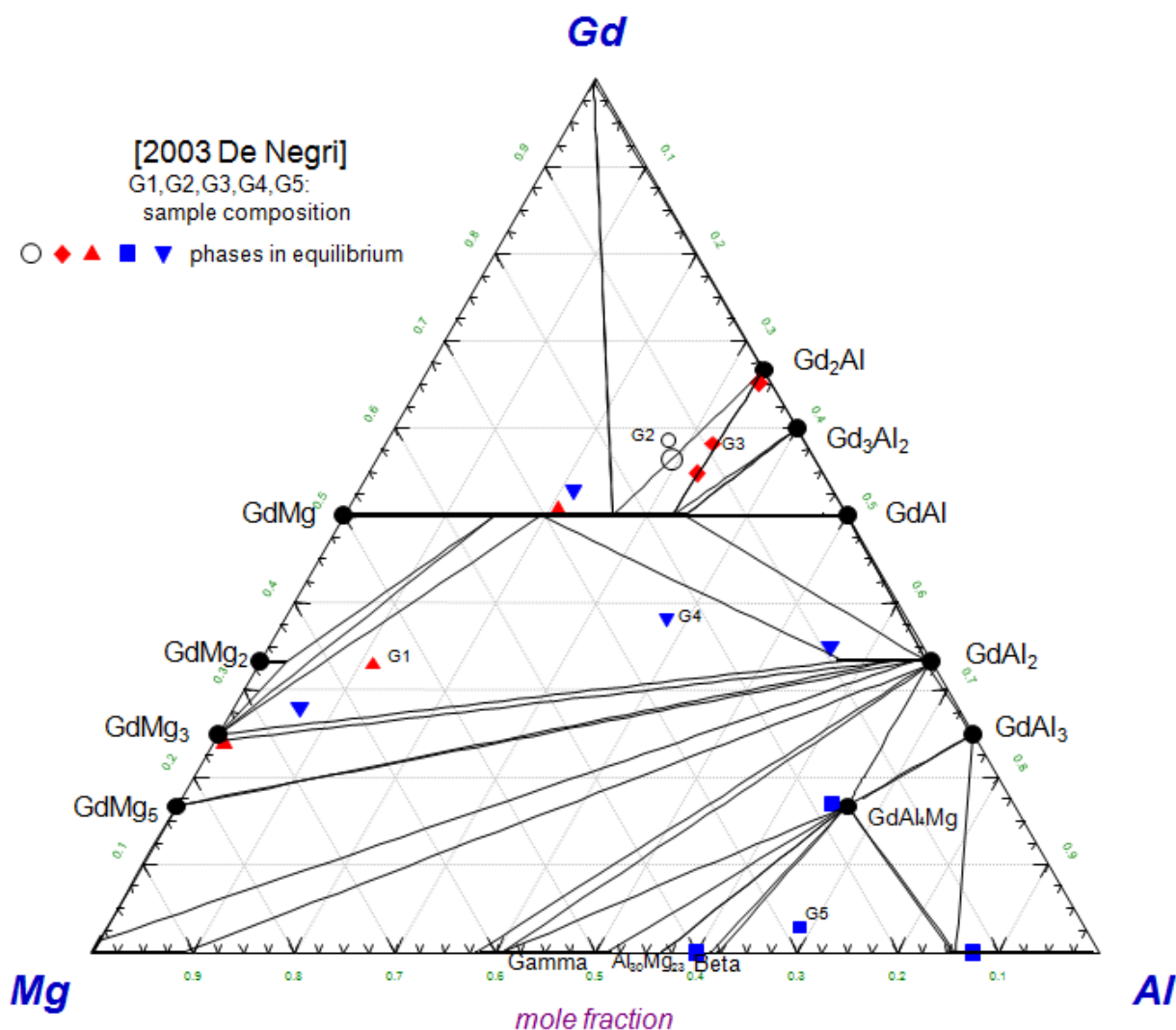
Figure 9.1 The calculated isothermal section of the Al–Gd–Mg ternary system at 673 K

The decomposition temperature of the ternary phase Al_4GdMg was calculated as 746 K, which is close to the value (about 723 K) suggested by De Negri *et al.*(De Negri et al., 2003). The solid solubility of Al in the GdMg (BCC_B2) phase, and of Mg in the $GdAl_2$ (Laves_C15) phase were calculated to be about 34 at.% and 9 at.%, respectively. They are in good agreement with the experimental investigations of De Negri *et al.*(De Negri et al., 2003), but differ from the experimental results of Gröbner *et al*. (Gröbner et al., 2001). The latter assumed no solid solubility in the GdMg (BCC_B2) and $GdAl_2$ (Laves_C15) phases. This disparity may be due to sample preparation. Gröbner *et al*. (Gröbner et al., 2001) arc-melted three samples (as-cast

state), then used X-ray powder diffraction analysis (XRD). The samples from De Negri *et al.*(De Negri et al., 2003) were annealed for 850 hours at 673 K. The calculated liquidus temperature at the composition of 38 wt % Al, 53 wt % Gd and 9 wt % (the third sample in Gröbner *et al.* (Gröbner et al., 2001) for which the DTA measurements were carried out) is not far from their reported temperature of 1527 K (T = 1440 K in our study), considering measurement error. It was pointed out by Gröbner *et al.* (Gröbner et al., 2001) that the calculated ternary liquidus temperatures were higher than what was assumed by Rokhlin *et al.*(Rokhlin et al., 1997), who did not measure as far as 1573 K. The thermal arrests below 973 K observed by Rokhlin *et al.*(Rokhlin et al., 1997) should relate to other phase equilibria. Similar discrepancies were also observed in calculations of the Al–Mg–La, Al–Mg–Ce, Al–Mg–Pr and Al–Mg–Nd (Jin & Chartrand, 2011b) systems. These differences might be due to experimental difficulties at high temperature; experimental details were not given by Rokhlin *et al.*(Rokhlin et al., 1997).
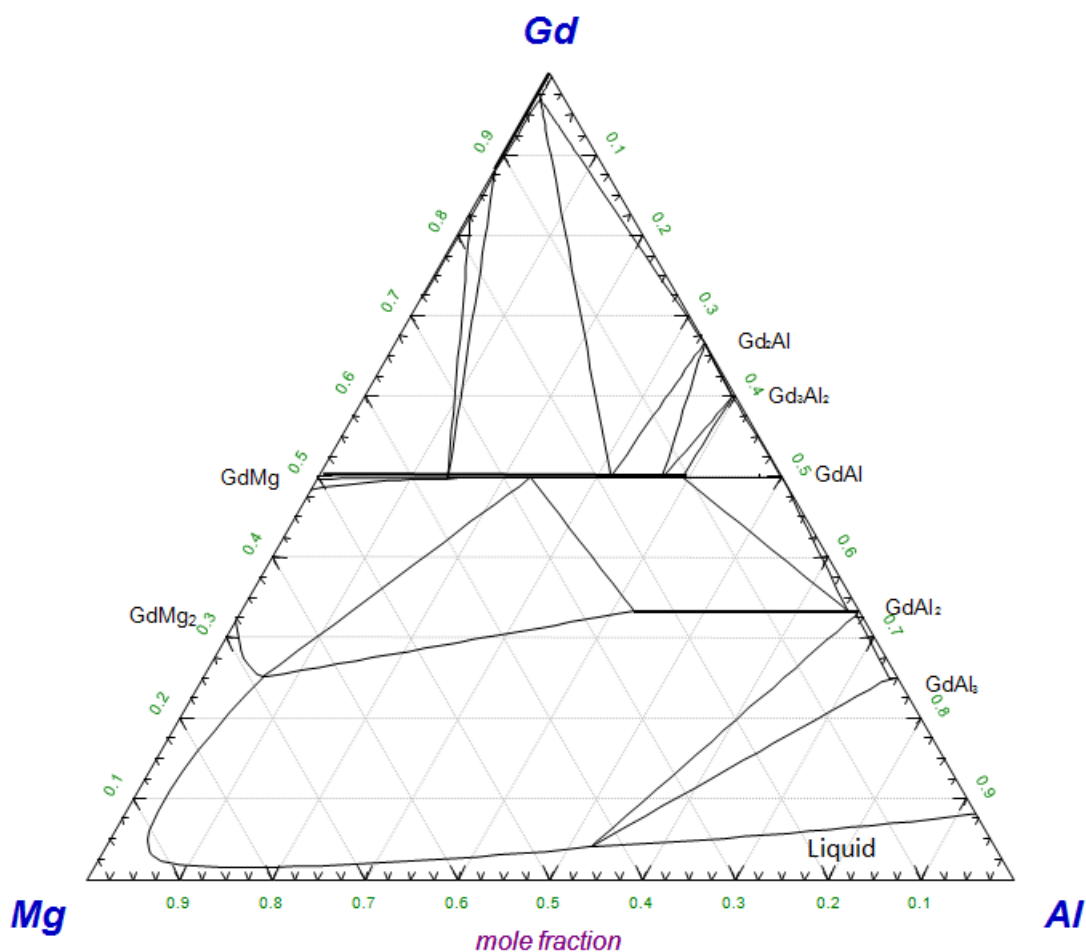
Figure 9.2 The calculated isothermal section of the Al–Gd–Mg ternary system at 1073 K

The calculated isothermal section of the Al–Gd–Mg ternary system at 1073 K is shown in Figure 9.2. It can be seen that the solid solubility limit of the Laves_C15 phase is greater than that at 673 K, as is also reported in Cacciamani *et al.* (Cacciamani et al., 2003b). GdMg and GdAl are only partially miscible since they have different crystal structures (CsCl and ErAl type, respectively). However, $GdMg_2$ and $GdAl_2$ form a Laves_C15 solid solution since they have the same structure (Cu_2Mg type).
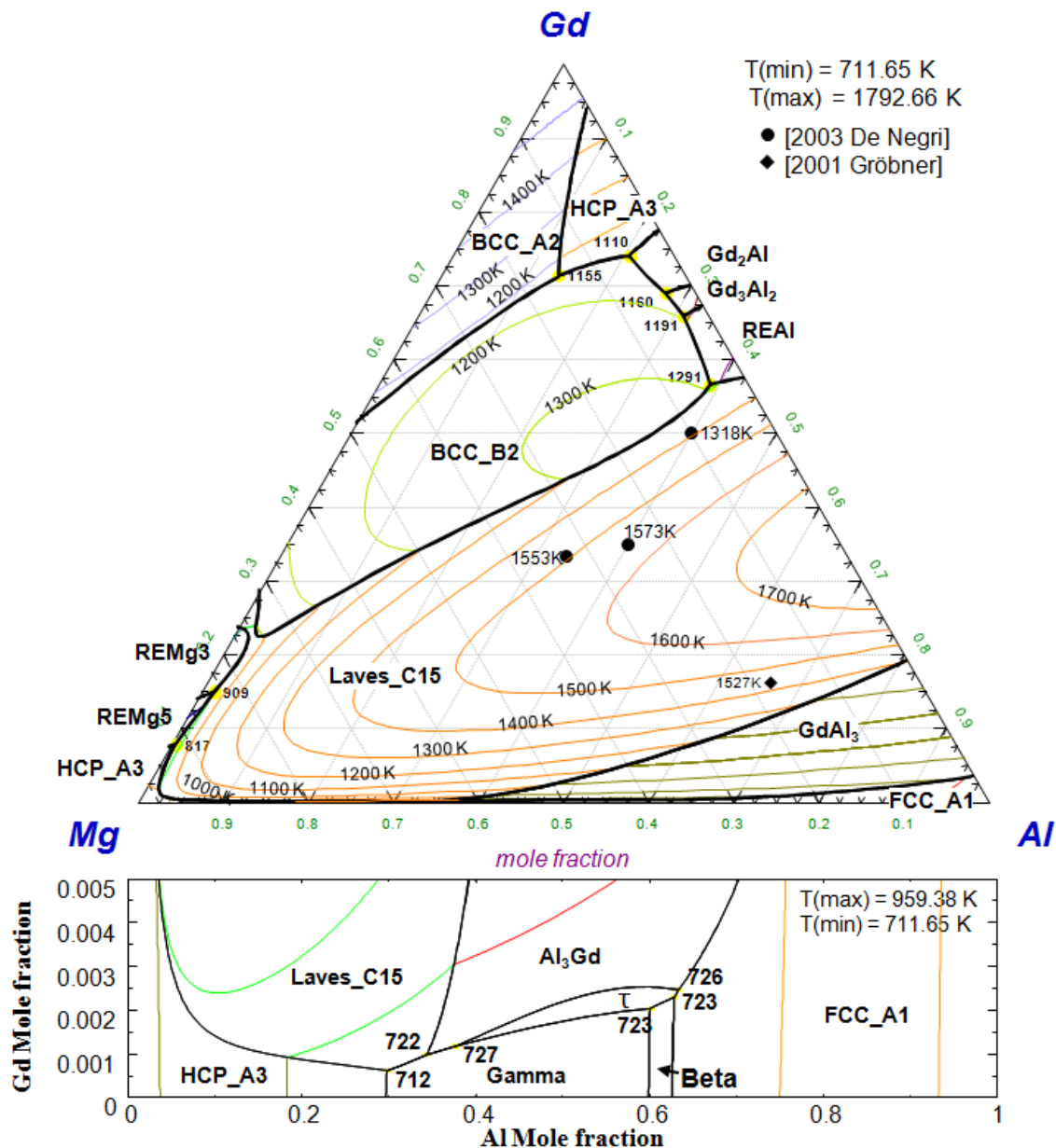
Figure 9.3 The calculated liquidus surface of the Al–Mg–Gd system with the experimental data from De Negri *et al.* (De Negri et al., 2003) and Gröbner *et al.* (Gröbner et al., 2001).

Figure 9.3 shows the calculated liquidus surface of the Al–Mg–Gd system, with experimental data from De Negri *et al*. (De Negri et al., 2003) and Gröbner *et al*. (Gröbner et al., 2001). A qualitative agreement is observed. However, as discussed by Cacciamani *et al*. (Cacciamani et al., 2003b), accurate experimental data in the Al-rich side were probably difficult to obtain due to side reactions [*e.g.,* rare earth elements react with Al_2O_3 crucibles (Ferro et al., 1998)] at high temperature in the Al-rich alloys. In the present study, no ternary interaction parameters in the liquid phase were used, considering the limited reliability of the experiments. The calculated liquidus surface is dominated by the Laves_C15 (almost pure $GdAl_2$) phases, which have high melting temperatures and very negative enthalpies of formation. The primary phase regions of the Laves_C15, $GdMg_5$ and $GdAl_3$ (Ni_3Sn structure) phases intersect that of Mg (HCP_A3). Therefore, these phases are likely to precipitate in the HCP phase during Mg alloy solidification.

9.2.2 The Al – Mg – Dy system

The only reported thermodynamic optimization of the Al–Mg–Dy system is by Cacciamani *et al.* (Cacciamani et al., 2003b) who based their evaluation on the experimental results of De Negri *et al.* (De Negri et al., 2003). In their study, one ternary interaction parameter for the liquid phase was used; no short-range ordering was considered and the Muggianu interpolation method (Pelton, 2001) was used for the ternary system. Seven ternary solid solutions (Laves_C15, BCC_B2, Dy(Mg,Al)₃, HCP_A3, FCC_A1, BCC_A2 and Gamma) were considered. Two sublattices were used for the Laves_C15 phase and the BCC_B2 phase. The ternary compound $Al_2Dy_{0.36}Mg_{0.64}$ (τ2) has a $MgNi_2$-type structure (De Negri et al., 2003) and it was assumed to be a stoichiometric (line) compound. The Gibbs energy of the liquid phase was calculated using the symmetric Kohler approximation with no ternary interaction parameters. The Gibbs energy of the $Al_2Dy_{0.36}Mg_{0.64}$ compound was optimized to reproduce the measured formation temperature (around 803 K) and phase equilibria at 673 K (De Negri et al., 2003). The calculated decomposition temperature of the ternary phase $Al_2Dy_{0.36}Mg_{0.64}$ is 784 K. The optimized model parameters in the Al – Mg – Dy system are summarized in Table 9.4.

Table 9.6 Calculated invariant reactions in the Al–Mg–Dy system

Reaction	T (K) Calc	Type†	Phase	Composition (at%) Calc		
				Al	Dy	Mg
L + Laves_C15 ↔ AlDy + BCC_B2	1339	U	L	41.4	54.2	4.4
L + AlDy ↔ Al$_2$Dy$_3$+ BCC_B2	1264	U	L	35.0	62.3	2.7
L + Al$_2$Dy$_3$↔ AlDy$_2$+ BCC_B2	1237	U	L	30.8	65.9	3.3
L+ AlDy$_2$ ↔ HCP_A3+ BCC_B2	1175	U	L	21.0	73.5	5.5
L + BCC_A2 ↔ BCC_B2+ HCP_A3	1226	U	L	14.2	71.1	14.7
L + Laves_C14 ↔ Dy$_5$Mg$_{24}$ + BCC_B2	873	U	L	1.1	18.6	80.3
L + BCC_B2 ↔ Laves_C15 + Dy$_5$Mg$_{24}$	867	U	L	1.6	16.9	81.5
L ↔ Laves_C15 + Dy$_5$Mg$_{24}$ + HCP_A3	830	E	L	0.7	10.4	88.9
L ↔ FCC_A1+DyAl$_3$ + Dy$_2$Al$_{10}$Mg$_3$	764	E	L	69.8	0.4	29.8
L ↔ FCC_A1+Beta + Dy$_2$Al$_{10}$Mg$_3$	724	E	L	62.7	0.1	37.2
L ↔ Gamma+ Beta + Dy$_2$Al$_{10}$Mg$_3$	724	E	L	60.0	0.1	39.9
L ↔ Gamma+ HCP_A3 + Dy$_2$Al$_{10}$Mg$_3$	712	E	L	29.85	0.05	70.1

† U: quasiperitectic, E: eutectic

Calculated invariant reactions in the Al–Mg–Dy system are listed in Table 9.6. The calculated isothermal section of the Al–Mg–Dy ternary system at 673 K is shown in Figure 9.4, with experimental data of De Negri *et al.*(De Negri et al., 2003). The calculated isothermal section of the Al–Mg–Dy ternary system at 1073 K is also shown in Figure 9.5. It can be seen that the solid

solubilities of the C15 phase is larger at 1073 K than those at 673 K, as is also shown in Cacciamani *et al.* (Cacciamani et al., 2003b). DyMg and DyAl are only partially miscible since they have different crystal structures (CsCl and ErAl type, respectively). However, $DyMg_2$ and $DyAl_2$ form a Laves_C15 solid solution because they have the same structure (Cu_2Mg type).
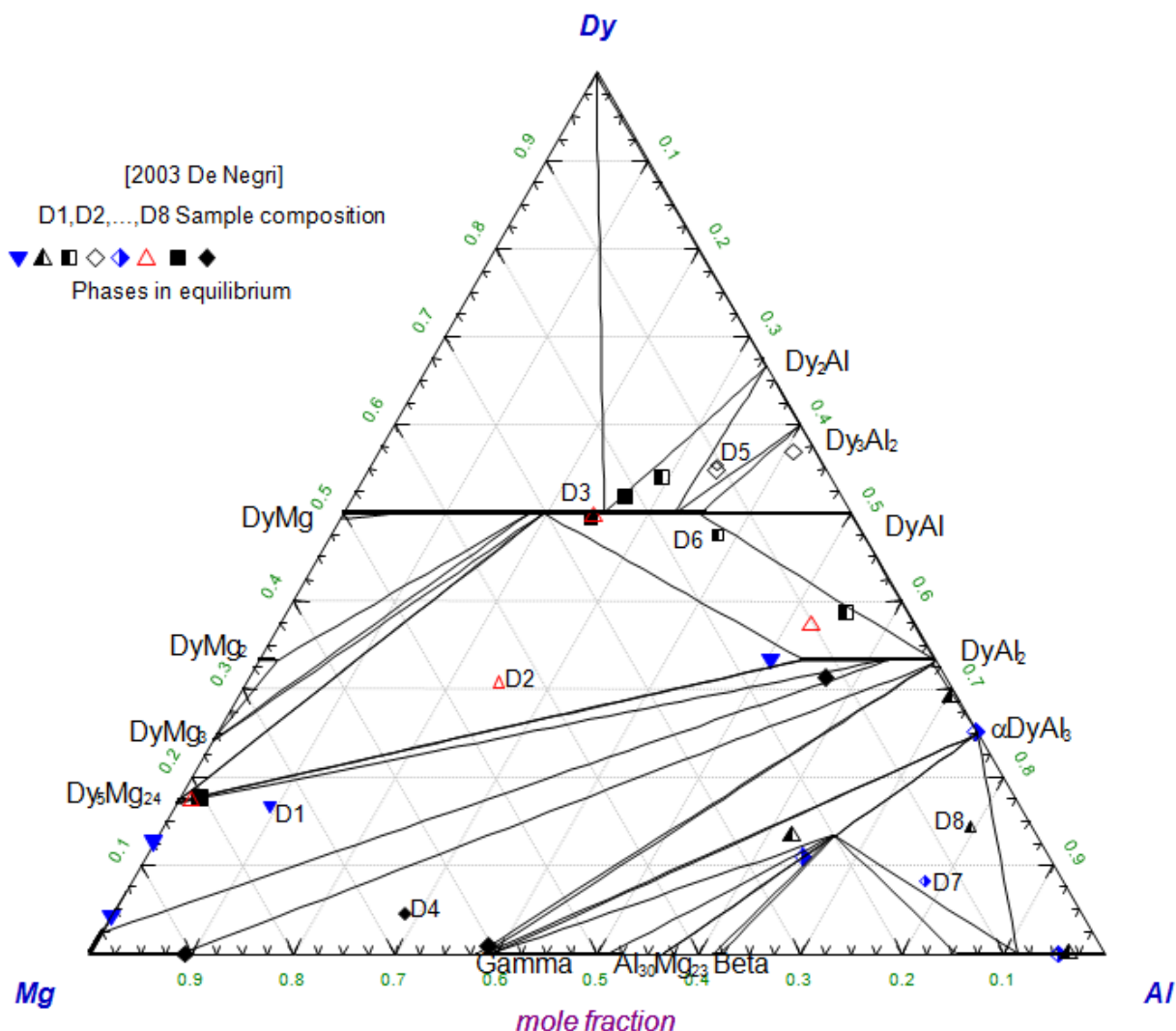
Figure 9.4 The calculated isothermal section of the Al–Mg–Dy ternary system at 673 K with experimental data of De Negri *et al.*(De Negri et al., 2003).
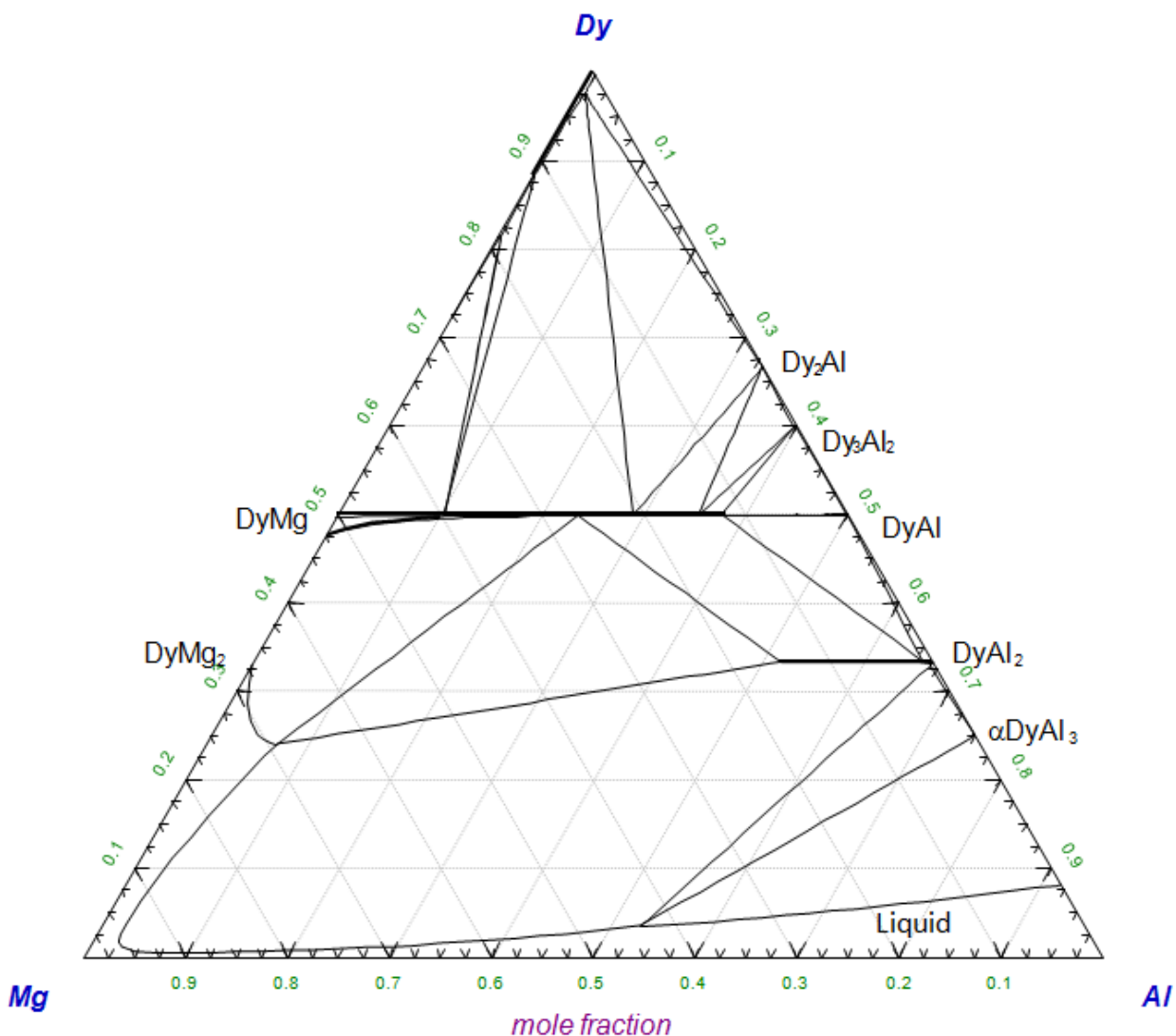
Figure 9.5 The calculated isothermal section of the Al–Mg–Dy ternary system at 1073 K

Figure 9.6 shows the calculated liquidus surface for the entire Al–Mg–Dy system. The liquidus surface is dominated by the Laves_C15 (almost pure Al_2Dy) phases, which have high melting temperature and very negative enthalpies of formation. The primary phase regions of Laves_C15, Dy_5Mg_{24} (Gamma) and $DyAl_3$ phases intersect that of Mg(HCP_A3). Therefore, these phases are likely to precipitate in the HCP phase during Mg alloy solidification.
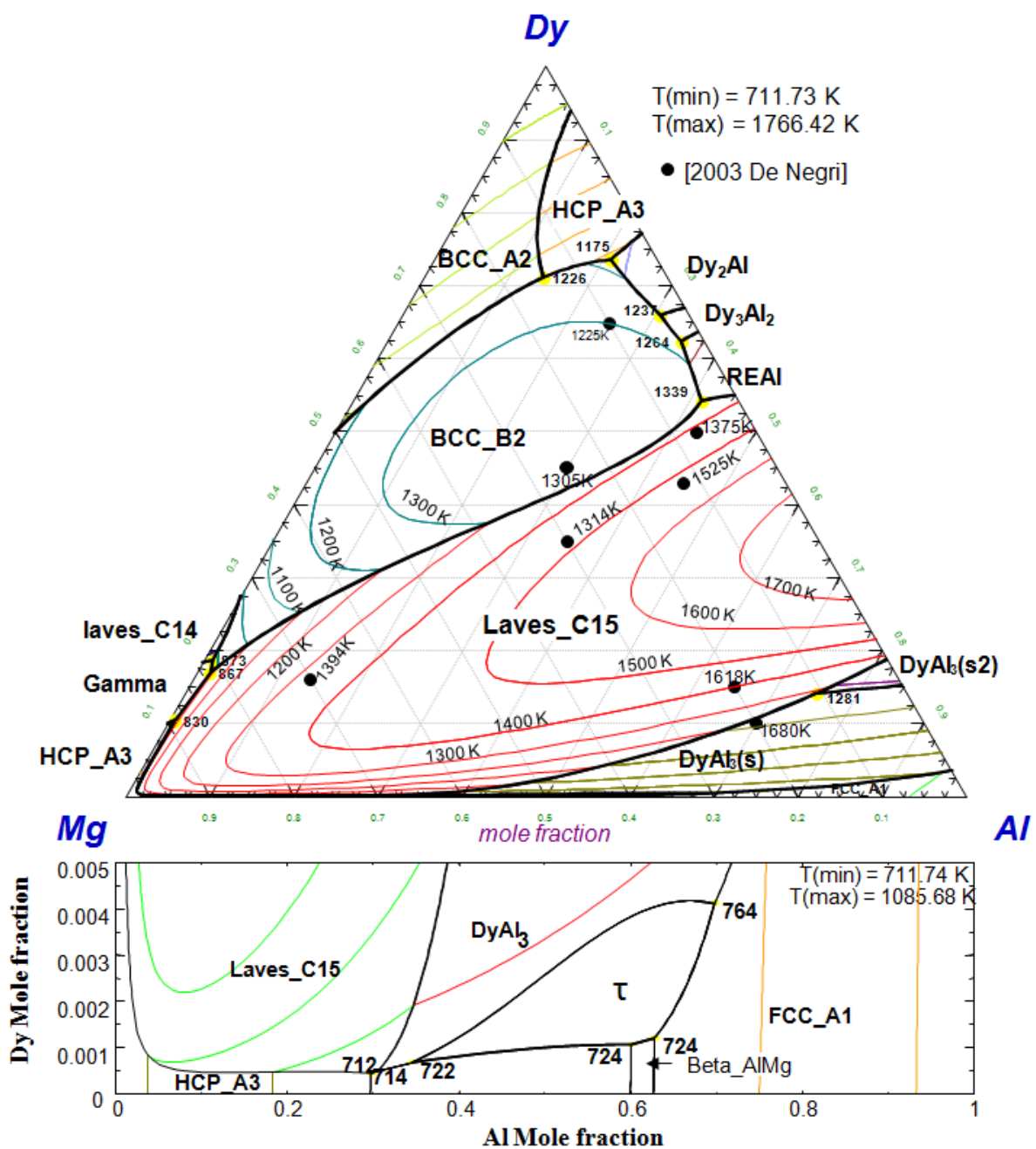
Figure 9.6 The calculated liquidus surface of the Al–Mg–Dy system with experimental data from De Negri *et al.* (De Negri et al., 2003).

4.3 The Al – Mg – Ho system

Cacciamani *et al.* (Cacciamani et al., 2003b) optimized the Al – Mg – Ho system based on the experimental results of De Negri *et al.* (De Negri et al., 2003) with one ternary interaction

parameter for the liquid phase. No short-range ordering was considered and the Muggianu interpolation method (Pelton, 2001) was employed for this ternary system. In this work, seven ternary solid solutions (Laves_C15, BCC_B2, Ho(Mg,Al)$_3$, HCP_A3, FCC_A1, BCC_A2 and Gamma) were considered. The ternary compound is Al$_{10}$Mg$_3$Ho$_2$ (τ3) of prototype MgNi$_2$ [identified as Al$_2$Ho$_{0.39}$Mg$_{0.61}$ (De Negri et al., 2003)]; it is assumed to be a stoichiometric (line) compound although slight solid solubility could not be ruled out. The Gibbs energy of the liquid phase was calculated using the symmetric Kohler approximation with no ternary interaction parameters. The optimized model parameters are summarized in Table 9.4.

The Gibbs energy of the Al$_2$Ho$_{0.39}$Mg$_{0.61}$ compound was optimized to reproduce the measured formation temperature (about 723 K) and phase equilibria at 673 K (De Negri et al., 2003). The calculated decomposition temperature of the ternary phase Al$_2$Ho$_{0.39}$Mg$_{0.61}$ is 745 K.

Table 9.7 Calculated invariant reactions in the Al–Mg–Ho system

| Reaction | T (K) | Type[†] | Composition (at%) | | |
| | | | Phase | Calc | | |
	Calc			Al	Ho	Mg
L + Laves_C15 ↔ AlHo + BCC_B2	1288	U	L	35.5	52.6	11.9
L + AlHo ↔ Al$_2$Ho$_3$+ BCC_B2	1244	U	L	32.5	59.5	8.0
L + Al$_2$Ho$_3$↔ AlHo$_2$+ BCC_B2	1232	U	L	30.3	60.9	8.8
L+ AlHo$_2$ ↔ HCP_A3+ BCC_B2	1167	U	L	19.4	66.5	14.1
L+ HCP_A3↔ BCC_B2 + BCC_A2	1182	U	L	10.4	58.8	30.8
L + Laves_C14 ↔ Ho$_5$Mg$_{24}$ + BCC_B2	871	U	L	1.5	20.6	77.9
L + BCC_B2 ↔ Laves_C15 + Ho$_5$Mg$_{24}$	870	U	L	2.0	19.5	78.5

|						
L ↔ Laves_C15 + Ho$_5$Mg$_{24}$ + HCP_A3	816	E	L	0.5	9.3	90.2
L ↔ FCC_A1+HoAl$_3$ + Ho$_2$Al$_{10}$Mg$_3$	737	E	L	65.1	0.3	34.6
L ↔ FCC_A1+Beta + Ho$_2$Al$_{10}$Mg$_3$	724	E	L	62.8	0.2	37.0
L ↔ Gamma+ Beta + Ho$_2$Al$_{10}$Mg$_3$	723	E	L	60.0	0.2	39.8
L ↔ Gamma+ HCP_A3 + HoAl$_3$	712	E	L	29.75	0.05	70.2

† U: quasiperitectic, E: eutectic

Calculated invariant reactions in the Al–Mg–Ho system are listed in Table 9.7. The calculated isothermal section of the Al–Mg–Ho ternary system at 673 K is shown in Figure 9.7 with experimental data of De Negri *et al.*(De Negri et al., 2003). The calculated isothermal section of the Al–Mg–Ho ternary system at 1073K is also shown in Figure 9.8. It can be seen that the solid solubility of the Laves_C15 phase is greater at 1073 K than that at 673 K, as is also demonstrated in Cacciamani *et al*. (Cacciamani et al., 2003b). HoMg and HoAl are only partially miscible since they have different crystal structures (CsCl and ErAl type, respectively). However, HoMg$_2$ and HoAl$_2$ form a Laves_C15 solid solution because they have the same structure (Cu$_2$Mg type).
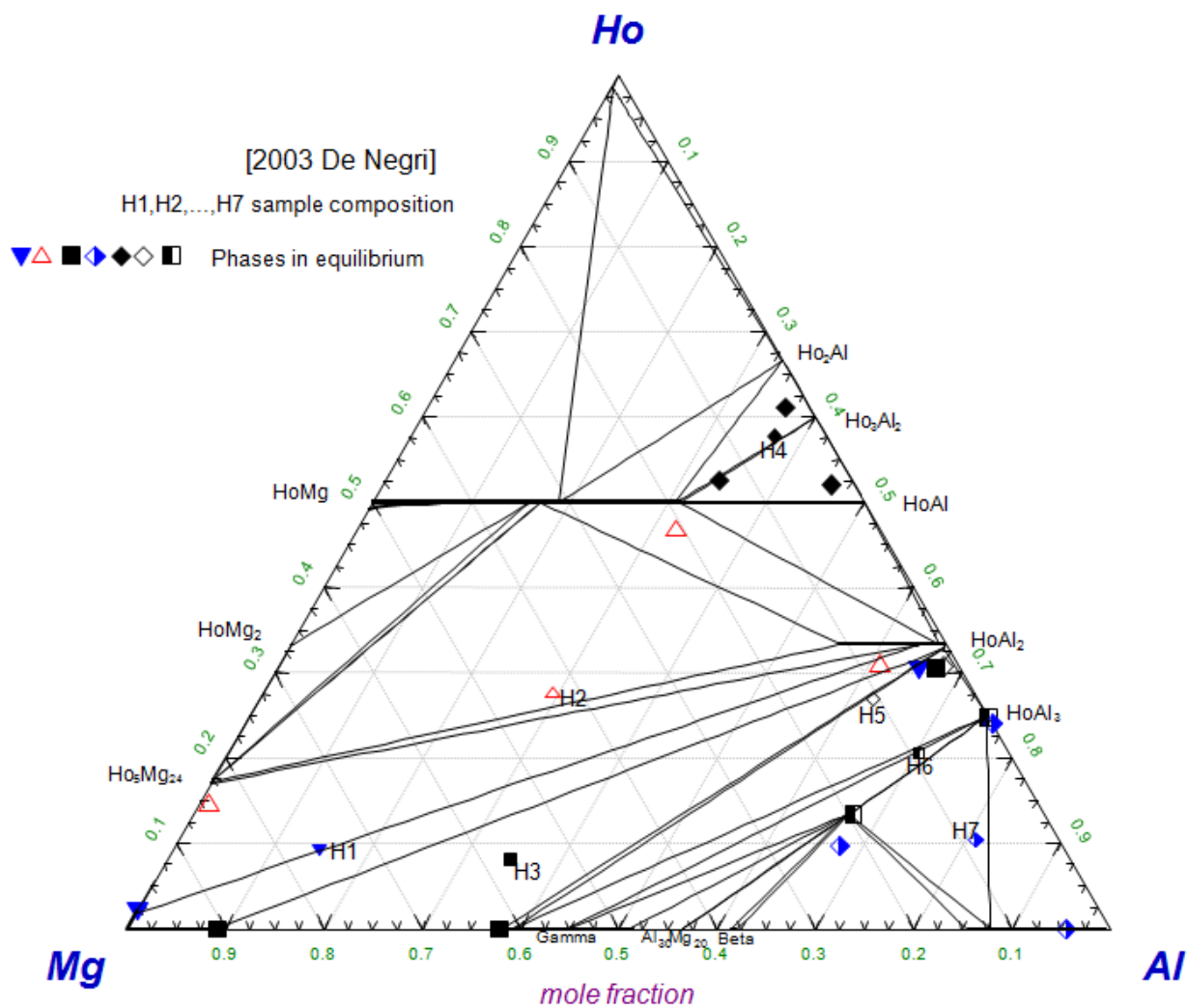
Figure 9.7 The calculated isothermal section of the Al–Mg–Ho ternary system at 673 K with experimental data of De Negri *et al.*(De Negri et al., 2003).
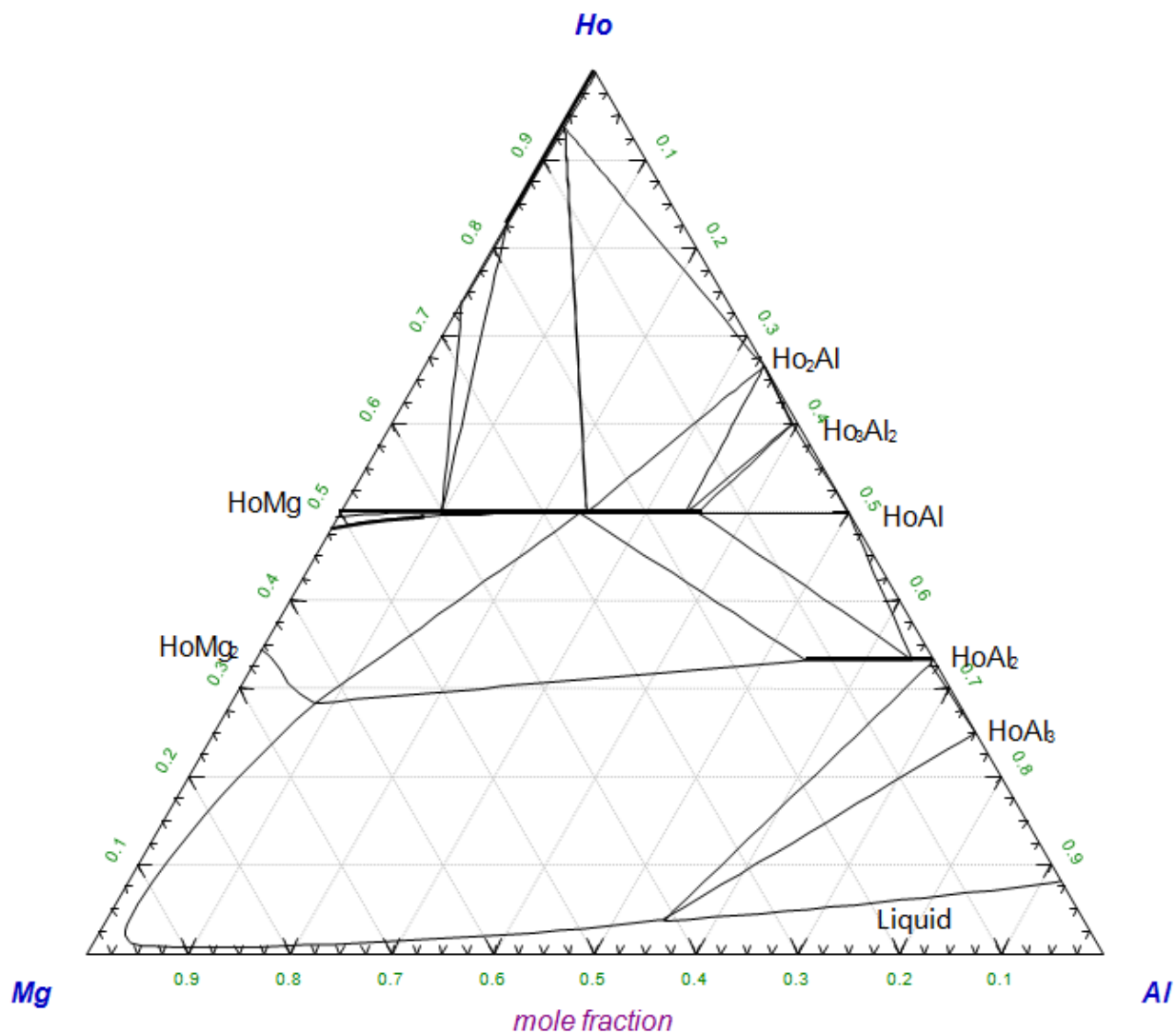
Figure 9.8 The calculated isothermal section of the Al–Mg–Ho ternary system at 1073 K

Figure 9.9 shows the calculated liquidus surface in the whole Al–Mg–Ho system. The liquidus surface is dominated by the Laves_C15 (almost pure Al_2Ho) phases, which have high melting temperature and very negative enthalpies of formation. The primary phase regions of Laves_C15, Ho_5Mg_{24} and Al_3Ho phases intersect that of Mg (HCP_A3). Therefore, these phases are likely to precipitate in the HCP phase during Mg alloy solidifcation.
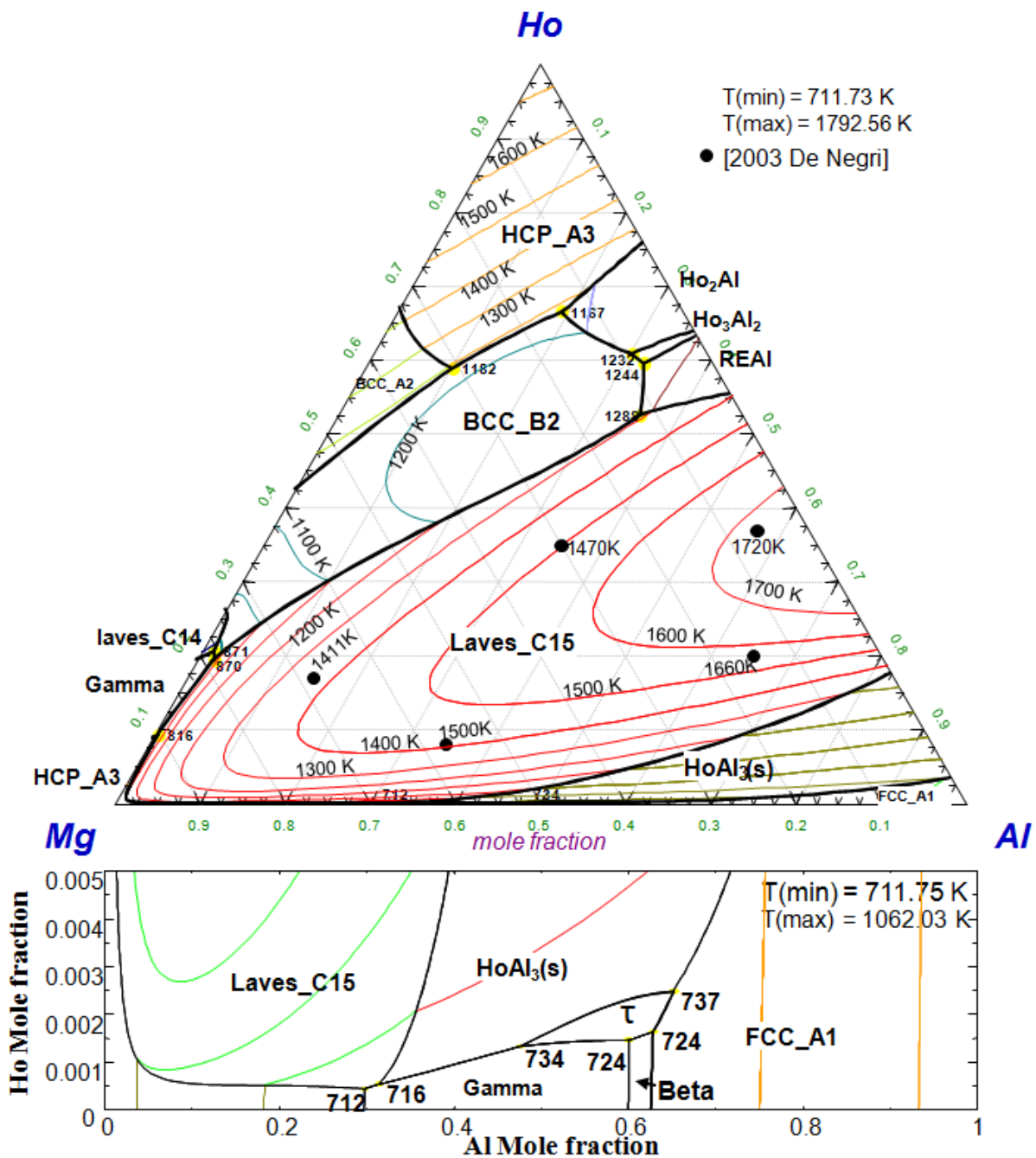
Figure 9.9 The calculated liquidus surface of the Al–Mg–Ho system with experimental data from De Negri *et al*. (De Negri et al., 2003).

9.2.3 The Al – Mg – Er system

Cacciamani *et al.* (Cacciamani et al., 2002) optimized the Al – Mg – Er system based on experimental results of Saccone *et al.* (Saccone et al., 2002) with ternary interaction parameters for the liquid phase. In the present work, seven ternary solid solutions (Laves_C15, BCC_B2, Er(Mg,Al)$_3$, HCP_A3, FCC_A1, BCC_A2 and Gamma) were considered. The ternary compound Al$_2$Er$_{0.3}$Mg$_{0.7}$ ($\tau4$) [the same composition as Al$_{66.7}$Er$_{10}$Mg$_{23.3}$ in Saccone *et al.* (Saccone et al., 2002)] has a MgZn$_2$-type structure (De Negri et al., 2003) and it was assumed to be a stoichiometric (line) compound because no solid solubility has been observed experimentally. The Gibbs energy of the liquid phase was calculated using the symmetric Kohler approximation with no ternary interaction parameters. The Gibbs energy of the Al$_2$Er$_{0.3}$Mg$_{0.7}$ compound was optimized to reproduce the measured formation temperature and phase equilibria at 673 K (Saccone et al., 2002). All the optimized model parameters in Al–Mg–Er system were summarized in Table 9.4. Calculated invariant reactions in the Al–Mg–Er system were listed in Table 9.8.

Table 9.8 Calculated invariant reactions in the Al–Mg–Er system

Reaction	T (K) Calc	Type[†]	Phase	Composition (at%) Calc		
				Al	Er	Mg
L + AlEr ↔ BCC_B2+ Al$_2$Er$_3$	1312	U	L	40.3	54.0	5.7
L ↔ HCP_A3+ BCC_B2+ AlEr$_2$	1221	E	L	21.8	67.4	10.8
L+ HCP_A3↔ BCC_B2 + BCC_A2	1234	U	L	9.1	56.2	34.7
L + Laves_C14 ↔ Er$_5$Mg$_{24}$ + BCC_B2	869	U	L	0.6	20	79.4
L + BCC_B2 ↔ Laves_C15 + Er$_5$Mg$_{24}$	858	U	L	1.4	15.2	83.4
L ↔ Laves_C15 + Er$_5$Mg$_{24}$+ HCP_A3	831	E	L	0.8	10.7	88.5

L ↔ FCC_A1+ErAl₃ + Er₃Al₂₀Mg₇	780	E	L	71.8	0.1	28.1
L ↔ FCC_A1+Beta + Er₃Al₂₀Mg₇	724	E	L	62.6	0.01	37.39
L ↔ Gamma+ Beta + Er₃Al₂₀Mg₇	724	E	L	59.95	0.01	40.04
L ↔ Gamma+ HCP_A3 + Laves_C15	712	E	L	29.71	0.01	70.28

† U: quasiperitectic, E: eutectic
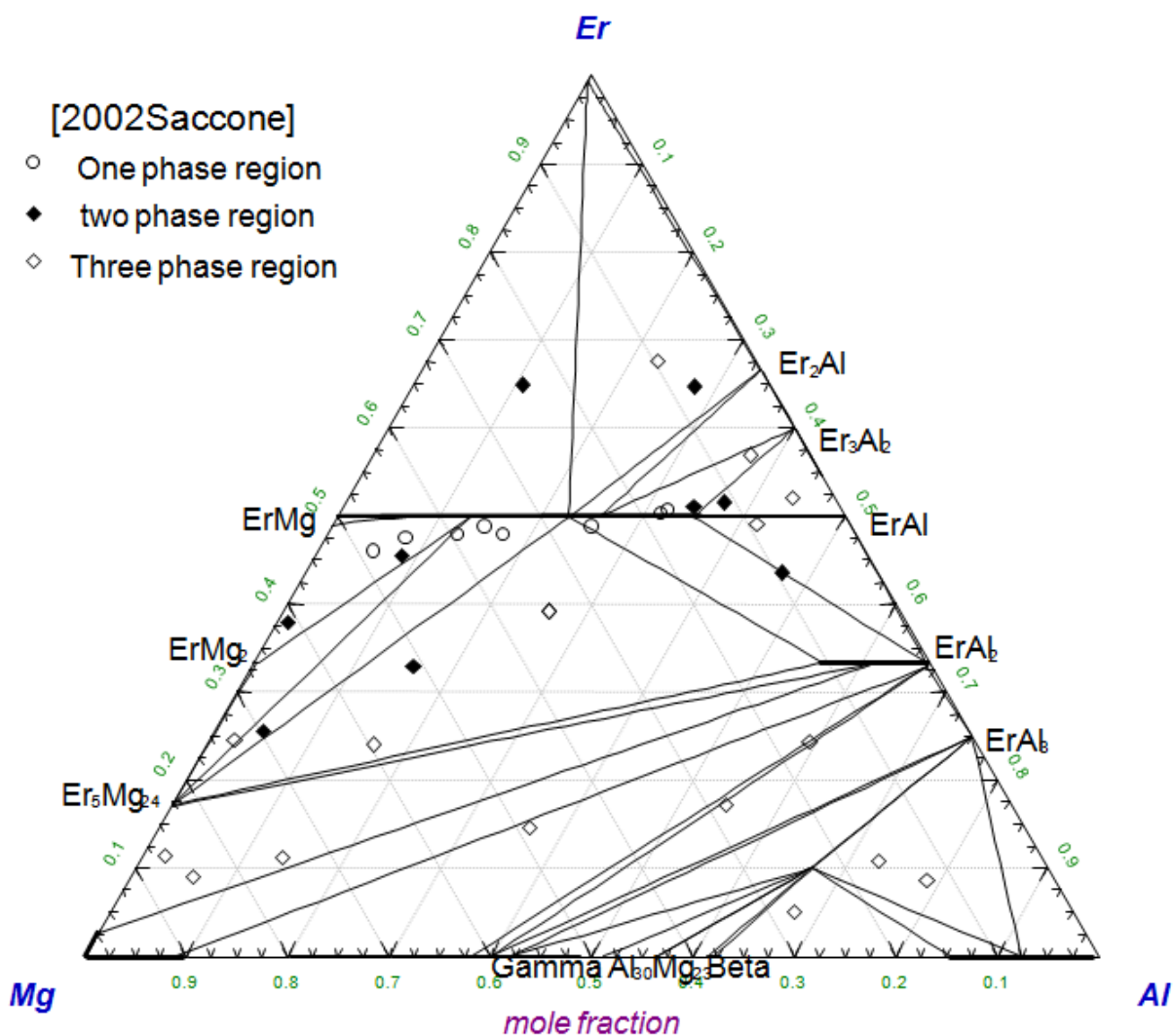
Figure 9.10 The calculated isothermal section of the Al–Mg–Er ternary system at 673 K with experimental data of Saccone *et al.* (Saccone et al., 2002).

The calculated isothermal section of the Al–Mg–Er ternary system at 673 K is shown in Figure 9.10 with experimental data of Saccone *et al.* (Saccone et al., 2002). The calculated isothermal section of the Al–Mg–Er ternary system at 1073 K is also shown in Figure 9.11. It can be seen that the solid solubility of the Laves_C15 phase is greater at 1073 K than that at 673 K, as is also demonstrated in Cacciamani *et al.* (Cacciamani et al., 2002). ErMg and ErAl are only partially miscible since they have different crystal structures (CsCl and ErAl type, respectively). However, $ErMg_2$ and $ErAl_2$ form a Laves_C15 solid solution because they have the same structure (Cu_2Mg type).
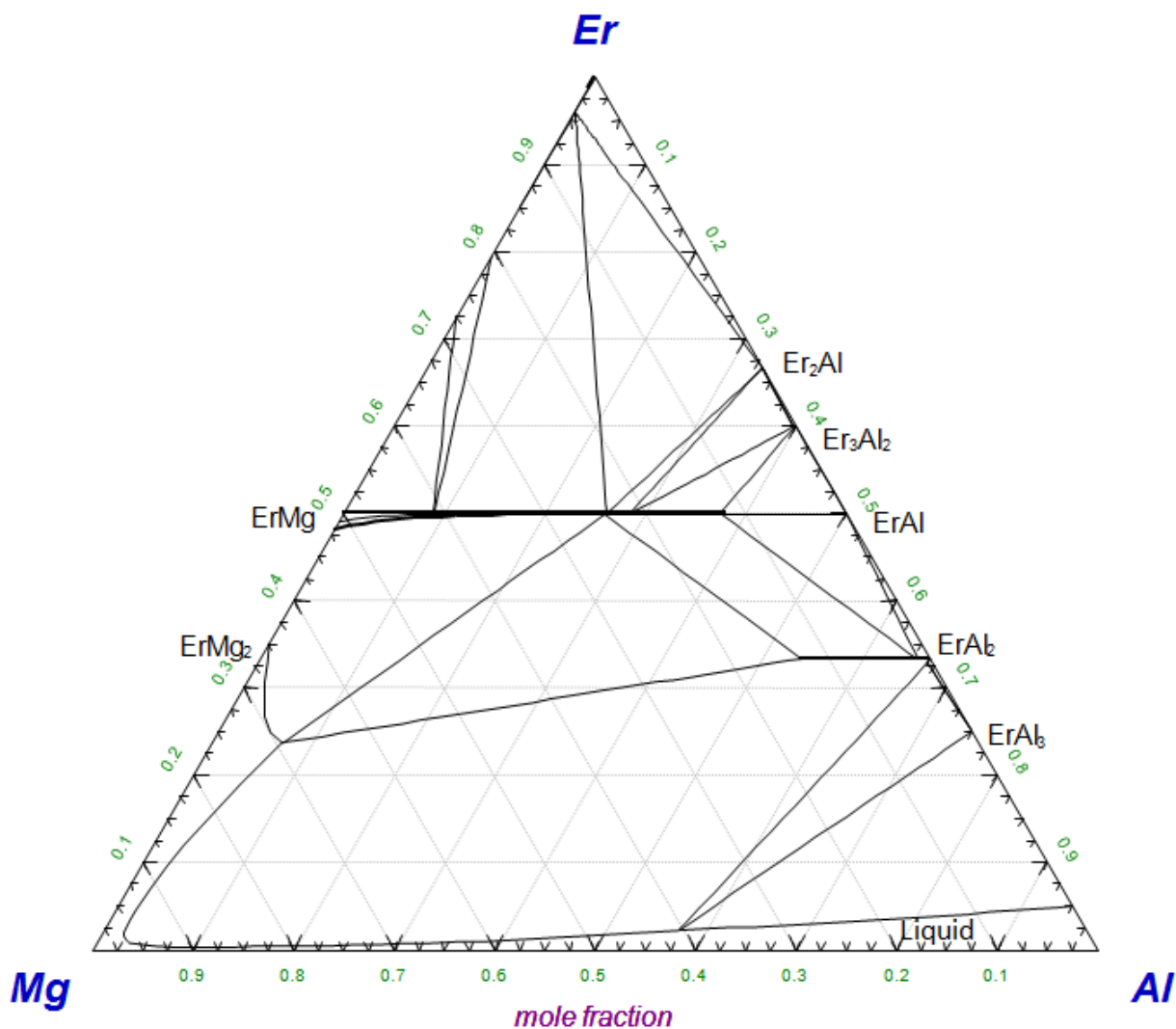
Figure 9.11 The calculated isothermal section of the Al–Mg–Er ternary system at 1073 K
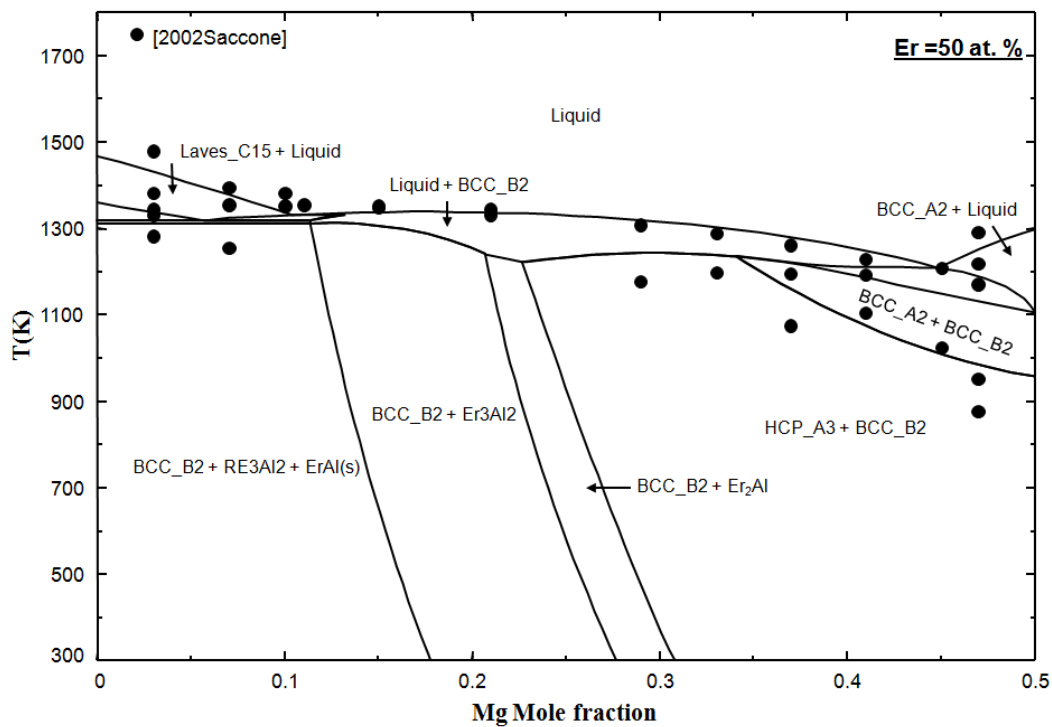
Figure 9.12 The calculated vertical section at a constant Er content of 50 at.%
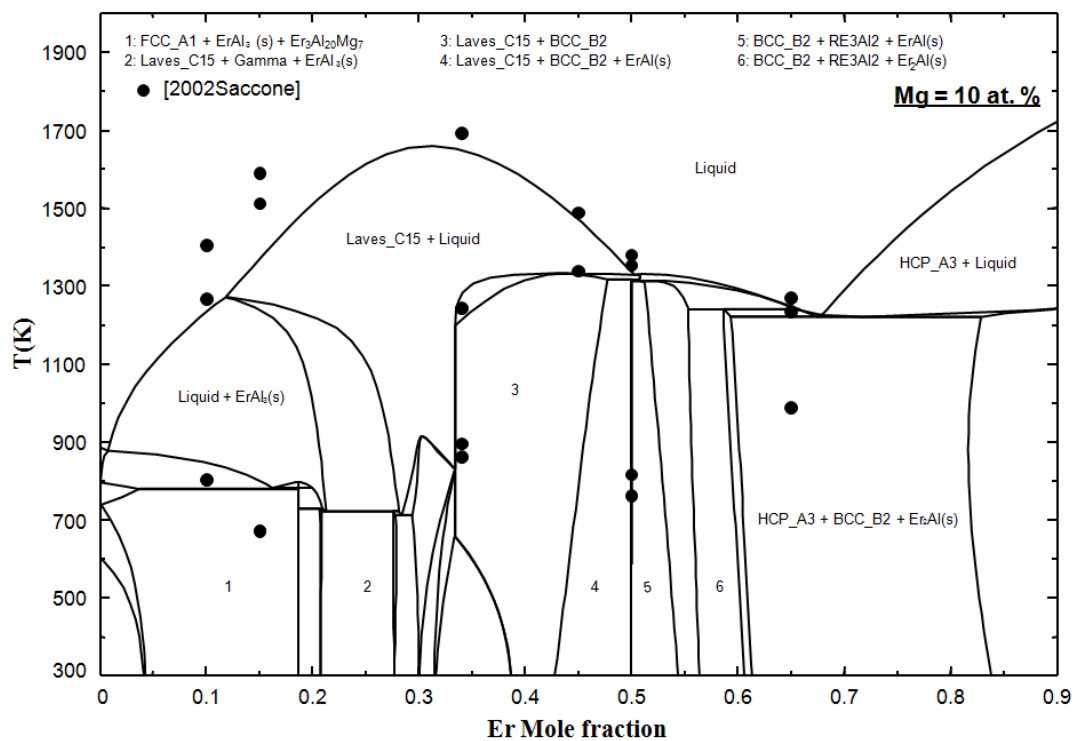
Figure 9.13 The calculated vertical sections at a constant Mg content of 10 at.%
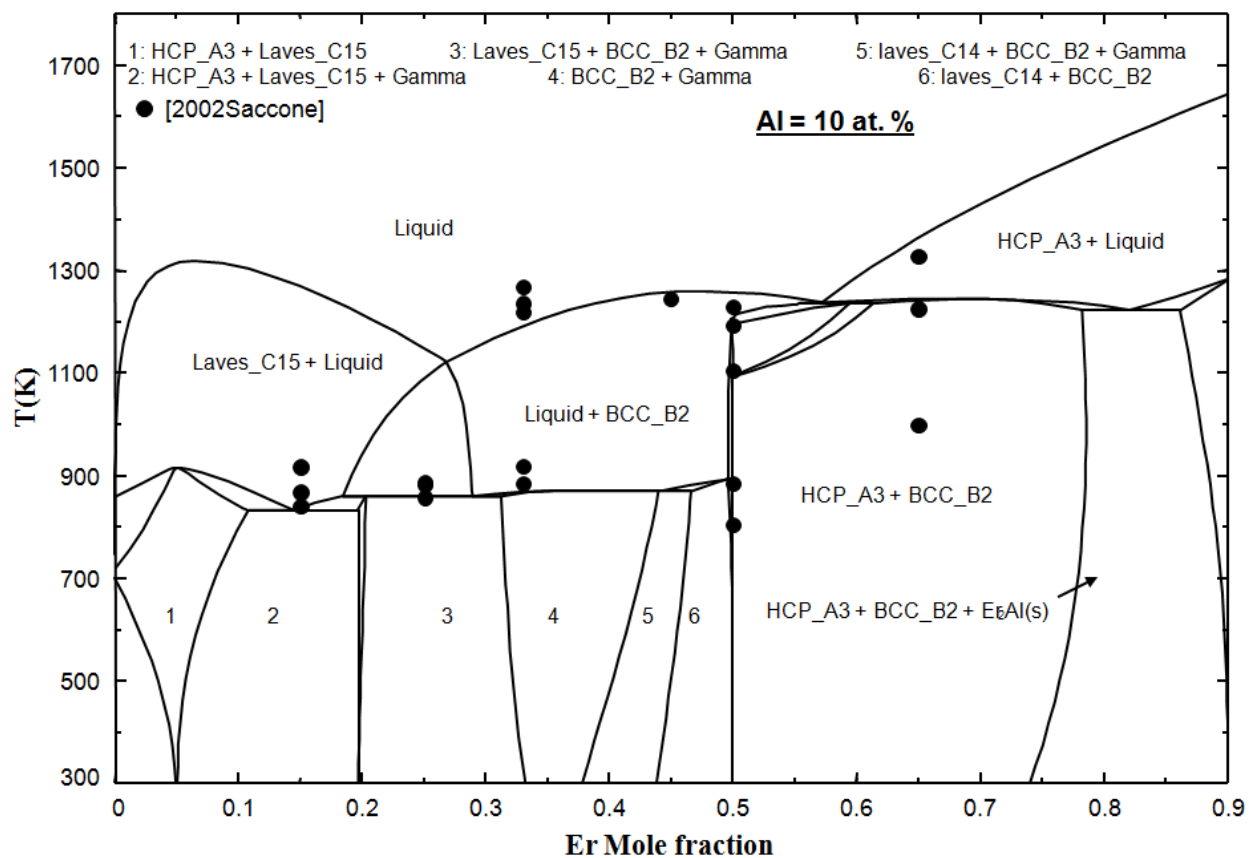
Figure 9.14 The calculated vertical sections at a constant Al content of 10 at.%

Figures 9.12 to 9.14 show three calculated vertical sections at a constant content of 50 at.% Er, of 10 at.% Mg and of 10 at.% Al, respectively. Figure 9.15 shows the calculated liquidus surface of the entire Al–Mg–Er system. The liquidus surface is dominated by the Laves_C15 (almost pure Al_2Er) phase, which has high melting temperature and very negative enthalpy of formation. The primary phase regions of the Laves_C15, Er_5Mg_{24} and $ErAl_3$ phases intersect that of Mg (HCP_A3). Therefore, these phases are likely to precipitate in the HCP phase during Mg alloy production.
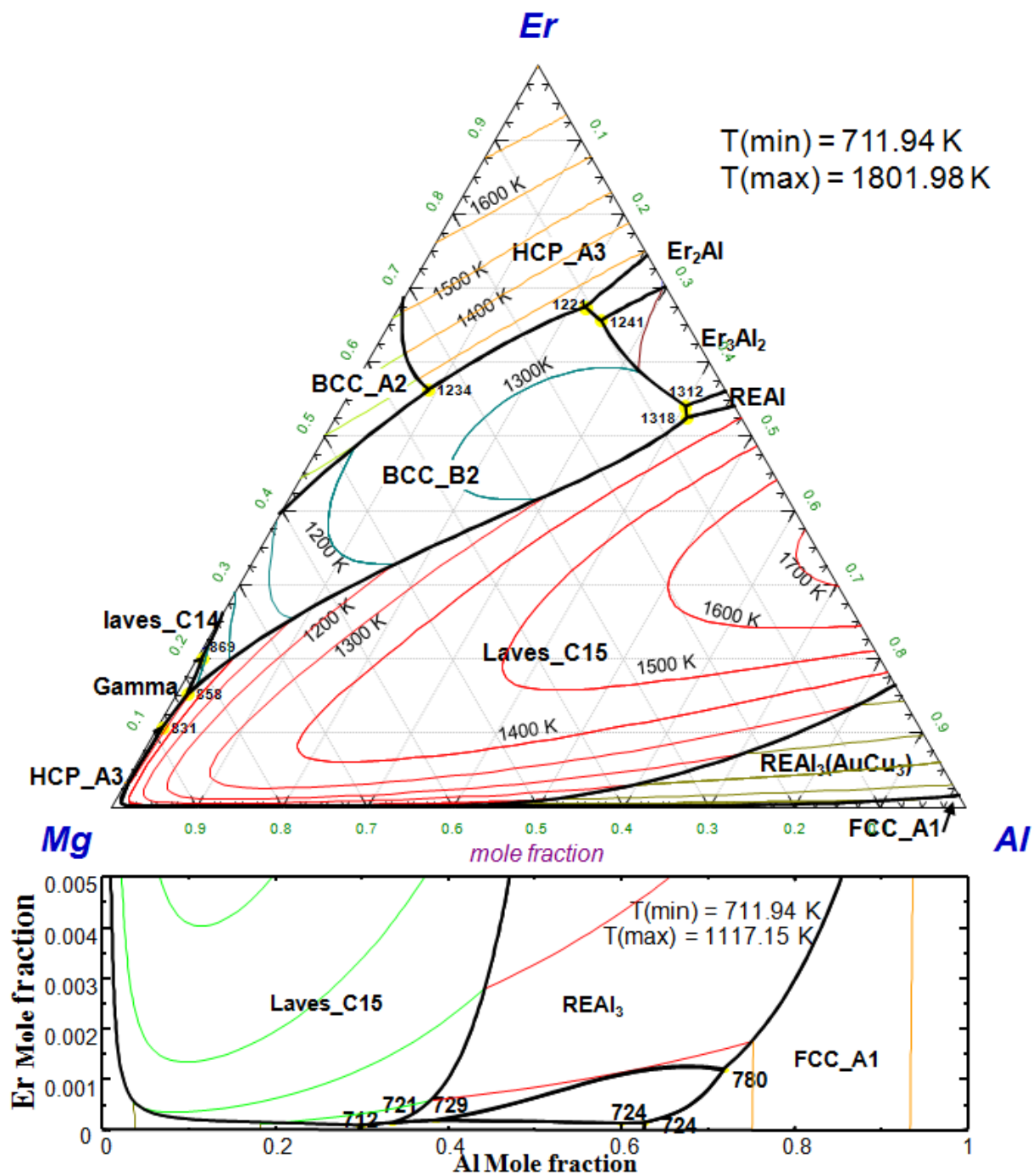
Figure 9.15 The calculated liquidus surface in the Al–Mg–Er system.

9.2.4 The Al – Mg – Tb system

As is mentioned earlier, thermodynamic properties of rare earth metal alloys show a smooth trend with RE atomic numbers. In the present study, it was assumed that the ternary compound Al$_4$MgTb exists at 673 K by taking into consideration the similarities among the Al–Mg–Tb, Al–Mg–Gd and Al–Mg–Dy systems. The enthalpy of formation for the ternary compound Al$_4$MgTb was optimized based on the calculation from the Miedema model. Similar model parameters were used for the solid solutions (BCC_B2, Laves_C14, Laves_C15) in the Al–Mg–Tb ternary system. The phase equilibria were assumed to be the same as in the Al–Mg–Dy system. Analogous to the Al–Mg–Gd and Al–Mg–Dy systems, the calculated isothermal section of the Al–Mg–Tb ternary system at 673 K is shown in Figure 9.16. The calculated isothermal section of the Al–Mg–Tb ternary system at 1073 K is also shown in Figure 9.17.
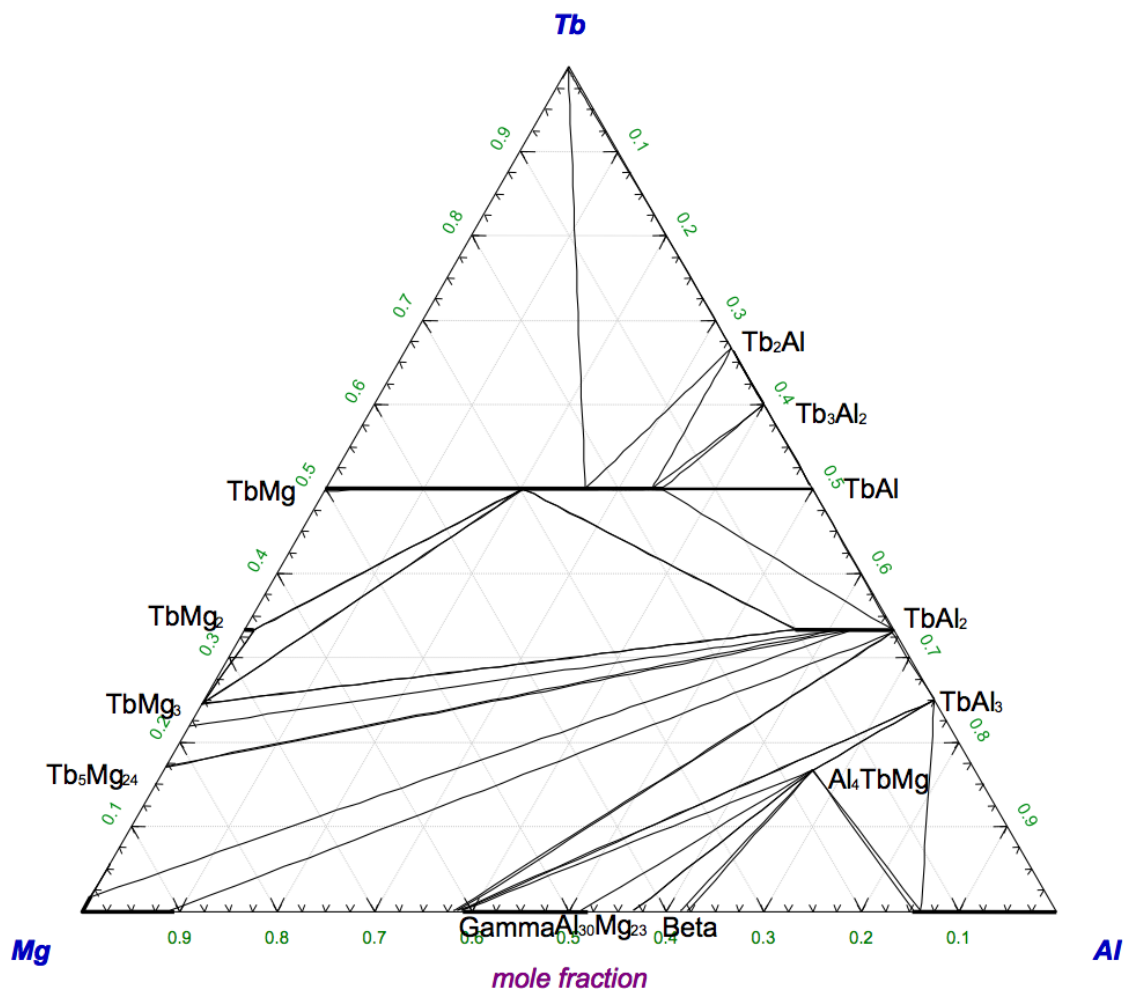
Figure 9.16 The calculated isothermal section of the Al–Mg–Tb ternary system at 673 K
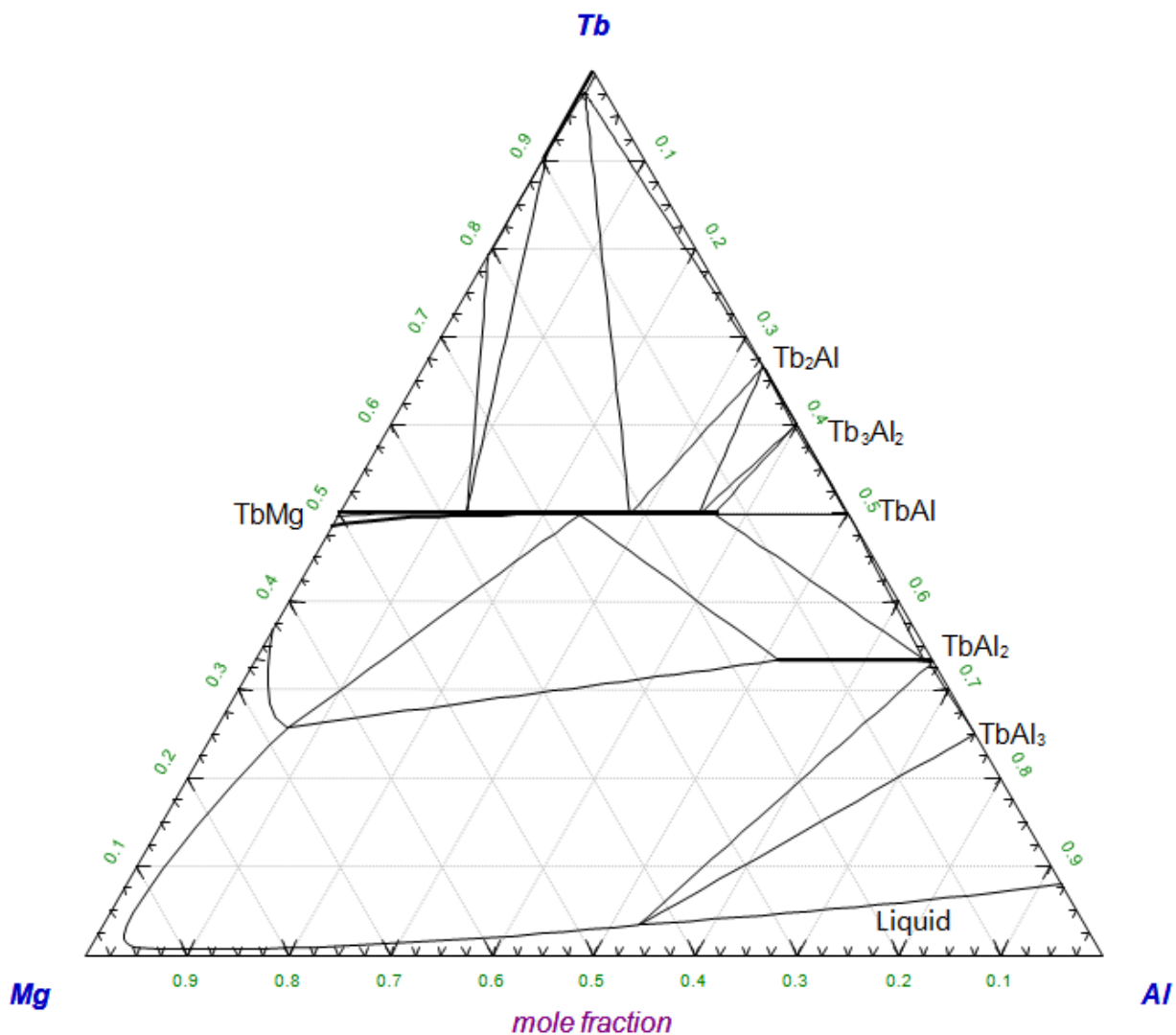
Figure 9.17 The calculated isothermal section of the Al–Mg–Tb ternary system at 1073 K

Shown in Figure 9.18 is the liquidus projection of Al–Mg–Tb ternary system. No ternary parameters are used for the liquid phase. All the optimized model parameters in Al–Mg–Tb system are summarized in Table 9.4 and calculated invariant reactions in the Al–Mg–Tb system are listed in Table 9.9.
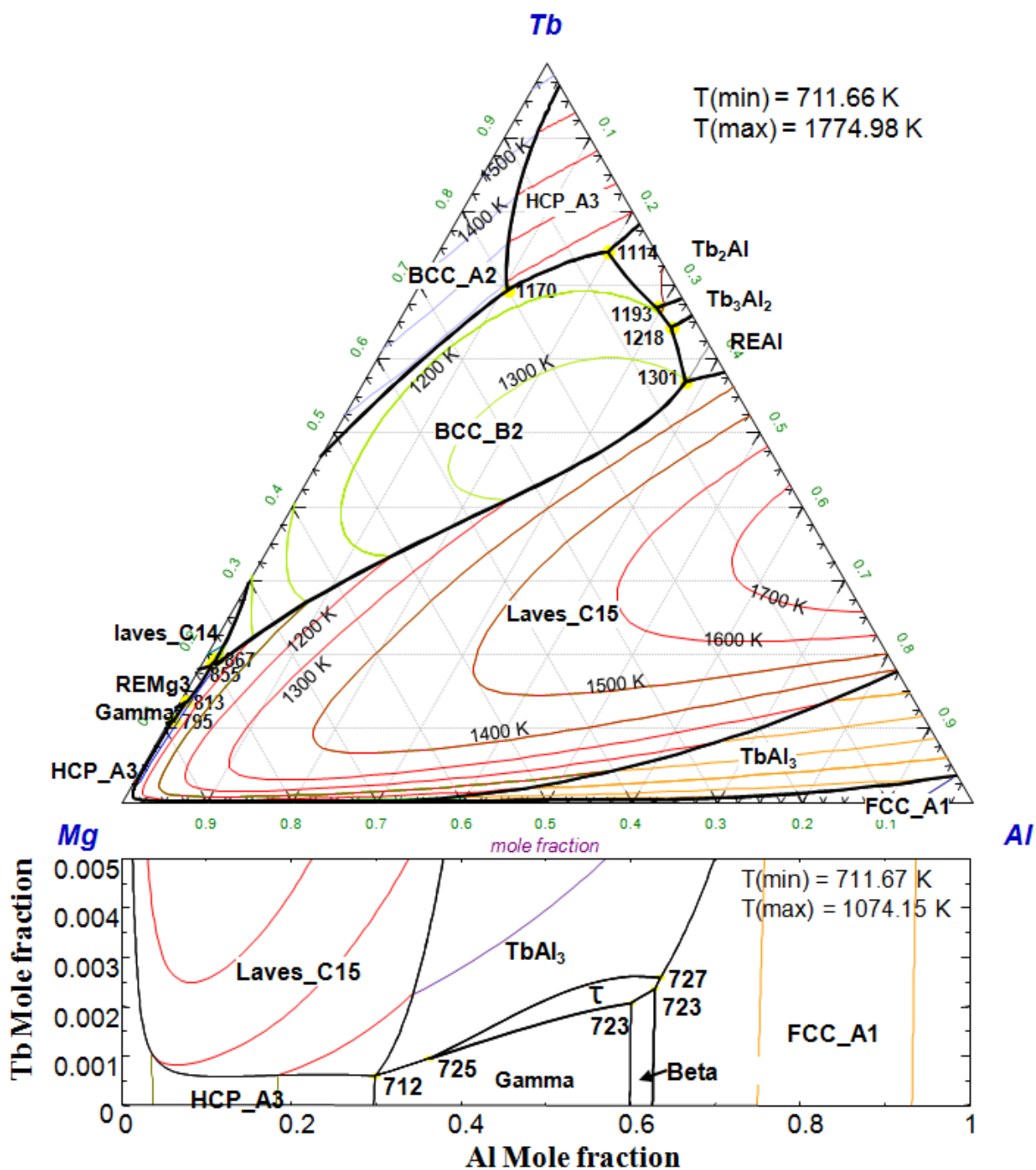
Figure 9.18 The calculated liquidus surface in the Al–Mg–Tb system

Table 9.9 Calculated invariant reactions in the Al–Mg–Tb system

Reaction	T (K) Calc	Type†	Composition (at%)			
			Phase	Calc		
				Al	Tb	Mg
L + Laves_C15 ↔ AlTb + BCC_B2	1301	U	L	37.9	57.0	5.1
L + AlTb ↔ Al$_2$Tb$_3$+ BCC_B2	1218	U	L	32.6	64.3	3.1
L + Al$_2$Tb$_3$↔ AlTb$_2$+ BCC_B2	1193	U	L	29.5	67.0	3.5
L+ AlTb$_2$ ↔ HCP_A3+ BCC_B2	1114	U	L	19.9	74.6	5.5
L + HCP_A3+ BCC_A2 ↔ BCC_B2	1170	P	L	10.7	69.4	19.9
L ↔ FCC_A1+TbAl$_3$ + TbAl$_4$Mg	727	E	L	63.4	0.3	36.3
L ↔ FCC_A1+Beta + TbAl$_4$Mg	723	E	L	62.9	0.2	36.9
L ↔ Gamma+ Beta + TbAl$_4$Mg	723	E	L	60.1	0.2	39.7
L ↔ Gamma+ HCP_A3 + Laves_C15	712	E	L	29.8	0.1	70.1

† P: peritectic, U: quasiperitectic, E: eutectic, D: degenerate

9.3 Conclusions

Systematic thermodynamic evaluations and optimizations of the Al–Mg–Gd, Al–Mg–Dy, Al–Mg–Ho, Al–Mg–Er, and Al–Mg–Tb systems have been presented on the basis of literature information. The Al–Mg–Tb system was optimized for the first time based on this systematic approach. Existence of Al$_4$TbMg ternary compound was assumed by comparing with Al–Mg–Gd, Al–Mg–Dy systems. The "RE5Mg24" phase and Gamma (Al$_{12}$Mg$_{17}$) phase have been modeled as one single phase (Gamma) using a three sub-lattice CEF with (Mg, RE)$_{10}$(Al, Mg)$_{24}$(Al, Mg)$_{24}$ formula. The same strategy was used to estimate Gibbs energy of meta-stable

end-members for Al–Mg–light rare earth and Al–Mg–heavy rare earth systems. Five Al–RE binary systems in the Al-rich side have been slightly re-adjusted in order to fit the ternary experimental data. No ternary parameters were used for the ternary liquids, indicating the accurate Gibbs energy data sets of the binary phases and that the extrapolation from the binary data produced a satisfactory agreement with the ternary experimental data. These five systems show similar characteristics.

CHAPTER 10   **GENERAL DISCUSSION**

Systematic thermodynamic evaluations and optimizations of the Al–Mg–La–Ce–Pr–Nd–Sm–Gd–Tb–Dy–Ho–Er group have been carried out on the basis of all available literature information. Experimental work on all the ternary Al–RE'–RE" and Mg–RE'–RE" (RE', RE" = La, Ce, Pr, Nd, Sm, Gd, Tb, Dy, Ho, Er) systems should be carried out in order to get the accurate thermodynamic properties. The thermodynamic database obtained for Mg and Al alloy design is of great use in order to quantify the effects of alloying elements on critical micro-structural elements which directly influence the properties of the material. The Factsage^{TM} thermochemical software permits calculation of the phase diagrams, phase equilibria, thermodynamic properties, and Scheil - Gulliver cooling behavior using the evaluated and optimized thermodynamic database. Some examples of Mg and Al alloys design are given here.

As is known, commercial cast magnesium alloys for automotive applications are often AZ (*i.e.* AZ91) and AM (*i.e.* AM60B) series alloys. These alloys offer a good combination of mechanical properties, corrosion resistance and die-castability. However, their poor creep resistance above 125 ℃ makes them inadequate for major powertrain applications. The poor creep resistance in these alloys can be explained by the discontinuous precipitation of the $Mg_{17}Al_{12}$ (Gamma) phase which has the poor thermal stability. This phase has a low eutectic temperature of 437 ℃. The following are some examples of the use of our developed Al–Mg–RE thermodynamic database.

The effect of RE on magnesium AE alloys

Adding RE metals to the Mg–Al alloys can improve the creep resistance by precipitating the thermally stable $Al_{11}RE_3$ phase and suppressing the detrimental $Mg_{17}Al_{12}$ phase. Rare earth alloying additions are expensive and therefore a cheaper substitute known as mischmetal (a mixture of rare earth elements, mainly Ce, La, Nd, Pr) is often used as alloying additions for magnesium alloys. Aluminum is added to improve castability and room temperature mechanical properties (Powell et al., 2002).

In order to determine the solidification paths and micro-segregation through the alloy design process by varying the alloy compositions, Scheil-Gulliver cooling calculations were performed. These can give more reasonable and realistic predictions of the as-cast microstructure than the thermodynamic equilibrium calculations. In the Scheil-Gulliver solidification model, the liquid phase is assumed to be homogeneous at all times during solidification, while no diffusion at all takes place within the solid phases involved. This causes the gradual formation of concentration gradients (micro-segregation) inside the solid phases as the solidification proceeds.

The AE41 and AE42 alloys were studied as examples.

Figures 10.1-10.4 show the calculated solidification behavior of the Mg - 4 wt. %Al - x wt. %RE (x = 1, 2, 3, 4) alloys assuming Scheil-Gulliver cooling, where no Mn, Zn or Si is included in the calculation. Here RE is the mixture of rare earth metals (mischmetal), which has the typical composition 50 wt% Ce - 25 wt% La - 20 wt% Nd -5 wt% Pr. According to the calculation, the as-cast microstructure of the alloys will consist of primary α-(Mg) dendrites with the RE_3Al_{11} phase.
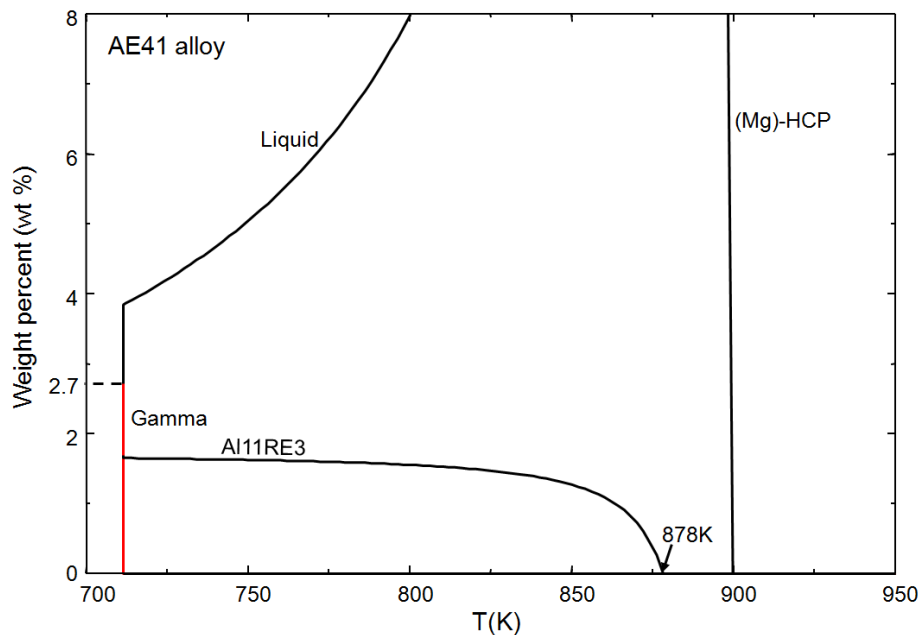
Figure 10.1 Scheil-Gulliver cooling of AE41 alloy
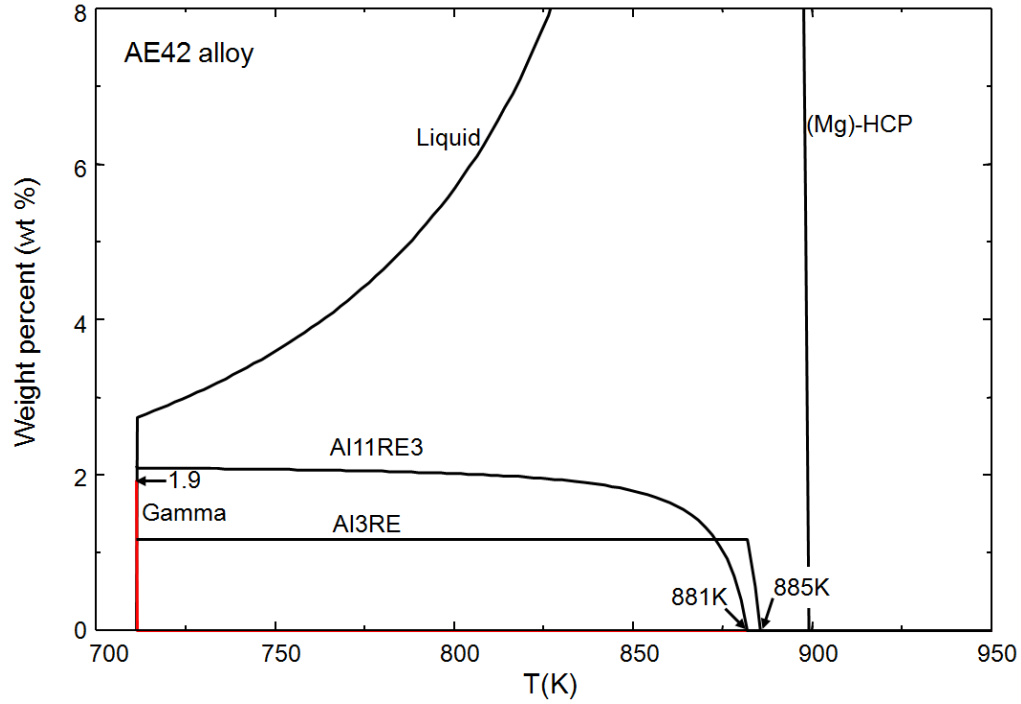
Figure 10.2 Scheil-Gulliver cooling of AE42 alloy
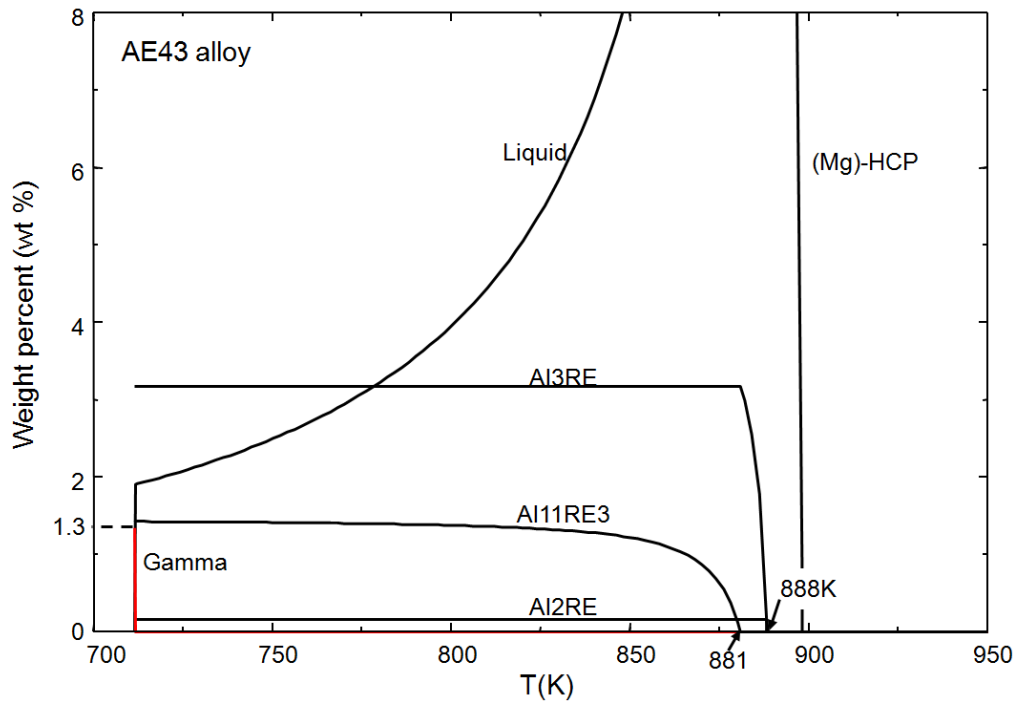
Figure 10.3 Scheil-Gulliver cooling of AE43 alloy
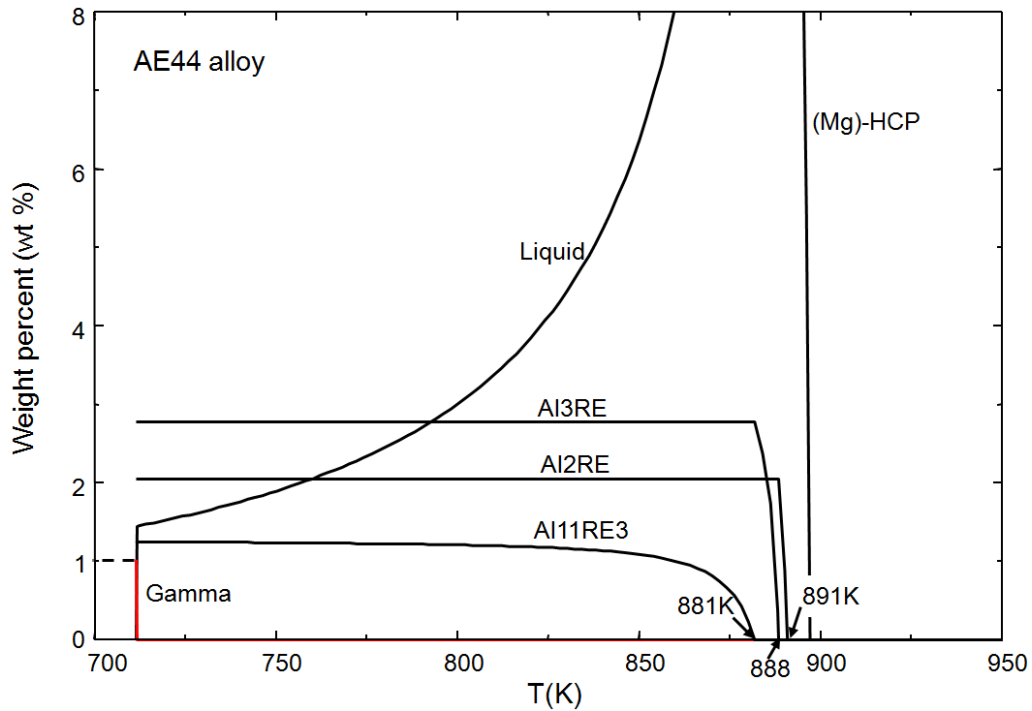
Figure 10.4 Scheil-Gulliver cooling of AE44 alloy

The effect of RE on aluminum alloys

Adding RE to Al alloys can improve the mechanical properties of aluminum alloys. For example, the hardness and strength can be increased by the addition of Er to high purity Al or Al–Mg alloy, since the precipitated $ErAl_3$ (cP4-$AuCu_3$) phase has a high melting point, good thermal stability, and is coherent or semi-coherent with the FCC matrix (Nie et al., 2004).
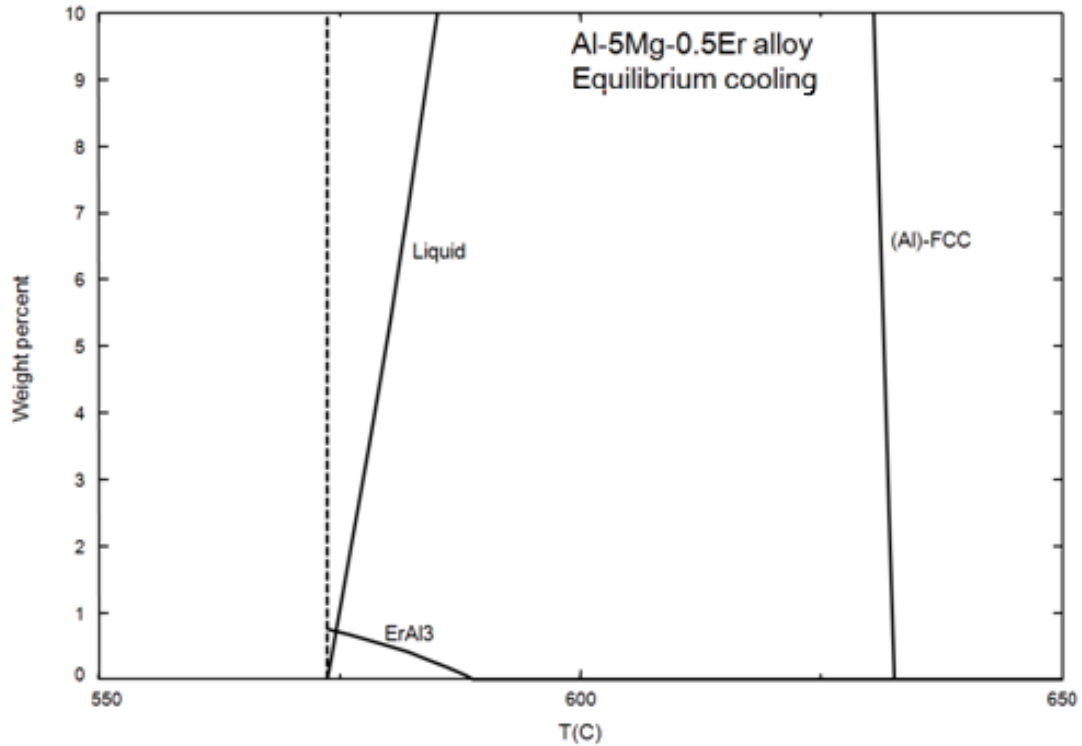
Figure 10.5 Equilibrium cooling of Al–5Mg–0.5Er alloy
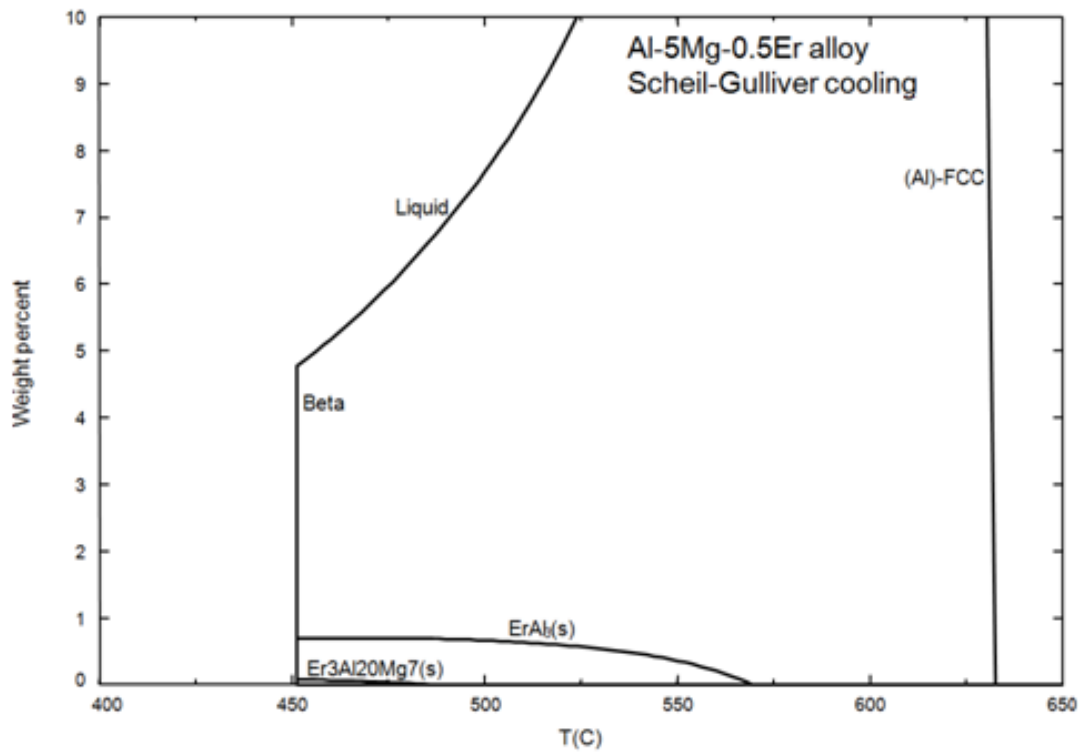
Figure 10.6 Scheil-Gulliver cooling of Al–5Mg–0.5Er alloy

<u>Short-range ordering in liquid solutions</u>

As discussed in chapters 5 and 6, Al–RE systems show a strong short-range ordering in liquid solutions. For the Al–La system as an example, Figure 10.7 shows the calculated pair fraction of Al–Al, Al–La, and La–La pairs in liquid at 2000 K using our optimized model parameters. It can be seen that the strongest short-range ordering occurs around $X_{La} = 0.33$.

As pointed out by Paliwal and Jung (Paliwal & Jung, 2009), the excess stability function (ES) as defined by Darken (Darken, 1967) is one indication of the tendency toward ordering:

$$ES = \left(\frac{\partial^2 G^E}{\partial X_i^2} \right)_{T,P}$$

eq. (10.1)

where G^E is the excess Gibbs energy of solution, X_i is the mole fraction of component i.

Figure 10.8 is the calculated ES versus mole fraction X_{La} in the stable or metastable liquid at different tempetures. The peak, which indicates the strongest short-range ordering shifts to the Al side as temperature increases. Furthermore, the short-range ordering tendency of liquid solutions decreases with increasing temperature.
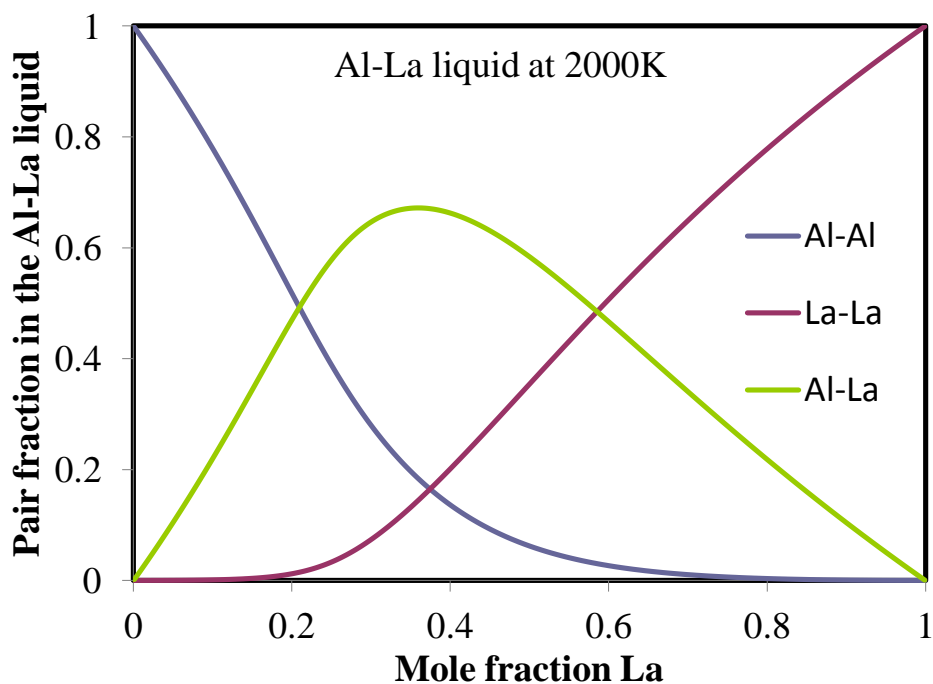
Figure 10.7 The calculated pair fraction in the Al–La liquid at 2000 K
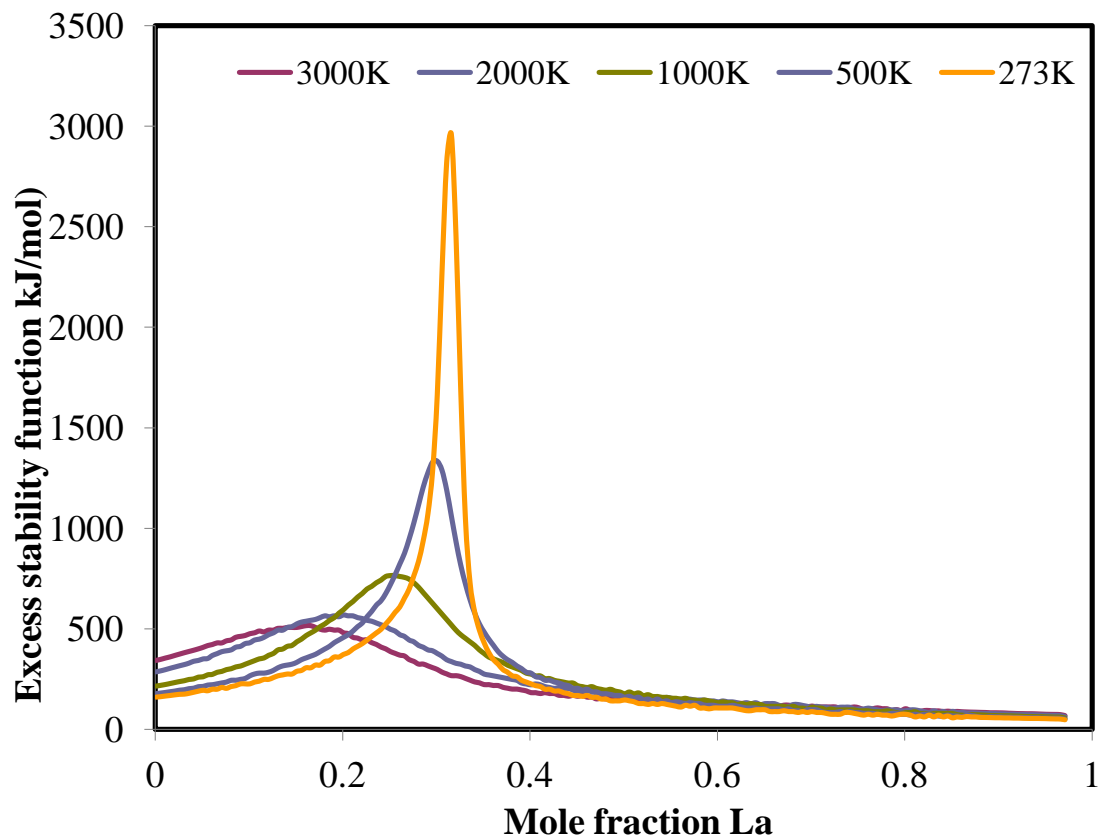
Figure 10.8 The calculated ES in the stable or metastable liquid at different tempetures

The calculations presented here are merely a few examples on what can be done with the thermodynamic database using the FactSage^{TM} software.

CONCLUSION AND RECOMMENDATIONS

The goal of the present study is to build a critically optimized thermodynamic database for Mg–Al–RE alloys. To this end, the Al–RE, Mg–RE, Al–Mg–RE, and Al–RE'–RE" systems were systematically optimized. The Al–Tm, Al–Lu and Al–Pm binary systems, which lack experimental data, are not included and the Al–Eu and Al–Yb systems that show anomalies compared with other Al–RE systems are not considered in this thesis. The Al–Sc and Al–Y systems, which were optimized previously and already available in our thermodynamic database, were not included in this work. All the available thermodynamic and phase equilibria data were evaluated in order to obtain a self-consistent thermodynamic database. The Modified Quasichemical Model, which takes short–range ordering into account, was used for the liquid phase and the Compound Energy Formalism (CEF) was used for the solid solutions in the binary and ternary systems.

The Al–RE (RE= La, Ce, Pr, Nd, Sm, Gd, Tb, Dy, Ho, Er) binary systems were optimized systematically taking into account the similar regularities across the lanthanide series. For the Al–Tb system, due to the lack of experimental data of thermodynamic properties and phase equilibria, one of the systematic methods—the reduced melting temperature proposed by Gschneidner—has been employed. The melting temperatures of intermetallic compounds in the Al–Tb system were then interpolated linearly according to this trend. Assuming the similarities between the Al–Gd and Al–Dy systems, the Al–Tb phase diagram was estimated and presented. The entropy of mixing of Al–RE liquid was considered to be better represented by MQM model than Bragg-William model.

The data on the Mg–light RE (RE= La, Ce, Pr, Nd, Sm) systems were critically reviewed and optimized in the present study. A high priority had been given to the solid solubility limits of RE elements in (Mg)-HCP in the thermodynamic optimizations. Since the reported solubility data in (Mg)-HCP were usually scattered or contradictory, the linear relationship between $\ln x_{RE}^{HCP}$ and $1/T$ when $\ln x_{RE}^{HCP}$ is very small (provided that γ_{RE}^{HCP} is only dependant on $1/T$ as is the case for

regular or sub-regular solutions with no excess entropy terms) served as a diagnostic tool to check trends among the solubility limits of the different light rare-earth elements. For enthalpy of formation of intermetallic compounds, the experimental data from vapor pressure measurement and solution calorimetry were sometimes quite different. For example, in the Mg–Ce system, the difference in enthalpy of formation data between Biltz and Pieper (Biltz & Pieper, 1924) using acid solution calorimetry and Ogren *et al*. (Ogren et al., 1967) using vapor pressure measurement is about 20 kJ/mole of atoms. The Miedema model was employed to estimate the enthalpy of formation for binary phases. The First-Principles calculations were also used to calculate the enthalpy of mixing in dilute Mg–RE systems and enthalpies of formation of intermetallic compounds. The calculations from the Miedema model, First-Principles and thermodynamic optimizations were compared and it was concluded that the calculated enthalpy of formation of compounds from ab-initio and from the Miedema model were comparable, although the latter may not be as accurate as the former.

The Miedema model was then used to calculate enthalpy of formation of ternary compounds in the Al–Mg–RE (RE= La, Ce, Pr, Nd, Sm) ternary systems. Moreover, key alloy experiments had were performed in the Mg-rich corners to check the phase equilibria and solid solubilities. The Al–Mg–RE systems were optimized based on available experimental data. No ternary parameters were used for the ternary liquid, which indicates reliable Gibbs energy data sets for the binary phases.

The Al–Mg–RE (RE= Gd, Tb, Dy, Ho, Er) ternary systems were systematically optimized. The Miedema model was also used to calculate the enthalpy of formation of ternary compounds and metastable phases. Considering the limited reliability of experimental data, no ternary parameters were used for the ternary liquid. It was worth noting that the Al–Mg–Tb system was estimated by assuming similarities with the Al–Mg–Gd and Al–Mg–Dy systems. That is, the existence of ternary compound Al_4MgTb was assumed and similar model parameters were used.

Finally, some examples of application were given using present developed thermodynamic database.

The hypothesis that the Modified Quasi-chemical Model (MQM) can well describe liquid solutions and that realistic results can be obtained for phase equilibria in multi-component systems (even without ternary parameters) was confirmed in this study.

This work contributes to materials engineering relevance for the thermodynamic database of Mg–Al–RE systems. The originality of this thesis includes:

1- All the Mg–Al–RE systems (including binary and ternary systems) were optimized for the first time using the Modified Quasichemical Model for liquid phases except the Al–Sc and Al–Y systems which were previously optimized by Kang et al. in CRCT, École Polytechnique de Montréal.

2- The Al–Mg–Pr and Al–Mg–Nd systems were optimized for the first time and the thermodynamic properties and phase equilibria of the Al–Tb, Al–Mg–Tb, Al–La–Nd, Al–Pr–Nd, Al–La–Pr, Al–Ce–La, and Al–Ce–Pr systems were estimated for the first time using systematic analysis. Estimation methods were used to approximate the enthalpy of formation of hypothetical or metastable phases, assuming the same trends as those calculated from first-principles.

3- The solid solubilities of RE (RE= La, Ce, Pr, Nd and Sm) in (Mg)–HCP solutions were critically reviewed and optimized systematically. This was done on the basis of the combination of recent solid solubility data for Mg–Nd system (Kopp) using atom probe tomography, the analysis of the solid solubility data in the $\ln x_{RE}^{HCP}$ versus $1/T$ relationship, the recent experimental enthalpy of formation data in Mg–La system and our First-Principles calculations for enthalpies of formation of the $Mg_{12}La$, $Mg_{12}Ce$, $Mg_{12}Pr$, $Mg_{41}Nd_5$, and $Mg_{41}Sm_5$ binary intermetallic compounds which greatly influence the solid solubility of RE (La, Ce, Pr, Nd and Sm) in (Mg)–HCP solutions.

4- The Miedema model was used for the first time to estimate the enthalpy of formation (ΔH_f) of ternary compounds in the Mg–Al–RE systems.

5- Key experiments were made in Mg-rich corner of Al–Mg–RE (La, Ce, Pr, Nd) systems.

6- A thermodynamic database for Mg–Al–RE alloys was constructed. This facilitates the development of Mg and Al alloys with RE additions, for practical industrial purposes.

Although a good agreement was reached between the experimental (or estimated) data and thermodynamically optimized data, some key experimental work remains to be done to fine-tune our model parameters.

The following recommendations are made regarding to the experimental work and First-Principles calculations:

For Mg–RE systems, it is known that acid solution calorimetry or vapor pressure measurements may result in large errors in obtaining the enthalpy of formation of compounds. It was pointed out by Ferro *et al*. (Ferro et al., 1998) that thermodynamic properties of Mg–RE systems obtained by these two methods may require revision. Therefore, other experimental methods (*e.g.* direct reaction calorimetry or the Smith method) have to be employed, at least for one Mg– light RE system and one Mg– heavy RE system, in order to verify or confirm the optimized model parameters.

For the Al–Mg–Sm system, no ternary compound at 673 K was found in the only available experimental report by Zheng *et al.* (Zheng et al., 1987). This contrasts with other Al–Mg–RE (RE= La, Ce, Pr, Nd, Gd, Dy, Ho, Er) systems where a ternary compound was found experimentally at 673 K. It would be worthwhile to perform more experiments on the Al–Mg–Sm system to verify this point.

For the Al–Mg–Tb system, liquidus temperatures have yet to be measured. The phase equilibria measurments, at least in Mg-rich area, remain to be done to verify assumptions of its similarities with Al–Mg–Gd and Al–Mg–Dy systems in the present work.

For the Al–La–Nd, Al–Pr–Nd, Al–La–Pr, Al–Ce–La, and Al–Ce–Pr systems, liquidus temperatures and phase equilibria remain to be measured.

Although the Al–Tm, Al–Lu, Al–Eu and Al–Yb systems are not considered in this thesis, preliminary results were obtained. However, new experimental measurements on their thermodynamic properties and phase equilibria are needed in order to fine-tune the model parameters.

Generally, the experimental work on the Mg–Al–RE systems demands careful sample preparation and careful measurement due to the evaporation of Mg or Al elements and oxidation of metals.

As to First-Principles calculations, the enthalpies of formation of ternary compounds in Al–Mg–RE systems and some metastable or hypothetic phases (*i.e.* RE_3Mg_{11} with α-La_3Al_{11} structure, $REAl_{12}$ with $CeMg_{12}$ structure) are needed for thermodynamic optimizations. The enthalpies of mixing in solutions could be of possible use if calculated from First-Principles, such as special quasi-random structures (SQS) or *ab initio* molecular dynamics (AMD).

The thermodynamic database obtained in this thesis will be integrated in Factsage^{TM} software and distributed to Factsage^{TM} users soon. It would greatly advance the development and design of new Mg and Al alloys with rare earth additions.

REFERENCES

Aljarrah, M., & Medraj, M. (2008). Thermodynamic modelling of the Mg-Ca, Mg-Sr, Ca-Sr and Mg-Ca-Sr systems using the modified quasichemical model. *CALPHAD: Computer Coupling of Phase Diagrams and Thermochemistry, 32*(2), 240-251.

Altunbas, M., & Harris, I. R. (1980). Structural and constitutional studies of some cerium-praseodymium alloys. *Journal of Materials Science, 15*, 693-701.

Ansara, I., Chart, T. G., Guillermet, A. F., Hayes, F. H., Kattner, U. R., Pettifor, D. G., & Saunders, N. (1997). Workshop on thermodynamic modelling of solutions and alloys: Schloβ Ringberg, March 10 to March 16, 1996 *Calphad* (Vol. 21, pp. 171-218).

Bakker, H. (1998). Enthalpies in alloys. Miedema's semi-empirical model. *Materials Science Foundations, 1*, i-ii, v, vii-x, 1-78.

Bale, C. W., Chartrand, P., Degterov, S. A., Eriksson, G., Hack, K., Ben Mahfoud, R., . . . Petersen, S. (2002). FactSage thermochemical software and databases. *CALPHAD: Computer Coupling of Phase Diagrams and Thermochemistry, 26*(2), 189-228.

Berche, A., Marinelli, F., Rogez, J., & Record, M. C. (2010). Enthalpy of formation of the La-Mg intermediate phases. *Thermochimica Acta, 499*(1-2), 65-70.

Biltz, W., & Pieper, H. (1924). Contributions to the systematic affinity principle. XXVII. The heats of formation of intermetallic compounds. IV. Cerium alloys. *Zeitschrift für anorganische und allgemeine Chemie, 134*, 13-24.

Blochl, P. E. (1994). Projector augmented-wave method. *Physical Review B, 50*(24), 17953.

Boer, F. R. D., Boom, R., Mattens, W. C. M., Miedema, A. R., & Niessen, A. K. (1988). *Cohesion In Metals: Transition Metal Alloys*. New York: North-Holland.

Born, M., & Oppenheimer, R. (1927). Zur Quantentheorie der Molekeln. *Annals of Physics*(84), 457-484.

Borzone, G., Borsese, A., & Ferro, R. (1983). A contribution to the study of the alloying behavior of the rare earths with tin. *Zeitschrift fuer Anorganische und Allgemeine Chemie, 501*, 199-208.

Borzone, G., Cacciamani, G., & Ferro, R. (1991). Heats of formation of aluminum-cerium intermetallic compounds. *Metallurgical Transactions A: Physical Metallurgy and Materials Science, 22A*(9), 2119-2123.

Borzone, G., Cardinale, A. M., Parodi, N., & Cacciamani, G. (1997). Aluminum compounds of the rare earths: enthalpies of formation of Yb-Al and La-Al alloys. *Journal of Alloys and Compounds, 247*(1-2), 141-147.

Borzone, G., Parodi, N., Ferro, R., Bros, J. P., Dubès, J. P., & Gambino, M. (2001). Heat capacity and phase equilibria in rare earth alloy systems. R-rich R-Al alloys (R=La, Pr and Nd). *Journal of Alloys and Compounds, 320*(2), 242-250.

Buschow, K. H. J. (1965a). the erbium-aluminum system and a comparison with the yttrium-aluminum system. *Zeitschrift für Metallkunde, 56*(1), 9-13.

Buschow, K. H. J. (1965b). Phase relations and intermetallic compounds in the systems neodymium-aluminum and gadolinium-aluminum. *Journal of the Less-Common Metals, 9*(6), 452-456.

Buschow, K. H. J., & Van Vucht, J. H. N. (1967). Systematic arrangement of the binary rare earth-aluminium systems. *Philips Research Reports, 22*(3), 233-245.

C. Bale, A. Pelton, & Thompson, W. (2008). Factsage thermochemical software and databases, from http://www.crct.polymtl.ca/

Cacciamani, G., Cardinale, A. M., Borzone, G., & Ferro, R. (2003a). Thermodynamic modelling and optimization of the Al-Ce-Nd system. *CALPHAD: Computer Coupling of Phase Diagrams and Thermochemistry, 27*(2), 227-233.

Cacciamani, G., De Negri, S., Saccone, A., & Ferro, R. (2003b). The Al-R-Mg (R = Gd, Dy, Ho) systems. Part II. Thermodynamic modelling of the binary and ternary systems. *Intermetallics, 11*(11-12), 1135-1151.

Cacciamani, G., Saccone, A., De Negri, S., & Ferro, R. (2002). The Al-Er-Mg ternary system. Part II: thermodynamic modeling. *Journal of Phase Equilibria, 23*(1), 38-50.

Cardinale, A. M., Cacciamani, G., Borzone, G., & Ferro, R. (2003). Experimental investigation of the Al-Ce-Nd system. *CALPHAD: Computer Coupling of Phase Diagrams and Thermochemistry, 27*(2), 221-226.

Casteels, F. (1967). Aluminum-rich parts of the aluminum-samarium and aluminum-dysprosium systems. *Journal of the Less-Common Metals, 12*(3), 210-220.

Ceperley, D. M., & Alder, B. J. (1980). Ground State of the Electron Gas by a Stochastic Method. *Physical Review Letters, 45*(7), 566.

Chartrand, P. (2006). Thermodynamic optimization of the Al-Mg system. *École Polytechnique de Montréal, Canada*, unpublished research.

Chartrand, P., & Pelton, A. (2001a). The modified quasi-chemical model: Part III. Two sublattices. *Metallurgical and Materials Transactions A, 32*(6), 1397-1407.

Chartrand, P., & Pelton, A. (2001b). Thermodynamic evaluation and optimization of the LiF-NaF-KF-MgF$_2$-CaF$_2$ system using the modified quasi-chemical model. *Metallurgical and Materials Transactions A, 32*(6), 1385-1396.

Chartrand, P., & Pelton, A. D. (2000). On the choice of \"geometric\" thermodynamic models. *Journal of Phase Equilibria, 21*(2), 141-147.

Chen, S. L., Daniel, S., Zhang, F., Chang, Y. A., Yan, X. Y., Xie, F. Y., . . . Oates, W. A. (2002). The PANDAT software package and its applications. *CALPHAD: Computer Coupling of Phase Diagrams and Thermochemistry, 26*(2), 175-188.

Colinet, C., Pasturel, A., & Buschow, K. H. J. (1985). Molar enthalpies of formation of lanthanide-aluminum (LnAl$_2$) compounds. *Journal of Chemical Thermodynamics, 17*(12), 1133-1139.

Colinet, C., Pasturel, A., & Buschow, K. H. J. (1988). Cohesive properties in the Al-Gd system. *Physica B+C, 150*(3), 397-403.

Cordfunke, E. H. P., & Konings, R. J. M. (2001a). The enthalpies of formation of lanthanide compounds : I. LnCl3(cr), LnBr3(cr) and LnI3(cr). *Thermochimica Acta, 375*(1-2), 17-50.

Cordfunke, E. H. P., & Konings, R. J. M. (2001b). The enthalpies of formation of lanthanide compounds : III. Ln2O3(cr). *Thermochimica Acta, 375*(1-2), 65-79.

Darken, L. S. (1967). Thermodynamics of binary metallic solutions. *Trans. metall. Soc. AIME, 239*, 80-89.

Davies, R. H., Dinsdale, A. T., Gisby, J. A., Robinson, J. A. J., & Martin, S. M. (2002). MTDATA - thermodynamic and phase equilibrium software from the national physical laboratory. *Calphad, 26*(2), 229-271.

De Negri, S., Saccone, A., Cacciamani, G., & Ferro, R. (2003). The Al-R-Mg (R = Gd, Dy, Ho) systems. Part I. Experimental investigation. *Intermetallics, 11*(11-12), 1125-1134.

Delfino, S., Saccone, A., & Ferro, R. (1984). Alloying behavior of indium with rare earths. *J. Less-Common Met. , 102*(2), 289-310.

Dinsdale, A. T. (1991). SGTE data for pure elements. *Calphad, 15*(4), 317-425.

Drits, M. E., Kadaner, E. S., Turkina, N. I., & Kuz'mina, V. I. (1978). Structure and properties of aluminum-terbium alloys. *Izvestiya Vysshikh Uchebnykh Zavedenii, Tsvetnaya Metallurgiya*(3), 157-158.

Du, Z., Yang, X., Ling, G., & Liu, H. (2004). Thermodynamic assessment of the Dy-Mg system *Z. Metallkd, 95*(12), 1115-1119.

Eriksson, G. (1975). Thermodynamic studies of high-temperature equilibriums. XII. SOLGASMIX, a computer program for calculation of equilibrium compositions in multiphase systems. *Chemica Scripta, 8*(3), 100-103.

Fabrichnaya, O. B., Lukas, H. L., Effenberg, G., & Aldinger, F. (2003). Thermodynamic optimization in the Mg-Y system. *Intermetallics, 11*(11-12), 1183-1188.

Ferro, R., Borzone, G., Cacciamani, G., & Parodi, N. (1998). Thermodynamics of rare earth alloys: systematics and experimental. *Thermochimica Acta, 314*(1-2), 183-204.

Ferro, R., & Delfino, S. (1979). Comments on the properties of silver-rich alloys in the silver-rare earth systems. *J. Less-Common Met. , 68*(2), 23-29.

Ferro, R., Delfino, S., Borzone, G., Saccone, A., & Cacciamani, G. (1993). Contribution to the evaluation of rare earth alloy systems. *Journal of Phase Equilibria, 14*(3), 273-279.

Ferro, R., & Saccone, A. (2008). *Intermetallic Chemistry*: Elsevier.

Franke, P., & Neuschütz, D. (Eds.). (2007). *Al-Dy (Aluminium - Dysprosium)* (Vol. (5a)).

Froes, F. H., Eliezer, D., & Aghion, E. (1998). the Science, Technology and Applications of Magnesium. *Journal of the Minerals, Metals, and Materials Society, 50*(9), 30-34.

Gao, M. C., Rollett, A. D., & Widom, M. (2007). Lattice stability of aluminum-rare earth binary systems: a first-principles approach. *Physical Review B: Condensed Matter and Materials Physics, 75*(17), 174120/174121-174120/174116.

Gorsse, S., Hutchinson, C. R., Chevalier, B., & Nie, J. F. (2005). A thermodynamic assessment of the Mg–Nd binary system using random solution and associate models for the liquid phase. *Journal of Alloys and Compounds, 392*(1-2), 253-262.

Greenwood, N. N., & Earnshaw, A. (1998). *Chemistry of the Elements (2nd Edition)*: Elsevier.

Gröbner, J., Kevorkov, D., Pisch, A., & Schmid-Fetzer, R. (2000). *Mg-Al-(Sc,Gd) alloy design using computational thermochemistry.* Paper presented at the Magnesium Alloys and Their Applications Conference, Munich, Germany.

Gröbner, J., Kevorkov, D., & Schmid-Fetzer, R. (2001). Thermodynamic calculation of Al-Gd and Al-Gd-Mg phase equilibria checked by key experiments. *Zeitschrift fuer Metallkunde, 92*(1), 22-27.

Gschneidner, K., & Calderwood, F. (1982a). The Ce−Nd (Cerium−Neodymium) system. *Journal of Phase Equilibria, 3*(1), 90-90.

Gschneidner, K., & Calderwood, F. (1982b). The Ce−Pr (Cerium−Praseodymium) system. *Journal of Phase Equilibria, 3*(2), 187-188.

Gschneidner, K., & Calderwood, F. (1982c). The La−Nd (Lanthanum-Neodymium) system. *Journal of Phase Equilibria, 2*(4), 452-453.

Gschneidner, K., & Calderwood, G. (1982d). The Nd−Pr (Neodymium−Praseodymium) system. *Journal of Phase Equilibria, 3*(2), 196-198.

Gschneidner, K. A. (1961). *Rare Earth Alloys; A Critical Review of the Alloy Systems of the Rare Earth, Scandium, and Yttrium Metals.*

Gschneidner, K. A., & Calderwood, F. W. (1989a). The Al-Tm (aluminum-thulium) system. *Bulletin of Alloy Phase Diagrams, 10*(1), 42-43.

Gschneidner, K. A., Jr. (1969). Interrelations of the physical properties of lanthanide compounds: the melting point, heat of formation, and lattice parameter(s). *Journal of the Less-Common Metals, 17*(1), 1-12.

Gschneidner, K. A., Jr. (1985). Systematics of the intra-rare-earth binary alloy systems. *J. Less-Common Met., 114*(Copyright (C) 2012 American Chemical Society (ACS). All Rights Reserved.), 29-42.

Gschneidner, K. A., Jr. (1990a). Physical properties of the Rare Earth Metals. *Bulletin of Alloy Phase Diagrams, 11*(3), 216-224.

Gschneidner, K. A., Jr. (1990b). Systematics of the thermochemistry of rare earth compounds. *Met., Mater. Processes, 1*(4), 241-251.

Gschneidner, K. A., Jr., & Calderwood, F. W. (1989b). The Al-Yb (aluminum-ytterbium) system. *Bulletin of Alloy Phase Diagrams, 10*(1), 47-49, 91-92.

Gschneidner, K. A., Pecharsky, V. K., Cho, J., & Martin, S. W. (1996). The [beta] to [gamma] transformation in cerium--A twenty year study. *Scripta Materialia, 34*(11), 1717-1722. doi: Doi: 10.1016/1359-6462(96)00035-8

Gschneidner, K. A. J., & Calderwood, F. W. (1982e). The Ce−La (Cerium−Lanthanum) system. *Bulletin of Alloy Phase Diagrams, 2*(4), 445-447.

Gulliver, G. H. (1913). The Quantitative Effect of Rapid Cooling on the Constitution of Binary Alloys. *Engineering (London), 95*, 380.

Guo, C., & Du, Z. (2004). Thermodynamic assessment of the La-Mg system. *Journal of Alloys and Compounds, 385*(1-2), 109-113.

Guo, C., & Du, Z. (2005). Thermodynamic assessment of the Mg-Pr system. *Journal of Alloys and Compounds, 399*(1-2), 183-188.

Hackenberg, R. E., Gao, M. C., Kaufman, L., & Shiflet, G. J. (2002). Thermodynamics and phase equilibria of the Al-Fe-Gd metallic glass-forming system. *Acta Materialia, 50*(9), 2245-2258.

Hillert, M. (2001). The compound energy formalism. *Journal of Alloys and Compounds, 320*(2), 161-176.

Jia, B. R., Liu, L. B., Yi, D. Q., Jin, Z. P., & Nie, J. F. (2008). Thermodynamic assessment of the Al-Mg-Sm system. *Journal of Alloys and Compounds, 459*(1-2), 267-273.

Jin, L.-L., & Chartrand, P. (2011a). Thermodynamic evaluation and optimizations of Al-Mg-La and Al-Mg-Ce systems with selected equilibrated-alloy experiments. *in preparation*.

Jin, L.-L., Chartrand, P., Kang, Y.-B., & Fuerst, C. D. (2010). Thermodynamic evaluation and optimization of Al-Gd, Al-Tb, Al-Dy, Al-Ho, and Al-Er systems using Modified Quasichemical Model for the liquid. *Calphad, 34*(4), 456-466.

Jin, L.-L., Kang, Y.-B., Chartrand, P., & Fuerst, C. D. (2011). Thermodynamic evaluation and optimization of Al-La,Al-Ce, Al-Pr, Al-Nd and Al-Sm systems using Modified Quasichemical Model for the liquid. *Calphad, 35*(1), 30-41.

Jin, L.-L., Kang, Y.-B., Chartrand, P., & Fuerst, C. D. (2012). Thermodynamic evaluation and optimization of Al-Mg-La, Al-Mg-Ce, Al-Mg-Pr, Al-Mg-Nd and Al-Mg-Sm systems with selected equilibrated-alloy experiments. *in preparation*.

Jin, L., & Chartrand, P. (2011b). Thermodynamic evaluation and optimizations of Al-Mg-Pr and Al-Mg-Nd systems with selected equilibrated-alloy experiments. *in preparation*.

Johansson, B., & Rosengren, A. (1975). Generalized phase diagram for the rare-earth elements: Calculations and correlations of bulk properties. *Physical Review B, 11*(8), 2836.

Johnson, Q. C., Smith, G. S., Wood, D. H., & Cramer, E. M. (1964). New structure in the Mg - rich region of the Ce - Mg system. *Nature, 201*, 600.

Jung, I.-H., Decterov, S. A., & Pelton, A. D. (2005). Critical thermodynamic evaluation and optimization of the CaO-MgO-SiO$_2$ system. *Journal of the European Ceramic Society, 25*(4), 313-333.

Jung, W. G., Kleppa, O. J., & Topor, L. (1991). Standard molar enthalpies of formation of PdAl, PtAl, ScAl$_{1.78}$, YAl$_2$ and LaAl$_2$. *Journal of Alloys and Compounds, 176*(2), 309-318.

Kang, Y.-B. (2008). Critical evaluation and thermodynamic optimization of the Mg- heavy rare earth binary systems. *École polytechnique de Montréal, Canada*, unpublished work.

Kang, Y.-B., Jin, L.-L., Chartrand, P., & Pelton, A. D. (2007a). *unpublished work., Ecole polytechnique de Montréal, Quebéc, Canada*.

Kang, Y.-B., Jin, L., & Chartrand, P. (2008a). Thermodynamic evaluation and optimization of Mg-RE and RE'-RE" binary systems using Modified Quasichemical Model for the liquid. *unpublished*.

Kang, Y.-B., Jin, L., Chartrand, P., Gheribi, A. E., Bai, K., & Wu, P. (2012). Thermodynamic evaluations and optimizations of binary Mg- light Rare Earth (La, Ce, Pr, Nd, Sm) systems. *Calphad, 38*, 100-116.

Kang, Y.-B., Jung, I.-H., Decterov, S. A., Pelton, A. D., & Lee, H.-G. (2004). Phase equilibria and thermodynamic properties of the $CaO-MnO-Al_2O_3-SiO_2$ system by critical evaluation, modeling and experiment. *ISIJ International, 44*(6), 975-983.

Kang, Y.-B., Pelton, A. D., Chartrand, P., & Fuerst, C. D. (2008b). Critical evaluation and thermodynamic optimization of the Al-Ce, Al-Y, Al-Sc and Mg-Sc binary systems. *Calphad, 32*(2), 413-422.

Kang, Y.-B., Pelton, A. D., Chartrand, P., Spencer, P., & Fuerst, C. D. (2007b). Critical evaluation and thermodynamic optimization of the binary systems in the Mg-Ce-Mn-Y system. *Journal of Phase Equilibria and Diffusion, 28*(4), 342-354.

Kang, Y.-B., Pelton, A. D., Chartrand, P., Spencer, P., & Fuerst, C. D. (2007c). Thermodynamic database development of the Mg-Ce-Mn-Y system for Mg alloy design. *Metallurgical and Materials Transactions A: Physical Metallurgy and Materials Science, 38*(6), 1231-1243.

Kirkaldy, J. S. (1958). Diffusion in multicomponent metallic systems. I. Phenomenological theory for substitutional solid-solution alloys. *Can. J. Phys., 36*, 899-906.

Kohler, F. (1960). Estimation of the thermodynamic data for a ternary system from the corresponding binary systems. *Monatsh. Chem., 91*, 738-740.

Kohn, W., & Sham, L. J. (1965). Self-Consistent Equations Including Exchange and Correlation Effects. *Physical Review, 140*(4A), A1133.

Kopp, V., Lefebvre, W., & Pareige, C. (2011). Determination of the Mg-Rich Phase Boundary of the Binary Mg-Nd Phase Diagram by Means of Atom Probe Tomography. *Journal of Phase Equilibria and Diffusion, 32*(4), 298-301.

Kresse, G., & Joubert, D. (1999). From ultrasoft pseudopotentials to the projector augmented-wave method. *Physical Review B, 59*(3), 1758.

Kresse, G., Marsman, M., & Furthmüller, J. VASP package, from http://cms.mpi.univie.ac.at/vasp/vasp/vasp.html

Kuzma, Y. B., Stelmakhovich, B. M., & Galamushka, L. I. (1992). Phase equilibriums and crystal structure of compounds in lutetium - aluminum and lutetium – copper - aluminum systems *Metally, 1*, 216-221.

Li, R., Yang, Q., Pang, S., Ma, C., & Zhang, T. (2008). Misch metal based metallic glasses. *Journal of Alloys and Compounds, 450*(1-2), 181-184.

Liu, Z.-K. (2008). Thermodynamic calculations and phase diagrams for magnesium and its alloys: part I. *JOM, 60*(12), 31.

Liu, Z.-K. (2009). First-Principles Calculations and CALPHAD Modeling of Thermodynamics. *Journal of Phase Equilibria and Diffusion, 30*(5), 517-534.

Lundin, C. E., Nachman, J. F., & Yamamoto, A. S. (1964). The praseodymium-neodymium system. *Proc. Conf. Rare Earth Res., 3rd, Clearwater, Florida, 1963*, 315-328.

Luo, Q., Zhao, D. Q., Pan, M. X., & Wang, W. H. (2006). Magnetocaloric effect in Gd-based bulk metallic glasses. *Applied Physics Letters, 89*(8), 081914-081913.

Markova, I. A., Terekhova, V. F., & Savitskii, E. M. (1963). Composition diagram of alloys in the praseodymium-neodymium system. *Zh. Neorg. Khim., 8*, 1998-2000.

Meschel, S. V., & Kleppa, O. J. (2001). Thermochemistry of alloys of transition metals and lanthanide metals with some IIIA and IVA elements in the periodic table. *Journal of Alloys and Compounds, 321*(2), 183-200.

Meyer, A. (1966). Aluminum-holmium system. *Journal of the Less-Common Metals, 10*(2), 121-129.

Meyer, A. (1970). On the Cubic and Rhombohedral Form of ErAl3. *Journal of Less-common Metals, 353*, 20.

Miedema, A. R., De Chatel, P. F., & De Boer, F. R. (1980). Cohesion in alloys - fundamentals of a semiempirical model. *Physica B+C: Physics of Condensed Matter + Atomic, Molecular and Plasma Physics, Optics (Amsterdam), 100*(1), 1-28.

Monkhorst, H. J., & Pack, J. D. (1976). Special points for Brillouin-zone integrations. *Physical Review B, 13*(12), 5188.

Nakaura, Y., Watanabe, A., & Ohori, K. (2006). Effects of Ca,Sr additions on properties of Mg-Al based alloys. *Mater. Trans., 47*, 1031-1039.

Nayeb-Hashemi, A. A., & Clark, J. B. (1988a). "Dy-Mg (Dysprosium-Magnesium)" *Phase diagrams of binary magnesium alloys* (pp. 104-108). Metals Park, Ohio: ASM International

Nayeb-Hashemi, A. A., & Clark, J. B. (1988b). "Er-Mg (Erbium-Magnesium)" *Phase diagrams of binary magnesium alloys* (pp. 108-112). Metals Park, Ohio: ASM International

Nayeb-Hashemi, A. A., & Clark, J. B. (1988c). "Gd-Mg (Gadolonium-Magnesium)" *Phase diagrams of binary magnesium alloys* (pp. 128-142). Metals Park, Ohio: ASM International

Nayeb-Hashemi, A. A., & Clark, J. B. (1988d). "Ho-Mg (Holmium-Magnesium)" *Phase diagrams of binary magnesium alloys* (pp. 157-160). Metals Park, Ohio: ASM International

Nayeb-Hashemi, A. A., & Clark, J. B. (1988e). "Mg-Pr (Magnesium-Praseodymium)" *Phase diagrams of binary magnesium alloys* (pp. 252-256). Metals Park, Ohio: ASM International

Nayeb-Hashemi, A. A., & Clark, J. B. (1988f). "Mg-Tb (Magnesium-Terbium)" *Phase diagrams of binary magnesium alloys* (pp. 313-316). Metals Park, Ohio: ASM International

Nie, Z. R., Fu, J. B., J.X, Z., Jin, T. N., Yang, J. J., Xu, G. F., . . . Zuo, T. Y. (2004). advanced alumimum alloys containing rare-earth erbium. *materials forum, 28*, 197-203.

Nie, Z. R., Jin, T., Fu, J., Xu, G., Yang, J., Zhou, J., & Zuo, T. (2002). research on rare earth in aluminum. *materials Science Forum, 396-402*, 1731-1736.

NIST. (2002). http://www.nist.gov/srd/thermo.cfm

Ogren, J., Magnani, N., & Smith, J. (1967). Thermodynamics of formation of binary rare earth-magnesium phases with CsCl-type structure. *Trans Soc AIME, 239*, 766–771.

Palenzona, A. (1972). Ytterbium-aluminum system. *Journal of the Less-Common Metals, 29*(3), 289-292.

Paliwal, M., & Jung, I.-H. (2009). Thermodynamic modeling of the Mg–Bi and Mg–Sb binary systems and short-range-ordering behavior of the liquid solutions. *Calphad, 33*(4), 744-754.

Pasturel, A., Chatillon-Colinet, C., Percheron-Guegan, A., & Achard, J. C. (1983). Thermodynamic study of the valence state of ytterbium in ytterbium-aluminum (YbAl2 and YbAl3) compounds. *Journal of the Less-Common Metals, 90*(1), 21-27.

Pekguleryuz, M. O., & Kaya, A. A. (2003). Creep Resistant Magnesium Alloys for Powertrain Applications *Magnesium: Proceedings of the 6th International Conference Magnesium Alloys and Their Applications* (pp. 74-93): Wiley-VCH

Pekguleryuz, M. O., & Renaud, J. (2000). *Creep resistance in Mg-Al-Ca casting alloys.* Paper presented at the Magnesium Technology 2000.

Pelton, A., & Chartrand, P. (2001a). The modified quasi-chemical model: Part II. Multicomponent solutions. *Metallurgical and Materials Transactions A: Physical Metallurgy and Materials Science, 32*(6), 1355-1360.

Pelton, A., & Chartrand, P. (2001b). Thermodynamic evaluation and optimization of the LiCl-NaCl-KCl-RbCl-CsCl-MgCl$_2$-CaCl$_2$ system using the modified quasi-chemical model. *Metallurgical and Materials Transactions A, 32*(6), 1361-1383.

Pelton, A. D. (2001). A general "geometric" thermodynamic model for multicomponent solutions. *Calphad, 25*(2), 319-328.

Pelton, A. D., & Blander, M. (1986). Thermodynamic analysis of ordered liquid solutions by a modified quasichemical approach-application to silicate slags. *Metall. Trans. B, 17B*(4), 805-815.

Pelton, A. D., & Chartrand, P. (2001c). The modified quasi-chemical model: Part II. Multicomponent solutions. *Metallurgical and Materials Transactions A: Physical Metallurgy and Materials Science, 32A*(6), 1355-1360.

Pelton, A. D., Degterov, S. A., Eriksson, G., Robelin, C., & Dessureault, Y. (2000). The modified quasichemical model I - binary solutions. *Metallurgical and Materials Transactions B: Process Metallurgy and Materials Processing Science, 31B*(4), 651-659.

Pettersen, G., Westengen, H., Hoier, R., & Lohne, O. (1996). Microstructure of a pressure die cast magnesium--4wt.% aluminium alloy modified with rare earth additions. *Materials Science and Engineering A, 207*(1), 115-120.

Pop, l., Dihoiu, N., Coldea, M., & Hăgan, C. (1979). The crystalline structure of the intermetallic compounds Gd$_2$Ni$_{17-x}$Al$_x$. *Journal of the Less-common Metals 64*, 64.

Powell, B., Rezhets, V., Balogh, M., & Waldo, R. (2002). Microstructure and creep behavior in AE42 magnesium die-casting alloy. *JOM 54*(8), 34-38.

Rokhlin, L. L. (1978). Regularities in the structure and properties of magnesium alloys with rare earth metals. *Probl. Metalloved. Tsvetn. Splavov*, 59-70.

Rokhlin, L. L. (1995). Regularities of the Mg sides of the Mg-RE (magnesium-rare earth metal) phase diagrams: comments on evaluations. *Journal of Phase Equilibria, 16*(6), 504-507.

Rokhlin, L. L. (2007). The regularities in the Mg-rich parts of the phase diagrams, phase transformations and mechanical properties of magnesium alloys with individual rare earth metals. *Arch. Metall. Mater., 52*, 5-11.

Rokhlin, L. L., Bochvar, N. R., & Lysova, E. V. (1996). Phase equilibria in the Al-Gd-Mg system in solid state. *Journal of Materials Science Letters, 15*(23), 2077-2079.

Rokhlin, L. L., Bochvar, N. R., & Lysova, E. V. (1997). Liquidus surface of the Al-Gd-Mg system. *Metally*(5), 122-126.

Saccone, A., Cacciamani, G., De Negri, S., & Ferro, R. (2002). The Al-Er-Mg ternary system. Part I: experimental investigation. *Journal of Phase Equilibria, 23*(1), 29-37.

Saccone, A., Cacciamani, G., Maccio, D., Borzone, G., & Ferro, R. (1998). Contribution to the study of the alloys and intermetallic compounds of aluminium with the rare-earth metals. *Intermetallics, 6*(3), 201-215.

Saccone, A., Cardinale, A. M., Delfino, S., & Ferro, R. (2000). Gd-Al and Dy-Al systems: phase equilibria in the 0 to 66.7 at.% Al composition range. *Zeitschrift fuer Metallkunde, 91*(1), 17-23.

Saccone, A., Delfino, S., Borzone, G., & Ferro, R. (1989). The samarium-magnesium system: a phase diagram. [10.1016/0022-5088(89)90169-0]. *J. Less-Common Met., 154*(Copyright (C) 2011 American Chemical Society (ACS). All Rights Reserved.), 47-60. doi: 10.1016/0022-5088(89)90169-0

Saccone, A., Delfino, S., & Ferro, R. (1988). Rare earth alloying systematics: thallium alloys, a review. *J. Less-Common Met. , 143*, 1-23.

Saccone, A., Delfino, S., Macciò, D., & Ferro, R. (1993). Magnesium-rare earth phase diagrams: Experimental investigation of the Ho-Mg system. *Journal of Phase Equilibria, 14*(3), 280-287.

Saccone, A., Macciò, D., Delfino, S., & Ferro, R. (1995). The interpolated Tm-Mg phase diagram. *journal of Alloys and Compounds, 220*(1–2), 161-166.

Shobu, K. (2009). CaTCalc: New thermodynamic equilibrium calculation software. *Calphad, 33*(2), 279-287.

Shukla, A., Kang, Y.-B., & Pelton, A. D. (2008). Thermodynamic assessment of the Si-Zn, Mn-Si, Mg-Si-Zn and Mg-Mn-Si systems. *CALPHAD: Computer Coupling of Phase Diagrams and Thermochemistry, 32*(3), 470-477.

Shukla, A., Kang, Y.-B., & Pelton, A. D. (2009). Thermodynamic assessment of the Ce-Si, Y-Si, Mg-Ce-Si and Mg-Y-Si systems. *International Journal of Materials Research, 100*(2), 208-217.

Sommer, F., & Keita, M. (1987). Determination of the enthalpies of formation of intermetallic compounds of aluminum with cerium, erbium and gadolinium. *Journal of the Less-Common Metals, 136*(1), 95-99.

Sommer, F., Keita, M., Krull, H. G., Predel, B., & Lee, J. J. (1988). Thermodynamic investigations of aluminum-lanthanum alloys. *Journal of the Less-Common Metals, 137*, 267-275.

Speight, J. D., Harris, I. R., & Raynor, G. V. (1968). Alloys of cerium with neodymium, samarium, and terbium, and of praseodymium with terbium. *Journal of the Less-Common Metals, 15*, 317-330.

Spencer, P. J. (2008). A brief history of CALPHAD. *CALPHAD: Computer Coupling of Phase Diagrams and Thermochemistry, 32*(1), 1-8.

Spencer, P. J., Pelton, A. D., Kang, Y.-B., Chartrand, P., & Fuerst, C. D. (2008). Thermodynamic assessment of the Ca-Zn, Sr-Zn, Y-Zn and Ce-Zn systems. *CALPHAD: Computer Coupling of Phase Diagrams and Thermochemistry, 32*(2), 423-431.

Strucheva, N. E., & Novozhenov, V. A. (2009). Investigation of the physical-chemical properties of the Tb-Mg-Al system alloys. *Izv. Altai. Gos. Univ.*, 87-90.

Sun, S. P., Yi, D. Q., Liu, H. Q., Zang, B., & Jiang, Y. (2010). Calculation of glass forming ranges in Al-Ni-RE (Ce, La, Y) ternary alloys and their sub-binaries based on Miedema's model. *Journal of Alloys and Compounds, 506*(1), 377-387.

Sundman, B., Jansson, B., & Andersson, J. O. (1985). The Thermo-Calc databank system. *CALPHAD: Computer Coupling of Phase Diagrams and Thermochemistry, 9*(2), 153-190.

Swift, W. M., & Wallace, W. E. (1968). Magnetic characteristics of Laves phase compounds containing two lanthanides with aluminum. *Journal of Physics and Chemistry of Solids, 29*(11), 2053-2061.

Tao, X., Ouyang, Y., Liu, H., Feng, Y., Du, Y., He, Y., & Jin, Z. (2011). Phase stability of magnesium-rare earth binary systems from first-principles calculations. *Journal of Alloys and Compounds, 509*(24), 6899-6907.

Toop, G. W. (1965). Predicting ternary activities using binary data. *Trans. Am. Inst. Min., Metall. Pet. Eng., 233*(5), 850-855.

Vengrenovich, R. D., & Psarev, V. I. (1969). Phase diagram of an aluminum-ytterbium system. *Izvestiya Vysshikh Uchebnykh Zavedenii, Tsvetnaya Metallurgiya, 12*(5), 117-119.

Vogel, R., & Klose, H. (1954). The phase diagrams cerium-lanthanum, lanthanum-antimony, and cerium-indium. *Zeitschrift für Metallkunde, 45*, 633-638.

Waldner, P., & Pelton, A. D. (2004). Critical thermodynamic assessment and modeling of the Fe-Ni-S system. *Metallurgical and Materials Transactions B: Process Metallurgy and Materials Processing Science, 35B*(5), 897-907.

Wasiur-Rahman, S., & Medraj, M. (2009). Critical assessment and thermodynamic modeling of the binary Mg-Zn, Ca-Zn and ternary Mg-Ca-Zn systems. *Intermetallics, 17*(10), 847-864.

Yang, Z., Li, J. P., Zhang, J. X., Lorimer, G. W., & Robson, J. (2008). Review on research and development of magnesium alloys. *Acta Metallurgica Sinica (English Letters), 21*(5), 313-328.

Zanicchi, G., Riani, P., Mazzone, D., Marazza, R., Rossi, D., & Ferro, R. (1994). On some ternary alloys R'-R"-Al with rare earths. *Journal of Alloys and Compounds, 215*, 181-186.

Zhang, T., Li, R., & Pang, S. (2009). Effect of similar elements on improving glass-forming ability of La-Ce-based alloys. *Journal of Alloys and Compounds, 483*(1-2), 60-63.

Zhang, Y. (2010). *Experimental investigation of the Ca-Mg-Zn system via diffusion couples and key experiments.* master of applied science, Concordia university, Montréal.

Zhao, J.-C. (Ed.). (2007). *Methods for Phase Diagram determination*: Elsevier Ltd.

Zheng, C., Chen, L., Tian, S., & Ye, Y. (1986). Phase diagram of the magnesium-samarium system and intermetallic compound Sm_2Mg_{13}. *Wuji Huaxue, 2*(2), 80-84.

Zheng, C., Chen, L., & Ye, Y. (1987). Phase equilibria in the aluminum-magnesium-samarium system at 400 Deg. *Jinshu Xuebao, 23*(3), B117-B120.

Zhou, S. H., & Napolitano, R. E. (2008). Modeling of thermodynamic properties and phase equilibria for the Al-Sm binary system. *Metallurgical and Materials Transactions A, 39A*(3), 502-512.

APPENDIX 1   Physical Properties of Rare Earth Metals

Table 1: Crystal Structures, Metallic Radius, Atomic Volume, and Density at 297K or Below (Gschneidner, 1990a)**.**

Rare earth metal	Crystal structure	Metallic radius (nm), CN=12	Atomic volume (cm³/mol)	Density (g/cm³)
αSc	hcp	0.16406	15.039	2.989
βSc	bcc	0.166	15.6	2.88
αY	hcp	0.18012	19.893	4.469
βY	bcc	0.183	20.8	4.28
αLa	dhcp	0.18791	22.602	6.146
βLa	fcc	0.1875	22.45	6.187
γLa	bcc	0.190	23.3	5.97
αCe	fcc	0.172	17.2	8.16
βCe	dhcp	0.18321	20.947	6.689
γCe	fcc	0.18247	20.696	6.770
δCe	bcc	0.184	21.1	6.65
αPr	dhcp	0.18279	20.803	6.773
βPr	bcc	0.184	21.2	6.64
αNd	dhcp	0.18214	20.583	7.008
βNd	bcc	0.184	21.2	6.80
αPm	dhcp	0.1811	20.24	7.264

βPm	bcc	0.183	20.8	6.99
αSm	rhomb	0.18041	20.000	7.520
βSm	hcp	0.18176	20.450	7.353
γSm	bcc	0.182	20.8	7.25
Eu	bcc	0.20418	28.979	5.244
αGd	hcp	0.18013	19.903	7.901
βGd	bcc	0.181	20.2	7.80
α'Tb at 220K	ortho	0.1784	19.34	8.219
αTb	hcp	0.17833	19.310	8.230
βTb	bcc	0.181	20.3	7.82
α'Dy at 86K	ortho	0.1774	19.00	8.551
αDy	hcp	0.17740	19.004	8.551
βDy	bcc	0.180	19.7	8.23
Ho	hcp	0.17661	18.752	8.795
Er	hcp	0.17566	18.449	9.066
Tm	hcp	0.17462	18.124	9.321
αYb at 296K	hcp	0.19451	25.067	6.903
βYb	fcc	0.19392	24.841	6.966
γYb	bcc	0.198	26.4	6.57
Lu	hcp	0.17349	17.779	9.841

fcc: face-centered cubic, bcc: body-centered cubic, hcp: hexagonal close-packed, dhcp: double hexagonal close-packed, ortho: orthogonal.

Table 2: Transition Temperatures, Heats of Transformation of Rare Earth Metals (Gschneidner, 1990a)**.**

Rare Earth Metal	Melting Point °C	Transition 1 (α-β)			Transition 2 (β-γ)		
		Temperature °C	Phases	ΔH$_{tr}$ kJ/mol	Temperature °C	Phases	ΔH$_{tr}$ kJ/mol
Sc	1541	1337	hcp-bcc	4.00	-	-	-
Y	1522	1478	hcp-bcc	4.99	-	-	-
La	918	277(a)	dhcp-fcc	0.36	865	fcc-bcc	3.12
Ce	798	-148(b)	fcc-dhcp	-	726	fcc-bcc (γ-δ)	2.99
		10(c)	dhcp-fcc	0.18(d)			
Pr	931	795	dhcp-bcc	3.17	-	-	-
Nd	1021	863	dhcp-bcc	3.03	-	-	-
Pm	1042	890	dhcp-bcc	3.0(b)	-	-	-
Sm	1074	734	rhomb-hcp	0.2(b)	922	hcp-bcc	3.11
Eu	822	-	-	-	-	-	-
Gd	1313	1235	hcp-bcc	3.91	-	-	-
Tb	1356	1289	hcp-bcc	5.02	-	-	-
Dy	1412	1381	hcp-bcc	4.16	-	-	-
Ho	1474	-	-	-	-	-	-
Er	1529	-	-	-	-	-	-
Tm	1545	-	-	-	-	-	-
Yb	819	795	fcc-bcc	1.75	-	-	-
Lu	1663	-	-	-	-	-	-

(a) Jin *et al*. (Jin et al., 2011). (b) On heating (Gschneidner, 1990a). (c) (Gschneidner et al., 1996).
(d) (Gschneidner et al., 1996)

Table 3 Electron configurations of rare earth elements.

Element	Atomic number	Gaseous atom configuration	Solid atom configuration	Ion configuration		
				Ln $^{2+}$	Ln $^{3+}$	Ln $^{4+}$
La	57	[Xe] $4f^0 5d^1 6s^2$	[Xe] $4f^0 5d^1 6s^2$	[Xe] $5d^1$	[Xe] $4f^0$	-
Ce	58	[Xe] $4f^1 5d^1 6s^2$	[Xe] $4f^1 5d^1 6s^2$	[Xe] $4f^2$	[Xe] $4f^1$	[Xe]
Pr	59	[Xe] $4f^3 6s^2$	[Xe] $4f^2 5d^1 6s^2$	[Xe] $4f^3$	[Xe] $4f^2$	[Xe] $4f^1$
Nd	60	[Xe]$4f^4 6s^2$	[Xe]$4f^3 5d^1 6s^2$	[Xe] $4f^4$	[Xe] $4f^3$	[Xe] $4f^2$
Pm	61	[Xe] $4f^5 6s^2$	[Xe] $4f^4 5d^1 6s^2$	[Xe] $4f^5$	[Xe] $4f^4$	-
Sm	62	[Xe] $4f^6 6s^2$	[Xe] $4f^5 5d^1 6s^2$	[Xe] $4f^6$	[Xe] $4f^5$	-
Eu	63	[Xe] $4f^7 6s^2$	[Xe] $4f^7 6s^2$	[Xe] $4f^7$	[Xe] $4f^6$	-
Gd	64	[Xe]$4f^7 5d^1 6s^2$	[Xe]$4f^7 5d^1 6s^2$	[Xe] $4f^8$	[Xe] $4f^7$	-
Tb	65	[Xe] $4f^9 6s^2$	[Xe] $4f^8 5d^1 6s^2$	[Xe] $4f^9$	[Xe] $4f^8$	[Xe] $4f^7$
Dy	66	[Xe] $4f^{10} 6s^2$	[Xe] $4f^9 5d^1 6s^2$	[Xe] $4f^{10}$	[Xe] $4f^9$	[Xe] $4f^8$
Ho	67	[Xe] $4f^{11} 6s^2$	[Xe] $4f^{10} 5d^1 6s^2$	[Xe] $4f^{11}$	[Xe] $4f^{10}$	-
Er	68	[Xe] $4f^{12} 6s^2$	[Xe] $4f^{11} 5d^1 6s^2$	[Xe] $4f^{12}$	[Xe] $4f^{11}$	-
Tm	69	[Xe] $4f^{13} 6s^2$	[Xe] $4f^{12} 5d^1 6s^2$	[Xe] $4f^{13}$	[Xe] $4f^{12}$	-
Yb	70	[Xe] $4f^{14} 6s^2$	[Xe] $4f^{14} 6s^2$	[Xe] $4f^{14}$	[Xe] $4f^{13}$	-
Lu	71	[Xe] $4f^{14} 5d^1 6s^2$	[Xe] $4f^{14} 5d^1 6s^2$	[Xe]$4f^{14} 5d^1$	[Xe] $4f^{14}$	-
Sc	21	[Ar] $3d^1 4s^2$	[Ar] $3d^1 4s^2$	[Ar] $3d^1$	[Ar]	-
Y	39	[Kr] $4d^1 5s^2$	[Kr] $4d^1 5s^2$	[Kr] $4d^1$	[Kr]	-

APPENDIX 2   Modeling   of   Thermodynamic Properties and Phase Equilibria in Mg–RE and Mg–Al–RE (RE=Rare Earth) Systems

Liling Jin[1], Youn-Bae Kang[2], Arthur D. Pelton[1], Patrice Chartrand[1]

[1]Centre for Research in Computational Thermochemistry (CRCT), Dept. of Chemical Engineering, École Polytechnique de Montréal, Montreal, QC, H3C 3A7, Canada
[2] Graduate Institute of Ferrous Technology (GIFT), Pohang University of Science and Technology, Pohang, 790-784, Korea

Keywords: Mg alloy, Rare earth, Thermodynamic database, Alloy design

ABSTRACT

Adding rare earth metals (RE) to Mg and Mg–Al alloys may improve the creep resistance and strength at elevated temperatures due to the precipitation of the intermetallic phases (Al_xRE_y and Mg_xRE_y phases) and suppression of the detrimental $Mg_{17}Al_{12}$ phase in the interdendritic or grain boundary region. Thermodynamic models and databases can provide invaluable information to elucidate the complex precipitation behavior involving RE. In the present study, recent progress of Mg alloy database development with FactSage[TM] for the systems Mg–RE, Al–RE (RE = La, Ce, Pr, Nd, Y, Sc, …), and a number of Mg–Al–RE systems (RE = La, Ce, Pr, Nd, Y, Sc…), is presented. Applications of the newly developed database to Mg alloy design are also illustrated.

Introduction

The thermodynamic database for Mg–Al–RE systems has been prepared by critical evaluation, modeling and optimization of available phase equilibrium and thermodynamic data. It contains model parameters giving the thermodynamic properties as functions of temperature and composition. Using the FactSage^{TM} software [1], one is able to calculate the amounts and compositions of all phases at equilibrium at any temperature and composition in multi-component alloys, to follow the course of equilibrium or non-equilibrium Scheil-Gulliver cooling, to calculate corresponding heat effects, *etc*. The new databases and software will help to develop new potential Mg alloys for the automotive, aeronautical and other industries. This will significantly reduce the amount of time and resources devoted to experimental work.

In the present study, many relevant thermodynamic assessments for RE-containing Mg– and Al–alloy binary systems and Mg–Al–RE ternary systems will be presented using our Modified Quasichemical Model [2] for the liquid phase. Much attention has been paid to the solid solubility of the rare-earth metals in solid Mg in the investigations because of its positive effect on the strength properties and plasticity of the magnesium alloys. It was confirmed from the recent study of Hantzsche *et al.* [3] that magnesium sheets with weak textures, which promise improved sheet formability [4], can be obtained by adding small amounts of alloying elements such as Nd, Ce and Y. In this regard, the solid solubilities of the different RE elements in the (Mg)–HCP phase are important.

Methodology

Experimental data for Mg–Al–RE systems, especially for thermodynamic properties, are not abundant. Selected key alloys were investigated by the present authors using EPMA (electron probe micro-analysis) techniques. Detailed experimental results can be found elsewhere [5]. Also in thermodynamic modeling, the Gibbs energies of metastable or unstable components (*e.g.*, La in the HCP structure) are often required in order to estimate solution behavior; these are generally not possible to be obtained experimentally. Therefore, when essential experimental data were not

available during the optimizations, results from theoretical calculations such as first-principles calculations or Miedema's model were used instead [6], or estimations based on the similarity between RE elements or trends among RE systems were used. Details have been presented by Jin *et al.*[6, 7]. It is well known that the RE elements and RE-containing binary systems show regularities or similarities [8-10]. Therefore, it was decided that a systematic thermodynamic modeling and database development of RE-containing systems should be carried out. Consequently, a systematic thermodynamic modeling of many Mg–RE and Al–RE binary systems (followed by Mg–Al–RE ternary systems, *etc*.) has been performed, and the RE elements are now included in our large Mg alloy thermodynamic database. This database can be used to explore phase equilibria and thermodynamic properties of Mg–RE and Mg–Al–RE alloys with mischmetal composed of several RE elements.

Examples of the Thermodynamic Evaluations and Optimizations

In the present study, the Modified Quasichemical Model (MQM) for the liquid phase was used [2, 11]. It has been shown that the MQM generally gives superior results compared to the conventional Bragg-Williams (BW) random mixing model [12] when strong short-range ordering (SRO) appears in the liquid alloys, as is the case for Al–RE alloys. For the many solid solution phases in binary, ternary and multi-component systems, the Compound Energy Formalism [13] was employed.

Shown in Fig. 1 are the calculated Mg-rich phase diagrams of the Mg–RE(La, Ce, Nd, Gd) systems. $Mg_{12}RE$, $Mg_{17}RE_2$, $Mg_{41}RE_5$, Mg_5RE, Mg_3RE, Mg_2RE and MgRE have been described as solid solutions in these systems. Most experimental phase diagram data are well reproduced [6].
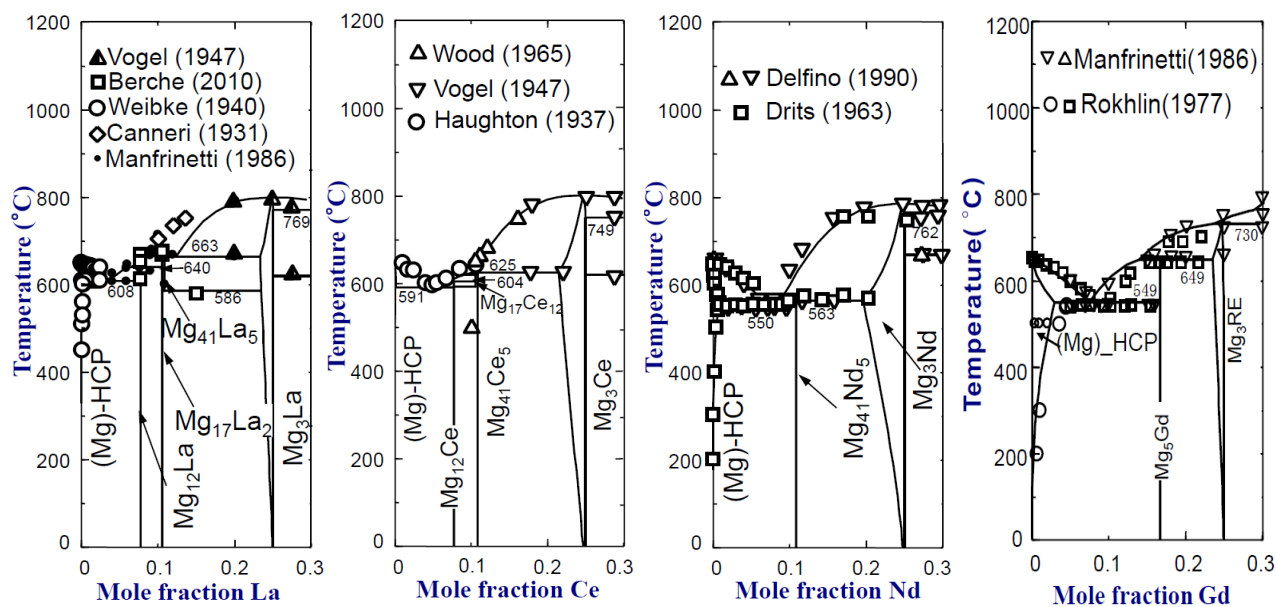
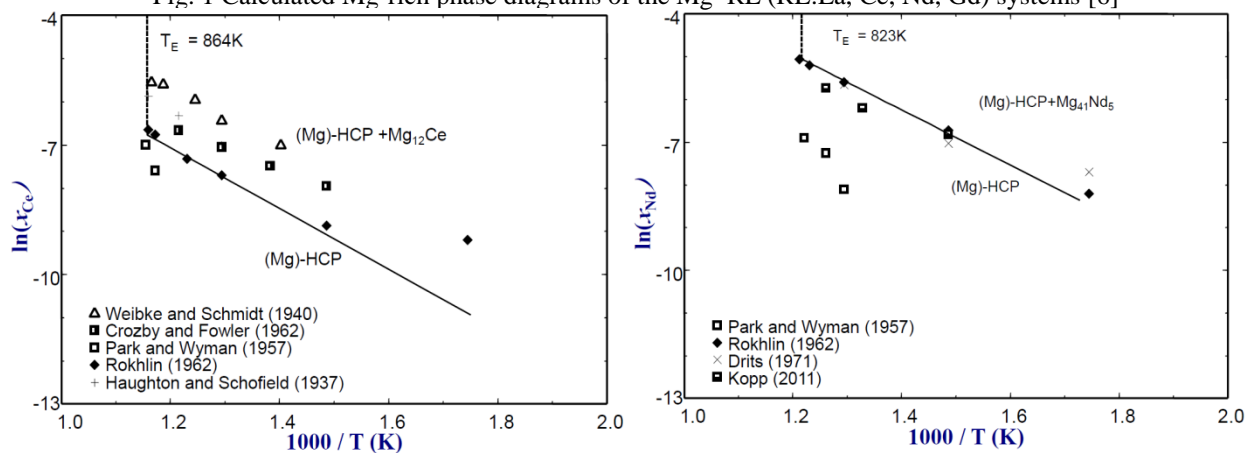Fig. 1 Calculated Mg-rich phase diagrams of the Mg–RE (RE:La, Ce, Nd, Gd) systems [6]

Fig. 2 Calculated solid solubility of Ce and Nd in (Mg)–HCP

Thermodynamic optimizations and database development for other Mg–RE binary systems have been carried out systematically, and the results have been described elsewhere [6]. Fig. 2 shows the calculated solubility of Ce and Nd in (Mg)–HCP [6], respectively. A linear relationship between $\ln x_{RE}^{HCP}$ versus $1/T$ was observed for light rare-earths, and this was used as one of the criteria to evaluate the experimental data for the dilute solid solubility.

In parallel to the thermodynamic modeling of the Mg–RE systems, critical evaluation and thermodynamic optimization of Al–RE systems have also been carried out [7, 14]. Fig. 3 shows the optimized phase diagram of the Al–Ce system along with experimental data [15-18]. A satisfactory agreement is obtained. Thermodynamic optimizations and database development for

other Al–RE binary systems have been carried out systematically, and the results have been described elsewhere [7, 14].

The thermodynamic modeling of the Mg–Ce and Al–Ce binary systems then was combined with thermodynamic modeling of the Al–Mg [19] system to describe the Gibbs energies of phases in the Mg–Al–Ce ternary system. In Fig. 4, a calculated isothermal section of the Mg–Al–Ce ternary system at 400 °C is shown [5]. According to the calculation, the (Mg)–HCP phase is in equilibrium with $Mg_{12}Ce$ ($Mg_{12}RE$), $(Al,Mg)_2Ce$ (Laves-C15), α-Al_3Ce(Al_3RE), α-$Al_{11}Ce_3$ ($Al_{11}RE_3$) and $Mg_{17}Al_{12}$ (Gamma) phases at 400 °C. This is generally in agreement with the experimental data of Odinaev et al. [20]. However, Odinaev et al. [20] reported a complete solid solution between Mg_2Ce and Al_2Ce with an intermediate miscibility gap at 400 °C even though Mg_2Ce is not stable at this temperature (Mg_2Ce decomposes to Mg_3Ce and MgCe at ~700 °C).
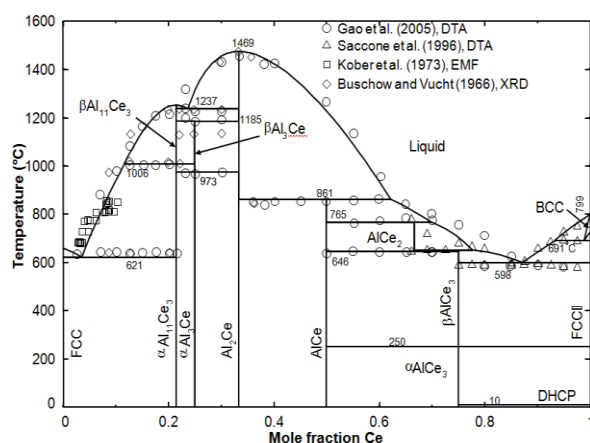

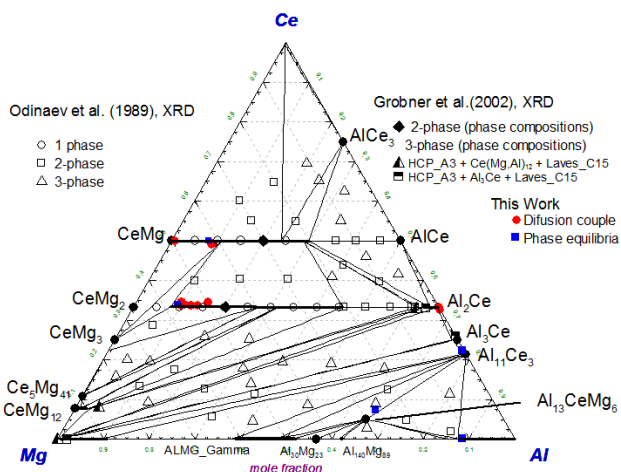Fig. 3 Calculated phase diagram of the Al–Ce system [7]

Fig. 4 Calculated isothermal section of the Mg–Al–Ce system at 400 °C [5]

Applications

Mischmetal (a mixture of rare earth elements, mainly Ce, La, Nd, Pr) is often used as alloying additions for magnesium alloys, while aluminum is added to improve castability and room temperature mechanical properties [21]. Shown in Fig. 5 is the liquidus projection at Mg-rich compositions for Mg–Al–mischmetal (RE: Ce, La, Nd, Pr) at weight ratios La/RE =0.25, Ce/RE =0.5 for AE alloys at Mg =94 wt%. The primary phase changes rapidly with the Al/RE ratio.
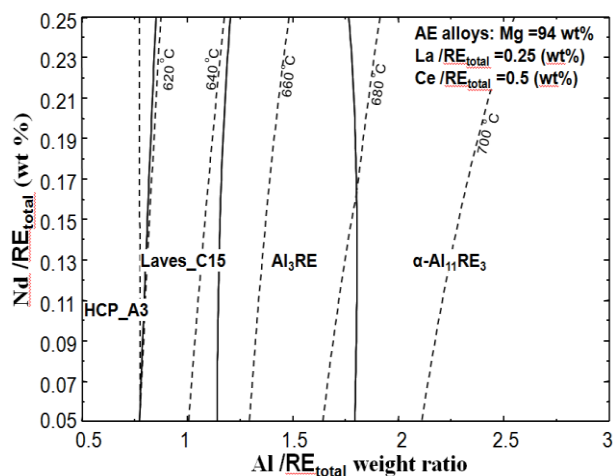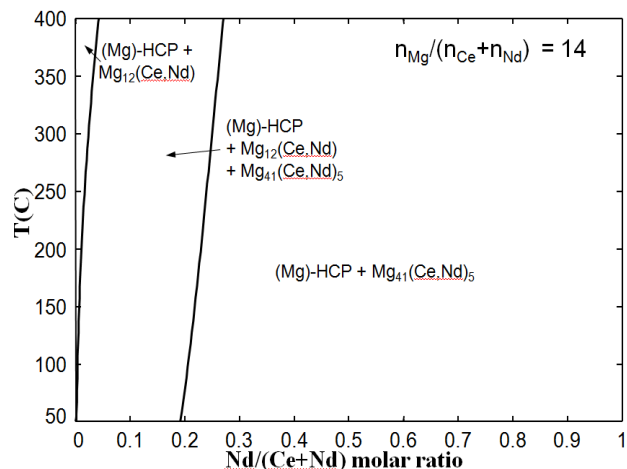
Fig. 5 Calculated liquidus projection of Mg–Al–RE system

Fig. 6 Calculated relative stability of $Mg_{12}RE_{(tI26)}$ and $Mg_{41}RE_{5\,(tI92)}$

As is known, the thermodynamic properties in Mg-rich alloys are very important for the Mg alloy design. In Mg–light RE systems, the equilibrium phase that saturates (Mg)–HCP is $Mg_{12}RE_{(tI26)}$ for La, Ce and Pr, while it is $Mg_{41}RE_{5(tI92)}$ for Nd and Sm. However, $Mg_{12}Nd_{(tI26)}$ is only observed in the quenched Mg–Nd samples [22], and is considered a metastable phase in the present study. The molar ratios of Nd+Sm over La+Ce+Pr in the mischmetal source will affect which of the $Mg_{12}RE_{(tI26)}$ or $Mg_{41}RE_{5\,(tI92)}$ solution phase will be stable during annealing. As an example, Fig. 6 shows the effect of the Rare Earth atomic ratio $\dfrac{Nd}{Nd+Ce}$ on the stability of $Mg_{12}RE_{(tI26)}$ and $Mg_{41}RE_{5\,(tI92)}$ phases for a Mg/RE molar ratio of 14 (*i.e.* at 93.33 at % Mg). Note that the diagram is quite insensitive to the Mg/RE molar ratio as long as it lies within the (Mg)–HCP + $Mg_{12}RE$ region.

Fig. 7 shows the predicted equilibrium cooling path for AE42 alloy (RE: $Ce_{0.5}La_{0.25}Nd_{0.2}Pr_{0.05}$) where no Mn, Zn or Si is included in the calculation. The HCP starts to solidify during cooling at 627 ℃. The Gamma phase ($Mg_{17}Al_{12}$) starts to precipitate in the HCP matrix at 195 ℃. The $Al_{11}Ce_3$ is the main constitution in $Al_{11}RE_3$ phase followed by $Al_{11}La_3$, $Al_{11}Nd_3$ and $Al_{11}Pr_3$.

It is known that Scheil-Gulliver cooling calculations can give reasonable predictions of the as-cast microstructure. Fig. 8 is the solidification behavior of the Mg - 4 wt. %Al - 2 wt. %RE ($Ce_{0.5}La_{0.25}Nd_{0.2}Pr_{0.05}$) (AE42) alloy assuming Scheil-Gulliver cooling. According to the calculation, the as-cast microstructure of the alloys will consist of primary α-(Mg) dendrites with 4% of the $Al_{11}RE_3$ phase.

The calculations presented here are merely a few examples on what can be done with the thermodynamic database using the FactSage^{TM} software.
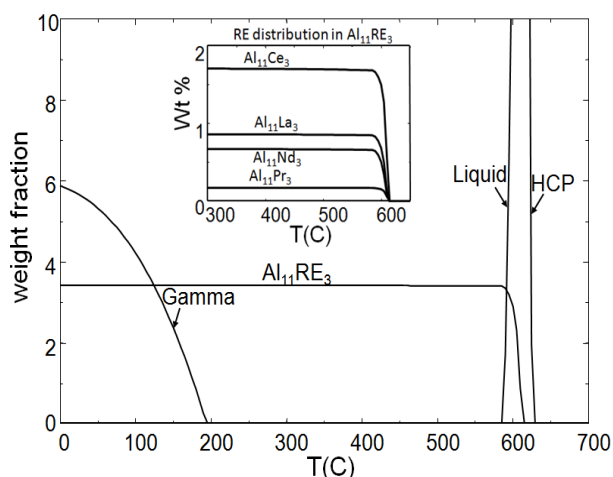

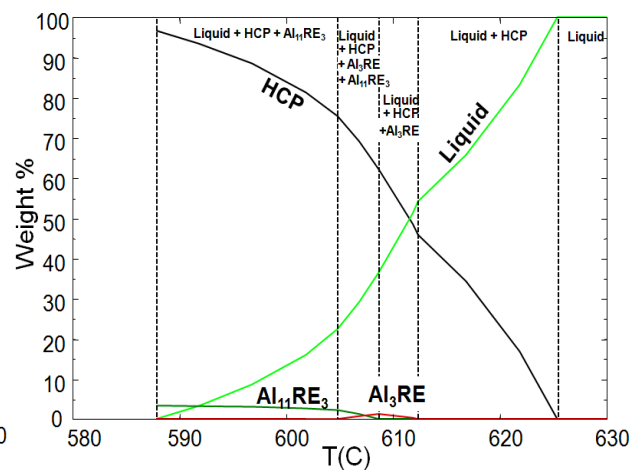Fig. 7 Calculated equilibrium cooling of AE42 alloys

Fig. 8 Scheil-Gulliver cooling of AE42 alloy

Summary

A thermodynamic database for Al–Mg–RE alloys has been developed through critical evaluation and thermodynamic optimization of relevant alloy systems. The solid solubility of RE in Mg–HCP was critically evaluated, and a linear relationship between $\ln x_{RE}^{HCP}$ versus $1/T$ was observed and used as one of the criteria to evaluate the experimental data of the dilute solid solubility for light rare-earths. Selected equilibrium alloys were investigated; first-principles and Miedema's model were employed to estimate the enthalpy of formation of the binary and ternary compounds. A few examples of applications of the thermodynamic database were illustrated. The developed thermodynamic dataset would be of great use to design new Mg and Al alloys with rare earth additions.

Acknowledgement

References

[1] C. W. Bale, P. Chartrand, S. A. Degterov, G. Eriksson, K. Hack, R. Ben Mahfoud, *et al.* FactSage thermochemical software and databases. CALPHAD: Computer Coupling of Phase Diagrams and Thermochemistry 26 (2002): 189-228.

[2] A. D. Pelton, S. A. Degterov, G. Eriksson, C. Robelin and Y. Dessureault. The modified quasichemical model I - binary solutions. Metallurgical and Materials Transactions B: Process Metallurgy and Materials Processing Science 31B (2000): 651-659.

[3] K. Hantzsche, J. Bohlen, J. Wendt, K. U. Kainer, S. B. Yi and D. Letzig. Effect of rare earth additions on microstructure and texture development of magnesium alloy sheets. Scripta Materialia 63 (2010): 725-730.

[4] S. Yi, J. Bohlen, F. Heinemann and D. Letzig. Mechanical anisotropy and deep drawing behaviour of AZ31 and ZE10 magnesium alloy sheets. Acta Materialia 58 (2010): 592-605.

[5] L.-L. Jin, Y.-B. Kang, P. Chartrand and C. D. Fuerst. Thermodynamic evaluation and optimization of Al-Mg-La, Al-Mg-Ce, Al-Mg-Pr, Al-Mg-Nd and Al-Mg-Sm systems with selected equilibrated-alloy experiments. in preparation (2011).

[6] Y.B.Kang, L. Jin, P. Chartrand, A. Gheribi, K. Bai and P. Wu. Thermodynamic evaluations and optimizations of Mg- light Rare Earth (RE: La, Ce, Pr, Nd, Sm) systems. Calphad (2012): submitted.

[7] L.-L. Jin, Y.-B. Kang, P. Chartrand and C. D. Fuerst. Thermodynamic evaluation and optimization of Al-La,Al-Ce, Al-Pr, Al-Nd and Al-Sm systems using Modified Quasichemical Model for the liquid. Calphad 35 (2011): 30-41.

[8] R. Ferro, S. Delfino, G. Borzone, A. Saccone and G. Cacciamani. Contribution to the evaluation of rare earth alloy systems. Journal of Phase Equilibria 14 (1993): 273-9.

[9] L. L. Rokhlin. The regularities in the Mg-rich parts of the phase diagrams, phase transformations and mechanical properties of magnesium alloys with individual rare earth metals. Arch. Metall. Mater. 52 (2007): 5-11.

[10] L. L. Rokhlin. Regularities of the Mg sides of the Mg-RE (magnesium-rare earth metal) phase diagrams: comments on evaluations. Journal of Phase Equilibria 16 (1995): 504-7.

[11] A. Pelton and P. Chartrand. The modified quasi-chemical model: Part II. Multicomponent solutions. Metallurgical and Materials Transactions A: Physical Metallurgy and Materials Science 32 (2001): 1355-1360.

[12] A. D. Pelton and Y.-B. Kang. Modeling short-range ordering in solutions. International Journal of Materials Research 98 (2007): 907-917.

[13] M. Hillert. The compound energy formalism. Journal of Alloys and Compounds 320 (2001): 161-176.

[14] L.-L. Jin, P. Chartrand, Y.-B. Kang and C. D. Fuerst. Thermodynamic evaluation and optimization of Al-Gd, Al-Tb, Al-Dy, Al-Ho, and Al-Er systems using Modified Quasichemical Model for the liquid. Calphad 34 (2010): 456-466.

[15] A. Saccone, A. M. Cardinale, S. Delfino and R. Ferro. Phase equilibria in the rare earth metals (R)-rich regions of the R-Al systems (R = La, Ce, Pr, Nd). Zeitschrift fuer Metallkunde 87 (1996): 82-7.

[16] K. H. J. Buschow and J. H. N. van Vucht. The binary systems cerium-aluminum and praseodymium-aluminum. Zeitschrift fuer Metallkunde 57 (1966): 162-6.

[17] M. C. Gao, N. Ünlü, G. J. Shiflet, M. Mihalkovic and M. Widom. Reassessment of Al-Ce and Al-Nd binary systems supported by critical experiments and first-principles energy calculations. Metallurgical and Materials Transactions A: Physical Metallurgy and Materials Science 36A (2005): 3269-3279.

[18] V. I. Kober, V. A. Lebedev, I. F. Nichkov, S. P. Raspopin and L. F. Yamshchikov. Thermodynamic properties of aluminum-rich cerium-aluminum alloys. Izv. Akad. Nauk SSSR, Metal. (1973): 217-20.

[19] P. Chartrand. Thermodynamic optimization of the Al-Mg system. École Polytechnique de Montréal, Canada (2006): unpublished research.

[20] K. O. Odinaev, I. N. Ganiev, V. V. Kinzhibalo and A. T. Tyvanchuk. Phase equilibrium diagram of the aluminum-magnesium-lanthanum system at 400 Deg. Izvestiya Vysshikh Uchebnykh Zavedenii, Tsvetnaya Metallurgiya (1988): 81-85.

[21] B. Powell, V. Rezhets, M. Balogh and R. Waldo. Microstructure and creep behavior in AE42 magnesium die-casting alloy. JOM Journal of the Minerals, Metals and Materials Society 54 (2002): 34-38.

[22] S. Delfino, A. Saccone and R. Ferro. Phase relationships in the neodymium-magnesium alloy system. Metallurgical Transactions A 21A (1990): 2109-14.

APPENDIX 3 Thermodynamic evaluations and optimization of Al–Ce–La, Al–Ce–Pr, Al–Ce–Nd, Al–La–Pr, Al–La–Nd and Al–Pr–Nd systems using the Modified Quasichemical Model for the liquid

All the present optimizations (La–Ce, La–Pr, La–Nd, Ce–Pr, Ce–Nd, Pr–Nd, Al–La–Ce, Al–La–Pr, Al–La–Nd, Al–Ce–Pr, Al–Ce–Nd, and Al–Pr–Nd) have been carried out by means of the FactSage thermodynamic software (Bale et al., 2002; C. Bale et al., 2008). The thermodynamic properties of pure Al and light rare earths (La, Ce, Pr and Nd) are taken from SGTE database (Dinsdale, 1991), except the Pr in the FCC–structure, together with La, Pr and Nd in the HCP–structure taken from Kang *et al.* (Kang et al., 2007a). The same models for the liquid and solid solutions are used. The optimized model parameters of liquid are shown in Table 1. The solid phases considered in this work are presented in Table 2.

Table 1: The coordination numbers and optimized model parameters of the MQM for the liquid in Mg-RE (RE= La, Ce, Pr, Nd, Sm) systems

| Coordination numbers				Gibbs energies of pair exchange reactions
i	j	Z^i_{ij}	Z^j_{ij}	(J/mol)
La	Nd	6	6	$\Delta g_{LaNd}= 174$
Ce	Pr	6	6	$\Delta g_{CePr}= 349$
Ce	La	6	6	$\Delta g_{CeLa}= 0$
Ce	Nd	6	6	$\Delta g_{CeNd}= 0$
La	Pr	6	6	$\Delta g_{LaPr}= 0$
Nd	Pr	6	6	$\Delta g_{NdPr}= 0$

Table 2: Crystal structures of the solid phases in Al-light RE (La, Ce, Pr, Nd) systems.

Proto-type	$\alpha Al_{11}La_3$	$BaAl_4$ [a]	Ni_3Sn	Cu_3Au	Cu_2Mg	AlCe	AlEr	Co_2Si	W	Cu	La
Pearson symbol	oI28	tI10	hP8	cP4	cF24	oC16	oP16	oP12	cI2	cF4	hP4
Al-La	$Al_{11}La_3$	$Al_{11}La_3$	Al_3La, La_3Al	✶	Al_2La	AlLa	✶	✶	BCC	FCC	DHCP
Al-Ce	$Al_{11}Ce_3$	$Al_{11}Ce_3$	Al_3Ce, Ce_3Al	Ce_3Al	Al_2Ce	AlCe	✶	✶	BCC	FCC	DHCP
Al-Pr	$Al_{11}Pr_3$	$Al_{11}Pr_3$	Al_3Pr, Pr_3Al	Pr_3Al	Al_2Pr	✶	AlPr	$AlPr_2$	BCC	FCC	DHCP
Al-Nd	$Al_{11}Nd_3$	$Al_{11}Nd_3$	Al_3Nd, Nd_3Al	✶	Al_2Nd	✶	AlNd	$AlNd_2$	BCC	FCC	DHCP

[a] $BaAl_4$: Al deficient. ✶: the phase is not a stable phase

1.1 The Ce–La, Ce–Nd, Ce–Pr, La–Pr, La–Nd and Pr–Nd binary systems

The Ce–La system is reviewed by Gschneidner and Calderwood (Gschneidner & Calderwood, 1982e). The optimized Ce–La system is based on the liquidus and FCC-to-BCC transformation data of Vogel and Klose (Vogel & Klose, 1954). Ce and La forms four continuous solid solutions: liquid, FCC_A1, BCC_A2, DHCP_A3'. The DHCP-to-FCC transformation for Ce occurs at 10 ℃ as suggested by Gschneidner *et al*. (Gschneidner et al., 1996). The lattice spacing for Ce–La alloys shows a small positive deviation from ideality (Vegard's law) for the whole compositions (Gschneidner & Calderwood, 1982e). The optimized phase diagram of the Ce–La system is shown in Figure 1, where no excess Gibbs energy parameter for the existing phases is used.
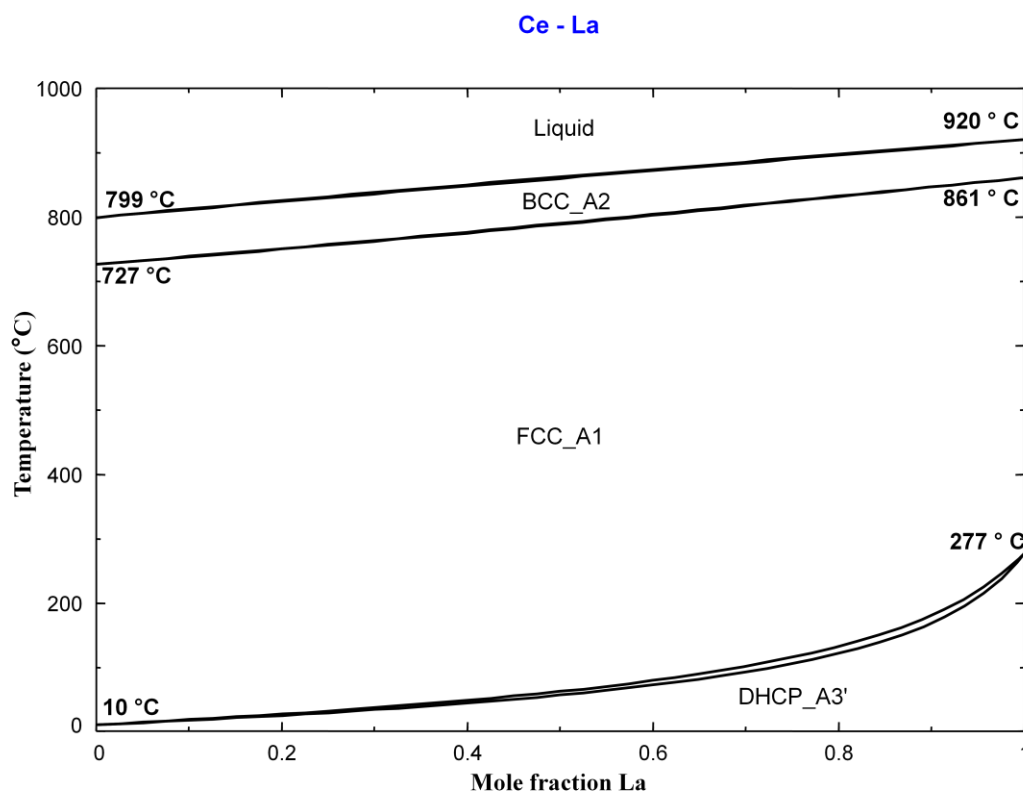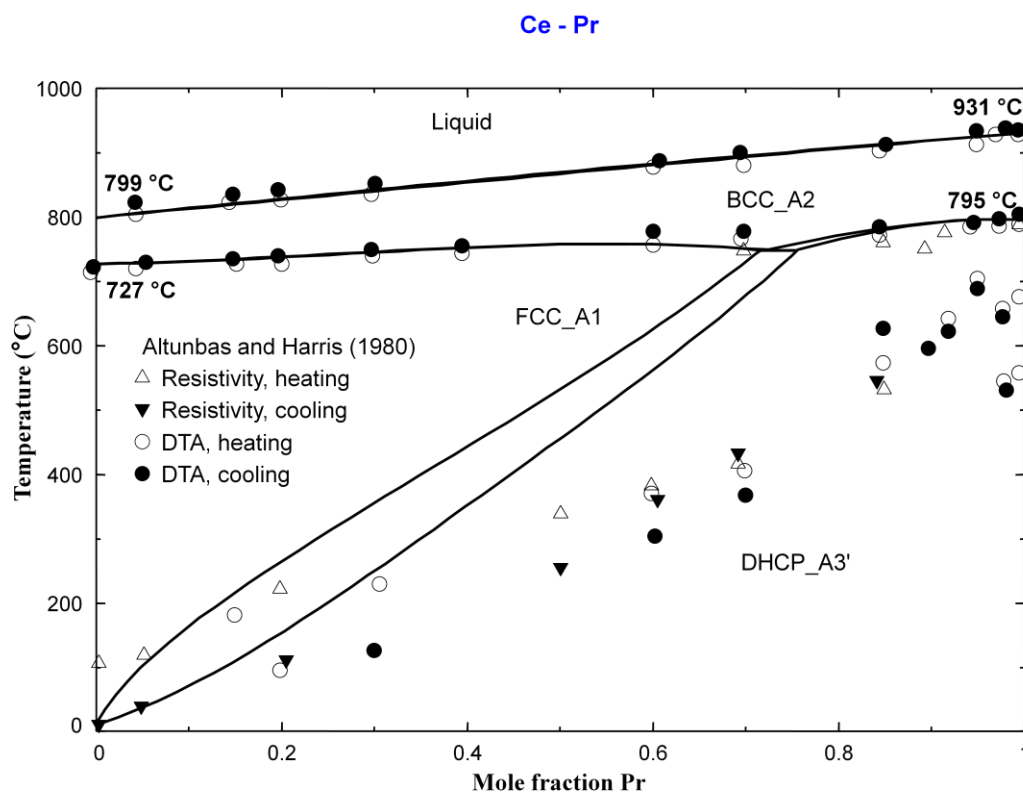
Ce - La

Figure 1. The calculated Ce–La phase diagram.

The Ce–Nd system is reviewed by Gschneidner and Calderwood (Gschneidner & Calderwood, 1982a). The assessed phase diagram is based on the lattice parameter studies investigated by Speight *et al*. (Speight et al., 1968), who observed a small deviation from ideality (Vegard's law) in the DHCP region. The optimized phase diagram of the Ce–Nd system is shown in Figure 2, where no excess Gibbs energy parameter for all the existing phases is used.
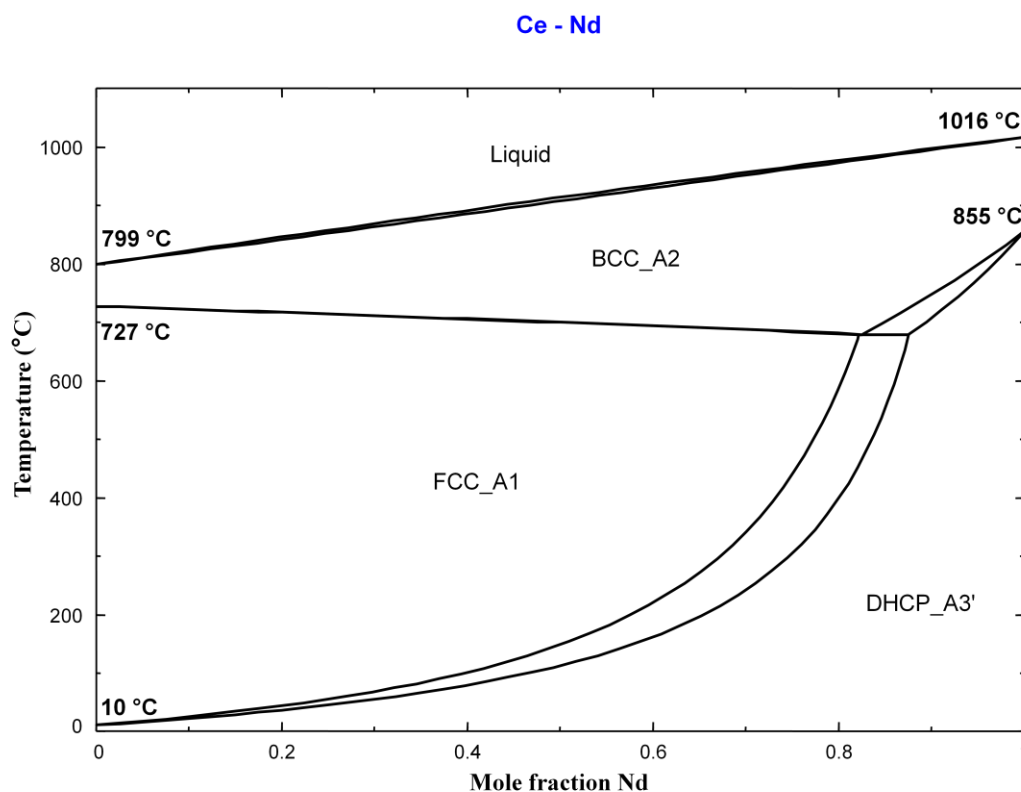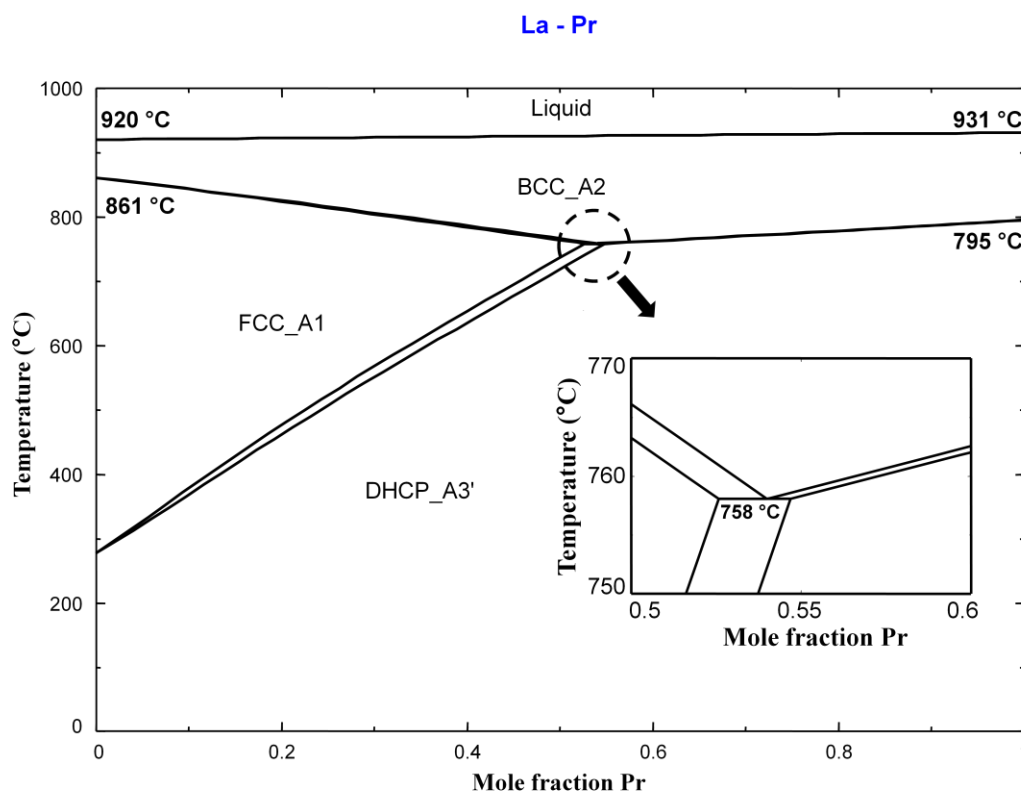
Figure 2. The calculated Ce–Nd phase diagram.

The Ce–Pr system is reviewed by Gschneidner and Calderwood (Gschneidner & Calderwood, 1982b). This system is investigated by Altunbas and Harris (Altunbas & Harris, 1980) using electrical resistivity, X-ray diffraction and DTA techniques. The optimized phase diagram of the Ce–Pr system is shown in Figure 3, where small excess Gibbs energy parameter for liquid, FCC and DHCP phase is used while BCC and HCP phases is ideal. The optimized model parameters of solid phases using CEF are summarized in Table 3.
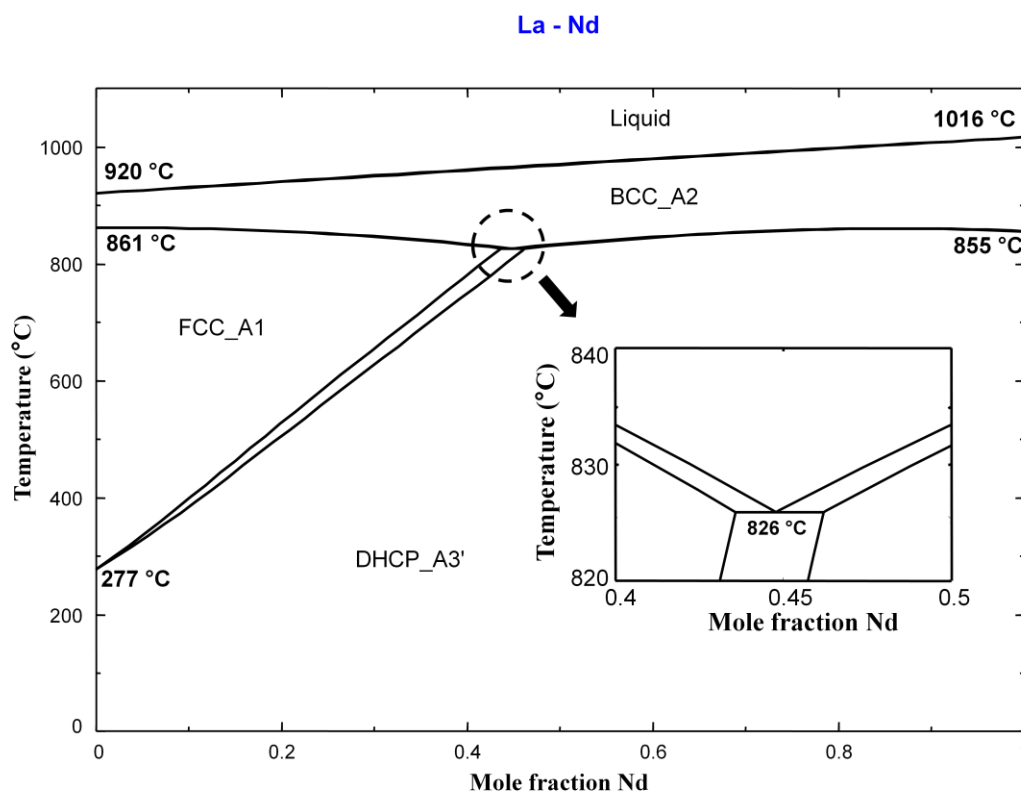
Figure 3. The calculated Ce–Pr phase diagram.

The La–Pr system is similar to Ce–Pr system. The qualitative feature of this system is proposed by Gschneidner (Gschneidner, 1985). The optimized phase diagram of the La–Pr system is shown in Figure 4, where no excess Gibbs energy parameter for any of the existing phases is used.

La - Pr

Figure 4. The calculated La–Pr phase diagram.

The La–Nd system is reviewed by Gschneidner and Calderwood (Gschneidner & Calderwood, 1982c). Gschneidner (Gschneidner, 1961) suggested that the BCC solid solution decomposes eutectoidally around 825 ℃ with FCC solid solution forming a close field and a complete DHCP solid solution below 310 ℃. The optimized phase diagram of the La–Nd system is shown in Figure 5, where small excess Gibbs energy parameter for liquid, FCC and DHCP phase is used while BCC, and HCP phases remains ideal. The DHCP-to-FCC phase transition for La occurs at 277 ℃ according to SGTE database (Dinsdale, 1991) instead of 310 ℃ from Gschneidner (Gschneidner, 1961).

Figure 5. The calculated La–Nd phase diagram.

The Pr–Nd system is reviewed by Gschneidner and Calderwood (Gschneidner & Calderwood, 1982d). The optimized phase diagram for Pr–Nd system is based on the work of Markova *et al*. (Markova et al., 1963) and Lundin *et al*. (Lundin et al., 1964). This system is proposed to be essentially ideal throughout the liquid and solid solutions (Lundin et al., 1964). The assessed phase diagram is shown in Figure 6, where no excess Gibbs energy parameter for any of the existing phases is used.

**Nd - Pr**
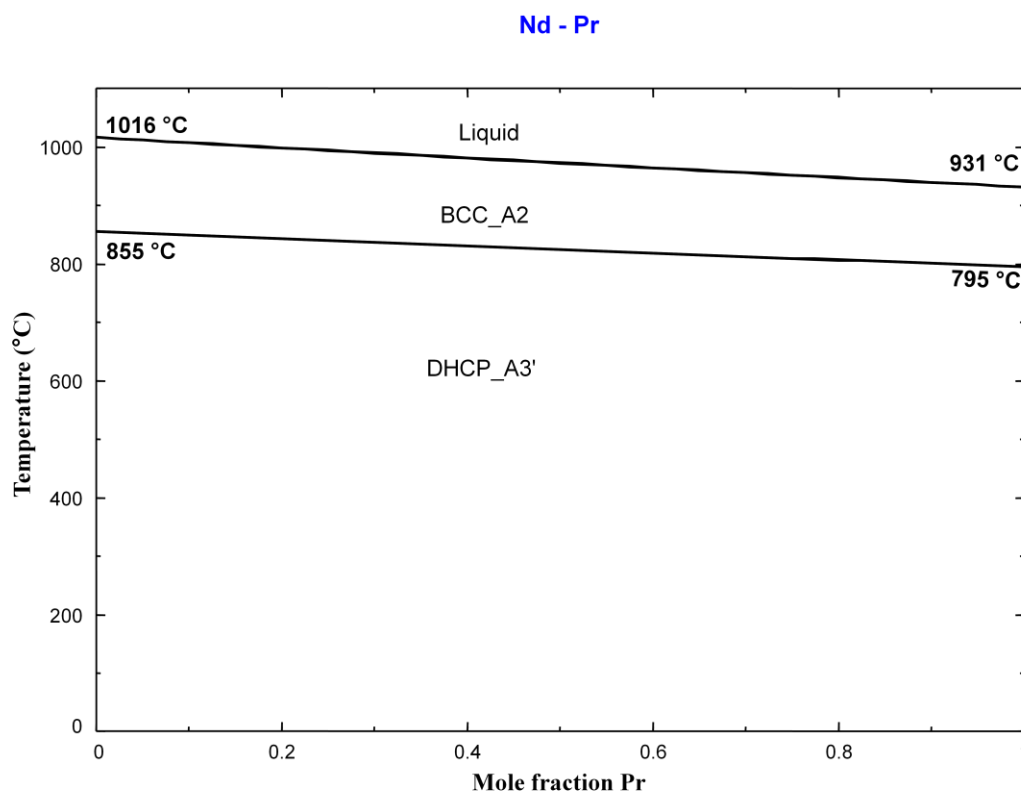
Figure 6. The calculated Pr–Nd phase diagram.

1.2 The Al–Ce–Nd system

This system has been optimized by Cacciamani *et al.* (Cacciamani et al., 2003a). Cardinale *et al.* (Cardinale et al., 2003) investigated Al–Ce–Nd isothermal section at 500 ℃ in the region of 25 to 67 at. % Al. the samples were characterized by metallographic microscopy, electron probe microanalysis (EPMA) and X-ray diffraction analysis. Three samples were subjected to differential thermal analysis (DTA), and three liquidus temperatures, 1118K, 1173K and 1123K, were reported for alloys $Ce_{0.3}Nd_{0.35}Al_{0.35}$, $Ce_{0.35}Nd_{0.25}Al_{0.4}$ and $Ce_{0.25}Nd_{0.45}Al_{0.3}$, respectively. No ternary compound was reported.

Since new optimizations for the Al–Ce and Al–Nd binary systems were carried out by using the Modified Quasichemical Model for the liquid phase (Jin et al., 2011), it is necessary to

recalculate the thermodynamic properties and phase diagram in the Al–Ce–Nd system by combining these new optimizations with the previous optimization for the Ce–Nd system by Kang (Kang et al., 2008a). The Ce–Nd system is considered as an ideal solution. The calculated isothermal section of the Al–Ce–Nd ternary system at 773K is shown in Figure 7 along with the experimental data of Cardinale *et al.* (Cardinale et al., 2003). The Gibbs energy of the liquid phase was calculated using the symmetric Kohler-Toop like approximation with no ternary interaction parameters. Since the enthalpy of mixing of the liquid in Al–Ce and Al–Nd systems are quite negative while that in Ce–Nd system is close to ideal, Al is considered as the asymmetrical element. Moreover, the Ce and Nd are chemically similar to each other and quite different to Al.
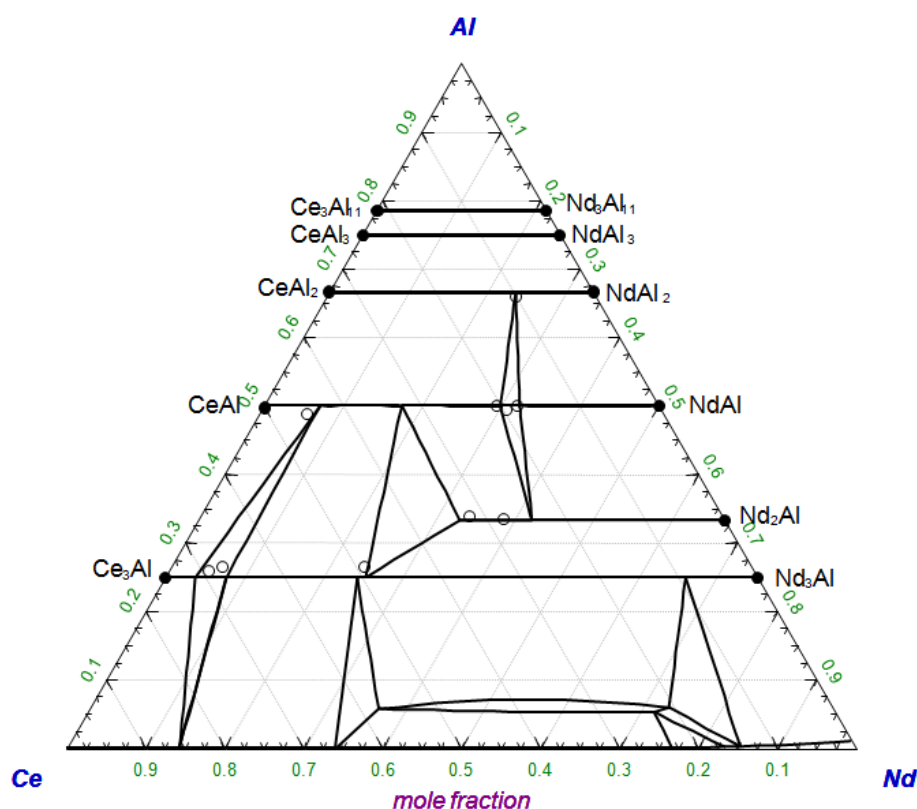
Figure 7. The calculated isothermal section of the Al–Ce–Nd ternary system at 773K compared with experimental data.

The calculated liquidus projection of the Al–Ce–Nd ternary system is shown in Figure 8 compared with the experimental data of Cardinale *et al.* (Cardinale et al., 2003).
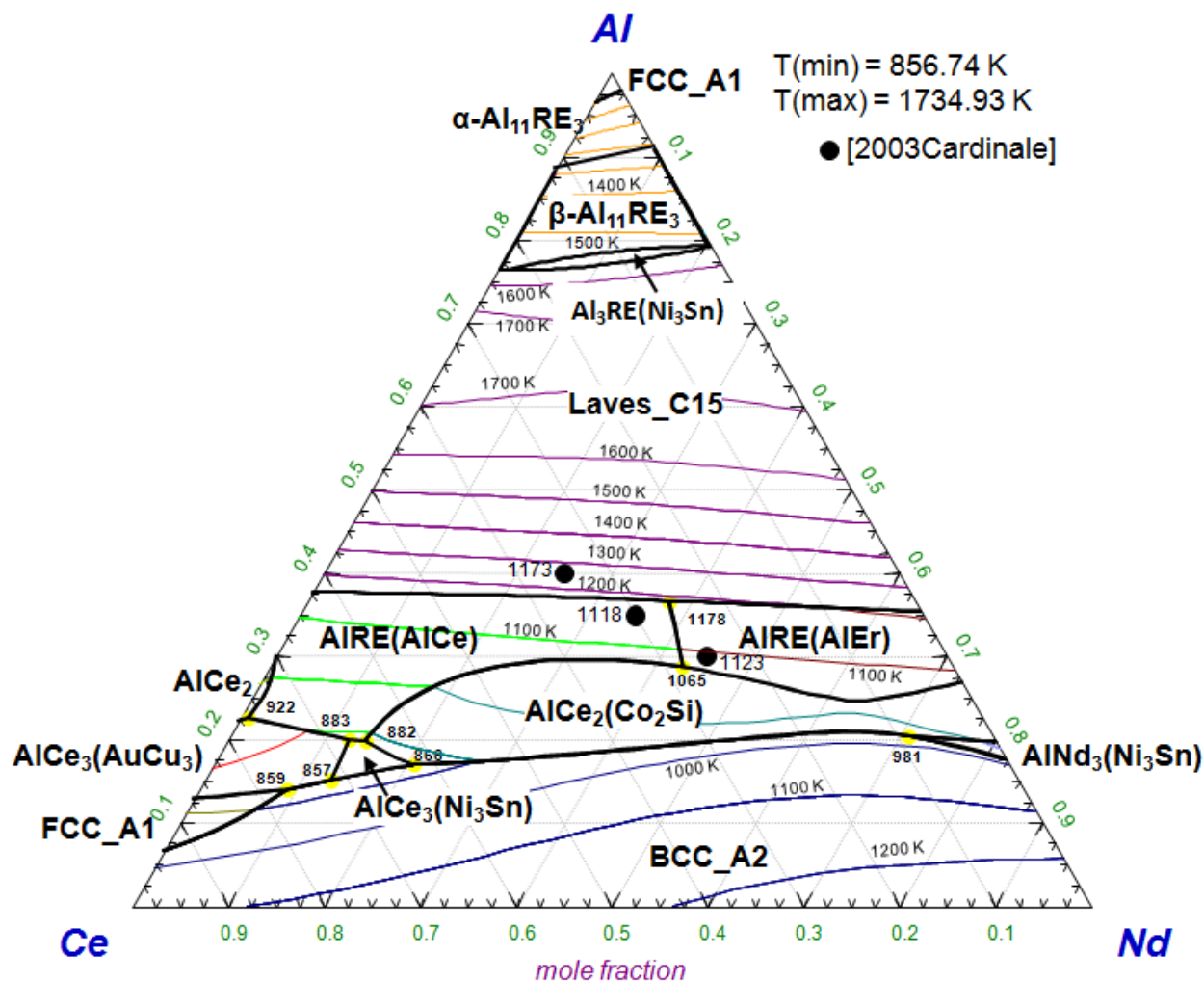
Figure 8. The calculated liquidus projection of the Al–Ce–Nd ternary system compared with experimental data.

1.3 The Al–La–Nd system

Zanicchi *et al.* (Zanicchi et al., 1994) observed three continuous solid solutions fields ($LaAl_2$-$NdAl_2$, $LaAl_3$-$NdAl_3$ and La_3Al_{11}-Nd_3Al_{11} sections) by metallographic microscopy and X-ray diffraction. No other experimental data is available. The calculated isothermal section of the Al–La–Nd ternary system at 773K is shown in Figure 9 considering the similarity to Al–Ce–Nd system.
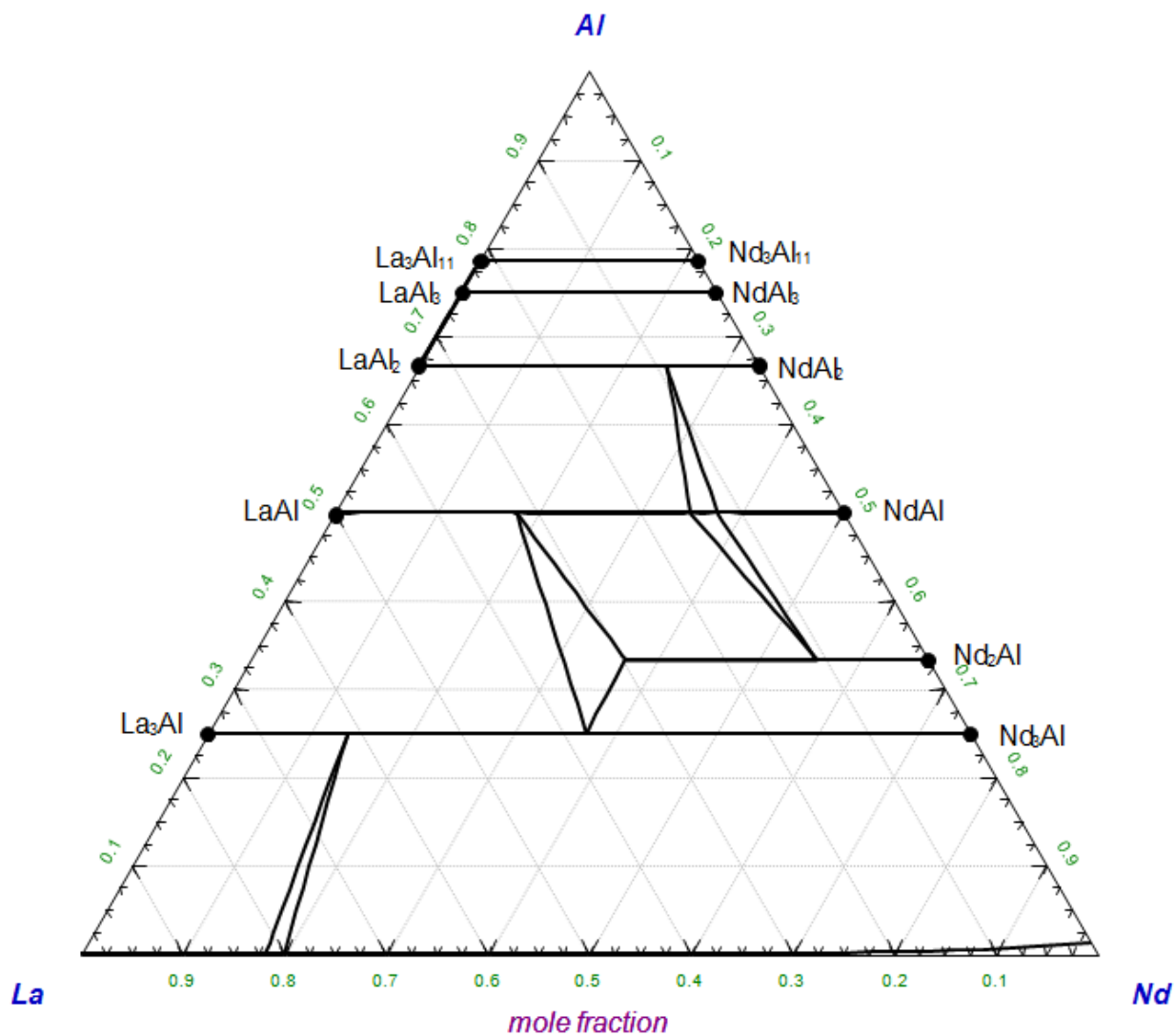
Figure 9. The calculated isothermal section of the Al–La–Nd ternary system at 773K compared with experimental data.

1.4 The Al–Pr–Nd system

Swift and Wallace (Swift & Wallace, 1968) reported a complete solid solution $PrAl_2$-$NdAl_2$. Zanicchi *et al.* (Zanicchi et al., 1994) studied the section $PrAl_3$-$NdAl_3$, where a complete solid solution were formed. The calculated isothermal section of the Al–Pr–Nd ternary system at 773K is shown in Figure 10 considering its similarity to Al–Ce–Nd system.
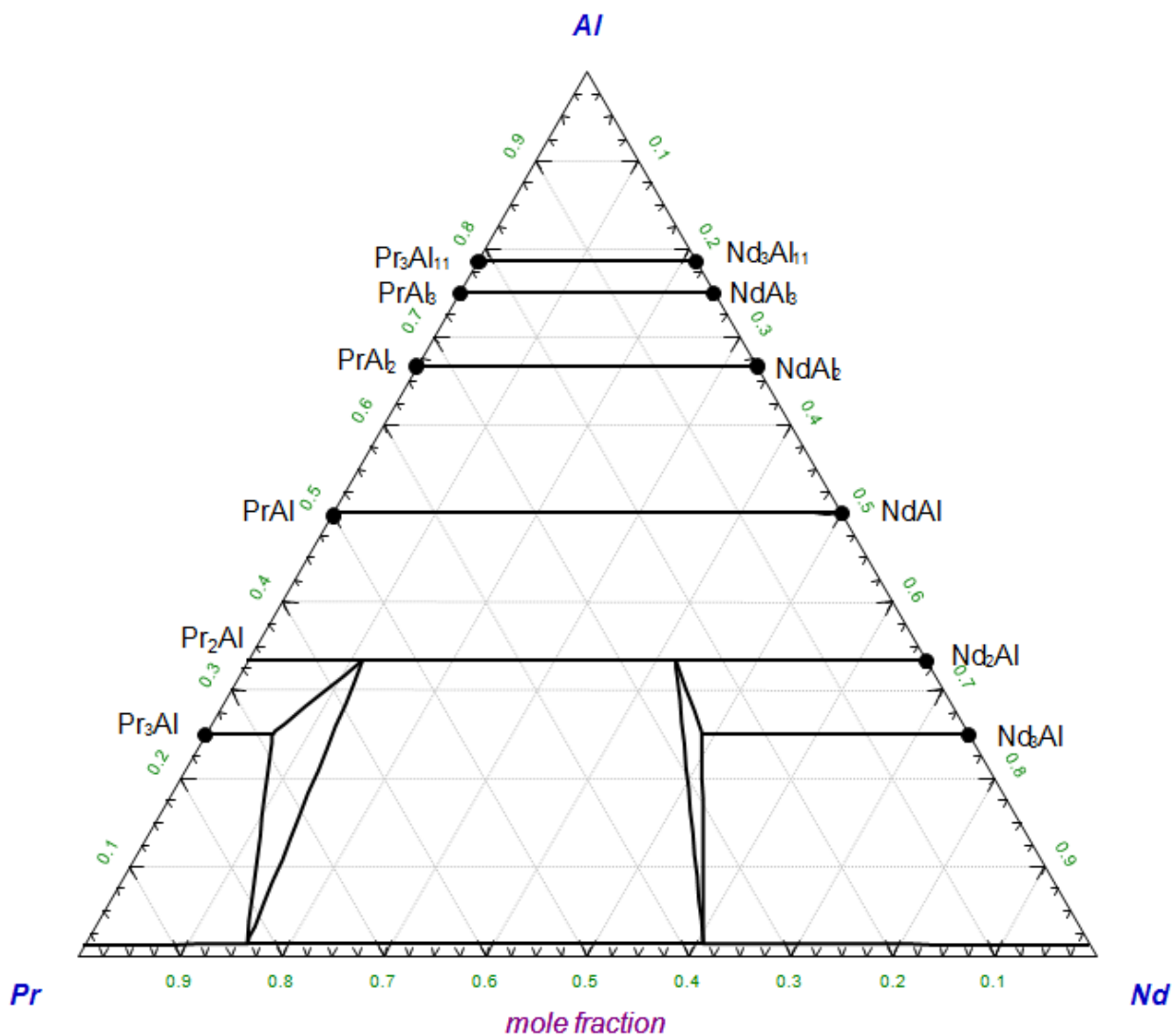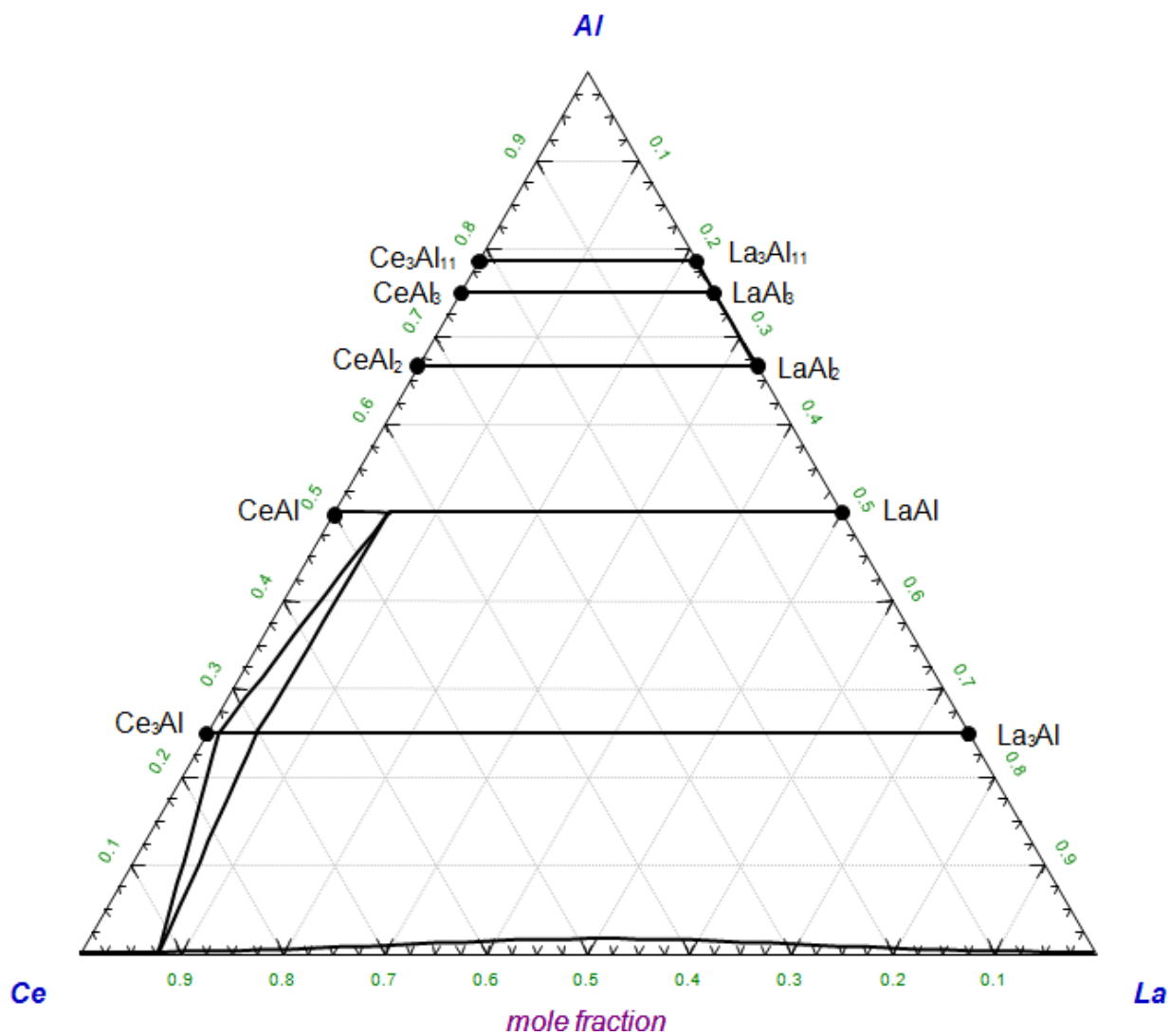
Figure 10. The calculated isothermal section of the Al–Pr–Nd ternary system at 773K compared with experimental data.

## 1.5 The Al–La–Pr, Al–Ce–La and Al–Ce–Pr systems

There is no experimental data available for Al–La–Pr, Al–Ce–La and Al–Ce–Pr systems. Considering the similarities among the rare earth elements, the complete solid solutions Laves_C15, $Al_{11}RE_3$, and Al_3RE may be expected. The isothermal sections for the Al–La–Pr, Al–Ce–La and Al–Ce–Pr systems are extrapolated directly from their subsystems and shown in Figs.11-13.
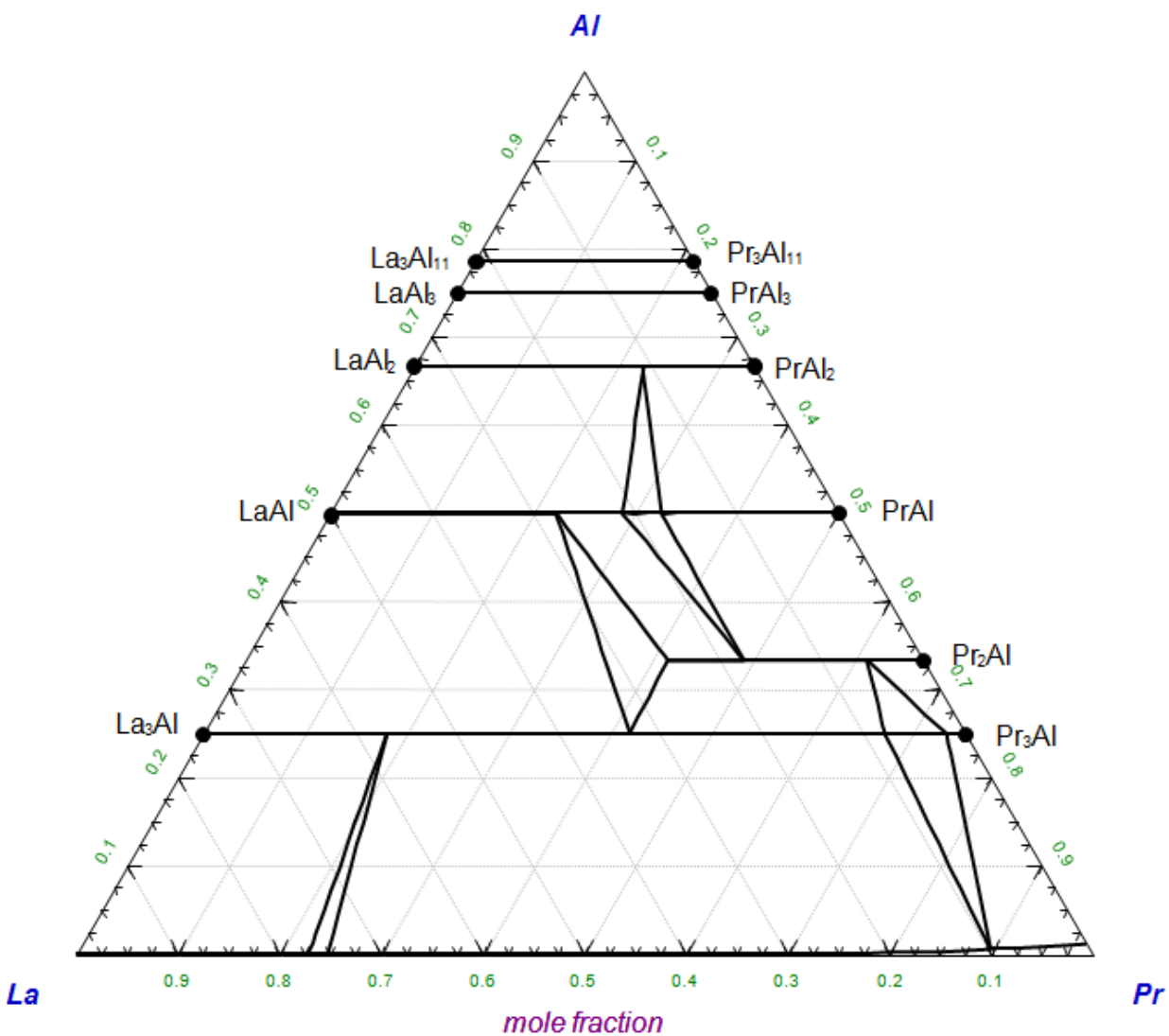
Figure 11. The calculated isothermal section of the Al–La–Pr ternary system at 773K compared with experimental data.

Figure 12. The calculated isothermal section of the Al–La–Ce ternary system at 773K compared with experimental data.
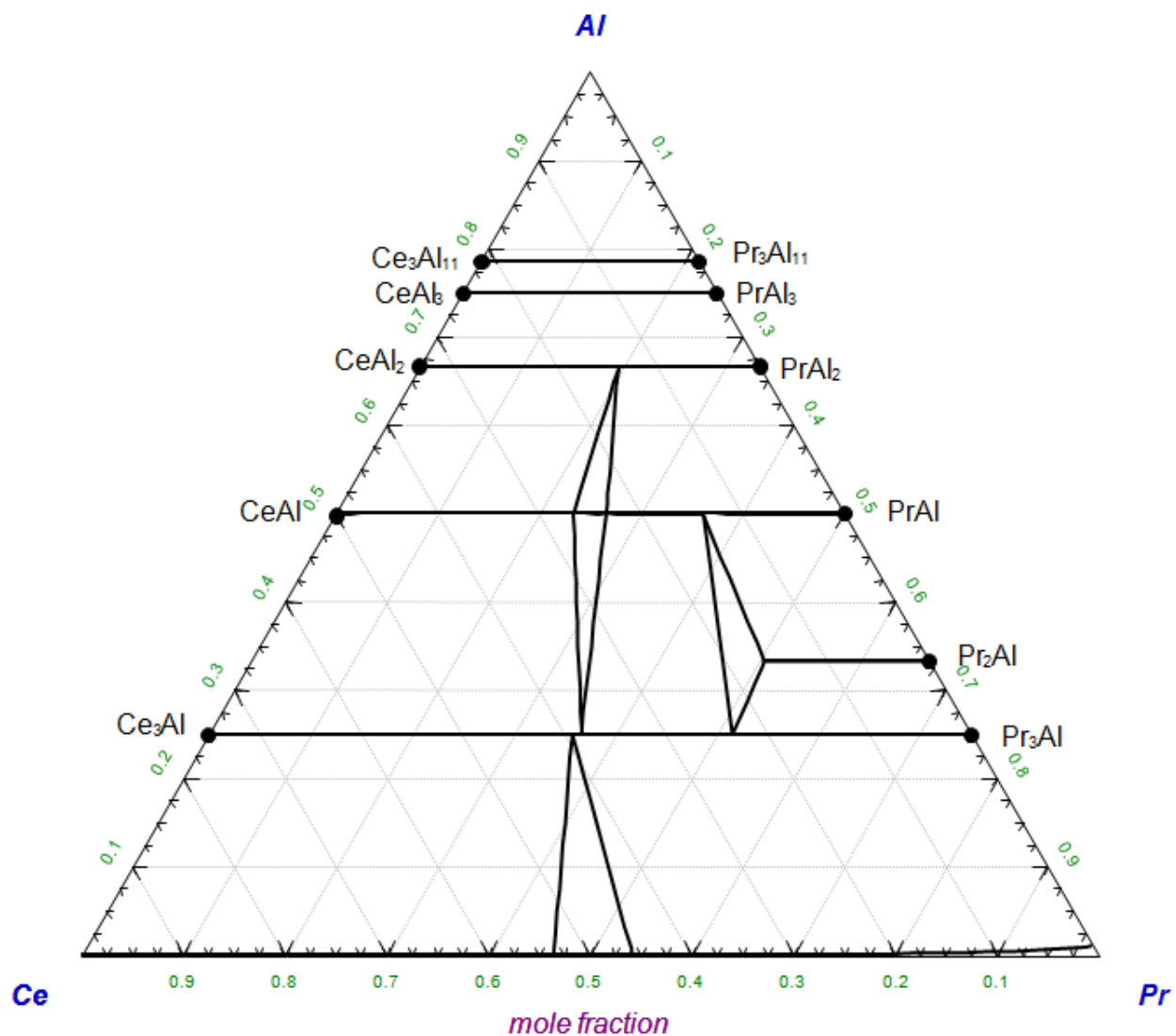
Figure 13. The calculated isothermal section of the Al–Ce–Pr ternary system at 773K compared with experimental data.

Table 3: Optimized model parameters for solid solutions in the present study (J/mole)

Al11RE3 (oI28-αAl₁₁La₃): [Al]₁₁(La, Ce, Pr, Nd)₃
Gibbs energies of end members and parameters
G(Al:La)　　= 11*GHSERAL* + 3*GHSERLA* -575,000+ 8.6*T*
G(Al:Ce)　　= 11*GHSERAL* + 3*GHSERCE* -610,000+ 39*T*
G(Al:Pr)　　= 11*GHSERAL*+ 3*GHSERPR* -614,974 + 59*T*

G(Al:Nd)	= 11$GHSERAL$+ 3$GHSERND$ -575,000 +53.5T

Al3RE (hP8-Ni$_3$Sn) : [Al]$_3$(La, Ce, Pr, Nd)

Gibbs energies of end members and parameters

G(Al:La)	= 3$GHSERAL$ +$GHSERLA$ − 176,552 + 3.5T
G(Al:Ce)	= 3$GHSERAL$ +$GHSERCE$ − 184,549+ 12.1T
G(Al:Pr)	= 3$GHSERAL$ +$GHSERPR$ − 187,760 + 18.3T
G(Al:Nd)	= 3$GHSERAL$ +$GHSERND$ − 181,100 + 19.7T

AlRE (oP16-AlEr): [Al](La, Ce, Pr, Nd)

Gibbs energies of end members and parameters

G(Al:La)	= $GHSERAL$ + $GHSERLA$ − 87,661 + 5.7T [a]
G(Al:Ce)	= $GHSERAL$ + $GHSERCE$ − 91,043 + 12.9T [a]
G(Al:Pr)	= $GHSERAL$ + $GHSERPR$ − 93,500 + 14.5T
G(Al:Nd)	= $GHSERAL$ + $GHSERND$ − 95,000 + 17.0T

AlRE (oC16-AlCe): [Al](La, Ce, Pr, Nd)

Gibbs energies of end members and parameters

G(Al:La)	= $GHSERAL$ + $GHSERLA$ − 89,000 + 5.7T
G(Al:Ce)	= $GHSERAL$ + $GHSERCE$ − 91,880 + 12.9T
G(Al:Pr)	= $GHSERAL$ + $GHSERPR$ − 92,663 + 14.5T [a]
G(Al:Nd)	= $GHSERAL$ + $GHSERND$ − 94,498 + 17.0T [a]

AlRE2 (oP12-Co$_2$Si): [Al](La, Ce, Pr, Nd)$_2$

Gibbs energies of end members and parameters

G(Al:La)	= $GHSERAL$ + 2$GHSERLA$ − 82,843
G(Al:Ce)	= $GHSERAL$ + 2$GHSERCE$ − 67,375-16.4 T
G(Al:Pr)	= $GHSERAL$ + 2$GHSERPR$ − 97,500 + 15.1T
G(Al:Nd)	= $GHSERAL$ + 2$GHSERND$ − 99,160 + 16.2T

AlRE3 (hP8-Ni₃Sn): [Al](La, Ce, Pr, Nd)₃	
Gibbs energies of end members and parameters	
G(Al:La)	= *GHSERAL* + 3*GHSERLA* − 77,300 − 12.0*T*
G(Al:Ce)	= *GHSERAL* + 3*GHSERCE* − 101,800 + 19.9*T*
G(Al:Pr)	= *GHSERAL* + 3*GHSERPR* − 99,326 + 17.2*T*
G(Al:Nd)	= *GHSERAL* + 3*GHSERND* − 98,660 + 13.9*T*
AlRE3 (cP4-AuCu₃): [Al](La, Ce, Pr, Nd)₃	
Gibbs energies of end members and parameters	
G(Al:La)	= *GHSERAL* + 3*GHSERLA* − 58,576 [a]
G(Al:Ce)	= *GHSERAL* + 3*GHSERCE* − 99,800 + 16.0*T*
G(Al:Pr)	= *GHSERAL* + 3*GHSERPR* − 101,000 + 17.2*T*
G(Al:Nd)	= *GHSERAL* + 3*GHSERND* − 75,230 + 13.9*T* [a]
FCC (cF4-Cu) : (Al, La, Ce, Pr, Nd)	
L(Ce, Pr)	= −627.6 − 418.4(X_{Pr}-X_{Ce})
DHCP (hP4-La) : (Al, La, Ce, Pr, Nd)	
L(Ce, Pr)	= −3765.6
L(La, Nd)	= −711.3

Parameters taken from Jin et al (Jin et al., 2011) except for those marked with [a] which is optimized in the present work.

APPENDIX 4   Adjusted Al-rich Corner in Al-RE(RE:Gd, Tb, Dy, Ho, Er) Systems and Model Parameters for Al-Mg System
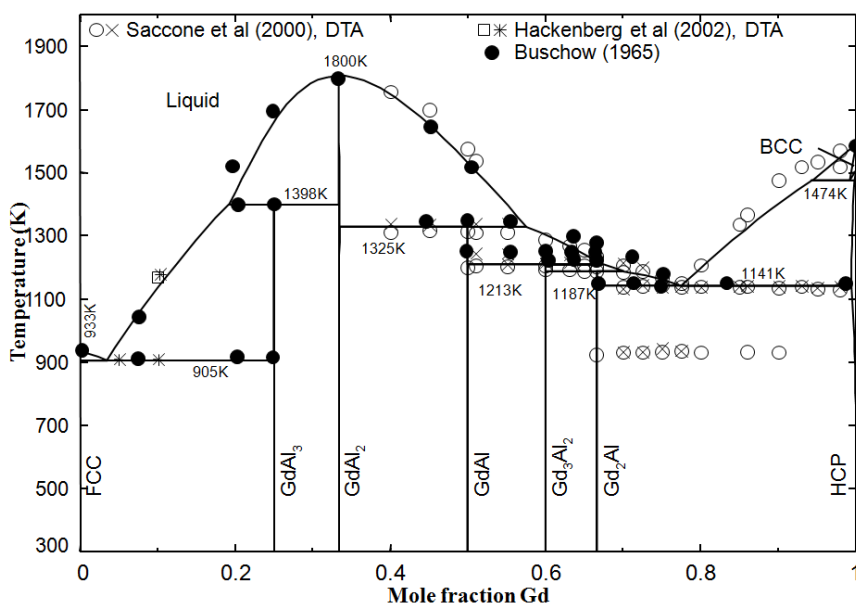

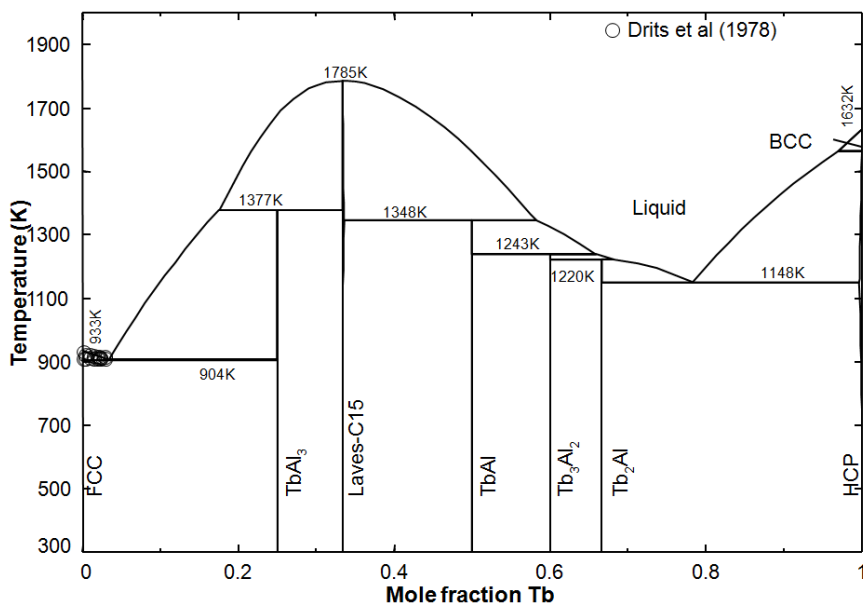Figure 1 Optimized phase diagram of Al-Gd system

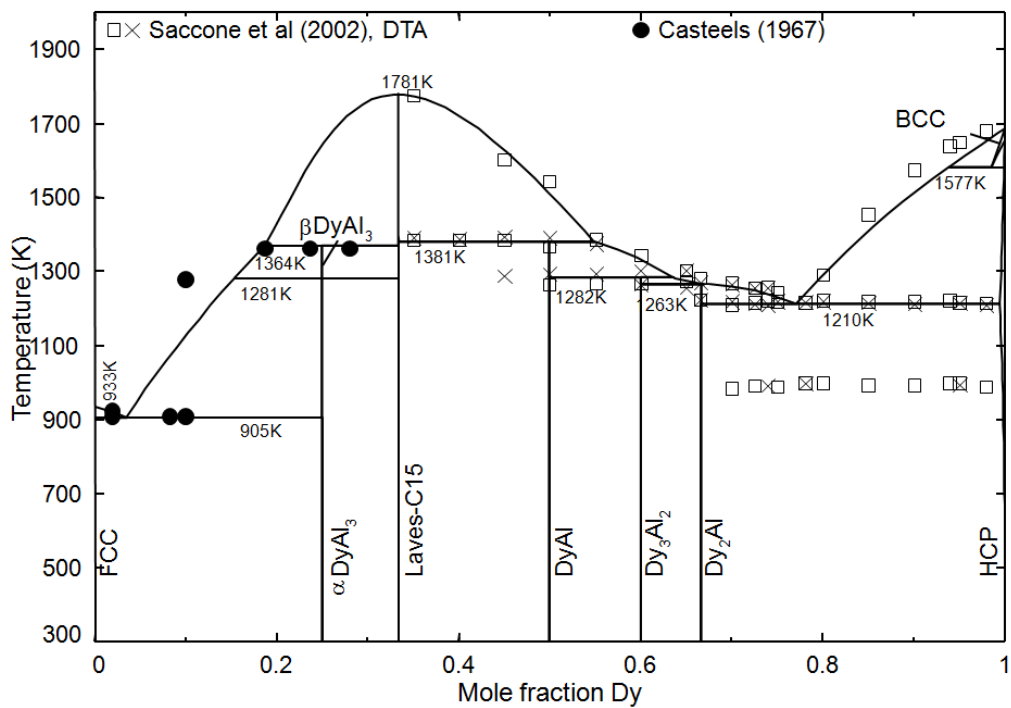Figure 2 Optimized phase diagram of Al-Tb system

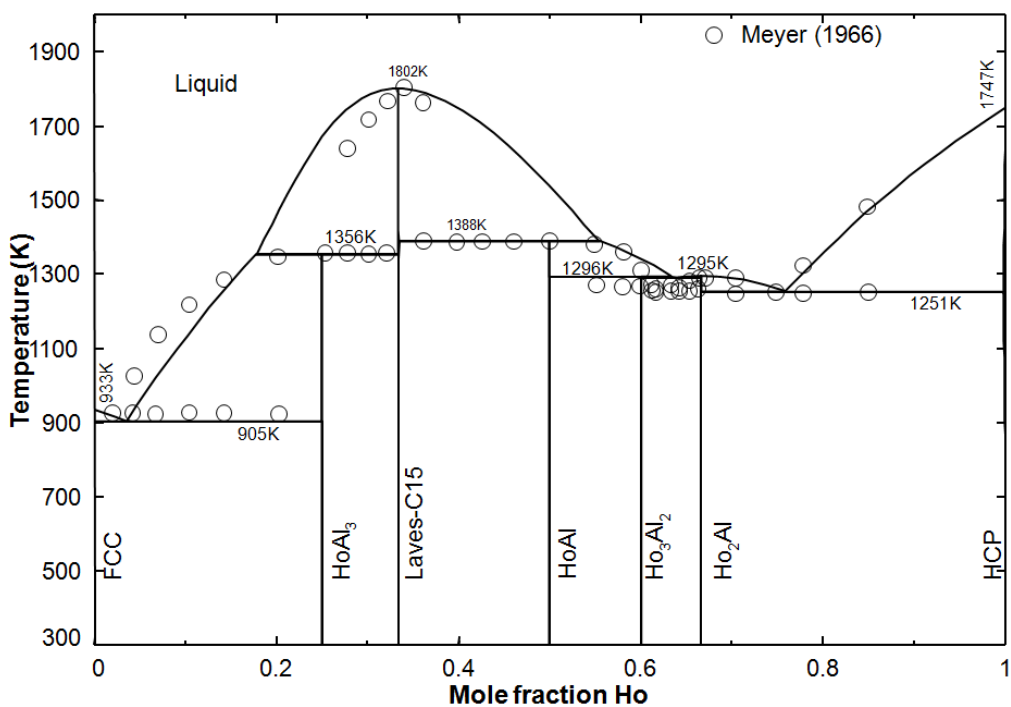Figure 3 Optimized phase diagram of Al-Dy system

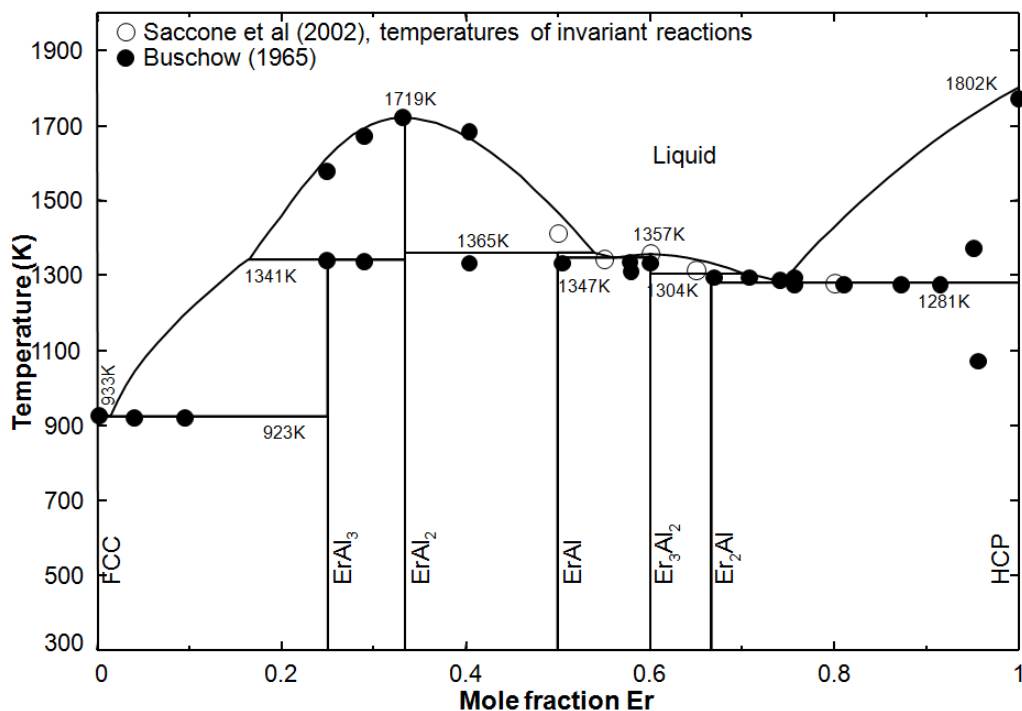Figure 4 Optimized phase diagram of Al-Ho system

Figure 5 Optimized phase diagram of Al-Er system

Table 1 Adjusted model parameters of stoichiometric phases in the Al–Gd, Al–Tb, Al–Dy, Al–Ho and Al–Er binary systems.

Compound	$\Delta H°_{25°C}$ (J/mol)	$S°_{25°C}$ (J/mol-K)	C_p (J/mol-K)
GdAl$_3$	-162,624	149.19	$C_p=C_p$ (Gd, HCP–A3) + 3C_p(Al,FCC–A1)
TbAl$_3$	-166,523	146.91	$C_p=C_p$ (Tb, HCP–A3) + 3C_p(Al,FCC–A1)
αDyAl$_3$	-164,431	152.81	$C_p=C_p$ (Dy, HCP–A3) + 3C_p(Al,FCC–A1)
βDyAl$_3$*	-163,431	153.59	$C_p=C_p$ (Dy, HCP–A3) + 3C_p(Al,FCC–A1)
HoAl$_3$	-165,059	152.64	$C_p=C_p$ (Ho, HCP–A3) + 3C_p(Al,FCC–A1)
ErAl$_3$	-160,000	156.86	$C_p=C_p$ (Er, HCP–A3) + 3C_p(Al,FCC–A1) - 9

note : * High-temperature stable compounds

Table 2 Adjusted model parameters of the Modified Quasichemical Model for liquid alloys in the Al-RE systems (RE: Gd, Dy, Ho) (J/mole) (* from Jin et al. (Jin et al., 2010))

Coordination numbers				Gibbs energies of pair exchange reactions
i	j	Z^i_{ij}	Z^j_{ij}	
Al	Gd	3	6	$\Delta g_{AlGd}= -48{,}116 +5.02T + (-3{,}264 -1.80T)X_{AlAl} -7{,}113X_{GdGd}$ *
Al	Gd	3	6	$\Delta g_{AlGd}= -48{,}116 +5.02T + (-2{,}008 -1.80T)X_{AlAl} -7{,}113X_{GdGd}$
Al	Dy	3	6	$\Delta g_{AlDy}= -47{,}279 +4.18T + (-3{,}347 -1.67T)X_{AlAl} -8{,}786X_{DyDy}$*
Al	Dy	3	6	$\Delta g_{AlDy}= -47{,}279 +4.18T + (-2{,}385 -1.67T)X_{AlAl} -8{,}786X_{DyDy}$
Al	Ho	3	6	$\Delta g_{AlHo}= -46{,}944 +4.18T + (-3{,}766 -2.09T)X_{AlAl} -11{,}715X_{HoHo}$*
Al	Ho	3	6	$\Delta g_{AlHo}= -46{,}944 +4.18T + (-3{,}347 -2.09T)X_{AlAl} -11{,}715X_{HoHo}$

Table 3 Model parameters of $Al_{30}Mg_{23}$ and liquid in the Al-Mg system optimized by Chartrand (Chartrand, 2006)

Compound	$\Delta H^\circ_{25\,°C}$ (J/mol)	$S^\circ_{25\,°C}$ (J/mol-K)	C_p (J/mol-K)
$Al_{30}Mg_{23}$	-116,328	1673.42	$C_p=30C_p$ (Al, FCC–A1) + $23C_p$(Mg, HCP–A3)

Coordination numbers				Gibbs energies of pair exchange reactions
i	j	Z^i_{ij}	Z^j_{ij}	
Al	Al	6	6	
Mg	Mg	6	6	$\Delta g_{AlMg}= -2{,}761 +1.53T + (-418.4 +0.628T)X_{AlAl}$
Al	Mg	6	6	

Table 4 Model parameters of FCC, HCP, Beta and Gamma phases in the Al-Mg system optimized by Chartrand (Chartrand, 2006)

Gamma (cI58-αMn)**: (Mg)$_{10}$(Mg, Al)$_{24}$(Mg, Al)$_{24}$**
Gibbs energies of end members and parameters
G(Mg:Mg:Mg) = 58*GHSERMG* + 359,155 – 174.6*T*
G(Mg:Mg:Al) = 34*GHSERMG* + 24*GHSERAL* – 208,742 + 78.5*T*
G(Mg:Al:Mg) = 34*GHSERMG* + 24*GHSERAL* + 568,249 – 276.1*T*
G(Mg:Al:Al) = 10*GHSERMG* + 48*GHSERAL* +178,763 - 203*T*
Beta (Mg$_2$Al$_3$)**: (Al)$_{19}$(Mg,Al)$_2$(Mg)$_{12}$**
Gibbs energies of end members and parameters
G(Al:Mg:Mg)   = 19*GHSERAL* + 14*GHSERLA*– 72,446 – 27.6*T*
G(Al:Al:Mg) = 21*GHSERAL* + 12*GHSERMG*– 82,111 – 13.8*T*
FCC_A1: (Al, Mg)
Gibbs energies of end members and parameters
G(Al,FCC) = *GHSERAL*   G(Mg,FCC) = *GFCCMG*
L(Al, Mg)   =4,144 - 4.379*T* +*(207.4 – 3.055T)(X$_{Mg}$ - X$_{Al}$)*
HCP_A3: (Al, Mg)
Gibbs energies of end members and parameters
G(Al, HCP) = *GHCPAL*   G(Mg,HCP) = *GHSERMG*
L(Al, Mg)   = 2,510